RADICAL AND RADICAL ION REACTIVITY IN NUCLEIC ACID CHEMISTRY

Wiley Series of Reactive Intermediates in Chemistry and Biology

Steven E. Rokita, Series Editor

Quinone Methides
Edited by Steven E. Rokita

Radical and Radical Ion Reactivity in Nucleic Acid Chemistry
Edited by Marc M. Greenberg

RADICAL AND RADICAL ION REACTIVITY IN NUCLEIC ACID CHEMISTRY

Edited by

MARC M. GREENBERG

WILEY

A John Wiley & Sons, Inc., Publication

Published by John Wiley & Sons, Inc., Hoboken, New Jersey

Published simultaneously in Canada

Library of Congress Cataloging-in-Publication Data:

Radical and radical ion reactivity in nucleic acid chemistry / editor, Marc M. Greenberg.

p. cm.

Includes index.

ISBN 978-0-470-25558-2 (cloth)

1. Nucleic acids–Effect of radiation on. 2. DNA. 3. Ionization. 4. Free radicals (Chemistry) I. Greenberg, Marc M.

QP620.R337 2009

572′.33–dc22

2009009770

Printed in the United States of America

10 9 8 7 6 5 4 3 2 1

CONTENTS

PREFACE TO SERIES

Most stable compounds and functional groups have benefited from numerous monographs and series devoted to their unique chemistry, and most biological materials and processes have received similar attention. Chemical and biological mechanisms have also been the subject of individual reviews and compilations. When reactive intermediates are given center stage, presentations often focus on the details and approaches of one discipline despite their common prominence in the primary literature of physical, theoretical, organic, inorganic, and biological disciplines. The *Wiley Series on Reactive Intermediates in Chemistry and Biology* is designed to supply a complementary perspective from current publications by focusing each volume on a specific reactive intermediate and endowing it with the broadest possible context and outlook. Individual volumes may serve to supplement an advanced course, sustain a special topics course, and provide a ready resource for the research community. Readers should feel equally reassured by reviews in their speciality, inspired by helpful updates in allied areas and intrigued by topics not yet familiar.

This series revels in the diversity of its perspectives and expertise. Where some books draw strength from their focused details, this series draws strength from the breadth of its presentations. The goal is to illustrate the widest possible range of literature that covers the subject of each volume. When appropriate, topics may span theoretical approaches for predicting reactivity, physical methods of analysis, strategies for generating intermediates, utility for chemical synthesis, applications in biochemistry and medicine, impact on the environmental, occurrence in biology, and more. Experimental systems used to explore these topics may be equally broad and range from simple models to complex arrays and mixtures such as those found in the final frontiers of cells, organisms, earth, and space.

Advances in chemistry and biology gain from a mutual synergy. As new methods are developed for one field, they are often rapidly adapted for application in the other. Biological transformations and pathways often inspire analogous development of new procedures in chemical synthesis, and likewise, chemical characterization and identification of transient intermediates often provide the foundation for understanding the biosynthesis and reactivity of many new biological materials. While individual chapters may draw from a single expertise, the range of contributions contained within each volume should collectively offer readers with a multidisciplinary analysis and exposure to the full range of activities in the field. As this series grows, individualized compilations may also be created through electronic access to highlight a particular approach or application across many volumes that together cover a variety of different reactive intermediates.

Interest in starting this series came easily, but the creation of each volume of this series required vision, hard work, enthusiasm, and persistence. I thank all of the contributors and editors who graciously accepted and will accept the challenge.

STEVEN E. ROKITA

University of Maryland

INTRODUCTION

More than a century ago, observations were reported in a period of less than five years from distinct fields that would comprise a large portion of the basis of radical mediated DNA damage. X-rays were discovered in 1895 and used to treat tumors shortly thereafter. In addition, by the turn of the twentieth century the Fenton reaction was reported and in 1900 Gomberg proposed the formation of the first carbon-centered radical. These seemingly disconnected reports were ultimately determined to overlap significantly. X-rays were found to kill tumor cells by oxidatively damaging DNA. Hydroxyl radical, which is produced from hydrogen peroxide in the Fenton reaction, was found to be a primary reactive species responsible for DNA damage mediated by gamma radiolysis. Finally, the connections are completed by the formation of radicals in DNA. The carbon-centered (and other) DNA radicals are produced from hydroxyl radical by hydrogen atom abstraction, as well as by addition to π-bonds.

The complexity of this chemistry becomes immediately apparent upon considering the size and heterogeneity of DNA, as well as the variety of experimental conditions (e.g., O_2, redox active metal ions, hydrogen atom donors) under which damage is induced.

Despite the complex nature of oxidative DNA damage, a broad range of scientists using a variety of physical and analytical methods have made significant contributions to our understanding of this chemistry during the latter half of the twentieth century. Clemens von Sonntag, a leader in this field, summarized much of this research in his seminal book *The Chemical Basis of Radiation Biology* (1987). By using ionizing radiation in conjunction with various techniques such as mass spectrometry and EPR spectroscopy, scientists were able to identify products, observe reactive intermediates, and proffer mechanisms of nucleic acid damage. Recent contributions describing significant advances in computational aspects of radiation damage, as well the direct

effects of ionizing radiation, the role of reactive species other than hydroxyl radical produced by ionizing radiation, the effects of electron affinic radiosensitizing agents on DNA radical chemistry, and the exciting realization of the role of low energy electrons in DNA damage, are described in this book.

Investigations in which ionizing radiation is used to initiate DNA damage face the limitation that they lack control over which reactive intermediates are produced or they cannot control where nucleic acids are damaged. The advent of solid phase oligonucleotides synthesis, modern mass spectrometry methods capable of analyzing biopolymers directly (e.g., MALDI-TOF MS and ESI-MS), and the assimilation of biochemical techniques such as gel electrophoresis and the utilization of nucleic acid modifying enzymes provided chemists with the wherewithal to probe oxidative DNA damage with greater precision. By utilizing these tools in conjunction with chemical synthesis of oligonucleotides containing modified nucleotides, chemists were able to simplify studies on nucleic acid damage and in the process uncover mechanistic complexities and unrecognized reaction pathways. In addition, the application of these and other state-of-the-art techniques facilitated elucidating the pathways for electron transfer in DNA that can be initiated directly or indirectly by ionizing radiation, as well as the utilization of DNA damage as a means for understanding protein–DNA interactions, the mechanisms of drugs and other species that target DNA, and the utilization of DNA damage as a chemical sensor. Experts on the respective topics also review advances in each of these areas in this compilation.

I am grateful to all of the contributors to this book. Their research and that of others described within have provided a deeper understanding of this biologically and technologically significant area of science and have also provided the basis for future investigations and applications of radicals in nucleic acid damage in general. Finally, I want to thank Professor Steven Rokita for having the vision and motivation to establish *Reactive Intermediates in Chemistry and Biology,* as well as for inviting me to participate in this project.

MARC M. GREENBERG

Johns Hopkins University

CONTRIBUTORS

William A. Bernhard, Department of Biochemistry and Biophysics, University of Rochester, Rochester, NY 14472, USA

Jean Cadet, Laboratoire Lésions des Acides Nucléiques, SCIB-UMR-E no. 3 (CEA/UJF), Institut Nanosciences et Cryogénie, CEA/Grenoble, F-38054 Grenoble Cedex 9, France; and Département de Médecine Nucléaire et Radiobiologie, Faculté de Médecine et des Sciences de la Santé, Université de Sherbrooke, Sherbrooke, Québec, Canada J1H 5N4

Chryssostomos Chatgilialoglu, ISOF, Consiglio Nazionale delle Richerche, 40129 Bologna, Italy

Conor Crean, Chemistry Department and Radiation and Solid State Laboratory, New York University, New York, NY 10003, USA

Thierry Douki, Laboratoire Lésions des Acides Nucléiques, SCIB-UMR-E no. 3 (CEA/UJF), Institut Nanosciences et Cryogénie, CEA/Grenoble, F-38054 Grenoble Cedex 9, France

Didier Gasparutto, Laboratoire Lésions des Acides Nucléiques, SCIB-UMR-E no. 3 (CEA/UJF), Institut Nanosciences et Cryogénie, CEA/Grenoble, F-38054 Grenoble Cedex 9, France

Nicholas E. Geacintov, Chemistry Department and Radiation and Solid State Laboratory, New York University, New York, NY 10003, USA

Marc M. Greenberg, Department of Chemistry, Johns Hopkins University, Baltimore, MD 21218, USA

Kiyohiko Kawai, The Institute of Scientific and Industrial Research (SANKEN), Osaka University, Ibaraki, Osaka 567-0047, Japan

Sean M. Kerwin, Division of Medicinal Chemistry, College of Pharmacy, The University of Texas at Austin, Austin, TX 78712, USA

Anil Kumar, Department of Chemistry, Oakland University, Rochester, MI 48309, USA

Tetsuro Majima, The Institute of Scientific and Industrial Research (SANKEN), Osaka University, Ibaraki, Osaka 567-0047, Japan

Richard A. Manderville, Departments of Chemistry and Toxicology, University of Guelph, Guelph, Ontario, Canada N1G 2W1

Jean-Luc Ravanat, Laboratoire Lésions des Acides Nucléiques, SCIB-UMR-E no. 3 (CEA/UJF), Institut Nanosciences et Cryogénie, CEA/Grenoble, F-38054 Grenoble Cedex 9, France

Léon Sanche, Centre de Recherche en Radiothérapie, Faculté de Médecine, Université de Sherbrooke, Sherbrooke, Québec Canada, J1H 5N4; and Department of Physics and Astronomy, The Open University, Walton Hall, Milton Keynes, MK7 6AA

Michael D. Sevilla, Department of Chemistry, Oakland University, Rochester, MI 48309, USA

Vladimir Shafirovich, Chemistry Department and Radiation and Solid State Laboratory, New York University, New York, NY 10003, USA

Hiroshi Sugiyama, Department of Chemistry, Graduate School of Science, Kyoto University, Kyoto 606-8502, Japan

Julie M. Sullivan, Department of Chemistry, University of North Carolina, Chapel Hill, NC 27599, USA

Ryu Tashiro, Faculty of Pharmaceutical Sciences, Suzuka University of Medical Science, Mie 513-8670, Japan

H. Holden Thorp, Department of Chemistry, University of North Carolina, Chapel Hill, NC 27599, USA

Reji Varghese, Institute of Organic Chemistry, University of Regensburg, D-93040 Regensburg, Germany

Hans-Achim Wagenknecht, Institute of Organic Chemistry, University of Regensburg, D-93040 Regensburg, Germany

J. Richard Wagner, Département de Médecine Nucléaire et Radiobiologie, Faculté de Médecine et des Sciences de la Santé, Université de Sherbrooke, Sherbrooke, Québec, Canada J1H 5N4

Peter Wardman, Gray Institute for Radiation Oncology and Biology, University of Oxford, Oxford OX3 7DQ, United Kingdom

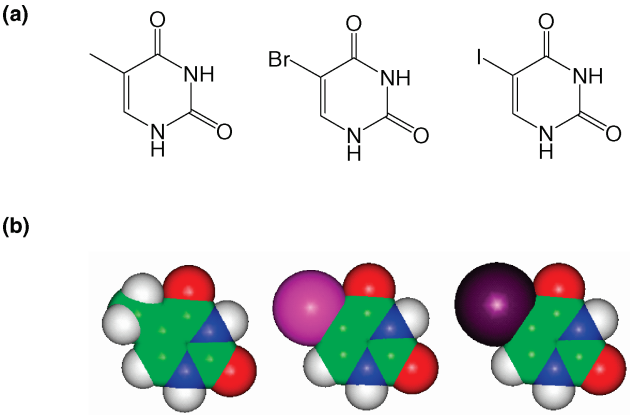

FIGURE 6.1. Chemical structures (**a**) and CPK models (**b**) of thymine, 5-bromouracil, and 5-iodouracil.

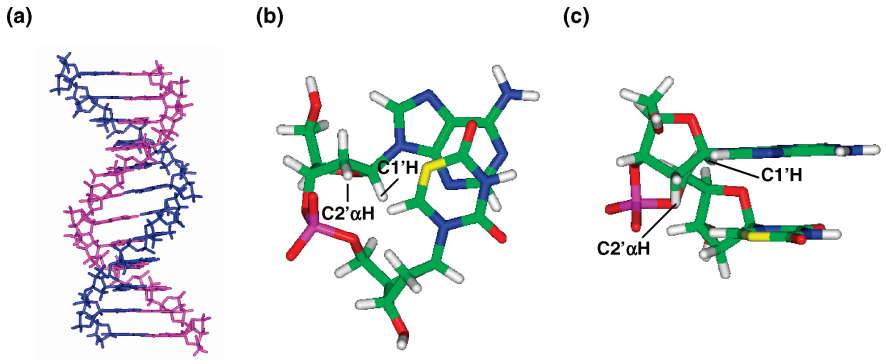

FIGURE 6.3. (**a**) Structure of B-form DNA. Close-up view of the $A^{Br}U$ sequence (**b**), and its side view (**c**). C5 of the uracil-5-yl radical is depicted in yellow.

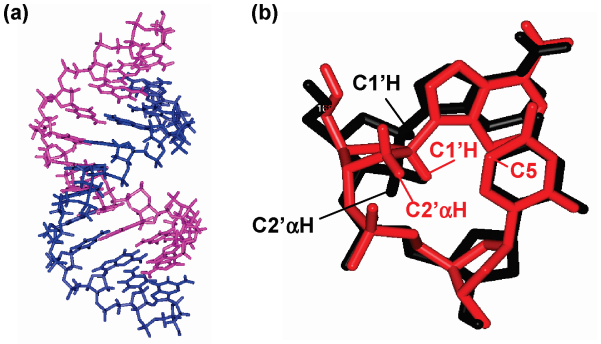

FIGURE 6.4. (**a**) Structure of A-form DNA. (**b**) Close-up view of $A^{Br}U$ step in the A-form (black) and the B-form (red).

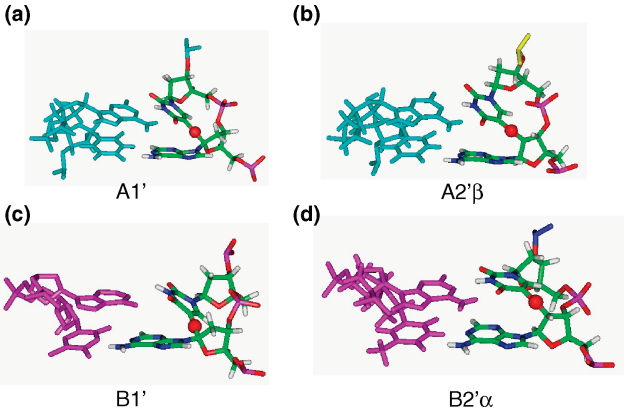

FIGURE 6.5. Estimated transition states of H abstraction in A- (**a**,**b**) and B-form (**c**,**d**) DNA. RNA and DNA are shown in blue and magenta, respectively. A red ball indicates an abstracting H atom.

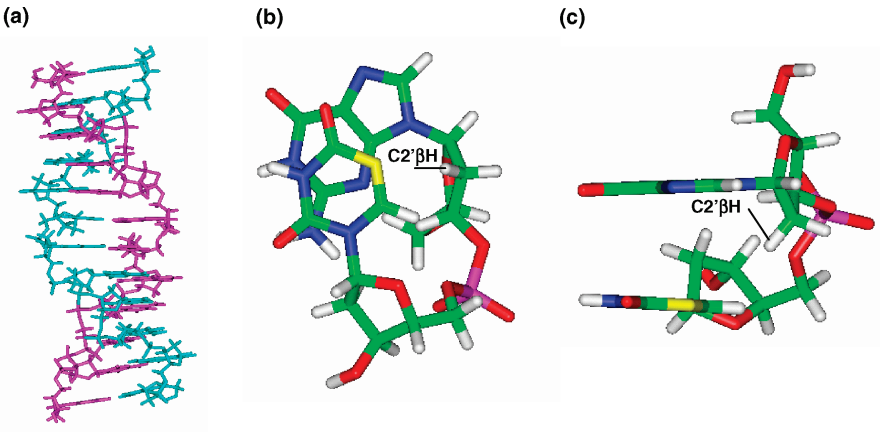

FIGURE 6.6. (**a**) Structure of Z-form DNA. (**b**) Close-up views of the GU sequence and its side view. (**c**) C5 of the uracil-5-yl radical is shaded yellow.

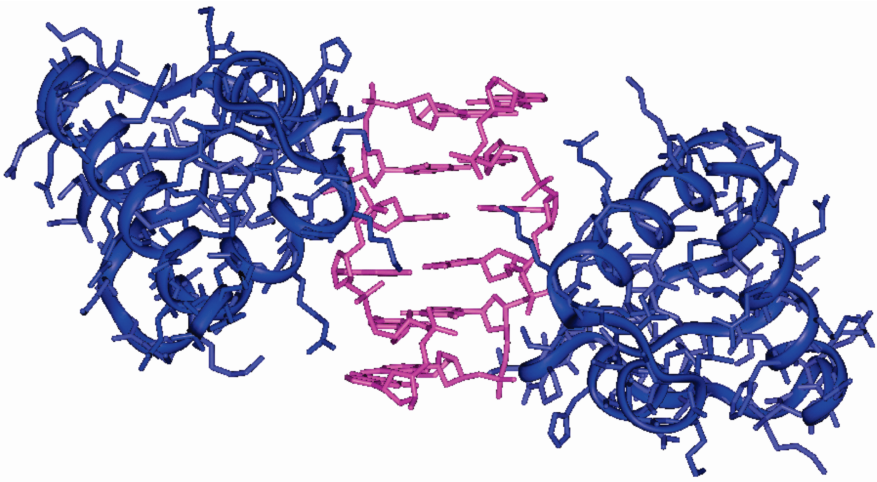

FIGURE 6.7. Structure of the d(CGCGCG)$_2$–Zα complex.

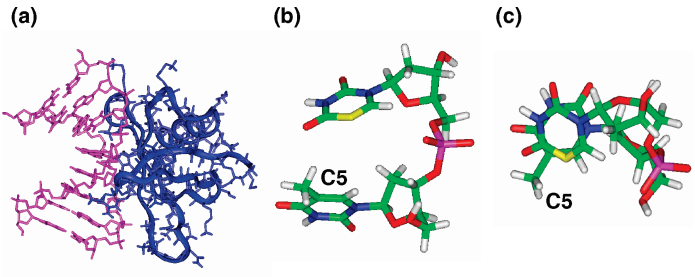

FIGURE 6.8. (**a**) Structure of the Sso7d–DNA complex. (**b**) Close-up view of the TU step and (**c**) its side view. C5 of the uracil-5-yl radical is shaded yellow.

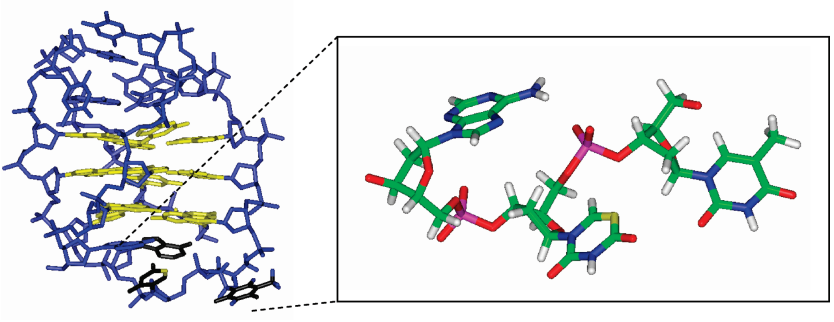

FIGURE 6.9. Structure of human telomere sequence 5′-AGGG(TTAGGG)$_3$-3′ in an NaCl solution and a close-up view of the diagonal TTA loop region. C5 of the uracil-5-yl radical is shaded yellow.

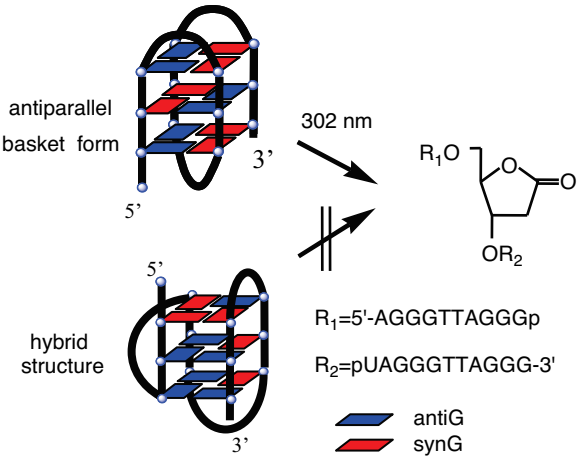

FIGURE 6.10. The ribonolactone residue is formed at the diagonal loop of the antiparallel basket form of the human telomere sequence, 5′-AGGGTTAGGGT^{I}UAGGGTTAGGG-3′, under irradiation at 302 nm. The hybrid structure does not produce ribonolactone residues in the presence of K^+ ions.

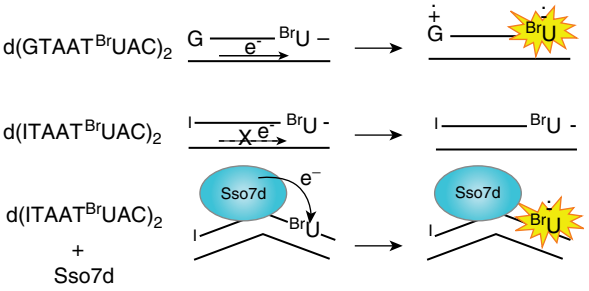

FIGURE 6.15. Electron transfer from Sso7d to ^{Br}U in the 5′-d(ITAAT^{Br}UAC)-3′ sequence.

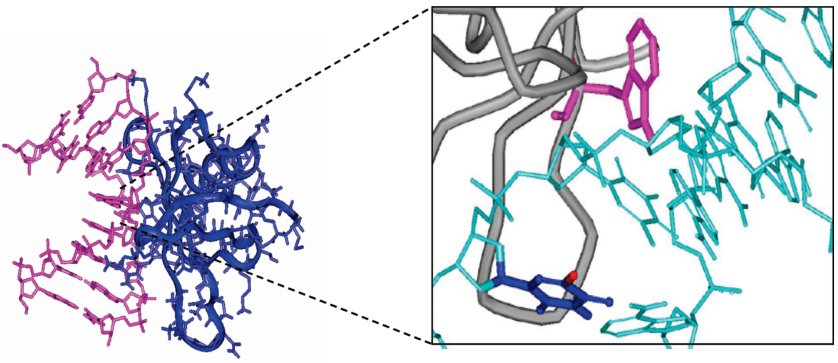

FIGURE 6.16. Close-up view of the structure of the Sso7d-d(GTAATTAC)$_2$ complex. Trp24 moiety (electron donnor) and ^{Br}U (acceptor) are shown in pink and blue, respectively.

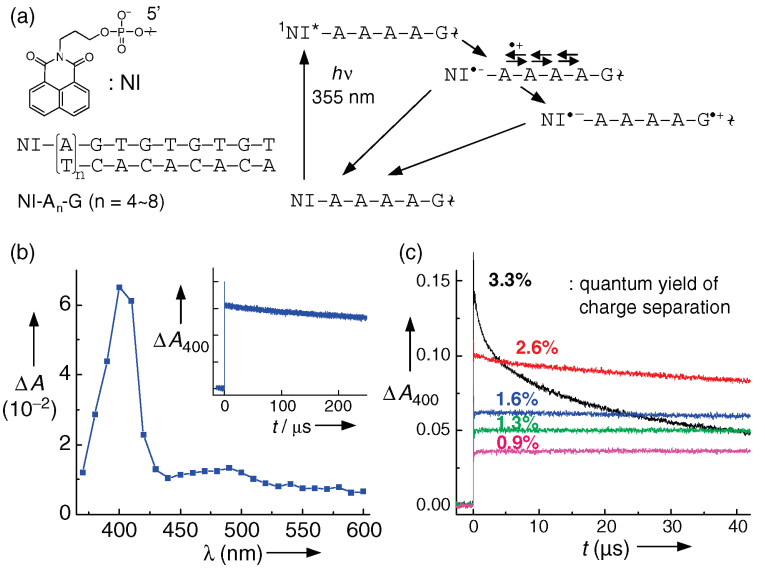

FIGURE 7.1. (**a**) Chemical structure of naphthalimide (NI) attached to the 5′-end of DNA, sequences of the NI-modified DNA, and the kinetic scheme for photoinduced one-electron oxidation of A, hole transfer through As, hole trapping at G, and charge recombination in DNA. (**b**) Transient absorption spectrum for NI–A_6–G, observed 200 ns after laser flash excitation (100 μM DNA in 20 mM Na phosphate buffer (pH 7.0) and 100 mM NaCl). **Inset**: Time profile monitored at 400 nm. (**c**) Decay profiles for NI–A_n–G ($n = 4$–8) monitored at 400 nm, following excitation of NI with a 355-nm laser pulse.

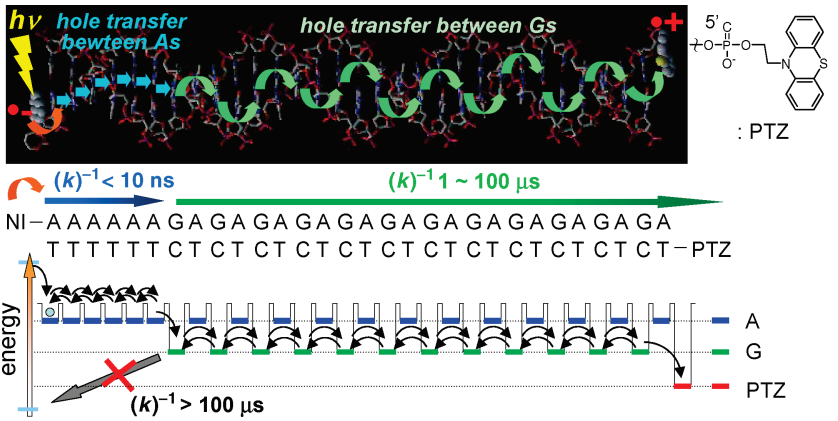

FIGURE 7.2. Strategy for the kinetic study of long-distance hole transfer process. Molecular representation for 30-mer DNA conjugated with naphthalimide (NI) and phenothiazine (PTZ), which work as a photosensitizer and hole acceptor, respectively, and schematic illustration for hole injection via hole transfer between As and long-distance hole transfer process via hole transfer between G through DNA.

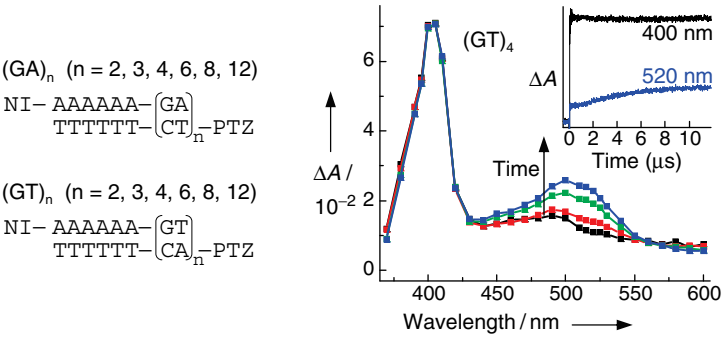

FIGURE 7.3. Transient absorption spectra observed at 200 ns (black), 2 (red), 5 (green), and 10 μs (blue) after a 355-nm laser flash (4 ns, 20 mJ pulse^{-1}) with excitation of the NI site during the laser flash photolysis of NI- and PTZ-modified DNA $(GT)_4$. **Inset**: Time profiles observed at 400 (black) and 520 nm (blue) assigned to the transient absorption peak for $NI^{\bullet -}$ and $PTZ^{\bullet +}$, respectively. Sample solution contained 100 μM duplex DNA, 20 mM Na phosphate buffer (pH 7.0), and 100 mM NaCl.

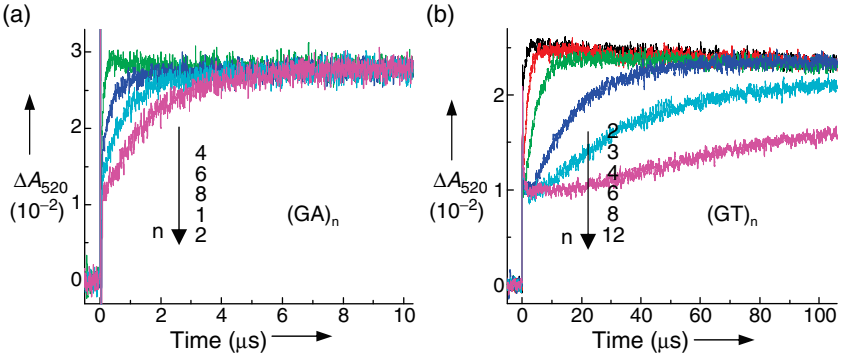

FIGURE 7.4. Time profiles of the transient absorption monitored at 520 nm assigned to $PTZ^{\bullet +}$ after the 355-nm laser flash excitation for (**a**) $(GA)_n$ and (**b**) $(GT)_n$ sequences. Sample solution contained 100 μM duplex DNA, 20 mM Na phosphate buffer (pH 7.0), and 100 mM NaCl.

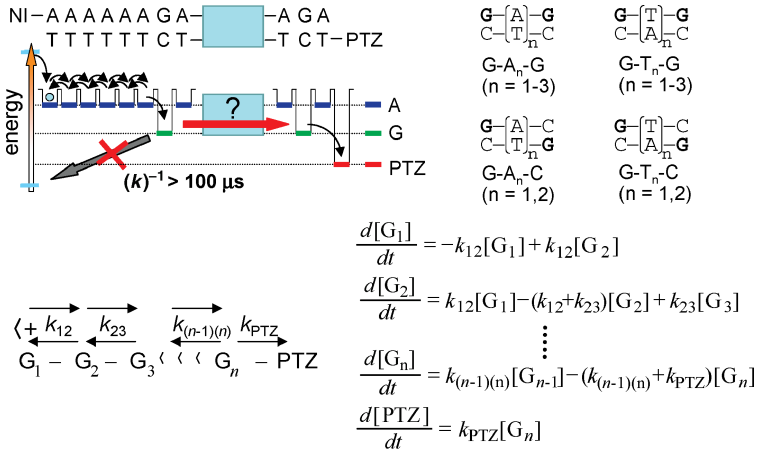

FIGURE 7.6. Schematic representation, kinetic model, and simultaneous differential equations for hole transfer process through DNA of various sequence patterns.

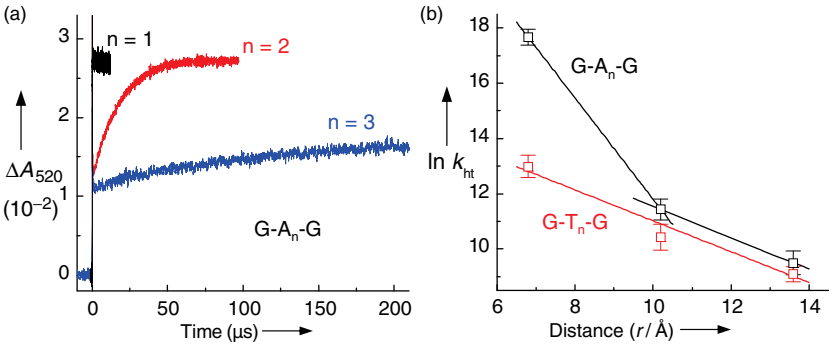

FIGURE 7.7. (**a**) Time profiles of the transient absorption of $PTZ^{\bullet+}$ monitored at 520 nm for G–A_n–G ($n = 1$–3). (**b**) Plots of logarithm of the hole transfer rate versus distance between Gs (r) for G–A_n–G (black) and G–T_n–G (red).

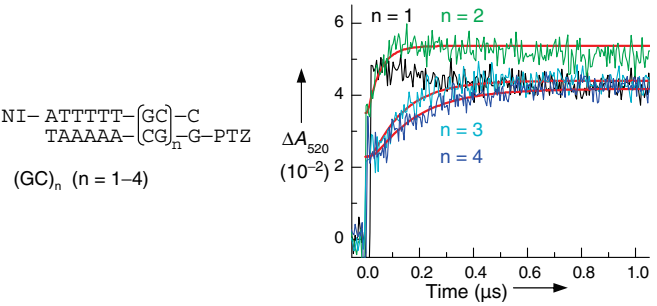

FIGURE 7.8. Sequences and time profiles of the transient absorption of $PTZ^{\bullet+}$ monitored at 520 nm during the 355-nm laser flash photolysis of an Ar-saturated solution of NI- and PTZ-modified DNAs with GC repeat sequences.

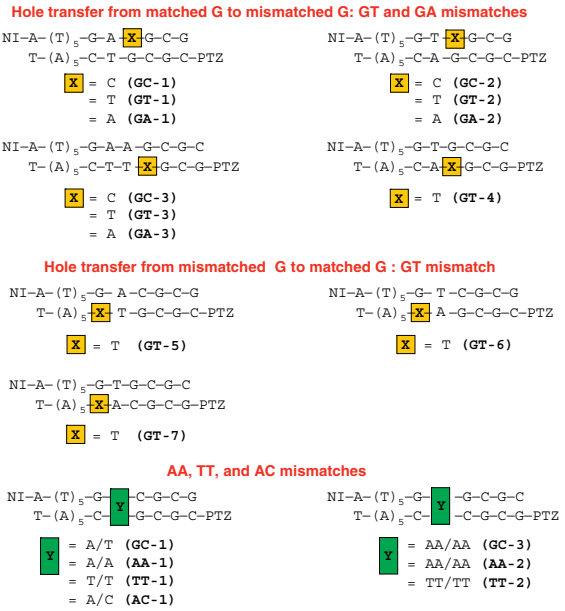

FIGURE 7.9. Sequences of NI- and PTZ-modified DNA used for the investigation of hole transfer through mismatched sequences.

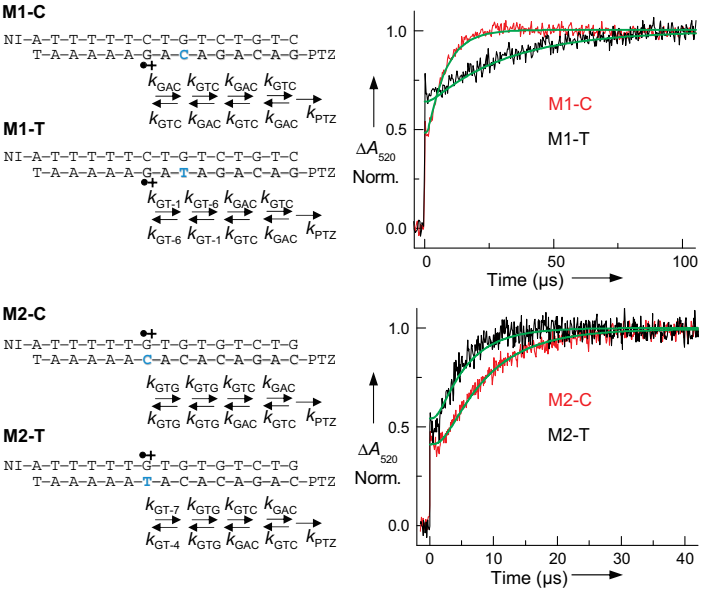

FIGURE 7.10. Discrimination of mismatch DNA related to SNP by hole transfer kinetics through DNAs. Bold letters shown in blue indicate the SNP sequences. Time profiles of the transient absorption of $PTZ^{\bullet+}$ at 520 nm during the 355-nm laser flash photolysis of Ar-saturated aqueous solution containing 100 mM NaCl and 20 mM sodium phosphate (pH 7.0) at a strand concentration of 50 μM. The green smooth curves superimposed on the curves are the fit derived from the kinetic model using the hole transfer rates depicted in Tables 7.1 and 7.2.

1

THEORETICAL MODELING OF RADIATION-INDUCED DNA DAMAGE

ANIL KUMAR AND MICHAEL D. SEVILLA
Department of Chemistry, Oakland University, Rochester, MI 48309, USA

1.1. INTRODUCTION

Ionizing radiation causes a variety of damages to DNA in living systems. Thus, the understanding of radiation-induced chemical processes leading to specific damage in DNA is of substantial biological importance.[1–10] Radiation ionizes each component of DNA (i.e., base, sugar, phosphate) and the surrounding water molecules in a random fashion and produces a cascade of secondary electrons, most of which are below 15 eV and are designated as low-energy electrons (LEE). LEE are produced in a large quantity (4×10^4 per MeV energy deposited)[11] along the tracks of the ionizing radiation and have been shown to result in direct DNA damage in model systems in the seminal work of Sanche and co-workers, who found that LEEs create single- and double-strand breaks (SSBs and DSBs) in DNA through dissociative electron attachment (DEA).[12–18] These findings having been substantiated by the work of others.[19–22] Only a small fraction of LEE result in DNA damage, because most electrons are thermalized and either recombine with positive charge ("hole") or are captured by the pyrimidines [thymine (T) and cytosine (C)], resulting in radical anion formation. During ionization events, all the bases are randomly ionized and "holes" (radical cations) are formed, which travel within DNA toward the base having lowest ionization potential, the order being guanine (G) < adenine (A) < cytosine (C) ≈ thymine (T).[2] Therefore, in a randomly ionized DNA double strand, the hole tunnels or hops from one base to

Radical and Radical Ion Reactivity in Nucleic Acid Chemistry, Edited by Marc M. Greenberg

the next, finally localizing on guanine to form the guanine radical cation ($G^{\bullet+}$).[1–3, 7–9] Ionization radiation also induces holes on the sugar–phosphate backbone site that lead to two competitive reactions: (i) deprotonation of the sugar cation radical at a carbon site resulting in the formation of neutral sugar radicals at carbon C_1' to C_5' sites[23–28] and (ii) transfer of hole to a nearby base in DNA.[28]

Since most sugar radicals lead to DNA strand breaks, sugar radical formation in DNA becomes of crucial importance to the biological consequences of radiation. Recently, it has been found that irradiation of DNA by a high LET (linear energy transfer) radiation, a high-energy argon ion beam,[23] produced a far higher yield of sugar radicals than was found by a low LET radiation, γ-irradiation. The authors report that the excess sugar radicals were created within the track core.[23] The energy density in the track core is high and results in ionizations and excitations in close proximity. For this reason, it was hypothesized that excited states of radical cations might result in the neutral sugar radicals in the core of the ion track. To test this hypothesis, recent experiments in our laboratory were performed on the photoexcitation of guanine and adenine radical cations ($G^{\bullet+}$, $A^{\bullet+}$) in DNA model systems.[24–27] It was found that excited DNA base cation radicals formed high yield of sugar radicals which confirmed the proposed hypothesis.[24–27]

While strand breaks are biologically significant, it is combinations of DNA damages known as multiple damage sites (MDS) that are the most lethal type of DNA damage. Such combinations of single- and double-strand breaks and base damages with 10 base pairs are known to lead to irreparable damage because of the loss of local structural information. High-LET radiations (α particles, atom ion beams, neutrons) are found to be about 10 times more damaging than the low-LET radiations such as β particles, X rays, and γ rays in the production of such damage.

From the above discussion, it is evident that ionization and excitation are the initial events in DNA damage. As the damage unfolds from these initial events, the processes may become complex in nature; however, the simplicity of the initial events allow for a clear understanding of these initial processes. Thus ionization, excitation, and electron addition to DNA bases have been extensively treated by theoretical calculations using a variety of methods with density functional theory (DFT) perhaps the most useful to large systems. The advent of substantial computing power and the availability of inexpensive computational resources[29] allows the application of more sophisticated level of theoretical calculation such as TD-DFT, Møller–Plesset perturbation theory (MP2), CCSD(T), and CASPT2 that can shed light on the underlying chemical processes controlling the DNA damage. A close agreement between theory and experiment is expected, given an appropriate use of theory. In this review we present recent investigations that employ theory to aid understanding of DNA base and sugar radical formation, via ionization, excitation, and electron attachment to DNA. Specific topics include (1) ionization energies and electron affinities of bases and base pairs, (2) excited states of radical DNA base cations and their roles in leading to sugar radicals, (3) the role of excited states of DNA base anion radicals in the formation of LEE (low-energy electron)-induced DNA single-strand breaks, (4) the nature of hole delocalization in adenine stacks systems including the usual stability of the dimer radical cation $(A_2)^{\bullet+}$ and its importance to the unusual long-range hole transfer within

A stacks in DNA, and (5) the prototropic equilibria found for the guanosine radical cation, which also modulates hole transfer in DNA.

1.2. DIRECT EFFECT OF IONIZING RADIATION IN RADICAL ION FORMATION

As described in the Introduction, the direct interaction of ionizing radiation with DNA initially creates "hole" (cation radical) in DNA and ejects an electron that is usually captured as an anion radical in DNA. Electron spin resonance (ESR) spectroscopy studies show that for γ-irradiated salmon testes DNA at 77 K, the relative amounts of the observed initial ion radicals are: 35% guanine radical cation ($G^{\bullet+}$) with a small amount (< 5%) of adenine radical cation ($A^{\bullet+}$) with nearly equal amounts of thymine and cytosine radical anions ($T^{\bullet-}$, $C^{\bullet-}$) summing to ~45%.[30, 10] The remaining fraction of 10–15% is made up of neutral radicals primarily on the sugar–phosphate backbone.[30, 10] The minimum energy required to form a radical cation is estimated from the ionization potential (IP), while the energy of formation for the anion radical is estimated from the electron affinity (EA) of the corresponding DNA base, sugar, and phosphate. The determination of these fundamental properties are of substantial importance, and much effort has been expended in this area.

Theoretical calculations of molecular structures of bases in their neutral and ionized radical states, their spin density distributions, and their IPs and EAs provide valuable information that aid interpretations of experiment. In Figure 1.1, the molecular structures of guanine (G), adenine (A), thymine (T), cytosine (C), uracil (U) (present in RNA), and sugar moiety are shown.

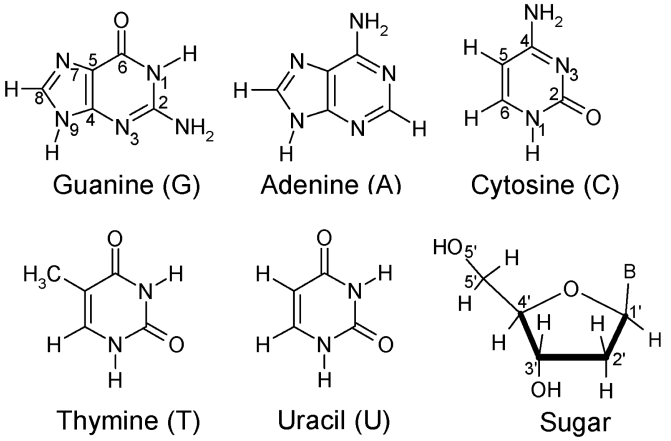

FIGURE 1.1. Molecular structures of guanine (G), adenine (A), cytosine (C), thymine (T), uracil (U) and sugar moiety, present in DNA/RNA. In the sugar moiety, B shows the site of base attachment.

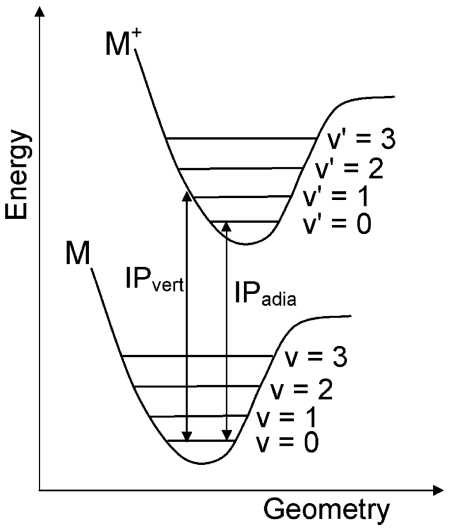

FIGURE 1.2. Diagram showing the definitions of vertical ionization potential (IP_{vert}) and adiabatic ionization potential (IP_{adia}).

1.2.1. Ionization Potential of DNA Bases and Base Pairs

The vertical ionization potential (IP_{vert}) of DNA bases G, C, A, and T in the gas phase has been measured experimentally using photoelectron spectroscopy by Hush and Cheung[31] while the corresponding adiabatic ionization potential (IP_{adia}) values were measured by Orlov et al.[32] using photoionization mass spectrometry in the gas phase. Recently, Kim and co-workers[33] reported the ionization potential of thymine (T) using the high-resolution vacuum ultraviolet mass-analyzed threshold ionization (VUV-MATI) spectroscopy. The ionization potential of a neutral molecule M is the energy required to remove an electron from the molecule. In Figure 1.2, theoretical estimates of the IP_{vert}, IP_{adia} are shown. If the energies are zero point energy (ZPE)-corrected, the ionization potentials are referred to as ZPE-corrected (IP_{zero}). Another quantity, the nuclear relaxation energy (NRE), calculated as the difference between IP_{vert} and IP_{adia}, is of interest because it provides an additional energetic barrier to "hole" transfer within DNA. Figure 1.3 shows the experimental IPs of A, T, G, and C along with their NRE energies. Using different theoretical methods, the gas-phase ionization potential of DNA bases were also calculated.[34–41] A comparison of the theoretically calculated IP values of G, A, C and T along with their corresponding experimental values are presented in Table 1.1. In Table 1.1, we see that both theory and experiment predict the same order of ionization potential of DNA bases as $G < A < C < T$.

The adiabatic ionization potentials of adenine and cytosine have been studied using CCSD(T)/6-311++G(3*df*, 2*p*) level of theory,[38] and the corresponding values are in an excellent agreement with those calculated using experiment, see Table 1.1. Recently, Cauët et al.[39] used the MP2 method to calculate the vertical and adiabatic ionization potentials of DNA bases. In their study, they added another polarization function (α_d)

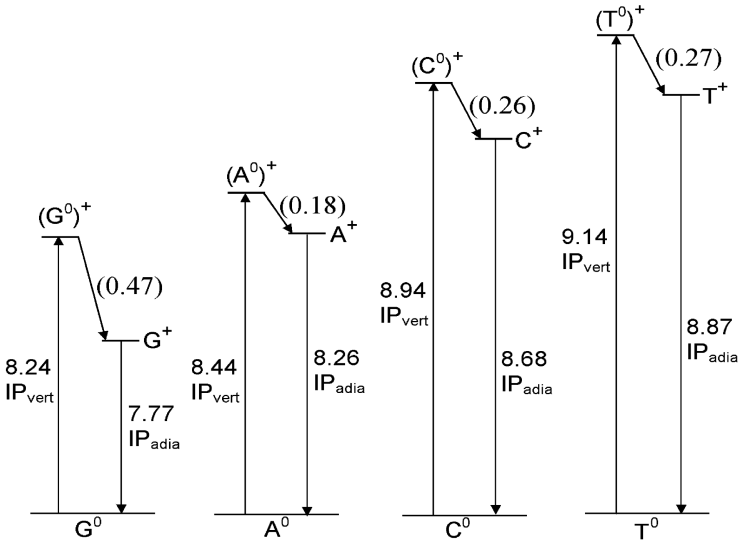

FIGURE 1.3. Experimentally estimated adiabatic and vertical ionization potentials of G, A, C, and T. The nuclear relaxation energy (NRE) is also shown in parentheses. G^0, A^0, C^0, and T^0 designate the neutral molecules.

for C, N, and O atoms to the standard 6-31G(*d*) basis set, resulting in the so-called 6-31G(2*d*(0.8, 0.1), *p*) basis set. Use of this basis set gave good values of IPs which are in close agreement to the experimental values, except for IP_{vert} of adenine. Generally, it is found that unrestricted MP2 (UMP2) method for open-shell systems (here cation doublet state) is largely spin contaminated and as a result the calculated IPs were found to be quite high.[40] In this context, Crespo-Hernandez et al.[40] used projected MP2 (PMP2) method for the calculation of IPs of DNA bases, see Table 1.1. Recently, Yang et al.[42] measured the ionization potentials of mono-, di-, and trinucleotide anions of A, T, G, and C using photodetachment–photoelectron (PD–PE) spectroscopy, and they found that 2′-deoxyguanosine 5′-monophosphate anion ($dGMP^-$) has the lowest ionization potential among all the DNA nucleotides. In their study, the electron detachment occurred from a π orbital of guanine base on $dGMP^-$; however, for the other three nucleotide anions, the lowest ionization takes place from the phosphate group. This observation is likely valid for the gas phase but is not relevant to solutions where the solvation of the phosphate group makes it the DNA component of highest IE. Furthermore, it is well known that bases are the sites of the lowest ionization in DNA from numerous experimental studies, and the presence of solvation and counterions near the phosphate groups when included show this to be the case by theory.[43,44]

There are several factors such as base pairing, base stacking, and solvation in DNA that significantly affect the ionization potential of bases in DNA. It is well known that solvation lowers the ionization potentials of bases by several electron volts when compared to the corresponding gas-phase values. In a study, Kim et al.[45] have found that ionization potentials of adenine and thymine decrease with the increasing number of hydrating water molecules and hydration by three water molecules decrease the

TABLE 1.1. Gas-Phase Ionization Potential and Nuclear Relaxation Energy (NRE) (eV) of A, T, G, and C Calculated Using Theory and Experiment

	Guanine			Adenine			Cytosine			Thymine		
Method	IP_{adia}	IP_{vert}	Δ	IP_{adia}	IP_{vert}	Δ	IP_{adia}	IP_{vert}	Δ	IP_{adia}	IP_{vert}	Δ
MP2/6-31+G(*d*)[a]	7.66	8.04	0.38	8.18	8.58	0.40	8.74	8.82	0.08	8.85	—	
CCSD(T)/6-311++G(3d*f*, 2*p*)[b]				8.25			8.71					
MP2/6-31G(2d(0.8, α_d), p)[c]	7.75	8.21	0.46	8.23	8.63	0.40	8.78	9.07	0.29	8.87	9.13	0.26
PMP2/6-31++G(*d*, *p*)[d]	7.90	8.33	0.43	8.23	8.62	0.39	8.78	8.69	−0.09	8.74	9.07	0.33
Experiment[e]	7.77	8.24	0.47	8.26	8.44	0.18	8.68	8.94	0.26	8.87	9.14	0.27
										8.9178 ± 0.0010		

[a]Geometries were optimized at HF/6-31G* level. Reference 34.
[b]Reference 38.
[c]The optimal value of $\alpha_d = 0.1$ was considered. Reference 39.
[d]Reference 40. The IP_{adia} are ZPE corrected using HF/6-31++G(*d*, *p*) method.
[e]Reference 31–33.

ionization potentials of A and T by 0.7 eV than their gas-phase values.[31–33] Recently, the vertical ionization potentials of A, T, G, and C in aqueous medium was calculated by Close[46] using polarized continuum model (PCM) and the projected MP2/6-31++G(d, p) and B3LYP/6-31++G(d, p) methods. After solvation energy correction of the electron (−1.3 eV), both the methods gave similar values of ionization potentials of guanine 4.77 (4.71), adenine 5.08 (5.05), cytosine 5.24 (5.32), and thymine 5.36 (5.41) (the numbers in parentheses are the PCM-B3LYP calculated values).[46] These calculated values use a unusual standard state for the ejected electron. An electron in water at the conduction band edge (V_0)[43] is employed as the final electron state not the gas-phase electron, and this lowers the IP by 1.3 eV. Without this correction the corresponding IP_{vet} values at B3LYP/6-31++G(d, p) level of calculation are 6.01 (G), 6.35 (A), 6.62 (C), and 6.71 (T).

The ionization potentials of DNA bases in GC and AT hydrogen-bonded base pairs were calculated by Colson et al.[47] using HF/3-21G and HF/6-31+G(d)//HF/3-21G methods in Koopmans' approximations which were further refined by Li et al.[48, 49] using the B3LYP method and the 6-31+G(d) basis set (Hutter and Clark[50] and Bertran et al.[51]). The calculated IP_{vert} for GC and AT base pairs, by Li et al.[48, 49], were found to be 7.23 and 7.80 eV; however, the zero-point energy (ZPE)-corrected adiabatic IP of GC and AT were found to be 6.90 and 7.68 eV, respectively. The IP_{adia} values of GC and AT pairs due to Li et al.[48, 49] are in good agreement (within 0.2 eV) with those earlier calculated by Hutter and Clark[50] and Bertran et al.[51]

The effect of hydration on the ionization potential of GC and AT base pairs was studied by Colson et al.[52, 53] using HF/3-21G and HF/6-31+G(d)//HF/3-21G methods and Koopmans' approximation. In the calculation, they used four water molecules to solvate the base pairs; and the calculated IP_{vert} of GC and AT base pairs, at HF/3-31G level of theory, were found to be 7.80 and 8.59 eV, respectively. However, the corresponding IP_{adia}, calculated at the HF/6-31+G(d)//HF/3-21G level of theory, was found to be 6.53 and 7.45 eV. Strangely, these values were higher than the corresponding gas-phase ionization potential values of the GC and AT base pairs.[52, 53] Each water molecule acting as a hydrogen-bond donor to the base increases the IP, while each water molecule in the hydrogen-bond acceptor configuration with the base lowers the IP.[52, 53] Therefore, it seems that four water molecules in the calculation of Colson et al.[52, 53] were not enough to fully account for the solvation shell surrounding the base pairs, and most of the waters act as hydrogen-bond donors.[53] Recently, Barnett et al.[54] studied the duplex DNA $d(5'\text{-(G)}n-3')$, for $n = 2$, 3, considering the crystallographic structures, counterions (Na^+) near the phosphate group, and solvating water molecules. Their calculated values of vertical and adiabatic IPs are substantially lower than expected, perhaps as a result of the involvement of nonequilibrium conformations in local minima which place counterions in sites to lower the IPs. The ionization potentials of base pairs in the stacked conformation have also been studied theoretically.[55–57] The vertical ionization potential of stacked bases and base-paired dinucleotides were calculated by Sugiyama and Saito[57] using 3-21G* and 6-31G* levels within Koopmans' approximation. With 6-31G* level of theory, the ionization potentials of G, GG, GGG, and GGGG were found to be 7.75, 7.28, 7.07, 6.98.[57] The above discussion clearly shows that base pairing, stacking, hydration, and

the local environment significantly affect the ionization potentials of the DNA bases, usually by lowering values.

1.2.2. Acid and Base Properties of Ionized DNA Bases and Base Pairs

Following radiation, the one-electron-oxidized purines ($G^{\bullet+}$, $A^{\bullet+}$) and one-electron-reduced pyrimidines ($C^{\bullet-}$, $T^{\bullet-}$) in DNA become quite reactive in comparison to their neutral forms. The oxidized purines become stronger acids and undergo deprotonation reactions, whereas the reduced pyrimidines become stronger bases and undergo protonation reactions. A competitive reaction to deprotonation for DNA base cation radicals is the addition of hydroxyl ions that form base hydroxyl adducts. This can lead to biologically significant damages such as 8-oxoG. In addition, electron–hole transfer and intra-base-pair proton transfer reactions also occur.[58–60] This intra-base pair proton (H^+) transfer in DNA can slow or stop charge transfer processes in DNA.[58–61] Such proton transfer process strongly depends on the pK_a value of the base radical ion involved. Steenken[58–60] first considered the proton transfer reactions between base-pair ion radicals from experimental measurements on nucleoside ion radicals and concluded that acidity of the complementary oxidized purine base and basicity of the radical anion (pyrimidine base) would affect the extent of such a proton transfer process.[58–61] Experimental values of the pK_a of $G^{\bullet+}$, $A^{\bullet+}$, $C^{\bullet+}$, and $T^{\bullet+}$ are 3.9, < 1 (strong acid), $\sim$4.0, and 3.6.[58–61] On the other hand, the pK_a of $C^{\bullet-}$ and $T^{\bullet-}$ were reported to be as $\geq$13.0 (strong base) and $\geq$ 6.9, respectively.[58–61]

Theoretical calculations of a pK_a is very sensitive and a modest change in energy can change the pK_a by several units. However, using the DFT method the pK_a values of oxidized DNA bases have also been calculated[62–64] to reasonable accuracy. In a recent study,[65] the pK_a of $A^{\bullet+}$ was calculated as -0.3 using B3LYP/6-31G* method in reasonable agreement with experiment and shows that $A^{\bullet+}$ should be a strong acid that deprotonates spontaneously in the presence of solvent. To confirm this, a hydration shell around the adenine base of deoxyadenosine radical cation ($dA^{\bullet+}$) was modeled by placing seven water molecules and optimized the geometry using the B3LYP/6-31G* method, shown in Figure 1.4a. In the optimized structure of ($dA^{\bullet+} + 7H_2O$), it was found that in the presence of solvent the N_6–H′ bond is elongated by $\sim$0.1 Å as compared to the corresponding bond length in gas phase (see Figure 1.4a). Furthermore, the potential energy surface (PES) of the deprotonation of N_6–H′ bond from the optimized structure of ($dA^{\bullet+} + 7H_2O$) was calculated by increasing the N_6–H′ bond in the step size of 0.1 Å from its equilibrium bond distance (1.127 Å), see Figure 1.4a. From the PES, it was found that N_6–H′ bond deprotonates in the presence of solvent without any barrier (for details see reference 65). Figure 1.4b, shows the formation of H_3O^+ from the deprotonation of $dA^{\bullet+}$. These theoretical results clearly predict that $dA^{\bullet+}$ is a strong acid in agreement with experiment.[58–61]

The proton transfer reactions in GC and AT base pairs in their radical cation and anion states have been studied using Hartree–Fock (HF) and DFT methods.[47, 49–52] In these calculations the proton transfer energies were calculated as the difference between total energies of the ionized radical base pair before and after proton transfer. For GC and AT radical cations a small proton transfer energy $\sim$2 kcal/mol was

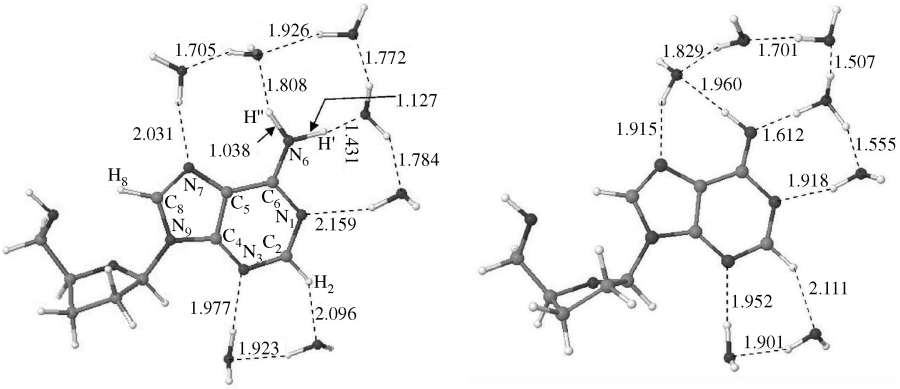

FIGURE 1.4. B3LYP/6-31G* optimized geometries of (**a**) deoxyadenosine cation radical in the presence of seven water molecules ($dA^{\bullet+} + 7H_2O$). The arrow on the elongated N_6–H′ bond in this figure indicates that the elongation of this N_6–H′ bond leads to deprotonation in the surrounding water shell (shown in **b**) and (**b**) hydronium ion (H_3O^+) formation from $A^{\bullet+}$ owing to deprotonation of the structure in **a**. (Reprinted with permission from reference 65, *J. Am. Chem. Soc*. copyright 2008, American Chemical Society.)

predicted at the HF/3-21G*[47,52] and B3LYP/6-31G*[50,51] level of theories. Li et al.[49] calculated the transition state and the corresponding enthalpy (ΔH) and the free energy (ΔE) for the inter-base proton transfer in GC and hypoxanthine–cytosine base pairs in their cation and anion states using the B3LYP/6-31+G(*d*) method. In their calculation, the forward barrier for the proton transfer in GC radical anion was calculated to be 0.84 kcal/mol; however, in GC radical cation, the corresponding barrier was found to be 2.96 kcal/mol.[49] Also, the proton transferred radical cation ($G^{\bullet+}C^{PT}$) was found to be unstable by ~1.25 kcal/mol compared to $G^{\bullet+}C$, while the proton transferred radical anion ($GC^{\bullet-PT}$) was more stable by 3.73 kcal/mol than $GC^{\bullet-}$.[49] Thus these calculations predict a highly favored proton transfer in GC anion radical and as predicted proton transfer from G to C has been observed on a nanosecond time scale using resonance-enhanced multiphoton ionization (REMPI) by Nir et al.[66]

1.2.3. Gase-Phase Electron Affinities of DNA Bases and Base Pairs

The electron affinity of a neutral molecule (M) is effectively the binding energy of an excess electron to the gas-phase molecule. The various processes that occur during electron molecule interactions are shown in Figure 1.5. Upon electron addition, the geometry of a neutral molecule undergoes nuclear relaxation to the geometry of the adiabatic anion (M^-). Electron attachment to the neutral molecule without nuclear relaxation yields the vertical electron affinity, and on relaxation the overall energy change gives the adiabatic electron affinity. If the anion is more stable than the neutral, positive electron affinities (VEA and AEA) are obtained, as shown in Figure 1.5. This topic has long been the subject of significant biological significance; and theoretical methods [including PPP, semiemperical (AM1), and DFT] and high-level methods

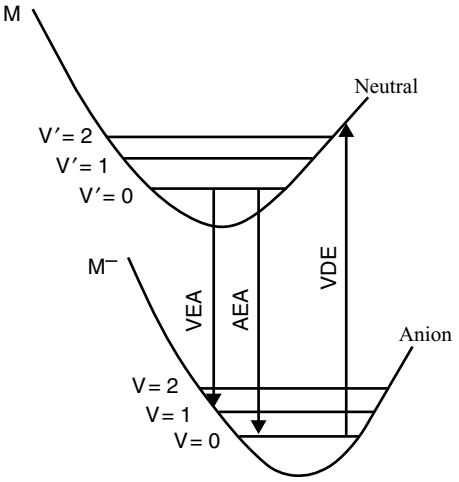

FIGURE 1.5. A diagram showing the potential energy surfaces (PES) of the formation of anionic molecule (M^-) after electron attachment (e^-) to the neutral molecule (M). Different processes occur during electron attachment: (i) Vertical electron affinity (VEA), (ii) adiabatic electron affinity (AEA), and (iii) vertical detachment energy (VDE) are shown. As can be inferred from the diagram, VEA and VDE represent the lower and upper bounds to AEA.

[such as MP2, and CCSD(T)] have been applied to evaluate the electron affinities of G, C, A, T, and U.[34, 67–73] From theory and experiment, it is well known that all the bases (A, T, G, C, and U) have negative vertical electron affinity values in gas phase.[34, 67, 74, 75] While all the bases have negative VEA, the adiabatic electron affinities (AEAs) of bases (C, T, and U) are found to be near zero[76–78] and still negative for A and G[34, 74, 79] (see Table 1.1). Under solvation, the radical anionic states of the bases become substantially stabilized and trap the excess electron, thereby preventing autodetachment. Although the DFT method has been widely used to evaluate the electron affinities of DNA bases and base pairs, it is noted that DFT calculated values are overestimated by about 0.15 eV over experimental values. The use of high-level ab initio methods such as CCSD(T) and CBS-Q are found to provide the best estimates of AEAs. The experimental electron affinity values of A, T, G, C, and U along with the best estimates from theory are presented in Table 1.1. In recent years, a number of reviews have appeared in the literature that cover the topic of DNA base EA.[7, 9, 72]

As described above, the vertical electron affinities (VEAs) of all the bases are negative, whereas their adiabatic electron affinities (AEAs) are near zero (Table 1.2). When the binding energy for "valence bound" anions is near zero or below, "dipole-bound" (DB) anions can form in gas phase when the dipole moment of the molecule is larger than 2.3 debye. Dipole-bound binding energies are small, generally less than a 100 meV[76, 78] with the electrons held in very diffuse states to the side of the molecule. Since each of the DNA bases have a sizeable dipole moment, each can form "dipole-bound" anions in the gas phase. Because of negative VEAs and substantially small AEAs ($\sim$0) of the bases, the accurate prediction of EAs of bases using theory is a complex task. Also, the use of diffuse functions in the basis set mix the valence states

TABLE 1.2. Experimental and Best Estimated Theoretical Gas-Phase Valence Electron Affinities of Bases (eV)

			Adiabatic			
	Vertical		Experiment		DFT	Ab Initio
Bases	Experiment	Theory	Valence	DB[e,g,l]	Valence	Valence
G	−0.74[a]	−1.25[c]	—		−0.75[h]	−0.52[i]
A	−0.54[a]	−0.74[d]	—		−0.35[h]	—
	−0.45[b]	—	—		—	—
C	−0.32[a]	−0.55[d]	—	85 ± 8[g]	−0.05[h]	−0.13[j]
	−0.55[b]	—			—	—
T	−0.29[a]	−0.30[d]	∼0[f]	69 ± 7[l]	0.15[h]	0.02[k]
	—	—		62 ± 8[g]	—	—
					—	—
U	−0.22[a]	−0.27[d]	∼0[f]	93 ± 7[l]	0.20[h]	0.002[j]
	−0.30[b]	—		86 ± 8[g]	—	0.040[m]
					—	—

[a]Electron transmission spectroscopy (ETS) results due to Aflatooni et al.[74] For G, VEA was estimated for keto tautomer from enol tautomer experimental value (−0.46 eV) plus the calculated difference in total energies between the two tautomers (0.28 eV).
[b]Rydberg electron transfer spectroscopy (RET) results due to Periquet et al.[79]
[c]Best estimate from B3LYP/D95V+(D) trends for other bases.[70]
[d]B3LYP/6-311G(2*df*, *p*) values due to Vera and Pierini[69] and Wetmore et al.[36]
[e]Values are in milli-electron volts.
[f]Estimated from stable valence anion complexes—for example, $U(Ar)^-$.
[g]Reference 78. Dipole-bound (DB).
[h]Best estimates from DFT basis set dependence study due to Li et al.[70] DFT values are generally overestimated by 0.15 eV.
[i]Reference 82.
[j]Calculated using CBS-Q. Reference 83.
[k]CCSD(T) correction to MP2 complete basis set (CBS) limit including ZPE correction. See Reference 84.
[l]References 76 and 78. Dipole-bound (DB).
[m]Reference 73.

with "dipole-bound" states and do not provide a good estimate of the valence electron affinities.[69, 70] A number of theoretical methods are available in the literature to deal with the negative electron affinities of molecules.[68–70] It is also found that use of a compact basis set that confines the electron to the molecular framework produces a good estimate of the VEA with absolute values estimated with interpolation techniques.[34] Li et al.[70] used the B3LYP method and several basis sets and show the trends when diffuse states (dipole bound) mix with the valence states. However, in the presence of aqueous medium, these diffuse states are destabilized and valence anions are stabilized by several electron volts. As expected, experiments in aqueous phases using electron spin resonance (ESR) spectroscopy show that stable anion base radicals are found for all DNA bases.[80, 81]

The electron affinities of isolated DNA bases change on base-pair formation. In this context, Bowen and co-workers[85] studied the radical anions of AT and 9-methyl-A:1-methyl-T (MAMT) using photoelectron spectroscopy (PES) and B3LYP/6-31+G**

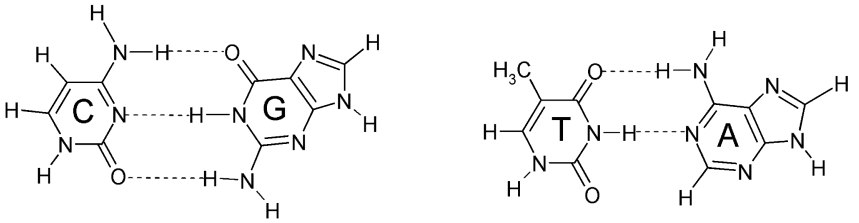

FIGURE 1.6. Diagram showing GC and AT base pairs in Watson–Crick conformation.

(6*d*) method. They calculated the vertical detachment energy (VDE) of the MAMT anion base pair as 0.77 eV, which corresponds very well to their experimental value. However, in AT radical anions the B3LYP/6-31+G**(6*d*) calculated value 0.89 eV was quite different from the experimental value of 1.7 eV.[85] However, they found a proton-transferred AT radical anion structure which has the VDE value comparable to the experimental value. The substantial positive VDE from this study demonstrates the occurrence of stable valence anion formation on base pairing. The excess electron was localized on the π^* orbitals of thymine in both AT and MAMT radical anions as expected. The gas-phase electron affinities of AT and GC base pairs have been calculated by several other workers.[48, 86–88] For AT the AEAs lie in the range 0.30–0.36 eV, while for GC base pair the AEAs lie in the range 0.49–0.60 eV, respectively. In each case the electron localizes on the pyrimidine; thus, base pairing increases the electron affinity of T by ~0.3 eV and C by ~0.6 eV. The larger increase in the EA of C over T on base pairing results from the fact that G provides two donor H bonds to C, whereas A provides only one donor H bond to T (see Figure 1.6). Each donor H bond raises the EA of the recipient molecule by 0.1–0.3 eV.

A large change in electron affinity values and the nature of excess electron binding with U, T, and C have been observed experimentally with the addition of water molecules by Bowen and co-workers,[77] Periquet et al.,[79] and Schiedt et al.[78] These studies show that the first water increases the EA by ~0.3 eV and that subsequent waters have decreasing contributions as the number of waters increases, and for up to 5 waters the EAs of T, C, and U were estimated to be 1.1, 1.0, and 1.4 eV,[78] respectively. Interestingly, the experimentally observed dipole bound states of all the pyrimidine (T, C, and U) radical anions in gas-phase transform to valence bound states on addition of a single water molecule and, as mentioned above, in an aqueous medium T, C, and U are predicted to have substantial positive valence electron affinities[77–79] as found experimentally.[80, 81]

The effect of bulk solvent on molecular ion radicals can be modeled by several methods including: (i) treating the solvent by the polarized continuum model (PCM) and (ii) placing a number of discrete water molecules around the molecule often followed by the PCM model for completeness. Though the former approach is simpler to study it lacks the hydrogen bonding between solute and solvent while the second approach takes into account the hydrogen bonding between solute and solvent (waters). However, this method is computationally very expensive and also misses the full effect of the solvent unless followed by a PCM calculation of the entire

structure. Using the above-mentioned approaches, the electron affinities of DNA bases and base pairs have been studied in a number of publications in recent years.[70, 89–98] Using B3LYP/DZP++ level of theory, Schaefer and co-workers[90–92] calculated the electron affinities of T, C, and U in the presence of 1–5 waters and their calculated ZPE-corrected absolute electron affinities of T, U, and C with 5 waters were calculated to be 0.65, 0.74, and 0.61 eV.[90–92] respectively. However, using the PCM model and the B3LYP/D95V+(D) method, Li et al.[70] calculated the AEAs of G, C, A, T, and U as 1.01, 1.89, 1.53, 2.06, and 2.15 eV, respectively. A large difference between these two calculations is obvious because former[90–92] calculations lack the bulk solvent effect. In another study, AEA of the thymidine monophosphate-adenine (5′-dTMPH-A) pair was calculated using the PCM model and the B3LYP/DZP++ method as 2.05 eV,[93] while the AEA of an AT base pair in the presence of 13 waters was predicted to be 0.97 eV at B3LYP/6-31+G* level of theory.[97] In a recent study,[98] the EA of GC base pair was also calculated using B3LYP/6-31+G* method in the presence of 6 and 11 waters and ZPE-corrected AEAs were found to be 0.74 and 0.95 eV, respectively. However, the incorporation of the bulk solvent (water) through the PCM model increased the AEAs of these ($GC + 6H_2O$ and $GC + 11H_2O$) complexes to 1.77 eV. In this study, surprisingly it was found that the hydration shell initially destabilizes the GC base pair toward electron capture as a transient anion. Energetically unstable diffuse states (σ^* orbitals) in the hydration shell were suggested to provide an intermediate state for the excess electron before molecular reorganization of the water molecules results in a stable base-pair anion formation. To confirm this conclusion, the first excited state of the vertical radical anion of $GC + 11H_2O$ complex was calculated using time-dependent density functional theory (TD-DFT) using TD-BHandHLYP/6-31 + G* level of theory, and a very small transition energy 0.33 eV having transition $SOMO(\pi) \rightarrow LUMO(\sigma^*)$ in nature with a small oscillator strength was found (see Figure 1.7). In adiabatic state, the excess electron localized on the π orbitals of the cytosine as expected. In the adiabatic state, it is also found that a water molecule was hydrogen-bonded with the C_6 atom of cytosine, as shown by an arrow in Figure 1.7c.

1.2.4. Role of Excited States in LEE-Induced Strand Break Formation

Interaction of low-energy electrons (LEEs) with DNA is a subject of significant biological importance, and in recent years it has been treated extensively using experiment[1–22, 99–102] and theory.[103–126] It is now recognized as a component of the complex processes leading to radiation induced DNA damage. In this context, the recent experiments of Sanche and co-workers[12, 100] showing that low-energy electrons in the energy range 0–4 eV (below the ionization threshold of DNA) can induce strand breaks in DNA attracted intense interest because it represents a new mechanism of strand breaks formation in DNA. Recent experiment by Illenberger and co-workers[11] also confirmed that LEEs in the subexcitation energy (< 3 eV) effectively decomposes uracil in gas phase. Thus, from these experiments it is well established that these LEEs induce a variety of DNA damage such as (i) hydrogen atom loss from base, (ii) single-strand break,[12, 13, 100] (iii) glycosidic bond cleavage,[13, 16] and (iv) fragmentation of

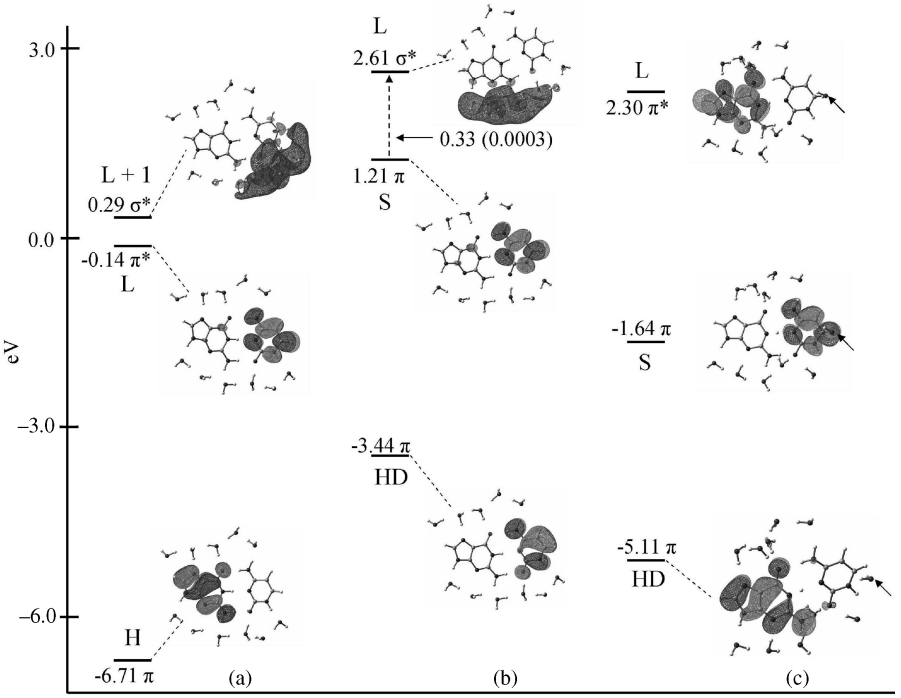

FIGURE 1.7. Plots of HOMO (H), HDMO (HD), LUMO (L), and SOMO (S) of GC-11H_2O in (**a**) neutral, (**b**) vertical (TNI), and (**c**) adiabatic radical anion along with respective molecular orbital (MO) energies (eV) calculated using the BHandHLYP/6-31+G**//B3LYP/6-31+G** method. The TD-BHandHLYP/6-31+G** calculated first vertical excitation energy (oscillator strength) between S(π) $\rightarrow$ L(σ^*) is also shown by a broken arrow in part b. In part c, an arrow shows the location of the water molecule hydrogen bonded with the C_6 atom of cytosine. HDMO = Doubly occupied highest molecular orbital. (Reprinted with permission from reference 98, *J. Phys. Chem.*, copyright 2008, American Chemical Society.)

deoxyribose.[21] Based on experiments, two types of mechanisms have been proposed which lead to dissociation processes: (i) Dissociative electron attachment (DEA) occurs in which LEEs are initially captured by the DNA components (bases, deoxyribose, and phosphate) to form transient negative ions (TNI)[19–22, 101, 102] resulting in dissociation at that site. (ii) LEEs are initially captured by the bases into their π^* MOs (shape resonance) and transferred to the sugar–phosphate group resulting in strand breaks.[100]

A number of theoretical papers have been appeared in the literature[103–126] that elucidate mechanisms of LEE-induced strand break formation in DNA. Simons's group[108–111] first proposed the "electron-induced" indirect mechanism of strand breaks formation using 5′-dTMP and 5′-dCMP as model systems. In their model,[108–111] they proposed that initially an excess electron is captured into the π^* MOs (shape resonance) of thymine or cytosine base in 5′-dTMP and 5′-dCMP; and during elongation of the C–O bond the electron transfers to the σ^* orbital of $C_{5'}$–$O_{5'}$

bond in the sugar–phosphate group, leading to C–O bond cleavage[108–111] Later, Gu et al.[112, 113] refined the calculations of Simons et al.[108–111] using the B3LYP/DZP++ level of theory and calculated the transition state for the dissociation of $C_{5'}$–$O_{5'}$ and $C_{3'}$–$O_{3'}$ bonds in pyrimidine nucleotides anion radicals in their adiabatic states and supported the proposed mechanism of Simons et al.[108–111] It is clearly evident that these studies proposed the occurrence of strand breaks from trapped electron into the π orbital on the base. However, it is well known that in a solvent environment, when an electron is stabilized in the π orbital on the base, no strand breaks are found.[127] This has also been supported by a recent study using B3LYP/6-31G** method, in which the $C_{5'}$–$O_{5'}$ bond cleavage of a 5′-dTMP radical anion was calculated in the presence of 11 water molecules, and the phosphate group was neutralized by a Na^+ counterion.[115] This study[115] clearly demonstrated that under solvation the barrier height of $C_{5'}$–$O_{5'}$ bond cleavage was calculated to be almost two times the corresponding gas-phase value. Also, from the singly occupied molecular orbital (SOMO) plot, it was found that transfer of excess electron from thymine to the C–O bond did not take place even at the transition state.[115] Li et al.[104] proposed the direct mechanism of strand breaks formation in DNA by considering the sugar–phosphate–sugar (S–P–S) model without a base moiety using B3LYP/6-31+G(*d*) level of theory and calculated the barrier height ($\sim$10 kcal/mol) for $C_{5'}$–$O_{5'}$ and $C_{3'}$–$O_{3'}$ bonds dissociation. In their model, they proposed the direct attachment of an excess electron to the sugar–phosphate group, leading to strand breaks. However, the calculated spin density distributions in this model showed a "dipole bound" anionic state rather than a valence bound state.[7, 104] Nevertheless, the low energy for dissociation shows that a weakly associated excess electron has the potential to fragment the deoxyribose backbone.

Though these theoretical models aid our understanding of strand break formation, they do not answer several important questions such as: (i) What is the role of initially formed transient negative ion (TNI)? and (ii) What is the role of various TNI excited states created during the low-energy electron–molecule interaction in strand breaks formation? These aspects have been investigated in recent studies.[115, 116] Using the B3LYP method and 6-31G* and 6-31++G** basis sets, the potential energy surfaces (PESs) of $C_{5'}$–$O_{5'}$ bond dissociation in 5′-dTMPH radical anion were calculated in both adiabatic (relaxed anion) and vertical (TNI) states.[115] It was found that the barrier height of $C_{5'}$–$O_{5'}$ bond dissociation in the vertical (TNI) state was lower than that in the adiabatic state. Since during TNI formation the unoccupied molecular orbitals (UMOs) of neutral 5′-dTMPH molecule are available to capture the excess electron, the first few UMOs of 5′-dTMPH were also calculated and their orbital energies were scaled to the available experimental values.[74] The scaled orbital energy values of five UMOs of 5′-dTMPH and their nature were calculated as 0.53(π_1^*), 1.56(π_2^*), 1.80(σ_1^*), 2.23(σ_2^*), and 2.64(σ_3^*), respectively, and π^* and σ^* orbitals were localized on the thymine base and on the sugar–phosphate group, respectively. Form this study,[115] it was evident that below 2 eV the orbitals on a phosphate group as well as on a base are available to capture the LEEs. Therefore, it seems that during TNI formation the lowest UMOs will excite the vibrational mode and result in the strand breaks.

It is well known that during electron–molecule interaction, different excited states are also involved. Their study can provide important information about the energy and

nature of these states, which are those produced after capture the electron. Using the time-dependent density functional theory (TD-DFT),[116] the excited states of the anion radical of 5′-dTMPH as a model of DNA were studied recently.[116] The geometries of 5′-dTMPH molecule in their neutral and radical anionic states were optimized using the B3LYP/6-31G* method, and the lowest vertical excited states were calculated using the B3LYP and BHandHLYP (BH&HLYP) methods using a 6-31G* basis set. In this study,[116] the use of a 6-31G* (compact) basis set was emphasized because LEE resonances form TNIs, which are equivalent to the excited states of electron adduct of the parent neutral molecule. Since these resonances can be in continuum, the use of a compact basis set avoids the mixing of valence states to the continuum states.[70] Also, the suitability of the TD-B3LYP/6-31G* and TD-BH&HLYP/6-31G* methods for the calculation of excited states were extensively tested for several anion radicals for which experimental or theoretically calculated values were available (for details see supporting information of reference 116). Furthermore, both the methods were also tested to calculate the excitation energies for DNA/RNA bases for which the experimental shape resonance values are available[74] (see Table 1.3). Both methods were found suitable for the test cases, but for the excited-state calculation of the 5′-dTMPH radical anion the TD-BH&HLYP/6-31G* method was found to be more appropriate than the TD-B3LYP/6-31G* method. The failure of the B3LYP method is well known because it underestimates the long-range Coulomb interactions in charge transfer states. However, the use of increased Hartree–Fock exchange 50% in BH&HLYP over 20% in B3LYP is found to be suitable to describe the long-range charge transfer states. Although in this class of study,[116] charge transfer states are not created during excitation and only electron transfer between the nominally neutral portions of the molecule occurs. In view of this, the excited states of 5′-dTMPH radical anions in vertical and adiabatic radical anion states were calculated using the TD-BH&HLYP/6-31G* method. In this work, the PESs of $C_{5'}$–$O_{5'}$ bond dissociation in 5′-dTMPH radical anions was stretched from their equilibrium bond length to 2.0 Å in the step size of 0.1 Å, respectively. At each fixed $C_{5'}$–$O_{5'}$ bond length on the PES, the lowest excited states were calculated. In Figure 1.8, the vertical excited states of 5′-dTMPH radical anions in the adiabatic state are shown. In the adiabatic state, TD-BH&HLYP predicted three lowest excitation energies as $\pi(T) \rightarrow \pi(T)^*$, $\pi(T) \rightarrow \sigma(PO4)^*$, and $\pi(T) \rightarrow \sigma(S)^*$ type (here T, PO_4, and S refer to thymine, phosphate, and sugar group as shown in Figure 1.8) having transition energies 3.03, 3.40, and 3.85 eV, respectively. Also, these transitions are dominant one-electron excitations having contributions of about 61%, 87%, 87%, respectively.

As already mentioned, TNI formation plays an important role in the DEA mechanism leading to strand breaks and resonance formation.[21,74,115] Thus, the excited states of 5′-dTMPH radical anions were calculated at the optimized geometry of neutral 5′-dTMPH (TNI formation) using the TD-BH&HLYP/6-31G* method as shown in Figure 1.9. The TD-BH&HLYP/6-31G*-calculated lowest three transitions were found to be $\pi(T) \rightarrow \sigma(PO4)^*$, $\pi(T) \rightarrow \pi(T)^*$, and $\pi(T) \rightarrow \sigma(S)^*$ in nature, having transition energies 1.42, 1.68, and 2.06 eV, respectively. The calculated second transition $\pi(T) \rightarrow \pi(T)^*$ (1.68 eV) is found to be in good agreement with the

TABLE 1.3. Vertical Excitation Energies (ΔE, eV) of Transient Negative Ion (TNI) of DNA/RNA Bases Calculated Using TD-B3LYP/6-31G* and TD-BH&HLYP/6-31G* Methods and Their Comparison with Available Experimental Values[a]

		ΔE		
Transition	Molecule	B3LYP	BH&HLYP	Experiment[b,c]
—	Uracil	—	—	0.22 (π_1^*)
$\pi \rightarrow \pi^*$		1.33	1.85	1.58 (π_2^*)
$\pi \rightarrow \pi^*$		4.27	4.73	3.83 (π_3^*)
—	Thymine	—	—	0.29 (π_1^*)
$\pi \rightarrow \pi^*$		1.38	1.89	1.71 (π_2^*)
$\pi \rightarrow \pi^*$		3.86	4.46	4.05 (π_3^*)
—	Cytosine	—	—	0.32 (π_1^*)
$\pi \rightarrow \pi^*$		1.55	1.91	1.53 (π_2^*)
$\pi \rightarrow \pi^*$		4.47	5.06	4.50 (π_3^*)
—	Adenine	—	—	0.54 (π_1^*)
$\pi \rightarrow \pi^*$		0.88	1.0	1.36 (π_2^*)
$\pi \rightarrow \pi^*$		1.89	1.86	2.17 (π_3^*)
—	5′-dTMPH[d]	—	—	(0.53 T)[d]
$\pi \rightarrow \pi^*$		1.16	1.68	(1.56 T)[d]
$\pi \rightarrow \sigma^{*e}$		0.18	1.42	(1.80 PO_4)[d]
$\pi \rightarrow \sigma^{*e}$		0.70	2.06	(2.23 S)[d]

[a]Transition energies of radical anions were calculated at the optimized neutral geometry of the molecules.
[b]Energies of the shape resonances in the electron transmission spectroscopy (ETS) experiment. Reference 74.
[c]π_1^* corresponds to the energy of the singly occupied molecular orbital (SOMO), and its difference with π_2^* and π_3^* orbital energies gives the estimate of the transition energies.
[d]Scaled B3LYP orbital energies (VOE). Reference 115.
[e]Electron transfers from thymine (π) to PO_4 and sugar (σ) part of 5′-dTMPH. (Reprinted with permission from reference 116, *J. Am. Chem. Soc.*, copyright 2008, American Chemical Society.).

experimental ETS value (1.71 π_2^*) of thymine[74] (see Table 1.3). This also confirms the accuracy of the TD-BH&HLYP/6-31G* calculated excitation energy for the second π^* surface (see Figure 1.9). Also, from Figures 1.8 and 1.9, it is clearly evident that SOMO is π type in ground state and is localized on the thymine base as found by others[103, 105, 108–115] and known from experiment. The barrier height for $C_{5'}$–$O_{5'}$ bond dissociation (in ground state) increases with the elongation of $C_{5'}$–$O_{5'}$ bond to the transition state (TS) and their values in adiabatic and in vertical (TNI) states are 23.3 and 18.7 kcal/mol as shown in Figures 1.8 and 1.9. It is also found that the first and second excited-state surfaces in the adiabatic state (Figure 1.8) and the second and third excited-state surfaces in the vertical state (Figure 1.9) show the bound character with the increase of $C_{5'}$–$O_{5'}$ bond. However, the second excited-state surface in the adiabatic state (Figure 1.8) and the first excited-state surface in the vertical state (Figure 1.9) show the dissociative nature. Such a dissociative nature of $\pi \rightarrow \sigma^*$ in the excited state has already been established for a number of molecules.[128–130] This study clearly predicts that a <2 eV electron can directly attach to the sugar–phosphate group during TNI formation (Figure 1.9) and cause

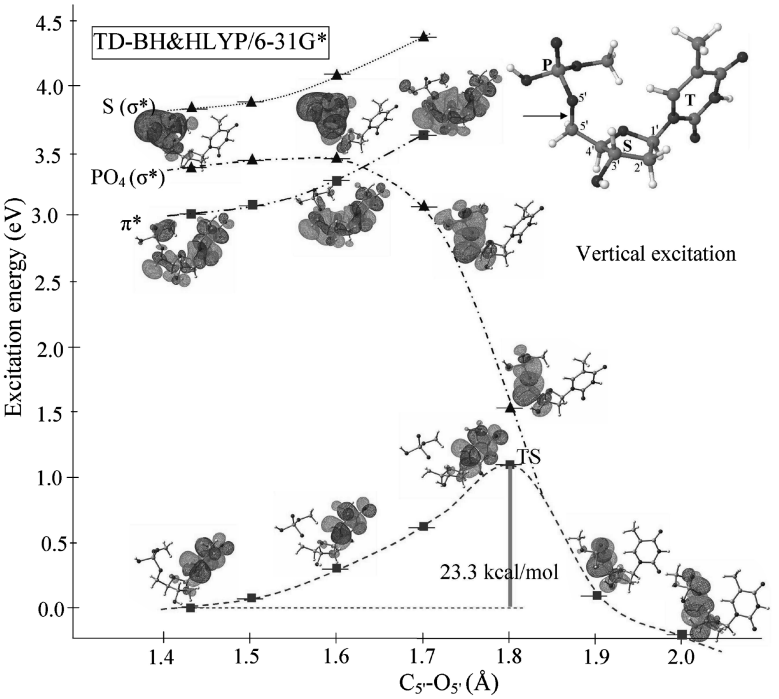

FIGURE 1.8. Lower curve shows the adiabatic ground-state potential energy surface for $C_{5'}$–$O_{5'}$ bond dissociation in the 5′-dTMPH radical anion calculated using BH&HLYP/6-31G*. Upper curves show the vertical excitation energies calculated using TD-BH&HLYP/6-31G* method. The lowest $\pi\pi^*$ state (■) and lowest $\pi\sigma^*$ states (▲) are shown. The SOMO in ground state and MOs involved in excitations are shown as well. Energies and distances are given in electron volts and angstroms, respectively. (Reprinted with permission from reference 116, *J. Am. Chem. Soc.*, copyright 2008, (American Chemical Society.)

strand breaks formation in DNA. The excited states of σ^* symmetry ($\pi(T) \rightarrow \sigma(PO4)^*$ transitions) are not populated directly, owing to their short lifetimes; however, they can be populated through vibronic coupling with the neighboring π^* states ($\pi(T) \rightarrow \pi(T)^*$). Thus, π^* and σ^* coupling would lead to a rapid dissociation process. The temporary anion states of trimethyl phosphate and several P=O group containing compounds were recently studied by Burrow et al.[131] using ETS, and the authors also concluded that resonances on phosphate groups are delocalized and σ^* in nature. Recently, the calculations on electron scattering from A and B forms of DNA model due to Caron and Sanche[122] concluded that irrespective of the internal electron diffractions in DNA, the capture probability of electron is much larger on the phosphate group than the other components. Also, the yields of single- and double-strand breaks induced by 0–4 eV incident electrons were studied by Martin et al.,[100] and they found two peaks at electron energies 0.8 ± 0.3 and 2.2 eV. The TD-BH&HLYP/6-31G*-calculated first transition energy $\pi(T) \rightarrow \pi(T)^*$ (1.7 eV) of TNI is in reasonable agreement with the observe second peak at 2.2 ± 0.3 eV.[100]

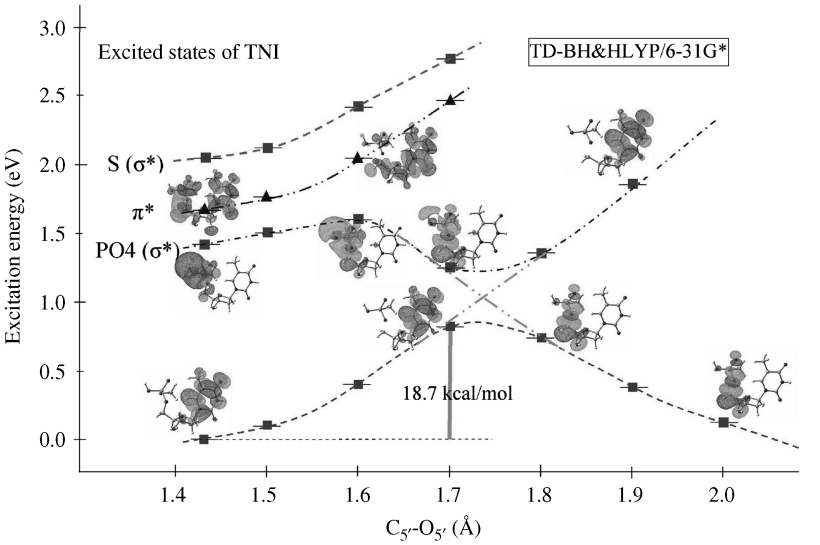

FIGURE 1.9. *Lower curve*: Potential energy surface (PES) of the 5′-dTMPH transient negative ion (TNI); calculated in the neutral optimized geometry of 5′-dTMPH with $C_{5'}$–$O_{5'}$ bond elongation. SOMO is shown at selected points. *Upper curves*: Calculated vertical excitation energies of the radical anion at each point along the PES, MOs involved in excitations are also shown. Energies and distances are given in electron volts and angstroms, respectively. The lowest $\pi\pi^*$ state (▲) and lowest $\pi\sigma^*$ states (■) are shown. (Reprinted with permission from reference 116, *J. Am. Chem. Soc*., copyright 2008, American Chemical Society.)

1.3. FORMATION OF SUGAR RADICALS VIA PHOTOEXCITATION OF ONE-ELECTRON OXIDIZED NUCLEOSIDES AND OLIGOMERS

Sugar radicals are formed in relatively low amounts (10–15% of all radicals) in γ-irradiated double-stranded DNA at 77 K while DNA base ion radicals constitute the major radical species (85–90%).[80, 23, 132] However, it is these carbon-centered sugar radicals that lead to the most important types of DNA damage (e.g., $C_{1'}^{\bullet}$ sugar radical results in an abasic site), while, $C_{3'}^{\bullet}$, $C_{4'}^{\bullet}$, and $C_{5'}^{\bullet}$ sugar radicals result in strand break formation[24, 133–136] There are two principal mechanisms for the sugar radical formation: (i) the abstraction of a hydrogen atom from the sugar moiety by the hydroxyl radical ($OH^{\bullet}$)[24, 133–136] and (ii) direct ionization of sugar–phosphate backbone followed by rapid deprotonation.[136] Recently, another mechanism of direct sugar radical formation from electronic excitation of one-electron-oxidized bases ($G^{\bullet+}$ and $A^{\bullet+}$) was proposed.[23–28, 132, 137, 138] In this mechanism,[23–28, 132, 137, 138] shown in Scheme 1.1, photoexcitation induces hole transfer from $G^{\bullet+}$ to the sugar ring, which is followed by a rapid deprotonation at specific carbon sites on the sugar ring.[23–28, 132, 137, 138]

As indicated in the Introduction, this mechanism originated from the work with ion beam irradiations in which high concentrations of sugar radicals were formed

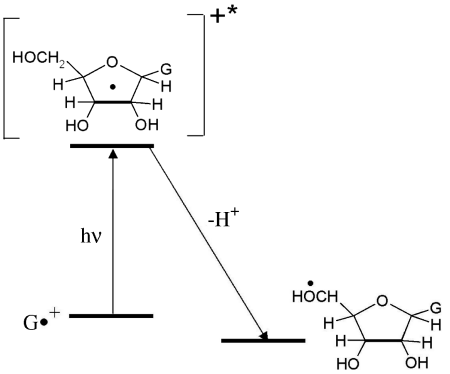

SCHEME 1.1. Proposed mechanism of the sugar radical formation (e.g., $C_{5'}^{\bullet}$) via photoexcitation of $G^{\bullet+}$. (Reprinted with permission from reference 138, *J. Phys. Chem.*, copyright 2008, American Chemical Society.)

predominantly along the ion track, where ionizations and excitations are in close proximity. The proposed hypothesis was experimentally verified using visible photoexcitation of $G^{\bullet+}$ and $A^{\bullet+}$ in DNA and a number of model systems of deoxyribonucleosides, dinucleoside phosphates, oligonucleotides, and RNA model systems and oligomers.[24–28, 137, 138] In model systems, a high yield of conversion of $G^{\bullet+}$ to sugar radical formation (80–100%) was found, while with oligos of increasing length and DNA the yield was found to fall off to ~50%.[24, 26, 27] This experimental observation was further supported by theoretical calculations using time-dependent density functional theory.[26–28] The excited states of $G^{\bullet+}$[26] and A(-H)$^{\bullet}$[27] were studied using TD-B3LYP/6-31G* method, which clearly shows the all the transitions in the near-UV–visible range originate from the inner shell (core) molecular orbitals (MOs), and many of them involved base-to-sugar hole transfer[26, 27] as proposed in Scheme 1.1. The experimental studies were further extended to larger model systems such as dinucleoside phosphate TpdG cation radical,[28] and the photoexcitation of $G^{\bullet+}$ in TpdG radical cations resulted in ~87% conversion of $G^{\bullet+}$ to sugar radicals which were found to be located at the $C_{1'}$ and $C_{3'}$ sugar sites.

Theoretical studies of excited states of a number of dinucleoside phosphates, such as TpdG, dGpdG, dApdA, dApdT, TpdA, and dGpdT in their cationic radical states, were also performed using TD-B3LYP/6-31G(d) method to gain a better understanding of several aspects of photoinduced hole transfer within DNA.[28, 139] In these studies, the ground-state geometries of dinucleoside phosphates in their radical cation states were optimized in the B-DNA conformation at the B3LYP/6-31G(d) level of theory.[28, 139] The effect of solvation of the dinucleoside phosphate radical cations was considered through the polarized continuum model (PCM), and the vertical excitations energies were calculated using the TD-B3LYP/6-31G(d) method (for details see reference 139). For each case, the 20 lowest electronic transition energies, arising from the inner shell (core) molecular orbitals (MOs) to the singly occupied molecular orbital (SOMO) of β-spin, were calculated.[28, 139] It was found that the first electronic transition in every case involving hole transfer from base to base is a $\pi \rightarrow \pi^*$

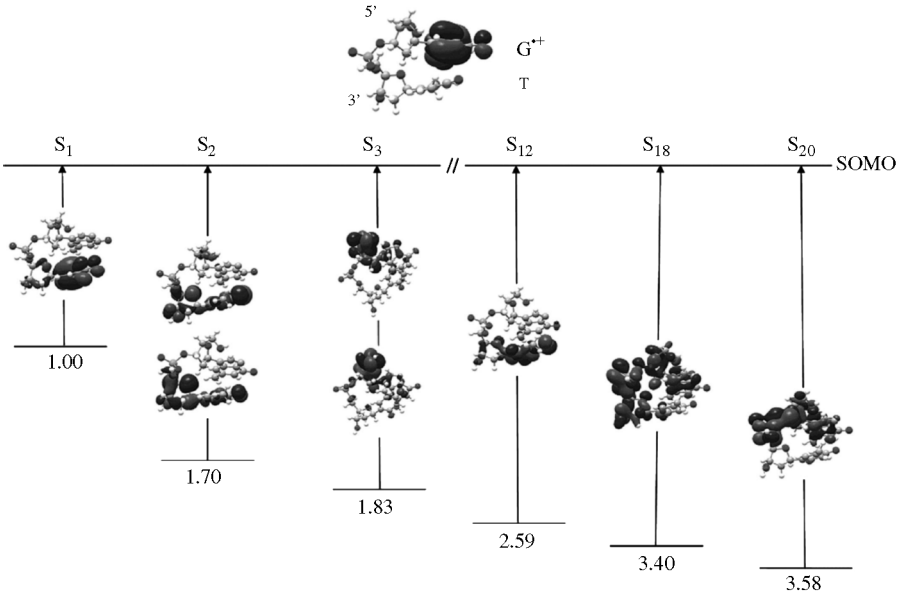

FIGURE 1.10. TD-B3LYP/6-31G(d)-computed transition energies of selected transitions of a dGpdT cation radical. Excitation energies are given in electron volts. (Reprinted with permission from reference 139, *J. Phys. Chem.*, copyright 2006, American Chemical Society.)

transition.[28, 139] However, other higher-energy transitions involved hole transfer from base to sugar–phosphate region. In this context, an experimental wavelength-dependence study of sugar radical formation from $G^{\bullet+}$ in 2′-deoxyguanosine (dGuo) and in DNA was also carried out by Adhikary et al.[26] by varying the photoexcitation wavelength from visible to UV range. Interestingly they found that while in dGuo the sugar radical formation was independent of wavelength of light, the formation of sugar radicals in dsDNA only occurred below 540 nm.[26] Thus, the TD-DFT study[28, 139] clearly supports the experimental observations.[26] As an example, in Figure 1.10, we present the selected transitions S_1, S_2, S_3, S_{12}, S_{18}, and S_{20}, which cover the visible to near-UV range for the dGpdT radical cation as calculated using the TD-B3LYP/6-31G(d) method.[139] All six transitions are from core MOs to SOMO, and they are also shown in Figure 1.10.

From molecular orbital plots in Figure 1.10, we see that SOMO as well as SOMO-1 are localized on guanine and thymine rings in the dGpdT radical cation. Also, in Figure 1.10, the first three transitions (S_1–S_3) correspond to the three lowest transitions, while the other three transitions (S_{12}, S_{18}, and S_{20}) have been chosen which correspond to the dominant molecular orbital contribution from a single inner MO. From Figure 1.10, it is clearly evident that the first transition (S_1) is $\pi \rightarrow \pi^*$ and involves the hole transfer from guanine to thymine (base-to-base) in $dG^{\bullet+}pdT$ with a transition energy of 1.0 eV. However, the other transitions involve hole transfer from base to sugar ring and occur at higher energies > 1.7 eV. In this study, it was also found that the computed first transition (S_1) energy in all the cases was comparable to those

calculated using the CAS-PT2 level of theory reported by Blancafort and Voityuk[140] except for $(dApdA)^{\bullet+}$. The TD-B3LYP method is not suitable for long-range charge transfer excited states as pointed out by Head-Gordon and co-workers.[141] However, a detailed analysis of transition energy calculation using an approximate approach[141] clearly demonstrates that the TD-B3LYP method works quite well for this class of molecules (for details see reference 139). This is because hole migration is not equivalent to a charge transfer state in which charge separation occurs (hole and excess electron). Only in the latter case is coulombic interaction between the induced charges a factor. It is this interaction that is poorly treated by DFT, whereas for hole migration no such interaction exists.

1.4. RADICALS AND TAUTOMERS OF DEPROTONATED GUANINE RADICAL CATION ($G^{\bullet+}$)

Guanine has the lowest ionization potential of the DNA bases, and for this reason it acts as a trap for the hole (positive charge) during oxidative processes on DNA such as ionization, followed by long-range hole transfer. It is well known that the acid and base properties of ionized bases (A, T, G, C, and U) are quite different from their corresponding neutral states[58–61] (see Section 1.2.2), with anion radicals undergoing protonation and cation radicals undergoing deprotonation reactions. Thus, one-electron-oxidized guanine ($G^{\bullet+}$) has a far lower pK_a value (~3.9) than its neutral guanine (9.0).[58–61] Prototropic equilibria involving $G^{\bullet+}$ in an aqueous environment (shown in Scheme 1.2) are therefore highly relevant to its subsequent chemistry.

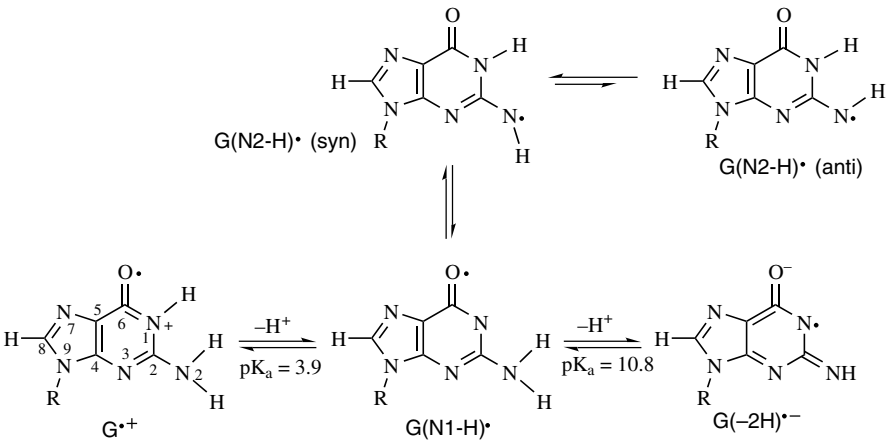

SCHEME 1.2. The numbering scheme and prototropic equilibria of one-electron-oxidized guanine cation radical ($G^{\bullet+}$), the monodeprotonated species, G(N1-H)$^{\bullet}$ and G(N2-H)$^{\bullet}$, in *syn*- and *anti*-conformers with respect to the N3 atom and the dideprotonated species, G(–2H)$^{\bullet-}$). (Reprinted with permission from reference 157, *J. Phys. Chem.*, copyright 2006), American Chemical Society.)

Upon deprotonation of $G^{\bullet+}$ (see Scheme 1.2), two isomeric radicals can form: (i) G(N1-H)$^{\bullet}$ resulting from deprotonation from N1 and (ii) G(N2-H)$^{\bullet}$ resulting from deprotonation from N2. Also, G(N1-H)$^{\bullet}$ and G(N2-H)$^{\bullet}$ (*syn*) have been suggested (from experiment) to be nearly isoenergetic because in aqueous environment the radical cations derived from 2′-deoxyguanosine (dGuo$^{\bullet+}$) and 1-methyl-2′-deoxyguanosine (1MedGuo$^{\bullet+}$) have similar pK_a values of 3.9 and 4.7, respectively.[142–144] Since N1 site in 1MedGuo$^{\bullet+}$ is blocked by a methyl group, only G(N2-H)$^{\bullet}$ forms upon deprotonation.[144] Pulse radiolysis studies[144–146] suggested the formation of G(N1-H)$^{\bullet}$ without any specific evidence. At higher pH, G(N1-H)$^{\bullet}$ further deprotonates from N2 site, which gives G(-2H)$^{\bullet-}$ with a pK_a of 10.8[144] (see Scheme 1.2). ENDOR studies of irradiated single crystals of guanine and their derivatives[147, 148] reported that G(N2-H)$^{\bullet}$ was the species form by deprotonation. These experimental observations[142–144] raised serious questions regarding the preferred site of deprotonation in $G^{\bullet+}$. These questions have been treated by a number of authors employing both theory and experiment[142–158] without definitive conclusions.

Recently, electron spin resonance (ESR) and the B3LYP/6-31G(d) level of theory have been used to identify the preferred site of deprotonation from guanine radical cation ($G^{\bullet+}$) in an aqueous medium at low temperatures as a function of pH.[157] In this study,[157] the various species and their pH ranges were identified as $G^{\bullet+}$ (pH 3–5), G(-H)$^{\bullet}$ (pH 7–9) and G(-2H)$^{\bullet}$ (>11). To be able to draw a definite conclusion about the presence of a specific species, the geometries of all the structures shown in Scheme 1.2 were fully optimized using the B3LYP/6-31G(d) method[157] in the presence of a single water molecule, placed near the N1 or NH2 sites of the molecule to compare the relative stabilities of these tautomers. The calculated relative stabilities of G(N1-H)$^{\bullet} + H_2O$, G(N2-H)$^{\bullet}$ (*syn*) $+ H_2O$ and G(N2-H)$^{\bullet}$ (*anti*) $+ H_2O$ were found to be 2.65, 0.0, and 3.63 kcal/mol,[157] respectively. These calculations therefore predict that G(N2-H)$^{\bullet}$ (*syn*) is the most stable species among all the three tautomers. Since a single water molecule was not enough to fully solvate the molecule, the relative stabilities were further calculated considering the effect of bulk solvent through polarized continuum model (PCM), and again G(N2-H)$^{\bullet}$ (*syn*) $+ H_2O$ was found to be ~1.00 kcal/mol more stable than G(N1-H)$^{\bullet} + H_2O$.[157] Using different theoretical models,[152, 154] G(N2-H)$^{\bullet}$ (*syn*) was found to be more stable than G(N1-H)$^{\bullet}$ by ~3.0–5.0 kcal/mol. These theoretical calculations clearly predict the presence of G(N2-H)$^{\bullet}$ (*syn*) species, but the B3LYP/6-31G(d) calculated hyperfine coupling constants (HFCCs) do match the ESR experimental HFCCs for single crystalline dG but not with those ESR experimental HFCCs found in solution.[157]

To rectify this problem, the theoretical model was further improved by including seven water molecules around the guanine base to consider the effect of the first hydration shell.[157] The geometries of $G^{\bullet+} + 7H_2O$, G(N1-H)$^{\bullet} + 7H_2O$, and G(N2-H)$^{\bullet}$ (*syn*) $+ 7H_2O$ were fully optimized at the B3LYP/6-31G(d) level of theory.[157] Interestingly, G(N1-H)$^{\bullet} + 7H_2O$ was found to be more stable than the G(N2-H)$^{\bullet}$ (*syn*) $+ 7H_2O$ by 3.26 kcal/mol; and using the PCM model, G(N1-H)$^{\bullet} + 7H_2O$ was found to be still more stable than G(N2-H)$^{\bullet}$ (*syn*) $+ 7H_2O$ by 3.0 kcal/mol.[157] In this study, the strong hydrogen bonding between G(N1-H)$^{\bullet}$ and seven water molecules was found to enhance the relative stability of G(N1-H)$^{\bullet}$ tautomers on hydration. It was also

noted that both the tautomers (G(N1-H)$^{\bullet}$ and G(N2-H)$^{\bullet}$ (*syn*)) had the same number of hydrogen bonds with the surrounding seven water molecules. Also, the B3LYP/6-31G (d)-calculated HFCCs for $G^{\bullet+} + 7H_2O$ and G(N1-H)$^{\bullet} + 7H_2O$ were found to be matched very well with the experimental ESR HFCCs.[157] This study strongly supports the existence of the G(N1-H)$^{\bullet}$ tautomer in the aqueous environment; and ^{15}N-substituted derivatives at N1, N2, and N3 atoms in dGuo and C-8 deuteration of dGuo confirms that N1-H is the preferred site for deprotonation in an aqueous environment. Similar conclusions were also drawn by Naumov and Sonntag[158] using UV–visible spectral properties and DFT study recently. Chatgilialoglu et al.[155, 156] also studied the tautomers of one-electron-oxidized guanosine using UV–visible spectral properties and the DFT method. Based on DFT results, they proposed the presence of a transient species G(N2-H)$^{\bullet}$ (*syn*) which in the presence of a water molecule transfers proton from N1 to N2 and becomes G(N1-H)$^{\bullet}$. Their calculated barrier height for the proton transfer using the B3LYP/6-31G* level of theory[155] was found to be 18.8 kJ/mol. However, the same calculation was repeated in reference 157 using B3LYP/6-31G* method and barrier height was found to be 18.9 kcal/mol, suggesting that units may have been incorrectly reported. Our work suggests that this transfer is not needed to produce G(N1-H)$^{\bullet}$[155] because the low-energy pathway is found to be directly from N1.

1.5. NATURE OF HOLE DELOCALIZATION IN ADENINE STACKS: THE DIMER RADICAL CATION $(A_2)^{\bullet+}$

The hole and electron transfer within DNA is of fundamental importance to many research and development areas such as radiation-induced DNA damage and repair, as well as DNA-based molecular devices and sensors.[8, 159, 160] Also, while of fundamental significance, the mechanism of charge transfer in DNA is complex, involving both tunneling and hopping with modulation by environment or proton transfer reactions. Intra-base proton transfer in DNA plays a crucial role in controlling the charge transfer process in DNA. Such proton transfer reactions in DNA either slow or stop the charge transfer process in DNA.[58, 61, 161–163] As already discussed in Sections 1.2.2 and 1.4, the proton transfer reactions will depend on the pK_a of the DNA bases. While the pK_a of the guanine radical cation is near 4, the pK_a of adenine radical cation ($A^{\bullet+}$) produced from dAdo in aqueous solution was estimated by Steenken and co-workers[58, 61] to be $\leq$ 1 (a very strong acid). However, another study[164] of the pH dependence of hole transfer from $A^{\bullet+}$ to guanine in dinucleosides phosphate ApG and GpA[164] suggested that the pK_a of $A^{\bullet+}$ increase in these systems to > 1. This result suggested an effect of base stacking on the pK_a of $A^{\bullet+}$. Many recent experiments[165–169] have shown that stacked adenine bases provide a route to long-range hole transfer in DNA. This work finds that hole migration in DNA through several intervening adenines transfer with little distance dependence. These results seem inexplicable, given the known pK_a of the adenosine cation radical. Indeed the rate constants of hole transfer between adjacent adenines was experimentally determined in the range 10^8–10^{10} s^{-1},[166] which is slower than the proton (H^+) transfer rate (estimated as < 1 ps).[58] This suggests that

deprotonation would occur before hole transfer and stop further hole transfer, which is contradictory to recent experiments.[165–169] Since deprotonation of $A^{\bullet+}$ would stop such transfer, these recent results suggest that the pK_a for $A^{\bullet+}$ in stacked DNA systems must be higher than for the isolated nucleoside in solution. In a study, Barton and coworkers[169] proposed that in adenine stacks the hole is delocalized over several adenines. Very recently, the effects of base stacking on the acid–base properties of $A^{\bullet+}$ were clarified by an investigation using electron spin resonance (ESR) and complementary DFT calculations.[65]

In this study,[65] $A^{\bullet+}$ was produced by one-electron oxidation of dAdo and the stacked DNA oligomer $(dA)_6$ by $Cl_2^{\bullet-}$ in aqueous glass. Using ESR, the presence of $A^{\bullet+}$ in dAdo was obtained in the pH range of 3–7, while in the pH range of 9–12 the presence of $A(-H)^{\bullet}$ (deprotonated $A^{\bullet+}$) was confirmed. As evident from Figure 1.11a, $A^{\bullet+}$ and $A(-H)^{\bullet}$ were found to be present in equal amounts at pH 8 at 150 K. This ESR study clearly shows that at 150 K, $A^{\bullet+}$ has a pK_a value of 8, which is quite different from the estimated pK_a (≤ 1) of $A^{\bullet+}$ as estimated by Steenken.[58] Furthermore, it is also well known that in an aqueous medium, dAdo tends to dimerize in the stacked conformation at ambient temperatures[170–173] having thermodynamic ΔG^0, ΔH^0, and ΔS^0 values as $-4.2\,\text{kJ mol}^{-1}$, $-27.2\,\text{kJ mol}^{-1}$, and $-75.2\,\text{J K}^{-1}\,\text{mol}^{-1}$, respectively. Based on these values,[170–173] it is clear that $A^{\bullet+}$ exists in stacked form in this low-temperature aqueous glass. DFT calculations also show that an adenine radical cation dimer $(A_2)^{\bullet+}$ is quite stable with a calculated pK_a of the dimer of 7 and that of the monomer of -0.3 (described below). Thus, the experimental pK_a value of 8 at 150 K was likely a result of base stacking, producing an adenine radical cation dimer or a

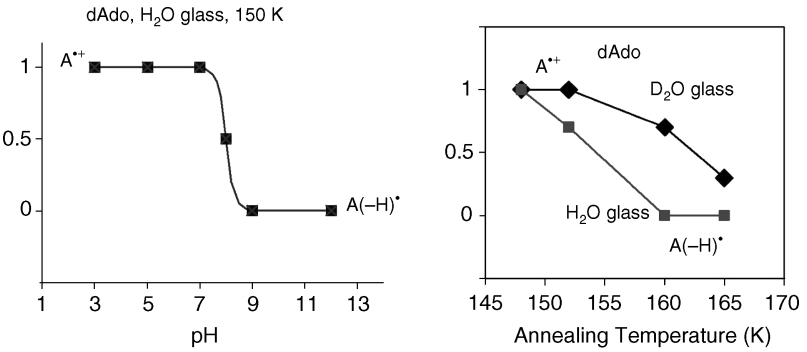

FIGURE 1.11. (**a**) The schematic diagram shows that $A^{\bullet+}$ is found for pHs up to 7 and $A(-H)^{\bullet}$ at pHs of 9 and above at 150 K in 7.5 M LiCl H_2O or D_2O glasses. At pH 8, equal amounts of $A^{\bullet+}$ and $A(-H)^{\bullet}$ are found; the pK_a of $A^{\bullet+}$ is therefore $\sim$8 at 150 K in these systems. In D_2O glassy samples, the corresponding pK_a of $A^{\bullet+}$ is $\sim$8.5. (**b**) The prototropic equilibrium of $A^{\bullet+}$ is found at 150 K. However, annealing to a slightly higher temperature of $\sim$160 K and above allows for molecular migration, and deprotonation is found at all pHs investigated (i.e., 3–12) in H_2O glasses. In D_2O glasses, which soften at slightly higher temperatures, deprotonation of $A^{\bullet+}$ is nearly complete at 165 K. (Reprinted with permission from reference 65, *J. Am. Chem. Soc.*, copyright (2008 American Chemical Society.)

higher multimer. At high annealing temperatures at 160 K in H_2O glass, this dimer breaks apart into monomer $A^{\bullet+}$ and deprotonates spontaneously to yield A(–H)$^{\bullet}$ as found by Steenken[58] and shown in Figure 1.11b. Similar behavior of $A^{\bullet+}$ in stacked oligomers $(dA)_6$[174] was found at 160 K.[65]

To better understand the nature of hole delocalization in the stacked adenine dimer, theoretical calculations were performed using B3LYP, MP2, BHandHLYP, MPWB95, and the 6-31G* basis set. The geometries of adenine (A), adenine radical cation ($A^{\bullet+}$), *syn*- and *anti*-adenine radical (deprotonated at NH_2 group, see Figure 1.1 for *syn*- and *anti*- convention with reference to N1 atom), adenine dimer $(A_B–A_B)_s$, and adenine dimer radical cation ($(A_B–A_B)_s^{\bullet+}$) in stacked conformations were fully optimized. Furthermore, to see the effect of an aqueous environment, the geometries of adenine radical cation ($A^{\bullet+}$) and ($(A_B–A_B)_s^{\bullet+}$) were fully optimized in the presence of 7 and 18 water molecules and designated as $A^{\bullet+} + 7H_2O$ and $(A_B–A_B)_s^{\bullet+} + 18H_2O$. Here A and A_B refer to dAdo (see Figure 1.4) and adenine base molecule, respectively (for a complete description, see reference 65).

As mentioned in Section 1.2.2 and shown in Figure 1.4, the pK_a of $A^{\bullet+}$ was calculated using the B3LYP/6-31G* (PCM) method and was found to be -0.3. The B3LYP/6-31G* calculation of $A^{\bullet+}$ in the presence of a solvent environment ($A^{\bullet+} + 7H_2O$) found that deprotonation from an NH_2 group occurs without a significant barrier (see Figure 1.4). This clearly shows the strongly acidic nature of $A^{\bullet+}$ reported previously for the monomer in aqueous solution. Furthermore, the pK_a of $(A_B–A_B)_s^{\bullet+}$ was also calculated at the same level of theory. Initially, the geometry of $(A_B–A_B)_s^{\bullet+}$ was fully optimized in the Cs symmetry using the B3LYP/6-31G* method, and it was found that $(A_B–A_B)_s^{\bullet+}$ was stabilized by -12.08 kcal/mol (basis set superposition error (BSSE) corrected). Since the B3LYP method is not suitable for estimation of stacking energies in stacked neutral systems (dispersion is not treated well), the calculations were further improved using the MP2 level of theory; and the BSSE-corrected stabilization energy was found to be -15.64 kcal/mol. This suggests the applicability of the B3LYP method for this class of molecules, stacked dimer cation radicals, in which the binding is a charge resonance interaction. Thus after this verification of the computational level, the B3LYP/6-31G*-calculated pK_a value of $(A_B–A_B)_s^{\bullet+}$ was performed and found to be 7, which is in close agreement with the estimated value of 8 (see Figure 1.11). Thus these theoretical calculations show the substantial binding interactions in stacked adenines such as the adenine radical cation dimer $(A_2)^{\bullet+}$.

The geometry of $(A_B–A_B)_s^{\bullet+} + 18H_2O$ was fully optimized at the B3LYP/6-31G* level of theory, and the potential energy surface (PES) for the stretching of N–H bond was calculated starting from the equilibrium N–H bond length to 1.45 Å in the step size of 0.05 Å. The same calculation was done for $A^{\bullet+} + 7H_2O$. The PESs of N–H bond stretching in $A^{\bullet+} + 7H_2O$ and of $(A_B–A_B)_s^{\bullet+} + 18H_2O$ are shown in Figure 1.12. In contrast to the $A^{\bullet+} + 7H_2O$ which showed no barrier to deprotonation, it is found that the barrier height for $(A_B–A_B)_s^{\bullet+} + 18H_2O$ increased with an increase of N–H bond length, showing a clear uphill process. This supports the high pK_a value of $A^{\bullet+}$ in stacked dimer conformation as estimated by the present experiment and calculations.[65]

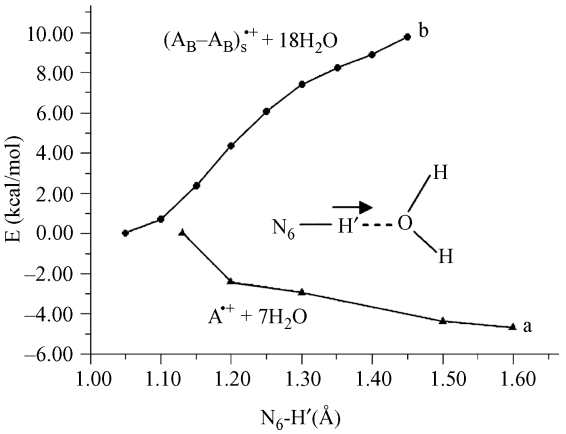

FIGURE 1.12. Potential energy surface (PES) of N_6–H′ bond dissociation of (**a**) $A^{\bullet+} + 7H_2O$ cation radical and (**b**) $(A_B–A_B)_s^{\bullet+} + 18H_2O$ cation radical in stacked conformation. The distances and energies are given in angstroms (Å) and kcal/mol, respectively. See Figures1.4 and 1.13 for structures. (Reprinted with permission from reference 65, *J. Am. Chem. Soc*., copyright 2008, American Chemical Society.)

After obtaining a very good match between theory and experiment[65] of pK_a values, the spin density distributions in adenine dimer radical cation $[(A_B–A_B)_s^{\bullet+}]$ in gas phase and in the presence of 18 water molecules were calculated using the B3LYP/6-31G* method. From the spin density distributions, it was found that spin densities were equally distributed on both of the adenine rings in $(A_B–A_B)_s^{\bullet+}$ (see Figure 1.13a), while in the presence of waters the spin density is more localized on one of the adenine rings (73%; see Figure 1.13b). It appears that on optimization, the relaxation of the surrounding water molecules tend to stabilize the hole (spin density) more on one of the adenine rings (see the upper adenine ring in Figure 1.13b). The B3LYP method is known to overestimate delocalization as a result of the self-interaction error, particularly, for odd electron containing molecular systems.[175] Therefore, the spin densities were also calculated using the HF/6-31G* method considering the B3LYP/6-31G* generated geometries. The HF/6-31G* method also shows the delocalization of spin density on both of the adenine rings in $(A_B–A_B)_s^{\bullet+}$ and localization of more spin density on one of the adenine ring in $(A_B–A_B)_s^{\bullet+} + 18H_2O$ as obtained with B3LYP method, see Figures 1.13c and 1.13d.

These results clearly indicate the peculiar behavior of adenine radical cation ($A^{\bullet+}$) in stacks of adenines that is quite different than the behavior of the guanine radical cation in guanine stacks where hole localization is found. In this context, the singly occupied molecular orbital (SOMO) of $dG^{\bullet+}pdG$, $(dApdA)^{\bullet+}$ and dA(–H)•pdA were calculated using the B3LYP/6-31G* method.[139] From Figure 1.14a, it is evident that in $dG^{\bullet+}pdG$, SOMO is localized on one of the guanines (84% spin density) at the 5′ end. In the $(dApdA)^{\bullet+}$ the SOMO is equally delocalized on both of the adenine rings (Figure 1.14b), while in the deprotonated dA(–H)•pdA the spin density is totally localized on the A(–H) adenine ring as expected (Figure 1.14c). This study shows that

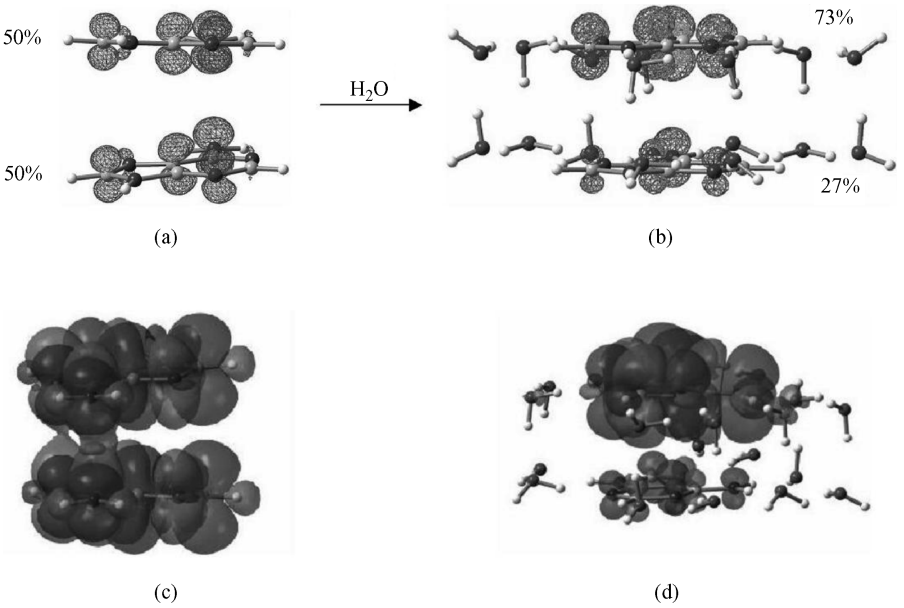

FIGURE 1.13. B3LYP/6-31G* calculated spin-density distribution shown in percentages in (**a**) the base-stacked adenine dimer cation radical $[(A_B–A_B)_s^{\bullet+}]$ in gas phase and (**b**) the base-stacked adenine dimer cation radical surrounded by 18 water molecules. On optimization, the water molecules adjust to favor spin on one of the adenine rings in $[(A_B–A_B)_s^{\bullet+} + 18H_2O]$ complex. (**c**) and (**d**) are the HF/6-31G*//B3LYP/6-31G* calculated spin-density distributions of systems shown in parts a and b, respectively. (Reprinted with permission from reference 65, *J. Am. Chem. Soc*., copyright 2008, American Chemical Society.)

in $dG^{\bullet+}pdG$ the hole is localized; however, in $(dApdA)^{\bullet+}$ the hole tends to be delocalized.

This study[65] also shows that the hole delocalization over the dimer cation resulted in substantial energy stabilization. For example, in comparison to the neutral adenine dimer which showed only weak interactions of a few kilocalories, $(A_2)^{\bullet+}$ was found to have a high binding energy of 12–16 kcal/mol depending on the level of calculation (see details in reference 65). As already mentioned in Section 1.2.1, the nuclear

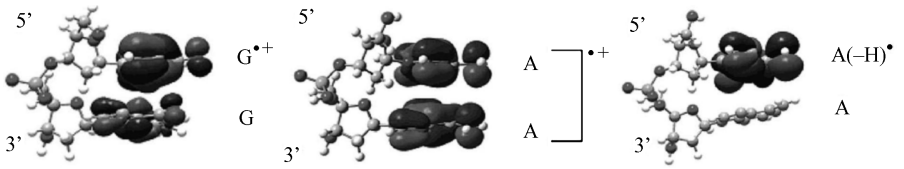

FIGURE 1.14. B3LYP/6-31G* calculated singly occupied molecular orbital (SOMO) plots of (**a**) $dG^{\bullet+}pdG$, (**b**) $(dApdA)^{\bullet+}$, and (**c**) $dA(–H)^{\bullet}pdA$. (Reprinted with permission from reference 139, *J. Phys. Chem*., copyright 2006 American Chemical Society.)

relaxation energy (NRE) of A, T, G, C, and U are experimentally estimated from the difference between their corresponding adiabatic and vertical ionization potential values (see Table 1.1). Among all the bases, adenine has the lowest NRE (0.18 eV) and guanine has the largest NRE (0.47 eV). These NRE values show that the geometrical change in adenine radical cation in comparison to neutral adenine is modest, while the geometrical change in guanine radical cation in comparison to neutral guanine is substantial. Calculations also predicted a very small NRE (0.1 eV) of adenine radical formation in the AT base pair; however, the corresponding value for the guanine radical cation in the GC base pair was found to be 0.3 eV.[48,49] Thus, adenine radical cation ($A^{\bullet+}$) has almost the same structure as it has in the neutral state. Thus in the DNA, adenine stack tends to delocalize the hole, while guanine stack tends to localize as a result of the large nuclear relaxation for $G^{\bullet+}$. Blancafort and Voityuk[140] calculated the transition energy of $A^{\bullet+}A$ using the CAS-PT2(11,12) level of theory and found a very small first transition energy 0.1 eV, and they assumed this small transition energy to be a problem in choosing the active space. But now it is clear from this study[65] that this small transition energy (0.1 eV) was due to hole delocalization on both the adenine rings. The B3LYP/6-31G* calculated transition energy (0.5 eV) of $(dApdA)^{\bullet+}$ was also found to be smallest among all the considered dinucleoside radical cations[139] because the hole in this case only was found to be delocalized (see Figure 1.14b).

1.6. CONCLUSIONS

The wide applications of theory to the studies of DNA radiation damage summarized in this review show that this area is of substantial and growing interest. Many successful theoretical studies have elucidated the detailed mechanisms that help to explain experiment. The agreement between theory and experiment is expected to improve as the theoretical model better mimics the experimental situation. With ever-increasing computing power and recent advances in theory, theory can be applied to more complex problems. For example, DFT is now used routinely for large molecular systems, even for substantial sections of DNA. DFT, especially with B3LYP, inherently has a number of limitations such as the self-interaction error that overestimates spin delocalization, the poor accounting for the coulombic term in charge transfer states, and poor treatment of dispersion interactions essential for DNA stacking. However, each of these problems is being treated, and progress is being made in corrections with new functionals. For example, recently, the development of new functionals in DFT has been found to be very suitable to study noncovalent and stacking interactions. Time-dependent density functional theory (TD-DFT) is found quite successful to describe the excited state properties of ionized DNA bases and base pairs. Furthermore, the DFT delocalization problem has been dealt with by functionals that increase the HF exchange contribution such as BH&HLYP which has a 50% HF exchange contribution. Thus such DFT calculations of hole delocalization in adenine stacks have led to a new understanding of hole transfer through adenine stacks within DNA.

ACKNOWLEDGMENTS

This work was supported by the NIH NCI under Grant R01CA045424. The authors are also grateful to the Arctic Region Supercomputing Center (ARSC) for generously providing the computational time to perform some of these calculations. Computational studies were also supported by a computational facilities grant NSF CHE-0722689.

REFERENCES

1. Sevilla, M. D.; Becker, D. ESR studies of radiation damage to DNA and related biomolecules. In *Royal Society of Chemistry Special Periodical Report, Vol. 19, Electron spin resonance*, London, **2004**, p. 243.
2. Becker, D.; Sevilla, M. D. The chemical consequences of radiation damage to DNA. In *Advances in Radiation Biology*, Vol. 17; Lett, J., ed.; Academic Press, New York, 1993, p. 121.
3. Burrows, C. J.; Muller, J. G. Oxidative nucleobase modifications leading to strand scission. *Chem. Rev.* **1998**, *98*, 1109–1152.
4. von Sonntag C. The chemistry of free-radical-mediated DNA damage. In *Physical and Chemical Mechanisms in Molecular Radiation Biology*; Glass, W. A.; Varma, M. N., Eds.; Plenum, New York, 1991, p. 287.
5. Swarts, S. G.; Sevilla, M. D.; Becker, D.; Tokar, C. J.; Wheeler, K. T. Radiation-induced DNA damage as a function of hydration. I. Release of unaltered bases. *Radiat. Res.* **1992**, *129*, 333–344.
6. Swiderek, P. Fundamental processes in radiation damage of DNA. *Angew. Chem. Int. Ed.* **2006**, *45*, 4056–4059.
7. Xifeng, L.; Sevilla, M. D. DFT treatment of radiation produced radicals in DNA model systems. *Adv. Quantum Chem.* **2007**, *52*, 59–87.
8. Becker, D.; Adhikary, A.; Sevilla, M. D. The role of charge and spin migration in DNA radiation damage. In *Charge Migration in DNA*; Chakraborty, T.,Ed.; Springer-Verlag, Berlin, 2007; pp. 139–175.
9. Kumar, A.; Sevilla M. D. Radiation effects on DNA: Theoretical investigations of electron, hole and excitation pathways to DNA damage. In *Radiation Induced Molecular Phenomena in Nucleic Acid: A Comprehensive Theoretical and Experimental Analysis*; Shukla, M. K.; Leszczynski, J.,Eds.; Springer-Verlag, Berlin, 2008, pp. 577–617.
10. Sevilla, M. D.; Bernhard, W. A. Mechanisms of direct radiation damage to DNA. In *Radiation Chemistry from Basics to Applications in Material and Life Sciences*; Spotheim-Maurizot, M.; Mostafavi, M.; Douki, T.; Belloni, J.,Eds.; EDP Sciences, Cedex A, France, 2008; pp. 191–201.
11. Hanel, G.; Gstir, B.; Denifl, S.; Scheier, P.; Probst, M.; Farizon, B.; Farizon, M.; Illenberger, E.; Märk, T. D. Electron attachment to uracil: Effective destruction at subexcitation energies. *Phys. Rev. Lett.* **2003**, *90*, 188–104.
12. Boudaïffa, B.; Cloutier, P.; Hunting, D.; Huels, M. A.; Sanche, L. Resonant formation of DNA strand breaks by low-energy (3 to 20 eV) electrons. *Science* **2000**, *287*, 1658–1660.

13. Huels, M. A.; Boudaïffa, B.; Cloutier, P.; Hunting, D.; Sanche, L. Single, double, and multiple double strand breaks induced in DNA by 3–100 eV electrons. *J. Am. Chem. Soc.* **2003**, *125*, 4467–4477.
14. Sanche, L. Low energy electron-driven damage in biomolecules. *Eur. Phys. J. D.* **2005**, *35*, 367–390.
15. Zheng, Y.; Cloutier, P.; Hunting, D. J.; Sanche, L.; Wagner, J. R. Chemical basis of DNA sugar–phosphate cleavage by low-energy electrons. *J. Am. Chem. Soc.* **2005**, *127*, 16592–16598.
16. Zheng, Y.; Wagner, J. R.; Sanche, L. DNA damage induced by low-energy electrons: Electron transfer and diffraction. *Phys. Rev. Lett.* **2006**, *96*, 208–101.
17. Ptasińska, S.; Sanche, L. Dissociative electron attachment to hydrated single DNA strands. *Phys. Rev. E* **2007**, *75*, 031915.
18. Ptasińska, S.; Sanche, L. Dissociative electron attachment to abasic DNA. *Phys. Chem. Chem. Phys.* **2007**, *9*, 1730–1735.
19. Baccarelli, I.; Gianturco, F. A.; Grandi, A.; Sanna, N. Lucchese, R. R.; Bald, I.; Kopyra, J.; Illenberger, E. Selective bond breaking in β-D-ribose by gas-phase electron attachment around 8 eV. *J. Am. Chem. Soc.* **2007**, *129*, 6269–6277.
20. Sulzer, P.; Ptasińska, S.; Zappa, F.; Mielewska, B.; Milosavljevic, A. R.; Scheier, P.; Märk, T. D.; Bald, I.; Gohlke, S.; Huels, M. A., Illenberger, E. Dissociative electron attachment to furan, tetrahydrofuran, and fructose. *J. Chem. Phys.* **2006**, *125*, 044304.
21. Bald, I.; Kopyra, J.; Illenberger, E. Selective excision of C5 from D-ribose in the gas phase by low-energy electrons (0–1 eV): Implications for the mechanism of DNA damage. *Angew. Chem., Int. Ed.* **2006**, *45*, 4851–4855.
22. König, C.; Kopyra, J.; Bald, I.; Illenberger, E. Dissociative electron attachment to phosphoric acid esters: The direct mechanism for single strand breaks in DNA. *Phys. Rev. Lett.* **2006**, *97*, 018105.
23. Becker, D.; Bryant-Friedrich, A.; Trzasko, C.; Sevilla, M. D. Electron spin resonance study of DNA irradiated with an argon-ion beam: Evidence for formation of sugar phosphate backbone radicals. *Radiat. Res.* **2003**, *160*, 174–185
24. Shukla, L. I.; Pazdro, R.; Huang, J.; DeVreugd, C.; Becker, D.; Sevilla, M. D. The formation of DNA sugar radicals from photoexcitation of guanine cation radicals. *Radiat. Res.* **2004**, *161*, 582–590.
25. Shukla, L. I.; Pazdro, R.; Becker, D.; Sevilla, M. D. Sugar radicals in DNA: Isolation of neutral radicals in gamma-irradiated DNA by hole and electron scavenging. *Radiat. Res.* **2005**, *163*, 591–602.
26. Adhikary, A.; Malkhasian, A. Y. S.; Collins, S.; Koppen, J.; Becker, D.; Sevilla, M. D. UVA–visible photo-excitation of guanine radical cations produces sugar radicals in DNA and model structures. *Nucleic Acids Res.* **2005**, *33*, 5553–5564.
27. Adhikary, A.; Collins, S.; Koppen, J.; Becker, D.; Sevilla, M. D. C5′- and C3′-sugar radicals produced via photo-excitation of one-electron oxidized adenine in 2′-deoxyadenosine and its derivatives. *Nucleic Acid Res.* **2006**, *34*, 1501–1511.
28. Adhikary, A.; Kumar, A.; Sevilla, M. D. Photo-induced hole transfer from base to sugar in DNA: Relationship to primary radiation damage. *Radiat. Res.* **2006**, *165*, 479–484.
29. Baker, J.; Wolinski, K.; Malagoli, M.; Kinghorn, D.; Wolinski, P.; Magyarfalvi, G.; Saebo, S.; Janowski, T.; Pulay, P. Quantum chemistry in parallel with PQS. *J. Comput. Chem.* **2009**, *30*, 317–335.

30. Sevilla, M. D.; Becker, D.; Yan, M.; Summerfield, S. R. Relative abundances of primary ion radicals in γ-irradiated DNA: Cytosine vs thymine anions and guanine vs adenine cations *J. Phys. Chem.* **1991**, *95*, 3409–3415.
31. Hush, N. S.; Cheung, A. S. Ionization potentials and donor properties of nucleic acid bases and related compounds. *Chem. Phys. Lett.* **1975**, *34*, 11–13.
32. Orlov, V. M.; Smirnov, A. N.; Varshavsky, Y. M. Ionization potentials and electron-donor ability of nucleic acid bases and their analogues. *Tetrahedron Lett.* **1976**, *17*, 4315–4394.
33. Choi, K.-W.; Lee, J.-H.; Kim, S. K. Ionization spectroscopy of a DNA base: Vacuum-ultraviolet mass-analyzed threshold ionization spectroscopy of jet-cooled thymine. *J. Am. Chem. Soc.* **2005**, *127*, 15674–15675.
34. Sevilla, M. D.; Besler, B.; Colson, A. O. Ab initio molecular orbital calculations of DNA radical ions. 5. Scaling of calculated electron affinities and ionization potentials to experimental values. *J. Phys. Chem.* **1995**, *99*, 1060–1063.
35. Russo, N.; Toscano, M.; Grand, A. Theoretical determination of electron affinity and ionization potential of DNA and RNA bases. *J. Comput. Chem.* **2000**, *21*, 1243–1250.
36. Wetmore, S. D.; Boyd, R. J.; Eriksson, L. A. Electron affinities and ionization potentials of nucleotide bases. *Chem. Phys. Lett.* **2000**, *322*, 129–135.
37. Rubio, M.; Roca-Sanjuán, D.; Merchán, M.; Serrano-Andrés, L. Determination of the lowest-energy oxidation site in nucleotides: 2′-Deoxythymidine 5′-monophosphate anion. *J. Phys. Chem. B* **2006**, *110*, 10234–10235.
38. Tureček, F. Computational studies of radicals relevant to nucleic acid damage. *Adv. Quantum Chem.* **2007**, *52*, 89–120.
39. Cauët, E.; Dehareng D.; Liévin, J. Ab initio study of the ionization of the DNA bases: Ionization potentials and excited states of the cations. *J. Phys. Chem. A* **2006**, *110*, 9200–9211.
40. Crespo-Hernandez, C. E.; Arce, R.; Ishikawa, Y.; Gorb, L.; Leszczynski, J.; Close, D. M. Ab initio ionization energy thresholds of DNA and RNA bases in gas phase and in aqueous solution. *J. Phys. Chem. A* **2004**, *108*, 6373–6377.
41. Zakjevskii, V. V.; King, S. J.; Dolgounitcheva, O.; Zakrzewski, V. G.; Ortiz, J. V. Base and phosphate electron detachment energies of deoxyribonucleotide anions. *J. Am. Chem. Soc.* **2006**, *128*, 13350–13351.
42. Yang, X.; Wang, X.-B.; Vorpagel, E. R.; Wang, L.-S. Direct experimental observation of the low ionization potentials of guanine in free oligonucleotides by using photoelectron spectroscopy. *Proc. Natl. Acad. Sci. USA* **2004**, *101*, 17588–17592.
43. Fernando, H.; Papadantonakis, G. A.; Kim, N. S.; Lebreton, P. R. Conduction-band-edge ionization thresholds of DNA components in aqueous solution. *Proc. Natl. Acad. Sci. USA* **1998**, *95*, 5550–5555.
44. Colson, A. O.; Besler, B.; Sevilla, M. D. Ab initio molecular orbital calculations on DNA radical ions. 3. Ionization potentials and ionization sites in components of the DNA sugar phosphate backbone. *J. Phys. Chem.* **1993**, *97*, 8092–8097.
45. Kim, S. K.; Lee, W.; Herschbach, D. R. Cluster beam chemistry: Hydration of nucleic acid bases; ionization potentials of hydrated adenine and thymine. *J. Phys. Chem.* **1996**, *100*, 7933–7937.
46. Close, D. M. Calculation of the ionization potentials of the DNA bases in aqueous medium. *J. Phys. Chem. A* **2004**, *108*, 10376–10379.

47. Colson, A. O.; Besler, B.; Sevilla, M. D. Ab initio molecular orbital calculations on DNA base pair radical ions: Effect of base pairing on proton-transfer energies, electron affinities, and ionization potentials. *J. Phys. Chem.* **1992**, *96*, 9787–9794.
48. Li, X. F.; Cai, Z. L.; Sevilla, M. D. Energetics of the radical ions of the AT and AU base pairs: A density functional theory (DFT) study. *J. Phys. Chem. A* **2002**, *106*, 9345–9351.
49. Li, X. F.; Cai, Z. L.; Sevilla, M. D. Investigation of proton transfer within DNA base pair anion and cation radicals by density functional theory (DFT). *J. Phys. Chem. B* **2001**, *105*, 10115–10123.
50. Hutter, M.; Clark, T. On the enhanced stability of the guanine–cytosine base-pair radical cation. *J. Am. Chem. Soc.* **1996**, *118*, 7574–7577.
51. Bertran, J.; Oliva, A.; Rodriguez-Santiago, L.; Sodupe, M. Single versus double proton-transfer reactions in Watson–Crick base pair radical cations. A theoretical study. *J. Am. Chem. Soc.* **1998**, *120*, 8159–8167.
52. Colson, A. O.; Sevilla, M. D. Elucidation of primary radiation-damage in DNA through application of ab-initio molecular-orbital theory. *Int. J. Radiat. Biol.* **1995**, *67*, 627–645.
53. Colson, A. O.; Besler, B.; Sevilla, M. D. Ab-initio molecular-orbital calculations an DNA radical ions. 4. Effect of hydration an electron-affinities and ionization-potentials of base-pairs. *J. Phys. Chem.* **1993**, *97*, 13852–13859.
54. Barnett, R. N.; Cleveland, C. L.; Joy, A.; Landman, U.; Schuster, G. B. Charge migration in DNA: Ion-gated transport. *Science* **2001**, *294*, 567–571.
55. Hutter, M. C. Stability of the guanine–cytosine radical cation in DNA base pairs triplets. *Chem. Phys.* **2006**, *326*, 240–245.
56. Prat, F.; Houk, K. N.; Foote, C. S. Effect of guanine stacking on the oxidation of 8-oxoguanine in B-DNA. *J. Am. Chem. Soc.* **1998**, *120*, 845–846.
57. Sugiyama, H.; Saito, I. Theoretical studies of GG-specific photocleavage of DNA via electron transfer: Significant lowering of ionization potential and 5′-localization of HOMO of stacked GG bases in B-form DNA. *J. Am. Chem. Soc.* **1996**, *118*, 7063–7068.
58. Steenken, S. Purine bases, nucleosides, and nucleotides: Aqueous solution redox chemistry and transformation reactions of their radical cations and e^- and OH adducts. *Chem. Rev.* **1989**, *89*, 503–520.
59. Steenken, S.; Telo, J. P.; Novais, H. M.; Candeias, L. P. One-electron-reduction potentials of pyrimidine bases, nucleosides, and nucleotides in aqueous solution. Consequences for DNA redox chemistry. *J. Am. Chem. Soc.* **1992**; *114*, 4701–4709.
60. Steenken, S.; Jovanovic, S. V. How easily oxidizable is DNA? One-electron reduction potentials of adenosine and guanosine radicals in aqueous solution. *J. Am. Chem. Soc.* **1997**, *119*, 617–618.
61. Steenken, S. Electron transfer in DNA? Competition by ultra-fast proton transfer? *Biol. Chem.* **1997**, *378*, 1293–1297.
62. Jang, Y. H.; GoddardIII, W. A.; Noyes, K. T.; Sowers, L. C.; Hwang, S.; Chung, D. S. First principles calculations of the tautomers and p*K*a values of 8-oxoguanine: Implications for mutagenicity and repair. *Chem. Res. Toxicol.* **2002**, *15*, 1023–1035.
63. Baik, M.-H.; Silverman, J. S.; Yang, I. V.; Ropp, P. A.; Szalai, V. A.; Yang, W.; Thorp, H. H. Using density functional theory to design DNA base analogues with low oxidation potentials. *J. Phys. Chem. B* **2001**, *105*, 6437–6444.

64. Chen, X.; Syrstad, E. A.; Nguyen, M. T.; Gerbaux, P.; Tureček, F. Distonic isomers and tautomers of the adenine cation radical in the gas phase and aqueous solution. *J. Phys. Chem. A* **2004**, *108*, 9283–9293.

65. Adhikary, A.; Kumar, A.; Khanduri, D.; Sevilla, M. D. Effect of base stacking on the acid–base properties of the adenine cation radical [$A^{\bullet+}$] in solution: ESR and DFT studies. *J. Am. Chem. Soc.* **2008**, *130*, 10282–10292.

66. Nir, E.; Kleinermanns, K.; de Vries, M. S. Pairing of isolated nucleic-acid bases in the absence of the DNA backbone. *Nature* **2000**, *408*, 949–951.

67. Desfrançois, C.; Periquet, V.; Bouteiller, Y.; Schermann, J. P. Valence and dipole binding of electrons to uracil. *J. Phys. Chem. A* **1998**, *102*, 1274–1278.

68. Puiatti, M.; Vera, D. M. A.; Pierini, A. B. Species with negative electron affinity and standard DFT methods. Finding the valence anions. *Phys. Chem. Chem. Phys.* **2008**, *10*, 1394–1399.

69. Vera, D. M. A.; Pierini, A. B. Species with negative electron affinity and standard DFT methods. *Phys. Chem. Chem. Phys.* **2004**, *6*, 2899–2903.

70. Li, X. F.; Cai, Z. L.; Sevilla, M. D. DFT Calculations of the electron affinities of nucleic acid bases: Dealing with negative electron affinities. *J. Phys. Chem. A* **2002**, *106*, 1596–1603.

71. Wesolowski, S. S.; Leininger, M. L.; Pentchev, P. N.; Schaefer, H. F. Electron affinities of the DNA and RNA bases. *J. Am. Chem. Soc.* **2001**, *123*, 4023–4028.

72. Svozil, D.; Jungwirth, P.; Havlas, Z. Electron binding to nucleic acid bases. Experimental and theoretical studies. A review. *Collect. Czech. Chem. Commun.* **2004**, *69*, 1395–1428.

73. Bachorz, A. R.; Klopper, W.; Gutowski, M. Coupled-cluster and explicitly correlated perturbation-theory calculations of the uracil anion. *J. Chem. Phys.* **2007**, *126*, 085101.

74. Aflatooni, K.; Gallup, G. A.; Burrow, P. D. Electron attachment energies of the DNA bases. *J. Phys. Chem. A* **1998**, *102*, 6205–6207.

75. Desfrançois, C.; Carles, S.; Schermann, J. P. Weakly bound clusters of biological interest. *Chem. Rev.* **2000**, *100*, 3943–3962.

76. Hendricks, J. H.; Lyapustina, S. A.; de Clercq, H. L.; Snodgrass, J. T.; Bowen, K. H.; Dipole bound, nucleic acid base anions studied via negative ion photoelectron spectroscopy. *J. Chem. Phys.* **1996**, *104*, 7788–7791.

77. Hendricks, J. H.; Lyapustina, S. A.; de Clercq, H. L.; Snodgrass, J. T.; Bowen, K. H. The dipole bound-to-covalent anion transformation in uracil. *J. Chem. Phys.* **1998**, *108*, 8–11.

78. Schiedt, J.; Weinkauf, R.; Neumark, D. M.; Schlag, E. W. Anion spectroscopy of uracil, thymine and the amino-oxo and amino-hydroxy tautomers of cytosine and their water clusters. *Chem. Phys.* **1998**, *239*, 511–524.

79. Periquet, V.; Moreau, A.; Carles, S.; Schermann, J. P.; Desfrançois, C. Cluster size effects upon anion solvation of N-heterocyclic molecules and nucleic acid bases. *J. Electron Spectrosc. Relat. Phenom.* **2000**, *106*, 141–151.

80. Wang, W.; Yan, M.; Becker, D.; Sevilla, M. D. The influence of hydration on the absolute yields of primary free radicals in gamma-irradiated DNA at 77 K. II. Individual radical yields. *Radiat. Res.* **1993**, *137*, 2–10.

81. Wang, W.; Sevilla, M. D. Protonation of nucleobase anions in gamma-irradiated DNA and model systems. Which DNA base is the ultimate sink for the electron? *Radiat. Res.* **1994**, *138*, 9–17.

82. Haranczyk, M.; Gutowski, M. Valence and dipole-bound anions of the most stable tautomers of guanine. *J. Am. Chem. Soc.* **2005**, *127*, 699–706.

83. Li, X. F.; Sevilla, M. D.; Sanche, L. Hydrogen atom loss in pyrimidine DNA bases induced by low-energy electrons: Energetics predicted by theory. *J. Phys. Chem. B* **2004**, *108*, 19013–19019.

84. Svozil, D.; Frigato, T.; Havlas, Z.; Jungwirth, P. Ab initio electronic structure of thymine anions. *Phys. Chem. Chem. Phys.* **2005**, *7*, 840–845.

85. Radisic, D.; Bowen, K. H.; Dabkowska, I.; Storoniak, P.; Rak, J.; Gutowski, M. AT base pair anions versus (9-Methyl-A)(1-Methyl-T) base pair anions. *J. Am. Chem. Soc.* **2005**, *127*, 6443–6450.

86. Richardson, N. A.; Wesolowski, S. S.; Schaefer, H. F. The adenine–thymine base pair radical anion: Adding an electron results in a major structural change. *J. Phys. Chem. B* **2003**, *107*, 848–853.

87. Gu, J. D.; Xie, Y. M.; Schaefer, H. F. Structural and energetic characterization of a DNA nucleoside pair and its anion: Deoxyriboadenosine (dA)–deoxyribothymidine (dT). *J. Phys. Chem. B* **2005**, *109*, 13067–13075.

88. Kumar, A.; Knapp-Mohammady, M.; Mishra, P. C.; Suhai, S. A theoretical study of structures and electron affinities of radical anions of guanine–cytosine, adenine–thymine, and hypoxanthine–cytosine base pairs. *J. Comput. Chem.* **2004**, *25*, 1047–1059.

89. Gu, J. A.; Xie, Y. M.; Schaefer, H. F. Electron attachment to nucleotides in aqueous solution. *Chem. Phys. Chem.* **2006**, *7*, 1885–1887.

90. Kim, S.; Wheeler, S. E.; Schaefer, H. F. Microsolvation effects on the electron capturing ability of thymine: Thymine–water clusters. *J. Chem. Phys.* **2006**, *124, 204310*.

91. Kim, S.; Schaefer, H. F. Effects of microsolvation on uracil and its radical anion: Uracil$^{\bullet}$ $(H_2O)_n$ (n = 1–5). *J. Chem. Phys.* **2006**, *125*, 144305.

92. Kim, S.; Schaefer, H. F. Microhydration of cytosine and its radical anion: Cytosine$^{\bullet}$ $(H_2O)_n$ (n = 1–5). *J. Chem. Phys.* **2007**, *126*, 064301.

93. Gu, J. A.; Xie, Y. M.; Schaefer, H. F. Understanding electron attachment to the DNA double helix: The thymidine monophosphate–adenine pair in the gas phase and aqueous solution. *J. Phys. Chem. B* **2006**, *110*, 19696–19703.

94. Harańczyk, M.; Gutowski, M. Finding adiabatically bound anions of guanine through a combinatorial computational approach. *Angew. Chem. Int. Ed.* **2005**, *44*, 6585–6588.

95. Bao, X. G.; Sun, H.; Wong, N. B.; Gu, J. D. Microsolvation effect, hydrogen-bonding pattern, and electron affinity of the uracil–water complexes U-$(H_2O)_n$ (n = 1, 2, 3). *J. Phys. Chem. B* **2006**, *110*, 5865–5874.

96. Bao, X. G.; Liang, G. M.; Wong, N. B.; Gu, J. Microsolvation pattern of the hydrated radical anion of uracil: $U^{-}(H_2O)_n$ (n = 3–5). *J. Phys. Chem. A* **2007**, *111*, 666–672.

97. Kumar, A.; Mishra, P. C.; Suhai, S. Adiabatic electron affinities of the polyhydrated adenine–thymine base pair: A density functional study. *J. Phys. Chem. A* **2005**, *109*, 3971–3979.

98. Kumar, A.; Sevilla, M. D.; Suhai, S. Microhydration of the guanine–cytosine (GC) base pair in the neutral and anionic radical states: A density functional study. *J. Phys. Chem. B* **2008**, *112*, 5189–5198.

99. Li, Z. J.; Zheng, Y.; Cloutier, P.; Sanche, L.; Wagner, J. R. Low energy electron induced DNA damage: Effects of terminal phosphate and base moieties on the distribution of damage. *J. Am. Chem. Soc.* **2008**, *130*, 5612–5613.
100. Martin, F.; Burrow, P. D.; Cai, Z.; Cloutier, P.; Hunting, D.; Sanche, L. DNA strand breaks induced by 0–4 eV electrons: The role of shape resonances. *Phys. Rev. Lett.* **2004**, *93*, 068101.
101. Ptasińska, S.; Denifl, S.; Gohlke, S.; Scheier, P.; Illenberger, E.; Märk, T. D. Decomposition of thymidine by low-energy electrons: Implications for the molecular mechanisms of single-strand breaks in DNA. *Angew. Chem., Int. Ed.* **2006**, *45*, 1893–1896.
102. Denifl, S.; Zappa, F.; Mauracher, A.; da Silva, F. F.; Bacher, A.; Echt, O.; Mark, T. D.; Bohme, D. K.; Scheier, P. Dissociative electron attachment to DNA bases near absolute zero temperature: Freezing dissociation intermediates. *Chem. Phys. Chem.* **2008**, *9*, 1387–1389.
103. Li, X.; Sanche, L.; Sevilla, M. D. Base release in nucleosides induced by low-energy electrons: A DFT study. *Radiat. Res.* **2006**, *165*, 721–729.
104. Li, X.; Sevilla, M. D.; Sanche, L. Density functional theory studies of electron interaction with DNA: Can zero eV electrons induce strand breaks? *J. Am. Chem. Soc.* **2003**, *125*, 13668–13669.
105. Li, X.; Sanche, L.; Sevilla, M. D. Low energy electron interactions with uracil: The energetics predicted by theory. *J. Phys. Chem. B* **2004**, *108*, 5472–5476.
106. Li, X.; Sevilla, M. D.; Sanche, L. DFT investigation of dehalogenation of adenine–halouracil base pairs upon low-energy electron attachment. *J. Am. Chem. Soc.* **2003**, *125*, 8916–8920.
107. Li, X.; Sanche, L.; Sevilla, M. D. Dehalogenation of 5-halouracils after low energy electron attachment: A density functional theory investigation. *J. Phys. Chem. A* **2002**, *106*, 11248–11253.
108. Simons, J. How do low-energy (0.1–2 eV) electrons cause DNA-strand breaks? *Acc. Chem. Res.* **2006**, *39*, 772–779.
109. Berdys, J.; Anusiewicz, I.; Skurski, P.; Simons, J. Damage to model DNA fragments from very low-energy (<1 eV) electrons. *J. Am. Chem. Soc.* **2004**, *126*, 6441–6447.
110. Barrios, R.; Skurski, P. Simons, J. Mechanism for damage to DNA by low-energy electrons. *J. Phys. Chem. B* **2002**, *106*, 7991–7994.
111. Berdys, J.; Skurski, P.; Simons, J. Damage to model DNA fragments by 0.25–1.0 eV electrons attached to a thymine π^* orbital. *J. Phys. Chem. B* **2004**, *108*, 5800–5805.
112. Bao, X.; Wang, J.; Gu, J.; Leszczynski, J. DNA strand breaks induced by near-zero-electronvolt electron attachment to pyrimidine nucleotides. *Proc. Natl. Acad. Sci. USA* **2006**, *103*, 5658–5663.
113. Gu, J.; Xie, Y.; Schaefer, H. F. Glycosidic bond cleavage of pyrimidine nucleosides by low-energy electrons: A theoretical rationale. *J. Am. Chem. Soc.* **2005**, *127*, 1053–1057.
114. Gu, J.; Wang, J.; Leszczynski, J. Electron attachment-induced DNA single strand breaks: $C_{3'}$–$O_{3'}$ σ-bond breaking of pyrimidine nucleotides predominates. *J. Am. Chem. Soc.* **2006**, *128*, 9322–9323.
115. Kumar, A.; Sevilla, M. D. Low-energy electron attachment to 5′-thymidine monophosphate: Modeling single strand breaks through dissociative electron attachment. *J. Phys. Chem. B* **2007**, *111*, 5464–5474.

116. Kumar, A.; Sevilla, M. D. The role of $\pi\sigma^*$ excited states in electron-induced DNA strand break formation: A time-dependent density functional theory study. *J. Am. Chem. Soc.* **2008**, *130*, 2130–2131.

117. Millen, A. L.; Archibald, L. A. B.; Hunter K. C., Wetmore, S. D. A Kinetic and hermodynamic study of the glycosidic bond cleavage in deoxyuridine. *J. Phys. Chem. B* **2007**, *111*, 3800–3812.

118. bo Zhang, R.; Zhang, K.; Eriksson, L. A. Theoretical studies of damage to 3′-uridine monophosphate induced by electron attachment. *Chem. Eur. J.* **2008**, *14*, 2850–2856.

119. Schyman, P.; Eriksson, L. A.; bo Zhang, R.; Laaksonen, A. Hydroxyl radical–thymine adduct induced DNA damages. *Chem. Phys. Lett.* **2008**, *458*, 186–189.

120. Xie, H.; Wu, R.; Xia, F.; Cao, Z. Effects of electron attachment on $C_{5'}$–$O_{5'}$ and $C_{1'}$–$N_{1'}$ bond cleavages of pyrimidine nucleotides: A theoretical study. *J. Comput. Chem.* **2008**, *29*, 2025–2032.

121. Liang, G.; Bao, X.; Gu, J. The possibility of the decomposition of 2′-deoxyribose moiety of thymidine induced by the low energy electron attachment. *J. Compu. Chem.* **2008**, *29*, 2648–2655.

122. Caron, L.; Sanche, L. Diffraction in resonant electron scattering from helical macromolecules: Effects of the DNA backbone. *Phys. Rev. A* **2005**, *72*, 032726.

123. Caron, L.; Sanche, L. Temporary electron localization and scattering in disordered single strands of DNA. *Phys. Rev. A* **2006**, *73*, 062707.

124. Caron, L.; Sanche, L. Diffraction in resonant electron scattering from helical macromolecules: *A*- and *B*-type DNA. *Phys. Rev. A* **2004**, *70*, 032719.

125. Caron, L.; Sanche, L. Low-energy electron diffraction and resonances in DNA and other helical macromolecules. *Phys. Rev. Lett.* **2003**, *91*, 113201.

126. Caron, L.; Sanche, L. Adapting gas-phase electron scattering *R*-matrix calculations to a condensed-matter environment. *Phys. Rev. A* **2007**, *76*, 032716.

127. von Sonntag C. *The Chemical Basis of Radiation Biology*; Taylor and Francis, London, New York, Philadelphia, 1987, pp. 262–265.

128. Domcke, W.; Sobolewski, A. L. Chemistry—Unraveling the molecular mechanisms of photoacidity. *Science* **2003**, *302*, 1693–1694.

129. Sobolewski, A. L.; Domcke, W. On the mechanism of nonradiative decay of DNA bases: Ab initio and TDDFT results for the excited states of 9H-adenine. *Eur. Phys. J., D* **2002**, *20*, 369–374.

130. Ashfold, M. N. R.; Cronin, B.; Devine, A. L.; Dixon, R. N.; Nix, G. D. The role of pi sigma* excited states in the photodissociation of heteroaromatic molecules. *Science* **2006**, *312*, 1637–1640.

131. Burrow, P. D.; Gallup, G. A.; Modelli, A. Are there π^* shape resonances in electron scattering from phosphate groups? *J. Phys. Chem. A* **2008**, *112*, 4106–4113.

132. Becker, D.; Razskazovskii, Y.; Callaghan, M. U.; Sevilla, M. D. Electron spin resonance of DNA irradiated with a heavy-ion beam ($^{16}O^{8+}$): Evidence for damage to the deoxyribose phosphate backbone. *Radiat. Res.* **1996**, *146*, 361–368.

133. Kim, J.; Kreller, C. R.; Greenberg, M. M. Preparation and analysis of oligonucleotides containing the C4′-oxidized abasic site and related mechanistic probes. *J. Org. Chem.* **2005**, *70*, 8122–8129.

134. Tronche, C.; Goodman, B. K.; Greenberg, M. M. DNA damage induced via independent generation of the radical resulting from formal hydrogen atom abstraction from the C1′-position of a nucleotide. *Chem. Biol.* **1998**, *5*, 263–271.

135. Dedon, P. C. The chemical toxicology of 2-deoxyribose oxidation in DNA. *Chem. Res. Toxicol.* **2008**, *21*, 206–219.

136. Pogozelski, W. K.; Tullius, T. D. Oxidative strand scission of nucleic acids: Routes initiated by hydrogen abstraction from the sugar moiety. *Chem. Rev.* **1998**, *98*, 1089–1107.

137. Adhikary, A.; Collins, S.; Khanduri, D.; Sevilla, M. D. Sugar radicals formed by photoexcitation of guanine cation radical in oligonucleotides. *J. Phys. Chem. B* **2007**, *111*, 7415–7421.

138. Khanduri, D.; Collins, S.; Kumar, A.; Adhikary, A.; Sevilla, M. D. Formation of sugar radicals in RNA model systems and oligomers via excitation of guanine cation radical. *J. Phys. Chem. B* **2008**, *112*, 2168–2178.

139. Kumar, A.; Sevilla, M. D. Photoexcitation of dinucleoside radical cations: A time-dependent density functional study. *J. Phys. Chem. B* **2006**, *110*, 24181–24188.

140. Blancafort, L.; Voityuk, A. A. CASSCF/CAS-PT2 study of hole transfer in stacked DNA nucleobases. *J. Phys. Chem. A* **2006**, *110*, 6426–6432.

141. Dreuw, A.; Weisman, J. L.; Head-Gordon, M. Long-range charge-transfer excited states in time-dependent density functional theory require non-local exchange. *J. Chem. Phys.* **2003**, *119*, 2943–2946.

142. Willson, R. L.; Wardman, P.; Asmus, K-D. Interaction of dGMP radical with cysteamine and promethazine as possible model of DNA repair. *Nature (London)* **1974**, *252*, 323–324.

143. Asmus, K.-D.; Deeble, D. J.; Garner, A.; Ali, K. M. I; Scholes, G. Chemical aspects of radiosensitization. Reaction of sensitizers with radicals produced in the radiolysis of aqueous solutions of nucleic acid components. *Br. J. Cancer* **1978**, *37* (Suppl. III), 46–49.

144. Candeias, L. P.; Steenken, S. Structure and acid–base properties of one-electron-oxidized deoxyguanosine, guanosine, and 1-methylguanosine. *J. Am. Chem. Soc.* **1989** *111*, 1094–1099.

145. Steenken, S.; Jovanovic, S. V.; Candeias, L. P.; Reynisson, Is "Frank" DNA-strand breakage via the guanine radical thermodynamically and sterically possible? *J. Chem. Eur. J.* **2001**, *7*, 2829–2833.

146. Kobayashi, K.; Tagawa, S. Direct observation of guanine radical cation deprotonation in duplex DNA using pulse radiolysis. *J. Am. Chem. Soc.* **2003**, *125*, 10213–10218.

147. Close, D. M.; Sagstuen, E.; Nelson, W. H. ESR study on the guanine cation. *J. Chem. Phys.* **1985**, *82*, 4386–4388.

148. Hole, E. O.; Sagstuen, E.; Nelson, W. H.; Close, D. M. Environmental effects on primary radical formation in guanine: Solid-state ESR and ENDOR of guanine hydrobromide monohydrate. *Radiat. Res.* **1991**, *125*, 119–128.

149. Jovanovic, S. V.; Simic, M. G. One-electron redox potentials of purines and pyrimidines. *J. Phys. Chem.* **1986**, *90*, 974–978.

150. Jovanovic, S. V.; Simic, M. G. The DNA guanyl radical: Kinetics and mechanisms of generation and repair. *Biochim. Biophys. Acta.* **1989**, *1008*, 39–44.

151. Wetmore, S. D.; Boyd, R. J.; Eriksson, L. A. Comparison of experimental and calculated hyperfine coupling constants. Which radicals are formed in irradiated guanine? *J. Phys. Chem. B* **1998**, *102*, 9332–9343.

152. Mundy, C. J.; Colvin, M. E.; Quong, A. A. Irradiated guanine: A Car-Parrinello molecular dynamics study of dehydrogenation in the presence of an OH radical. *J. Phys. Chem. A* **2002**, *106*, 10063–10071.

153. Gervasio, F. L.; Laio, A.; Iannuzzi, M.; Parrinello, M. Influence of DNA structure on the reactivity of the guanine radical cation. *Chem. Eur. J.* **2004**, *10*, 4846–4852.

154. Luo, Q.; Li, Q. S.; Xie, Y.; Schaefer, H. F. Radicals derived from guanine: Structures and energetics. *Collect. Czech. Chem. Commun.* **2005**, *70*, 826–836.

155. Chatgilialoglu, C.; Caminal, C.; Guerra, M.; Mulazzani, Q. G. Tautomers of one-electron-oxidized guanosine. *Angew. Chem. Int. Ed.* **2005**, *44*, 6030–6032.

156. Chatgilialoglu, C.; Caminal, C.; Altieri, A.; Vougiokalakis, G. C.; Mulazzani, Q. G.; Gimisis, T.; Guerra, M. Tautomerism in the guanyl radical. *J. Am. Chem. Soc.* **2006**, *128*, 13796–13805.

157. Adhikary, A.; Kumar, A.; Becker, D.; Sevilla, M. D. the guanine cation radical: investigation of deprotonation states by ESR and DFT. *J. Phys. Chem. B* **2006**, *110*, 24171–24180.

158. Naumov, S.; von Sonntag, C. Guanine-derived radicals: Dielectric constant-dependent stability and UV/Vis spectral properties: A DFT study. *Radiat. Res.* **2008**, *169*, 364–372.

159. Wagenknecht, H.-A.,Ed.; *Charge Transfer in DNA: From Mechanism to Application*; Wiley-VCH Verlag GmbH & Co. KGaA, Weiheim, 2005, pp. 1–26.

160. Cai, Z.; Sevilla, M. D. Electron and hole transfer from DNA base radicals to oxidized products of guanine in DNA. *Radiat. Res.* **2003**, *159*, 411–419.

161. Colson, A.-O.; Besler, B.; Close, D. M.; Sevilla, M. D. Ab initio molecular-orbital calculations of DNA bases and their radical ions in various protonation states—Evidence for proton-transfer in GC base pair radical-anions. *J. Phys. Chem.* **1992**, *96*, 661–668.

162. Bertran, J.; Oliva, A.; Rodriguez-Santiago, L.; Sodupe, M. Single versus double proton-transfer reactions in Watson–Crick base pair radical cations. A theoretical study. *J. Am. Chem. Soc.* **1998**, *120*, 8159–8167.

163. Nelson, W. H.; Sagstuen, E.; Hole, E. O.; Close, D. M. Electron spin resonance and electron nuclear double resonance study of X-irradiated deoxyadenosine: Proton transfer behavior of primary ionic radicals. *Radiat. Res.* **1998**, *149*, 75–86.

164. Candeias, L. P.; Steenken, S. Electron transfer in di(deoxy)nucleoside phosphates in aqueous solution: Rapid migration of oxidative damage (via adenine) to guanine. *J. Am. Chem. Soc.* **1993**, *115*, 2437–2440.

165. Giese, B.; Amaudrut, J.; Köhler, A.- K.; Spormann, M.; Wessely, S. Direct observation of hole transfer through DNA by hopping between adenine bases and by tunneling. *Nature* **2001**, *412*, 318–320.

166. Kawai, K.; Majima, T. In *Charge Transfer in DNA: From Mechanism to Application*; Wagenknecht, H.-A.,Ed.; Wiley-VCH Verlag GmbH & Co. KGaA, Weiheim, 2005, pp. 117–151.

167. Lewis, F. D.; Daublain, P.; Zhang, L.; Cohen, B.; Vura-Weis, J.; Wasielewski, M. R.; Shafirovich, V.; Wang, Q.; Raytchev, M.; Fiebig, T. Reversible bridge-mediated excited-state symmetry breaking in stilbene-linked DNA dumbbells. *J. Phys. Chem. B.* **2008**, *112*, 3838–3843.

168. Augustyn, K. E.; Genereux, J. C.; Barton, J. K. Distance-Independent DNA Charge Transport across an Adenine Tract. *Angew. Chem., Int. Ed.* **2007**, *46*, 5731–5733.

169. Shao, F.; O'Neill, M. A.; Barton, J. K. Long-range oxidative damage to cytosines in duplex DNA. *Proc. Natl. Acad. Sci. U. S.A.* **2004**, *101*, 17914–17919.

170. Ts'o, P. O. P. In *Fine Structure of Proteins and Nucleic Acids*; Fasman, G. D.; Tiemasheff, S. N.,Eds.; Marcel Dekker, New York, 1970, p. 151.

171. Broom, A. D.; Schweizer, M. P.; Ts'o, P. O. P. Interaction and association of bases and nucleosides in aqueous solutions. V. Studies of the association of purine nucleosides by vapor pressure osmometry and by proton magnetic resonance. *J. Am. Chem. Soc.* **1967**, *89*, 612–3622.

172. Olsthoorn, C. S. M.; Bostelaar, L. J.; De Rooij, J. F. M.; Van Boom, J. H.; Altona, C. Circular dichroism study of stacking properties of oligodeoxyadenylates and polydeoxyadenylate. A three-state conformational model. *Eur. J. Biochem.* **1981**, *115*, 309–321.

173. Itahara, T.; Imaizumi, K. Role of nitrogen atom in aromatic stacking *J. Phys. Chem. B* **2007**, *111*, 2025–2032.

174. Leonard, N. J. Trimethylene bridges as synthetic spacers for the detection of intramolecular interactions. *Acc. Chem. Res.* **1979**, *12*, 423–429.

175. Cohen, A. J.; Mori-Sánchez, P.; Yang, W. Insights into current limitations of density functional theory. *Science* **2008**, *321*, 792–794.

2

RADICAL REACTION PATHWAYS INITIATED BY DIRECT ENERGY DEPOSITION IN DNA BY IONIZING RADIATION

WILLIAM A. BERNHARD

Department of Biochemistry and Biophysics, University of Rochester, Rochester, NY 14472, USA

2.1. INTRODUCTION

Ionizing radiation—for example, X rays or γ rays—can deposit energy by ionization and excitation. In the case of DNA, the predominant source of chemical damage is ionization. Each ionization results in a radical cation and a radical anion, more generally referred to as a "hole" and an "electron-gain site." The focus of this chapter is on the reactions initiated by formation of holes and electron-gain sites produced directly in DNA by ionizing radiation.

Understanding the mechanisms of direct radiation damage to DNA is important in areas such as radiation risk assessment, radiation oncology, radiation sterilization, and nanotechnology. Direct damage is radiobiologically important because about half of the DNA damage arises from the direct effect.[1,2] The other half arises from the indirect effect, in which energy absorbed by the water results in OH radicals and aqueous electrons that react with the DNA. It is important to note that the direct deposition of ionizing energy does not break the bonds of DNA indiscriminately. Rather, it selectively generates a relatively small set of radical cations and radical anions. Interest in the reactivity and mobility of these radical ions extends well beyond fields

Radical and Radical Ion Reactivity in Nucleic Acid Chemistry, Edited by Marc M. Greenberg

related to radiation biology into applications such as the potential use of DNA in the construction of nanoscale circuits.

The goal of this chapter is to provide an overview of the primary reaction pathways initiated in DNA by the direct effect of ionizing radiation. The initial radical ion species, the reaction pathways stemming from the initial radicals, and the mobility of the DNA radicals are described in the context of a working model. This model is supported mainly by findings that come from the application of electron paramagnetic resonance (EPR) and electron nuclear double resonance (ENDOR) spectroscopy to solid-state DNA samples. Other reviews[3–6] on this topic have been published over the past decade.

By studying DNA in the solid state, the indirect effect is excluded and information on the direct effect can be selectively obtained. EPR is exquisitely suited for identifying radical species, measuring radical concentrations, and monitoring radical reactions. The high sensitivity of EPR is critically important because radical concentrations are typically very low, about one radical per 500 base pairs. Also, because of the transient nature of the radical species, it is advantageous to employ low temperatures to trap the reactive radical intermediates. Irradiating DNA at 4 K or 77 K traps radical species that are closely related to the radicals that are initially formed. Annealing the samples to higher temperatures mobilizes these trapped species and activates radical reactions. Because this approach reveals only the primary radical species and their successor products, it does not account for *all* of the chemistry initiated by ionizing radiation, but it does account for a major fraction of the direct damage in DNA.

The radical reactions initiated in DNA frequently go forward to form stable end products, often referred to as DNA lesions. These lesions are not radicals; they are diamagnetic and cannot be detected by EPR. Fortunately, given the high sensitivity of methodologies such as gel electrophoresis, HPLC, and GC/MS, progress has been made recently on determining the yields of some of the major lesions produced in DNA by the direct effect. How these products correlate with the presumed radical precursors is part of the working model described below. Note that these lesions are produced whether the DNA is irradiated at 4 K or at room temperature. There can be little doubt that the mechanistic understandings gained by studying DNA radical processes between 4 K and room temperature are applicable to the process that occurs when either a hole or electron is introduced into DNA at room temperature.

2.2. RADICAL CATIONS

2.2.1. Initial Distribution

The probability of ionizing a constituent atom or any molecular constituent is directly proportional to the number of electrons contained by that atom or constituent. This is directly related to Bragg's rule and is therefore often referred to as Bragg's rule. Using this rule, the probability of initially forming a radical cation (a hole) at each of the six DNA constituents is shown in Figure 2.1. Following ionization, the newly generated hole is rapidly thermalized, producing five different types of radical cation and, at

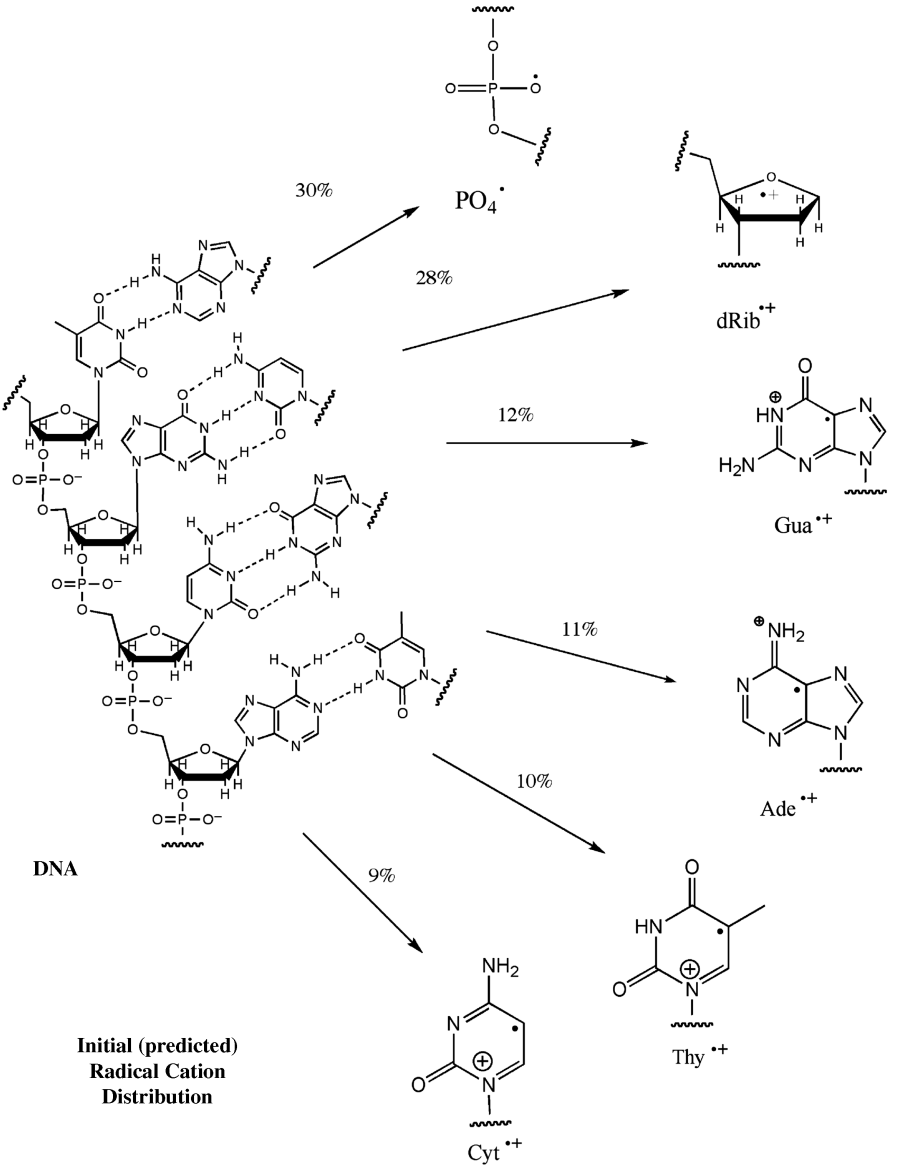

FIGURE 2.1. Direct deposition of ionizing radiation creates initial sites of hole (radical cation) formation at each of the six DNA constituents. The probability (expressed as a percentage) of hole information at a given constituent is directly related to the number of electrons comprising the constituent.

PO_4^-, a neutral phosphate radical, $PO_4^{\bullet}$. Electron loss from either phosphate (PO_4^-) or deoxyribose (dRib) is more than twice as likely as electron loss from any one of the four bases. The DNA backbone, PO_4^- + dRib, accounts for ~58% of the holes initially deposited in DNA. None of these initial electron-loss sites generated by ionizing

radiation, however, have been directly observed in ds-DNA containing a mixture of all four bases, not even at 4 K. This is because all of these sites rapidly undergo electron transfer and/or deprotonation reactions.

However, some of the radical cations shown in Figure 2.1 have been observed in DNA components under conditions that inhibit both electron and proton transfer. For example, $Thy^{\bullet+}$ has been trapped in low-temperature glasses[7] and at 4 K in pellets of both poly d(AT) and poly d(A):poly d(T).[8] Indeed much of our understanding of radical reaction mechanisms is based on such studies of isolated DNA components.[9] The mechanistic model described below is based on (i) the initial distribution of electron-loss sites shown in Figure 2.1, (ii) findings from isolated DNA components, (iii) radicals known to be trapped in ds-DNA, and (iv) the redox potentials of components determined in aqueous solution and by computational chemistry.

2.2.2. Purines

The oxidation potentials of the four DNA bases have been measured for each of the bases in aqueous solution at RT. The rank was found to be Gua < Ade < Cyt < Thy with values of 1.29, 1.42, 1.6, and 1.7 V (versus NHE), respectively (see references 10 and 11 and references therein). The redox values are influenced by base stacking and base pairing in duplex DNA.[12] In particular, the proton-accepting power of the base conjugate to a base radical cation moderates the expected lifetime of that radical cation.[13] But the rank given above, based on computation[14] and EPR results,[15] remains the same. Guanine is the primary, but not the only, hole trapping site in DNA.

The guanine radical cation, $Gua^{\bullet+}$, is a strong acid, with a pK_a of 2; and its conjugate base, Cyt, is a fair proton acceptor. As a result, proton transfer across the N1–H $\cdots$ N3 hydrogen bond is slightly favored,[12] with a predicted equilibrium of $K = 10^{0.4}$. Proton transfer results in a neutral radical, $Gua(N1–H)^{\bullet}$ (reaction **1** in Figure 2.2). While definitive evidence that the hole is trapped as $Gua(N1–H)^{\bullet}$ and not $Gua^{\bullet+}$ in solid DNA at low temperatures (<78 K) is lacking,[16] deprotonation has been observed for DNA in aqueous solution.[17] It is a good operating assumption that the hole trapped at low temperatures by Gua is the neutral $Gua(N1–H)^{\bullet}$ radical.[18] As discussed further below, reaction **1** is reversible; therefore, as DNA samples are warmed to higher temperatures, back transfer is activated. Back transfer reforms $Gua^{\bullet+}$, liberating the hole to tunnel to nearby purines, preferentially Gua. In the solid state, OH^- addition to form Gua $(C8 + OH)^{\bullet}$ (reaction **2** in Figure 2.2) appears to be the dominate irreversible reaction.[19, 20] While the Gua$(C8 + OH)^{\bullet}$ radical has not been observed directly by EPR in solid-state DNA, the yield of 8OxoGua and FapyGua, derived via oxidation (ox) or reduction (red) of the Gua$(C8 + OH)^{\bullet}$ radical (reactions **3** and **4,** respectively), has been measured in herring sperm DNA.[19] The yield of 8OxoGua has also been measured for the oligomer $d(GCACGCGTGC)_2$.[20] In both experiments, DNA is irradiated in the solid state and end products measured after dissolving the sample in water. In the later experiment, the yield of 8OxoGua was shown to exceed the yield of trapped precursor radical. This point will be considered again in Section 2.5. With respect to damage initiated by one-electron oxidation, Gua is both a major trapping site for the hole and the primary lesion site on the ds-DNA base stack.

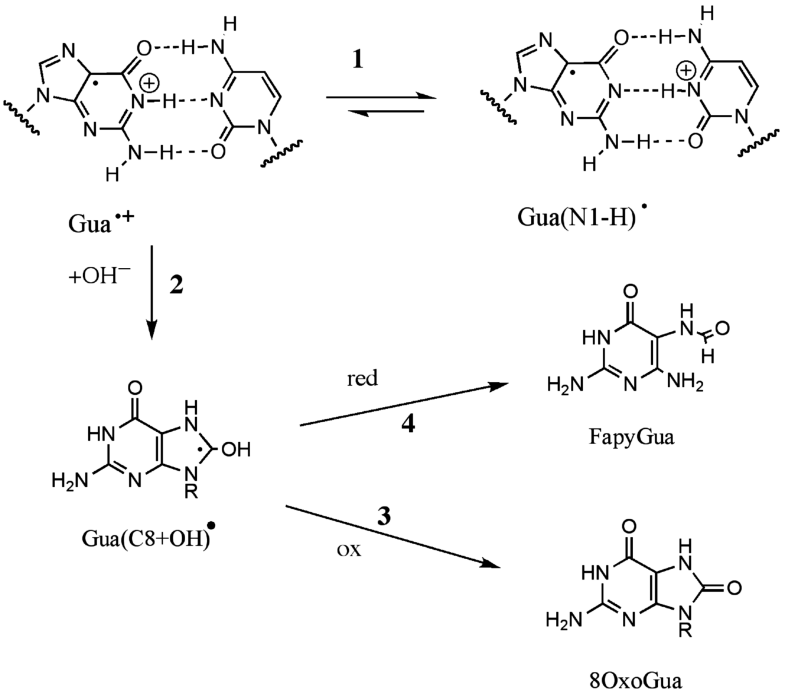

FIGURE 2.2. For the guanine radical cation produced by the direct effect, two major reaction pathways are shown.

Hole transfer from the adenine radical cation, $Ade^{\bullet+}$, to a nearby guanine (**5** in Figure 2.3) is favored as a consequence of guanine's lower oxidation potential. But if guanine is not within a few base pairs distance, there are three other reactions that potentially compete with hole transfer to Gua. One reaction is **6**, deprotonation from the amino group giving $Ade(N6'–H)^{\bullet}$, which has been observed in crystals of adenosine at 10 K.[21,22] But, as Steenken has pointed out for duplex DNA, thymine is a very poor proton receptor and the equilibrium should strongly favor adenine in the radical cation state.[12] A second reaction is **7**, irreversible deprotonation from C1′ of dRib to form $Ade(C1'–H)^{\bullet}$. This type of reaction has been observed in adenine derivatives containing either a methyl or ethyl group instead of dRib at N9,[23,24] but so far it has not been observed in DNA. The third reaction, **8**, is also irreversible. Addition of OH^- to the radical cation forms $Ade(C8 + OH)^{\bullet}$. Formation of the later radical is deduced from the production of 8OxoAde (via reaction **9**) and FapyAde (via reaction **10**) in herring sperm DNA[19] as well as production of 8OxoAde in $d(GCACGCGTGC)_2$.[20] In the study of $d(GCACGCGTGC)_2$, the yield of 8OxoAde is surprising large. Adjusting for low AT content, it was found that the probability of an Ade giving rise to 8OxoAde is about one-seventh that of Gua giving rise to 8OxoGua. These results indicate that in a base context where Ade is flanked by pyrimidines and Gua is just one base away, the rate of hole trapping at Ade, as detected by OH^- addition, is competitive with the rate of hole transfer to Gua.

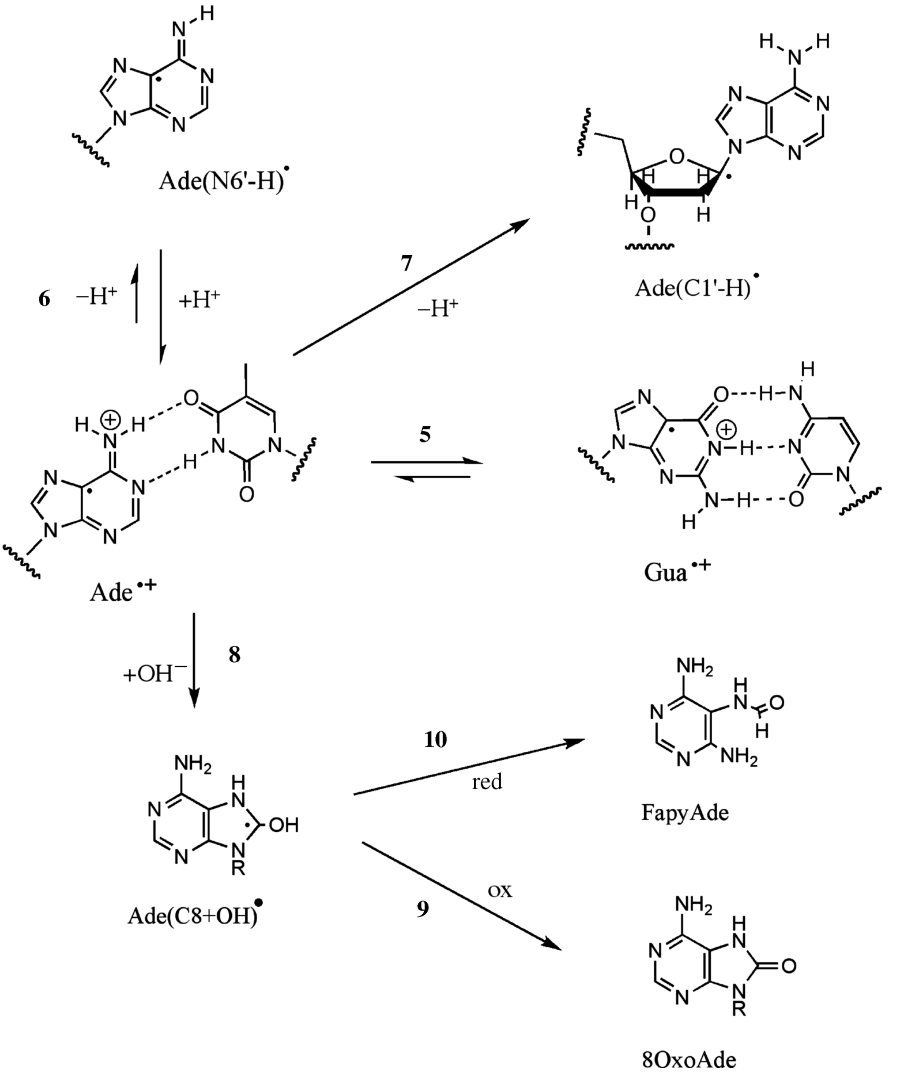

FIGURE 2.3. Hole transfer from the adenine radical cation to guanine, competes with deprotonation reactions **6** and **7** and with hydroxide addition **8**. The later leads to stable end products via reaction **9** or **10**. These products are analogous to those shown for guanine in **Figure 2** but the product yields are decreased by reaction **5** if guanine is in close proximity.

2.2.3. Pyrimidines

It can be seen from Figure 2.1 that the probability of forming either of the pyrimidine radical cations, $Cyt^{\bullet+}$ and $Thy^{\bullet+}$, is comparable to forming either of the purine radical cations. In spite of this, the yield of pyrimidine radicals, and the yield of pyrimidine products derived from one-electron oxidation of DNA, is small compared to the yield of 8OxoGua. This is because hole transfer from the pyrimidines to Gua (**11** in Figure 2.4 and **14** in Figure 2.5) is favored over alternative reactions. But there is

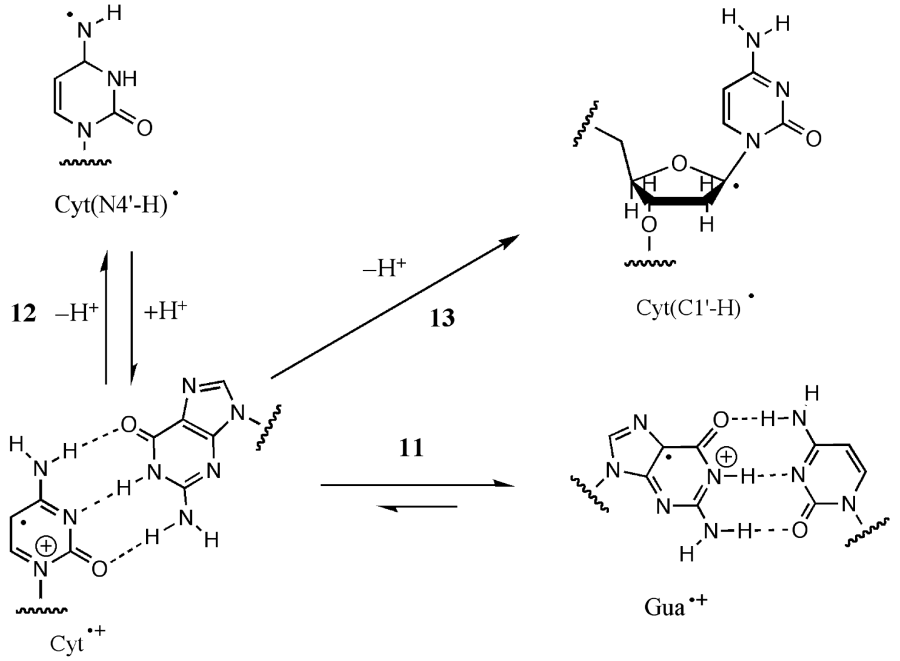

FIGURE 2.4. Hole transfer from the cytosine radical cation to guanine, competes with deprotonation reactions **12** and **13**. Because forward reactions from **13** result in strand breakage, this reaction scheme predicts that the yield of strand breaks at cytosine will increase when there are no guanines adjacent to cytosine.

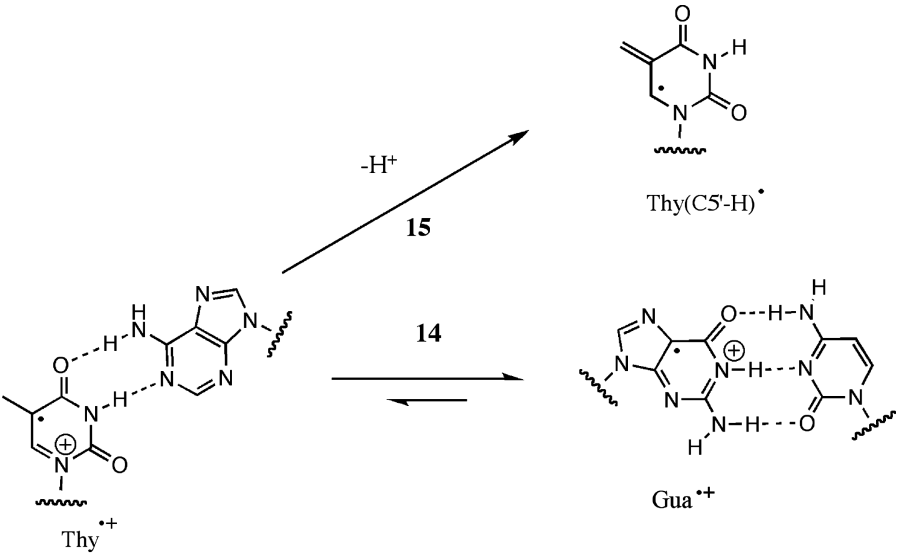

FIGURE 2.5. Hole transfer from the thymine radical cation to guanine, competes with deprotonation from the methyl group. Forward reactions from this allyl radical include 5-hydroxymethyl-uracil.

evidence that hole transfer is not absolute, stemming from identified lesions that are believed to originate from one-electron oxidation of pyrimidines.

The most likely reactions stemming from $Cyt^{\bullet+}$ are shown in Figure 2.4. If Gua is adjacent to Cyt, hole transfer to Gua (reaction **11**) will dominate. As the intrastrand distance between Cyt and Gua increases, the rate of hole transfer will decrease and other reactions may become competitive. One such reaction is deprotonation by C1′ of the deoxyribose, giving the Cyt(C1′–H)$^{\bullet}$ radical (**13** in Figure 2.4). Clear evidence of Cyt (C1′–H)$^{\bullet}$ formation comes from studies of deoxycytidine[25] and deoxycytidine-5′-phosphate[26] and there are indications that it is also formed in salmon testes DNA.[27] This reaction is of interest because it represents a transfer of oxidative damage from the bases to the backbone. As described in Section 2.2.5, holes (oxidative damage) are generally viewed as flowing from the DNA backbone to the bases, not the other way around. If electron loss from cytosine (or adenine) leads to oxidative damage of its dRib, then that dRib damage is base-specific. Such a possibility is of interest because there are DNA sequences where base sequence appears to influence the probability of deoxyribose damage.[28]

The $Cyt^{\bullet+}$ radical may also undergo reversible deprotonation to yield the iminyl radical, Cyt(N4′−H)$^{\bullet}$ shown in Figure 2.4. Evidence for reaction **12** comes from an EPR study of cytosine monohydrate in which the original assignment to the $Cyt^{\bullet+}$ radical [29] was reassigned to the Cyt(N4′–H)$^{\bullet}$.[9] It is of interest to note that in dilute aqueous solutions, loss of $Gua^{\bullet+}$ generated by oxidation of DNA using $SeO_3^{\bullet-}$ leads to a Cyt(N4′−H)$^{\bullet}$ intermediate that may gate the creation and migration of holes through DNA bases.[30]

Hole transfer from the thymine radical cation, $Thy^{\bullet+}$, will dominate if a Gua lies close by (**14** in Figure 2.5). Absence of a nearby Gua results in an increased likelihood that irreversible deprotonation from the methyl will occur, giving the Thy(C5′–H)$^{\bullet}$ radical. Evidence of **15** comes from studies of thymidine in glasses,[31] in poly d(AT),[8] and in DNA.[27] This is likely to be one of the most thermally stable radicals generated in DNA by direct ionization. In crystals of 1-methyl-thymine the Thy(C5′–H)$^{\bullet}$ radical has been detected at 200°C.[32] In an oxygenated solution, this radical gives rise to 5-hydroxymethyl-uracil, a product known to be formed by the indirect effect and one that is observed at very low yields for the direct effect in DNA.[19]

2.2.4. Deoxyribose-Phosphate Backbone

Most of the holes, ∼58%, are initially produced on the DNA backbone. Irreversible deprotonation of the backbone ionization sites competes with transfer of the hole to the base stack. By measuring the yield of radicals trapped on the deoxyribose, it was possible to determine that ∼2/3 of the initial backbone holes transfer into the base stack. The remaining ∼1/3 result in neutral deoxyribose radicals.[33]

The main source of deoxyribose radicals is ionization of PO_4^-. The hole so formed, $PO_4^{\bullet}$ in Figure 2.6, is presumed to be transient. It either transfers to the base stack (reaction **16**), deprotonates from C3′ giving dRib(C3′–H)$^{\bullet}$ (reaction **17**), or deprotonates from C5′ giving dRib(C5′–H)$^{\bullet}$ (reaction **18**). Evidence that electron loss from

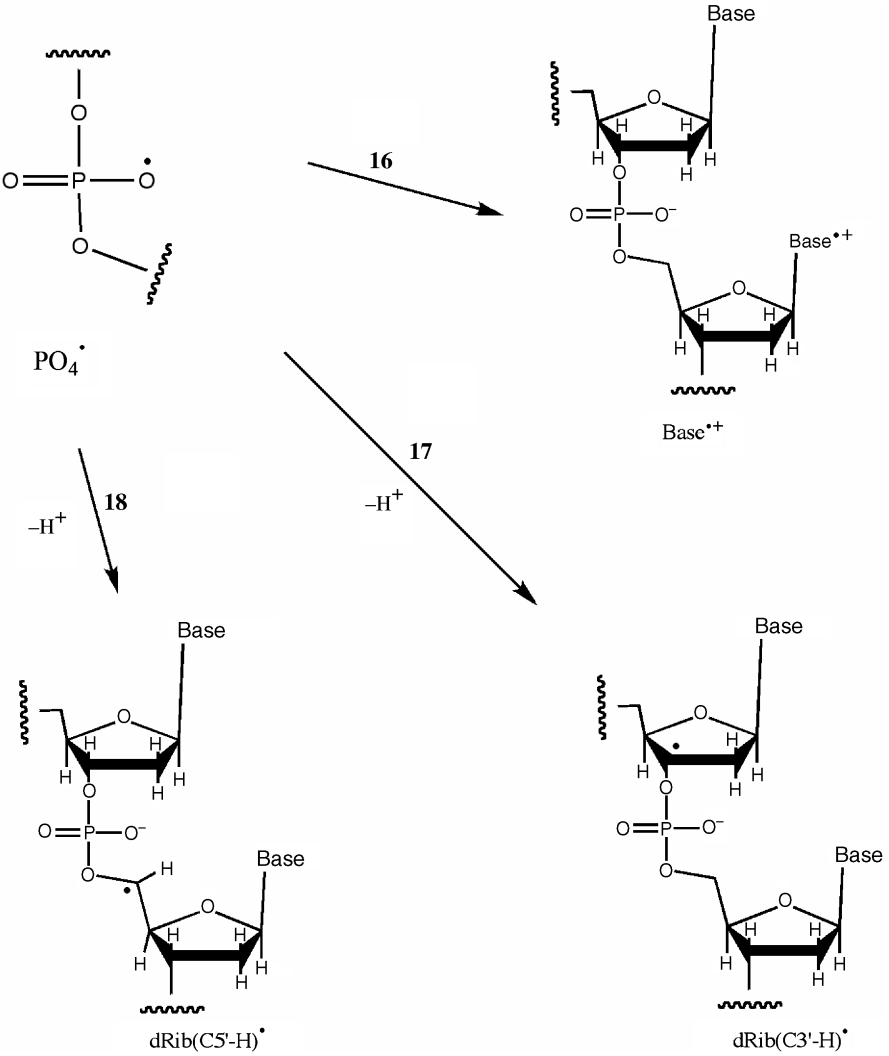

FIGURE 2.6. The phosphate centered hole transfers into the base stack, **16**, or deprotonates via reaction **17** or **18**.

the phosphate leads to deprotonation of the alpha carbons comes from studies of diethyl phosphate crystals.[34]

Ionization of the deoxyribose moiety should also lead to formation of dRib (C5′–H)•, dRib(C3′–H)•, and three other carbon-centered radicals, dRib(C4′–H)•, dRib(C2′–H)•, and dRib(C1′–H)• (reaction **19** in Figure 2.7). Given that ionization of either the phosphate or deoxyribose will result in C5′ and C3′ radicals, one predicts radical formation with the likelihood dRib(C5′–H)• > dRib(C3′–H)• ≫ dRib (C4′–H)• > dRib(C2′–H)•. While both C5′ and C3′ radical formation should be

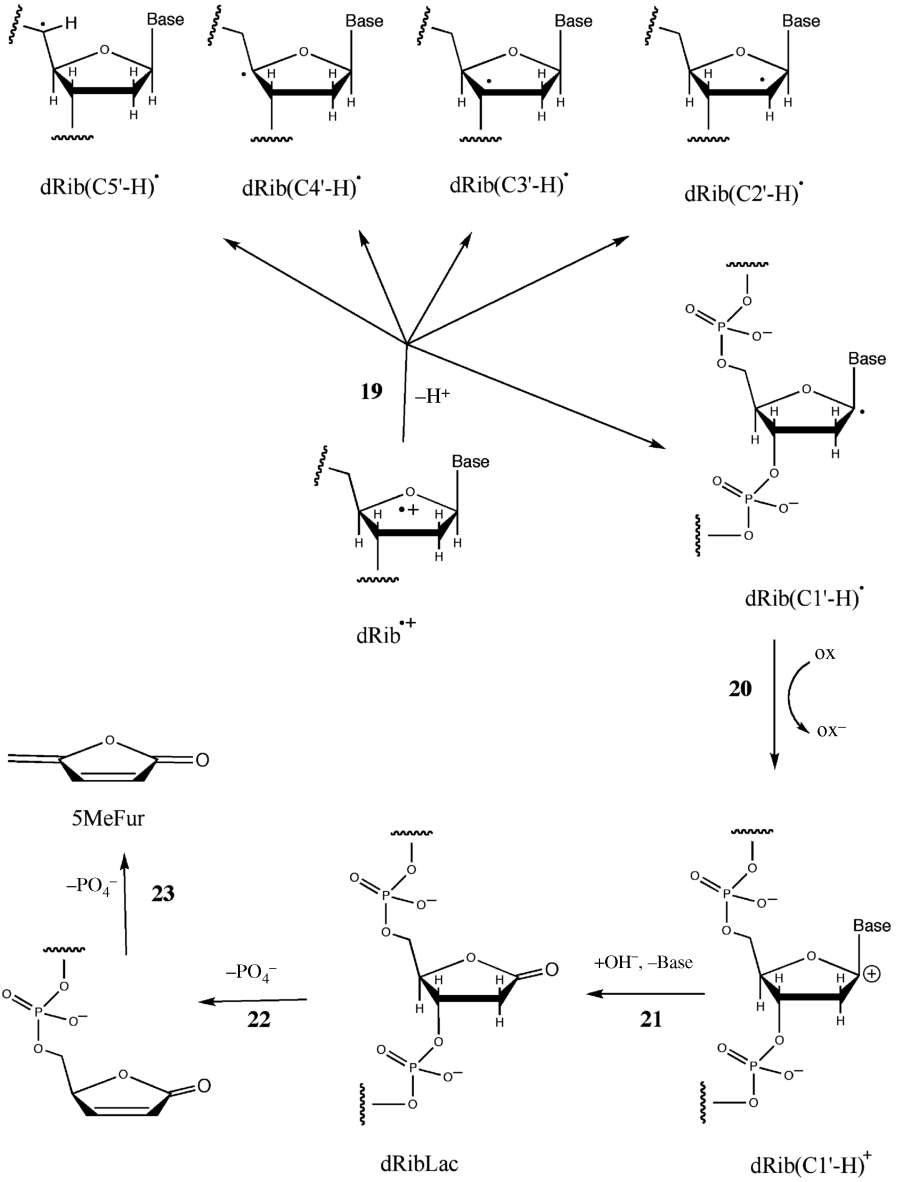

FIGURE 2.7. The deoxyribose centered hole deprotonates at any one of the carbons, **19**. Forward reactions from each of these five neutral carbon radicals result in strand breaks. As an example, one such reaction pathway is shown for the neutral C1' radical, reactions **20**–**23**.

enhanced via hole transfer from PO_4^-, the presence of two H's on C5′ compared to one H on C3′ increases the likelihood of deprotonation at C5′. The dRib(C1′–H)• radical is absent from this ranking because it should vary depending on base type and context. For example, if Cyt is the base and it is not adjacent to Gua, the probability of C1′ radical formation is enhanced.

Reactions **20–23** in Figure 2.7 lead from dRib(C1′–H)$^{\bullet}$ to 5-methylenefuranone (5MeFur), an end product characteristic of C1′ chemistry.[35,36] 5MeFur is formed in high yields when DNA is irradiated in either the solid state (direct effect) or in aqueous solution (indirect effect). In aqueous solution under air, it is a good assumption that the oxidant in Reaction **20** is molecular oxygen. But in the solid state, oxygen is effectively absent. In the absence of oxygen, it has been suggested that base-centered holes serve as an oxidant (see Section 2.5.1). Upon dissolution of the solid DNA sample, hydrolysis at of the C1′–base bond (Reaction **21**) produces free base plus deoxyribonolactone (dRibLac). The dRibLac lesion is relatively stable under ambient conditions but undergoes beta and gamma phosphate elimination upon heating in the presence of strong phosphate-binding cations at higher temperatures (70–90°C).[35] In aqueous solution, Xue and Greenberg[37] found dRibLac (C1′ chemistry) to be a major component of backbone damage generated by γ-radiolysis and >75% of its formation was oxygen-dependent.

Products derived from the other four dRib radicals have not been measured in solid-state systems. It appears likely, however, that the chemistry for each carbon-centered radical will be similar to that observed in aqueous systems under anaerobic conditions.[38] With only minor exceptions, all five of the dRib radicals lead to free base release in aqueous systems. It is quite likely that the yield of free base, obtained by direct ionization of DNA, is a good measure of the yield of total deoxyribose damage.[39]

2.3. RADICAL ANIONS

2.3.1. Initial Distribution

For nearly every site of electron loss on DNA, there is a corresponding site of electron gain. One-electron reduction of each of the four bases has been observed in solid-state systems consisting of isolated bases, nucleosides, and nucleotides.[2–4,6] It is assumed, therefore, that initially all four base radical anions are formed, as shown in Figure 2.8. But not quite all of the ejected electrons enter into these electron addition reactions; other types of chemistry are initiated by low-energy electrons (LEE). A small fraction of LEE undergo dissociative electron attachment (DEA), with one of the end results being strand breaks.[40,41] The yields of products generated by DEA, however, are estimated to be on the order of a few nanomoles per joule[42] as compared to the yields of products due to base radical anion formation, measured to be a few hundred nanomoles per joule.[20]

The redox order, Gua > Ade > Thy > Cyt, favors reduction of the pyrimidines over the purines.[12] After electron addition to the DNA base stack, base-to-base electron transfer funnels the excess electrons from the purines to the pyrimidines. In solid-state DNA, there are no radicals trapped that might be derivates of the guanine radical anion, Gua$^{\bullet-}$, whereas there are radicals trapped that are related directly to Ade$^{\bullet-}$, Thy$^{\bullet-}$, and Cyt$^{\bullet-}$. The preferred sites of one-electron reduction were determined by EPR of palindromic oligodeoxynucleotides in LiCl glasses irradiated at 4 K.[43] In these glasses, DNA selectively traps the excess electron while the holes are trapped as $Cl_2^{\bullet-}$. The resulting spectra give a clear view of the components due to the one-electron reduced bases. Electron capture by cytosine dominates, accounting for

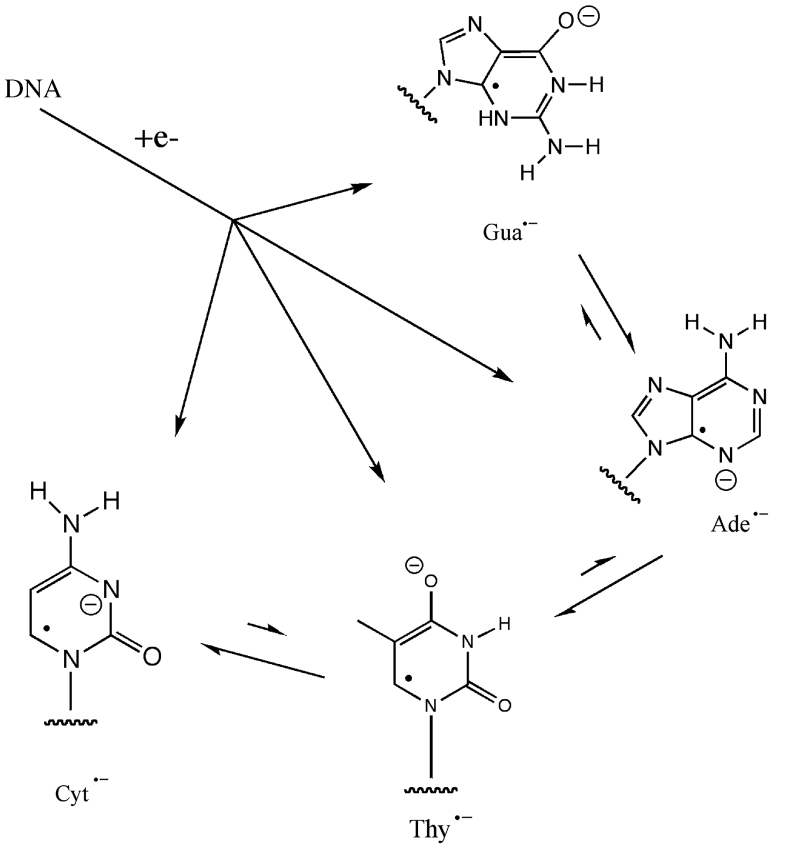

FIGURE 2.8. Direct deposition of ionizing radiation creates initial sites of electron gain (radical anion) at each of the four bases. Transfer of the excess electron favors capture primarily by cytosine and secondarily by thymine (and perhaps adenine).

~80% of radicals produced by one-electron reduction. The remaining ~20% of electron capture is by thymine and adenine, with thymine greater than adenine. Studies of high-molecular-weight DNA, in frozen aqueous solution irradiated at 77 K, confirm that cytosine is the major electron trapping site and thymine is secondary.[44,45] In these studies, where the EPR spectra of radicals due to both electron gain and electron loss are superimposed, it would be difficult to ascertain whether or not one-electron reduced adenine is formed or not.

2.3.2. Pyrimidines

The $Thy^{\bullet -}$ radical anion, formed in thymidine using pulse radiolysis, has a pK_a of 6.9.[12] The site of protonation is O4′, giving the $Thy(O4' + H)^{\bullet}$ radical shown in reaction **23** of Figure 2.9. EPR studies of thymine derivatives in the solid state report both radical forms, $Thy^{\bullet -}$ and $Thy(O4' + H)^{\bullet}$ but only in the studies where electron nuclear double resonance (ENDOR) was applied could the actual protonation

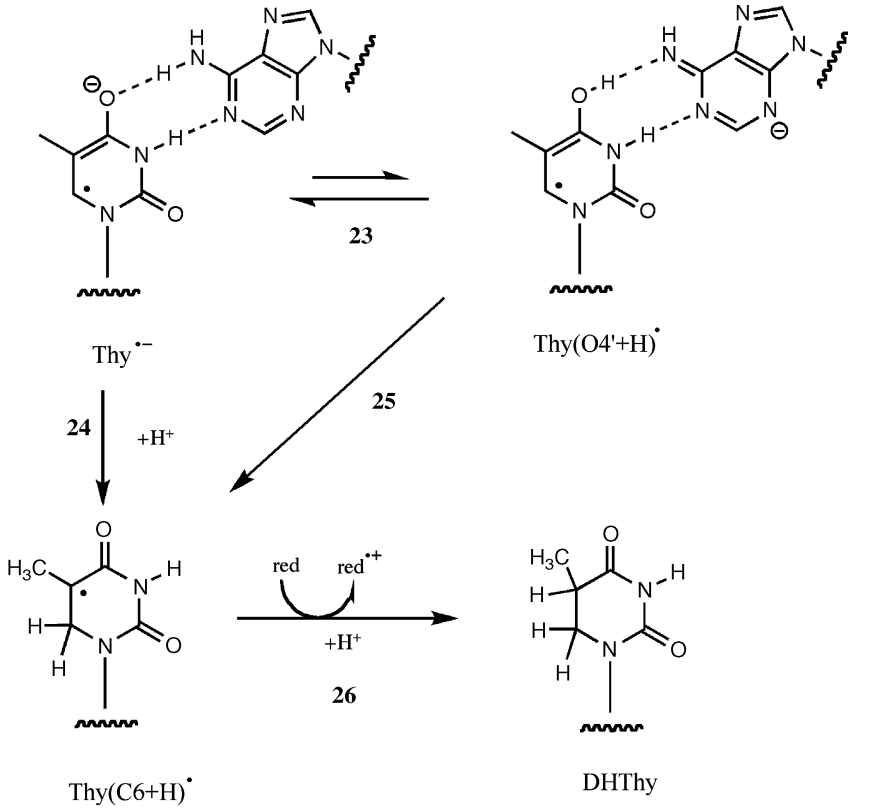

FIGURE 2.9. The thymine radical anion may reversibly protonate, **23**, or irreversibly protonate, **24**. In the later case, forward reactions lead to DHThy, one of the two major reductions products in DNA.

state be definitively discerned. In the ENDOR studies, the Thy(O4′ + H)• radical, not the Thy•−, is observed.[46–48] In duplex DNA, however, it is argued that because Ade is a relatively poor proton donor, the anionic state of one-electron-reduced Thy should be favored.[12] Thy•−, upon warming DNA irradiated at 77 K to >130 K, converts via reaction **24** to the relatively stable Thy(C6 + H)• radical.[44] Alternatively, Thy (C6 + H)• may be formed via reaction **25**. The irreversible protonation of the C5–C6 bond was first observed by Ormerod.[49] Because of its stability and distinctive EPR spectrum, Thy(C6 + H)• was the first radical identified in DNA.[50] Reduction of Thy(C6 + H)• leads to the end product DHThy (reaction **26**). The reductive step in **26** may be due to radical–radical disproportionation or electron transfer from a near by one-electron-reduced base. Using GC/MS, the yield of DHThy was measured for $d(GCACGCGTGC)_2$ films at $\Gamma = 2.5$ mol water/mol nucleotide: $G(DHThy) = 39 \pm 60$ nmol/J.[20]

The Cyt•− radical has not been observed in DNA. Protonation at N3, to give Cyt (N3 + H)•, is highly favorable (**27** in Figure 2.10). As predicted by Steenken from studies of cytosine and guanine derivatives, protonation of Cyt•− by Gua across the

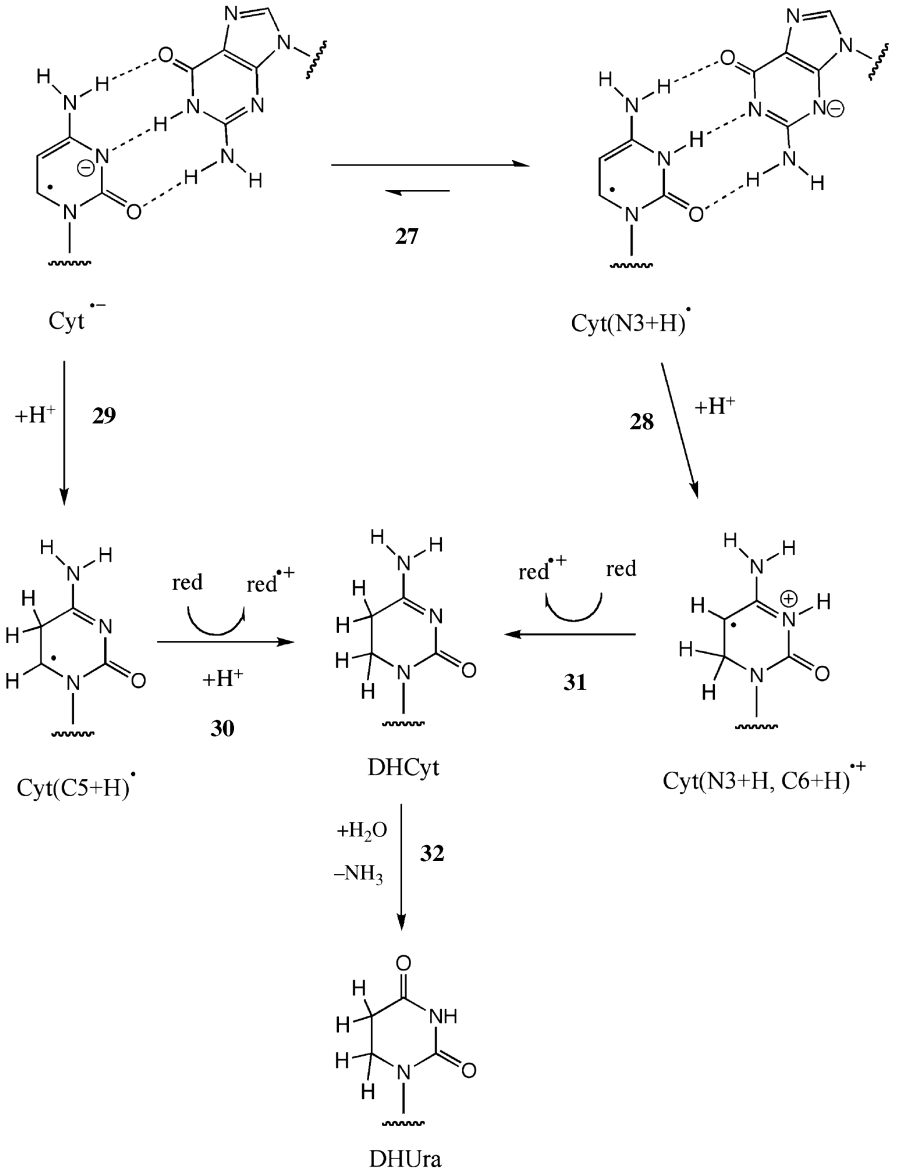

FIGURE 2.10. The cytosine radical anion may reversibly protonate, **27**, or irreversibly protonate at C5, **29** or at C6, **28**. Forward reactions **30** and **31** lead to DHCyt, which deaminates to give DHUra, the other major reduction product in DNA.

N3 · · · H−N1 hydrogen bond is strongly favored with a driving force of 52 kJ/mol.[12] This prediction is supported by *ab initio* calculations.[14]

Even at 4 K, a variety of monomeric systems show that N3 of one-electron reduced cytosine is protonated.[9,51] With respect to duplex DNA, one-electron reduced

pyrimidines were studied in crystalline oligodeoxynucleotides between 4 K and 240 K.[52, 53] These studies provide evidence that, while Cyt(N3 + H)$^{\bullet}$ is the dominant trapping site at 4 K, the doubly protonated radical anion, Cyt(N3 + H, C6 + H)$^{\bullet+}$ is also formed at 4 K (reactions **28** and **29**). The addition of a proton to C6 is irreversible and, like the Thy(C6 + H)$^{\bullet}$ radical, the Cyt(N3 + H, C6 + H)$^{\bullet+}$ radical is stable at higher temperatures. Upon annealing to 240 K, the Cyt(N3 + H)$^{\bullet}$ radical is annealed out and two types of cytosine radicals remain, Cyt(N3 + H, C6 + H)$^{\bullet+}$ and Cyt (C5 + H)$^{\bullet}$, the later is presumably formed by proton addition to C5 as shown in reaction **29**. Subsequent reduction of these two radicals, reactions **30** and **31**, leads to 5,6-dihydrocytosine (DHCyt). In aqueous solutions, DHCyt deaminates (reaction **32**) to give 5,6-dihydrouracil (DHUra).

The three radicals produced by the net addition of hydrogen to the C5–C6 bond of Thy and Cyt account for 85% of the reductive damage in d(GCACGCGTGC)$_2$ films.[20] Based on the yields of these three radicals and assuming that all of the radicals present at 240 K convert to the corresponding dihydropyrimidine end products, it was predicted that in B-form DNA the yield of DHUra and DHThy should be 40–60 nmol/J and 30–50 nmol/J, respectively. Thus, in spite of an initial distribution of trapped electrons being ~80% at Cyt, there is a final distribution of reductive damage that is ~50 : 50 between Cyt and Thy. This agrees with the observed mobilization of trapped electrons at temperatures > ~130 K and preferential retrapping of the excess electron to form Thy(C6 + H)$^{\bullet}$.[44]

2.4. RADICAL MOBILITY, COMBINATION REACTIONS, AND TRAPPING

2.4.1. DNA Is an Insulator

The mobility of holes and excess electrons through the stacked bases of DNA has been of central interest in radiation chemistry for over three decades. Motivating this interest is the fact that biological effects are determined by the degree to which the damage in DNA is clustered.[54, 55] By its very nature, energy deposition by ionizing radiation is nonhomogeneous. Radical ions are produced in tracks consisting of spurs, blobs, and short tracks, referred to collectively as clusters.[56] The main reaction following deposition is radical–radical combination, and the predominate type of combination reaction is return of the excess electron to the hole. Electron return re-creates the parent structure in an electronic excited state. These excited states, as well as the excited states produced directly by photon and fast charged particle interaction, relax without measurable amounts of chemistry occurring.[57] Combination reactions—that is, any reaction between two radicals—accounts for the fate of about half of the initial radicals.[58] The other half of the initial radicals escape recombination and either go on to form lesions in the DNA or recombine at a later stage.

If DNA lesions are isolated (separated from one another by at least 10 bp), they are repaired with extraordinarily high fidelity. If the lesions are clustered (less than 10 bp separation), repair fidelity decreases and biological effects increase.[59, 60] Further- more, the number and type of lesion trapped within a cluster determines it complexity; lesions

of high complexity are more likely to alter biological function. The mobility of holes and excess electrons determines the degree to which clustering is diffused and is, therefore, at the very heart of understanding and evaluating risk of exposure to ionizing radiation.

EPR studies have provided clear evidence that both the hole and electron are mobile,[16,61] but their mobility is very limited.[15,62] These early findings were in direct contradiction to the proposal that DNA is a molecular wire.[63–65] Proof that DNA is actually an insulator comes from the straightforward observation that when radical ions are formed in DNA, they are trapped with exceptional efficiency. The trapping efficiency improves as the temperature is lowered such that at 4 K over half of the ion radicals initially formed in DNA are trapped by DNA.[66]

If DNA were a conductor (a wire), effectively all of the radicals formed on the base stack would recombine with one another. Free radicals would be trapped only on the backbone, and there would be no base damage produced via the direct effect. The yield of trapped radicals would be very low. The facts that base damage yield is relatively high (200–300 nmol/J),[20] that radical trapping is extraordinarily high (600–700 mol/J), [67] and that radical trapping increases as the temperature decreases[68] all argue persuasively that DNA is an insulator—that is, a poor semiconductor. In addition, it is important to note that the insulator quality of DNA persists over a wide range of base sequences and forms A, B, and Z.[67,69] This indicates that the insulator properties are relatively independent of base sequence.

As described in Sections 2.2 and 2.3, holes and excess electrons are trapped preferentially by the purines and pyrimidines, respectively. This requires short migration distances for both the hole and electron, even at 4 K. In Figure 2.11, a hole and electron are shown on the DNA base stack, trapped initially at the base labeled B_2 and B_{N-2}, respectively. The hole and electron migrate at the respective rates of k_h and k_e. These rates are a function of base type and the distance between participating bases. If the migration distance of either the hole or excess electron is large, the probability of recombination at some base, B_i, is high. The yield of trapped radicals can only be high if the migration distances are relatively short. EPR studies show that the migration distance before trapping at 4 K is around 10 base pairs.[15,62] This short distance is readily understood in terms of a competition between hole–electron transfer and trapping by proton transfer reactions.[13]

Both hole and electron migration are governed by two distinctly different processes, tunneling and hopping. Migration over long distances is governed by multistep hopping and not by single-step long-distance tunneling.[70,71] Tunneling over long distances is simply too slow to compete with the rate of trapping. The tunneling rate, k_t, decreases exponentially as a function of distance, $k_t = k_{t0}e^{-\beta x}$, where k_{t0} is the rate at tunneling distance $x = 0$. A small exponential factor, $\beta > \sim 0.1$ Å^{-1}, is characteristic of a conductor; a larger value, $\beta > \sim 0.6$ Å^{-1}, is characteristic of a poor semiconductor. In an elegant set of experiments, Sevilla and co-workers[72–78] directly monitored electron and hole tunneling in solid state DNA. They proved that the observed reactions were due to tunneling by demonstrating that the hole and excess electron transfer rates were independent of temperature from 4 K to 130 K. For the excess electron, they found a β of 0.7 ± 0.1 Å^{-1} for one-electron-reduced Thy and a β of 1.4 ± 0.1 Å^{-1} for one-electron-reduced Cyt, using $k_{t0} \sim 10^{11}$ s^{-1}. For the hole, they found a β of 1.1 Å^{-1} using $k_{t0} \sim 10^{11}$ s^{-1}. Employing approximate values,

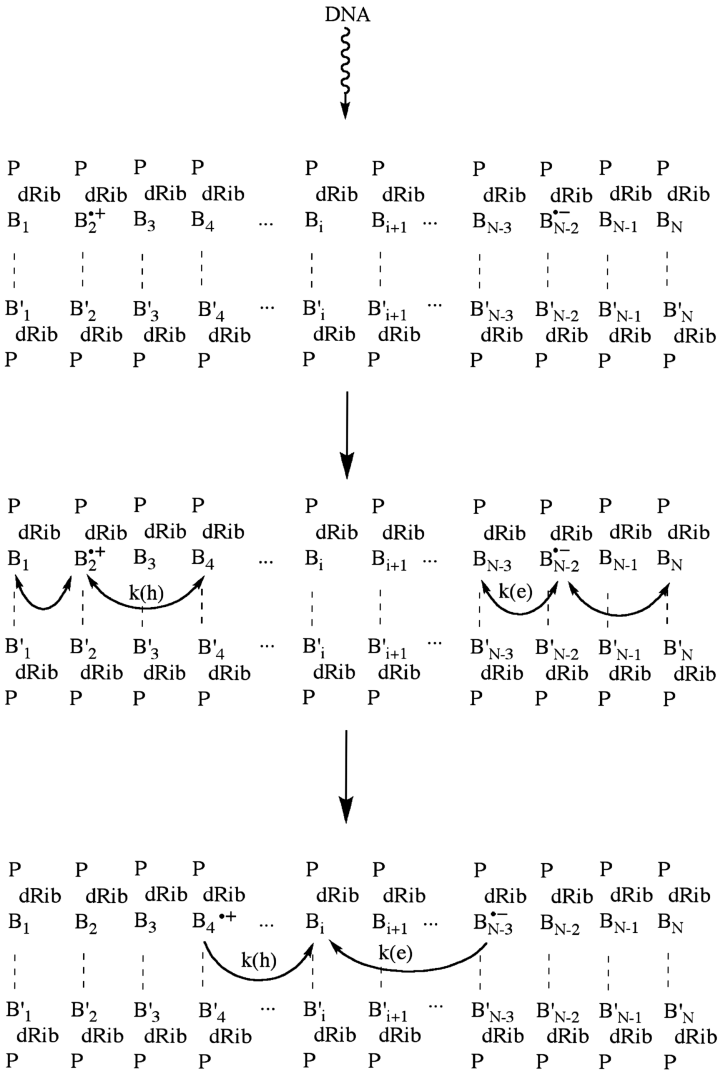

FIGURE 2.11. Direct ionization creates a hole at B2 and electron gain center at BN-2 in duplex DNA that is N bp long. The hole and excess electron diffuse at rates k(h) and k(e), respectively. If this one-dimensional diffusion brings the hole and excess electron back together, the outcome is no damage. Such combination reactions between opposite charges is the most likely outcome of the direct effect, returning > 60 % of the initial ionizations to their parent state.

$\beta = 1$ Å^{-1} and $k_{t0} = 10^{11}$ s^{-1}, it is easy to see that tunneling rates between two adjacent bases ($x = 3.4$ Å) would be relatively fast, $k_t = 3 \times 10^9$ s^{-1}, but the rate drops off quickly with distance. A 4-bp separation results in a $k_t = 1 \times 10^5$ s^{-1}. As pointed out by Steenken,[13] proton transfer rates for Reactions **1** in Figure 2.2 and **27** in Figure 2.10 are expected to be on the order of 10^{14} s^{-1}. Proton transfer reactions are certainly fast enough to trap holes and excess electrons and, thereby, curtail tunneling.

Hopping occurs when the hole (or excess electron) transfers from one base to another by passing over an energy barrier. An activation energy controls the rate with an Arrhenius-type behavior, the rate increasing exponentially with temperature. Proton transfer reactions are thermally activated; those that are reversible (e.g., **1** in Figure 2.2 and **27** Figure 2.10) gate electron and hole transfer, while those that are irreversible (e.g., **2** in Figure 2.2 and **28**, **29** in Figure 2.10) terminate migration.[68] At a high enough temperature and in the absence of terminal reactions, hopping can carry the hole or excess electron unlimited distances.

2.4.2. Reactions that Compete with Hole Transfer

The base-centered radicals, although efficiently trapped at 4 K, are mobilized upon warming. Between 4 K and ~100 K, the concentration of DNA-trapped radicals decreases monotonically.[68] In this same temperature range, the qualitative features of the EPR spectra remain relatively constant, indicating that the distribution of radical types remains relatively constant. The loss of radicals, therefore, must be a direct consequence of hole and/or excess electron hopping. Only radical mobility can bring radicals together in combination reactions. Predominantly, it is the hole and excess electron that combine, as illustrated in Figure 2.11 and as illustrated by reaction **33** in Figure 2.12. A less likely, but not inconsequential, combination reaction brings two holes together. Two examples are shown in Figure 2.12, reaction **34**, where the deprotonated radical cation, $B_i(-H)^{\bullet}$, is oxidized by a second base radical cation, and in reaction **35**, where the neutral deoxyribose radical, $dRib(-H)^{\bullet}$, is oxidized by a base radical cation.

The annealing properties of the DNA-trapped radicals indicate that the activation energy for hopping is highly disperse.[68] Trapping of holes and excess electrons requires dielectric relaxation around the trapping site to compensate for the change in charge at that site. A large component of the dielectric relaxation is the shift of a proton across the Watson–Crick hydrogen bond—for example, reaction **1** in Figure 2.2. The hole, now in the form of $Gua^{\bullet+}$, may tunnel to any neighboring purine at a rate strongly dependent on distance. The migration of the hole through DNA consists of tunneling steps gated by reversible proton transfer. Evidence of proton-gated hole transfer has been reported for DNA in aqueous solution.[79] Because there is a large dispersion in activation energies, detrapping of the holes occurs over a wide temperature, starting at ~10 K and extending to beyond 100 K.[68]

The distance over which the hole hops through DNA is limited by irreversible reactions. Guanine is special, not just because it has the deepest trapping well, but because of the nature of the reactions that compete with hopping. Detrapping the guanine-centered hole requires only a small activation energy, reversible proton transfer requiring just 2.3 kJ/mol.[12,13] Thus, the hopping rate at RT should be fast relative to irreversible trapping by OH^- addition (**2** in Figure 2.2). Indeed it has been proposed that holes can transfer over long distances, permitting "chemistry at a distance."[80,81] It would be surprising, however, if such long-range transfers are probable for DNA *in vivo*. In chromatin, the amino acid tyrosine, which lies in close proximity to DNA, is a deeper hole trap than guanine; it protects DNA against

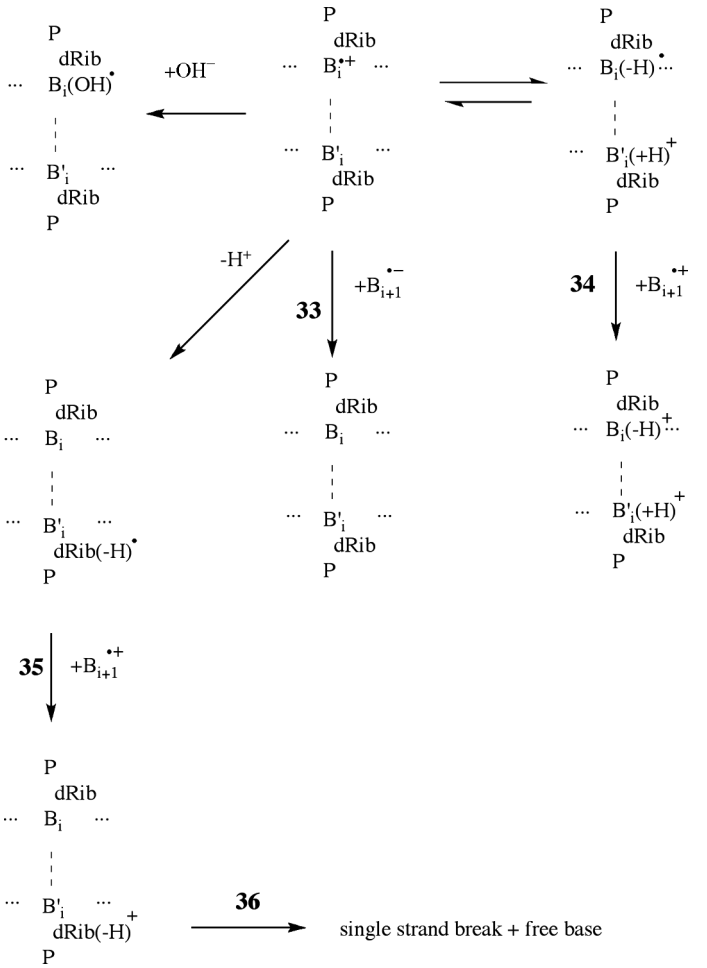

FIGURE 2.12. Not all combination reactions are between holes and excess electrons, shown here as reaction 33. Reaction 34 shows the case where the deprotonated base radical cation is one-electron oxidized to give a base cation. Reaction 35 shows the case where a neutral deoxyribose radical is one-electron oxidized by a base radical cation. In both examples, the resultant carbocation will go forward to products.

oxidative damage.[82] This makes sense since long-range electron transfer in DNA could prove problematic for DNA enzymes that function via one-electron transfer.

Although guanine is the main conduit for hole migration over long distances, it does not follow that the other three bases are uninvolved. Adenine is an important alternative site for localization of the hole. Studies on aqueous DNA indicate that the hole can migrate through large stretches of ATs.[83] In the solid state, the formation of 8OxoAde indicated that Ade trapped a significant fraction of holes in $d(GCACGCGTGC)_2$. In order to produce 8OxoAde, a hole on Ade must be

irreversibly trapped—as, for example, in reaction **8** of Figure 2.3. The fate of the hole generated on the pyrimidines is similar to Ade but with a stronger bias toward hole transfer from Pyr to Gua (Figures 2.4 and 2.5). Transfer of a hole formed on Cyt to another base competes with deprotonation at C1′ (**13** in Figure 2.4); and, for a hole on Thy, the competition is with deprotonation at the methyl group (**15** in Figure 2.5).

2.4.3. Reactions that Compete with Excess Electron Transfer

Migration of the excess electron is predominantly from Pyr to Pyr with a possible minor role of Ade. The excess electron is viewed as tunneling between bases producing transient radical anions. Reversible proton transfer deepens the electron trap site in the case of Cyt (**27** in Figure 2.10), explaining why this is the predominant trapping site at temperatures below 100 K. The transfer of the N1 Gua proton to N3 of Cyt is favored by 20 kJ/mol.[12, 13] Comparing this to the case of a hole on Gua where the same proton transfer (**1** in Figure 2.2) is favored by 2.3 kJ/mol supports the argument that migration of trapped electrons requires higher temperatures than migrations of holes. This fits with the conclusions drawn from EPR studies that the mobile species between 4 K and 100 K is the hole and between 120 and 200 K is the excess electron.[68]

As the DNA sample temperature was raised above 130 K, irreversible proton transfer to the C5–C6 position permanently trapped the excess electron at the pyrimidine bases.[45] The excess electron was irreversibly trapped at cytosine by reactions **28** and **29** in Figure 2.10 and at thymine by reactions **24** and **25** in Figure 2.9. The concentration of Thy(C6 + H)$^{\bullet}$ increased upon annealing from 140 K to 180 K. It appeared that the Cyt(C5 + H)$^{\bullet}$ radical was formed by heating while most, if not all, of the Cyt(N3 + H, C6 + H)$^{\bullet+}$ radical was formed as a spur reaction at 4 K. Because the yields of the two end products, DHUra and DHThy, were found to be nearly the same,[20] it can be deduced that electrons initially trapped by Cyt are, upon heating, transferred to Thy. Thus, even though reductive damage initially favors Cyt, it ends up partitioned rather equally between Thy and Cyt. This requires a net transfer of electrons from Cyt to Thy, and those transfer reactions are not activated until reaching temperatures above 130 K.

2.4.4. Summary on Radical Mobility

In summary, (i) the primary trapping site for both the hole and excess electron is initially the GC base pair, with holes centered on Gua and the excess electron centered on Cyt, (ii) reversible proton transfer plays a major role in trapping at the GC base pair, (iii) reversible proton transfer results in the excess electron being more deeply trapped than the hole, (iv) irreversible trapping of the excess electron is due to protonation of the pyrimidine C5–C6 bond, (v) irreversible trapping of the hole is due to OH^- addition to C8 of the purines, and (vi) the energy of activation for irreversible trapping by hydrogenation of a Pyr carbon is significantly lower than the activation energy for hydroxylation of a Pur carbon; consequently, the hole is able to migrate longer distances than the excess electron.

2.5. REACTIONS STEMMING FROM NONTRAPPABLE RADICALS

It had been long presumed that the radical population trapped in DNA—that is, the radicals escaping recombination—would quantitatively account for the lesions observed in DNA. Recent results indicate that this is not the case. The yield of DNA lesions exceeds the yield of trappable radicals.

2.5.1. Strand Breaks

The chemical yield of free radicals trapped in DNA X-irradiated at 4 K was measured by EPR.[84,85] DNA samples were prepared as transparent films from pUC18 plasmids. In these films the level of DNA hydration, Γ, was varied from 2.5 to 22 moles of water per mole of nucleotide. By taking advantage of the different dose–response characteristics of base radicals versus deoxyribose radicals, the yield was partitioned into these two types of radicals. It was found for DNA at $\Gamma = 2.5$ that the yield of deoxyribose radicals was 33 ± 5 nmol/J, increasing to 79 ± 12 nmol/J at $\Gamma = 22$.

Each of the five carbon-centered deoxyribose radicals (Figure 2.7) are known precursors to strand breaks and free base release.[38] In addition, the forward reactions of base-centered radicals in duplex DNA result in base damage, not deoxyribose damage.[57] Consequently, it is predicted that if trappable deoxyribose radicals are the only precursor to strand breaks, then the yield of strand breaks should equal the yield of deoxyribose radicals.

The chemical yield of strand breaks was measured in the same pUC18 films used for the radical yield measurements.[86] Gel electrophoresis was used to measure the loss of the supercoiled form. This highly sensitive technique takes advantage of the transition from the compact supercoiled form to the relaxed open circle form that occurs when just one of the duplex strands is broken. In addition, free base release was measured using HPLC.[39] Free base release is expected to provide a tighter correlation with strand break events than does loss of supercoil because multiple single strand breaks in one plasmid is scored as only one strand break. In contrast, for each strand break, regardless of where it occurs, a release of free base is expected. The yield of free base release for pUC18 at $\Gamma = 2.5$ and 22 was 134 ± 4 nmol/J and 212 ± 21 nmol/J, respectively. Thus, the yield of strand breaks exceeds the yield of deoxyribose trapped radicals. The difference between these two yields (e.g., $134 - 33 = 101 \pm 4$ nmol/J at $\Gamma = 2.5$) is termed the shortfall.

In order to explain the shortfall between the deoxyribose radical yield and single strand break yield, formation of molecular products was proposed. There are three central aspects to the proposed mechanism. One is that a significant fraction of the initially formed deoxyribose radicals, shown as dRib(−H)$^{\bullet}$ in Figure 2.12, are oxidized by a nearby base radical cation, $B_{i+1}{}^{\bullet+}$, forming a deoxyribose carbocation, dRib(−H)$^{+}$, as shown in reaction **35** of Figure 2.12. The second aspect is that this doubly oxidized site is produced in a spur reaction; that is, the initial two radicals, dRib(−H)$^{\bullet}$ and $B_{i+1}{}^{\bullet+}$, react within a spur (cluster) of ionizations. And the

third aspect is that when the DNA film is dissolved in water, the carbocation reacts (reaction **36**) to give strand breaks and free base release. This mechanism would then explain the shortfall between deoxyribose end products and deoxyribose trapped radicals.[39, 85]

2.5.2. Base Damage

The standard deviation in base damage yields is much larger than for deoxyribose damage yields. Keeping the large standard errors in mind, it appears that a molecular pathway similar to that invoked for deoxyribose damage may produce a significant amount of base damage. There appears to be a shortfall between the yield of base radical precursors and the yield of stable base products. Two examples are given below. The first entails two one-electron reductions and the second entails two one-electron oxidations.

The formation of DHThy (Figure 2.9) requires two one-electron reductions. In films of $d(GCACGCGTGC)_2$, the yield of DHThy was 36 ± 52 nmol/J.[20] The total trapped radical yield at 4 K is 618 ± 60 nmol/J. The fraction of this total due to one-electron-reduced thymine trapped at 4 K is estimated to be $\sim$60 nmol/J. Upon warming to room temperature, combination reactions reduce the radical concentration to 10% of that observed at 4 K; therefore, the RT yield of $Thy(C6 + H)^{\bullet}$ is less than $\sim$6 nmol/J. Upon dissolution in water, $Thy(C6 + H)^{\bullet}$ will be one-electron reduced to yield DHThy, but at this stage the yield of $Thy(C6 + H)^{\bullet}$ ($\sim$6 nmol/J) is insufficient to account for the yield of DHThy (36 ± 52 nmol/J). This shortfall can be explained if $Thy(C6 + H)^{\bullet}$ is one-electron reduced prior to dissolution. The two one-electron reduction mechanism may occur as part of a spur reaction or upon warming the sample. In the latter case, warming mobilizes the excess electron so as allow for reduction of $Thy(C6 + H)^{\bullet}$ by either a nearby $Cyt(N3 + H)^{\bullet}$ or $Thy^{\bullet -}$. In Figure 2.9, this assigns the reducing agent, **red** in reaction **26**, to a neighboring Pyr radical.

The formation of 8OxoGua requires two one-electron oxidations. In films of $d(GCACGCGTGC)_2$, the yield of 8OxoGua was 101 ± 49 nmol/J.[20] But the maximum yield of precursor radical at RT is $\sim$25 nmol/J. The yield of Gua-centered radical present when the sample is dissolved in water is insufficient to account for the yield of 8OxoGua product. Also, there were only 2.5 waters per nucleotide in these DNA films, greatly reducing the likelihood of an OH^- addition reaction (**2** in Figure 2.2) occurring prior to dissolution. In spite of such a reaction appearing to be energetically unfavorable, this raises the possibility that a large fraction of 8OxoGua proceeds through two one-electron oxidations of Gua prior to OH^- addition.

2.6. FUTURE PROSPECTS

The reactions given in Figures 2.1–2.12 constitute a working model that potentially explains much of what is known about the free radical intermediates and stable end products generated directly in DNA by ionizing radiation. Two aspects of this model are particularly provocative. One aspect is that holes generated on bases, Cyt in

particular, may result in C1′ deoxyribose damage. The idea that a hole may be transferred from a base to the backbone in ds-DNA is counter to most current thinking. But the observation that free base release is base-dependent requires an explanation; deprotonation at C1′ of base radical cations is one possibility. The other aspect is the proposal that carbocation (and carbanion) intermediates play a significant role in product formation. It is a hope of the author that this chapter might stimulate ideas and experiments that can provide direct evidence for, or against, formation of the proposed $dRib(-H)^+$ carbocation.

ACKNOWLEDGMENTS

The author thanks Steven Swarts and Paul Black for their helpful suggestions. The author's research program is supported by PHS Grant 2-R01-CA32546, awarded by the National Cancer Institute, DHHS. The contents of this chapter are solely the responsibility of the author and do not necessarily represent the official views of the National Cancer Institute.

REFERENCES

1. Krisch, R. E.; Flick, M. B.; Trumbore, C. N. Radiation chemical mechanisms of single- and double-strand break formation in irradiated SV40 DNA. *Radiat. Res.* **1991**, *126*, 251–259.
2. Bernhard, W. A.; Purkayastha, S.; Milligan, J. R. Which DNA damage is likely to be relevant in hormetic responses? *Dose–Response* **2008**, *6*, 184–195.
3. Becker, D.; Sevilla, M. D. In *Specialist Periodical Reports: Electron Paramagnetic Resonance*; Gilbert, B. C., Ed.; The Royal Society of Chemistry: Cambridge, UK, 1998; Vol. 16; pp 79–115.
4. Bernhard, W. A.; Close, D. M. In *Charged Particle and Photon Interactions with Matter*; Mozumder, A.; Hatano, Y., Eds.; Marcel Dekker, New York, 2003, pp. 471–489.
5. Sevilla, M. D.; Bernhard, W. A. *In Radiation Chemistry: From Basics to Applications in Material and Life Sciences*; Spotheim-Maurizot, M., Mostafavi, M., Douki, T., Belloni, J., Eds.; EDP Sciences: Les Ulis, France, 2008; pp 191–202.
6. Sevilla, M. D.; Becker, D. In *Specialist Periodical Reports: Electron Paramagnetic Resonance*; Gilbert, B. C., Ed.; The Royal Society of Chemistry: Cambridge, UK, 2004; Vol. 19; pp 243–278.
7. Sevilla, M. D.; Engelhardt, M. L. Mechanisms for radiation damage in DNA constituents and DNA. Reactions of the N1-substituted thymine π-cation radicals. *Faraday Discuss. Chem. Soc.* **1977**, *63*, 255–263.
8. Spalletta, R. A.; Bernhard, W. A. Influence of primary structure on initial free radical products trapped in A:T polydeoxynucleotides x-irradiated at 4 K. *Radiat. Res.* **1993**, *133*, 143–150.
9. Bernhard, W. A. In *Advances in Radiation Biology*, Vol. 9; Lett, J. T.; Adler, H., Eds.; Academic Press, New York, 1981, pp. 199–280.

10. Steenken, S. Purine bases, nucleosides, and nucleotides: Aqueous solution redox chemistry and transformation reactions of their radical cations and e^- and OH adducts. *Chem. Rev.* **1989**, *89*, 503–520.
11. Steenken, S. Structure, acid/base properties and transformation reaction of purine radicals. *Free Radical Commun.* **1989**, *6*, 117–120.
12. Steenken, S. Electron-transfer-induced acidity/basicity and reactivity changes of purine and pyrimidine bases. Consequences of redox processes for DNA base pairs. *Free Radical Res. Commun.* **1992**, *16*, 349–379.
13. Steenken, S. Electron transfer in DNA? Competition by ultra-fast proton transfer? *Biol. Chem.* **1997**, *378*, 1293–1297.
14. Colson, A. O.; Besler, B.; Sevilla, M. D. *Ab initio* molecular orbital calculations on DNA base pair radical ions: effect of base pairing on proton-transfer energies, electron affinities, and ionization potentials. *J. Phys. Chem.* **1992**, *96*, 9787–9794.
15. Wang, W.; Becker, D.; Sevilla, M. D. The influence of hydration on the absolute yields of primary ionic free radicals in γ-irradiated DNA at 77 K. I. Total radical yields, *Radiat. Res.* **1993**, *135*, 146–154.
16. Becker, D.; Sevilla, M. D. In *Advances in Radiation Biology*; Lett, J. T., Sinclair, W. K., Eds.; Academic Press: San Diego, 1993; Vol. 17; pp 121–180.
17. Hildenbrand, K.; Schulte-Frohlinde, D. ESR spectra of radicals of single-stranded and double-stranded DNA in aqueous solution. Implications for $^{\bullet}$OH-induced strand breakage, *Free Radical Res. Commun* **1990**, *11*, 195–206.
18. Nelson, W. H.; Sagstuen, E.; Hole, E. O.; Close, D. M. On the proton transfer behavior of the primary oxidation product in irradiated DNA. *Radiat. Res.* **1992**, *131*, 10–17.
19. Swarts, S. G.; Becker, D.; Sevilla, M.; Wheeler, K. T. Radiation-induced DNA damage as a function of hydration. II. Base damage from electron-loss centers, *Radiat. Res.* **1996**, *145*, 304–314.
20. Swarts, S. G.; Gilbert, D. C.; Sharma, K. K.; Razskazovskiy, Y.; Purkayastha, S.; Naumenko, K. A.; Bernhard, W. A. Mechanisms of direct radiation damage in DNA, based on a study of the yields of base damage, deoxyribose damage, and trapped radicals in d(GCACGCGTGC.$_2$. *Radiat. Res.* **2007**, *168*, 367–381.
21. Close, D. M.; Nelson, W. H. ESR and ENDOR study of adenosine single crystals x-irradiated at 10 K. *Radiat. Res.* **1989**, *117*, 367–378.
22. Nelson, W. H.; Sagstuen, E.; Hole, E. O.; Close, D. M. Electron spin resonance and electron nuclear double resonance study of X-irradiated deoxyadenosine: Proton transfer behavior of primary ionic radicals. *Radiat. Res.* **1998**, *149*, 75–86.
23. Flossmann, W.; Mueller, A.; Westhof, E. Radicals in irradiated monocrystals of the base-pair complex 9-ethyl adenine:1-methyl uracil, *Int. J. Radiat. Biol. Relat. Stud. Phys., Chem. Med.* **1974**, *26*, 481–492.
24. Hole, E. O.; Sagstuen, E.; Nelson, W. H.; Close, D. M. Free radical formation in single crystals of 9-methyladenine x-irradiated at 10 K. An electron paramagnetic resonance and electron nuclear double resonance study. *Radiat. Res.* **1995**, *144*, 258–265.
25. Hole, E. O.; Sagstuen, E.; Nelson, W. H.; Close, D. M. Free radical formation in X-irradiated crystals of 2′-deoxycytidine hydrochloride. Electron magnetic resonance studies at 10 K. *Radiat. Res.* **2000**, *153*, 823–834.
26. Herak, J. N.; Krilov, D.; McDowell, C. A. ENDOR study of the stable radicals in γ- or x-ray-irradiated single crystal of deoxycytidine-5′-phosphate. *J. Magn. Reson.* **1976**, *23*, 1–7.

27. Weiland, B.; Hüttermann, J. Free radicals from x-irradiated "dry" and hydrated lyophilized DNA as studied by electron spin resonance spectroscopy: Analysis of spectral components between 77 K and room temperature, *Int. J. Radiat. Biol.* **1998**, *74*, 341–358.
28. Sharma, K. K.; Purkayastha, S.; Bernhard, W. A. Unaltered free base release from $d(CGCGCG)_2$ produced by the direct effect of ionizing radiation at 4 K and room temperature. *Radiat. Res.* **2007**, *167*, 501–507.
29. Flossmann, W.; Westhof, E.; Mueller, A. Radical formation in salts of pyrimidines. III. Cytosine. H_2O crystals, *Int. J. Radiat. Biol. Relat. Stud. Phys., Chem. Med.* **1976**, *30*, 301–315.
30. Anderson, R. F.; Shinde, S. S.; Maroz, A. Cytosine-gated hole creation and transfer in DNA in aqueous solution, *J. Am. Chem. Soc.* **2006**, *128*, 15966–15967.
31. Sevilla, M. D. Electron spin resonance study of N1-substituted thymine π-cation radicals, *J. Phys. Chem.* **1976**, *80*, 1898–1901.
32. Schmidt, J. An ESR analysis of a heat-stable radical in gamma-irradiated single crystals of 1-methylthymine. *J. Chem. Phys* **1975**, *62*, 370–375.
33. Purkayastha, S.; Milligan, J. R.; Bernhard, W. A. The role of hydration in the distribution of free radical trapping in directly ionized DNA. *Radiat. Res.* **2006**, *166*, 1–8.
34. Ezra, F. S.; Bernhard, W. A. Electron spin resonance of γ-irradiated salts of diethyl phosphoric acid. *Radiat. Res.* **1974**, *60*, 350–354.
35. Roginskaya, M.; Bernhard, W. A.; Marion, R. T.; Razskazovskiy, Y. The release of 5-methylene-2-furanone from irradiated DNA catalyzed by cationic polyamines and divalent metal cations. *Radiat. Res.* **2005**, *163*, 85–89.
36. Roginskaya, M.; Razskazovskiy, Y.; Bernhard, W. A. 2-deoxyribonolactone lesions in X-ray-irradiated DNA: Quantitative determination by catalytic 5-methylene-2-furanone release. *Angew. Chem. Int. Ed.* **2005**, *44*, 6210–6213.
37. Xue, L.; Greenberg, M. M. Use of fluorescence sensors to determine that 2-deoxyribonolactone is the major alkali-labile deoxyribose lesion produced in oxidatively damaged DNA. *Angew. Chem.* **2007**, *119*, 567–570.
38. Pogozelski, W. K.; Tullius, T. D. Oxidative strand scission of nucleic acids: Routes initiated by hydrogen abstraction from the sugar moiety. *Chem. Rev.* **1998**, *98*, 1089–1107.
39. Sharma, K. K. K.; Milligan, J. R.; Bernhard, W. A. Multiplicity of DNA single-strand breaks produced in pUC18 exposed to the direct effects of ionizing radiation. *Radiat. Res.* **2008**, *170*, 156–162.
40. Boudaiffa, B.; Hunting, D.; Cloutier, P.; Huels, M. A.; Sanche, L. Induction of single- and double-strand breaks in plasmid DNA by 100–1500 eV electrons. *Int. J. Radiat. Biol.* **2000**, *76*, 1209–1221.
41. Huels, M. A.; Boudaiffa, B.; Cloutier, P.; Hunting, D.; Sanche, L. Single, double, and multiple double strand breaks induced in DNA by 3–100 eV electrons. *J. Am. Chem. Soc.* **2003**, *125*, 4467–4477.
42. Purkayastha, S.; Milligan, J. R.; Bernhard, W. A. Correlation of free radical yields with strand break yields produced in plasmid DNA by the direct effect of ionizing radiation. *J. Phys. Chem. B* **2005**, *109*, 16967–16973.
43. Bernhard, W. A. Sites of electron trapping in DNA as determined by ESR of one-electron reduced oligonucleotides. *J. Phys. Chem.* **1989**, *93*, 2187–2189.
44. Wang, W.; Sevilla, M. D. Protonation of nucleobase anions in gamma-irradiated DNA and model systems. Which DNA base is the ultimate sink for the electron? *Radiat. Res.* **1994**, *138*, 9–17.

45. Yan, M.; Becker, D.; Summerfield, S.; Renke, P.; Sevilla, M. D. Relative abundance and reactivity of primary ion radicals in γ-irradiated DNA at low temperatures. 2. Single- vs double-stranded DNA. *J. Phys. Chem.* **1992**, *96*, 1983–1989.

46. Hole, E. O.; Sagstuen, E.; Nelson, W. H.; Close, D. M. Primary reduction and oxidation of thymine derivatives: ESR/ENDOR of thymidine and 1-methylthymine x-irradiated at 10 K. *J. Phys. Chem.* **1991**, *95*, 1494–1503.

47. Sagstuen, E.; Hole, E. O.; Nelson, W. H.; Close, D. M. Radiation-induced free-radical formation in thymine derivatives: EPR/ENDOR of anhydrous thymine single crystals x-irradiated at 10 K. *J. Phys. Chem.* **1992**, *96*, 1121–1126.

48. Sagstuen, E.; Hole, E. O.; Nelson, W. H.; Close, D. M. Radiation damage to DNA base pairs. I. Electron paramagnetic resonance and electron nuclear double resonance study of single crystals of the complex 1-methylthymine.cntdot.9-methyladenine x-irradiated at 10 K. *Radiat. Res.* **1996**, *146*, 425–435.

49. Ormerod, M. G. Free radical formation in irradiated deoxyribonucleic acid, *Int. J. Radiat. Biol.* **1965**, *9*, 291–300.

50. Salovey, R.; Shulman, R. G.; Walsh, W. M., Jr. Electron spin resonance of irradiated DNA. *J. Chem. Phys.* **1963**, *39*, 839–840.

51. Sagstuen, E.; Hole, E. O.; Nelson, W. H.; Close, D. M. Protonation state of radiation-produced cytosine anions and cations in the solid state: EPR/ENDOR of cytosine monohydrate single crystals x-irradiated at 10 K. *J. Phys. Chem.* **1992**, *96*, 8269–8276.

52. Debije, M. G.; Bernhard, W. A. Thermally stable sites for electron capture in directly ionized DNA: Free radicals produced by the net gain of hydrogen at C5/C6 of cytosine and thymine in crystalline oligodeoxynucleotides. *J. Phys. Chem. A* **2002**, *106*, 4608–4615.

53. Debije, M. G.; Close, D. M.; Bernhard, W. A. Reductive damage in directly ionized DNA: saturation of the C5=C6 bond of cytosine in dCGCG)2 crystals. *Radiat. Res.* **2002**, *157*, 235–242.

54. Goodhead, D. T. Initial events in the cellular effects of ionizing radiations: Clustered damage in DNA. *Int. J. Radiat. Biol.* **1994**, *65*, 7–17.

55. Ward, J. F. DNA damage produced by ionizing radiation in mammalian cells: Identities, mechanisms of formation, and reparability. *Prog. Nucleic Acid Res. Mol. Biol.* **1988**, *35*, 95–125.

56. Mozumder, A.; Magee, J. L. Theory of radiation chemistry. VII. Structure and reactions in low LET tracks. *J. Chem. Phys* **1966**, *45*, 3332–3341.

57. von Sonntag, C. *The Chemical Basis of Radiation Biology*; Taylor and Francis, New York, 1987.

58. Bernhard, W. A.; Mroczka, N.; Barnes, J. Combination is the dominant free radical process initiated in DNA by ionizing radiation: An overview based on solid-state EPR studies, *Int. J. Radiat. Biol.* **1994**, *66*, 491–497.

59. Wallace, S. S. Enzymic processing of radiation-induced free radical damage in DNA. *Radiat. Res.* **1998**, *150*, S60–S79.

60. Weinfeld, M.; Rasouli-Nia, A.; Chaudhry, M. A.; Britten, R. A. Response of base excision repair enzymes to complex DNA lesions. *Radiat. Res.* **2001**, *156*, 584–589.

61. Sevilla, M. D.; Becker, D. Radiation damage in DNA. *Electron Spin Reson.* **1994**, *14*, 130–165.

62. Spalletta, R. A.; Bernhard, W. A. Free radical yields in A:T polydeoxynucleotides, oligodeoxynucleotides, and monodeoxynucleotides at 4 K. *Radiat. Res.* **1992**, *130*, 7–14.
63. Barton, J. K. Photoinduced electron transfer through the double helix: Is DNA a wire? *Proc. Robert A. Welch Found. Conf. Chem. Res.* **1993**, *37TH*, 171–179.
64. Dandiliker, P. J.; Holmlin, R. E.; Barton, J. K. Oxidative thymine dimer repair in the DNA helix. *Science* **1997**, *275*, 1465–1468.
65. Kelley, S.; Barton, J. DNA-mediated electron transfer from a modified base to ethidium: π-stacking as a modulator of reactivity, *Chem. Biol.* **1998**, *5*, 413–425.
66. Debije, M. G.; Milano, M. T.; Bernhard, W. A. DNA responds to ionizing radiation as an insulator, not as a "molecular wire." *Angew. Chem., Int. Ed.* **1999**, *38*, 2752–2756.
67. Debije, M. G.; Bernhard, W. A. Free radical yields in crystalline DNA X-irradiated at 4 K, *Radiat. Res.* **1999**, *152*, 583–589.
68. Debije, M. G.; Bernhard, W. A. Electron and hole transfer induced by thermal annealing of crystalline DNA X-irradiated at 4 K, *J. Phys. Chem. B* **2000**, *104*, 7845–7851.
69. Debije, M. G.; Strickler, M. D.; Bernhard, W. A. On the efficiency of hole and electron transfer from the hydration layer to DNA: An EPR study of crystalline DNA X-irradiated at 4 K. *Radiat. Res.* **2000**, *154*, 163–170.
70. Giese, B. Electron transfer in DNA. *Curr. Opin. Chem. Biol.* **2002**, *6*, 612–618.
71. Schuster, G. B. Long-range charge transfer in DNA: Transient structural distortions control the distance dependence. *Acc. Chem. Res.* **2000**, *33*, 253–260.
72. Cai, Z.; Gu, Z.; Sevilla, M. D. Electron spin resonance study of the temperature dependence of electron transfer in DNA: Competitive processes of tunneling, protonation at carbon, and hopping. *J. Phys. Chem. B* **2000**, *104*, 10406–10411.
73. Cai, Z.; Sevilla, M. D. Electron Spin Resonance Study of Electron Transfer in DNA: Inter-Double-Strand Tunneling Processes, *J. Phys. Chem. B* **2000**, *104*, 6942–6949.
74. Cai, Z.; Gu, Z.; Sevilla, M. D. Electron spin resonance study of electron and hole transfer in DNA: Effects of hydration, aliphatic amine cations, and histone proteins. *J. Phys. Chem. B* **2001**, *105*, 6031–6041.
75. Cai, Z.; Li, X.; Sevilla, M. D. Excess electron transfer in DNA: Effect of base sequence and proton transfer. *J. Phys. Chem. B* **2002**, *106*, 2755–2762.
76. Cai, Z.; Sevilla, M. D. Electron and hole transfer from DNA base radicals to oxidized products of guanine in DNA. *Radiat. Res.* **2003**, *159*, 411–419.
77. Cai, Z.; Sevilla, M. D. In *Long Range Transfer in DNA*, Vol. II; Shuster, G., Ed.; Springer-Verlag, New York, **2004**, Vol. 237 of Topics in Current Chemistry, pp. 103–128.
78. Messer, A.; Carpenter, K.; Frozley, K.; Buchanan, J.; Yang, S.; Razskazovskii, Y.; Cai, Z.; Sevilla, M. Electron spin resonance study of electron transfer rates in DNA: Determination of the tunneling constant β for single-step excess electron transfer. *J. Phys. Chem. B* **2000**, *104*, 1128–1136.
79. Shafirovich, V.; Dourandin, A.; Geacintov, N. E. Proton-coupled electron-transfer reactions at a distance in DNA duplexes: Kinetic deuterium isotope effect. *J. Phys. Chem. B* **2001**, *105*, 8431–8435.
80. Barton, J. K. DNA -mediated electron transfer: Chemistry at a distance. *Pure Appl. Chem.* **1998**, *70*, 873–879.
81. Odom, D. T.; Barton, J. K. Long-range oxidative damage in DNA/RNA duplexes. *Biochem.* **2001**, *40*, 8727–8737.

82. Ly, A.; Bullick, S.; Won, J.-H.; Milligan, J. R. Cationic peptides containing tyrosine protect against radiation-induced oxidative DNA damage. *Int. J. Radiat. Biol.* **2006**, *82*, 421–433.

83. Giese, B.; Spichty, M.; Wessely, S. Long-distance charge transport through DNA. An extended hopping model. *Pure Appl. Chem.* **2001**, *73*, 449–453.

84. Purkayastha, S.; Bernhard, W. A. What is the initial chemical precursor of DNA strand breaks generated by direct-type effects? *J. Phys. Chem. B* **2004**, *108*, 18377–18382.

85. Purkayastha, S.; Milligan, J. R.; Bernhard, W. A. An investigation into the mechanisms of DNA strand breakage by direct ionization of variably hydrated plasmid DNA. *J. Phys. Chem. B* **2006**, *110*, 26286–26291.

86. Purkayastha, S.; Milligan, J. R.; Bernhard, W. A. On the chemical yield of base lesions, strand breaks, and clustered damage generated in plasmid DNA by the direct effect of X rays. *Radiat. Res.* **2007**, *168*, 357–366.

3

CHEMICAL REACTIONS OF THE RADICAL CATIONS OF NUCLEOBASES IN ISOLATED AND CELLULAR DNA. FORMATION OF SINGLE-BASE LESIONS

JEAN CADET,[*,†] THIERRY DOUKI,[*] DIDIER GASPARUTTO,[*] JEAN-LUC RAVANAT,[*] AND J. RICHARD WAGNER[†]

[*] *Laboratoire Lésions des Acides Nucléiques, SCIB-UMR-E no. 3 (CEA/UJF), Institut Nanosciences et Cryogénie, CEA/Grenoble, F-38054 Grenoble Cedex 9, France*

[†] *Département de Médecine Nucléaire et Radiobiologie, Faculté de Médecine et des Sciences de la Santé, Université de Sherbrooke, Sherbrooke, Québec, Canada J1H 5N4*

3.1. INTRODUCTION

In the last two decades, much attention has been devoted to the elucidation of mechanisms implicated in the oxidative degradation pathways of DNA base[1] and 2-deoxyribose moieties[1e, 2] upon exposure of isolated and cellular DNA to both endogenous and exogenous oxidizing agents. Comprehensive oxidation reaction schemes are available for several reactive oxygen species (ROS), including ubiquitous and highly reactive hydroxyl radical ($OH^{\bullet}$),[1, 2,] specific singlet oxygen ($^1O_2$),[3] and less biologically relevant ozone.[4] It may be added that peroxynitrite, arising from the reaction of nitric oxide with superoxide anion radical, a poorly reactive species toward DNA bases, has been shown to have both oxidative and

Radical and Radical Ion Reactivity in Nucleic Acid Chemistry, Edited by Marc M. Greenberg

nitrative properties for DNA components.[5] In contrast, an inflammation release product, HOCl, is able to halogenate amino substituted nucleobases.[6] Other oxidation reactions that are not mediated by ROS or nitrogen reactive species are accounted for by one-electron abstraction from DNA components, whose oxidation potential decreases in the following order: guanine $<$ adenine $<$ thymine $\sim$ cytosine $<$ 2-deoxyribose.[7] One of the strongest one-electron oxidants is ionizing radiation, which, through the direct effect, is able to efficiently abstract one electron from any DNA component at least in the dry state or in frozen solutions.[8] High-intensity nano- and picosecond UVC laser pulses have been shown to be a suitable means to ionize purine and pyrimidine bases with similar efficiency according to a two-photon mechanism.[9] Another suitable method to generate nucleobase radical cations is to use UVA triplet-excited sensitizers operating through the type I mechanism.[10] Most type I photosensitizers are able to selectively oxidize guanine by charge transfer, whereas riboflavin also has the capability to abstract one electron from adenine.[10] Several quinone derivatives including 2-methyl-1,4-naphthoquinone, also called menadione (MQ),[11] and anthraquinone[12] upon UVA excitation are able to efficiently oxidize pyrimidine bases by one-electron abstraction. Similar results can be obtained with aromatic ketones.[13] Inorganic ions that can be generated by either UV photolysis or gamma irradiation are also efficient one-electron oxidants of guanine.[14] Among them, evidence is growing for the biological relevance of $CO_3^{\bullet -}$[15] that is likely generated in cells by the decomposition of nitrosoperoxycarbonate, the addition product of peroxynitrite and CO_2.[16] Exposure of DNA components to ionizing radiation in the solid state, either as dry samples or as frozen aqueous solutions, has allowed ESR detection of purine and pyrimidine radicals.[8] Upon warming of the irradiated samples, positive holes are located on guanine, as observed in aqueous solutions at room temperature, due to charge migration within DNA,[12,17] whereas electrons attach to pyrimidine bases.[18] Although the solid-state approach is suitable for the detection and structural assignment of radicals initially formed by the ionization of nucleobase and 2-deoxyribose components, it is not a biologically relevant model system in terms of final degradation products.[19] This is related primarily to the fact that molecular oxygen does not diffuse in the solid state to react with DNA radicals. Moreover, water molecules are necessary in the conversion of initial radicals into diamagnetic compounds. Consequently, the final product distribution obtained upon the irradiation of DNA in the dry state is drastically different from that observed upon one-electron oxidation of DNA in aerated aqueous solutions at room temperature.[1f] For these reasons, only results of model studies performed in aerated aqueous liquid solutions are discussed in the first section of the chapter, which is devoted to one-electron oxidation reactions of the main pyrimidine and purine nucleobases and three oxidized bases. Emphasis is placed on the oxidation reactions of nucleobases giving rise to single lesions since the formation of clustered damage initiated by a single radical is the topic of another chapter.[20] Recently available information on the oxidation reactions of cellular DNA induced by two-quantum photoionization of DNA bases is also reported and discussed in the second part of the chapter.

3.2. ONE-ELECTRON OXIDATION REACTIONS OF NORMAL PYRIMIDINE AND PURINE BASES IN MODEL COMPOUNDS AND ISOLATED DNA

Relevant mechanistic insights toward one-electron oxidation reactions of nucleobases in aerated aqueous solutions have been gained from extensive studies that initially mostly involved pyrimidine and purine 2′-deoxyribonucleosides used as DNA model compounds. This was inferred from the characterization of final DNA base oxidation products and the structural assignment of several radical precursors and unstable intermediates. It may be added that at least for the formation of single oxidation products, most of the degradation pathways that were thus determined have been validated in oligonucleotides and/or in isolated DNA. As a general observation, the formation of one-electron oxidation products of pyrimidine and purine bases may be rationalized in terms of two competitive reactions including hydration and deprotonation of initially generated base radical cations.

3.2.1. Thymine

Comprehensive mechanistic information on the one-electron oxidation reactions of the thymine moiety has been gained from the characterization of both transient radicals and final degradation products of MQ-mediated sensitization of thymidine (**1**) to UVA radiation in aerated aqueous solutions. Two main decomposition pathways of thymidine radical cations (**2**) generated upon one electron transfer from the base moiety of **1** to triplet-excited MQ[11] have been identified (Scheme 3.1). Evidence for the highly specific hydration of **2** was inferred from ESR-spin-trapping experiments of the oxidizing 6-hydroxy-5,6-dihydrothymid-5-yl radicals (**3**).[21] These results were confirmed from the isolation of the four *cis* and *trans* diastereomers of 5-hydroperoxy-6-hydroxy-5,6-dihydrothymidine **6**[22] whose formation is accounted for by fast addition of O_2 to **3** at a rate controlled by diffusion[23] and subsequent reduction of the resulting hydroperoxyl radicals **5** by $O_2^{\bullet -}$ (Scheme 3.2). The assignment of the four diastereomers of **6** that was achieved on the basis of extensive ^1H and ^{13}C NMR

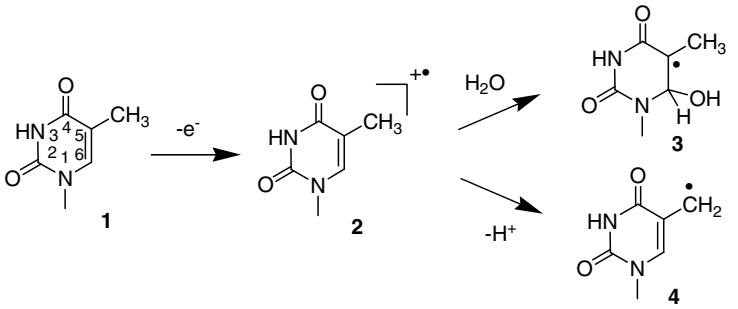

SCHEME 3.1. Mechanisms of decomposition of thymidine radical cation (**2**) generated by one electron oxidation of thymidine (**1**).

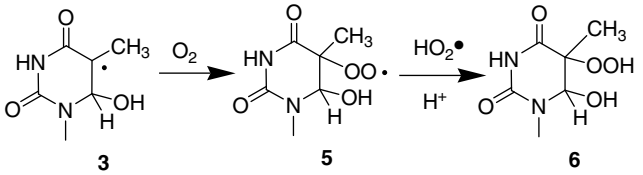

SCHEME 3.2. Mechanisms of formation of thymine hydroperoxides (**6**).

measurements received further support from their stereospecific synthesis.[24] The absolute configuration of each of the four diastereomers of **6** and the related 6-hydroperoxide position isomers was inferred from earlier structural assignment of related 6-hydroxylayed 5,6-dihydrothymidine derivatives,[25] data that were further confirmed for the site of the peroxidic function by X-ray crystallographic analysis of *cis*-5-hydroperoxy-6-hydroxy-5,6-dihydrothymine.[26] Since the hydroperoxides **6** are relatively stable in aqueous solutions at neutral pH, with a half-life at 37°C of 8–10 h and 16–35 h for *cis* and *trans* diastereomers, respectively,[25] the formation of stable thymidine degradation products including the four *cis* and *trans* diastereomers of 5,6-dihydroxy-5,6-dihydrothymidine (**7**), the 5*R** and 5*S** forms of 1-(2-deoxy-ß-D-*erythro*-pentofuranosyl)-5-hydroxy-5-methylhydantoin (**10**) and *N*-(2-deoxy-ß-D-*erythro*-pentofuranosyl) formamide (**11**) cannot be solely explained by hydrolytic degradation of the latter hydroperoxides **6** but also by the fate of alkoxyl radical intermediates **8** (Scheme 3.3). The latter reactive radicals **8** are likely to be generated by disproportionation of tertiary peroxyl radicals **5** that are not involved in a concerted Russell decomposition mechanism.[1e,27] The ß-scission mechanism, a typical reaction of alkoxyl radicals, is expected to lead to cleavage of the 5,6-pyrimidine bond with subsequent loss of the pyruvyl group from transiently generated *N*-formyl-*N*′-pyruvylurea nucleoside **9**.[22] Cyclization of the resulting ureide likely explains the formation of **10**, whereas hydrolysis gives rise to formamide nucleoside **11**.[22] The reduction of **6** by a S_N2 type mechanism involving the peroxide bond cannot be totally

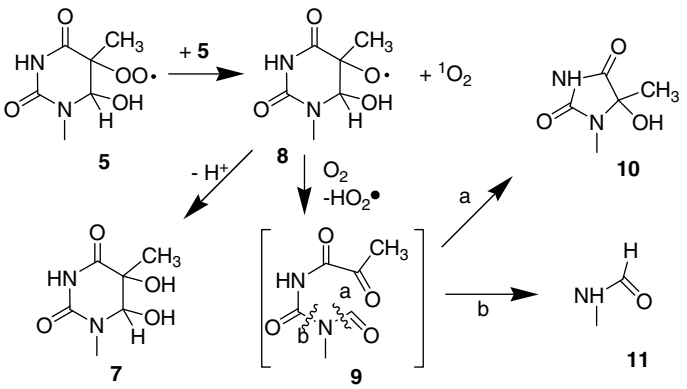

SCHEME 3.3. Proposed mechanisms for the decomposition of thymidine hydroperoxides through the transient formation of alkoxy radicals (**8**).

excluded, likely catalyzed by metals, to explain the formation of the four diastereomers of **7**, but also the alkoxyl radical **8** may mediate hydrogen abstraction reactions. Altogether, the hydration pathway accounts for 60% of the total degradation products of thymidine (**1**).

The other competitive deprotonation pathway has been shown to involve the exocyclic methyl group with a slightly lower efficiency (40%) than the hydration pathway (*vide supra*) (Scheme 3.1). Interestingly, the relative importance of the pathways is dependent on the photosensitizer used since it was found to be significantly favored upon benzophenone-mediated UVA sensitization. An influence of the pK_a of the radical anion of the sensitizer was proposed to account for this result.[13] Deprotonation of the radical cation of thymine gives rise to allylic 5-methyl-(2′-deoxyuridylyl) radical (**4**).[22] It may be noted that for isolated thymine, deprotonation occurs quantitatively at N1 leading to the formation of aminyl radicals that are able to add to the 5,6-pyrimidine bond of thymine bases with the subsequent formation of biadducts.[28] Efficient addition of O_2 to **4** is the first step of a sequence of reactions, that through the intermediacy of peroxyl radicals **12**, and their subsequent reduction, leads to the generation of highly stable 5-(hydroperoxymethyl)-2′-deoxyuridine (**13**) (Scheme 3.4). This hydroperoxide exhibits a relatively long half-life of 8 weeks at 37°C.[24] The formation of two methyl oxidation products including 5-(hydroxymethyl)-2′-deoxyuridine (**15**) and formyl-2′-deoxyuridine (**16**) may be rationalized in terms of a Russell mechanism that operates for both primary and secondary peroxyl radicals.[27] Bimolecular reaction of **12** is expected to give rise to linear tetroxides **14** (Scheme 3.4) as recently proposed for the decomposition of peroxyl radicals of linoleic acid.[29] The thermal decomposition of **14** is likely to involve a cyclic mechanism with subsequent formation of alcohol **15** and aldehyde **16** products together with concomitant release of singlet oxygen.

Hydration and deprotonation reactions of thymine radical cations previously identified in 2′-deoxyribonucleosides (*vide supra*) have been shown to occur as well in isolated DNA and double-stranded oligonucleotides.[30] This was achieved

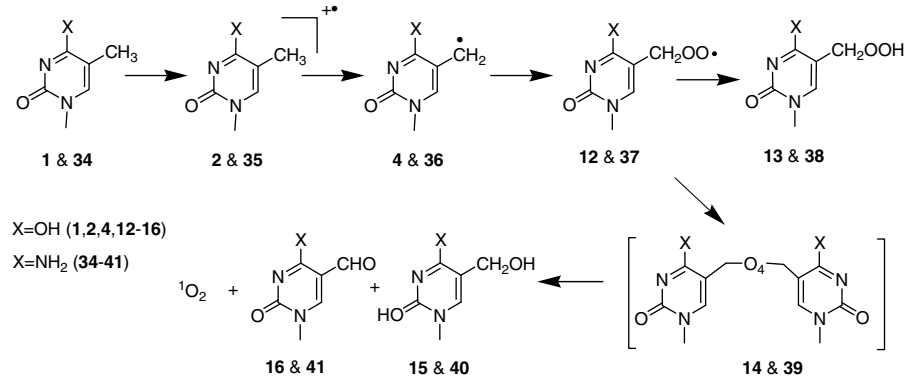

SCHEME 3.4. Decomposition reactions of 5-methyl-(2′-deoxyuridylyl) radical (**4**) and 5-methyl-(2′-deoxycydylyl) radical (**35**).

upon suitable digestion of oxidized DNA to 2′-deoxyribonucleosides followed by high-performance liquid chromatography coupled to versatile and sensitive tandem mass spectrometry (HPLC-MS/MS) detection.[31] Thus, several oxidized nucleosides, including thymidine 5,6-glycols (**7**), 5-(hydroxymethyl)-2′-deoxyuridine (**15**), and 5-formyl-2′-deoxyuridine (**16**), were generated in DNA- and AT-containing oligonucleotides exposed to high-intensity UVC laser pulses[30a] and UVA-excited anthraquinone,[30b] respectively. It is interesting to note that in the latter case, final damage was localized on thymine rather than on adenine, probably as the result of the higher reactivity of pyrimidine radical cations. Evidence for the one-electron oxidation-mediated formation of **15** and **16** in isolated DNA was gained from previous studies with menadione, riboflavin, and nitro derivatives of lysine, as type I photosensitizers.[30a, 32]

3.2.2. Cytosine

A convenient method to generate the radical cations of cytosine derivatives is by photosensitization with menadione and UVA light. Triplet-excited MQ undergoes charge transfer with 2′-deoxycytidine (**17**) to give the corresponding radical cation with a quantum yield of 0.33.[11] Using MQ-photosensitized oxidation, the radical cation **18** transforms into a mixture of products in aqueous aerated solutions that have been characterized by detailed NMR and mass spectrometry.[22b,33] The stable products may be divided into those that arise from deprotonation ($-H^+$) and those from hydration ($+H_2O$) of initial radical cation **18** (intermediates **19**–**22**; Scheme 3.5).

There are two competitive pathways of deprotonation for radical cation **18**: (i) deprotonation from the exocyclic *N*4 group giving rise to 2′-deoxyuridine (**23**) by way of *N*4-aminyl radical **19** and (ii) deprotonation from the C1′ position of the sugar moiety leading to the release of cytosine (**24**) and 2-deoxyribono-1,4-lactone (**25**).[34] The yield of **23** was 36%, while that of cytosine was only 4% based on the total decomposition of **17**. In a computational study, the most likely pathway of deamination—that is, that with the lowest free energy barrier—involved addition of water to the N3–C4 imine bond followed by cleavage of the C4–N4 bond.[35] The release of cytosine involves *N*-glycosidic bond cleavage and may be accounted for by deprotonation of the anomeric proton and subsequent transformation of **20** into alkali-labile **25**.[36] This pathway is rationalized in terms of formation of related peroxyl radicals, loss of superoxide radical anion, and further hydrolysis of the resulting sugar carbocation.[2a]

The competitive hydration of radical cation **18** takes place at either the C5 or C6 position of the pyrimidine ring, leading to the corresponding hydroxyl-substituted radicals (**21** and **22**); the same species are generated by the addition of $OH^{\bullet}$ to **17**. The resulting radicals rapidly incorporate O_2 to give the corresponding β-hydroxyperoxyl radicals. Thus, the hydration of **18** followed by addition of O_2 generates two different types of β-hydroxyperoxyl radicals depending on the position of hydroxyl and peroxyl groups (either C5 or C6). The mechanism of formation of 5,6-glycols (**26**), 5-hydroxyhydantoin (**30**), and formamide (**11**) likely involves the reduction

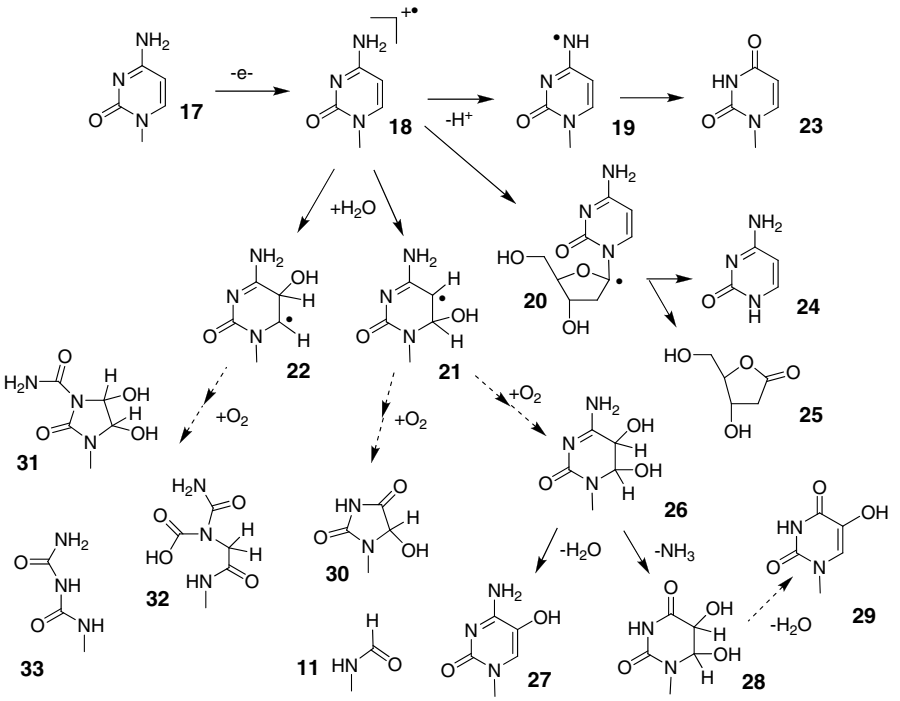

SCHEME 3.5. Proposed mechanism of formation of products from one-electron oxidation of cytosine and its derivatives.

of β-hydroxyperoxyl radicals to 5(6)-hydroxy-6(5)-hydroperoxides, followed by their decomposition, as well as the bimolecular decay of β-hydroxyperoxyl radicals. Although labile hydroperoxides have been detected in aqueous solutions of DNA exposed to ionizing radiation,[37] the 5(6)-hydroxy-6(5)-hydroperoxides of **17** are too unstable in aqueous solution to allow for their direct characterization. Experiments in the presence of $^{18}O_2$ showed that heavy oxygen atoms are incorporated at C5 and C6 in the structure of **11**, **27**, and **28**.[33] These results suggest that the addition of water occurs with the similar efficacy at both C5 and C6 positions of **18**, in contrast to the very specific addition of water at the C6 position of thymidine radical cation **2**.[10]

The formation of 5,6-glycols **26**[38] may be explained by the decomposition of initial β-hydroxyperoxyl radicals or the corresponding 5(6)-hydroxy-6(5)-hydroperoxides. Saturation of the 5,6-double bond renders the molecule susceptible to undergo either dehydration to 5-hydroxy-2′-deoxycytidine (**27**) or deamination to 5,6-dihydroxy-5,6-dihydro-2′-deoxyuridine (**28**) (Scheme 3.5). In aqueous solution (pH 3–8), the predominant pathway is dehydration to the 5,6-unsaturated product **27** (half-life = 1 h at 37°C; 5 h at 22°C). In contrast, the decomposition of cytosine 5,6-glycols **26** is dramatically altered in double-stranded DNA. The half-life of **26** increases 6.5-fold in poly(dG-dC) and 28-fold in double-stranded calf-thymus DNA while the extent of deamination increases 20–30%.[38] These effects have serious repercussions in cellular

DNA because deamination may cause C-to-T transition mutations. However, the dehydration of 2′-deoxyuridine 5,6-glycols (**28**) to 5-hydroxy-2′-deoxyuridine (**29**), which is only a minor reaction for the nucleoside under neutral conditions, does not detectably occur in DNA.[38a]

The formation of N1-(2-deoxy-β-D-*erythro*-pentofuranosyl)-1-carbamoyl-3, 4-dihydroxy-2-oxoimidazolidine (**31**), aminocarbonyl[N1-(2-deoxy-β-D-*erythro*-pentofuranosyl]-2-oxomethylcarbamic acid (**32**), and N1-(2-deoxy-β-D-*erythro*-pentofuranosyl)biuret (**33**) represents a unique pathway of oxidation for pyrimidine derivatives containing an internal N3–C4 imine group (Scheme 3.5). The imidazolidine-4,5-glycols **31** were obtained from the decomposition of 5-hydroxy-6-hydroperoxy-5,6-dihydro-2′-deoxycytidine, prepared *in situ* by peroxidation of *trans*-5-bromo-6-hydroxy-5,6-dihydro-2′-deoxycytidine.[39] The formation of **31** likely involves intramolecular rearrangement of 5-hydroxy-6-hydroperoxides (or the corresponding β-hydroxyperoxyl radicals) to C6–C4 endoperoxides followed by concerted O–O and C4–C5 bond cleavage.[40] Additional evidence for this pathway was provided by [$^{18}O_2$]-labeling experiments showing the incorporation of two ^{18}O atoms into the structure of **31**—that is, one atom on each at the side of O–O bond cleavage. The formation of other products in this pathway, **32** and **33**, may be explained by either dehydration or fragmentation of the imidazolidine ring of **31**, respectively. Alternatively, an open-chain ureide has been proposed in the formation of imidazolidine-4,5-glycols obtained by oxidation of the nucleobase.[40] Imidazolidine-4,5-glycols **31** exist as four distinct diastereomers depending on the configuration of C4 and C5. The structure of diastereomers was determined by ^{1}H-NMR, ^{13}C-NMR, and 2D-NOESY analyses.[39] A remarkable feature of the diastereomers is their ability to interconvert via single and successive cycles of ring-chain tautomerism at N1–C5 and N3–C4, leading to epimerization of C5 and C4, respectively. Although the *cis* diastereomers were the initial products of decomposition, they appeared to rapidly isomerize into the *trans* diastereomers with a half-life of 14 min at 37°C and pH 7. Likewise, the *cis* diastereomers probably undergo isomerization to give the more stable *trans* diastereomers in DNA. However, the *trans*-imidazolidine 4,5-glycols (**31**) have been detected in γ-irradiated oligonucleotides and calf-thymus DNA.[41] Further studies are in progress to determine the yield of these products in relation to other modifications in DNA.

3.2.3. 5-Methylcytosine

5-Methyl-2′-deoxycytidine (**34**) is a minor DNA base that plays an important role in regulating gene expression at CpG sequences. Interestingly, the properties of related radical cation **35** are different from those of 2′-deoxycytidine radical cation **18** (Scheme 3.4) in some respects. The main site of deprotonation of **35** is the methyl group accounting for as much as 60% of the total products. The resulting 5-methyl-(2′-deoxycytidylyl) radical (**36**) likely incorporates O_2 to give rise to the corresponding peroxyl radicals, which subsequently undergo either reduction and protonation to 5-(hydroperoxymethyl)-2′-deoxycytidine (**38**) or bimolecular decay to stable products (via tetroxide **39**). The half-life of the primary hydroperoxides (**38**) is

9.5 ± 0.5 h at 24°C.[42] In addition, two stable methyl oxidation products have been isolated and assigned as 5-(hydroxymethyl)-2′-deoxycytidine (**40**) and 5-formyl-2′-deoxycytidine (**41**). The mechanism of formation of the stable products, **40** and **41**, is likely analogous to that of the corresponding oxidation products of 1 (Schemes 3.1 and 3.4). It should be added that **40** is susceptible to further oxidation during menadione photosensitization and that subsequent oxidation gives rise to 5-formyl-2′-deoxycytidine (**41**). Similar to 2′-deoxycytidine radical cation **18**, the deprotonation of radical cation **35** at C1′ is a minor process leading to 2-deoxyribono-1,4-lactone (**25**) and the concomitant release of free 5-methylcytosine.

Other hydroperoxides, although not yet identified, were generated upon menadione photosensitized oxidation of **34**. The decomposition of these hydroperoxides led to the formation of several degradation products as observed by HPLC, including the *cis*-(5*R*,6*R*)- and (5*S*,6*S*)-diastereomers of 5,6-dihydroxy-5,6-dihydro-5-methyl-2′-deoxycytidine (the 5-methyl derivatives of 2′-deoxycytidine 5,6-glycols **26**). When the reaction was carried out in $^{18}O_2$, mass spectrometry analysis revealed that ^{18}O was incorporated at C5 in the structure of *cis* and *trans* diastereomers of the latter 5,6-glycols. This indicates that water and O_2 addition of transient pyrimidine radical cations takes place at C6 and C5, respectively. This contrasts to the initial addition of water at both C5 and C6 in the case of cytosine radical cation **18**, but it is similar to the hydration of thymine radical cation **2** that exclusively occurs at C6. Following the addition of water and O_2, the resulting β-hydroxyperoxyl radicals are likely reduced/protonated to the corresponding 6-hydroxy-5-hydroperoxides and/or take part in bimolecular modes of decay to stable products. The two *cis* diastereomers of 5-methyl-2′-deoxycytidine-5,6-glycols were generated upon exposure of **34** to γ rays in aerated aqueous solutions as the result of the initial addition of $OH^{\bullet}$ addition at C6 and C5 of the base moiety.[43] An interesting feature of 5-methylcystosine-5,6-glycols is the much higher stability toward hydrolytic deamination compared to cytosine homologues **26**, with the *cis* diastereomers being more easily converted into the corresponding thymine-5,6-glycols **7** compared to the *trans* forms.[38b,43] The absence of imidazolidine-4,5-glycols (the methyl derivatives of **31**) in menadione-photosensitized oxidation of **34** suggests that these products are preferentially formed by the decomposition of the corresponding 5-hydroxy-6-hydroxperoxides rather than 6-hydroxy-5-hydroperoxides. Indeed, imidazolidine-4,5-glycols derived from **34** were produced in relatively large amounts from the γ-irradiation of aerated aqueous solution of **34** in which $OH^{\bullet}$ mainly adds to C5 to give 5-hydroxy-5,6-dihydro-5-methyl-2′-deoxycytid-6-yl radicals, the corresponding 5-hydroxy-6-peroxyl radicals, and then 5-hydroxy-6-hydroperoxides in aerated aqueous solutions.

The development of methods to specifically oxidize methylated cytosine in DNA is relevant because of their utility in mapping the genomic methylation patterns. 5-Methylcytosine has a slightly lower oxidation potential compared to cytosine and thymine, and thus it has been shown to be a preferential target of certain single and double oxidizing agents.[44] In particular, V_2O_5/LiBr and $NaIO_4$/LiBr were found to specifically target methylated cytosine in oligonucleotides through a mechanism involving electrophilic addition of bromonium cation.[44a] The susceptibility of 5-methylcytosine toward oxidation was recently demonstrated in naphthoquinone-

tethered oligonucleotides.[44b] Efficient piperidine-induced cleavage was observed with 5-methylcytosine opposite naphthoquinone. Surprisingly, however, no cleavage was observed in the sequence at neighboring GG doublets, which have a much lower oxidation potential than 5-methylcytosine. These results indicate that photosensitizer radical anion efficiently undergoes recombination with radical cations centered at GG doublets, whereas the radical cation of 5-methylcytosine reacts rapidly, probably by deprotonation, to irreversibly transform into oxidation products. 5-Formyl-2′-deoxyuridine (**41**) was proposed as the precursor to strand breaks after piperidine treatment. A possible mechanism of formation of **41** in the photosensitized oxidation of quinone-tethered oligonucleotides involves the deprotonation of radical cation **35** followed by the incorporation of O_2 and subsequent reduction and protonation of peroxyl radicals to diamagnetic hydroperoxides **38**. The complete transformation of **34** to **41** may involve the reaction of quinone radical anions or secondary photosensitized oxidation.

3.2.4. Guanine

Similar to pyrimidine bases, there are two main competitive degradation pathways of guanine radical cations (**43**), which includes deprotonation and hydration and gives rise to oxidizing G(−H)$^{\bullet}$ (**44**) and reducing 8-hydroxy-7,8-dihydroguanyl **45** radicals in aqueous solutions, respectively (Scheme 3.6). The two predominant one-electron oxidation products of the purine moiety of free 2′-deoxyguanosine (**42**) arising from **44**

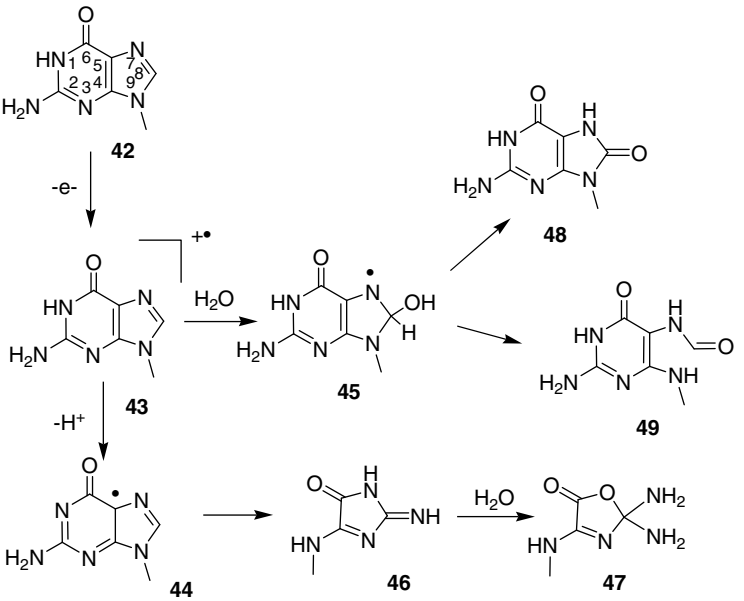

SCHEME 3.6. Degradation pathways of guanine radical cations (**43**) arising from one-electron oxidation of 2′-deoxyguanosine (**42**).

have been identified as 2,2-diamino-4-[(2-deoxy-ß-D-*erythro*-pentofuranosyl)amino]-5(2*H*)-oxazolone (**47**) and its precursor, 2-amino-5-[(2-deoxy-ß-D-*erythro*-pentofuranosyl)amino]-4*H*-imidazol-4-one (**46**).[45] The mechanism of their production (Scheme 3.6) has been rationalized in terms of multistep reactions of **44**, the transient product of deprotonation of guanine radical cation **43**[46] that occurs with a rate constant of $1.8 \times 10^7\ s^{-1}$ for the nucleoside.[47] It should be mentioned that **44**, which exhibits a pK_a of 3.9,[48] and shows a low reactivity, if any, toward O_2,[49] may also be generated by either dehydration of the $OH^\bullet$ adduct at C4 ($k = 6 \times 10^3\ s^{-1}$)[46] or protonation of the electron adduct of 8-bromoguanine[50] with rapid loss of Br^-. Thus, the addition of $O_2^{\bullet -}$ to tautomeric C(5) carbon-centered radicals whose rate constant has been estimated to be $3 \times 10^9\ M^{-1}\ s^{-1}$ and $4.7 \times 10^8\ M^{-1}\ s^{-1}$ for the nucleoside[46] and DNA duplexes, respectively,[51] leads after protonation to the transient formation of 5-hydroperoxides. This reaction is followed by an α-hydroperoxide type cleavage of the 5,6-bond and subsequent decarboxylation of the resulting opened-pyrimidine ring moiety. At this point, nucleophilic addition of a water molecule may take place across the 7,8-unsaturated bond prior to further rearrangement. This reaction involves the release of a formamide molecule through ring chain tautomerism[52] leading, after cyclization and quantitative hydrolysis of an unstable imidazolone **46** precursor (half-life = 10 h in aqueous solution at 20°C), to the formation of oxazolone nucleoside **47**.[45] It may be added that the oxidation of 8-oxo-7,8-dihydro-2′-deoxyguanosine **48** by reaction with highly oxidizing oxyl radical **44**[53] may also contribute to the formation of **46** and **47** (*vide infra*). The latter lesions are both highly alkali-labile lesions[54] in contrast to **48** which is relatively stable.[54a,55] Interestingly, the nucleophilic addition of a water molecule in the sequence of events giving rise to **47** is supported by the competitive formation of an anhydronucleoside upon one-electron oxidation of **42**.[56] This represents a relevant model system for investigating the mechanism for the radical-mediated oxidative formation of DNA-protein cross-links as illustrated in previous studies.[57]

Hydration of **43** whose pseudo-first-order rate constant was estimated to be $6 \times 10^4\ s^{-1}$ in double-stranded DNA[58] gives rise to the 8-hydroxy-7,8-dihydroguanyl radical **45**[46] (Scheme 3.6) according to a counterion-assisted proton shuttle mechanism as proposed from molecular dynamics and *ab initio* quantum simulations.[59] Support for the nucleophilic addition of H_2O to C8 of **43** was provided by the incorporation of ^{18}O into the structure of **48** upon riboflavin photosensitized oxidation of calf thymus DNA in $H_2{}^{18}O$ solutions.[60] Two major competitive reactions have been described for the conversion of **45** in aqueous solution that may also be generated by $OH^\bullet$ radical addition with a yield of 17%.[46] It should be added that the relative importance of the last two reactions is strongly dependent on the redox status of the environment, and in particular, on the extent of oxygenation of aqueous solutions. Therefore, oxidation of **45** gives rise to **48** while one-electron reduction of the latter guanine radical leads to the formation of 2,6-diamino-4-hydroxy-5-formamidopyrimidine (**49**) (Scheme 3.6). This is rationalized by scission of the saturated C8–N9 bond of 8-hydroxy-7,8-dihydroguanine intermediates that takes place with a rate of $k = 2 \times 10^5\ s^{-1}$ as determined by pulse radiolysis measurements.[46] It may be noted that other degradation pathways of **45** recently proposed on the basis of density

functional theory computation to explain the formation of **49** need to be further challenged experimentally.[61] The formation of **48** was the predominant pathway of decay for the intermediate radical **45** in double-stranded DNA in aerated aqueous solutions, whereas the formation of **49** was four-fold lower.[62] In contrast, only traces of **48** were detected upon one-electron oxidation of **42** as a monomer or in single-stranded DNA. This may be accounted for by the efficient oxidation of **48** as soon as it is generated from **42** ($k = 0.46 \times 10^9\,M^{-1}\,s^{-1}$ at pH 7.0)[63] and also by the efficient deprotonation of **43** that occurs more readily in the absence of base stacking and pairing in contrast to what is observed in double-stranded DNA.[60]

Similar to hydration, other examples of nucleophilic reactions of **43** have become available more recently from the isolation and characterization of novel guanine adducts. Thus, a guanine–lysine cross-link was shown to be generated upon riboflavin photosensitization of TGT trinucleotide and KKK trilysine peptide that form a tight complex.[64] The formation of the latter damage is accounted for by efficient addition of the central lysine residue of KKK to C8 of **43** followed by an oxidation step in a similar way as that for the generation of **48**. This appears to be more likely than an alternative mechanism that has ben recently proposed and that involves initial generation of a lysine radical cation prior to its addition to the guanine moiety.[65] Another example of nucleophilic addition involving guanine radical cations was provided by the isolation in single-stranded oligonucleotides of intrastrand cross-links between guanine and either thymine or uracil bases separated from the guanine moiety by cytosine.[66] The formation of these adducts was rationalized in terms of nucleophilic addition of the N3 atom of pyrimidine bases to C8 of guanine.

A major difference between the chemistry of base radical cations as free nucleosides compared to those within double-stranded helix is the occurrence of efficient charge transfer reactions from initially generated base radical cations of DNA, and additionally, from direct ionization of 2-deoxyribose in the case of ionizing radiation. The proposed mechanisms of transfer include polaron-mediated hopping, two-step hopping with superexchange, and coherent long-range tunneling.[17] This leads to the generation of oxidatively damaged bases mostly at guanines and to a lesser extent at adenines[9a] because guanine bases may be considered as preferential sinks for positive hole migration. On the basis of both experimental and theoretical investigations, intra- but not interstrand charge migration was shown to be implicated in the formation of damage at guanine following 193-nm laser pulse-mediated ionization of double-stranded DNA.[67] Kinetic information is also available for the two competitive reactions of guanine radical cations **43**, namely hydration and hole transfer to other guanine sites.[58] Thus, the pseudo-order rate for the hydration of guanine radical cations, **43**, was estimated to be about $6 \times 10^4\,s^{-1}$ or two orders of magnitude lower than the rate of hole migration between two isolated guanines separated by two AT base pairs.[58]

3.2.5. Adenine

Adenine radical cations (**51**) generated by one-electron oxidation reactions of adenine (**50**) have been shown to lead to the formation of 8-hydroxy-7,8-dihydroadenyl

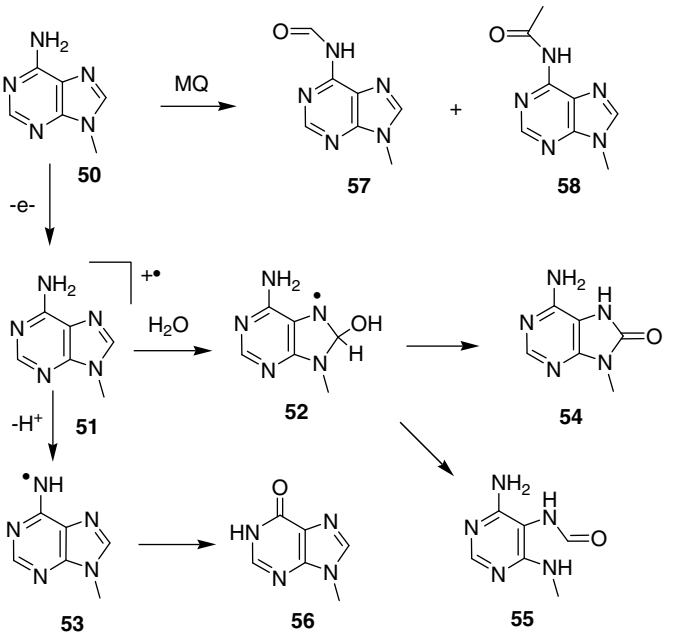

SCHEME 3.7. One-electron-oxidation-mediated decomposition of 2′-deoxyadenosine (**50**).

radicals (**52**) or to oxidizing 6-aminyl radicals **53** by hydration and deprotonation, respectively (Scheme 3.7). The reducing radical **52**, as already discussed for the related guanine radical **45**, is able to undergo two competitive reactions in aqueous solutions. Oxidation of **52** promoted by oxygen leads to the formation of 8-oxo-7,8-dihydroadenine (**54**), while reduction gives rise to 4,6-diamino-5-formamidopyrimidine (**55**).[68] The main final degradation product of the deprotonation pathway has been shown to be hypoxanthine (**56**), resulting from deamination of 6-aminyl radicals **53**.[10] As a striking observation, the yield of **54** and **55** in isolated DNA upon exposure to either $OH^{\bullet}$ or one-electron oxidants was about 10-fold lower than that of related guanine degradation products including **48** and **49**.[69] It was also shown that photoexcited menadione-mediated one-electron oxidation of adenine within several dinucleoside monophosphates, including d(ApA), d(CpA), and d(ApC), produced N^6-formyladenine (**57**) and N^6-acetyladenine (**58**) residues.[70]

3.3. ONE-ELECTRON OXIDATION REACTIONS OF OXIDIZED PYRIMIDINE AND PURINE DNA BASES

Several modified bases, including 5-hydroxycytosine (**27**), 5-hydroxyuracil (**29**), 8-oxo-7,8-dihydroguanine (**48**), 8-oxo-7,8-dihydroadenine (**54**), and the related formamidopyrimidine, exhibit lower oxidation potentials than those of normal pyrimidine and purine nucleobases, and thus they are also efficient targets for one-electron oxidants.

3.3.1. Hydroxypyrimidines: 5-Hydroxyuracil and 5-Hydroxycytosine

Oxidation of 2′-deoxycytidine (**17**) by $OH^{\bullet}$ and MQ-sensitization to UVA radiation leads to the formation of intermediate *cis*- and *trans*-5,6-glycols (**26**), which readily undergo dehydration to 5-hydroxy-2′-deoxycytidine (**27**).[71] In addition, 5-hydroxy-2′-deoxyuridine (**29**) may be produced by the dehydration of 5,6-glycols **28** (although this reaction is minor under neutral conditions for the nucleoside) and the decomposition of intermediate β-hydroxyhydroperoxides or the corresponding 5(6)-hydroxy-6(5)-hydroperoxides. Using HPLC on line with an ESA electrochemical detector, the oxidation potentials at half-maxima (versus Pd reference electrode) are 70 and 150 mV for **27** and **29**, respectively.[71,72] Using this detector, the oxidation potentials of 8-oxo-7,8-dihydro-2′-deoxyguanosine (**48**) is 190 mV, whereas that of nonmodified DNA bases is considerable higher (>700 mV). Several studies have reported the ability of $KMnO_4$ to transform 5-hydroxypyrimidines within oligonucleotides into strand breaks.[73,74] The incorporation of 5-hydroxypyrimidine nucleoside triphosphates by PCR followed by site specific oxidation of the modified base with $KMnO_4$ has been proposed as a method to detect single nucleotide polymorphism.[74] On the other hand, the susceptibility of 5-hydroxypyrimidines to further oxidation may be a serious problem in the analysis of these products in cellular DNA, and as well in studies concerning DNA repair and mutagenesis.

The mechanism of oxidation of **29** was recently investigated using modified nucleosides and oligonucleotides.[75–77] The oxidation of **29** by Br_2, iridium salts (Na_2IrCl_6), and $KMnO_4$ gave 1-(2-deoxy-β-D-*erythro*-pentofuranosyl)-isodialuric acid (**59**; Scheme 3.8). Remarkably, initial oxidation of **29** induces a sequence of transformations from **59** to 1-(2-deoxy-β-D-*erythro*-pentofuranosyl)-dialuric acid (**60**), followed by the conversion of **60** to 1-(2-deoxy-β-D-*erythro*-pentofuranosyl)-5-hydroxyhydantoin (**30**) and 1-(2-deoxy-β-D-*erythro*-pentofuranosyl)-4-hydroxyimidazolidine-2,5-dione (**61**).[75] Each product (**30**, **59–61**) existed as a pair of diastereomers, which were separated by reversed-phase HPLC. An interesting feature of the diastereomers of **59** was that they existed as fully hydrated hemiacetal derivatives in aqueous solution. The mechanism of oxidation of **29** by Br_2 likely involves the formation of intermediate bromohydrins, which transform into unstable 5,6-glycol-related products upon elimination of Br anion.[25,43] The oxidation of **27** by Br_2 resulted in the same products **30, 59–61** as the oxidation of **29**. Most interestingly, analogous products containing an exocyclic amino group were also detected in the product mixture, suggesting that the deamination of products in the sequence competes with their transformation.

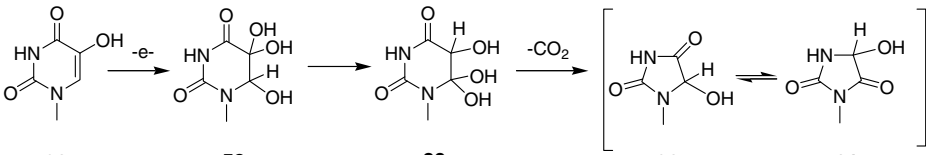

29 **59** **60** **30** **61**

SCHEME 3.8. One-electron oxidation reactions of 5-hydroxy-2′-deoxyuridine (**29**).

The isodialuric acid product **59** transforms into the dialuric acid nucleoside **60** after 2 h at 37°C in neutral aqueous solution.[75,76] The transformation of **59** takes place in a stereospecific manner, indicating a mechanism involving a α-hydroxyketone rearrangement with a concerted transfer of a proton from C6 to C5. In turn, **60** subsequently transforms, after 72 h at 37°C, into an equilibrium of four products including two diastereomers of the hydantoin product **30** and two diastereomers of the isohydantoin product **61**.[75,76] The mechanism of decomposition of **60** probably involves initial ring opening between N1 and C6 followed by decarboxylation from an intermediate ureid, which contains a terminal α-hydroxycarboxylic acid group. In contrast, the formation of the hydantoin product **30** from the $OH^{\bullet}$-induced oxidation of pyrimidine nucleosides **1**,**17** may also take place by another pathway involving the decomposition of intermediate 6-hydroxy-5-hydroperoxides.[24,33] The isomerization of **30** to **61**, and vice versa, may be accounted for by three possible reactions: (1) α-hydroxyketone rearrangement, (2) ring-chain tautomerism at N1–C5, and (3) ring-chain tautomerism at N3–C4. When the individual diastereomers were incubated at 37°C for 72 h under neutral conditions, they predominantly transformed into the corresponding diastereomer resulting from α-hydroxyketone rearrangement (80%), whereas the diastereomers resulting from ring-chain tautomerism were formed to a lesser extent (20%).

Treatment of trimers as well as longer oligonucleotides (<15 mer) containing 5-hydroxyuracil (**29**) with Na_2IrCl_6 led to the quantitative conversion of **29** to isodialuric acid (**59**) as inferred by MALDI-TOF analysis of the intact oligonucleotide.[77] Interestingly, whereas the fully hydrated form of the isodialuric acid product (**59**) exists as free nucleosides in aqueous solution, the dehydrated carbonyl form prevails in double-stranded DNA oligomers. Similar to the modified nucleoside, a trimeric oligonucleotide that contains **59** was observed to undergo a series of transformation from **59** to **60** and then at later times appeared to reach an equilibrium with the hydantoin products **30** and **61** as monitored by HPLC. The estimated half-life of **59** in the trimer was 10 h at pH 7 and 25°C. The preparation of oligonucleotides containing **59** permitted an initial assessment of its stability and DNA repair. Alkali treatment (30 min in 1 M piperidine) of DNA oligomers (15-mers) containing **59** led to complete cleavage of the phosphodiester bond next to the modification consistent with β,δ-elimination. The study of *in vitro* DNA repair with double-stranded DNA oligomers (15 mers) demonstrated that **59** was a substrate for *N*-glycosylases from *E. coli* [including formamidopyrimidine DNA *N*-glycosylase (Fpg), endonuclease III (endo III), and, to a lesser extent, endonuclease VIII (endo VIII)] and for homologous enzymes from *Saccharomyces cerevisiae* (including yNTG1 and NTG2), whereas no repair activity was observed with yOGG1.

3.3.2. 8-Oxo-7,8-dihydroguanine

8-Oxo-7,8-dihydroguanine (**48**), a ubiquitous oxidation product of DNA in cells, is highly susceptible to a wide variery of one-electron oxidation agents, including inorganic and organic radicals, peroxyl radicals, high-valent chromium complex, triplet ketones, oxyl radicals, and type I photosensitizers.[14,78,79] This may be

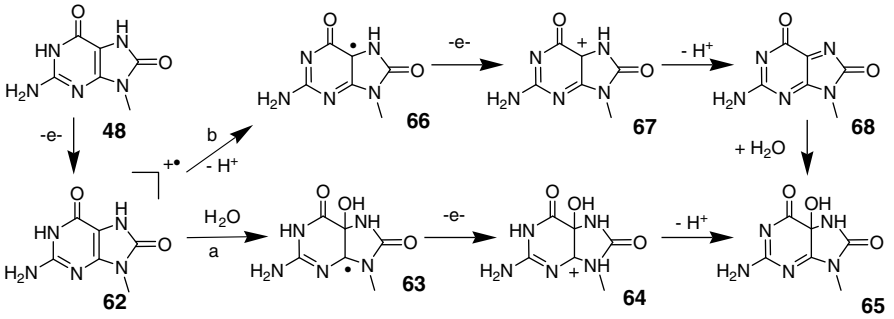

SCHEME 3.9. One-electron oxidation of 8-oxo-7,8-dihydro-2′-deoxyguanosine.

accounted for by the low redox potential of **48** (0.74 V versus NHE)[7] in comparison with that of **42** (1.29 versus NHE).[62] Detailed information is now available on (a) the degradation pathways of the resulting radical cations, whose pK_a is 6.6, and (b) 8-oxo-7,8-dihydroguanine's deprotonated neutral radical, whose chemistry mimics, at least partly, that of related guanine radicals. Thus, hydration of the radical cation **62** will likely generate 5-hydroxy-4-yl radical **63** that upon one-electron oxidation gives rise to 2-amino-5-hydroxy-7,9- dihydropurine-6,8-dione (**65**)[80] after deprotonation of the cationic intermediate **64** (Scheme 3.9), pathway a). An alternative reaction scheme (Scheme 3.9), pathway b), which is kinetically favored over pathway a on the basis of extensive DFT theoretical calculations,[81] may also explain the formation of **65**. Pathway b involves the initial deprotonation of **62**, leading to neutral radical **66** that upon one-electron oxidation and subsequent deprotonation of the resulting cation **67** is expected to generate a quinonoid intermediate (**68**). The addition of a water molecule across the 5,7 double bond of **68** leads to **65**, which was unambiguously characterized by low-temperature ^{1}H and ^{13}C NMR as a singlet oxygen product of a suitably derivatized ribonucleoside derivative of **48**.[82] It may be added that nucleophilic addition to either the cation (**64**, pathway a) or the quinonoid compound (**68**, pathway b) received further support from the isolation of addition products at C5 of the purine ring with several amino- and hydroxy-substituted compounds including spermidine, lysine, and tyrosine.[83] Intermediate **63** and related substituted compounds at C5 were found to be unstable at room temperature, undergoing two types of pH-dependent rearrangements as proposed by DFT studies. At neutral and slightly alkaline pH, the formation of the two diastereomers of spiroiminodihydantoin (**71**) (Scheme 3.10), whose absolute configuration is still a matter of debate,[84] was favored for both free nucleosides and oligonucleotides. It was recently proposed that the formation of **71** may be rationalized in terms of initial deprotonation of the hydroxyl group of **65** to generate **69**, which subsequently is converted into **70** through a 1,2-acyl shift mechanism. Under acidic conditions (pH < 6.5), cleavage of N1–C6 pyrimidine bond (**72**) appears to be the preferential route giving rise to a guanidinohydantoin compound (**75**) as a mixture of two diastereomers. This requires decarboxylation of the resulting open pyrimidine base (**73**) prior and subsequent to the tautomerization of **74**.

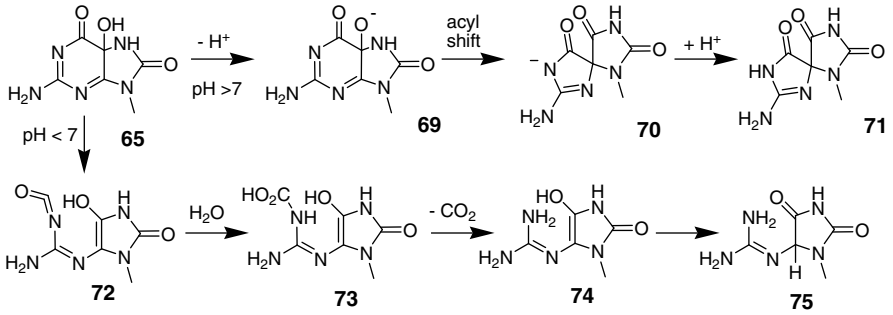

SCHEME 3.10. pH-dependent decomposition reaction of **65**.

Evidence has been provided for the reaction of oxidizing radicals **66** obtained by 2-aminopurine-mediated bi-photonic electron abstraction from **48** in DNA fragments on the one hand and $O_2^{\bullet -}$ formed by quenching of photo-ejected electrons with molecular oxygen on the other hand.[85] The rate constant of the reaction of $O_2^{\bullet -}$ with **66** was determined by flash photolysis to be $(1.3 \pm 0.2) \times 10^8\,M^{-1}\,s^{-1}$ and $(1.0 \pm 0.5)\,x\,10^8\,M^{-1}\,s^{-1}$ in single- and double-stranded DNA, respectively.[86] The dehydrated guanidinohydantoin **78** is generated through opening of the 5,6 bond of the resulting 5-hydroperoxide **76** followed by decarboxylation of **77** to give **78**. The transformation of unstable **78** into oxaluric acid (**82**) has been established for the monosubstituted isomer of oxaluric acid once **78** is generated by specific singlet oxygen oxidation of an 8-oxoGua-containing 15-mer. It was shown that the incubation of modified oligonucleotides leads to the quantitative conversion of **78** into **82**, which may be accounted for by the initial formation of carbinolamine **79**. In a subsequent step, tautomerization of **79** gives rise to parabanic acid (**81**) with the concomitant release of guanidine **80** (Scheme 3.11). In turn, the hydrolysis of **81** occurs in a specific way by cleavage of the 1,5 bond to generate **82**.[87, 88] A competitive degradation pathway of 5-hydroperoxide, shown to be favored at alkali pH, appears to be at the origin of the formation of imidazolone (**46**), through an as yet not fully identified mechanism. These few examples illustrate the complexity in chemical terms of purine radicals derived from the one-electron oxidation of **48**. If O_2 is not able to

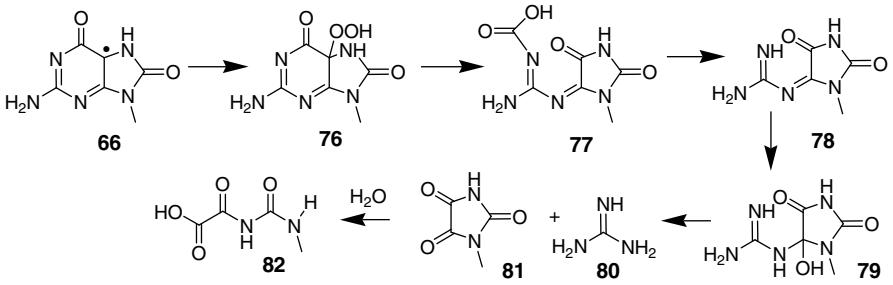

SCHEME 3.11. Proposed mechanism of formation of oxaluric acid (**82**) upon one-electron oxidation of **44** in oligonucleotides.

significantly react with **62** ($k < 10^2\ M^{-1}\ s^{-1}$), C5 adducts may be observed in the presence of either $CO_3^{\bullet -}$ or $NO_2^{\bullet}$,[89] which are both decomposition radicals of nitrosoperoxycarbonate, the product of the reaction of peroxynitrite and bicarbonate.

The reactivity of 8-oxo-7,8-dihydroguanine (**48**) residues toward various oxidizing agents was investigated in defined DNA fragments with different sequence contexts.[90] Thus, when **48** was stacked in a duplex with a 3′ neighboring guanine, it was more susceptible to one-electron oxidation than the other possible doublets involving the three other normal bases. This finding, which parallels the previously observed higher reactivity of the 5′ guanine in a GG doublet toward one-electron oxidants, is in agreement with *ab initio* calculations of the ionization potential of nucleobases. Insight into the one-electron oxidation at distant 8-oxo-7,8-dihydroguanine (**48**) residues in duplex DNA was gained from a time-resolved photolysis study using inserted 2-aminopurine (AP) as the one-electron oxidant.[89] The rate constants of electron transfer between the deprotonated radical cation of the photosensitizer and **48** were found to be strongly dependent on the distance between the two targeted bases. The rate constant for AP and **48** separated by two molecules of thymidine (**1**) was estimated to be $3.8 \pm 0.5 \times 10^4\ s^{-1}$. Interestingly, the rate was found to decrease by more than 10-fold with the presence of four intervening nucleosides **1**.[89]

3.4. ONE-ELECTRON OXIDATION REACTIONS OF CELLULAR DNA

It may be pointed out as a general remark that the measurement of oxidatively generated base lesions in cellular DNA has been hampered until recently by the use of inappropriate methods. As a typical example, application of the GC-MS assay for more than 15 years led to an overestimation of the measured level of DNA lesions, particularly with respect to ubiquitous 8-oxo-7,8-dihydro-2′-deoxyguanosine (**48**), by two to three orders of magnitude.[1f] Use of the more reliable HPLC with either electrochemical detection[91] or tandem mass spectrometry technique,[92] combined with optimized conditions of DNA extraction that minimize adventitious metal-mediated oxidation of normal DNA bases,[93] represents a suitable alternative as shown by the cooperative efforts of ESCODD network.[94]

3.4.1. Primary Oxidation Pathways

Only a few examples of one-electron oxidation reactions of cellular DNA are available in contrast to the more abundant literature concerning oxidative pathways mediated by $OH^{\bullet}$ and $^1O_2$.[1f] This is partly due to the difficulty of specifically inducing ionization processes in the absence of reactive oxygen species such as $OH^{\bullet}$. Thus, potassium bromate ($KBrO_3$), a renal carcinogen, when reduced by thiol compounds, such as glutathione and cysteine, was shown to preferentially oxidize 5′-guanine in GG and GGG of double-stranded DNA fragments.[95] These results are a strong indication for the one-electron oxidation of guanine, since neither $OH^{\bullet}$ nor $^1O_2$ exhibits the same specificity. This conclusion received further support from the observation that the incubation of mammalian cells with $KBrO_3$ in the presence of GSH induced

the predominant formation of Fpg-sensitive sites, mostly 8-oxo-7,8-dihydro-2′-deoxyguanosine (**48**) as detected by HPLC with electrochemical detection, which was more abundant than either DNA strand breaks or endonuclease III type lesions.[96] Pretreatment of mice with buthionine-(*S*,*R*)-sulfoximine, a GSH-depleting agent, was found to increase the levels of **48** in both kidney and liver DNA upon exposure to $KBrO_3$.[97] These various observations are in agreement with the formation of a reactive intermediate such as BrO_2, a reduction product of BrO_3^- that is able to abstract one electron from guanine. However, further work is required to substantiate this possibility or to assess the eventual role of other species, such as $BrO^\bullet$ or $Br^\bullet$.[98]

Another way to generate guanine radical cation **43** and other one-electron oxidized base intermediates in cellular DNA involves photolysis with high intensity 266-nm nanosecond pulses. Detailed model studies have shown that UVC laser irradiation of free nucleosides and isolated DNA induces efficient bi-photonic photoionization of purine and pyrimidine nucleobases. This may be accounted for by subsequent UV photon absorption of nucleobases in their triplet state generated within the duration of the UV pulse.[9] The overall energy level of the excited species thus generated is higher than the ionization threshold, and as a result, base radical cations are produced. Exposure of THP1 neoplastic human monocytes to nanosecond UVC pulses led to the predominant formation of **48** as measured by HPLC-MS/MS.[99] In addition, smaller amounts of three other oxidized nucleosides, including 5,6-dihydroxy-5,6-dihydrothymidine (**7**), 5-(hydroxymethyl)-2′-deoxyuridine (**15**) and 5-formyl-2′-deoxyuridine (**16**) were also detected albeit their overall formation represented only 10% of the amount of **48**. The distribution pattern of photooxidized nucleosides is not consistent with any significant contribution of $OH^\bullet$ to the molecular effects of laser irradiation since this radical induces higher levels of damage to thymine (**1**) than to guanine (**42**).[92a,100] Therefore, the photoinduced formation of **48** and **7** may be rationalized in terms of the hydration of initially generated guanine and thymine radical cations, respectively, followed by reaction pathways that have been depicted in previous sections. Competitive deprotonation of thymine radical cations followed by fast addition of O_2 to the resulting 5-methyl-centered thymine radicals is the sequence of reactions giving rise to **15** and **16** through the intermediacy of 5-(hydroperoxymethyl)uracil (**13**). The preferential formation of **48** is most likely explained in terms of charge transfer of initially generated purine and pyrimidine radical cations to guanine sites that act as sinks of positive holes as previously shown in model studies involving double-stranded DNA fragments.

3.4.2. Secondary Oxidation Reaction of 8-Oxo-7,8-dihydroguanine

The well-documented high susceptibility of 8-oxo-7,8-dihydroguanine (**48**) to one-electron oxidants has led one to consider the possible occurrence of secondary oxidation of this ubiquitous marker of oxidative stress. The previous characterization of diastereomeric spiroiminodihydantoin nucleosides **71** as the main degradation products of **48** in oligonucleotides at neutral pH has facilitated the development of HPLC-MS-based assays aimed at searching for a relevant marker of oxidation of **48** in DNA. Thus, the formation of **71** was observed in isolated DNA exposed to Cr(VI) in

the presence of ascorbic acid as a reducing agent.[101] In a subsequent study, again using HPLC-MS measurements performed in the selective ion monitoring mode, six residues of oxidized nucleosides **71** per 10^3 guanines were detected in the DNA of chromate-treated TK3D11 *E. coli* cells deficient in Nei,[102] the base excision repair enzyme able to excise **71**. This amount of damage is about 20-fold higher than the yield determined in wild bacterial cells while the level of **48**, the likely precursor of **71**, is much lower in both cell types. From a kinetic point of view, however, taking into consideration the relative levels of **48** and **42** together with the reactivity of the two bases toward chromate ions, the secondary oxidation of **48** is likely to be a rare event unless the oxidant is located in close proximity to its target. A major concern is the questionable use of HPLC-MS, which is much less specific than MS/MS, for measuring low amounts of modified nucleosides due to the lack of specificity of SIM detection under these conditions and thus the possible presence of interfering compounds. In this respect, it may be noted that HPLC-MS/SIM measurements of several radiation-induced oxidized nucleosides, including **48**, **54**, and purine 5′,8-cyclonucleosides, in the DNA of human cells have led to overestimated values by factors varying between two and three orders of magnitude.[103] Therefore, it would be of interest to search for the formation of **71** using the HPLC-MS/MS technique as a more reliable analytical method.

It has also been suggested that due to the possible occurrence of hole migration within DNA, the presence of **48** may have a sacrificial role allowing protection of normal nucleobases against the damaging effects of one-electron oxidants.[104] However, this hypothesis has been recently questioned.[105] It is difficult to rationalize how **48**, with a frequency in human cells that does not exceed a few residues per 10^6, can be preferentially oxidized with respect to overwhelming nucleobases because efficient hole transfer processes within DNA helix are limited to distances of less than 20 bp, depending on the sequence.

3.5. CONCLUSIONS AND PERSPECTIVES

Comprehensive one-electron oxidation pathways are now available for the five main DNA bases and two oxidatively generated base lesions that exhibit low ionization potentials. This was inferred in most cases from extensive studies of transient base radical intermediates and characterization of final oxidation products using nucleobases and/or nucleosides as model compounds. However, the situation is more complex in DNA because of the occurrence of hole transfer, which may lead to a general redistribution of the initially generated radical damage from purine and pyrimidine bases to guanine sites. In addition, there is evidence that peroxyl radical generated at pyrimidine bases may induce the formation of tandem lesions by interacting with vicinal bases. There remains much work to assess the relative importance of the formation of single and tandem lesions in duplex DNA upon one-electron oxidation. Formation of oxidized bases mostly involving guanine has been shown to occur in cellular DNA upon exposure to one-electron oxidants. There is also a need for further studies to search more thoroughly for the formation of tandem lesions.

REFERENCES

1. (a) Cadet, J.; Berger, M.; Douki, T.; Ravanat, J.-L. Oxidative damage to DNA: Formation, measurement and biological significance. *Rev. Physiol. Biochem. Pharmacol.* **1997**, *131*, 1–87. (b) Cadet, J.; Douki, T.; Gasparutto, D.; Ravanat, J.-L. Oxidative damage to DNA: Formation, measurement and biochemical features. *Mutat. Res.* **2003**, *531*, 5–23. (c) Gimisis, T.; Cismas, C. Isolation, characterization, and independent synthesis of guanine oxidation products. *Eur. J. Org. Chem.* **2006**, 1351–1378. (d) Pratviel, G.; Meunier, B. Guanine oxidation: one- and two-electron reactions. *Chem. Eur. J.* **2006**, *12*, 6018–6030. (e) von Sonntag C. in *Free-Radical Induced DNA Damage and Its Repair. A Chemical Perspective*, Springer, Heidelberg, **2006**. (f) Cadet, J.; Douki, T.; Ravanat, J.-L. Oxidatively generated damage to the guanine moiety of DNA: Mechanistic aspects and formation in cells. *Acc. Chem. Res.* **2008**, *41*, 1075–1083.
2. (a) Chatgilialoglu, C., Ferreri, C.; Bazzanini, R.; Guerra, M.; Choi, S.-Y.; Emanuel, C. J.; Horner, J. H. Newcomb, M. Models of DNA C1′ radicals. Structural, spectral, and chemical properties of the thyminylmethyl radical and the 2′-deoxyuridin-1′-yl radical. *J. Am. Chem. Soc.* **2002**, *122*, 9525–9533. (b) Dedon, P.C. The chemical toxicology of 2-deoxyribose oxidation in DNA. *Chem. Res. Toxicol.* **2008**, *21*, 206–219.
3. Cadet, J., Ravanat, J.-L, Martinez, G.R., Medeiros, M.H.G., Di Mascio, P. Singlet oxygen oxidation of isolated and cellular DNA: Product formation and mechanistic insights. *Photochem. Photobiol.* **2006**, *82*, 1219–1225.
4. Girault, I.; Fort, S.; Molko, D.; Cadet, J. Ozonolysis of 2′-deoxycytidine: isolation and identification of the main oxidation products. *Free Radic. Res.* **1997**, *26*, 257–266.
5. (a) Dedon, P. C.; Tannenbaum, S. R. Reactive nitrogen species in the chemical biology of inflammation. *Arch. Biochem. Biophys.* **2004**, *423*, 12–22. (b) Niles, J. C.; Wishnok, J. S.; Tannenbaum, S. R. Peroxynitrite-induced oxidation and nitration products of guanine and 8-oxoguanine: structures and mechanisms of product formation. *Nitric Oxide* **2006**, *14*, 109–121. (c) Neeley, W. L.; Essigmann, J. M. Mechanisms of formation, genotoxicity, and mutation of guanine oxidation products. *Chem. Res. Toxicol.*, **2006**, *19*, 491–505.
6. (a) Masuda, M.; Suzuki, T.; Friesen, M. D.; Ravanat, J.-L.; Cadet, J.; Pignatelli, B.; Nishino, H.; Ohshima, H. Chlorination of guanosine and other nucleosides by hypochlorous acid and myeloperoxidase of activated human neutrophils. Catalysis by nicotine and trimethylamine. *J. Biol. Chem.* **2001**, *276*, 40486–40496. (b) Badouard, C.; Masuda, M.; Nishino, H.; Cadet, J.; Favier, A.; Ravanat, J.-L. Detection of chlorinated DNA and RNA nucleosides by HPLC coupled to tandem mass spectrometry as potential biomarkers of inflammation. *J. Chromatogr. B* **2005**, *827*, 26–31.
7. Steenken, S.; Jovanovic, S. V. How easily oxidizable is DNA? One-electron reduction potentials of adenosine and guanosine radicals in aqueous solutions. *J. Am. Chem. Soc.* **1997**, *119*, 617–618.
8. (a) Becker, D.; Sevilla, M. *Adv. Radiat. Biol.* **1993**, *17*, 121–180. (b) Symons, M. C. R. Electron-spin-resonance studies of radiation-damage to DNA and proteins. *Radiat. Phys. Chem.* **1995**, *45*, 837–845. (c) Debije, M.G.; Bernhard, W. A. Free radical yields in crystalline DNA X-irradiated at 4K. *Radiat. Res.* **1999**, *152*, 583–589. (d) Adhikary, A.; Kumar, A.; Becker, Sevilla, M. D. The guanine cation radical: investigation of deprotonation states by ESR and DFT. *J. Phys. Chem B* **2006**, *110*, 24171–24180.
9. (a) Angelov, D.; Spassky, A.; Berger, M. Cadet, J. High-intensity UV laser photolysis of DNA and purine 2′-deoxyribonucleosides: Formation of 8-oxopurine damage and

oligonucleotide strand cleavage as revealed by HPLC and gel electrophoresis studies. *J. Am. Chem. Soc.* **1997**, *119*, 11373–11360. (b) Douki, T.; Angelov, D.; Cadet, J. UV laser photolysis of DNA: Effect of duplex stability on charge transfer efficiency. *J. Am. Chem. Soc.* **2001**, *123*, 11360–11366.

10. Cadet, J.; Vigny, P. The photochemistry of nucleic acids. In *Bioorganic Photochemistry, Photochemistry and the Nucleic Acid*, Vol. *1;* Morrison, H., Ed.; John Wiley & Sons, New York, 1990, pp. 1–272.
11. (a) Fisher, G. J.; Land, E. J. Photosensitization of pyrimidines by 2-methylnaphthoquinone in water: A laser flash photolysis study. *Photochem. Photobiol.* **1983**, *37*, 27–32. (b) Wagner, J. R.; van Lier, J. E.; Johnston, L. J. Quinone sensitized electron transfer photooxidation of nucleic acids: Chemistry of thymine and thymidine radical cations in aqueous solution. *Photochem. Photobiol.* **1990**, *52*, 333–343.
12. Schuster, G. B. Long-range charge transfer in DNA: Transient structural distortions control the distance dependence. *Acc. Chem. Res.* **2000**, *33*, 2253–2260.
13. Delatour T.; Douki, T.; D'Ham C.; Cadet, J. Photosensitization of thymine nucleobase by benzophenone through energy transfer, hydrogen abstraction and one-electron oxidation. *J. Photochem. Photobiol. B: Biol.* **1998**, *44*, 191–198.
14. Cadet, J.; Douki, T.; Ravanat, J.-L. The human genome as a target of oxidative modification: Damage to nucleic acids. In *Redox–Genome Interactions in Health and Disease*; Fuchs, J.; Podda, M.; Packer, L., Eds.; Marcel Dekker, New York, 2004, pp. 145–192.
15. Joffe, A.; Geacintov, N.E.; Shafirovich, V. DNA lesions derived from the site selective oxidation of guanine by carbonate radical anions. *Chem. Res. Toxicol.* **2003**, *16*, 1528–1538.
16. Medinas, D. B.; Cerchiaro, G.; Trindale, D. F.; Augusto, O. The carbonate radical and related oxidants derived from bicarbonate buffer. *IUBMB Life* **2007**, *59*, 255–262.
17. (a) Giese, B.; Amaudrut, J.; Köhler, A.-K.; Spormann, M.; Wessely, S. Direct observation of hole transfer through DNA by hopping between adenine bases and by tunnelling. *Nature* **2001**, *412*, 318–320. (b) Boon, E. M.; Barton, J. K. Charge transfer in DNA. *Curr. Opin. Struct. Biol.* **2002**, *12*, 320–329. (c) Roginskaya, M.; Bernhard, W.A.; Razskazovskiy, Y. Diffusion approach to long distance charge migration in DNA: Time dependent and steady-state analytical solutions for the product yield. *J. Phys. Chem. B* **2004**, *108*, 2432–2437. (d) Osakada, Y.; Kawai, K.; Fujitsuka, M.; Majima, T. Charge transfer through DNA nanoscaled assembly programmable with DNA building blocks. *Proc. Natl. Acad. Sci. USA* **2006**, *103*, 18072–18076.
18. Debje, M. G.; Close, D. M.; Bernhard, W. A. Reductive damage in directly ionized DNA: saturation of the C5–C6 bond of cytosine in $d(CGCG)_2$ crystals. *Radiat. Res.* **2002**, *157*, 235–242.
19. (a) Swarts, S. G.; Becker, D.; Sevilla, M.; Wheeler, K. T. *Radiat. Res.* **1996**, *145*, 304–314. (b) Shaw, A. A.; Cadet, J. Radical combination processes under the direct effect of gamma radiation on thymidine. *J. Chem. Soc. Perkin Trans. 2* **1990**, 2063–2070. (c) Gromova, M.; Balanzat, E.; Gervais, B.; Nardin, R.; Cadet, J. The direct effect of heavy ions and electrons on thymidine in the solid state. *Int. J. Radiat. Biol.* **1998**, *74*, 81–97. (d) Gromova, M.; Nardin, R.; Cadet, J. Direct effects of heavy ions and electrons on 2′-deoxyguanosine in the solid state. *J. Chem. Soc. Perkin Trans. 2* **1998**, 1365–1374. (c) Swarts, S. G.; Gilbert, D. C.; Sharma, K. K.; Razskazovskiy, Y.; Purkayastha, S.; Naumenko, K. A.; Bernhard, W. A. Mechanisms of direct radiation damage in DNA, based on a study of the yields of base damage, deoxyribose damage, and trapped radicals in d(GCACGCGTGC)2, *Radiat. Res.* **2007**, *168*, 367–381.

20. Greenberg, M. M. Pyrimidine nucleobase radical reactivity. Chapter 5, present volume.
21. Krishna, C. M.; Decarroz, C., Wagner, J. R.; Cadet, J.; Riesz, P. Menadione sensitized photooxidation of nucleic acid and protein constituents. An ESR and spin-trapping study. *Photochem. Photobiol.* **1987**, *46*, 175–182.
22. (a) Decarroz, C.; Wagner, J. R.; van Lier, J. E.; Krishna, C. M.; Riesz, P.; Cadet, J. Sensitized photo-oxidation of thymidine by 2-methyl-1,4-naphthoquinone. Characterization of the stable photoproducts. *Int. J. Radiat. Biol.* **1986**, *50*, 491–505; (b) Wagner, J. R.; van Lier, J. E.; Decarroz, C.; Berger, M.; Cadet, J. Photodynamic methods for oxy radical-induced DNA damage. *Methods Enzymol*. **1990**, *186*, 502–511.
23. Isildar, M.; Schuchmann, M. N.; Schulte-Frohlinde, D.; von Sonntag, C. V. Oxygen uptake in the radiolysis of aqueous solutions of nucleic acids and their constituents. *Int. J. Radiat. Biol.* **1982**, *41*, 525–533.
24. Wagner, J. R.; van Lier, J. E.; Berger, M.; Cadet, J. Thymidine hydroperoxides, structural assignment, conformational features and thermal decomposition in water. *J. Am. Chem. Soc.* **1994**, *116*, 2235–2242.
25. (a) Cadet, J.; Ducolomb, R..; Téoule, R. Préparation, isomérisation et configuration absolue des hydrates de thymidine. *Tetrahedron* **1977**, *33*, 1603–1607. (b) Cadet, J.; Ducolomb, R.; Hruska, F. E. Proton magnetic resonance studies of 5,6-saturated thymidine derivatives produced by ionizing radiation. Conformational studies of 6-hydroxylated diastereoisomers. *Biochim. Biophys. Acta* **1979**, *563*, 206–215.
26. Jolibois, F.; D'Ham, C.; Grand, A.; Subra, R.; Cadet, J. Cis-5-Hydroperoxy-6-hydroxy-5,6-dihydrothymine crystal structure and theoretical investigations of the electronic properties by DFT. *J. Mol. Struct. (Theochem)* **1998**, *427*, 143–155.
27. Russell, G. A. Deuterium-isotope effects in the autoxidation of aralkyl hydrocarbons. Mechanisms of the interaction of peroxy radicals. *J. Am. Chem. Soc.* **1957**, *79*, 3871–3877.
28. Wagner, J. R; Cadet, J.; Fisher, G. J. Photo-oxidation of thymine sensitized by 2-methyl-1,4-naphthoquinone: Analysis of products including three novel photodimers. *Photochem. Photobiol.* **1984**, *40*, 589–597.
29. Miyamoto, S.; Marques, S. A.; Retton, D.; Augusto, O.; Medeiros, M. H; Di Mascio, P. Linoleic acid hydroperoxide reacts with hypochlorous acid to generate peroxyl radical intermediate and singlet oxygen. *Proc. Natl. Acad. Sci. USA* **2006**, *103*, 293–298.
30. (a) Douki, T.; Cadet, J. Modification of DNA bases by photosensitized one-electron oxidation. *Int. J. Radiat. Biol.* **1999**, *75*, 571–581. (b) Gosh, A.; Joy, A.; Schuster, G. B.; Douki, T.; Cadet, J. Selective one-electron oxidation of duplex DNA oligomers: Reaction at thymines. *Org. Biomol. Chem.* **2008**, *6*, 916–928.
31. Frelon, S.; Douki, T.; Ravanat, J.-L.; Pouget, J.-P.; Tornabene, C.; Cadet, J. High performance liquid chromatography—Tandem mass spectrometry measurement of radiation-induced base damage to isolated and cellular DNA. *Chem. Res. Toxicol.* **2000**, *13*, 1002–1010.
32. Saito, I.; Takayama, M.; Kawanishi, S. Photoactivable DNA-cleaving amino acids: High sequence-selective DNA photocleavage by novel L-lysine derivatives. *J. Am. Chem. Soc.* **1995**, *117*, 5590–5591.
33. Wagner, J. R.; Decarroz, C.; Berger, M.; Cadet, J. Hydroxyl radical-induced decomposition of 2′-deoxycytidine in aerated aqueous solutions. *J. Am. Chem. Soc.* **1999**, *121*, 4101–4110.

34. Decarroz, C.; Wagner, J. R.; Cadet, J. Specific deprotonation reactions of the pyrimidine radical cation resulting from menadione mediated photosensitization of 2′-deoxycytidine. *Free Rad. Res. Commun.* **1987**, *2*, 295–301.

35. Labet, V., Grant, A., Cadet, J., Eriksson, L. A. Deamination of the radical cation of the base moiety of 2′-deoxycytidine: A theoretical study. *ChemPhysChem* **2008**, *9*, 1195–1203.

36. (a) Urata, H.; Yamamoto, K.; Akagi, M.; Hiroaki, H.; Uesugi, S. A 2-deoxyribonolactone-containing nucleotide: Isolation and characterization of the alkali-sensitive photoproduct of the trideoxyribonucleotide d(ApCpA). *Biochemistry* **1989**, *28*, 9566–9569. (b) Roupioz, Y.; Lhomme, J.; Kotera, M. Chemistry of the 2-deoxyribonolactone lesion in oligonucleotides: cleavage kinetics and products analysis. *J. Am. Chem. Soc.* **2002**, *124*, 9129–9135. (c) Xue, L.; Greenberg, M. M. Use of fluorescence sensors to determine that 2-deoxyribonolactone is the major alkali-labile deoxyribose lesion produced in oxidatively damaged DNA. *Angew. Chem. Int. Ed. Engl.* **2007**, *46*, 561–564.

37. Schweibert, M.C; Daniels, M. ^{60}Co gamma-ray-induced peroxidation of DNA in aqueous solution. *Int. J. Radiat. Phys. Chem.* **1971**, *3*, 353–366.

38. (a) Tremblay, S.; Wagner, J. Dehydration, deamination, and enzymatic repair of cytosine glycols from oxidized poly(dC-dG) and poly(dC-dI). *Nucleic Acids Res.* **2008**, *36*, 284–293. (b) Tremblay, S.; Douki, T.; Cadet, J.; Wagner, J. R. 2′-Deoxycytidine glycols, a missing link in the free radical-mediated oxidation of DNA. *J. Biol. Chem.* **1999**, *274*, 20833–20838.

39. Tremblay, S.; Gantchev, T.; Tremblay, L.; Lavigne, P.; Cadet, J.; Wagner, J. R. Oxidation of 2′-deoxycytidine to four interconverting diastereomers of N-1-carbamoyl-4,5-dihydroxy-2-oxoimidazolidine nucleosides. *J. Org. Chem.* **2007**, *72*, 3672–3678.

40. (a) Polverelli, M.Modification radio-induites de la cytosine en solution aqueuse aérée et après irradiation gamma *d'Escherichia coli*, Thesis Université Joseph Fourier, Grenoble, **1983**. (b) Leonard, N. J., Wiemer, D. F. Synthesis of cytosine radiolysis products: *cis*- and *trans*-1-carbamoyl-4,5-dihydroxyimidazolidin-2-one. *J. Am. Chem. Soc.* **1976**, *98*, 8218–8221.

41. (a) Paul, C. R.; Arakali, A. V.; Wallace, J. C.; McReynolds, J.; Box, H. C. Radiation chemistry of 2′-deoxycytidylyl-'3′-5′)-2′-deoxyguanosine and its sequence isomer in N_2O and O_2-saturated solutions. *Radiat. Res.* **1987**, *112*, 464–477. (b) Wagner, J. R.; Blount, B. C.; Weinfeld, M. Excision of oxidative cytosine modifications from gamma irradiated DNA by *Escherichia coli* endonuclease III and human whole cell extracts. *Anal. Biochem.* **1996**, *233*, 73–86. (c) Paul, C. R.; Wallace, J. C.; Alderfer, J. L.; Box, H. C. Radiation chemistry of d(TpApCpG) in oxygenated solutions. *Int. J. Radiat. Biol.* **1988**, *54*, 403–415.

42. Bienvenu, C.; Wagner, J. R.; Cadet, J. Photosensitized oxidation of 5-methyl-2′-deoxycytidine by 2-methyl-1,4-naphthoquinone—Characterization of 5-(hydroperoxymethyl)-2′-deoxycytidine and stable methyl group oxidation products. *J. Am. Chem. Soc.* **1996**, *118*, 11406–11411.

43. Bienvenu, C.; Cadet, J. Synthesis and kinetic study of the deamination of the cis diastereomers of 5,6-dihydroxy-5,6-dihydro-5-methyl-2′-deoxycytidine. *J. Org. Chem.* **1996**, *61*, 2632–2637.

44. (a) Bareyt, S.; Carell, T. Selective detection of 5-methylcytosine sites in DNA. *Angew. Chem. Int. Engl. Ed.* **2008**, *47*, 181–184. (b) Tanabe, K.; Yamada, H.; Nishimoto, S. One-electron photooxidation and site-selective strand cleavage at 5-methylcytosine in DNA by

sensitization with 2-methyl-1,4-naphthoquinone-tethered oligonucleotides. *J. Am. Chem. Soc.* **2007**, *129*, 8034–8040.

45. (a) Cadet, J.; Berger, M.; Buchko, G. W.; Joshi, P.; Raoul, S.; Ravanat, J.-L. 2,2-Diamino-4-(3,5-di-*O*-acetyl-2-deoxy-β-D-*erythro*-pentofuranosyl)amino]-5-(2*H*)-oxazolone: A novel and predominant radical oxidation product of 3′,5′-di-*O*-acetyl-2′-deoxyguanosine. *J. Am. Chem. Soc.* **1994**, *116*, 7403–7404. (b) Raoul, S.; Berger, M.; Buchko, G. W.; Joshi, P. C.; Morin, B., Weinfeld, M., Cadet, J. ^{1}H, ^{13}C and ^{15}N NMR analysis and chemical features of the two main radical oxidation products of 2′-deoxyguanosine: Oxazolone and imidazolone nucleosides. *J. Chem. Soc. Perkin Trans. 2* **1996**, 371–381.
46. Candeias, L. P.; Steenken, S. Reaction of $HO^{\bullet}$ with guanine derivatives in aqueous solution: formation of two different redox-active OH-adduct radical and their unimolecular transformation reactions. Properties of $G(-H)^{\bullet}$. *Chem. Eur. J.* **2000**, *6*, 475–484.
47. Kobayashi, K.; Tagawa, S. Direct observation of guanine radical cation deprotonation in duplex DNA using pulse radiolysis. *J. Am. Chem. Soc.* **2003**, *125*, 10213–10218.
48. Steenken, S. Purine bases, nucleosides, and nucleotides: aqueous solution redox chemistry and transformation reactions of their radical cations and e- and OH adducts. *Chem. Rev.* **1989**, *89*, 503–520.
49. Al-Sheikhly, M. The reactivity of adenyl and guanyl radicals towards oxygen. *Rad. Phys. Chem.* **1994**, *44*, 297–301.
50. Chatgiglialoglu, C.; Caminal, C.; Altieri, A.; Vougiokalakis, G. C.; Mulazzani, Q. G.; Gimisis, T.; Guerra, M. Tautomerism in the guanyl radical. *J. Am. Chem. Soc.* **2006**, *128*, 13796–13805.
51. Misiaszek, R.; Crean, C.; Joffe, A.; Geacintov N. E.; Shafirovich, V. Oxidative DNA damage associated with combination of guanine and superoxide radicals and repair mechanisms via radical trapping. *J. Biol. Chem.* **2004**, *279*, 32106–32115.
52. Vialas, C.; Pratviel, G.; Claparols, C.; Meunier, B. Efficient oxidation of 2′-deoxyguanosine by Mn-TMPyP/$KHSO_5$ to imidazolone dIz without formation of 8-Oxo-dG. *J. Am. Chem. Soc.* **1998**, *120*, 11548–11553.
53. Ravanat, J.-L., Saint-Pierre, C.; Cadet, J. One-electron oxidation of the guanine moiety of 2′-deoxyguanosine: Influence of 8-oxo-7,8-dihydroguanine. *J. Am. Chem. Soc.* **2003**, *125*, 2030–2031.
54. (a) Gasparutto, D.; Ravanat, J.-L.; Gérot, O.; Cadet, J. Characterization and chemical stability of photooxidized oligonucleotides that contain 2,2-diamino-4-[(deoxy-β-D-*erythro*-pentofuranosyl)-amino]-5(2*H*)-oxazolone. *J. Am. Chem. Soc.* **1998**, *120*, 10283–10286. (b) Kino, K.; Saito, I.; Sugyiama, H. Product analysis of GG-specific photooxidation of DNA via electron transfer: 2-aminoimidazolone as a major guanine oxidation product. *J. Am. Chem. Soc.* **1998**, *120*, 7373–7374.
55. Cullis, P. M., Malone, M. E., Merson-Davies, L. A. Guanine radical cations are precursors of 7,8-dihydro-8-oxo-2′-deoxyguanosine but are not precursors of immediate strand breaks in DNA. *J. Am. Chem. Soc.* **1996**, *118*, 2775–2781.
56. Buchko, G. W.; Cadet, J.; Ravanat, J.-L.; Labataille, P. Isolation and characterization of a new product produced by ionizing radiation and type I photosensitization of 2′-deoxyguanosine in oxygen-saturated aqueous solution: (2*S*)-2,5′-anhydro-1-(2′-deoxy-β-D-*erythro*-pentofuranosyl)-5-guanidinylidene-2-hydroxy-4-oxoimidazolidine. *Int. J. Radiat. Biol.* **1993**, *63*, 669–676.
57. (a) Morin, B.; Cadet, J. Type I benzophenone mediated nucleophilic reaction of 5′-amino-2′,5′-dideoxyguanosine. *Chem. Res. Toxicol.* **1995**, *8*, 792–799. (b) Morin, B.; Cadet, J.

Chemical aspects of the benzophenone photosensitized formation of two lysine-2′-deoxyguanosine crosslinks. *J. Am. Chem. Soc.* **1995**, *117*, 12408–12415.

58. Giese, B.; Spichy, M. Long-distance charge transport through DNA: Quantification and extension of the hopping model. *ChemPhysChem.* **2000**, *1*, 195–198.
59. Barnett, R. N.; Bongiorno, A.; Cleveland, C. L.; Joy, A.; Landman, U.; Schuster, G. B. Oxidative damage to DNA: Counterion-assisted addition of water to ionized DNA. *J. Am. Chem. Soc.* **2006**, *128*, 10795–10800.
60. Kasai, H.; Yamaizumi, Z.; Berger, M.; Cadet, J. Photosensitized formation of 7,8-dihydro-8-oxo-2′-deoxyguanosine (8-hydroxy-2′-deoxyguanosine) in DNA by riboflavin: A non-singlet oxygen mediated reaction. *J. Am. Chem. Soc.* **1992**, *114*, 9692–9694.
61. Munk, B. H.; Burrows, C. J.; Schlegel, H. B. Exploration of mechanisms for the transformation of 8-hydroxy guanine radical to FAPyG by density functional theory. *Chem. Res. Toxicol.* **2007**, *20*, 432–444.
62. Steenken, S.; Jovanovic, S. B.; Bietti, M.; Bernhard, K. The trap death (in DNA) of 8-oxo-7,8-dihydro-2′-deoxyguanosine as derived from electron transfer equilibria in aqueous solution. *J. Am. Chem. Soc.* **2000**, *122*, 2373–2374.
63. Douki, T.; Cadet, J. Modification of DNA bases by photosensitized one-electron oxidation. *Int. J. Radiat. Biol.* **1999**, *75*, 571–581.
64. Perrier, S.; Hau, J.; Gasparutto, D.; Cadet, J.; Favier, A.; Ravanat, J.-L. Characterization of lysine-guanine cross-links upon one-electron oxidation of a guanine-containing oligonucleotides in the presence of a trilysine peptide. *J. Am. Chem. Soc.* **2006**, *128*, 5703–5710.
65. Xu, X.; Muller, J. G.; Ye, Y.; Burrows, C. J. DNA-protein cross-links between guanine and lysine depend on the mechanism of oxidation for formation of C5 Vs C8 guanosine adducts. *J. Am. Chem. Soc.* **2008**, *130*, 703–709.
66. (a) Crean, C.; Uvaydov, Y.; Geacintov, N. E.; Shafirovich, V. Oxidation of single-stranded oligonucleotides by carbonate radical anions: Generating intrastrand cross-links between guanine and thymine bases separated by cytosines. *Nucleic Acids Res.* **2008**, *36*, 742–755. (b) Crean, C.; Geacintov, N. E.; Shafirovich, V. Intrastrand G-U cross-links generated by the oxidation of guanine in 5′-d(GCU) and 5′-r(GCU). *Free Radic. Biol. Med.* **2008**, 45, 1125–1134.
67. O'Neill, P.; Parker, A. W.; Plumb, M. A., Siebbeles, L. D. A. Guanine modifications following ionization of DNA occurs predominantly via intra- and not interstrand charge migration: An experimental and theoretical study. *J. Phys. Chem. B* **2001**, *105*, 5283–5290.
68. (a) Berger, M.; de Hazen, M.; Nejjari, A.; Fournier, J.; Guignard, J.; Pezerat, H.; Cadet, J. Radical oxidation reactions of the purine moiety of 2′-deoxyribonucleosides and DNA by iron-containing minerals. *Carcinogenesis* **1993**, *14*, 41–46. (b) Raoul, S.; Bardet, M.; Cadet, J. Gamma irradiation of 2′-deoxyadenosine in oxygen-free aqueous solutions: Identification and conformational features of formamidopyrimidine nucleoside derivatives. *Chem. Res. Toxicol.* **1995**, *8*, 924–933.
69. Frelon, S.; Douki, T.; Cadet, J. Radical oxidation of the adenine moiety of nucleoside and DNA: 2-hydroxy-2′-deoxyadenosine is a minor decomposition product. *Free Radic. Res.* **2002**, *36*, 499–508.
70. Wang, Y.; Liu, Z.; Dixon, C. Major adenine products from 2-methyl-1,4-naphthoquinone-sensitized photoirradiation at 365 nm. *Biochem. Biophys. Res. Commun.* **2002**, *91*, 1252–1257.

71. Wagner, J. R.; Hu, C. C.; Ames, B.N. Endogenous oxidative damage of deoxycytidine in DNA. *Proc. Natl. Acad. Sci. U.S.A.*, **1992**, *89*, 3380–3384.

72. Rivière, J.; Ravanat, J.L.; Wagner, J.R. Ascorbate and H_2O_2 induced oxidative DNA damage in Jurkat cells. *Free Rad. Biol. Med.* **2006**, *40*, 2071–2079.

73. Fujimoto, J.; Tran, L.; Sowers, L.C. Synthesis and cleavage of oligodeoxynucleotides containing a 5-hydroxyuracil residue at defined site. *Chem. Res. Toxicol.* **1997**, *10*, 1254–1258.

74. Wolfe, J. L.; Kawate, T.; Sarracino, D. A.; Zillmann, M.; Olson, J.; Stanton, V. P.; Verdine, G. L. A genotyping strategy based on incorporation and cleavage of chemically modified nucleotides. *Proc. Natl. Acad. Sci. U.S.A.* **2002**, *99*, 11073–11078.

75. Rivière, J.; Bergeron, F.; Tremblay, S.; Gasparutto, D.; Cadet, J.; Wagner, J.R. Oxidation of 5-hydroxy-2′-deoxyuridine into isodialuric acid, dialuric acid, and hydantoin products. *J. Am. Chem. Soc.* **2004**, *126*, 6548–6549.

76. Rivière, J.; Klarskov, K.; Wagner, J.R. Oxidation of 5-hydroxypyrimidine nucleosides to 5-hydroxyhydantoin and its alpha-hydroxy-ketone isomer. *Chem. Res. Toxicol.* **2005**, *18*, 1332–1338.

77. Simon, P.; Gasparutto, D.; Gambarelli, S.; Saint-Pierre, C.; Favier, A.; Cadet, J. Formation of isodialuric acid lesion within DNA oligomers via one-electron oxidation of 5-hydroxyuracil: Characterization, stability and excision repair. *Nucleic Acids Res.* **2006**, *34*, 3660–3669.

78. Joffe, A.; Geacintov, N. E.; Shafirovich, V. DNA lesions derived from the site selective oxidation of guanine by carbonate radical anions. *Chem. Res. Toxicol.* **2003**, *16*, 1528–1538.

79. Cadet, J.; Douki, T.; Ravanat, J.-L. Onet-electron oxidation of DNA and inflammation processes. *Nat. Chem. Biol.* **2006**, *2*, 348–349.

80. (a) Luo, W.; Muller, J. G.; Burrows, C.J. The pH-dependent role of superoxide in riboflavin-catalyzed photooxidation of 8-oxo-7,8-dihydroguanosine. *Org. Lett.* **2001**, *3*, 2801–2804. (b) Luo, W.; Muller, J. G.; Rachlin, E. M.; Burrows, C. J. Characterization of hydantoin products from one-electron oxidation of 8-oxo-7,8-dihydroguanosine in a nucleoside model. *Chem. Res. Toxicol.* **2001**, *14*, 927–938.

81. Munk, B. H.; Burrows, C. J.; Schlegel, H. B. An exploration of mechanisms for the transformation of 8-oxoguanine to guanidinohydantoin and spiroiminodihydantoin by density functional theory. *J. Am. Chem. Soc.* **2008**, *130*, 5245–5256.

82. McCallum, J. E.; Kuniyoshi, C. Y.; Foote, C. S. Characterization of 5-hydroxy-8-oxo-7,8-dihydroguanosine in the photosensitized oxidation of 8-oxo-7,8-dihydroguanosine and its rearrangement to spiroiminodihydantoin. *J. Am. Chem. Soc.* **2004**, *126*, 16777–16782.

83. (a) Hosford, M. E.; Muller, J. G.; Burrows, C. J. Spermine participates in oxidative damage of guanosine and 8-oxoguanosine leading to deoxyribosylurea formation. *J. Am. Chem. Soc.* **2004**, *126*, 9540–9541. (b) Johansen, M. E., Muller, J. G.; Xu, X.; Burrows, C. J. Oxidatively induced DNA-protein cross-linking between single-stranded binding protein and oligodeoxynucleotides containing 8-oxo-7,8-dihydro-2′-deoxyguanosine. *Biochemistry* **2005**, *44*, 5660–5671.

84. (a) Durandin, A.; Jia, L.; Crean, C.; Kolbanovskiy, A.; Ding, S.; Shafirovich, V.; Broyde, S.; Geacintov, N. E. Assignment of absolute configuration of the enantiomeric spiroiminodihydantoin nucleobase by experimental and computational optical rotatory dispersion methods. *Chem. Res. Toxicol.* **2006**, *19*, 908–913. (b) Karwowski, B.; Dupeyrat, F.; Bardet, M.; Ravanat, J.-L.; Krajewski, P.; Cadet, J. Nuclear magnetic resonance studies of

the 4*R* and 4*S* diastereomers of spiroiminodihydantoin 2′-deoxyribonucleosides: Absolute configuration and conformational features. *Chem. Res. Toxicol.* **2006**, *19*, 1357–1365.

85. Shafirovich, V.; Cadet, J.; Gasparutto, D.; Dourandin, A.; Huang, W.; Geacintov, N. E. Direct spectroscopic observation of 8-oxo-7,8-dihydro-2′-deoxyguanosine radicals in double-stranded DNA generated by one-electron oxidation at a distance by 2-aminopurine radicals. *J. Phys. Chem. B* **2001**, *105*, 586–592.
86. Misiaszek, R.; Uvaydov, Y.; Crean, C.; Geacintov, N. E.; Shafirovich, V. Combination reactions of superoxide with 8-oxo-7,8-dihydroguanine radicals in DNA: Kinetics and end products. *J. Biol. Chem.* **2005**, *280*, 6293–6300.
87. Buchko, G. W.; Cadet, J. Identification of the alpha and beta anomers of 1-(2-deoxy-D-erythro-pentofuranosyl)-oxaluric acid at the site of riboflavin-mediated photooxidation of guanine in 2′-deoxyguanosine and thymidylyl-(3′-5′)-2′-deoxyguanosine. *J. Photochem. Photobiol.* **2006**, *82*, 191–199.
88. Duarte, V.; Gasparutto, D.; Yamaguchi, Y. F.; Ravanat, J.-F.; Martinez, G. R.; Medeiros, M. H. G.; Di Mascio, P.; Cadet, J. Oxaluric acid as the major product of singlet oxygen-mediated oxidation of 8-oxo-7,8-dihydroguanine in DNA. *J. Am. Chem. Soc.* **2000**, *122*, 12622–12628.
89. Shafirovich, V.; Cadet, J.; Gasparutto, D.; Durandin, A.; Geracintov, N. E. Nitrogen dioxide as an oxidizing agent of 8-oxo-7,8-dihydro-2′-deoxyguanosine oxidation but not of 2′-deoxyguanosine. *Chem. Res. Toxicol.* **2001**, *14*, 233–241.
90. Hickerson, R. P.; Prat, F.; Muller, J. G.; Foote, C. S.; Burrows, C. J. Sequence and stacking dependence of 8-oxoG oxidation: Comparison of one-electron vs singlet oxygen mechanisms. *J. Am. Chem. Soc.* **1999**, *121*, 9423–9428.
91. (a) Floyd, R. A.; Watson, J. J.; Wong, P.K.; Atmiller, D. H.; Rickard, R. C. Hydroxyl free radical adduct of deoxyguanosine: Sensitive detection and mechanism of formation. *Free Rad. Res Commun.* **1986**, *1*, 163–172. (b) Kasai, H. Analysis of a form of oxidative DNA damage, 8-hydroxy-2′-deoxyguanosine, as a marker of cellular oxidative stress during carcinogenesis. *Mutat. Res.* **1997**, *387*, 147–163.
92. (a) Frelon, S.; Douki, T.; Ravanat, J.-L.; Pouget, J.-P.; Tornabene, C.; Cadet, J. High-performance liquid chromatography–tandem mass spectrometry measurement of radiation-induced base damage to isolated and cellular DNA. *Chem. Res. Toxicol.* **2000**, *13*, 1002–1010. (b) Singh, R.; McEwan, M.; Lamb, J.H.; Santella, R. M.; Farmer, P. B. An improved liquid chromatography/tandem mass spectrometry method for the determination of 8-oxo-7,8-dihydro-2′-deoxyguanosine in DNA samples using immunoaffinity column purification. *Rapid Commun. Mass Spectrom.* **2003**, *17*, 126–134.
93. Ravanat, J.-L.; Douki, T.; Duez, P.; Gremaud, E.; Herbert, K.; Hofer, T.; Lasserre, L.; Saint-Pierre, C.; Favier, A.; Cadet, J. Cellular background of 8-oxo-7,8-dihydro-2′-deoxyguanosine: An isotope based method to evaluate artefactual oxidation of DNA during its extraction and subsequent work-up. *Carcinogenesis* **2002**, *23*, 1911–1918.
94. (a) ESCODD. Measurement of DNA oxidation in human cells by chromatographic and enzymic methods. *Free Radic. Biol. Med.* **2003**, *34*, 1089–1099. (b) Collins, A. R.; Cadet, J.; Möller, L.; Poulsen, H. E.; Viña, J. Are we sure we know how to measure 8-oxo-7,8-dihydroguanine in DNA from human cells? *Arch. Biochem. Biophys.* **2004**, *423*, 57–65.
95. (a) Murata M., Bansho Y., Inoue S., Ito K., Ohnishi S., Midorikawa K., Kawanishi S. Requirement of glutathione and cysteine in guanine-specific oxidation of DNA by

carcinogenic potassium bromate. *Chem. Res. Toxicol.* **2001**, *14*, 678–685. (b) Kawanishi, S.; Murata, M. Mechanism of DNA damage induced by bromate differs from general types of oxidative stress. *Toxicology* **2006**, *221*, 172–178.

96. (a) Ballmaier, D.; Epe, B. Oxidative DNA damage induced by potassium bromate under cell-free conditions and in mammalian cells. *Carcinogenesis* **1995**, *16*, 335–342. (b) Ballmaier, D.; Epe, B. DNA damage by bromate: mechanism and consequences. *Toxicology* **2006**, *221*, 166–171.
97. Jałoszyński, P.; Murata, S.; Shinkai, Y.; Takahashi, S.; Kumagai, Y.; Nishimura, S.; Yamamoto, M. Dysfunction of Nrf2 decreases KBrO3-induced oxidative DNA damage in Ogg1-null mice. *Biochem. Biophys. Res. Commun.* **2007**, *364*, 966–971.
98. Chipman, J. K.; Parsons, J. L.; Beddowes, E. J. The multiple influences of glutathione on bromate genotoxicity: Implications for the dose–response relationship. *Toxicology* **2006**, *221*, 187–189.
99. Douki, T.; Ravanat, J.-L; Pouget, J.-P.; Testard, I.; Cadet, J. Minor contribution of direct ionization to DNA base damage induced by heavy ions. *Int. J. Radiat. Biol.* **2006**, *82*, 119–127.
100. Pouget, J. P.; Frelon, S.; Ravanat, J.-L.; Testard, I.; Odin, F.; Cadet, J. Formation of modified DNA to DNA in cells exposed to either gamma radiation or high-LET particles. *Radiat. Res.* **2002**, *157*, 589–595.
101. Slade, P. G.; Hailer, M. K.; Martin, B. D.; Sugden, K. D. Guanine-specific oxidation of double-stranded DNA by Cr(VI) and ascorbic acid forms spiroiminodihydantoin and 8-oxo-2′-deoxyguanosine. *Chem. Res. Toxicol.* **2005**, *18*, 1140–1149.
102. Hailer, M. K.; Slade, P. G.; Martin, B. D.; Sugden, K. D. Nei deficient *Escherichia coli* are sensitive to chromate and accumulate the oxidized guanine lesion spiroiminodihydantoin. *Chem. Res. Toxicol.* **2005**, *18*, 1378–1383.
103. (a) Tuo, J.; Jaruga, P.; Rodriguez, H.; Dizdaroglu, M.; Bohr, V. A. The Cockayne syndrome group B gene product is involved in cellular repair of 8-hydroxyadenine in DNA. *J. Biol. Chem.* **2002**, *277*, 30832–30837. (b) Tuo, J.; Jaruga, P.; Rodriguez, H.; Bohr, V. A.; Dizdaroglu, M. Primary fibroblasts of Cockayne syndrome patients are defective in cellular repair of 8-hydroxyguanine and 8-hydroxyadenine from oxidative stress. *FASEB J.* **2003**, *17*, 668–674.
104. (a) Friedman, K. A.; Keller, A. On the nonuniform distribution of guanine in introns of human genes: Possible protection of exons against oxidation by proximal introns poly-G sequences. *J. Phys. Chem. B* **2001**, *105*, 11859–11865. (b) Friedman, K. A.; Keller, A. Guanosine distribution and oxidation resistance in eight eukaryotic genomes. *J. Am. Chem. Soc.* **2004**, *126*, 2368–2371.
105. Kanvah, S.; Schuster, G. B. The sacrificial role of easily oxidizable sites in the protection of DNA from damage. *Nucleic Acids Res.* **2005**, *33*, 5133–5138.

4

REACTIVITY OF NUCLEIC ACID SUGAR RADICALS

CHRYSSOSTOMOS CHATGILIALOGLU
ISOF, Consiglio Nazionale delle Ricerche, 40129 Bologna, Italy

4.1. INTRODUCTION

Reactive oxygen species (ROS)—and, in particular, $OH^{\bullet}$ derived from the metabolism of oxygen[1]—are known to cause chemical modifications to DNA through the formation of strand breaks and nucleobase modifications. However, the majority of cells also possess defense mechanisms against oxidative damage, such as base excision repair (BER) and nucleotide excision repair (NER) enzymes, which remove these lesions to maintain the integrity of the genome.[2] Some of the lesions, particularly those due to poorly repaired oxidative damage, may accumulate in cells over time through errors in repair, replication, and recombination, and the levels of repair proteins may decrease with the cell aging.[3] In addition to the induction of DNA damage through the metabolism of oxygen, DNA damage may also be induced through other environmental insults such as ionizing radiation, UV light and chemical mutagens. Although the majority of DNA lesions induced through oxidative metabolism are single lesions, there are also types of multiple lesions such as tandem DNA lesions and clustered DNA damage that may challenge the repair machinery of the cell.

Diffusible hydroxyl radicals ($HO^{\bullet}$) are known to react with DNA either by hydrogen abstraction from the 2-deoxyribose units or by addition to the base moieties. The majority of $HO^{\bullet}$ attacks occur at the base moieties. However, there is growing evidence that the oxidation of 2-deoxyribose in DNA plays a critical role in the genetic toxicology of oxidative stress and inflammation.[4] The order of reactivity of $HO^{\bullet}$

Radical and Radical Ion Reactivity in Nucleic Acid Chemistry, Edited by Marc M. Greenberg

radical toward the various hydrogen atoms of the 2-deoxyribose moiety is currently under debate.[4] A proposed order that also parallels the exposure to solvent of the 2-deoxyribose hydrogen atoms (i.e., $H5' > H4' > H3' \approx H2' \approx H1'$) is generally accepted.[5] Indeed, the positioning of the C4′ and C5′ hydrogen atoms on the edge of the minor groove renders them accessible to diffusible species. Experimental data on the reaction of $HO^{\bullet}$ radicals with simple nucleosides like 2′-deoxyadenosine and 2′-deoxyguanosine indicated that ~25% of H-atom abstraction occurs at the sugar moiety, ~40% of which is at the H5′ position.[6] On the other hand, C1′-, C4′-, and C5′-hydrogen atoms are abstracted by several minor groove-binding molecules.[7–9]

Abstraction of a hydrogen atom from 2-deoxyribose produces a carbon-centered radical whose fate depends upon the environment. Many of the recent studies focus on the selective generation of these species that allowed quantitative data to be obtained. Although the chemistry of all possible sugar radicals (i.e., C1′, C2′, C3′ C4′, and C5′) from nucleosides to DNA will be discussed in this chapter, only the literature from the last ten years has been covered due to space limitations. The reader is referred to some excellent reviews[7–11] and books[12, 13] for more details of earlier work. The chemistry of 2-deoxyribose oxidation in DNA has its roots in the literature of ionizing radiation, as summarized in two books by von Sonntag.[12, 13]

4.2. OXIDATION OF THE C1′ POSITION

The 2-deoxyribonolactone lesion (or C1′-oxidized abasic site) results from oxidation of the C1′ position of DNA nucleotides and has been implicated in DNA strand scission, mutagenesis, and covalent cross-linking to DNA binding proteins.[3, 4] A variety of toxic agents have been shown to produce the deoxyribonolactone lesion, including enediyne antibiotics (e.g., neocarzinostatin chromophore, NCS), bis(phenanthroline) copper, cationic manganese porphyrins, oxoruthenium complexes, ultraviolet irradiation, and ionizing irradiation.[7–9, 11–13] The chemical mechanisms for oxidized abasic site generation by these agents have been the subject of intensive investigation. Although the details vary among damage reagents and conditions, central features of the damage process include hydrogen abstraction at the C1′ position, nucleotide oxygenation, and extrusion of the nucleobase to produce the 2-deoxyribonolactone (**L**) lesion in duplex DNA.

In the last decade, significant efforts have been devoted to creating a site-specific radical generating system and to the incorporation of the **L** lesion in duplex DNA. Significant developments have also increased our understanding of its biological implications.

4.2.1. Structural and Chemical Properties of C1′ Radicals

The specific generation of the C1′ radical has been achieved by two independent synthetic routes of the corresponding *tert*-butyl ketone **1** subjected to photoinduced cleavage (Scheme 4.1).[14, 15] The 2′-deoxyuridin-1′-yl radical, generated by photolysis of *tert*-butyl ketone **1** or **2** in water, was studied spectroscopically by electron

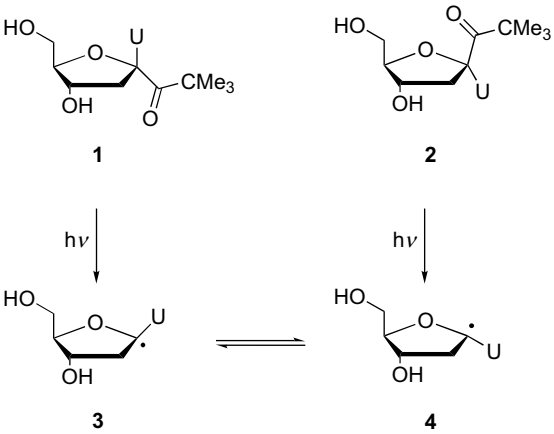

SCHEME 4.1

paramagnetic resonance (EPR) and laser flash photolysis (LFP) methods.[15, 16] DFT calculations at the UB3LYP/6-311G** level have also been carried out on this radical to obtain information on its structural properties and to assign the hyperfine coupling (hfs) constants determined by EPR and the optical transitions observed in the UV–vis region of the LFP spectrum.[15, 16] The radical center is not planar and the energy profile for the interconversion of the two anomeric forms **3** and **4** (Scheme 4.1) was determined computationally. A broad band in the region 290–370 nm with $\lambda_{max} = 320$ nm is characteristic of 2′-deoxyuridin-1′-yl radical. The vertical optical transitions {spin} SOMO $\rightarrow \pi^*$(uracil){α} and π(uracil) $\rightarrow$ SOMO{β} are computed at 296 nm (oscillator strength $f = 0.010$) and 378 nm ($f = 0.06$), respectively.[16]

The 2′-deoxyuridin-1′-yl radical abstracts hydrogen from β-mercaptoethanol, cysteine, and glutathione (GSH) with rate constants of 2.3×10^6, 2.9×10^6, and $4.4 \times 10^6\ M^{-1}\ s^{-1}$, respectively, to give a β:α anomeric ratio in the 1.3–2.0 range.[16] Since the β:α ratio was insensitive to the initial concentration of thiol and the precursor, it was suggested that the C-1′ radical rapidly inverts (Scheme 4.1) and that the β/α distribution depends on the degree of the shielding effect of the two γ-substituents in the sugar ring—that is, OH versus CH_2OH. The *tert*-butyl ketone **1** has been incorporated into oligonucleotide sequences and the reactivity of the C1′-nucleotide radical toward thiols has been addressed.[17] The β:α ratios were found to be about 4.2 and 6.5 for trapping of radical **5** (B = uracil) in single- and double-strand oligonucleotides, respectively, using β-mercaptoethanol (Scheme 4.2). This increase in stereoselectivity favors the restoration of the naturally occurring β-deoxynucleotide. It is worth mentioning that α-deoxynucleotides, produced during γ-radiolysis of DNA under anaerobic conditions, have shown to be premutagenic *in vitro*.[18, 19] It has been proposed that the C1′ radical **5** abstracts a hydrogen atom from a thiol to give a mixture of β-anomer **6** and α-anomer **7** (Scheme 4.2).

In the presence of O_2, radical **5** leads to abasic site damage with the formation of the 2-deoxyribonolactone residue **10**.[4, 8, 11, 20] The reaction of selectively generated

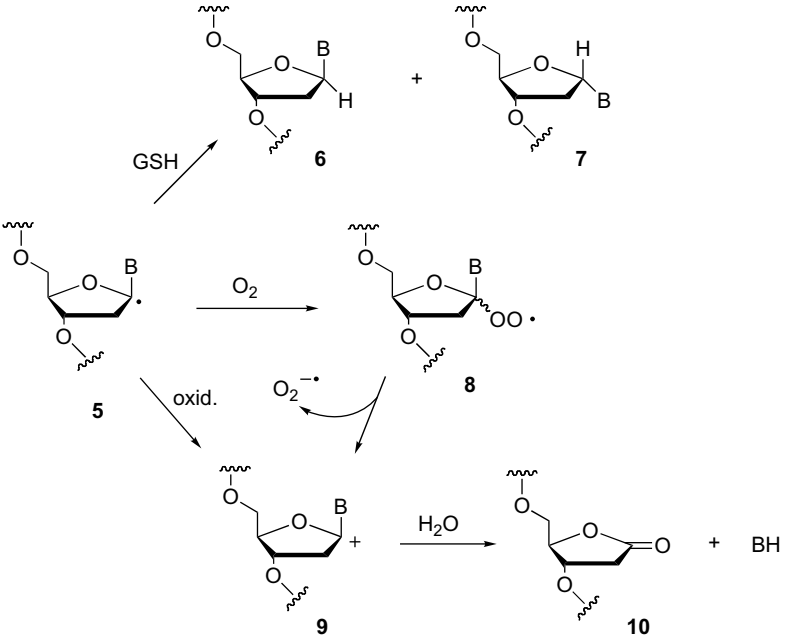

SCHEME 4.2

2′-deoxyuridin-1′-yl radical with molecular oxygen gives the corresponding peroxyl radical with a rate constant of $1 \times 10^9\,M^{-1}\,s^{-1}$ (cf. structure **8** in Scheme 4.2).[16] The fate of this peroxyl radical has been investigated in some detail by ^{18}O-labeling and LFP experiments.[21,22] The labeled experiments demonstrated the partition between two channels where the carbonyl oxygen in the ribonolactone derives from molecular oxygen and a water molecule.[21] In the LFP experiment, the rapid release of $O_2^{\bullet-}$ from the peroxyl radical corresponds to a rate constant of $1.5 \times 10^4\,s^{-1}$.[22] Evidence that similar reactions occur in double-stranded DNA was also reported earlier.[17]

Under biological conditions, oxygen and GSH trapping of C1′ radicals are competitive processes, due to the low O_2 concentration in the nucleus. Since the rate constant for reaction of the DNA-peroxyl radicals with GSH is $\leq 400\,M^{-1}\,s^{-1}$,[23] at physiological GSH concentrations (approximately 5 mM), superoxide release from C1′ nucleotide peroxyl radicals is orders of magnitude faster than peroxyl trapping. Once formed, the C1′ peroxyl radicals **8** expel superoxide radical anion to give C1′ cations **9** that lead to **10** much faster than the respective trapping by GSH to give hydroperoxides.[24]

As a strongly reducing species, the C1′ radical **5** in the presence of metal complexes undergoes oxidation to the corresponding cation **9** (Scheme 4.2).[10,11] Rate constants for the reaction of the 2′-deoxyuridin-1′-yl radical **3** with $CuCl_2$ and $FeCl_3$ are reported as 7.9×10^7 and $1 \times 10^8\,M^{-1}\,s^{-1}$, respectively.[16]

Therefore, 2-deoxyribonolactone (**L**) has been identified as the only C1′ oxidation product. Many radical-based DNA studies suggest radical translocation from the base

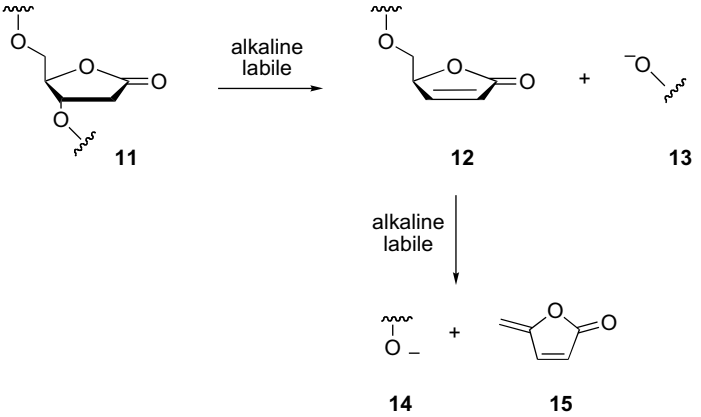

SCHEME 4.3

unit to C1′ position as the process for the **L** formation. For example, the photochemical dehalogenation of 5-halouracil-containing DNA (see also Section 4.3) has been investigated in detail.[25] Hydrogen abstraction from the resulting uracil-5-yl radicals is atom-specific and highly dependent on the DNA structure, suggesting that this approach could also be applied as a probe for the DNA conformations in living cells.

4.2.2. Synthesis and Fate of the 2-Ribonolactone Lesion

2-Deoxyribonolactone (**L**) is an alkali-labile lesion and results in strand scission upon subjection to alkaline conditions (Scheme 4.3), with formation of 3′-phosphate **13** and 5′-phosphate **14** termini. Therefore, **L** cannot be incorporated into chemically synthesized oligonucleotides that are deprotected under basic conditions.

In addition to the photolysis of the corresponding oligonucleotides containing the *tert*-butyl ketone **1**,[17,24] a general method has been developed for the *in situ* generation of the lesion at a defined site of oligonucleotides using known radical translocation approaches. Efficient 1,5-radical translocation protocols for the selective generation of C1′ radicals **17** (Scheme 4.4) and the subsequent trapping of these radicals in nucleosides were proposed.[26,27] In particular, an efficient synthesis based upon the photochemical conversion of a nitroindole nucleoside **18**, selectively incorporated in an oligonucleotide, to **19** with simultaneous expulsion of nitrosoindole **20** (Scheme 4.5) has been reported.[28,29] The single strands containing **L** were hybridized with the complementary strand for biophysical and

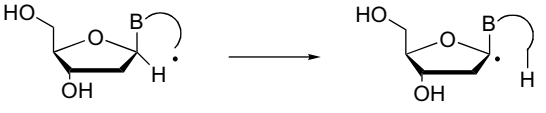

SCHEME 4.4

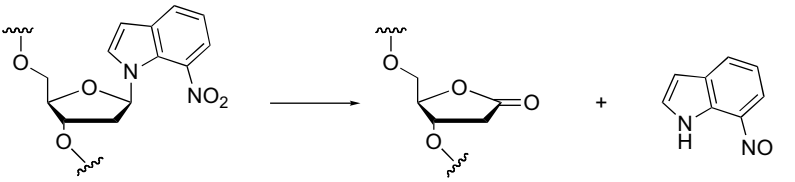

SCHEME 4.5

biochemical studies. NMR structural studies have illuminated aspects of the conformation of the DNA containing this lesion.[30] The procedure was also extended to double-strand synthesis by irradiation of the performed duplex in which one strand contains the nitroindole residue.[31]

An alternative photochemical approach for the introduction of **L** in double-strand oligonucleotides has also been developed.[32,33] A C1′ nitroveratryl cyanohydrin phosphoramidite analogue (**21**) was synthesized and used for the preparation of single-strand oligonucleotides. Irradiation at 350 nm quantitatively converted **21** to the 2-deoxyribonolactone lesion.

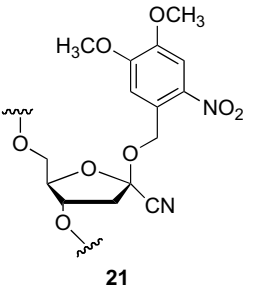

21

The chemistry of the degradation of **L**-containing DNA was investigated in some detail.[31,32] The cleavage through α,β- and γ,δ-elimination at the site of the lesion has been established with identification of the reaction products (Scheme 4.3). The degradation kinetics were investigated as a function of pH, temperature, length and ionic strength.[31] Incubation of **L**-containing DNA under simulated physiological conditions gave rise to DNA fragmentation by two consecutive elimination reactions: DNA cleavage occurred with a half-life of ~20 h in single-stranded DNA and 32–54 h in duplex DNA, depending on the identity of the deoxynucleotide paired opposite to the lesion site (A > C > G > T).[33] The initial α,β-elimination reaction was shown to be the rate-determining step for the formation of methylene furanone and phosphorylated DNA products.

In the case of the minor groove binding copper-phenanthroline conjugate, $Cu(OP)_2$, the formation of 5-methylene furanone (**15**) and 3′- and 5′-terminus phosphates occurs without alkali-labile conditions in a much faster kinetic regime than that expected (cf. Scheme 4.3).[24] A double-stranded oligonucleotide containing **L** was produced by photolysis of the corresponding oligonucleotide containing the *tert*-butyl ketone **1**

(Scheme 4.1).[17,24] It was shown that $Cu(OP)_2$ produces direct strand scission by effecting α,β-elimination from **10** (Scheme 4.3).[34]

Using the above-described approaches for the synthesis of DNA-containing **L** lesions, several features of the toxicity, mutagenesis, and the biochemical fate of the **L** lesion have been elucidated. This lesion is incised by AP endonucleases, suggesting a BER pathway for **L** removal.[35] The **L** lesion was found to induce DNA polymerase-mediated mutagenesis[36] and transcriptional inhibition.[37] It was shown that **L** lesions form covalent adducts with DNA repair proteins that metabolize AP sites suggesting potential toxicity mechanisms,[38,39] and it was also reported that long-patch base excision DNA repair of the **L** lesion prevents the formation of DNA–protein cross-links with DNA pol β.[40] The **L** lesion has been shown to have mutagenic properties different from those of native abasic sites,[41,42] although caution is needed for the interpretation of the experiments.[4] It should also be mentioned that research toward the development of analytical methods for quantifying 2-deoxyribose oxidation products in isolated DNA and cells has been carried out.[43,44]

4.3. OXIDATION OF THE C2′ POSITION

4.3.1. Model Studies

The photoreaction of 2′-α-iodo-2′-deoxyuridine (**22**) as a site-specific radical generating system has been explored. The reaction affords a large number of products that involve the formation of C2′ radical **23** and C2′ cation **24** (Scheme 4.6).[45] It is well known that photoinduced homolytic cleavage of the C–I bond is followed by single electron transfer in the cage before the diffusion of some reactive species. Under

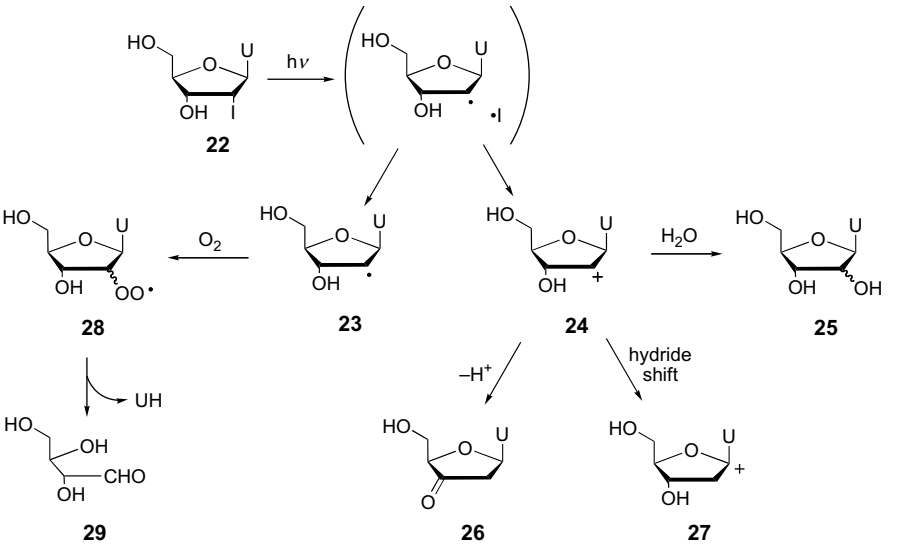

SCHEME 4.6

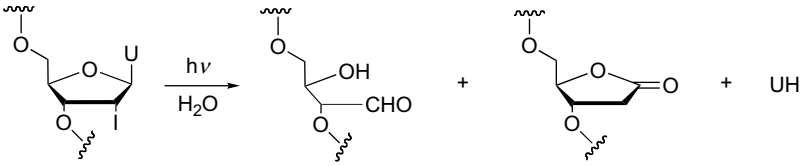

30 **31** **32**

SCHEME 4.7

anaerobic conditions, the solvolysis product **25** as an anomeric mixture prevails together with other products derived from proton elimination or cation translocation to give **26** and **27**, respectively. In the presence of oxygen, the conversion of the C2′ radical to the corresponding peroxyl radical **28** is a consistent path that ultimately leads to the formation of erythose **29** and uracil as well as to the C2′-hydroxylated product **25**.

The photoirradiation of **30** in a double-stranded oligonucleotide produced **31** (11%) and **32** (5.6%) under aerobic conditions, whereas in the absence of oxygen the yield of **31** decreased upon the increase of **32** (Scheme 4.7).[45] Detailed investigations have focussed on the photochemical dehalogenation of 5-halouracil-containing DNA, where the hydrogen abstraction from the resulting uracil-5-yl radicals is atom-specific and highly dependent on the DNA structure.[25] Competitive C1′ and C2′ hydrogen abstraction were observed from the 2-deoxyribose of the 5′ side in the B-form DNA, affording the oligonucleotides **31** and **32**.[45,46] In analogous experiments with Z-form DNA, the product **32** is significantly suppressed and the formation of **31** is accompanied by C2′α-hydroxylation.[47]

Therefore, the formation of D-erythrose abasic site **31** and the hydroxylation at C2′ position have been identified as the key C2′ oxidation products. Early studies on the γ-irradiation of DNA also included a report of the formation of erythrose-containing sites.[48] Several mechanistic paths for the formation of **31** from the C2′–OO• radicals have been suggested, but confirmation/proof is not yet available.[46,47]

4.3.2. Synthesis and Fate of the Erythrose Abasic Site

In addition to the 5-halouracil photochemical system described above for the synthesis of oligonucleotides containing an erythrose abasic site, a system for the *in situ* generation of the lesion at a defined of oligonucleotide site has been developed.[49] A phosphoramidite derivative of a protected ribitol was prepared, which, following the incorporation into oligonucleotides, can be deprotected to give **33**. Periodate oxidization of the vicinal diol affords the erythrose abasic site **34**, as shown in Scheme 4.8.

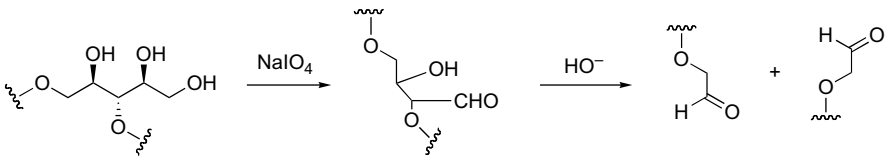

33 **34** **35** **36**

SCHEME 4.8

While incorporation of the precursor into oligonucleotides has only a 50% efficiency, the conversion of the precursor to the erythrose abasic site *in situ* was found to be virtually quantitative.

This lesion is rapidly cleaved by piperidine at 90°C.[49] One chemically interesting feature of this abasic site is that heating under alkaline conditions causes a retroaldol reaction, resulting in a strand break with formation of oligonucleotides 3′-phosphoglycolaldehyde **35** and 5′-phosphoglycolaldehyde **36** (Scheme 4.8).[46,50] However, cleavage by 0.1 M NaOH at 37°C shows that the erythrose abasic site is considerably less labile to hydrolysis (half-life of 3.3 h) than other abasic lesions.[49] It is worth noting that the 3′-residue (**35**) is chemically identical, but mechanistically unrelated, to the 3′-phosphoglycolaldehyde residue arising from the oxidation of C3′ radical (*vide infra*).

The results of two *in vitro* studies suggest possible biological consequences for the erythrose abasic lesion.[50,51] Like other abasic lesions, deoxyadenosine is preferentially incorporated opposite to the abasic site, but the lesion is a strong inhibitor to polymerase extension. This lesion is incised by phosphodiesterases, but is not a substrate for endonuclease III, even though a Schiff base is formed.

4.3.3. Ribo-Nucleosides

Compound **37** was synthesized as site-specific adenosin-2′-yl radical-generating system upon photolysis. The radical **38** was generated and was trapped by glutathione (GSH) (Scheme 4.9),[52] leading to the *ribo*- and *arabino*-products **39** and **40**, respectively, in a 1:3.5 ratio. The preferred attack of the thiol from the α-face of the C2′ radical is due to the efficient β-face shielding by the adenine moiety. Adenine was also a reaction product. Competition kinetics afforded the ratio $k_H/k_f = 4.3\ M^{-1}$, suggesting a relatively fast β-elimination.

The same adenosin-2′-yl radical was obtained by one-electron reduction of 8-bromoadenosine (see Section 4.6) in pulse radiolysis experiments (Scheme 4.10).[52] A value of $k_f = 1.1 \times 10^5\ s^{-1}$ is obtained by measuring the oxidizing radical formed

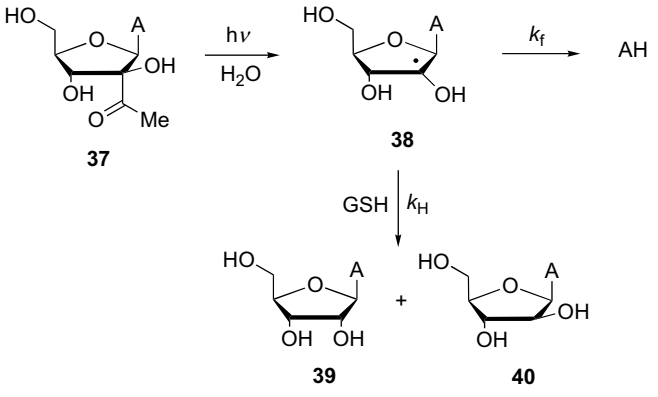

SCHEME 4.9

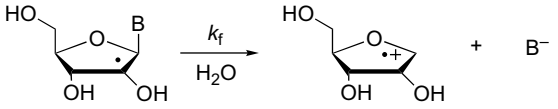

41 B = A or Hy **42**

SCHEME 4.10

upon adenine release. It was suggested that the heterolysis of the glycosidic bond in radical **41** produces the radical cation **42** and the adenine. Similar experiments and results were reported for inosin-2′-yl radical that produces the same radical cation **42** and hypoxanthine (Hy) upon heterolysis of the glycosidic bond.[53]

4.4. OXIDATION OF THE C3′ POSITION

4.4.1. Model Studies

Metallointercalators generally bind to the minor groove of double-stranded DNA and abstract mainly C1′, C4′, and C5′ H atoms from the sugar backbone. However, phenanthrenequinone diimine complexes of rhodium(III) intercalate in the major groove of double-stranded DNA and, upon photoactivation, have been postulated to abstract C3′ H atoms from deoxyribose,[54] although evidence suggests that H2′ may be abstracted during photocleavage.[55] The C3′ chemistry of **43** under aerobic conditions has thus been linked to the formation of 3′-phosphoglycolaldehyde **44**, base propenoate **45**, free base, and the oligonucleotide 3′-phosphate and 5′-phosphate termini at the site of strand scission (Scheme 4.11).

Some research on site-specific radical generating systems has been carried out. Initial work described the synthesis of *tert*-butyl ketone **46** or **47** and the conditions in which Norrish-type I photocleavage gave the desired C3′ radical **48**.[56] In the presence of Bu_3SnH as a hydrogen donor, both derivatives gave **49** a 1:1 mixture of isomers (Scheme 4.12).

The *tert*-butyl ketone **47** (or its analogous acetyl derivative) has been incorporated into oligonucleotides and used as a photoactivated precursor of C3′ radicals in single-stranded DNA.[57, 58]

Some products have been successfully identified, although the mechanism of their formation is far from being understood. The thymidin-3′-yl radical abstracts hydrogen from GSH to give the reduced product in an undetermined β:α anomeric ratio.[57]

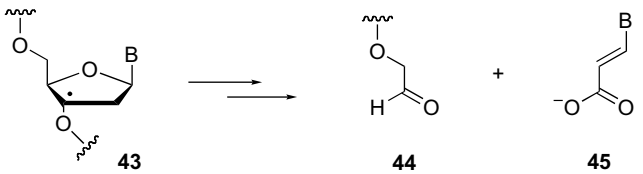

43 **44** **45**

SCHEME 4.11

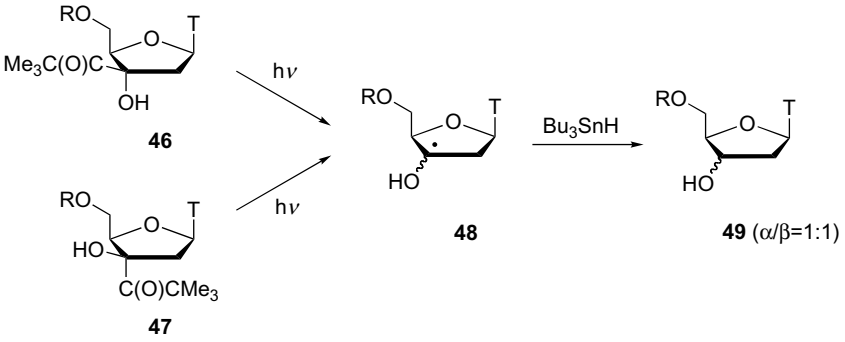

SCHEME 4.12

Under aerobic conditions, the thymidin-3′-yl radical was found to produce the labile 3′-ketodeoxynucleotide **51**, which gives **53** and free base, as well as the 5′- and 3′-phosphate-terminated oligomers (**52** and **54**) (Scheme 4.13).[58] The expected 3′-phosphoglycolaldehyde (3′-PGA) is accompanied by 3′-phosphoglycolate (3′-PG), and 5′-aldehyde terminated oligonucleotides. The formation of the last two fragments has been explained by oxidation of the C4′ radicals of the same nucleotide and by oxidation of the C5′ radicals of the 3′-adjacent nucleotide. The authors suggested the radical translocations from **56** shown in Scheme 4.14 with formation of radicals **57** and **58**, respectively. It should be noted that these findings are based on single-stranded oligonucleotide experiments. From a mechanistic point of view, the transformation of peroxyl radical **50** to 3′-ketodeoxynucleotide **51** still remains unclear. It could be suggested that the fate of this peroxyl radical is be similar to that observed in the oxidation of C1′ radicals—that is, release of $O_2^{\bullet -}$ from the peroxyl radical, trap of the corresponding cation by water, and β-elimination of the phosphate. Since the electronic environment of the C1′ cation versus the C3′ cation is

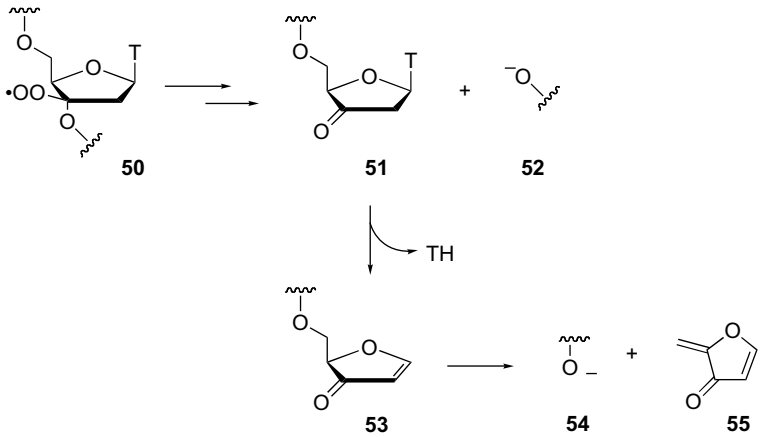

SCHEME 4.13

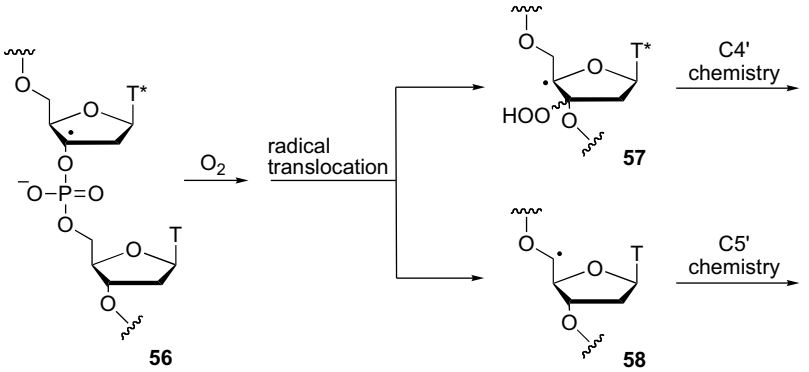

SCHEME 4.14

quite different, the $O_2^{\bullet -}$ release in radical **50** should be much slower, thereby allowing the intramolecular processes depicted in Scheme 4.14.

The mechanism of formation of 3′-phosphoglycolaldehyde (3′-PGA, **44**) is not very clear. It was suggested that after formation of the hydroperoxide, a molecular rearrangement occurs with insertion of an oxygen atom into the deoxyribose ring, which further decomposes to form 3′-PGA together with other products.[54] The degradation of the C3′ radical may not be the only pathway leading to 3′-PGA. However, a method for the quantification of 3′-PGA residues has also been reported. After DNA irradiation and enzymatic digestion, this method exploits the aldehyde moiety in 3′-PGA by derivatization as a stable oxime with pentafluorobenzylhydroxylamine, followed by solvent extraction and gas chromatography/negative chemical ionization/mass spectrometry.[59,60] A stable isotopically labeled [$^{13}C_2$]PGA was synthesized and used as an internal standard. The limit of detection in the presence of DNA was 30 fmol per sample, corresponding to two molecules of PGA in 10^6 nucleotides for 170 μg of DNA. The application of this method for quantifying 3′-PGA residues revealed different yields for γ- and α-radiations.[59]

4.4.2. Ribo-Nucleosides

Ribonucleotide reductases are enzymes that catalyze the conversion of 5′-(di or tri) phosphate esters of *ribo*-nucleosides **59** to 2′-deoxynucleotides **60** in all organisms (Scheme 4.15). A radical-based mechanism derived from the information obtained from numerous biological studies has been established.[61,62] The key steps involve

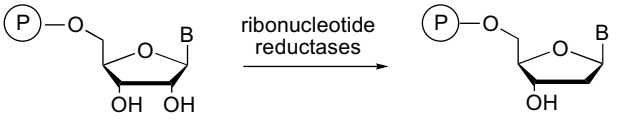

SCHEME 4.15

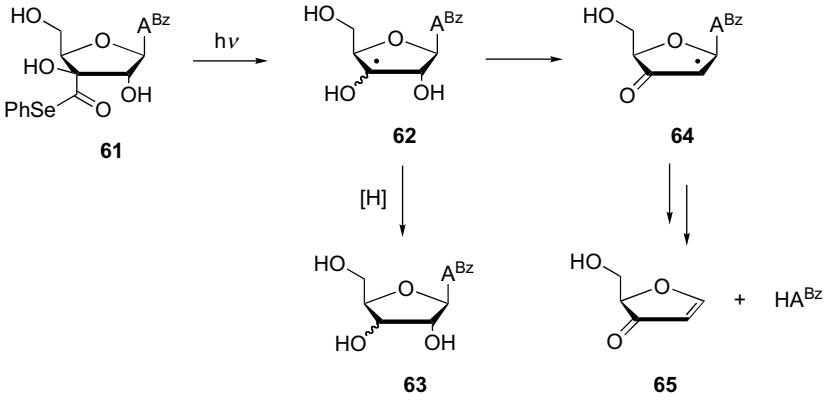

SCHEME 4.16

formation of C-3′ radical via hydrogen atom abstraction by a cofactor-induced thiyl radical, and elimination of water prior to return of a hydrogen atom.

Biomimetic simulations of the free radical-initiated cascade reactions, postulated to occur at the active site of ribonucleoside reductases, have also been performed.[63, 64] Site-specific generation of adenosin-3′-yl radical was obtained by the synthesis of selenol ester **61** and subsequent photolysis (Scheme 4.16).[63] Using competition kinetic methods, it could be demonstrated that this radical effects the rapid elimination of the 2′-hydroxy group, which is subjected to general base catalysis. The rate coefficient for this reaction was determined as $1.5 \times 10^6\,s^{-1}$ by competition kinetics in the presence of 1 M triethylammonium acetate buffer at pH 7. Without the catalyst, the elimination rate is about 10^3 times slower. It was suggested that a similar mechanism is also feasible for the key steps of the enzyme-catalyzed reaction.

4.5. OXIDATION OF THE C4′ POSITION

The chemistry of 4′ oxidation can follow several pathways depending on the experimental conditions. For example, only the 4′-hydrogen abstraction to give **66** has been observed with duplex DNA and iron bleomycin, and resulted mainly in two paths (Scheme 4.17).[65] Path A gives the C4′-oxidized abasic site **67** (or 2-deoxy-pentos-4-ulose lesion) and free base, whereas path B leads to a strand break with formation of 3′-phosphoglycolate residue **68**, base propenal **69** and 5′-phosphate terminus **70**.

4.5.1. Model Studies

The fate of the C4′ radical, either in nucleosides or in oligonucleotides, has been investigated in some detail under oxygen-free or aerobic conditions.[66]

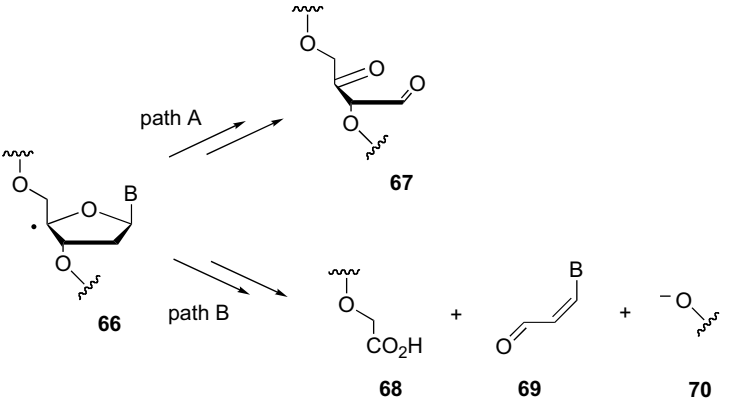

SCHEME 4.17

Oligonucleotides containing a modified unit **71** or **72**, which allowed for the selective generation of the C4′ radical under photolytic conditions, were synthesized.

71 **72**

In the absence of added traps, the C4′ radical **73** in ss- or ds-oligonucleotides yields the oligonucleotide phosphates **77** and **80** as main products (Scheme 4.18). The reaction starts with a heterolytic cleavage to give radical cation **76** and 5′-phosphate **77** with a rate constant of about $10^3\ s^{-1}$ for a ss-oligonucleotide, whereas the analogous reaction in a ds-oligonucleotide was found to be about 10 times slower.[67] Spectroscopic evidence for the radical cation intermediate was obtained by ESR and CIDNP techniques.[68, 69] This radical cation has oxidizing properties and is capable of oxidizing a neighboring guanine base.[70] The heterolytic cleavage is favored over a homolytic β-cleavage due to the effective solvation of the ensuing ions.[71] Trapping of **76** by H_2O generates radical **78**, which undergoes a second heterolytic cleavage to give phosphate **80** and radical cation **81**. In the presence of GSH, the heterolytic cleavage of radicals **73** and **78** is in competition with hydrogen abstraction from GSH, when present at millimolar levels (Scheme 4.18). Radical **73** abstracts hydrogen from a thiol with a rate constant of $1.9 \times 10^6\ M^{-1}\ s^{-1}$.[72] The stereoselectivity of the H-trapping reaction is remarkable. Radical **73** in ss-oligonucleotides reacts nearly unselectively with GSH (**74**:**75** $\approx$ 1.5), whereas radical **73** in ds-oligonucleotides leads predominantly to the natural 2′-deoxyribonucleotides (**74**:**75** $\approx$ 9).[67]

In the presence of O_2, C4′ radical **82** is trapped very rapidly ($2 \times 10^9\ M^{-1}\ s^{-1}$) to give peroxyl radical **83** (Scheme 4.19). However, this reaction was found to be reversible. The rate constant from single-stranded 4′-DNA peroxyl radical is $1.0\ s^{-1}$ at ambient temperature.[72] Peroxyl radicals, detected by ESR,[71] abstract hydrogen from

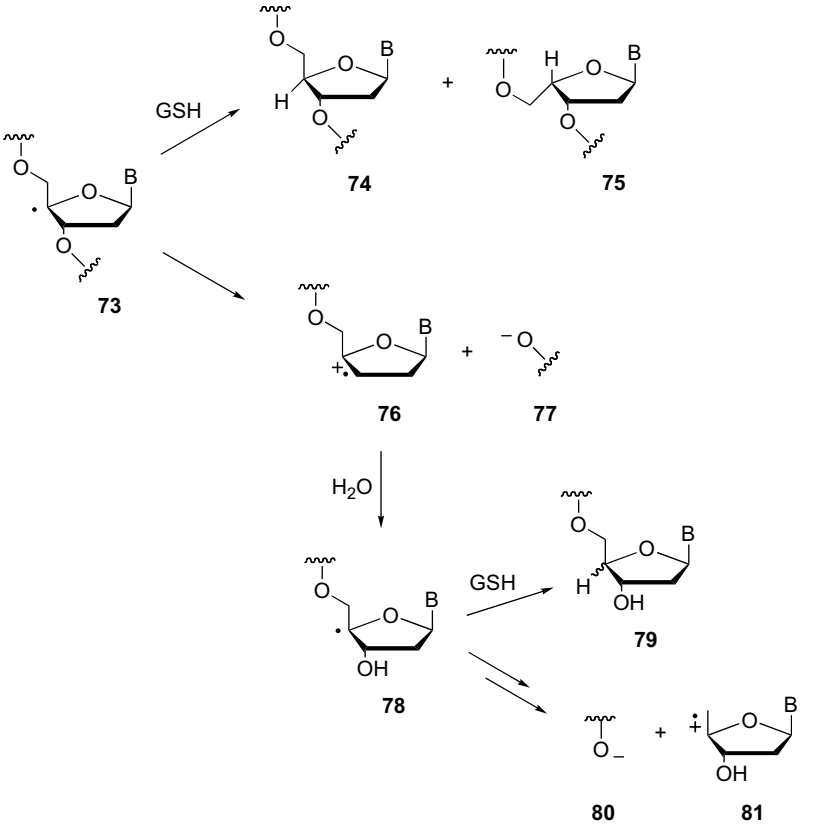

SCHEME 4.18

GSH with a rate constant of $\leq 400\,M^{-1}\,s^{-1}$,[23] and the product hydroperoxide **84** has been isolated and characterized.[72, 73] Subsequently, the hydroperoxide **84** is converted to cation **85** (Criegee rearrangement), which after β-elimination (**86**) and subsequent hydrolysis leads to 5′-phosphate **89** and 3′-phosphoglycolate **87** as oligomeric cleavage products together with base propenal **88**. Therefore, strand cleavage depends on the concentration of the hydrogen donor. At low GSH concentration, the strand scission is the result of a spontaneous heterolytic cleavage that occurs even under aerobic conditions. It should be emphasized that the 5′-phosphate strand terminus (**77** or **89**) is formed under both aerobic and anaerobic conditions (cf. Schemes 4.18 and 4.19). On the other hand, 3′-phosphoglycolate **87** and 3′-phosphate **80** strand termini are the characteristic cleavage products, respectively, under aerobic and anaerobic conditions.

According to the mechanism proposed by Stubbe et al.[65], the 2-deoxypentos-4-ulose lesion **93** is produced by oxidation of the C4′ radical **90** to cation **91** that is trapped by H_2O to give the cyclic hemiacetal **92**. Hydrolysis of **92** affords the observed lesion (Scheme 4.20). The oxidation step was suggested to be carried out by the bleomycin/Fe^{2+}/O_2 complex after H-abstraction from DNA. The subsequent partition

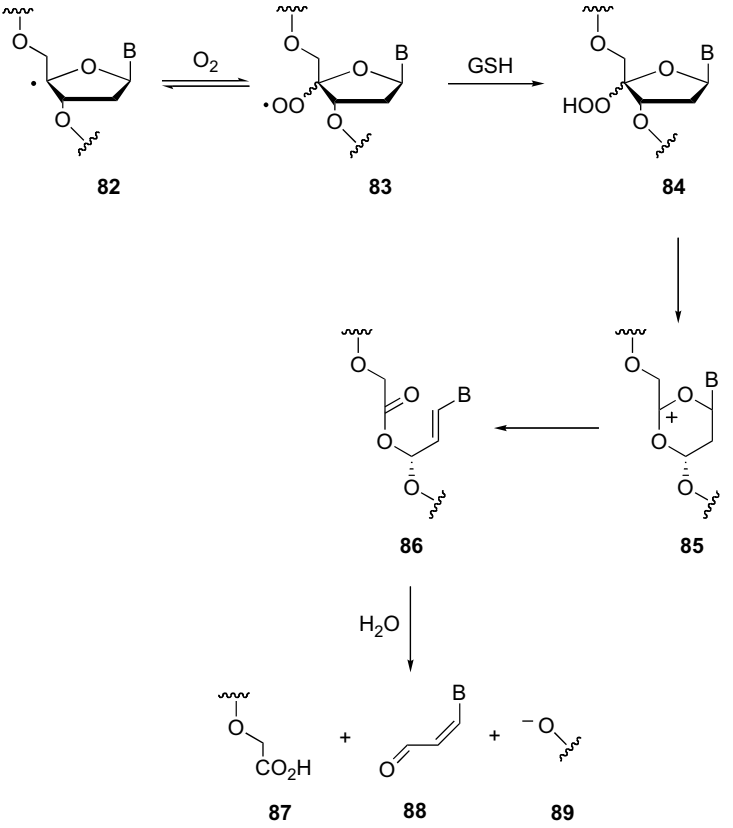

SCHEME 4.19

ratio depends on the concentration of O_2 (cf. Scheme 4.17). Support in favor of the mechanism in Scheme 4.20 comes also from model studies, suggesting that oxygen does not oxidize C4′ radical **90** to cation, while metal oxides can easily induce the oxidation step.[74]

4.5.2. Synthesis and Fate of the 2-Deoxypentos-4-ulose Lesion

The C4′-oxidized abasic site (know also as the 4′-keto abasic site) is produced by a variety of DNA damaging agents. It accounts for ~40% of the lesions produced by the antitumor agent bleomycin and exhibits interesting and unique biochemical and biological effects in DNA. The 4′-keto abasic site, or 2-deoxypentos-4-ulose residue **94**, may exist in the hydrated form **95**, which is expected to be in equilibrium with the cyclic form **96** (Scheme 4.21).

Methods for the accessibility of oligonucleotides containing the C4′-oxidized abasic site at a defined position along the sequence have been developed, and investigation of the lesion's effects on DNA have been reported. Greenberg and co-workers[75] reported the first general method for the synthesis of oligonucleotide

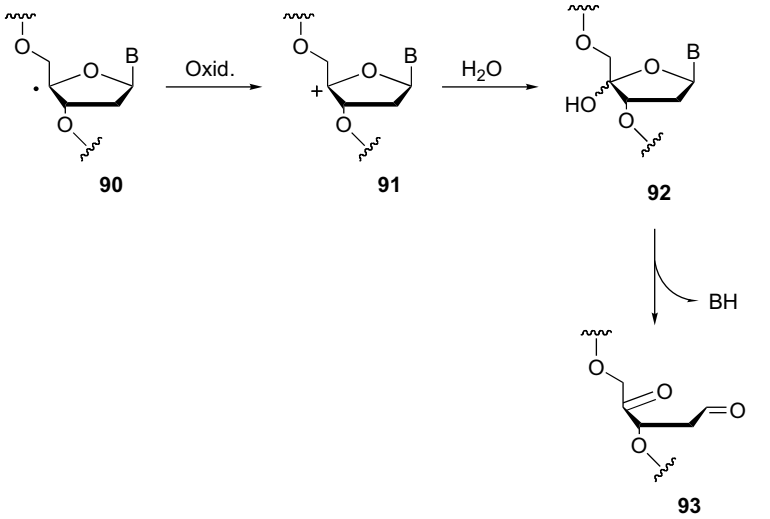

SCHEME 4.20

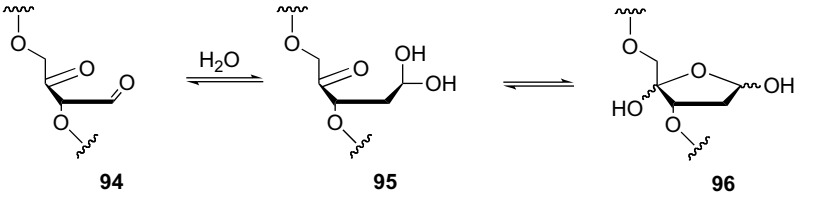

SCHEME 4.21

containing this lesion. Modified oligonucleotides **97** incorporating the nitroveratryl group as protection were prepared and subsequent photolysis of the desired ss- or ds-oligonucleotides afforded the C4′-oxidized abasic site **98** (Scheme 4.22).

An alternative general method for the preparation of the C4′-oxidized abasic site was also reported.[76] 4′-Azido-2′-deoxyuridine-5′-triphosphate is incorporated into

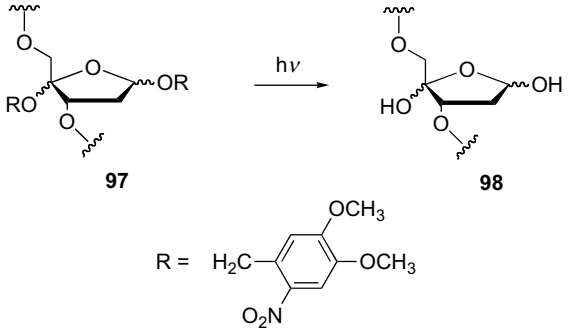

SCHEME 4.22

duplex DNA using a primer and HIV-1 reverse transcriptase. The two strands of the duplex are separated based on size after cleavage with the restriction enzyme. The ss-DNA containing 4′-azido-2′-deoxyuridine **99**, when treated with uracil-DNA glycosylase, resulted in the quantitative release of uracil and azide and the generation of ss-DNA containing the C4′-oxidized abasic site. This lesion was characterized directly by MALDI-TOF MS and indirectly by subsequent reduction, enzymatic digestion, and GC/MS. Synthetic methods for the preparation of gapped 3′-PG/5′-P lesions and the study of their structures by 2-D NMR methods were also reported.[77]

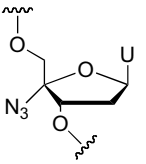

99

The stability of the C4′-oxidized abasic site in both ss- and ds-DNA has been studied. A half-life of 7.8 h (37°C, 100 mM NaCl at pH 7.5)[75] was found in ss-DNA and 26 h (37°C, 100 mM NaCl at pH 7) in ds-DNA.[76] The rate constant is faster by a factor of 3 in ss-DNA, suggesting that duplex DNA stabilizes the lesion, although pH conditions and the sequences were different in the two studies. A similar effect due to DNA structure has recently been reported for the 2-deoxyribonolactone lesion, whose half-life was found to be 20 h in ss-DNA and 32-54 h in ds-DNA. Thus, the stability of sugar lesions appears to be sensitive to both sequence and sequence context (ss-DNA versus ds-DNA).

A GC/MS approach was proposed for the quantification of 2-deoxypentos-4-ulose and 3′-phosphoglycolate pathways.[78] Another selective method for detecting femtomole amounts of the C4′-oxidized abasic site in DNA, which takes advantage of the selective reactivity of the 1,4-dicarbonyl groups in the lesions with a biotinylated probe, has also been reported.[79] The adducts are quantified using a fluorescent assay.

The ability to generate the 2-deoxypentos-4-ulose or the 3′-PG/5′-P lesions in any sequence context should elucidate the lesions' structure (both ss- and ds-DNA lesions). The efficiency with which these lesions are repaired *in vitro* by the Ape1 protein (the major human abasic site endonuclease) and β-polymerase was observed.[80] Ape1 catalyzed effective incision at the C4′-oxidized abasic site at a rate that may be only a few-fold less than the for incision of hydrolytic native abasic sites at the same location. Ape1 hydrolyzed 3′-phosphoglycolates (3′-PG) 25 times more slowly than the abasic site. The repair of C4′-oxidized abasic site lesion has been studied with a variety of DNA polymerases *in vitro*.[81]

The C4′-oxidized abasic site from intrastrand or interstrand cross-links in cellular DNA was detected by mass spectrometry.[82] In particular, cyclic adducts were formed with deoxycytidine. DNA interstrand cross-links are deleterious to cells because they are potent blocks to replication and transcription.[83] By means of duplexes in which **98** is produced from a synthetic precursor, the lesion was shown to produce interstrand

cross-links in which both strands were intact and cross-links in which the strand containing the C4′-oxidized abasic site were cleaved.[84] The yields of these products depend upon the surrounding nucleotide sequence. When the lesion **98** is opposed by dA, cross-link formation occurs exclusively with an adjacent dA on the 5′ side.

4.5.3. Ribo-Nucleotides

The site-specific generation of C4′ radical in *ribo*-nucleosides and RNA has received much less attention. It should be noted that iron bleomycin cleaves RNA much less efficiently than DNA.[85] An oligonucleotide containing the modified methyl ketone **100** as photolytic precursor (Scheme 4.23) has been synthesized.[86] In the presence of GSH and in competition with hydrogen abstraction from GSH to give **102**, the 4′-RNA radical **101** cleaves heterolytically to give the radical cation **103** and phosphate **104**. Assuming a $k_H = 1 \times 10^7\ M^{-1}\ s^{-1}$ for the reaction of radical **101** with GSH, a rate constant of $k_f = 5 \times 10^2\ s^{-1}$ is calculated for the heterolytic cleavage of **101**. The cleavage rate of the corresponding 4′-DNA radical is more than three times faster. This decrease in the rate of cleavage of *ribo*-nucleotide radical has been attributed to a destabilizing effect of the additional 2′-OH group.[87]

Experiments carried out under aerobic conditions afforded the expected products **104** and **105** (Scheme 4.23).[66] However, the relative percentage changes substantially, since the **105/104** ratio goes from 0.33 for 4′-DNA radical to 3.0 for 4′-RNA radical **101**. This effect was assigned to the retardation of β-elimination after the Criegee rearrangement (cf. Scheme 4.19).

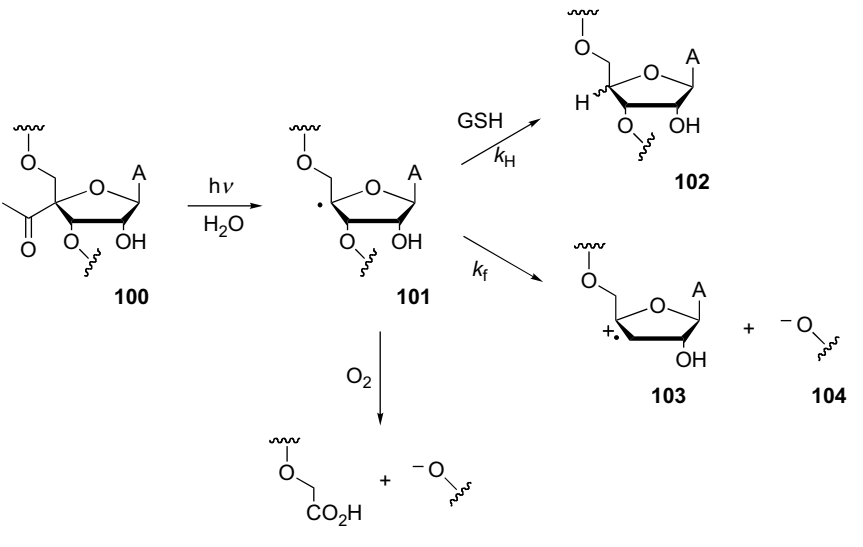

SCHEME 4.23

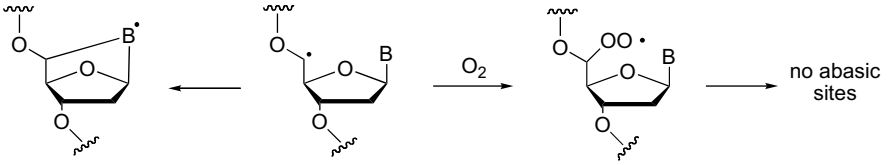

108 **106** **107**

SCHEME 4.24

4.6. OXIDATION OF THE C5′ POSITION

The chemistry of C5′ radical **106** is very peculiar with respect to the other positions of 2-deoxyribose in the sense that (i) the peroxyl radical **107** does not generate an abasic site and (ii) unique cyclic base–sugar adducts are formed (Scheme 4.24). In particular, 5′,8-cyclo-2′-deoxyadenosine and 5′,8-cyclo-2′-deoxyguanosine moieties, generally referred to as 5′,8-cyclopurines, are the result of the attack of C5′ radical to the purine moiety to give **108** more rapidly than its reaction with oxygen. These lesions are observed among the DNA modifications.[88,89] They have also been identified in mammalian cellular DNA *in vivo*.[90,91] The chemistry of C5′ oxidation has not received the same attention as that of the C1′ or C4′ positions until recently. One reason may be the lack of an abasic site and the associated interest in the polymerase bypass and mutagenesis.[4] The difficult access to 5′,8-cyclopurines and their incorporation in oligonucleotides are additional factors.

4.6.1. Model Studies

The typical 5′-*tert*-butyl ketone modification as the site-specific generation of model sugar radicals has recently been extended to the C5′ position. Photolysis of derivatives **109** and **112** leads to the formation of thymidin-5′-yl (**110**) and 2′-deoxyguanosin-5′-yl (**113**) radicals, respectively (Schemes 4.25 and 4.26).[92] In the thymidine system, the C5′ radical **110** is fully quenched to give **111** in the presence of physiological concentrations of thiols. In the 2′-deoxyguanosine system, the C5′ radical **113** is partially quenched to give **114** and in competition undergoes intramolecular attack onto the C8–N7 double bond of guanine, leading ultimately to the 5′,8-cyclo-2′-deoxyguanosine derivative **116**. The cyclization **112** → **115** occurs with a rate constant of $\sim 1 \times 10^6\,s^{-1}$ (based on $k_H = 5 \times 10^6\,M^{-1}\,s^{-1}$) and is highly stereoselective, affording only the (5′*S*)-isomer.

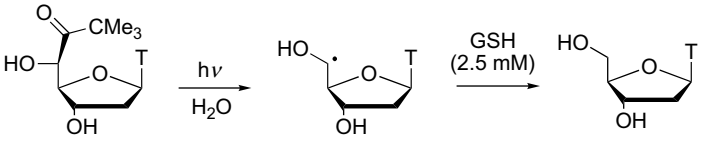

109 **110** **111**

SCHEME 4.25

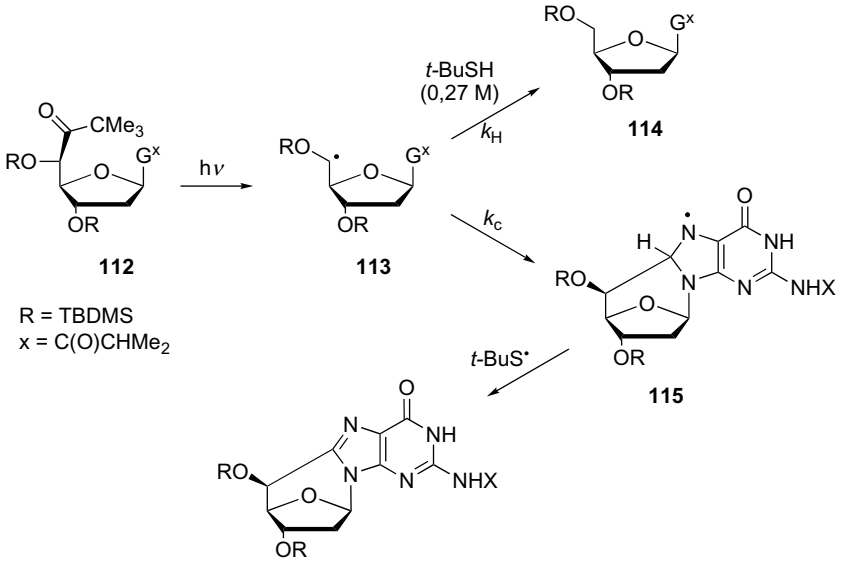

SCHEME 4.26

Both 5′,8-cyclo-2′-deoxyadenosine (**117**, **118**) and 5′,8-cyclo-2′-deoxyguanosine (**119**, **120**) have two diastereoisomeric forms, the (5′*S*) and (5′*R*) isomers, which differ in the configuration of the C5′ position (Chart 4.1).

Both sets of diastereomeric forms have been synthesized and fully characterized. The first report involves a multistep synthesis, but in overall poor yield.[93, 94] A one-pot

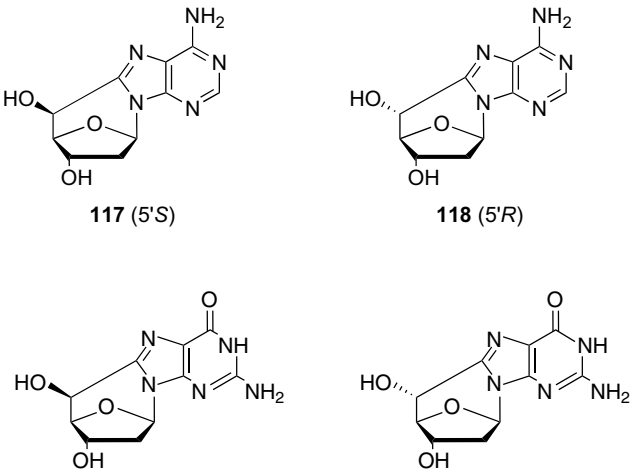

117 (5′*S*) **118** (5′*R*)

119 (5′*S*) **120** (5′*R*)

CHART 4.1

synthesis was developed starting from the commercially available 8-bromopurine derivatives under continuous radiolysis or photolysis.[95–99] These procedures involve a radical cascade reaction that mimics the DNA damage causing the formation of these lesions. Furthermore, the mechanism of these reactions was investigated by time-resolved spectroscopy to provide important information on the fate of C5′ radicals.[96,97] Some of these findings, summarized in Scheme 4.27, are as follows: 8-Bromo-2′-deoxyadenosine **121** captures electrons and rapidly loses a bromide ion to give the corresponding C8 radical **122**.[96] Radical **122** can also be obtained by homolytic cleavage of C–Br bond under photolysis.[97] This intermediate intramolecularly abstracts a hydrogen atom from the C5′ position selectively affording the 2′-deoxyadenosin-5′-yl radical **123**. Radical **123** undergoes cyclization with a rate constant of $k_c = 1.6 \times 10^5\ s^{-1}$ to give the heteroaromatic radical **124**. Furthermore, the reactivity of C5′ radical **123** toward GSH ($k = 4.9 \times 10^7\ M^{-1}\ s^{-1}$), O_2 ($1.8 \times 10^9\ M^{-1}\ s^{-1}$), and $K_3Fe(CN)_6$ ($4.2 \times 10^9\ M^{-1}\ s^{-1}$) was examined in competition

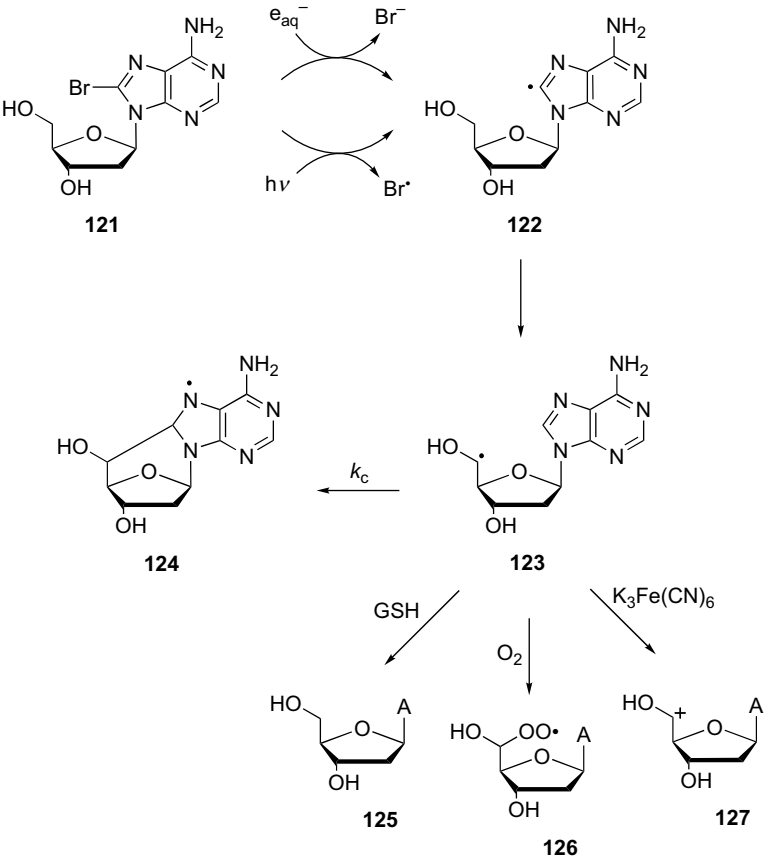

SCHEME 4.27

with the cyclization process as shown in Scheme 4.2[6,96] Similar experiments and results were reported for 2′-deoxyinosin-5′-yl radical.[53]

Depending on the substrate and the experimental conditions, the isomeric ratio (5′*S*)/(5′*R*) substantially changes in both sets. The effect of the solvent and the nature of the substituents at the O5′ position play an important role in the stereoselectivity of the C5′-radical cyclization.[92,98,99] The (5′*S*)/(5′*R*) ratio depends on the bulkiness of the C5′-OR substituent and the water solvation through intermolecular hydrogen bonding. Structures **128** and **129** show the chair transition states of the *pro*-(5′*S*) and *pro*-(5′*R*) conformers, which have the 5′- OH in the equatorial in the axial position, respectively. In aqueous solution only the *pro*-(5′*R*) conformer can be stabilized by hydrogen bonding, involving either the N3 of the base (**129**) or the oxygen of the sugar ring (not shown). The (5′*R*)/(5′*S*) ratios of 6:1 and 8:1 isomers were obtained in water for 5′,8-cyclo-2′-deoxyadenosine and 5′,8-cyclo-2′-deoxyguanosine, respectively. In contrast, the (5′*S*) stereoselectivity of the cyclization reaction in Scheme 4.26 can be explained by the steric hindrance between the guanine moiety and the 5′-O-TBDMS substituent that forces the 5′-O-TBDMS into the equatorial position. The (5′*R*)/(5′*S*) ratios of approximately 2 and 0.3 were reported for 5′,8-cyclo-2′-deoxyadenosine and 5′,8-cyclo-2′-deoxyguanosine lesions, respectively, in double-stranded DNA.[88,89]

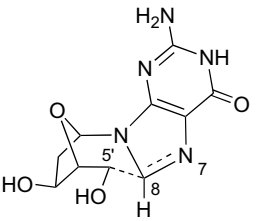

128

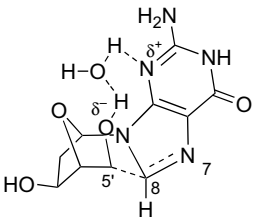

129

Two interesting properties of (5′*S*)-5′,8-cyclo-2′-deoxyadenosine (**117**) were recently evidenced in aqueous medium. The glycosidic bond was found to be <40-fold more resistant to acidic hydrolysis than that in 2′-deoxyadenosine, and no adenine was released, as evidenced by the intact C5′–C8 covalent bond.[100] Under sunlight irradiation, **117** photoisomerizes to the (5′*R*) isomer **118**, whereas the latter compound does not isomerize under the same conditions.[101] This one-way photoisomerization of **117** to **118** has been explained by invoking a heterolytic cleavage of the C–O bond leading to benzyl-type cations, which subsequently undergo nucleophilic trapping by water with concomitant isomerization. The isomer **118** is more easily repaired when these cyclopurine lesions are formed in DNA (see below), and it would be interesting to extend this study in ss- or ds-DNA.

The C5′ radicals of pyrimidine nucleosides are also cyclized to give the analogous diastereomeric mixtures of 5′,6-cyclopyrimidines.[102,103] In addition, some of these derivatives have been incorporated in oligonucleotides and their properties have been

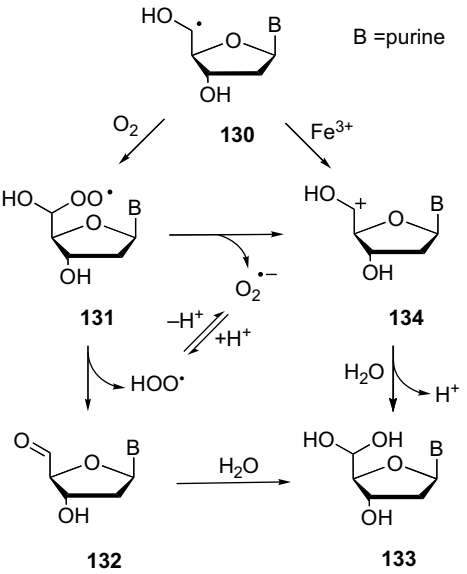

SCHEME 4.28

investigated.[103, 104] However, there is no evidence of 5′,6-cyclopyrimidines formation *in vitro* or *in vivo* in either ss- or ds-DNA. In this context, the rate constant of the cyclization of the substituted thymid-5′-yl radical was measured and found to be two to three orders of magnitude slower than the analogous substituted 2-deoxyguanosin-5′yl radical (cf. Scheme 4.25).[102] In the pyrimidine series, therefore, the cyclization of C5′ radicals remains an interesting reaction for synthetic applications in medicinal chemistry,[105] whereas in oxidative DNA damage the chemistry of C5′ peroxyl radicals is better understood (see below).

The reactivity of purine-substituted C5′ radicals **130** under aerobic conditions has also been elucidated (Scheme 4.28).[6] Using an oxygen concentration in the range of 13–266 mM (typical for oxygenated tissues), the hydrated 5′-aldehyde **133** is accompanied by the 5′,8-cyclopurine nucleoside (Chart 4.1). The formation of 5′,8-cyclopurines is relevant in all experiments, and the yields increased with decreasing O_2 concentration. The proposed mechanism involving the formation of peroxyl radical **131** that decays either via a cyclic transition state leading to HOO$^\bullet$ radical and aldehyde **132** or via heterolytic cleavage to generate carbocation **134** and superoxide radical anion is given in Scheme 4.27. The two pathways are formally identical. Trapping C5′ radicals with $Fe(CN)_6^{3-}$ gave the corresponding hydrated 5′-aldehydes in good yields (Scheme 4.28).[6] Similar experiments and results were reported for 2′-deoxyinosin-5′-yl radical.[6]

4.6.2. Biochemical Features of 5′,8-Cyclopurine Lesions

Synthetic oligonucleotides containing (5′*S*)- and (5′*R*)-5′,8-cyclo-2′-deoxyadenosine at selected sites were prepared using solid-phase synthesis to investigate the

biochemical features of such lesions.[106, 107] In 2000, two groups independently reported that (5′*S*)- and (5′*R*)-5′,8-cyclo-2′-deoxyadenosine are substrates of the nucleotide excision repair (NER) pathway, but not of other repair pathways.[106, 107] Indeed, neither the (5′*S*)- nor the (5′*R*)-isomer is recognized by human DNA glycosylases active in the base excision repair (BER) pathway. Furthermore, both isomers were found to be relatively poor substrates for the NER pathway, the (5′*S*)-isomer being repaired more efficiently than the (5′*R*)-isomer. The (5′*S*)-isomer was found to strongly block gene expression[107] and to cause transcriptional mutagenesis.[108] It was also reported that stereospecific differences between the (5′*S*)- and (5′*R*)-isomer residues affect the relative resistance to exonucleolytic activity and give rise to different efficiencies of translesion synthesis by human polymerase η.[109] These observations led both groups to propose that these lesions may be responsible for the neurodegeneration suffered by xeroderma pigmentosum (XP) patients who lack the capacity to carry out NER.[106, 107] The clinical and neuropathological aspects of the XP disease were recently described, and a reasonable set of criteria that indicate the 5′,8-cyclopurine lesion as the best candidate of any currently known DNA lesions for a role in this neurological disease is provided.[90, 110] The 5′,8-cyclopurine lesions have also been identified in mammalian cellular DNA *in vivo*, where their levels are enhanced by conditions of oxidative stress.[90, 91]

4.6.3. The 5′-Aldehyde Terminus and Other Oxidation Lesions

5′-Aldehyde-terminated DNA, or oligonucleotide **137**, has been observed during the analysis of DNA oxidized by chemical nucleases, such as metalloporphyrins, or natural products, such as enediyne compounds (Scheme 4.29). A second lesion produced in lower yield results from cleavage of C4′–C5′ bond is the 2-phosphoryl-1,4-dioxo butane residue **142**. Several mechanistic aspects of the 5′-oxidation pathways under aerobic conditions are not well understood. All the proposed intermediates are based on rationalization of the products observed in DNA degradation by NCS-Chrom in the presence of glutathione.[7, 8, 11] The forming C5′ radical **135** (where B = thymine) reacts with oxygen to generate the peroxyl radical **136**. The peroxyl radical **136** should partition between two reaction channels to give the corresponding hydroperoxide by reaction with GSH and the corresponding alkoxyl radical by disproportionation. The hydroperoxide produces the 5′-aldehyde terminus **137** and fragment **138**, while the alkoxyl intermediate could be responsible for the 3′-formyl phosphate residue **141** and the 5′-(2-phosphoryl-1,4-dioxobutane) residue **142** with the concomitant loss of base (Scheme 4.28). In other studies, a 5′-aldehyde-terminated oligonucleotide arising from the hydroxylation at C5′ of a 2-deoxyribose to give **143**, where B = guanine.[111] This hydroxylation promotes the spontaneous elimination of the attached phosphate group and the cleavage of DNA accompanied by the formation of two DNA products: a 5′-aldehyde end (**137**) and a 3′-phosphate end (**138**).

Upon heating at 90°C for 30 min or upon alkaline treatment, the 5′-aldehyde **137** undergoes β,δ-elimination reactions with the release of furfural **139** and of the corresponding nucleobase, resulting in the formation of a one-nucleotide shorter

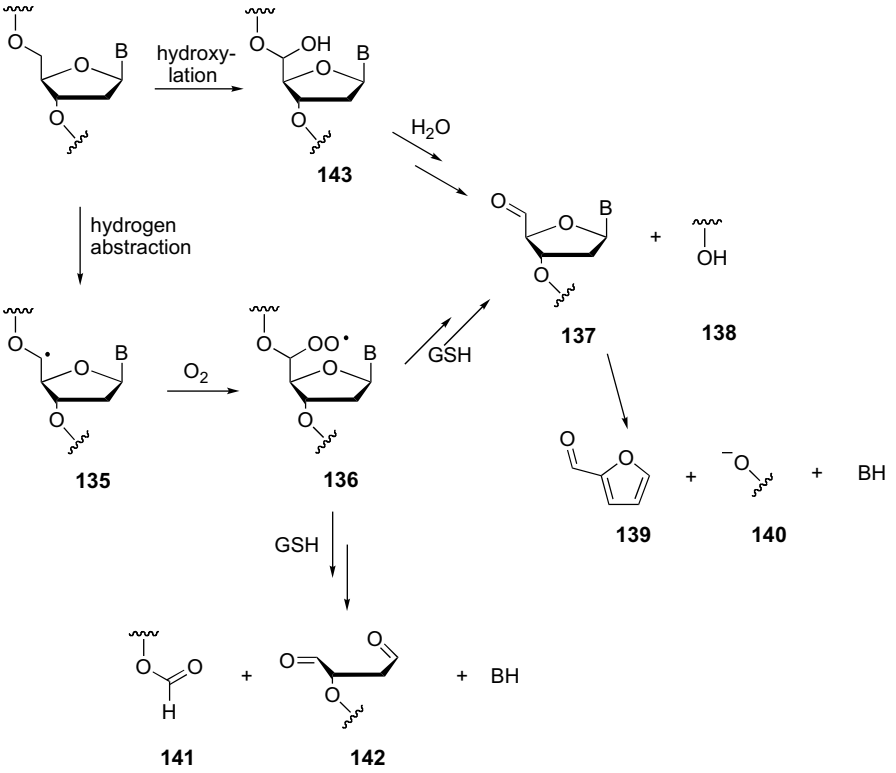

SCHEME 4.29

5′-phosphate DNA fragment (Scheme 4.29).[111] Furthermore, the 5′-aldehyde **137** is found to give adducts with nucleophiles.

The 2-phosphoryl-1,4-dioxo butane residue **144** may exist in a hydrated form, which is expected to be in equilibrium with the cyclic form **145** (Scheme 4.30). The dialdehydic structure and β-elimination reaction that gives 2-phosphoryl-1,4-dioxo

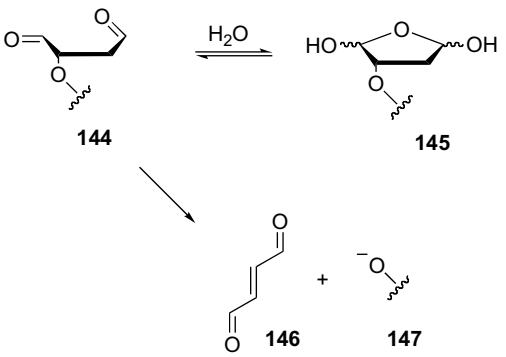

SCHEME 4.30

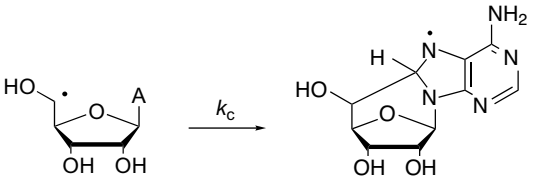

148 **149**

SCHEME 4.31

butane **146** and 5′- phosphate-terminated oligomers **147** was investigated in detail. [112, 113] Two analytical methods have also been developed for the detection and quantification of **146**.[112] It was recently shown that **146** forms adducts with dA and dC in oxidized DNA.[113]

Methods for the synthesis of oligonucleotides containing 5′-aldehyde or 2-phosphoryl-1,4-dioxo butane termini, resulting from the C5′-oxidation of thymidine in DNA, have been developed and their cleavage labilities were determined.[114] 5′-Aldehyde **137** does not destabilize duplex DNA compared to thymidine, whereas **144** affects the thermal stability of a duplex to an extent similar to that of the tetrahydrofuran model of an abasic site.

4.6.4. Ribo-Nucleosides

The chemistry of 5′,8-cyclopurine nucleosides has its origin in the literature of ionizing radiation since they have been first observed as products in the reaction of $HO^{\bullet}$ radicals with adenosine.[12, 13, 91]

The site-specific generation of adenosin-5′-yl radical **148** was obtained by one-electron reduction of 8-bromoadenosine in pulse radiolysis experiments (Scheme 4.31).[52] 8-Bromoadenosine captures electrons and rapidly loses a bromide ion to give the corresponding C8 radical which intramolecularly abstracts a hydrogen atom (cf. **122** in Scheme 4.27 for the analogous 2′-deoxyadenosine). The reaction is partitioned between the C5′ and C2′ positions in a 60:40 ratio leading to adenosin-5′-yl radical **148** and adenosin-2′-yl radical (*vide infra*). Radical **148** attacks adenine with a rate constant of $1.0 \times 10^4\ s^{-1}$ and gives the aromatic aminyl radical **149**. This rate constant is more than one-order of magnitude slower than the cyclization of the analogous 2′-deoxyadenosin-5′-yl radical, probably as a consequence of the conformational changes in going from *ribo* to 2′-deoxy*ribo* derivatives. Product analysis of these reactions evidenced the formation of 5′,8-cycloadenosine in a (5′*R*)/(5′*S*) diastereomeric ratio of 3.5:1. Similar experiments and results were reported for the inosin-5′-yl radical.[53]

4.7. CONCLUSIONS

In the last decade, the reactivity of nucleic acid sugar radicals has been an intensive research subject as evidenced by the literature surveyed in this chapter. The site-

specific generation of sugar radicals has been the key approach for a better understanding of chemical molecular mechanisms occurring at the biological level. It is now clear that once a certain sugar radical is formed, it can partition among various pathways. Unimolecular processes, such as fragmentations or cyclizations, compete with bimolecular processes, such as reactions with oxygen, thiols, oxidants, or reductants. Therefore, the local concentration of these components and pH are extremely important in selecting the preferred pathway. However, important information is still missing regarding radical reactions occurring at the supramolecular level in duplex DNA. For example, questions concerning the role of oxygen in the formation of 5′,8-cyclopurines and their diastereomeric ratio and the fate of DNA–peroxyl radicals in the presence of thiols remain unanswered.

The last decade has also been characterized by (a) the development of methods for the synthesis of oligonucleotides incorporating specific lesions, which are of great importance for clarifying the biochemical and biophysical aspects of these lesions, and (b) the development of methods for the measurement of 2-deoxyribose oxidation products in DNA. Research in these areas is also expected to expand in view of the importance of metabolic fate of sugar oxidation products in genetic toxicology.

REFERENCES

1. Halliwell, B.; Gutteridge, J. M. C. *Free Radicals in Biology and Medicine*, 4th ed.; Oxford University Press, Oxford, 2007.
2. Friedberg, E. C.; Walker, G. C.; Siede, W. *DNA Repair Mutagenesis*; ASM Press, Washington, DC, 1995.
3. Delaney, J. C.; Essigmann, J. M. Biological properties of single chemical–DNA adducts: A twenty year perspective. *Chem. Res. Toxicol.* **2008**, *21*, 232–252.
4. Dedon, P. C. The chemical toxicology of 2-deoxyribose oxidation in DNA. *Chem. Res. Toxicol.* **2008**, *21*, 206–219.
5. Sy, D.; Savoye, C.; Begusova, M.; Michalik, V.; Charlier, M.; Spotheim-Maurizot, M. Sequence-dependent variations of DNA structure modulate radiation-induced strand breakage. *Int. J. Radiat. Biol.* **1997**, *72*, 147–155.
6. Boussicault, F.; Kaloudis, P.; Caminal, C.; Mulazzani, Q. G.; Chatgilialoglu, C. The fate of C5′ radicals of purine nucleosides under oxidative conditions. *J. Am. Chem. Soc.* **2008**, *130*, 8377–8385.
7. Goldberg, I. H. Mechanism of neocarzinostatin action: Role of DNA microstructure in determination of chemistry of bistranded oxidative damage. *Acc. Chem. Res.* **1991**, *24*, 191–198.
8. Pratviel, G.; Bernadou, J.; Meunier, B. Carbon–hydrogen bonds of DNA sugar units as targets for chemical nucleases and drugs. *Angew. Chem. Int. Ed. Eng.l* **1995**, *34*, 746–769.
9. Dedon, P. C.; Goldberg, I. H. Free-radical mechanisms involved in the formation of sequence-dependent bistranded DNA lesions by the antitumor antibiotics bleomycin, neocarzinostatin, and calicheamicin. *Chem. Res. Toxicol.* **1992**, *5*, 311–332.

10. O'Neill, P.; Fielden, E. M. Primary free radical processes in DNA. *Adv. Radiat. Biol.* **1993**, *17*, 53–120.
11. Pogozelski, W. K.; Tullius, T. D. Oxidative strand scission of nucleic acids: Routes initiated by hydrogen abstraction from the sugar moiety. *Chem. Rev.* **1998**, *98*, 1089–1107.
12. von Sonntag, C. *The Chemical Basis of Radiation Biology*; Taylor & Francis, Philadelphia, 1987.
13. von Sonntag, C. *Free-Radical-Induced DNA Damage and Its Repair: A Chemical Persective*; Springer-Verlag, Berlin, 2006.
14. Tallman, K. A.; Tronche, C.; Yoo, D. J.; Greenberg, M. M. Release of superoxide from nucleoside peroxyl radicals, a double-edged sword? *J. Am. Chem. Soc.* **1998**, *120*, 4903–4909.
15. Chatgilialoglu, C.; Gimisis, T.; Guerra, M.; Ferreri, C.; Emanuel, C. J.; Horner, J. H.; Newcomb, M.; Lucarini, M.; Pedulli, G. F. Spectra and structure of the 2′-deoxyuridin-1′-yl radical. *Tetrahedron Lett*. **1998**, *39*, 3947–3950.
16. Chatgilialoglu, C.; Ferreri, C.; Bazzanini, R.; Guerra, M.; Choi, S.-Y.; Emanuel, C. J.; Horner, J. H.; Newcomb, M. Model of DNA C1′ radicals. Structural, spectral and chemical properties of the thyminylmethyl radical and the 2′-deoxyuridin-1′-yl radical. *J. Am. Chem. Soc.* **2000**, *122*, 9525–9533.
17. Hwang, J.-T.; Greenberg, M. M. Kinetic and stereoselectivity of thiol trapping of deoxyuridin-1′-yl in biopolymers and their relationship to the formation of premutagenic α-deoxynucleotides. *J. Am. Chem. Soc.* **1999**, *121*, 4311–4315.
18. Lesiak, K. B.; Wheeler, K. T. Formation of α-deoxyadenosine in polydeoxynucleotides exposed to ionising radiation under anoxic conditions. *Radiat. Res.* **1990**, *121*, 328–337.
19. Ide, H.; Yamaoka, T.; Kimura, Y. Replication of DNA templates containing the α-anomer of deoxyadenosine, a major adenine lesion produced by hydroxyl radicals. *Biochemistry* **1994**, *33*, 7127–7133.
20. Tronche, C.; Goodman, B. K.; Greenberg, M. M. DNA damage induced via independent generation of the radical resulting from formal hydrogen atom abstraction from the C1′-position of a nucleotide. *Chem. Biol.* **1998**, *5*, 263–271.
21. Chatgilialoglu, C.; Gimisis, T. Fate of the C-1′ peroxyl radical in the 2′-deoxyuridine system. *Chem. Commun.* **1998**, 1249–1250.
22. Emanuel, C. J.; Newcomb, M.; Ferreri, C.; Chatgilialoglu, C. Kinetics of 2′-deoxyuridin-1′-yl radical reactions. *J. Am. Chem. Soc.* **1999**, *121*, 2927–2928.
23. Hildenbrand, K.; Schulte-Frohlinde, D. Time-resolved EPR studies on the rates of peroxyl radicals of poly(acrylic acid) and of calf thymus DNA with glutathione. Re-examination of a rate constant for DNA. *Int. J. Radiat. Biol.* **1997**, *71*, 377–385.
24. Greenberg, M. M. Elucidating DNA damage and repair processes by independently generating reactive and metastable intermediates. *Org. Biomol. Chem.* **2007**, *5*, 18–30.
25. Xu, Y.; Sugiyama, H. Photochemical approach to probing different DNA structures. *Angew. Chem. Int. Ed.* **2006**, *45*, 1354–1362.
26. Gimisis, T.; Chatgilialoglu, C. 1,5-Radical translocation protocol for the generation of C-1′ radicals in nucleosides. Synthesis of spiro nucleosides through a rare 5-*endo-trig* cyclization. *J. Org. Chem.* **1996**, *61*, 1908–1909.
27. Gimisis, T.; Castellari, C.; Chatgilialoglu, C. A new class of anomeric spironucleosides. *Chem. Commun.* **1997**, 2089–2090.

28. Kotera, M.; Bourdat, A.-G.; Defraneq, E.; Lhomme, J. A highly efficient synthesis of oligodeoxyribonucleotides containing the 2′-deoxyribonolactone lesion. *J. Am. Chem. Soc.* **1998**, *120*, 11810–11811.

29. Defrancq, E.; Lhomme, J.; Dumy, P.; Kotera, M. 3-Nitro-3-deaza-2′-deoxyadenosine as a versatile photocleavable 2′-deoxyadenosine mimic. *J. Am. Chem. Soc.* **2004**, *126*, 9532–9533.

30. Jourdan, M.; Garcia, J.; Defrancq, E.; Kotera, M.; Lhomme, J. 2′-Deoxyribonolactone lesion in DNA: Refined solution structure determined by nuclear magnetic resonance and molecular modeling. *Biochemistry* **1999**, *38*, 3985–3995.

31. Roupioz, Y.; Lhomme, J.; Kotera, M. Chemistry of the 2-deoxyribonolactone lesion in oligonucleotides: Cleavage kinetics and products analysis. *J. Am. Chem. Soc.* **2002**, *124*, 9129–9135.

32. Lenox, H. J.; McCoy, C. P.; Sheppard, T. L. Site-specific generation of deoxyribonolactone lesions in DNA oligonucleotides. *Org. Lett.* **2001**, *3*, 2415–2418.

33. Zheng, Y.; Sheppard, T. L. Half-life and DNA strand scission products of 2-deoxyribonolactone oxidative DNA damage lesions. *Chem. Res. Toxicol.* **2004**, *17*, 197–207.

34. Bales B. C.; Pitié, M.; Meunier, B.; Greenberg, M. M. A minor groove binding copper-phenanthroline conjugate produces direct strand breaks via β-elimination of 2-deoxyribonolactone. *J. Am. Chem. Soc.* **2002**, *124*, 9062–9063.

35. Greenberg, M. M.; Weledji, Y. N.; Kim, J.; Bales, B. C. Repair of oxidized abasic sites by exonuclease III, endonuclease IV, and endonuclease III biochemistry. *Biochemistry* **2004**, *43*, 8178–8183.

36. Berthet, N.; Roupioz, Y.; Constant, J. F.; Kotera, M.; Lhomme, J. Translesional synthesis on DNA templates containing the 2′-deoxyribonolactone lesion. *Nucleic Acids Res.* **2001**, *29*, 2725–2723.

37. Wang, Y.; Sheppard, T. L.; Tornaletti, S.; Maeda, L. S.; Hanawalt, P. C. Transcriptional inhibition by an oxidized abasic site in DNA. *Chem. Res. Toxicol.* **2006**, *19*, 234–241.

38. DeMott, M. S.; Beyret, E.; Wong, D.; Bales, B. C.; Hwang, J. T.; Greenberg, M. M.; Demple, B. Covalent trapping of human DNA polymerase b by the oxidative DNA lesion 2-deoxyribonolactone. *J. Biol. Chem.* **2002**, *277*, 7637–7640.

39. Kroeger, K. M.; Hashimoto, M.; Kow, Y. W.; Greenberg, M. M. Cross-linking of 2-deoxyribonolactone and its β-elimination product by base excision repair enzymes. *Biochemistry* **2003**, *42*, 2449–2455.

40. Sung, J. S.; DeMott, M. S.; Demple, B. Long-patch base excision DNA repair of 2-deoxyribonolactone prevents the formation of DNA-protein cross-links with DNA polymerase beta. *J. Biol. Chem.* **2005**, *280*, 39095–39103.

41. Faure, V.; Constant, J. F.; Dumy, P.; Saparbaev, M. 2′-Deoxyribonolactone lesion produces G $\rightarrow$ A transitions in *Escherichia coli*. *Nucleic Acids Res.* **2004**, *32*, 2937–2946.

42. Kow, Y. W.; Bao, G.; Minesinger, B.; Jinks-Robertson, S.; Siede, W.; Jiang, Y. L.; Greenberg, M. M. Mutagenic effects of abasic and oxidized abasic lesions in *Saccharomyces cerevisiae*. *Nucleic Acids Res.* **2005**, *33*, 6196–6202.

43. Roginskaya, M.; Razskazovskiy, Y.; Bernhard, W. A. 2-Deoxyribonolactone lesions in X-ray-irradiated DNA: Quantitative determination by catalytic 5-methylene-2-furanone release. *Angew. Chem. Int. Ed.* **2005**, *44*, 6210–6213.

44. Xue, L.; Greenberg, M. M. Use of fluorescence sensors to determine that 2-deoxyribonolactone is the major alkali-labile deoxyribose lesion produced in oxidatively damaged DNA. *Angew. Chem. Int. Ed.* **2007**, *46*, 561–564.
45. Sugiyama, H.; Fujimoto, K.; Saito, I. Stereospecific 1,2-hydride shift in ribonolactone formation in the photoreaction of 2′-iododeoxyuridine. *J. Am. Chem. Soc.* **1995**, *117*, 2945–2946.
46. Sugiyama, H.; Tsutsumi, Y.; Fujimoto, K.; Saito, I. Photoinduced deoxyribose C2′ oxidation in DNA. Alkali-dependent cleavage of erythrose-containing sites via a retro-aldol reaction. *J. Am. Chem. Soc.* **1993**, *115*, 4443–4448.
47. Kawai, K.; Saito, I.; Sugiyama, H. Conformation-dependent photochemistry of 5-halouracil-containing DNA: Stereospecific 2′α-hydroxylation of deoxyribose in Z-form DNA. *J. Am. Chem. Soc.* **1999**, *121*, 1391–1392.
48. Dizdaroglu, M.; Schulte-Frohlinde, D.; von Sonntag, C. Z. γ-Radiolysis of DNA in oxygenated aqueous solution. Structure of an alkali labile site. *Naturforsch.* **1977**, *32C*, 1021–1022.
49. Kim, J.; Weledji, Y. N.; Greenberg, M. M. Independent generation and characterization of a C2′-oxidized abasic site in chemically synthesized oligonucleotides. *J. Org. Chem.* **2004**, *69*, 6100–6104.
50. Greenberg, M. M.; Kreller, C. R.; Young, S. E.; Kim, J. Reactivity of the C2′-oxidized abasic lesion and its relevance to interactions with Type I base excision repair enzymes. *Chem. Res. Toxicol.* **2006**, *19*, 463–468.
51. Greenberg, M. M.; Weledji, Y. N.; Kroeger, K. M.; Kim, J. *In vitro* replication and repair of DNA containing a C2′-oxidized abasic site. *Biochemistry* **2004**, *43*, 15217–15222.
52. Chatgilialoglu, C.; Duca, M.; Ferreri, C.; Guerra, M.; Ioele, M.; Mulazzani, Q. G.; Strittmatter, H.; Giese, B. Selective generation and reactivity of 5′-adenosinyl and 2′-adenosinyl radicals. *Chem. Eur. J.* **2004**, *10*, 1249–1255.
53. Russo, M.; Jimenez, L. B.; Mulazzani, Q. G.; D'Angelantonio, M.; Guerra, M.; Miranda, M. A.; Chatgilialoglu, C. Chemical radiation studies of 8-bromo-2′-deoxyinosine and 8-bromoinosine in aqueous solutions. *Chem. Eur. J.* **2006**, *12*, 7684–7693.
54. Sitlani, A.; Long, E. C.; Pyle, A. M.; Barton, J. K. DNA photocleavage by phenanthrenequinone diimine complexes of rhodium(III): Shape-selective recognition and reaction. *J. Am. Chem. Soc.* **1992**, *114*, 2303–2312.
55. Hudson, B. P.; Barton, J. K. Solution structure of a metallointercalator bound site specifically to DNA. *J. Am.Chem. Soc.* **1998**, *120*, 6877–6888.
56. Körner, S.; Bryant-Friedrich, A. C.; Giese, B. C-3′-branched thymidines as precursors for the selective generation of C-3′-nucleoside radicals. *J. Org. Chem.* **1999**, *64*, 1559–1564.
57. Bryant-Friedrich, A. C. Generation of a C-3′-thymidinyl radical in single-stranded oligonucleotides under anaerobic conditions. *Org. Lett.* **2004**, *6*, 2329–2332.
58. Lahoud, G. A.; Hitt, A. L.; Bryant-Friedrich, A. C. Aerobic fate of the C-3′-thymidinyl radical in single-stranded DNA. *Chem. Res. Toxicol.* **2006**, *19*, 1630–1636.
59. Collins, C.; Zhou, X.; Wang, R.; Barth, M. C.; Jiang, T.; Coderre, J. A.; Dedon, P. C. Differential oxidation of deoxyribose in DNA by γ - and α-radiation. *Radiat. Res.* **2005**, *163*, 654–662.
60. Collins, C.; Awada, M. M.; Zhou, X.; Dedon, P. C. Analysis of 3′-phosphoglycolaldehyde residues in oxidized DNA by gas chromatography/negative chemical ionization/mass spectrometry. *Chem. Res. Toxicol.* **2003**, *16*, 1560–1566.

61. Stubbe, J; van der Donk, W. A. Protein radicals in enzyme catalysis. *Chem. Rev.* **1998**, *98*, 705–762.
62. Lawrence C. C.; Bennati, M.; Obias, H. V.; Bar, G.; Griffin, R. G.; Stubbe, J. High-field EPR detection of a disulfide radical anion in the reduction of cytidine 5′-diphosphate by the E441Q R1 mutant of Escherichia coli ribonucleotide reductase. *Proc. Natl. Acad. Sci. U.S.A.* **1999**, *96*, 8979–8984.
63. Lenz, R.; Giese, B. Studies on the mechanism of ribonucleotide reductases. *J. Am. Chem. Soc.* **1997**, *119*, 2784–2794.
64. Robins, M. J.; Guo, Z.; Samano, M. C.; Wnuk, S. F. Biomimetic simulation of free radical-initiated cascade reactions postulated to occur at the active site of ribonucleotide reductases. *J. Am. Chem. Soc.* **1999**, *121*, 1425–1433.
65. Stubbe, J.; Kozarich, J. W.; Wu, W.; Vanderwall, D. E. Bleomycins: a structural model for specificity, binding, and double strand cleavage. *Acc. Chem. Res.* **1996**, *29*, 322–330.
66. Giese, B.; Beyrich-Graf, X.; Erdmann, P.; Petretta, M.; Schwitter, U. The chemistry of single-stranded 4′-DNA radicals: influence of the radical precursor on anaerobic and aerobic strand cleavage. *Chem. Biol.* **1995**, *2*, 367–375.
67. Giese, B.; Dussy, A.; Meggers, E.; Petretta, M.; Schwitter, U. Conformation, lifetime, and repair of 4′-DNA radicals. *J. Am. Chem. Soc.* **1997**, *119*, 11130–11131.
68. Peukert, S.; Batra, R.; Giese, B. ESR evidence for a heterolytic C,O-bond cleavage in models of 4′-DNA radicals. *Tetrahedron Lett.* **1997**, *38*, 3507–3510.
69. Gugger, A.; Batra, R.; Rzadek, P.; Rist, G.; Giese, B. Spectroscopic evidence for a radical cation as intermediate in a model reaction of the 4′-DNA radical strand cleavage. *J. Am. Chem. Soc.* **1997**, *119*, 8740–8741.
70. Giese, B. Long-distance charge transport in DNA: The hopping mechanism. *Acc. Chem. Res.* **2000**, *33*, 631–636.
71. Glatthar, R.; Spichty, M.; Gugger, A.; Batra, R.; Damm, W.; Mohr, M.; Zipse, H.; Giese, B. Mechanistic studies in the radical induced DNA strand cleavage—Formation and reactivity of the radical cation intermediate. *Tetrahedron* **2000**, *56*, 4117–4128.
72. Dussy, A.; Meggers, E.; Giese, B. Spontaneous cleavage of 4′-DNA radicals under aerobic conditions: Apparent discrepancy between trapping rates and cleavage products. *J. Am. Chem. Soc.* **1998**, *120*, 7399–7403.
73. Giese, B.; Beyrich,-Graf, X.; Erdmann, P.; Giraud, L.; Imwinkelried, P.; Müller, S. N.; Schwitter, U. Cleavage of single-stranded 4′-oligonucleotide radicals in the presence of O_2. *J. Am. Chem. Soc.* **1995**, *117*, 6146–6147.
74. Beyrich,-Graf, X.; Müller, S. N.; Giese, B. Oxidation of 4′-deoxyribonucleoside radicals to 4′-deoxyribonucleoside cations. A model for the function of bleomycin. *Tetrahedron Lett.* **1998**, *39*, 1553–1556.
75. Kim, J.; Gil, J. M.; Greenberg, M. M. Synthesis and characterization of oligonucleotides containing the C4′-oxidized abasic site produced by bleomycin and other DNA damaging agents. *Angew. Chem. Int. Ed.* **2003**, *42*, 5882–5885.
76. Chen, J.; Stubbe, J. Synthesis and characterization of oligonucleotides containing a 4′-keto abasic site. *Biochemistry* **2004**, *43*, 5278–5286.
77. Junker, H.-D.; Hoehn, S. T.; Bunt, R. C.; Marathius, V.; Chen, J.; Turner, C. J.; Stubbe, J. Synthesis, characterization and solution structure of tethered oligonucleotides containing an internal 3′-phosphoglycolate, 5′-phosphate gapped lesion. *Nucleic Acids Res.* **2002**, *30*, 5497–5508.

78. Chen, B.; Zhou, X.; Taghizadeh, K.; Chen, J.; Stubbe, J.; Dedon, P. C. GC/MS methods to quantify the 2-deoxypentos-4-ulose and 3′-phosphoglycolate pathways of 4′ oxidation of 2-deoxyribose in DNA: Application to DNA damage produced by γ radiation and bleomycin. *Chem. Res. Toxicol.* **2007**, *20*, 1701–1708.
79. Dhar, S.; Kodama, T.; Greenberg, M. M. Selective detection and quantification of oxidized abasic lesions in DNA. *J. Am. Chem. Soc.* **2007**, *129*, 8702–8703.
80. Xu, Y. J.; Kim, E. Y.; Demple, B. Excision of C-4′-oxidized deoxyribose lesions from double-stranded DNA by human apurinic/apyrimidinic endonuclease (ape1 protein) and DNA polymerase beta. *J. Biol. Chem.* **1998**, *273*, 28837–28844.
81. Greenberg, M. M.; Weledji, Y. N.; Kroeger, K. M.; Kim, J.; Goodman, M. F. *In vitro* effects of a C4′-oxidized abasic site on DNA polymerases. *Biochemistry* **2004**, *44*, 2656–2663.
82. Regulus, P.; Duroux, B.; Bayle, P.-A.; Favier, A.; Cadet, J.; Ravanat, J.-L. Oxidation of the sugar moiety of DNA by ionizing radiation or bleomycin could induce the formation of a cluster DNA lesion. *Proc. Natl. Acad. Sci. U.S.A.* **2007**, *104*, 14032–14037.
83. Noll, D. M.; Mason, T. M.; Miller, P. S. Formation and repair of interstrand cross-links in DNA. *Chem. Rev.* **2006**, *106*, 277–301.
84. Sczepanski, J. T.; Jacobs, A C.; Greenberg, M. M. Self-promoted DNA interstrand cross-Link formation by an abasic site. *J. Am. Chem. Soc.* **2008**, *130*, 9646–9647.
85. Hecht, S. M. RNA degradation by bleomycin, a naturally occurring bioconjugate. *Bioconjugate Chem.* **1994**, *5*, 513–526.
86. Strittmatter, H.; Dussy, A.; Schwitter, U.; Giese, B. Differences between 4′-RNA and 4′-DNA radicals during anaerobic and aerobic strand cleavage. *Angew. Chem. Int. Ed.* **1999**, *38*, 135–137.
87. Crich, D.; Mo, X.-S. Nucleotide C3′,4′-radical cations and the effect of a 2′-oxygen substituent. The DNA/RNA paradox. *J. Am. Chem. Soc.* **1997**, *119*, 249–250.
88. Dizdaroglu, M.; Jaruga, P.; Rodriguez, H. Identification and quantification of 8,5′-cyclo-2′-deoxyadenosine in DNA by liquid chromatography-mass spectrometry. *Free Radic. Biol. Med.* **2001**, *30*, 774–784.
89. Jaruga, P.; Birincioglu, M.; Rodriguez, H.; Dizdaroglu, M. Mass spectrometric assays for the tandem lesion 8,5′-cyclo-2′-deoxyguanosine in mammalian DNA. *Biochemistry* **2002**, *41*, 3703–3711.
90. Brooks, P. J. The 8,5′-cyclopurine-2′-deoxynucleosides: Candidate neurodegenerative DNA lesions in xeroderma pigmentosum, and unique probes of transcription and nucleotide excision repair. *DNA Repair* **2008**, *7*, 1168–1179.
91. Jaruga, P.; Dizdaroglu, M. 8,5′-Cyclopurine-2′-deoxynucleosides in DNA: Mechanisms of formation, measurement, repair and biological effects. *DNA Repair* **2008**, *7*, 1413–1425.
92. Manetto, A.; Georganakis, D.; Gimisis, T.; Leondiadis, L.; Mayer, P.; Carell, T.; Chatgilialoglu, C. Independent generation of C-5′ nucleosidyl radicals in thymidine and 2′-deoxyguanosine. *J. Org. Chem.* **2007**, *72*, 3659–3666.
93. Romieu, A.; Gasparutto, D.; Molko, D.; Cadet, J. Site-specific introduction of (5′S)-5′,8-cyclo-2′-deoxyadenosine into oligodeoxyribonucleosides. *J. Org. Chem.* **1998**, *63*, 5245–5249.
94. Romieu, A.; Gasparutto, D.; Cadet, J. Synthesis and characterization of oligonucleotides contaning 5′,8-cyclopurine 2′-deoxyribonucleosides: (5′R)- 5′,8-cyclo-2′-deoxyadenosine, (5′S)- 5′,8-cyclo-2′-deoxyadenosine, and (5′R)- 5′,8-cyclo-2′-deoxyguanosine. *Chem. Res. Toxicol.* **1999**, *12*, 412–421.

95. Flyunt, R.; Bazzanini, R.; Chatgilialoglu, C.; Mulazzani, Q. G. Fate of the 2′-deoxyadenosin-5′-yl radical under anaerobic conditions. *J. Am. Chem. Soc.* **2000**, *122*, 4225–4226.

96. Chatgilialoglu, C., Guerra, M.; Mulazzani, Q. G. Model studies of DNA C5′ radicals. Selective generation and reactivity of 2′-deoxyadenosin-5′-yl radical. *J. Am. Chem. Soc.* **2003**, *125*, 3839–3848.

97. Jimenez, L. B.; Encinas, S.; Miranda, M. A.; Navacchia, M. L.; Chatgilialoglu, C. The photochemistry of 8-bromo-2′-deoxyadenosine. A direct entry to cyclopurine lesions. *Photochem. Photobiol. Sci.* **2004**, *3*, 1042–1046.

98. Navacchia M. L.; Chatgilialoglu, C.; Montevecchi, P. C. C5′-Adenosinyl radical cyclization. A stereochemical investigation. *J. Org. Chem.* **2006**, *71*, 4445–4452.

99. Chatgilialoglu, C.; Bazzanini, R.; Jimenez, L. B.; Miranda, M. A. (5′*S*)- and (5′*R*)-5′,8-cyclo-2′-deoxyguanosine: Mechanistic insights on the 2′-deoxyguanosin-5′-yl radical cyclization. *Chem. Res. Toxicol.* **2007**, *20*, 1820–1824.

100. Theruvathu, J. A.; Jaruga, P.; Dizdaroglu, M.; Brooks, P. J. The oxidatively-induced DNA lesions 8,5′-cyclo-2′-deoxyadenosine and 8-hydroxy-2′-deoxyadenosine are strongly resistant to acid-induced hydrolysis of the glycosidic bond. *Mech. Ageing Dev.* **2007**, *128*, 494–502.

101. Jimenez, L. B.; Encinas, S.; Chatgilialoglu, C.; Miranda, M. A. Solar one-way photoisomerisation of 5′,8-cyclo-2′-deoxyadenosine. *Org. Biomol. Chem.* **2008**, *6*, 1083–1086.

102. Navacchia, M. L.; Manetto, A.; Montevecchi, P. C.; Chatgilialoglu, C. Radical cyclization approach to cyclonucleosides. *Eur. J. Org. Chem.* **2005**, 4640–4648.

103. Romieu, A.; Gasparutto, D.; Cadet, J. Synthesis and characterization of oligodeoxynucleotides containing the two 5*R* and 5*S* diastereomers of (5′*S*,6*S*)-5′,6-cyclo-5,6-dihydrothymidine; radiation-induced tandem lesions of thymidine. *J. Chem. Soc., Perkin Trans. 1* **1999**, 1257–1263.

104. Muller, E.; Gasparutto, D.; Cadet, J. Chemical synthesis and biochemical properties of oligonucleotides that contain the (5′*S*,5*S*,6*S*)-5′,6-cyclo-5-hydroxy-5,6-dihydro-2′-deoxyuridine DNA lesion. *ChemBioChem* **2002**, *3*, 534–542.

105. Len, C.; Mondon, M.; Lebreton, J. Synthesis of cyclonucleosides having a C–C bridge. *Tetrahedron* **2008**, *64*, 7453–7475.

106. Kuraoka, I.; Bender, C.; Romieu, A.; Cadet, J.; Wood, R. D.; Lindahl, T. Removal of oxygen free-radical-induced 5′,8-purine cyclodeoxynucleosides from DNA by the nucleotide excision-repair pathway in human cells. *Proc. Natl. Acad. Sci. USA* **2000**, *97*, 3832–3837.

107. Brooks, P. J.; Wise, D. S.; Berry, D. A.; Kosmoski, J. V.; Smerdon, M. J.; Somers, R. L.; Mackie, H.; Spoonde, A. Y.; Ackerman, E. J.; Coleman, K.; Tarone, R. E.; Robbins, J. H. The oxidative DNA lesion 8,5′-(S)-cyclo-2′-deoxyadenosine is repaired by the nucleotide excision repair pathway and blocks gene expression in mammalian cells. *J. Biol. Chem.* **2000**, *275*, 22355–22362.

108. Marietta, C. Brooks, P. J. Transcriptional bypass of bulky DNA lesions causes new mutant RNA transcripts in human cells. *EMBO Rep*. **2007**, *8*, 388–393.

109. Kuraoka, I.; Robins, P.; Masutani, C.; Hanaoka, F.; Gasparutto, D.; Cadet, J.; Wood, R. D.; Lindahl, T. Oxygen free radical damage to DNA. Translesion synthesis by human DNA polymerase eta and resistance to exonuclease action at cyclopurine deoxynucleoside residues. *J. Biol. Chem.* **2001**, *276*, 49283–49288.

110. Brooks, P. J. The case for 8,5′-cyclopurine-2′-deoxynucleosides as endogenous DNA lesions that cause neurodegeneration in xeroderma pigmentosum. *Neuroscience* **2007**, *145*, 1407–1417.

111. Angeloff, A.; Dubey, I; Pratviel, G.; Bernadou, J.; Meunier, B. Characterization of a 5′-aldehyde terminus rsulting from the oxidative attack at C5′ of a 2-deoxyribose on DNA. *Chem. Res. Toxicol.* **2001**, *14*, 1413–1420.

112. Chen, B.; Bohnert, T.; Zhou, X.; Dedon, P. C. 5′-(2-Phosphoryl-1,4-dioxobutane) as a product of 5′-oxidation of deoxyribose in DNA: Elimination as *trans*-1,4-dioxo-2-butene and approaches to analysis. *Chem. Res. Toxicol.* **2004**, *17*, 1406–1413.

113. Chen, B.; Vu, C. C.; Byrns, M. C.; Dedon, P. C.; Peterson, L. A. Formation of 1,4-dioxo-2-butene-derived adducts of 2′-deoxyadenosine and 2′-deoxycytidine in oxidized DNA. *Chem. Res. Toxicol.* **2006**, *19*, 982–985.

114. Kodama, T.; Greenberg, M. M. Preparation and analysis of oligonucleotides containing lesions resulting from C5′-oxidation. *J. Org. Chem.* **2005**, *70*, 9916–9924.

5

PYRIMIDINE NUCLEOBASE RADICAL REACTIVITY

MARC M. GREENBERG
Department of Chemistry, Johns Hopkins University, Baltimore, MD 21218, USA

5.1. INTRODUCTION

Radical-mediated DNA damage is a ubiquitous process whose importance is evident in chemistry and biology. Oxidative DNA damage can affect transcription and/or replication, resulting in carcinogenesis. DNA damage can also result in cell death and is the mechanism of action employed by some anticancer agents. Oxidative DNA damage is also used for analytical purposes, to study the structure, macromolecular interactions, and folding of nucleic acids. Nucleobase radicals are an important family of reactive intermediates formed when DNA is oxidatively damaged. The reactivity of pyrimidine nucleobase radicals is the focus of this chapter. Please note that for simplicity a common identifying number regardless of whether they are present as monomers, dinucleotides, oligonucleotides, and so on, is used to refer to all molecules.

Nucleobase radicals are produced in a variety of ways, including radical addition and hydrogen atom abstraction. Highly reactive σ-radicals are produced upon irradiation of nucleosides containing halogenated nucleobases. Nucleobase radicals are the major species produced when nucleic acids react with hydroxyl radical (OH•).[1] Hydroxyl radicals are produced during the reaction of some metal complexes, such as Fe•EDTA, with hydrogen peroxide.[2] They are also produced from water by γ-radiolysis in what is termed the indirect effect of ionizing radiation. Consequently, nucleobase radicals are typically associated with ionizing radiation and are generally believed to be the major family of reactive intermediates formed from the indirect effect of γ-radiolysis.

Radical and Radical Ion Reactivity in Nucleic Acid Chemistry, Edited by Marc M. Greenberg

Nucleobase radical reactivity is complex. Nucleobase radicals may react with the sugar backbone to produce strand breaks and alkali-labile lesions. They also yield inter- and intrastrand cross-links by reacting with other nucleobases. In order to avoid overlap with material covered in other chapters of this collection, this chapter focuses on the reactivity of pyrimidine nucleobase radicals resulting from addition to the π-bond and from hydrogen atom abstraction from the methyl group of thymidine and 5-methyl-2′-deoxycytidine. The reactivity of purine nucleobase radicals is described in Chapters 3, 4, and 11. The radical chemistry resulting from photolysis of 5-bromo-2′-deoxycytidine and to a lesser extent 5-bromo-2′-deoxyuridine is also discussed in this chapter. However, most of the reactivity of the 2′-deoxyuracil-5-yl radical produced from 5-bromo- and 5-iodo-2′-deoxyuridine are described by Professor Sugiyama (Chapter 6).

5.1.1. DNA Damage by γ-Radiolysis

Exogenous alkylating and/or oxidizing reagents constantly attack nucleic acids. In addition, reactive oxygen species that ultimately lead to nucleic acid damage are produced as a consequence of respiration.[3–6] One can think of DNA damage as collateral damage resulting from living. Determining how nucleic acids are oxidatively damaged is a challenging endeavor because they are heterogeneous polymers that are available in small quantities. Mechanistic studies are also complicated because many DNA damaging agents generate multiple intermediates with little selectivity or even randomly throughout the biopolymer. For instance, γ-radiolysis, the most commonly used cancer treatment that targets DNA, is also the most chemically complex. Radiation scientists have contributed significantly to our understanding of radiation induced DNA damage.[1,7] However, the unselective nature of ionizing radiation limits what can be learned about DNA damage chemistry by using it to generate reactive intermediates. During the past 15 years, organic chemistry has been used successfully to independently generate the reactive and metastable intermediates formed in DNA during oxidative stress under controlled conditions.[8–16]

5.1.2. Nucleobase-Centered Reactive Intermediates Resulting from Addition to Double Bonds

Hydroxyl radical (OH•) adds to double bonds about an order of magnitude faster than it abstracts hydrogen atoms from carbon–hydrogen bonds. The inherent differences in rate constants are reflected in the distribution of reactive intermediates produced when hydroxyl radical reacts with DNA. By some estimates, nucleobase radicals are believed to account for as much as 90% of the reactive intermediates formed (e.g., **1** and **2**, Figure 5.1).[7] Nucleobase radicals are also produced by the direct ionization of DNA, followed by reaction with water. (See Chapter 3 for more information.)

Radiation chemists have studied the reactivity of nucleobase radicals using biopolymers, monomers, and short oligonucleotides substrates. The reactivity of these substrates has been examined using an assortment of analytical and

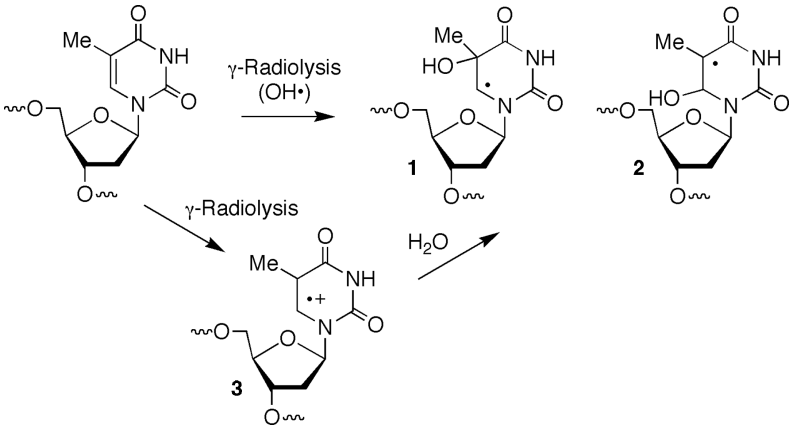

FIGURE 5.1. Formation of thymidine nucleobase radicals resulting from formal addition of OH•.

spectroscopic tools, including pulse radiolysis, EPR spectroscopy, and mass spectrometry.[7,17–20] Based on these studies, it has been proposed that ~40% of the reactions between OH• and nucleic acids result in direct strand scission.[21] If this estimate for strand scission efficiency and the proposed predominance of nucleobase radical formation are accurate, some of these reactive intermediates must lead to strand cleavage. In order to yield a strand break, the radical center must be transferred to the sugar backbone. Verification of such a process is difficult to come by using ionizing radiation to generate radicals.

5.1.2.1. Nucleobase Radical Reactivity in Nucleosides and Dinucleotides. Photolabile, synthetic nucleosides have been very useful for studying the reactivity of pyrimidine nucleobase radicals. For instance, addition of electrophilic OH• to the C5 position (**1**) is favored over formation of the C5 radical (**2**) by as much as 4 or 5:1 (Figure 5.1). The major OH• adduct of thymidine (**1**) was originally generated from trifluoromethyl benzoate **4** via a photochemical single-electron transfer process (Figure 5.2).[22,23] The instability of **4** to the alkaline conditions of oligonucleotide deprotection and mechanism of radical formation from it precludes it use to generate **1** under aerobic conditions or within oligonucleotides. However, the trifluoromethyl benzoate ester (**4**) was useful for examining the ability of **1** to effect intranucleotidyl hydrogen atom abstraction (**6**), as well as its ability to generate the cation radical (**3**). The latter has also been proposed to be an intermediate in direct strand scission.[19] Isotopic labeling and ^{2}H NMR experiments indicated that neither of these processes is competitive with the reaction of **1** with O_2 or hydrogen atom donors such as 1,4-cyclohexadiene and thiols that produced **5**.[22,23]

More recently, **1** was produced by direct photolysis of a phenyl sulfide (**7**) (Figure 5.3). Initial studies in di- and trinucleotides upon 254-nm irradiation led to the proposal that the nucleobase radical added to the adjacent guanine (**8**), but that an abasic site (**9**) was the major product.[24] The reaction with an adjacent nucleotide

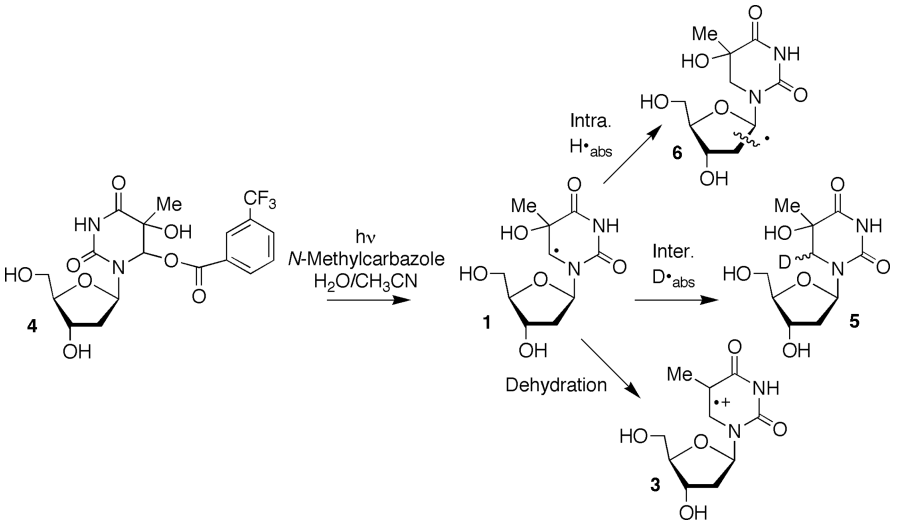

FIGURE 5.2. Independent generation of 5,6-dihydro-5-hydroxythymidin-6-yl (**1**) via photoinduced electron transfer.

produces two contiguously damaged nucleotides and is referred to as a tandem lesion.[25,26] Tandem lesions are a subset of well-studied clustered lesions, which are defined as two damaged nucleotides within ∼1.5 turns of duplex DNA.[27–30] Although subsequent experiments in duplex DNA did not corroborate the initial studies, it is possible that lesions such as **8** are formed, but were not detectable under the reported conditions.[31]

The formal C5-hydrogen atom addition product of 2′-deoxyuridine (**10**), which was designed to model the major OH• radical adduct of a pyrimidine (e.g., **1**) was generated via a Norrish Type I photochemical reaction from **11** (Figure 5.4).[32,33] The 5′-benzoyl group was used to facilitate HPLC detection. Radical **10** was generated instead of the actual OH• adduct in part because of the greater ease with which **11** could be synthesized. Competitive kinetic studies between O_2 (**12**) and β-mercaptoethanol (BME, **13**) established that monomeric 5,6-dihydro-2′-deoxyuridin-6-yl (**10**) reacts with the thiol with a rate constant ($k_{BME} = 8.8 \pm 0.5 \times 10^6\,M^{-1}\,s^{-1}$) that is typical of an alkyl radical.[34,35] Similar experiments were carried out to estimate

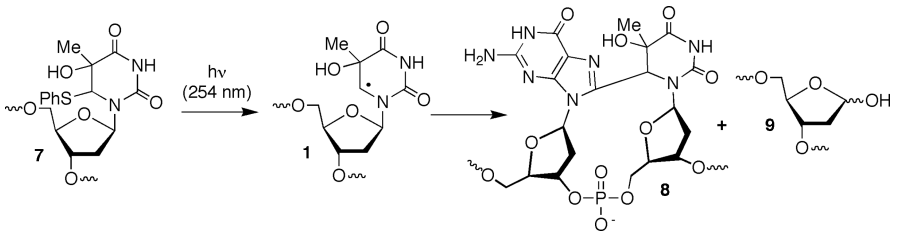

FIGURE 5.3. Independent generation of 5,6-dihydro-5-hydroxythymidin-6-yl (**1**) via 254-nm irradiation of a phenyl sulfide and tandem lesion formation.

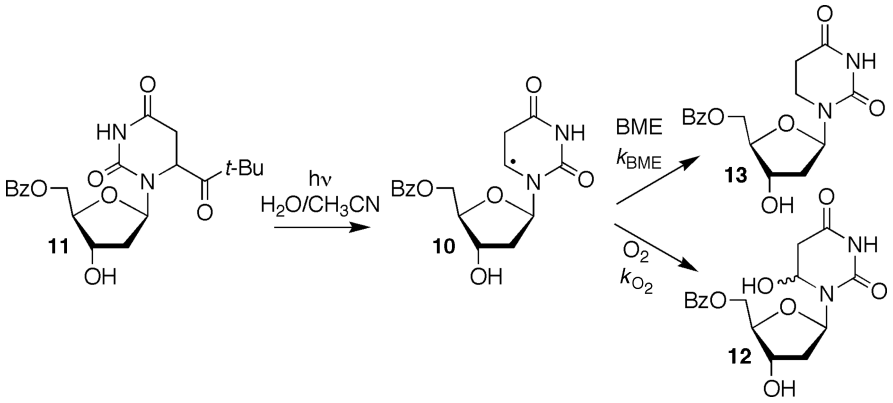

FIGURE 5.4. Independent generation of 5,6-dihydro-2′-deoxyuridin-6-yl radical (**10**) and its competitive reactions with O_2 and thiol.

the rate constant for reaction of **10** with 2,5-dimethyltetrahydrofuran (MTHF, $k_{MTHF} = 31.0 \pm 2.5\,M^{-1}\,s^{-1}$). MTHF was used as a volatile model of deoxyribose in DNA. The rate constant for hydrogen atom abstraction from MTHF (k_{MTHF}) is sufficiently slow, such that even if the effective molarity of the adjacent deoxyribose ring(s) in DNA is as high as 10 M, radical transfer from the nucleobase to the sugar will not compete with trapping by O_2 or thiol.

Photochemical generation of **10** under aerobic conditions enabled characterization of the reactivity of the respective peroxyl radical (**14**, Figure 5.5).[34] There was no evidence for $O_2^{\bullet -}$ (or OOH•) elimination from **14**. However, 2-deoxyribonolactone formation suggested that the peroxyl radical abstracts the C1′-hydrogen atom. Competition experiments with BME indicated that the rate constant for the product determining abstraction step was comparable to that of related reactions ($<1\,s^{-1}$).[36, 37]

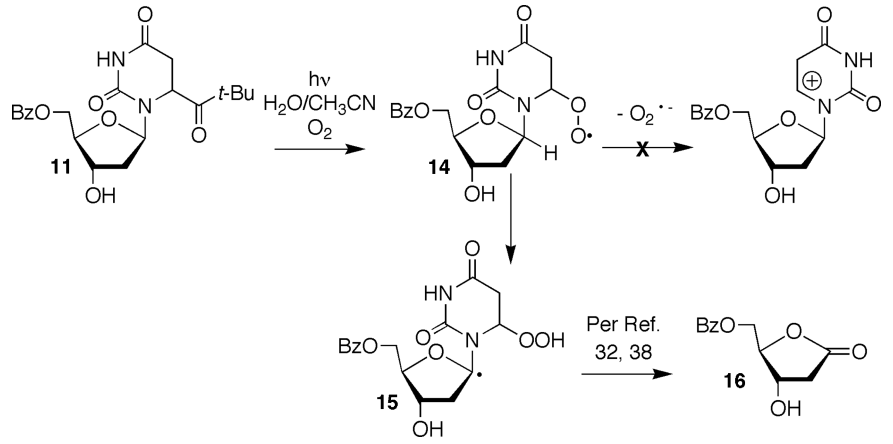

FIGURE 5.5. Reactivity of the peroxyl radical (**14**) derived from 5,6-dihydro-2′-deoxyuridin-6-yl radical (**10**).

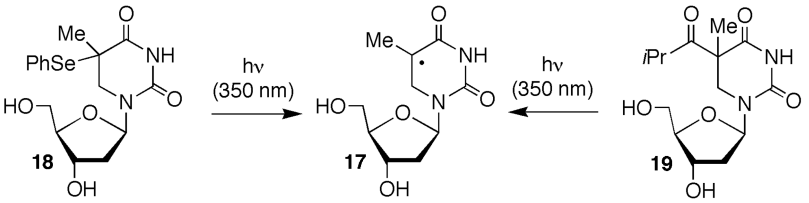

FIGURE 5.6. Independent generation of 5,6-dihydrothymidin-5-yl radical (**17**).

The detailed mechanism for the conversion of **15** into 2-deoxyribonolactone (**16**) is discussed in Chapter 4.[32,38] The formation of **16** is potentially significant because this oxidized abasic lesion exhibits interesting and unusual biochemical properties, including cross-link formation with repair proteins.[39–41]

The regioisomeric formal C6-hydrogen atom addition product of thymidine (**17**) was also generated instead of the respective OH• adduct because of synthetic expediency. The 5,6-dihydrothymidin-5-yl radical (**17**) was generated from **18** and **19** (Figure 5.6).[32, 33] The reactivity of **17** with hydrogen atom donors was similar to that of 5,6-dihydro-2′-deoxyuridin-6-yl (**10**). For instance, reaction of **17** with volatile hydrogen atom donors chosen to mimic the strength of the carbon–hydrogen bonds in 2-deoxyribose suggested that it too was highly unlikely to lead to direct strand breaks and/or lesions resulting from hydrogen atom abstraction from the 2′-deoxyribose in DNA.[33] Under aerobic conditions, **17** yielded a diastereomeric mixture of hydroperoxide **21**, which could be reduced to thymidine C5-hydrate (**22**). Mechanistic studies using **18** revealed the formation of superoxide ($O_2^{\bullet -}$) purportedly from the intermediate peroxyl radical (**20**) (Figure 5.7). The peroxyl radical was proposed to formally eliminate hydroperoxyl radical (OOH•), which deprotonates at physiological pH.[32] Elimination of OOH• from **20** produces thymidine and is competitive with reduction

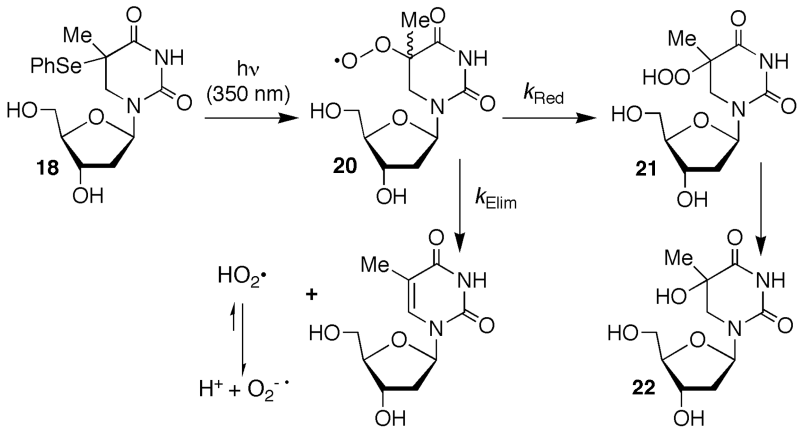

FIGURE 5.7. Superoxide elimination from the peroxyl radical of 5,6-dihydrothymidin-5-yl radical (**20**).

by hydrogen atom donors ($k_{Elim}/k_{Red} = 1.3 \times 10^{-2}$ M). This interesting reaction protects the DNA against oxidative damage.

5.1.2.2. Nucleobase Radical Reactivity in Single- and Double-Stranded DNA. Direct strand breaks and alkali-labile lesions were not observed when **19** was photolyzed in single stranded oligonucleotides under anaerobic conditions, confirming that 5,6-dihydrothymidin-5-yl radical (**17**) does not abstract hydrogen atoms from nucleotides.[42,43] In contrast, under aerobic conditions, alkali labile lesions were produced at the nucleotide where **17** was generated (intranucleotidyl) and at the 5′- and 3′-adjacent nucleotides (internucleotidyl). Deuterium labeling of the 5′-adjacent nucleotide indicated that **19** selectively abstracted the C1′-hydrogen atom from this site.

The 5,6-dihydro-2′-deoxyuridin-6-yl radical (**10**) exhibited similar dependency of strand scission on O_2, and its reactivity in DNA largely paralleled the chemistry described in the monomer.[34,44,45] For instance, there was no evidence for radical transfer from the nucleobase in **10** to its sugar or the deoxyribose of an adjacent nucleotide.[44] In contrast, tandem lesions were the major types of damage resulting from 5,6-dihydro-2′-deoxyuridin-6-yl radical (**10**) in duplex DNA under aerobic conditions via the respective peroxyl radical (**23**) (Figure 5.8).[44] Tandem lesions

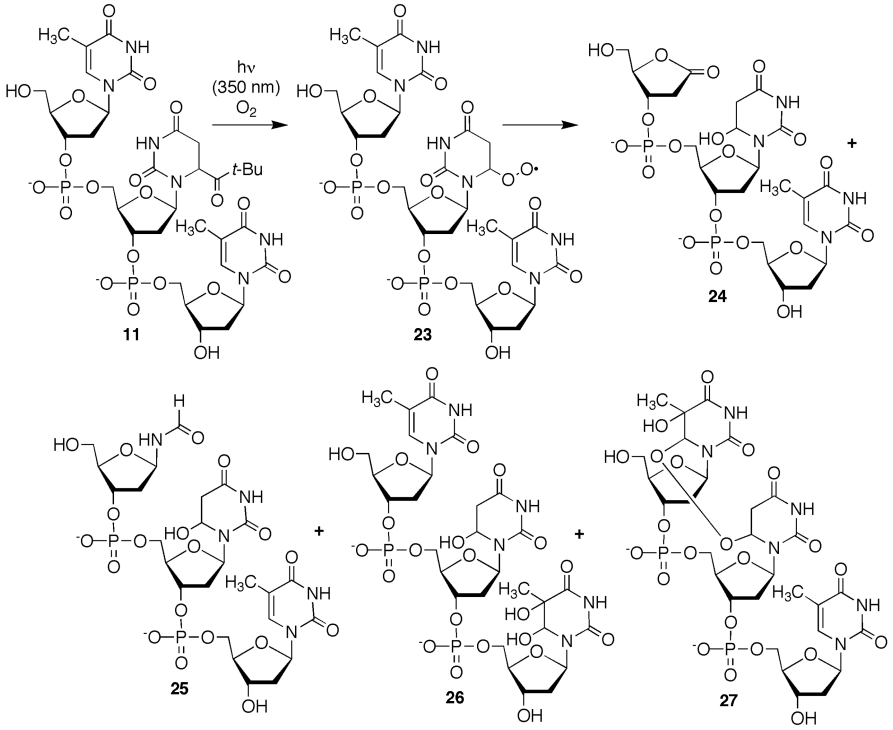

FIGURE 5.8. Representative tandem lesions produced from the peroxyl radical (**23**) of 5,6-dihydro-2′-deoxyuridin-6-yl radical (**10**).

involving the 5′-adjacent and 3′-adjacent nucleotides were detected by gel electrophoresis and accounted for at least 65% of the alkali-labile lesions derived from **23**. Modulation of the alkaline conditions indicated that tandem lesions involving the 5′-adjacent nucleotide resulted from addition to the pyrimidine ring and hydrogen atom abstraction from the deoxyribose portion of the nucleotide; whereas reaction with the 3′-adjacent nucleotide involved only reaction with the pyrimidine.

Deuterium isotope effects indicated that C1′-hydrogen atom abstraction from the 5′-adjacent nucleotide occurred selectively. Using previous studies as a guide, the C1′ radical was expected to yield 2-deoxyribonolactone (**16**).[32,38] Several subsequent experiments confirmed this hypothesis. 2-Deoxyribonolactone was detected by gel electrophoresis using a series of fingerprint reactions diagnostic for this oxidized abasic site and subsequently by a biotinylated reagent that reacted selectively with it.[46–48] Unambiguous identification of this product was obtained via MALDI-TOF MS analysis of photolyzed single-stranded DNA. Additional MS evidence, including ^{2}H and ^{18}O isotopic labeling, was obtained by analyzing photolyses of a trinucleotide containing **11** via ESI-MS/MS (Figure 5.8). These experiments also confirmed that the lactone (**16**) was produced via elimination of superoxide from the corresponding C1′-peroxyl radical and that **23** reacts with the 5′-adjacent nucleotide but not the 3′-adjacent nucleotide to produce 2-deoxyribonolactone.[32,38] The ESI-MS/MS experiments also provided positive proof for a variety of novel tandem lesions. Some of the lesions contained peroxide bonds between adjacent nucleobases (e.g., **27**), while others were consistent with the intermediacy of peroxyl radical addition products (e.g., **25**, **26**). Deuterium-labeling experiments also confirmed gel electrophoresis observations, which indicated that **23** abstracted the C1′-hydrogen atom from the 5′-adjacent nucleotide but not from the 3′-nucleotide.

Gel electrophoresis analysis indicated that 2-deoxyribonolactone (**16**) containing tandem lesions (e.g., **24**) account for ~15–25% of the tandem lesions derived from **23**. Selective C1′ hydrogen atom abstraction by **23** was consistent with predicted carbon–hydrogen bond strengths and the proximity of the peroxyl radical oxygen atom, which is able to reach into the minor groove from its position in the major groove.[49,50] The peroxyl radical oxygen of **23** can approach to within 1.5 Å of the C1′-hydrogen atom of the 5′-adjacent nucleotide without distorting the duplex. Importantly, formation of 2-deoxyribonolactone (**16**) as part of a tandem lesion via **23** provides a mechanism to explain the high yields of this lesion when DNA is exposed to diffusible species, despite the C1′-hydrogen atom's poor solvent accessibility.[49,51–53] Studies on the mutagenicity of this tandem lesion have not been reported. However, a related lesion significantly alters the activity of some base excision repair enzymes and is a substrate for nucleotide excision repair.[54]

Molecular modeling also revealed why tandem lesions involving the 3′-adjacent nucleotide resulted exclusively from reaction with the respective nucleobase. The deoxyribose hydrogen atoms of the 3′-adjacent nucleotide are considerably further (>5 Å) from the diastereomeric peroxyl radical (6*S*-**23**) due to the helical twist of

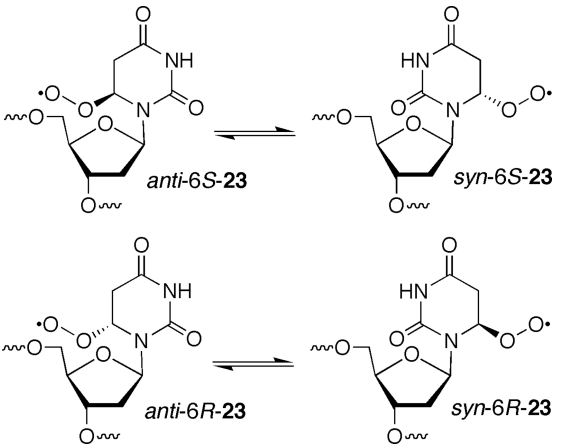

FIGURE 5.9. Conformational isomers of diastereomeric nucleobase peroxyl radicals.

the duplex.[44] Furthermore, glycosidic bond rotation in the peroxyl radicals (6*R*-**23**, 6*S*-**23**) to adopt the *syn*- and *anti*-conformations, which trapping experiments indicate are kinetically feasible, does not increase the accessibility of the 3′-adjacent nucleotide's deoxyribose ring (Figure 5.9).[45] Overall, these experiments revealed that tandem lesions are produced in higher yield than previously recognized and that the reactivities of nucleobase peroxyl radicals are strongly influenced by conformational constraints. The studies also suggest that direct strand breaks may be formed less efficiently from γ-radiolysis than is generally accepted if nucleobase radicals are the major family of reactive species produced by ionizing radiation.

5.1.3. Nucleotide Methyl Radicals Resulting from Formal Hydrogen Atom Abstraction from C5-Pyrimidine Methyl Groups

Ionizing radiation experiments have suggested that 5-(2′-deoxyuridinyl)methyl radical (**28**) can account for as much as 7% of the reactions of OH• with thymidine. Thermodynamics and DNA structure suggest that 5-(2′-deoxyuridinyl)methyl (**28**) and 5-(2′-deoxycytidinyl)methyl radicals (**29**) are viable candidates for reactive intermediates produced by OH•. The methyl group carbon–hydrogen bonds in the nucleotides are the weakest such bonds in DNA because **28** and **29** are stabilized by delocalization of the unpaired electrons into the respective pyrimidine rings. In addition, the methyl group hydrogen atoms are readily accessible in the major groove of DNA to diffusible species such as OH•. The nucleotide methyl radicals can also be produced by deprotonation of the radical cations that are formed by one-electron oxidation of the nucleotides. This pathway was recently proposed to explain 5-(2′-deoxyuridinyl)methyl radical (**28**) formation during electron transfer through DNA.[55,56]

Radicals **28** and **29** have been independently produced from multiple photolabile precursors (Figure 5.10). Although **28** was produced from a benzyl ketone (**30**) via a Norrish Type I reaction, most studies on it and the 5-(2′-deoxycytidinyl)methyl radical

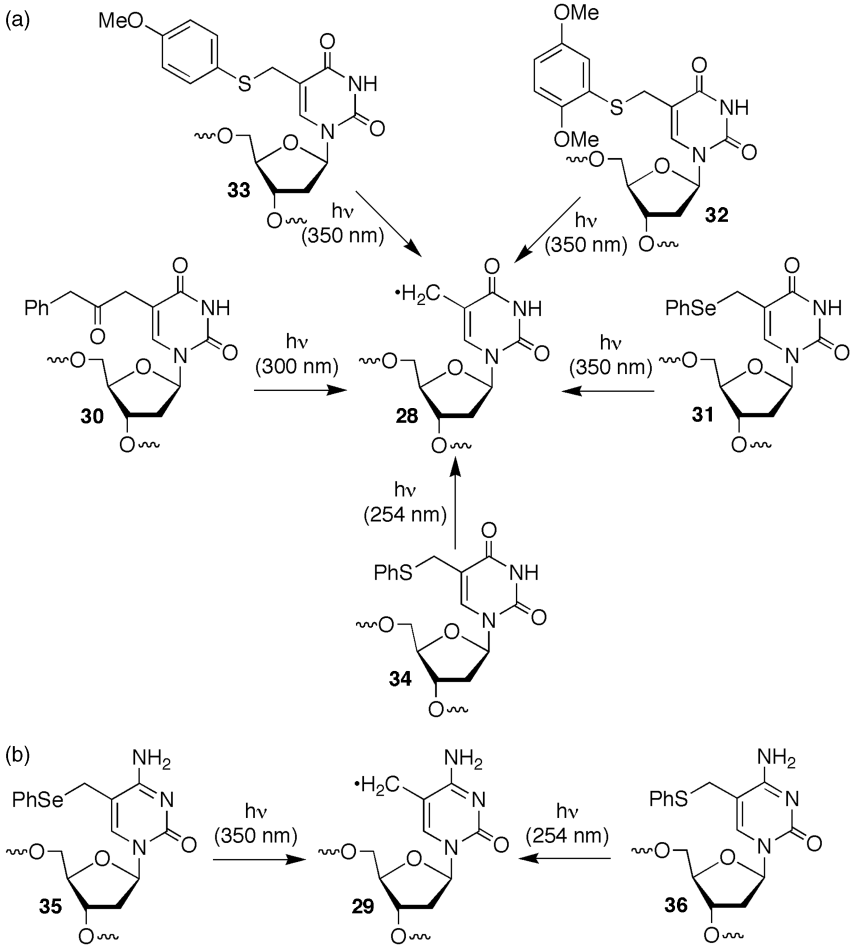

FIGURE 5.10. Independent generation of (**A**) 5-(2′-deoxyuridinyl)methyl (**28**) and (**B**) 5-(2′-deoxycytidinyl)methyl (**29**) radicals.

(**29**) have utilized phenyl selenides (**31**, **35**) or aryl sulfides (**32**–**34**, **36**) as stable photochemical precursors.[57–60] Phenyl sulfides **34** and **36** require irradiation at 254 nm to produce the corresponding radicals.[61–63] However, the phenyl selenides (**31**, **35**) and electron-rich aryl sulfides (**32**, **33**) produce **28** and **29** when photolyzed at 350 nm, which is less likely to generate random damage throughout the DNA.

5.1.4. Tandem Lesion Formation from 5-(2′-Deoxyuridinyl)methyl (28) and 5-(2′-Deoxycytidinyl)methyl Radicals (29)

Prior to the advent of methods for independently generating reactive intermediates within DNA, tandem lesions resulting from the formal addition of 5-(2′-deoxyuridinyl)

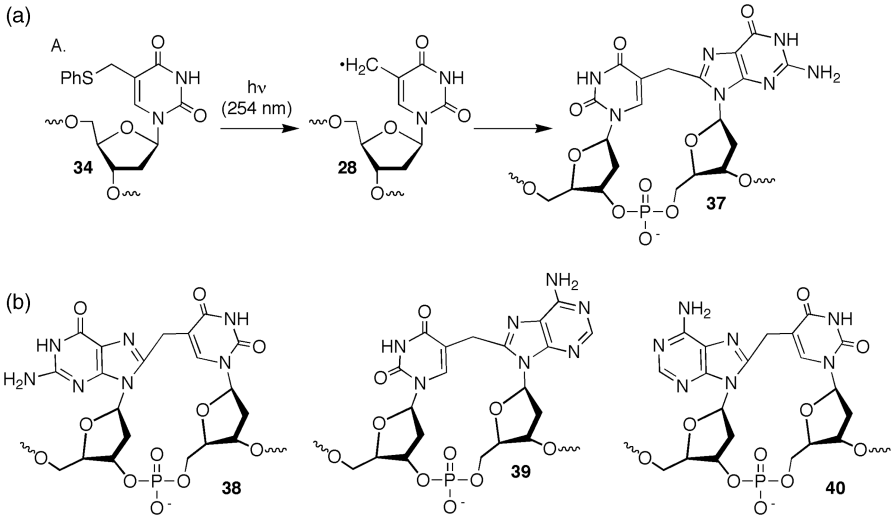

FIGURE 5.11. A. Tandem lesion formation from reaction of 5-(2′-deoxyuridinyl)methyl radical (**28**) and a 3′-dG. B. Other purine tandem lesions from **28**.

methyl radical (**28**) to adjacent purines were identified in ionizing radiation experiments.[64,65] Formal addition of **28** to a 3′-adjacent 2′-deoxyguanosine (**37**) was observed upon 254-nm irradiation of **34** in single-stranded oligonucleotides (Figure 5.11A).[61,62,66,67] The respective tandem lesions between **28** and a 3′-dA (**39**), as well purine adducts bound to the 5′-phosphate of **28** (**38**, **40**), have also been identified (Figure 5.11B).[68] All four lesions were identified in DNA samples subjected to ionizing radiation under anaerobic conditions or Fenton-type conditions that are known to produce OH•.[66,68] However, dG containing tandem lesions are produced in greater amounts than those involving reaction of dA. Furthermore, both purines form tandem lesions more efficiently when they are bonded to the 5′-phosphate of thymidine. The regioselectivity for the proposed addition of the methyl radical into the adjacent purine is consistent with the smaller distance between the radical center of the 5-(2′-deoxyuridinyl)methyl radical (**28**) and C8 of the 5′-purine (∼3.6 Å) compared to the respective carbon of the 3′-purine (∼6.3 Å). The preferences observed during *in vitro* studies are reflected in cellular experiments. Of the four possible purine adducts, only **38** was detected when Hela-S3 cells were exposed to γ-,radiolysis.[67]

Similarly, tandem lesions resulting from addition of the respective radical derived from 5-methyl-2′-deoxycytidine (**29**) into 2′-deoxyguanosine bonded to either phosphate (**41**, **42**) were also detected when **36** was photolyzed at 254 nm (Figure 5.12).[14,69] Tandem lesions were obtained in ∼15-fold higher yields when the purine was in the 5′ position (**41**) than when the radical was bonded to dG via its 3′-phosphate (**42**). In addition, the relative yields of the tandem lesions were similar

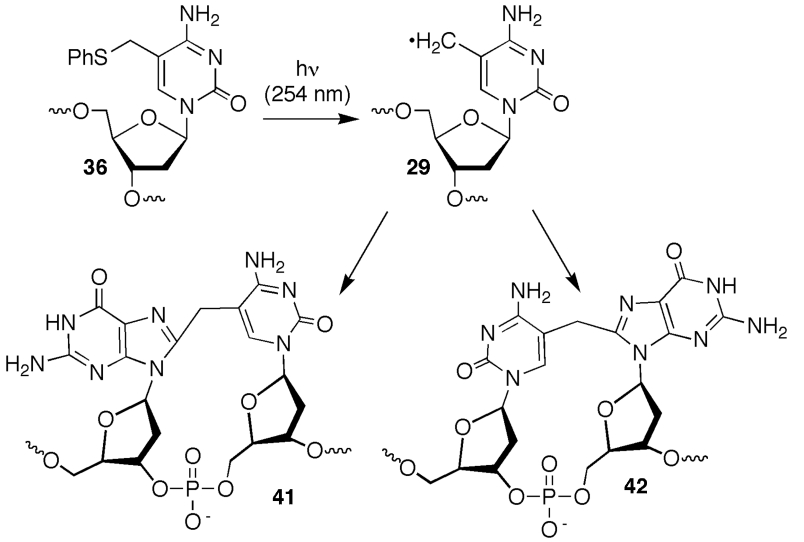

FIGURE 5.12. Tandem lesion formation from reaction between 5-(2′-deoxycytidinyl)methyl radical (**29**) and an adjacent dG.

to this when **29** was produced randomly in DNA by γ-radiolysis or Fenton-type reagents.[70]

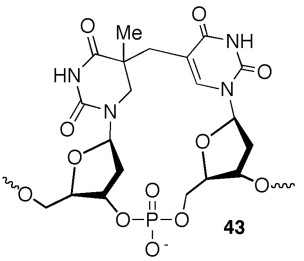

Tandem lesions involving the addition of **28** or **29** into the double bond of dC or dT have not been detected when DNA is irradiated in aqueous solution, and the spore photoproduct (**43**) is not formed under these conditions.[71,72] The reason for selective reaction with adjacent purines is not explained. However, molecular modeling indicates that conformational constraints are not the limitation. It is interesting to note that analogous lesions involving C5′-radical addition into intranucleotidyl nucleobases are also more favorable for purines than for pyrimidines, suggesting that the pyrimidine rings are inherently less reactive.[73,74]

Tandem lesions involving hydrogen atom abstraction from the deoxyribose components of adjacent nucleotides also have not been detected. Studies on the monomeric radical support the apparent kinetic inefficiency of these reactions.[57] Kinetic competition studies involving **28** were carried out under anaerobic conditions using 2,5-dimethyltetrahydrofuran (k_{MTHF}) and 2-propanol (k_{Pr}) as deoxyribose models. The estimated bimolecular rate constants ($k_{MTHF} = 46.1 \pm 15.4\,M^{-1}\,s^{-1}$, $k_{Pr} = 13.6 \pm 3.5\,M^{-1}\,s^{-1}$)

for hydrogen atom abstraction by **28** were too slow to compete with O_2 trapping or thiol quenching of the radical. However, the data indicated that the radical could abstract hydrogen atoms from an adjacent nucleotide in DNA in the absence of these reactants with comparable efficiency as other nucleobase radicals. The absence of such products suggested that another, much more rapid process must exist.

5.1.5. Interstrand Cross-Link Formation from 5-(2′-Deoxyuridinyl)methyl (28) and 5-(2′-Deoxycytidinyl)methyl Radicals (29)

Interstrand cross-links (ICLs) are an important family of DNA damage because of their ability to block replication and transcription. They are produced by a number of antitumor agents that bind in the minor groove and alkylate DNA or rearrange to biradicals and are strongly associated with these molecules' cytotoxic effects.[75,76] Surprisingly, generation of **28** upon 350-nm photolysis of duplexes containing phenyl selenide **31** or the more electron rich aryl sulfides (**32**, **33**) produced interstrand cross-links in high yield.[58,59] ICLs are produced in very low yield when DNA is exposed to γ-radiolysis and the structure(s) or formation mechanism(s) had not been previously characterized.

Because of the unusual nature of the ICL, extensive studies were undertaken to verify that the interstrand cross-links were due to 5-(2′-deoxyuridinyl)methyl radical (**28**).[59] Hydrogen atom donor (e.g., glutathione, β-mercaptoethanol) quenching of ICL formation was consistent with a radical mediated process. In addition, cross-link formation by all three photochemical precursors (**31**–**33**) was strong evidence for the involvement of a common intermediate. An unusual attribute for a radical reaction was the observation that cross-linking was independent of O_2, which typically traps radicals close to the diffusion controlled limit ($k_{O_2} = 2 \times 10^9\ M^{-1}\ s^{-1}$). This unusual observation was reconciled with a radical mechanism by using the monomeric radical precursor (**31**) to demonstrate that O_2 trapping of **28** was reversible (Figure 5.13). The

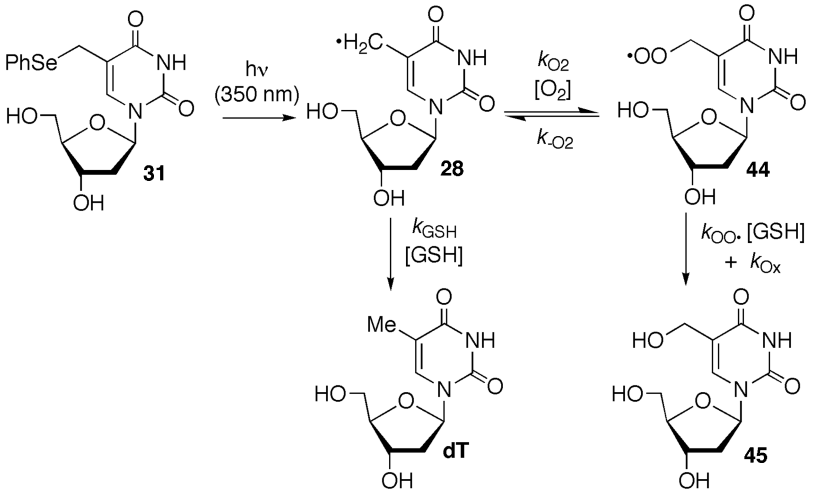

FIGURE 5.13. Reversible O_2 trapping of 5-(2′-deoxyuridinyl)methyl radical (**28**).

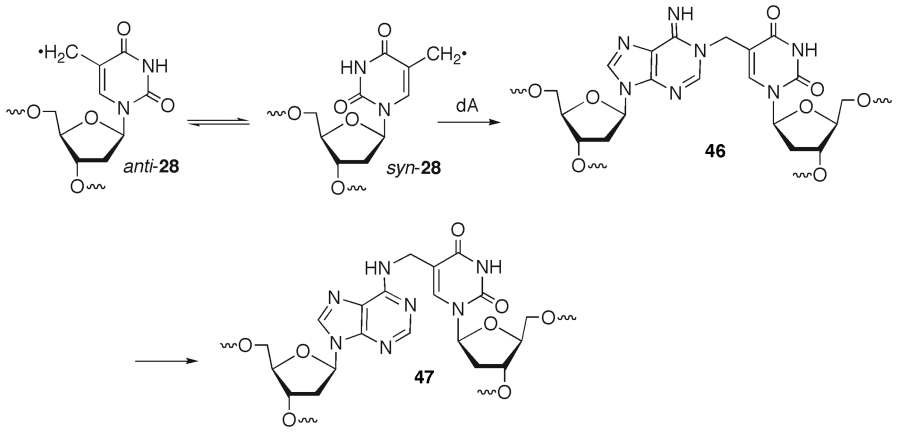

FIGURE 5.14. Interstrand cross-link formation between 5-(2′-deoxyuridinyl)methyl radical (**28**) and dA.

rate constant determined for loss of O_2 ($k_{O_2} = 3.4\ s^{-1}$) from **44** by measuring the ratio of dT:**45** as a function of glutathione concentration (GSH) was consistent with that determined for other peroxyl radicals of similar structure.[11,77]

Multinuclear NMR, ESI-MS, and the OH• cleavage method developed by Hopkins were used to characterize the structure of the cross-linked product.[58,78] ESI-MS analysis of the isolated ICL formed under aerobic conditions revealed that O_2 is not incorporated in the product. This is consistent with the lack of ICL formation dependence on O_2. Hydroxyl radical cleavage revealed another unusual aspect of cross-linking by **28**. In contrast to alkylating agents, which typically react with nucleotides that are 1–2 base pairs apart, the radical reacted exclusively with the opposing deoxyadenosine.[76] The atomic level structure of the cross-link was determined following digestion of the duplex. The product (**47**) obtained was the result of formal addition to the *N6*-amino group of 2′-deoxyadenosine (Figure 5.14). The identical product was isolated when monomeric **28** was generated in the presence of 2′-deoxyadenosine. It is difficult to formulate a mechanism by which **28** would produce **47** directly, and kinetic studies revealed that it is not the primary product.[59]

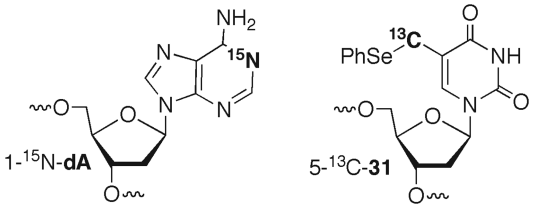

Examination of molecular models led to the proposal that *syn*-**28** added to the N1 position of the opposing dA resulting in **46**, which ultimately rearranged to **47**.[59] Multinuclear NMR analysis of ICL formed from duplex DNA containing 5-^{13}C-**31**

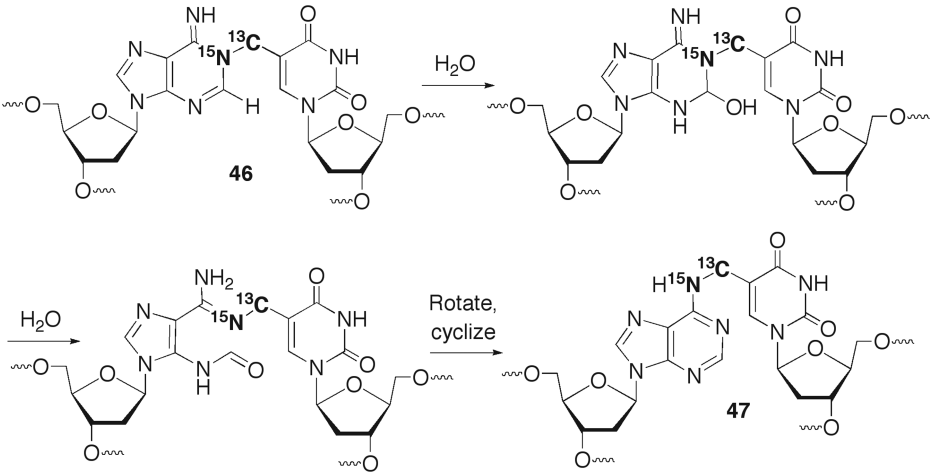

FIGURE 5.15. Associative mechanism for rearrangement of ICL **46** to **47** using isotopic labeling.

and 1-^{15}N-dA confirmed the structure of **46** by taking advantage of the coupling between magnetically active labels.[60] Furthermore, the labeling studies confirmed that **46** rearranged to **47** via an associative mechanism in which the carbon derived from the radical center and N_1-dA remain bonded to one another (Figure 5.15). The relevance of this elaborate mechanism was substantiated in γ-radiolysis studies on oligonucleotides, in which tritium was used to verify formation of **47**.[79]

ICL formation requires rotation about the glycosidic bond to the less stable *syn* conformation. The rate constant for ICL formation from **28** was estimated by using thiols as competitors. The rate constants (k_{ICL}) showed some dependence on local sequence but varied from $1.2 \times 10^3\ s^{-1}$ when flanked by dT to $\sim 5–6 \times 10^3\ s^{-1}$ when flanked by dC.[60] The estimated k_{ICL} were in the range of what is expected for nucleotide flipping and suggests that rotation about the glycosidic bond to populate the *syn*-conformation of **26** is the rate-determining step.[80–82]

5.1.5.1. Protein Binding Effects on Interstrand Cross-Link Formation. Protein–DNA interactions are important and prevalent in cells. For instance, the wrapping of chromosomal DNA around histone proteins creates nucleosomes.[83] More transient protein binding controls transcription. Protein binding can affect the accessibility of DNA to diffusible species such as OH•.[84,85] However, the structural alteration of DNA upon protein binding may also influence the reactivity of radicals formed in the biopolymer. DNA bending is a common consequence of protein binding.[86] For instance, the histone like family of bacterial integration host factor DNA bending proteins significantly reduce base stacking at the kink site.[87,88] One such protein, Hbb, from the species (*Borrelia burgdorferi*) responsible for Lyme disease in humans was used to demonstrate how a disruption in base stacking can have a profound effect on DNA radical reactivity.

Interstrand cross-linking by 5-(2′-deoxyuridinyl)methyl radical (**28**) produced at the Hbb bending site was significantly increased in the presence of the protein.[89] The approximately four-fold increase in the rate constant for cross-linking was ascribed to a reduction in the barrier to adopt the *syn*-conformation, which as discussed above is the rate determining step in ICL formation from **28**. Hbb had an even more striking effect on the reactivity of 5-(2′-deoxycytidinyl)methyl radical (**29**).[89] 5-(2′-Deoxycytidinyl)methyl radical (**29**) does not yield ICLs in the absence of protein. The absence of ICLs is attributed to the higher barrier to rotation about the glycosidic bond due to the presence of 3 hydrogen bonds instead of 2, as is the case for **28**. However, the ICL yield is $>10\%$ when **29** is generated at the Hbb kink site in the presence of protein.

5.1.5.2. A Change in Mechanism for Interstrand Cross-Link Formation and Its Application. Dioxygen "fixes" DNA damage by trapping the alkyl radicals formed and preventing their repair by hydrogen atom donors. The requirement for O_2 is why radiation therapy is less effective in hypoxic (O_2-deficient) tumor cells, and it provides the driving force for the development of molecules (radiosensitizing agents) that can enhance radical mediated DNA damage under O_2-deficient conditions.[90] The observation that ICL formation by **28** was independent of O_2 suggested that radical precursors such as **31** could be useful as radiosensitizing agents if γ-radiation could substitute for ultraviolet light as radical generator. 5-(2′-Deoxyuridinyl)methyl radical (**28**) would have an advantage over other radiosensitizers, such as 5-bromo- and 5-iodo-2′-deoxyuridine because cross-links are more deleterious than the single strand breaks and alkali-labile lesions produced by the 5-halopyrimidines.[91–95] Irradiation (^{137}Cs) of DNA containing **31** produced cross-links in good yield.[96] However, ICL formation was dependent on O_2, indicating a change in mechanism to one involving reactive oxygen species (ROS). Experiments utilizing selective probes for various ROS revealed that H_2O_2, produced from water by ionizing radiation, was required for ICL formation.

A variety of experiments using monomeric and oligonucleotide substrates have firmly established that H_2O_2 (and a variety of other oxidants) oxidizes **31** to the selenoxide (**48**), which undergoes a [2,3]-sigmatropic rearrangement to form a highly electrophilic quinone methide-like species (**49**, Figure 5.16).[59] The monomeric quinone methide like species (**49**) was detected directly by ^{1}H NMR. The *syn*-conformation of this molecule produces the identical primary product generated from **28** (Figure 5.14) by alkylating N_1 of the opposing deoxyadenosine. The N_1-alkylation product was observed directly in duplex DNA using ^{15}N- and ^{13}C-labeled DNA, as described above in the experiments in which the radical is produced photochemically.[60] Furthermore, kinetic studies on the monomer using azide as a model nucleophile confirmed that alkylation occurs via an S_N2 mechanism.[60]

These mechanistic studies revealed other potential applications for **31**. For instance, cross-linking through **31** under oxidative conditions suggested that $^1O_2$ should also initiate this reaction, because this ROS oxidizes phenyl selenides to selenoxides.[97] Indeed, photosensitization by Rose Bengal produced high yields of

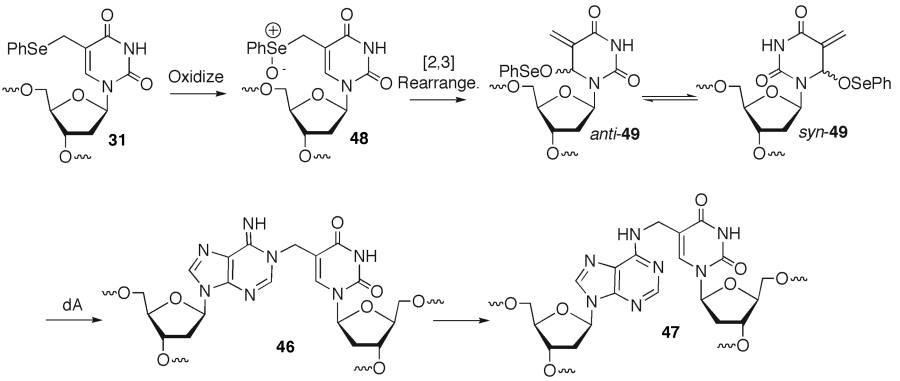

FIGURE 5.16. Interstrand cross-link formation via a quinone-methide like intermediate produced from **31** under oxidative conditions.

cross-links, suggesting that **31** incorporated in DNA could be a useful adjuvant in photodynamic therapy.[98–100] The ability of Klenow fragment, a replicative DNA polymerase to incorporate the phenyl selenide, is a positive sign that this reaction could be used in cells. Although the polymerase accepts the respective nucleotide triphosphate as a substrate ~150 times less efficiently than dTTP, this is sufficient for achieving sufficient incorporation levels of **31** in DNA.[96]

The requirement to incorporate **31** into cellular DNA is a demanding one that has not yet been satisfied. However, facile oxidatively induced ICL formation from the phenyl selenide (**31**) has proven useful in chemical applications, such as selective detection of DNA sequences.[101] Oligonucleotide probes containing **31** and a 5′-biotin facilitated SNP detection by enabling one to use stringent washing conditions to remove excess probe. Single nucleotide discrimination and fluorescent detection of target sequences was achieved at femtomole levels without PCR by exploiting biotin binding to streptavidin conjugated horseradish peroxidase to amplify the signal.

The facile cross-linking reaction was also extended to triplex forming oligonucleotides (TFOs), although not without additional surprises.[89] Molecular models suggested that incorporating **31** or **35** into the Hoogsteen strand of the triplex would result in alkylation of the N7 position of dA or dG, respectively (Figure 5.17). The 5-methyl-2′-deoxycytidine derivative's (**35**) reactivity under oxidative conditions proceeded as expected. The opposing dG was alkylated at the N7 position, and the ICL yield was unaffected by generation of the electrophile at an internal site or 5′-terminus of the TFO. In contrast, the ICL yield produced from **31** was much lower when the electrophile was generated at an internal position than at the 5′-terminus of the TFO. Determination that N_1 and not N_7 of the opposing dA was alkylated by the TFO explained this unexpected result. Reaction at this position requires disruption of the triplex, which will be more energetically demanding at an internal site than when the quinone methide-like species is at the terminus of the TFO. Finally, ICL formation through **31** was also useful for resolving a mechanistic controversy concerning the termination of DNA replication.[102]

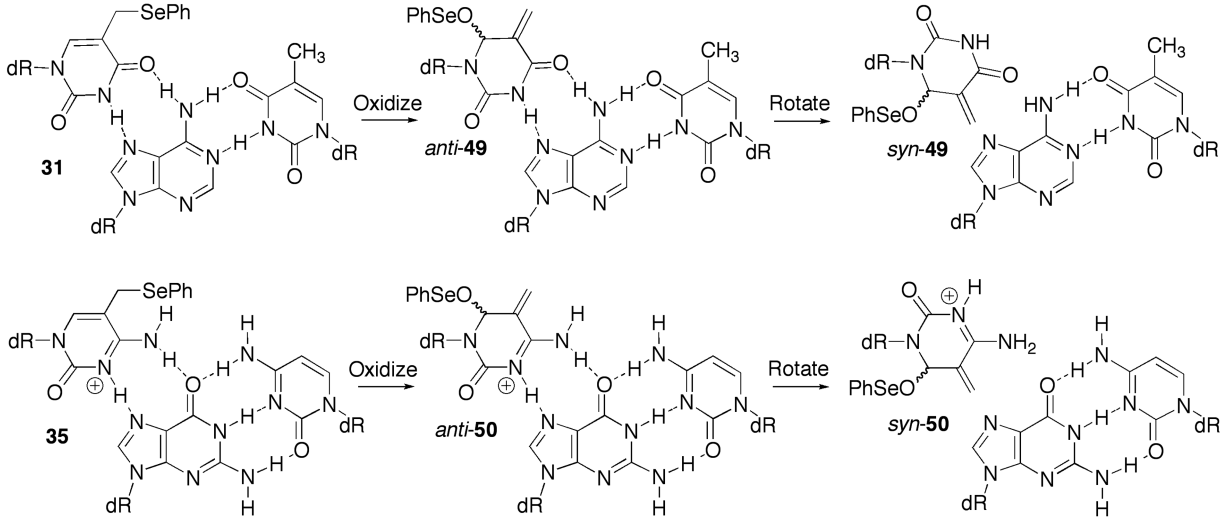

FIGURE 5.17. Juxtaposition of quinone methide like electrophiles to the N7 positions of purines via Hoogsteen base pairing of (**A**) **31** and (**B**) **35**.

5.2. FORMAL TANDEM LESION FORMATION FROM NUCLEOBASE σ-RADICALS

UV-irradiation of 5-halopyrimidines produces the respective σ-radicals, which are more reactive than the π-radicals discussed thus far (Figure 5.18). A significant amount of the chemistry of 2′-deoxyuridin-5-yl radical (**52**) is described in Chapter 6. However, one recently elucidated reactivity mode that is not described in Chapter 6 concerns the addition of **52** and 2′-deoxycytidin-5-yl radical (**54**) into the double bonds of adjacent purines. The possibility for such a reaction was originally uncovered by Box in ionizing radiation studies of short oligonucleotides.[64,103] The structures of these tandem lesions produced from photolysis of the halogenated nucleosides, as well as their formation from native DNA exposed to ionizing radiation, have been thoroughly studied by Wang.

Several types of products that contain covalent bonds between nucleobases have been detected when either 5-bromo-2′-deoxycytidine (**53**) (Figure 5.19) or 5-bromo-2′-deoxyuridine (**51**) (Figure 5.20) flanked by purines is photolyzed. In initial studies, five products (**55**–**59**) attributable to 2′-deoxycytidin-5-yl (**54**) were identified when dinucleotides and/or oligonucleotides containing **53** flanked by dA were photolyzed (Figure 5.19).[104, 105] Formal products resulting from σ-radical addition to C8 (**55**, **56**) and C2 of adenine (**57**, **58**) were detected. In addition, a coupling product between the pyrimidine's C5 carbon and adenine's exocyclic amine (**59**) was also detected. In a subsequent study, products resulting from addition of **54** to C8 of guanine and coupling to the N2 amino group were also identified (**60**–**62**).[106] The products were proposed to result from generation of the σ-radical and the respective purine cation radical following photoinduced electron transfer involving the 5-halopyrimidine (**53**). Coupling to the purines' exocyclic amines (**59**, **62**) is proposed to involve prior deprotonation of the cation radical. Formation of the aminyl radical is required for

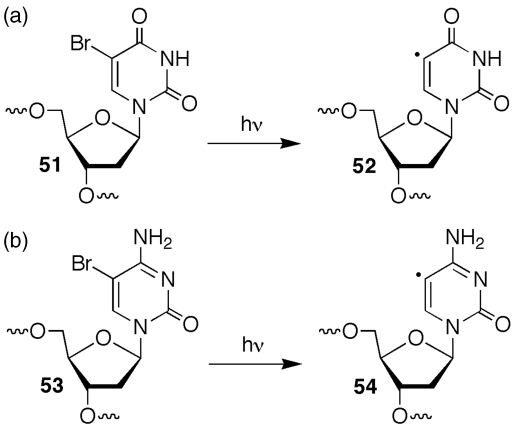

FIGURE 5.18. Photochemical generation of (A) 2′-deoxyuridin-5-yl radical (**52**) and (B) 2′-deoxycytidin-5-yl radical (**54**) from the respective 5-halopyrimidines.

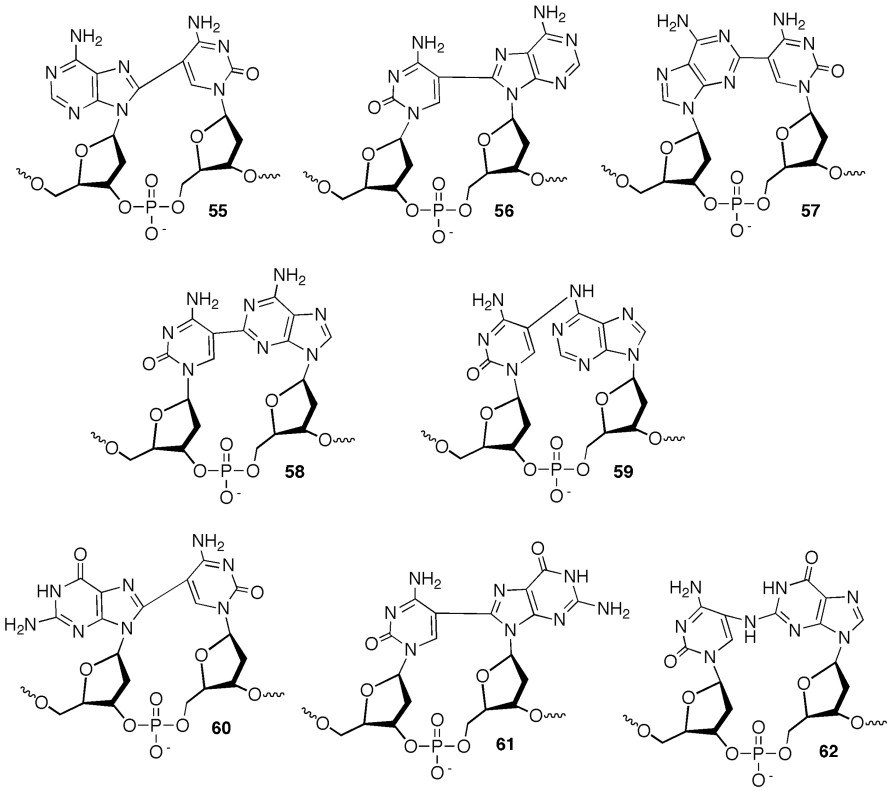

FIGURE 5.19. Tandem lesions produced from reaction of 2′-deoxycytidin-5-yl radical (**54**) with dA and dG.

coupling to the σ-radical. This is important in a broader sense concerning the formation of this family of products from other reactive intermediates that are produced from the native nucleotides (*vide infra*). In contrast, tandem lesions containing carbon–carbon bonds between nucleobases while suggested to involve coupling

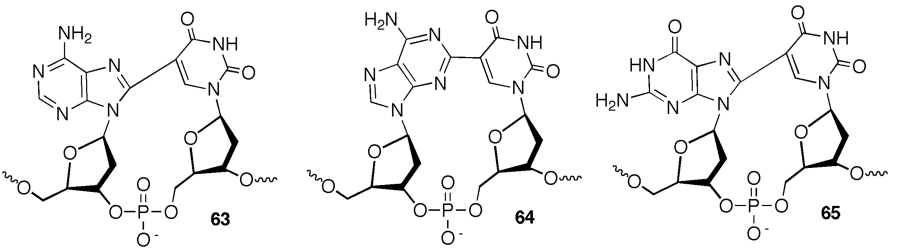

FIGURE 5.20. Tandem lesions produced from reaction of 2′-deoxyuridin-5-yl radical (**52**) with dA and dG.

between pyrimidine radicals and purine cation radicals could form under other conditions via radical addition directly to the undamaged purine.

Reaction between the pyrimidine and purine bases is directional. Coupling products produced by carbon–carbon bond formation are formed in higher yield when the purine is in the 5′ position (e.g., **60** versus **61**).[105] These observations are postulated to result from more favorable π-overlap in this arrangement, which yields more efficient photochemical conversion. In addition, the proximity of the reactive centers is greater in a 5′-purine 3′-pyrimidine sequence due to the helical nature of duplex DNA. A subset of analogous tandem lesions (**63**–**65**) was detected in photolyses of DNA containing 5-bromo-2′-deoxyuridine (**51**) (Figure 5.20).

One of these lesions, **60**, was detected in DNA treated with Fenton reagents that generate OH• and was also detected in cellular DNA isolated from HeLA cells exposed to γ-radiolysis.[70,107] Under these conditions, and in the absence of **53**, the lesion is believed to result from the C6-hydroxyl radical adduct of dC instead of directly from the σ-radical **54**. The yield of **60** in cells was much lower than single lesions. However, it had a significant effect on replication in *E. coli*. 2′-Deoxyadenosine or dG were misincorporated opposite the portion of the lesion derived from dG almost 10% of the time, resulting in 8.7% G → T transversions and 1.2% G → C transversions.[107] These mutation frequencies are significantly greater than the well-studied DNA lesion 8-oxoguanine (**66**) in *E. coli*.[108,109] In addition, as one would expect for lesion that must distort the local duplex structure, **60** is incised by UvrABC.[110]

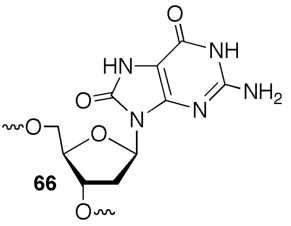

66

5.3. SUMMARY AND FUTURE DIRECTIONS

Nucleobase radicals are major components of the collection of reactive intermediates produced in nucleic acids by diffusible species, such as OH•. Their chemistry has perhaps been somewhat obscured by their indirect connection to direct strand scission. However, recent studies, many of which utilize organic photochemistry to independently generate radical intermediates, have revealed the rich and biologically relevant chemistry of nucleobase radicals. There is still much to learn about these radicals, including their reactivity in the more biologically relevant context in which they are bound by proteins. In addition, the more varied structure of RNA, as well as the effects of an additional hydroxyl group, may significantly alter the reactivity of the respective nucleobase radicals of this biopolymer of increasing importance.

ACKNOWLEDGMENTS

I thank my past and present co-workers, many of whose names are listed in the reference list, without whose contributions to the portion of the research described here from our own group would not be possible. We are grateful for support of this research by the National Institute of General Medical Sciences (GM-054996 and GM-063028).

REFERENCES

1. von Sonntag, C. *The Chemical Basis of Radiation Biology*; Taylor & Francis, London, 1987.
2. Pogozelski, W. K.; McNeese, T. J.; Tullius, T. D. What species is responsible for strand scission in the reaction of $[FeIIEDTA]^{2-}$ and H_2O_2 with DNA? *J. Am. Chem. Soc.* **1995**, *117*, 6428–6433.
3. Trzupek, J. D.; Gottesfeld, J. M.; Boger, D. L. Alkylation of duplex DNA in nucleosome core particles by duocarmycin SA and yatakemycin. *Nat. Chem. Biol.* **2006**, *2*, 79–82.
4. Boger, D. L.; Garbaccio, R. M. Shape-dependent catalysis: Insights into the source of catalysis for the CC-1065 and duocarmycin DNA alkylation reaction. *Acc. Chem. Res.* **1999**, *32*, 1043–1052.
5. Chen, J.; Stubbe, J. Bleomycins: Towards better therapeutics. *Nature Rev. Cancer* **2005**, *5*, 102–112.
6. Xi, Z.; Goldberg, I. H. In *Comprehensive Natural Products Chemistry*, Vol. *7;* Kool, E. T., Ed.; Elsevier, Amsterdam, 1999, pp. 553–592.
7. von Sonntag, C. *Free-Radical-Induced DNA Damage and Its Repair*; Springer-Verlag, Berlin, 2006.
8. Greenberg, M. M. Investigating nucleic acid damage processes via independent generation of reactive intermediates. *Chem. Res. Toxicol.* **1998**, *11*, 1235–1248.
9. Greenberg, M. M. In *Comprehensive Natural Products Chemistry*, Vol. *7*, *DNA and Aspects of Molecular Biology*; Kool, E. T., Ed.; Elsevier, Amsterdam, 1999, pp. 371–426.
10. Giese, B.; Dussy, A.; Meggers, E.; Petretta, M.; Schwitter, U. Conformation, lifetime, and repair of 4′-DNA radicals. *J. Am. Chem. Soc.* **1997**, *119*, 11130–11131.
11. Dussy, A.; Meggers, E.; Giese, B. Spontaneous cleavage of 4′-DNA radicals under aerobic conditions: Apparent discrepancy between trapping rates and cleavage products. *J. Am. Chem. Soc.* **1998**, *120*, 7399–7403.
12. Giese, B. Long-distance charge transport in DNA: The hopping mechanism. *Acc. Chem. Res.* **2000**, *33*, 631–636.
13. Bryant-Friedrich, A. C. Generation of a C-3′-thymidinyl radical in single-stranded oligonucleotides under anaerobic conditions, *Org. Lett.* **2004**, *6*, 2329–2332.
14. Zhang, Q.; Wang, Y. Independent generation of 5-(2′deoxycytidinyl)methyl radical and the formation of a novel cross-link lesion between 5-methylcytosine and guanine. *J. Am. Chem. Soc.* **2003**, *125*, 12795–12802.
15. Greenberg, M. M. Elucidating DNA damage and repair processes by independently generating reactive and metastable intermediates. *Org. Biomol. Chem.* **2007**, *5*, 18–30.

16. Wang, Y. Bulky DNA lesions induced by reactive oxygen species. *Chem. Res. Toxicol.* **2008**, *21*, 276–281.
17. Dizdaroglu, M.; Jaruga, P.; Birincioglu, M.; Rodriguez, H. Free radical-induced damage to DNA: Mechanisms and measurements. *Free Rad. Biol. Med.* **2002**, *32*, 1102–1115.
18. Adhikary, A.; Kumar, A.; Sevilla, M. D.; Adhikary, A.; Malkhasian, A. Y. S.; Collins, S.; Koppen, J.; Becker, D.; Sevilla, M. D. Photo-induced hole transfer from base to sugar in DNA: Relationship to primary radiation damage UVA–visible photo-excitation of guanine radical cations produces sugar Radicals in DNA and model structures. *Radiat. Res.* **2006**, *165*, 479–484.
19. Hildenbrand, K.; Schulte-Frohlinde, D. E.S.R. Studies on the mechanism of hydroxyl radical-induced strand breakage of polyuridylic acid. *Int. J. Radiat. Biol.* **1989**, *55*, 725–738.
20. Hildenbrand, K.; Behrens, G.; Schulte-Frohlinde, D. Comparison of the reaction of $^{\bullet}OH$ and of $SO_4^{-\bullet}$ radicals with pyrimidine nucleosides. An electron spin resonance study in aqueous solution. *J. Chem. Soc. Perkin Trans. II* **1989**, 283–289.
21. Lemaire, D. G. E.; Bothe, E.; Schulte-Frohlinde, D. Yields of radiation-induced main chain scission of poly U in aqueous solution: Strand break formation via base radicals. *Int. J. Radiat. Biol.* **1984**, *45*, 351–358.
22. Barvian, M. R.; Greenberg, M. M. Independent generation of the major adduct of hydroxyl radical and thymidine. Examination of intramolecular hydrogen atom transfer in competition with thiol trapping. *Tetrahedron Lett.* **1992**, *33*, 6057–6060.
23. Barvian, M. R.; Barkley, R. M.; Greenberg, M. M. Reactivity of 5,6-dihydro-5-hydroxythymid-6-yl generated via photoinduced single electron transfer and the role of cyclohexa-1,4-diene in the photodeoxygenation process. *J. Am. Chem. Soc.* **1995**, *117*, 4894–4904.
24. Zhang, Q.; Wang, Y. Independent generation of the 5-hydroxy-5,6-dihydrothymidin-6-yl radical and its reactivity in dinucleoside morophosphates. *J. Am. Chem. Soc.* **2004**, *126*, 13287–13297.
25. Box, H. C.; Wallace, J. C. Free radical-induced double base lesions, *Radiat. Res.* **1995**, *141*, 91.
26. Box, H. C.; Patrzyc, H. B.; Dawidzik, J. B.; Wallace, J. C.; Freund, H. G.; Iijima, H.; Budzinski, E. E. Double base lesions in DNA X-irradiated in the presence or absence of oxygen, *Radiat. Res.* **2000**, *153*, 442–446.
27. Dianov, G. L.; O'Neill, P.; Goodhead, D. T. Securing genome stability by orchestrating DNA Repair: Removal of Radiation-induced clustered lesions in DNA, *BioEssays* **2001**, *23*, 745–749.
28. Lomax, M. E.; Gulston, M. K.; O'Neill, P. Chemical aspects of clustered DNA damage induction by ionising radiation. *Radiation Protection Dosimetry* **2002**, *99*, 63–68.
29. Weinfeld, M.; ResouliNia, A.; Chaudhry, M. A.; Britten, R. A. Response of base excision repair enzymes to complex DNA lesions. *Radiat. Res.* **2001**, *156*, 584–589.
30. Jenner, T. J.; Fulford, J.; O'Neill, P. Contribution of base lesions to radiation-induced clustered DNA damage: Implication for models of radiation response. *Radiat. Res.* **2001**, *156*, 590–593.
31. Zhang, Q.; Wang, Y. The reactivity of the 5-hydroxy-5,6-dihydrothymidin-6-yl radical in oligodeoxyribonucleotides. *Chem. Res. Toxicol.* **2005**, *18*, 1897–1906.

32. Tallman, K. A.; Tronche, C.; Yoo, D. J.; Greenberg, M. M. Release of superoxide from nucleoside peroxyl radicals, a double-edged sword? *J. Am. Chem. Soc.* **1998**, *120*, 4903–4909.
33. Barvian, M. R.; Greenberg, M. M. Independent generation of 5,6-dihydrothymid-5-yl and investigation of its ability to effect nucleic acid strand scission via hydrogen atom abstraction. *J. Org. Chem.* **1995**, *60*, 1916–1917.
34. Carter, K. N.; Greenberg, M. M. Independent generation and study of 5,6-dihydro-2′-deoxyuridin-6-yl, a member of the major family of reactive intermediates formed in DNA from the effects of γ-radiolysis, *J. Org. Chem.* **2003**, *68*, 4275–4280.
35. Newcomb, M. Competition methods and scales for alkyl radical reaction kinetics. *Tetrahedron* **1993**, *49*, 1151–1176.
36. Janik, I.; Ulanski, P.; Rosiak, J. M.; Von Sonntag, C. Hydroxyl-radical-induced reactions of the poly(vinyl methyl ether) model 2,4-dimethoxypentane in the absence and presence of dioxygen: A pulse radiolysis and product study, *J. Chem. Soc. Perkin Trans. 2* **2000**, 2034–2040.
37. Schuchmann, M. N.; Von Sonntag. Hydroxyl radical-induced oxidation of diisopropyl ether in oxygenated aqueous solution. A product and pulse radiolysis study. C. *Z. Naturforsch. B* **1987**, *42*, 495–502.
38. Emanuel, C. J.; Newcomb, M.; Ferreri, C.; Chatgilialoglu, C. kinetics of 2′-deoxyuridin-1′-yl radical reactions. *J. Am. Chem. Soc.* **1999**, *121*, 2927–2928.
39. Hashimoto, M.; Greenberg, M. M.; Kow, Y. W.; Hwang, J.-T.; Cunningham, R. P. The 2-deoxyribonolactone lesion produced in DNA by neocarzinostatin and other DNA damaging agents forms cross-links with the base-excision repair enzyme endonuclease III. *J. Am. Chem. Soc.* **2001**, *123*, 3161–3162.
40. DeMott, M. S.; Beyret, E.; Wong, D.; Bales, B. C.; Hwang, J.-T.; Greenberg, M. M.; Demple, B. Covalent trapping of human DNA polymerase β by the oxidative DNA lesion 2-deoxyribonolactone. *J. Biol. Chem.* **2002**, *277*, 7637–7640.
41. Huang, H.; Greenberg, M. M. Hydrogen bonding contributes to the selectivity of nucleotide incorporation opposite an oxidized abasic lesion, *J. Am. Chem. Soc.* **2008**, *130*, 6080–6081.
42. Barvian, M. R.; Greenberg, M. M. Independent generation of 5,6-dihydrothymid-5-yl in single-stranded polythymidylate. O2 is necessary for strand scission. *J. Am. Chem. Soc.* **1995**, *117*, 8291–8292.
43. Greenberg, M. M.; Barvian, M. R.; Cook, G. P.; Goodman, B. K.; Matray, T. J.; Tronche, C.; Venkatesan, H. DNA damage induced via 5,6-dihydrothymidin-5-yl in single-stranded oligonucleotides. *J. Am. Chem. Soc.* **1997**, *119*, 1828–1839.
44. Carter, K. N.; Greenberg, M. M. Tandem lesions are the major products resulting from a pyrimidine nucleobase radical. *J. Am. Chem. Soc.* **2003**, *125*, 13376–13378.
45. Hong, I. S.; Carter, K. N.; Greenberg, M. M. Evidence for glycosidic bond rotation in a nucleobase peroxyl radical and its effect on tandem lesion formation. *J. Org. Chem.* **2004**, *69*, 6974–6978.
46. Hwang, J.-T.; Tallman, K. A.; Greenberg, M. M. The reactivity of the 2-deoxyribonolactone lesion in single-stranded DNA and its implication in reaction mechanisms of DNA damage and repair. *Nucleic Acids Res.* **1999**, *27*, 3805–3810.
47. Sato, K.; Greenberg, M. M. Selective detection of 2-deoxyribonolactone in DNA. *J. Am. Chem. Soc.* **2005**, *127*, 2806–2807.

48. Hong, I. S.; Carter, K. N.; Sato, K.; Greenberg, M. M. Characterization and mechanism of formation of tandem lesions in DNA by a nucleobase peroxyl radical. *J. Am. Chem. Soc.* **2007**, *129*, 4089–4098.

49. Miaskiewicz, K.; Osman, R. Theoretical study on the deoxyribose radicals formed by hydrogen abstraction. *J. Am. Chem. Soc.* **1994**, *116*, 232–238.

50. Colson, A. O.; Sevilla, M. D. Structure and relative stability of deoxyribose radicals in a model DNA backbone: *Ab initio* molecular orbital calculations. *J. Phys. Chem.* **1995**, *99*, 3867–3874.

51. Dizdaroglu, M.; Schulte-Frohlinde, D.; Von Sonntag, C. Isolation of 2-deoxy-D-erythro-pentonic acid from an alkali-labile site in g-irradiated DNA. *Int. J. Radiat. Biol.* **1977**, *32*, 481–483.

52. Roginskaya, M.; Razskazovskiy, Y.; Bernhard, W. A. 2-Deoxyribonolactone lesions in X-ray-irradiated DNA: Quantitative determination by catalytic 5-methylene-2-furanone release. *Angew. Chem. Int. Ed.* **2005**, *44*, 6210–6213.

53. Xue, L.; Greenberg, M. M. Use of fluorescence sensors to determine that 2-deoxyribonolactone is the major alkali-labile deoxyribose lesion produced in oxidatively damaged DNA. *Angew. Chem. Int. Ed.* **2007**, *46*, 561–564.

54. Imoto, S.; Bransfield, L. A.; Croteau, D. L.; Van Houten, B.; Greenberg, M. M. DNA tandem lesion repair by strand displacement synthesis and nucleotide excision repair. *Biochemistry* **2008**, *47*, 4306–4316.

55. Joy, A.; Ghosh, A. K.; Schuster, G. B. One-electron oxidation of DNA oligomers that lack guanine: Reaction and strand cleavage at remote thymines by long-distance radical cation hopping. *J. Am. Chem. Soc.* **2006**, *128*, 5346–5347.

56. Ghosh, A.; Joy, A.; Schuster, G. B.; Douki, T.; Cadet, J. Selective one-electron oxidation of duplex DNA oligomers: Reaction at thymines. *Org. Biomol. Chem.* **2008**, *6*, 916–928.

57. Anderson, A. S.; Hwang, J. T.; Greenberg, M. M. Independent generation and reactivity of 2′-Deoxy-5-methyleneuridin-5-yl, a significant reactive intermediate produced from thymidine as a result of oxidative stress. *J. Org. Chem.* **2000**, *65*, 4648–4654.

58. Hong, I. S.; Greenberg, M. M. Efficient DNA interstrand cross-link formation from a nucleotide radical. *J. Am. Chem. Soc.* **2005**, *127*, 3692–3693.

59. Hong, I. S.; Ding, H.; Greenberg, M. M. Oxygen independent DNA interstrand cross-link formation by a nucleotide radical. *J. Am. Chem. Soc.* **2006**, *128*, 485–491.

60. Ding, H.; Majumdar, A.; Tolman, J. R.; Greenberg, M. M. Multinuclear NMR and kinetic analysis of DNA interstrand cross-link formation. *J. Am. Chem. Soc.***in press**, *130*.

61. Romieu, A.; Bellon, S.; Gasparutto, D.; Cadet, J. Synthesis and UV photolysis of oligodeoxynucleotides that contain 5-(phenylthiomethyl)-2′-deoxyuridine: A specific photolabile precursor of 5-(2′-deoxyuridilyl)methyl radical. *Org. Lett.* **2000**, *2*, 1085–1088.

62. Bellon, S.; Gasparutto, D.; Romieu, A.; Cadet, J. 5-(Phenylthiomethyl)-2′-deoxyuridine as an efficient photoreactive precursor to generate single and multiple lesions within DNA fragments. *Nucleosides, Nucleotides & Nucleic Acids* **2001**, *20*, 967–971.

63. Zhang, Q.; Wang, Y. Independent generation of 5-(2′-deoxycytidinyl)methyl radical and the formation of a novel cross-link lesion between 5-methylcytosine and guanine. *J. Am. Chem. Soc.* **2003**, *125*, 12795–12802.

64. Box, H. C.; Budzinski, E. E.; Dawidzik, J. B.; Wallace, J. C.; Iijima, H. Tandem lesions and other products in X-irradiated DNA oligomers. *Radiat. Res.* **1998**, *149*, 433–439.

65. Delatour, T.; Douki, T.; Gasparutto, D.; Brochier, M.-C.; Cadet, J. A novel vicinal lesion obtained from the oxidative photosensitization of TpdG: Characterization and mechanistic aspects. *Chem. Res. Toxicol.* **1998**, *11*, 1005–1013.

66. Hong, H.; Cao, H.; Wang, Y. Identification and quantification of a guanine–thymine intrastrand cross-link lesion induced by Cu(II)/H_2O_2/ascorbate. *Chem. Res. Toxicol.* **2006**, *19*, 614–621.

67. Jiang, Y.; Hong, H.; Cao, H.; Wang, Y. *In vivo* formation and *in vitro* replication of a guanine–thymine intrastrand cross-link lesion. *Biochemistry* **2007**, *46*, 12757–12763.

68. Bellon, S.; Ravanat, J.-L.; Gasparutto, D.; Cadet, J. Cross-linked thymine–purine base tandem lesions: Synthesis, characterization, and measurement in gamma-irradiated isolated DNA. *Chem. Res Toxicol.* **2002**, *15*, 598–606.

69. Zhang, Q.; Wang, Y. Generation of 5-(2′-deoxycytidyl)methyl radical and the formation of intrastrand cross-link lesions in oligodeoxyribonucleotides. *Nucleic Acids Res.* **2005**, *33*, 1593–1603.

70. Cao, H.; Wang, Y. Quantification of oxidative single-base and intrastrand cross-link lesions in unmethylated and CpG-methylated DNA Induced by Fenton-type reagents. *Nucleic Acids Res*. **2007**, *35*, 4833–4844.

71. Cheek, J.; Broderick, J. B. Direct H atom abstraction from spore photoproduct C-6 initiates DNA repair in the reaction catalyzed by spore photoproduct lyase: Evidence for a reversibly generated adenosyl radical intermediate. *J. Am. Chem. Soc.* **2002**, *124*, 2860–2861.

72. Friedel, M. G.; Pieck, J. C.; Klages, J.; Dauth, C.; Kessler, H.; Carell, T. Synthesis and stereochemical assignment of DNA spore photoproduct analogues. *Chem. Eur. J.* **2006**, *12*, 6081–6094.

73. Boussicault, F.; Kaloudis, P.; Caminal, C.; Mulazzani, Q. G.; Chatgilialoglu, C. The fate of C5′ radicals of purine nucleosides under oxidative conditions. *J. Am. Chem. Soc.* **2008**, *130*, 8377–8385.

74. Chatgilialoglu, C.; Bazzanini, R.; Jimenez, L. B.; Miranda, M. A. (5′ *S*)- and (5′ *R*)-5′, 8-cyclo-2′-deoxyguanosine: Mechanistic insights on the 2′-deoxyguanosin-5′-yl radical cyclization. *Chem. Res. Toxicol.* **2007**, *20*, 1820–1824.

75. Tomasz, M.; Palom, Y. The mitomycin bioreductive antitumor agents: Crosslinking and alkylation of DNA as the molecular basis of their activity. *Pharmacol. Therapeut.* **1997**, *76*, 73–87.

76. Noll, D. M.; Mason, T. M.; Miller, P. S. Formation and repair of interstrand cross-links in DNA, *Chem. Rev.* **2006**, *106*, 277–301.

77. von Sonntag, C.; Schuchmann, H.-P. The elucidation of peroxyl radical reactions in aqueous solution with the help of radiation-chemical methods. *Angew. Chem. Int. Ed.* **1991**, *30*, 1229–1253.

78. Millard, J. T.; Weidner, M. F.; Kirchner, J. J.; Ribeiro, S.; Hopkins, P. B. Sequence preferences of DNA interstrand crosslinking agents: Quantitation of interstrand crosslink locations in DNA duplex fragments containing multiple crosslinkable sites. *Nucleic Acids Res.* **1991**, *19*, 1885–1892.

79. Ding, H.; Greenberg, M. M. Gamma-radiolysis and hydroxyl radical produce interstrand cross-links in DNA involving thymidine. *Chem. Res. Toxicol.* **2007**, *20*, 1623–1628.

80. Guéron, M.; Leroy, J. Studies of base pair kinetics by NMR measurement of proton exchange. *Methods Enzymol.* **1995**, *261*, 383–413.

81. Snoussi, K.; Leroy, J. L. Alteration of A•T base-pair opening kinetics by the ammonium cation in DNA A-tracts. *Biochemistry* **2002**, *41*, 12467–12474.

82. Parker, J. B.; Bianchet, M. A.; Krosky, D. J.; Friedman, J. I.; Amzel, L. M.; Stivers, J. T. Enzymatic capture of an extrahelical thymine in the search for uracil in DNA. *Nature* **2007**, *449*, 433–437.

83. Luger, K.; Mader, A. W.; Richmond, R. K.; Sargent, D. F.; Richmond, T. J. Crystal structure of the nucleosome core particle at 2.8 Å resolution. *Nature* **1997**, *389*, 251–260.

84. Pogozelski, W. K.; Tullius, T. D. Oxidative strand scission of nucleic acids: Routes initiated by hydrogen abstraction from the sugar moiety. *Chem. Rev.* **1998**, *98*, 1089–1107.

85. Price, M. A.; Tullius, T. D. Using hydroxyl radical to probe DNA structure, *Methods Enzymol*. **1992**, *212*, 194–219.

86. Rees, W. A.; Keller, R. W. Evidence of DNA bending in transcription complexes imaged by scanning force microscopy. *Science* **1993**, *260*, 1646.

87. Mouw, K. W.; Rice, P. A. Shaping the *Borrelia burgdorferi* genome: crystal structure and binding properties of the DNA-bending protein Hbb, *Mol. Microbiol.* **2007**, *63*, 1319–1330.

88. Swinger, K. K.; Rice, P. A. IHF and HU: Flexible architects of bent DNA. *Curr. Op. Struct. Biol.* **2004**, *14*, 28–35.

89. Peng, X.; Hong, I. S.; Li, H.; Seidman, M. M.; Greenberg, M. M. Interstrand cross-link formation in duplex and triplex DNA by modified pyrimidines. *J. Am. Chem. Soc.* **2008**, *130*, 10299–10306.

90. Brown, J. M.; Wilson, W. R. Exploiting tumor hypoxia in cancer treatment. *Nature Reviews: Cancer* **2004**, *4*, 437–447.

91. Sugiyama, H.; Saito, I. Highly sequence selective photoreaction of 5-bromouracil-containing deoxyhexanucleotides. *J. Am. Chem. Soc.* **1990**, *112*, 6720.

92. Cook, G. P.; Greenberg, M. M. A novel mechanism for the formation of direct strand breaks upon anaerobic photolysis of duplex DNA containing 5-bromodeoxyuridine. *J. Am. Chem. Soc.* **1996**, *118*, 10025–10030.

93. Sugiyama, H.; Fujimoto, K.; Saito, I. Evidence for intrastrand C2′ hydrogen abstraction in photoirradiation of 5-halouracil-containing oligonucleotides by using stereospecifically C2′-deuterated deoxyadenosine. *Tetrahedron Lett*. **1996**, *37*, 1805–1808.

94. Franken, N. A. P.; Bree, C. V.; Veltmaat, M. A. T.; Rodermond, H. M.; Haveman, J.; Barendsen, G. W. Radiosensitization by bromodeoxyuridine and hyperthermia: Analysis of linear and quadratic parameters of radiation survival curves of two human tumor cell lines. *J. Radiat. Res.* **2001**, *42*, 179–190.

95. Ling, L. L.; Ward, J. F. Radiosensitization of Chinese hamster V79 cells by bromodeoxyuridine substitution of thymidine: Enhancement of radiation-induced toxicity and DNA strand break production by monofilar and bifilar substitution. *Radiat. Res.* **1990**, *121*, 76–83.

96. Hong, I. S.; Ding, H.; Greenberg, M. M. Radiosensitization by a modified nucleotide that produces DNA interstrand cross-links under hypoxic conditions. *J. Am. Chem Soc.* **2006**, *128*, 2230–2231.

97. Krief, A.; Lonez, F. Singlet oxygen oxidation of selenides to selenoxides. *Tetrahedron Lett*. **2002**, *43*, 6255–6257.

98. Hong, I. S.; Greenberg, M. M. DNA Interstrand cross-link formation initiated by reaction between singlet oxygen and a modified nucleotide. *J. Am. Chem. Soc.* **2005**, *127*, 10510–10511.

99. Sharman, W. M.; Allen, C. M.; van Lier, J. E. Role of activated oxygen species in photodynamic therapy. *Methods Enzymol*. **2000**, *319*, 376–400.

100. Dolmans, D. E.; Fukumura, D.; Jain, R. Photodynamic therapy for cancer. *Nature Rev. Cancer* **2003**, *3*, 380–387.

101. Peng, X.; Greenberg, M. M. Facile SNP detection using bifunctional, cross-linking oligonucleotide probes. *Nucleic Acids Res*. **2008**, *36*, e31.

102. Bastia, D.; Zzaman, S.; Krings, M.; Peng, X.; Greenberg, M. M. Replication termination mechanism as revealed by Tus-mediated polar arrest of a sliding helicase. *Proc. Natl. Acad. Sci. USA* **2008**, *105*, 12831–12836.

103. Box, H. C.; Budzinski, E. E.; Dawidzik, J. B.; Gobey, J., S.; Freund, H. G. Free radical-induced tandem base damage in DNA oligomers. *Free Rad. Biol. Med.* **1997**, *23*, 1021–1030.

104. Zeng, Y.; Wang, Y. Facile formation of an intrastrand cross-link lesion between cytosine and guanine upon Pyrex-filtered UV light irradiation of d(^{Br}CG) and duplex DNA containing 5-bromocytosine. *J. Am. Chem. Soc.* **2004**, *126*, 6552–6553.

105. Hong, H.; Wang, Y. Formation of intrastrand cross-link products between cytosine and adenine from UV irradiation of d(BrCA) and duplex DNA containing a 5-bromocytosine. *J. Am. Chem. Soc.* **2005**, *127*, 13969–13977.

106. Zeng, Y.; Wang, Y. Sequence-dependent formation of intrastrand crosslink products from the UVB irradiation of duplex DNA containing a 5-bromo-2′-deoxyuridine or 5-bromo-2′-deoxycytidine. *Nucleic Acids Res*. **2006**, *34*, 6521–6529.

107. Hong, H.; Cao, H.; Wang, Y. Formation and genotoxicity of a guanine-cytosine intrastrand cross-link lesion *in vivo*. *Nucleic Acids Res*. **2007**, *35*, 7118–7127.

108. Delaney, J. C.; Essigmann, J. M. Biological properties of single chemical-DNA adducts: A twenty year perspective. *Chem. Res. Toxicol.* **2008**, *21*, 232–252.

109. Patro, J. N.; Wiederholt, C. J.; Jiang, Y. L.; Delaney, J. C.; Essigmann, J. M.; Greenberg, M. M. Studies on the replication of the ring opened formamidopyrimidine, Fapy.dG in *Escherichia coli*, *Biochemistry* **2007**, *46*, 10202–10212.

110. Gu, C.; Zhang, Q.; Yang, Z.; Wang, Y.; Zou, Y.; Wang, Y. Recognition and incision of oxidative intrastrand cross-link lesions by UvrABC nuclease. *Biochemistry* **2006**, *45*, 10739–10746.

6

REACTIVITY OF 5-HALOPYRIMIDINES IN NUCLEIC ACIDS

RYU TASHIRO[*] AND HIROSHI SUGIYAMA[†]

[*] *Faculty of Pharmaceutical Sciences, Suzuka University of Medical Science, Mie 513-8670, Japan*

[†] *Department of Chemistry, Graduate School of Science, Kyoto University, Kyoto 606-8502, Japan*

5-Halouracils are analogues of thymine in which the methyl group of thymine has been replaced with a halogen atom. The photoreactive 5-halouracils, bromouracil (^{Br}U) and iodouracil (^{I}U), are widely used in medical applications and biological and chemical research. Because of the similarity in size of 5-halouracils and thymine (Figure 6.1), the thymine moiety of DNA can be replaced with a 5-halouracil without impairing the *in vivo* functionality of DNA. Such replacement enhances the UV sensitivity of the cell with respect to DNA–protein cross-linking, DNA strand breakage, and the creation of alkali-labile sites by forming uracil-5-yl radicals when exposed to UV irradiation.[1] 5-Halouracil-based photocrosslinking and photofootprinting methods have been used to investigate specific DNA–protein interfaces.[2] The photoreactions of 5-halouracil-containing DNAs have been extensively studied using DNA oligonucleotides and DNA fragments with defined sequences. The reactivities of 5-halouracils in DNA differ significantly from those of monomeric model systems. It has been demonstrated that hydrogen (H) abstraction by uracil-5-yl is atom specific and is highly dependent on local DNA conformation (Figure 6.2). It has been suggested that the photoreactivity of 5-halouracils could be used to detect various DNA structures.[3] Oxidative lesions generated by H abstraction and subsequent oxidation allow us to investigate stability and reactivity of these sites in DNA, which could provide useful information to

Radical and Radical Ion Reactivity in Nucleic Acid Chemistry, Edited by Marc M. Greenberg

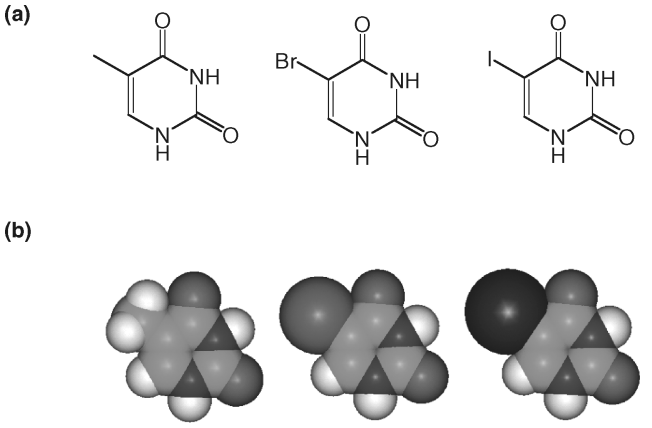

FIGURE 6.1. Chemical structures (**a**) and CPK models (**b**) of thymine, 5-bromouracil, and 5-iodouracil. (See color insert.)

understand molecular mechanisms of DNA damage. In addition to their H abstraction properties, 5-halouracil residues in DNA can be used as electron acceptors 4 as they rapidly eliminate halide anions and generate uracil-5-yl radicals when reduced to an anion radical (Figure 6.2).[4] The electron transfer and back electron transfer processes are highly dependent on DNA conformation. This chapter discusses specific H abstraction by uracil-5-yl radicals in various DNA conformations, and it also discusses 5-halouracil studies on electron transfer in the B and Z forms of DNA and between DNA–protein interfaces.

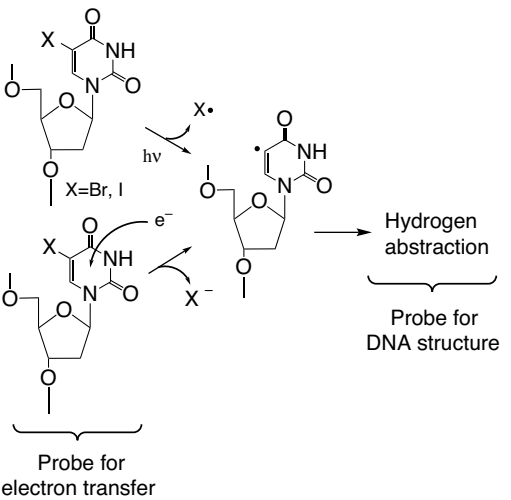

FIGURE 6.2. Generation of the uracil-5-yl radical from 5-halouracil and its utilization as a DNA probe.

6.1. ELUCIDATION OF DNA STRUCTURE USING THE 5-HALOURACIL PHOTOREACTION

When DNA that contains ^{Br}U or ^{I}U is irradiated with UV light, the uracil-5-yl radical is generated from 5-halouracil and abstracts H from the deoxyribose backbone of DNA. Appropriate orbital overlapping of the uracil-5-yl radical and the target H–C bond during the transition state of H abstraction is necessary for efficient H abstraction. As local DNA structures differ in the proximity of H atoms to the uracil-5-yl radical, the site of uracil-5-yl radical-induced H abstraction and its degradation products is highly dependent on the surrounding DNA conformation. Therefore, analysis of the degradation products of DNA that contains 5-halouracil can provide information on its structure. H abstraction reactions in DNA conformations such as the B, A, and Z forms, bent DNA, and the G quadruplex have been studied and their degradation products have been identified.[3] The mechanisms by which these degradation products are produced, and their properties, are described in the following sections.

6.1.1. H Abstraction in B-Form DNA

It has been shown that the major reactions that occur when B-form DNA that contains ^{Br}U or ^{I}U is irradiated are formation of deoxyribonolactone- (**1**) and erythrose-containing sites (**2**) on the 5′ side of 5-halouracil (Scheme 6.1).[5] Therefore, the formation of these residues in irradiated DNA is indicative of a B-form structure. As shown in Figure 6.3, the uracil-5-yl radical in B-form DNA is close enough to the C1′ and C2′α Hs of the 5′ side residue of the uracil-5-yl radical to induce H abstraction at these sites. Fujimoto et al. proved that the ribonolactone residue in DNA is derived from direct C1′ H abstraction using a C1′-deuterated deoxyadenine-containing oligonucleotide with a kinetic isotope effect (kH/kD) of 1.7.[6]

Mass spectrometry of the ribonolactone-containing oligonucleotide (**1**) isolated after photoreaction in $H_2{}^{18}O$ indicated that the 1′ oxygen atom of ribonolactone is derived from H_2O. The proposed mechanism for the formation of ribonolactone shown in Scheme 6.2 is based on these observations. After H abstraction of the C1′ H by the uracil-5-yl radical, the C1′ radical is oxidized, presumably by the cation radical of G or molecular O_2, and the C1′ cation that is formed reacts with water to give **1**. Because the formation of the uracil-5-yl radical and the subsequent oxidation of the C1′ radical by a base cation radical is related to the electron transfer process, this mechanism is described in Section 6.2.1. Upon heating at neutral pH (90°C, 5–20 min), the

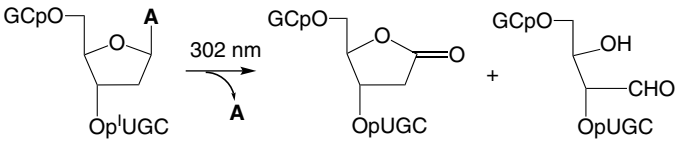

SCHEME 6.1

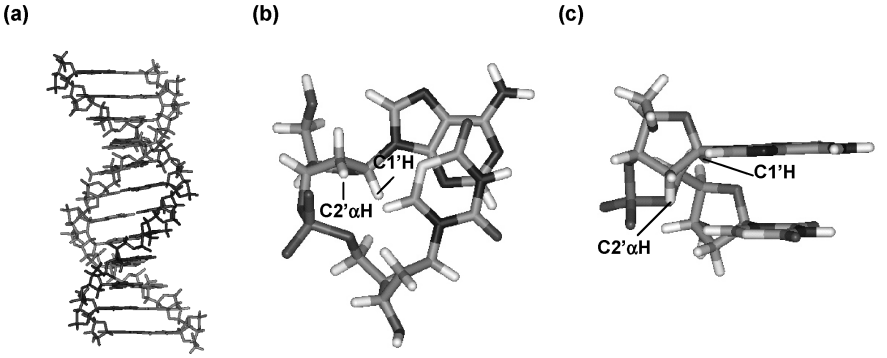

FIGURE 6.3. (**a**) Structure of B-form DNA. Close-up view of the $A^{Br}U$ sequence (**b**), and its side view (**c**). C5 of the uracil-5-yl radical is depicted in yellow. (See color insert.)

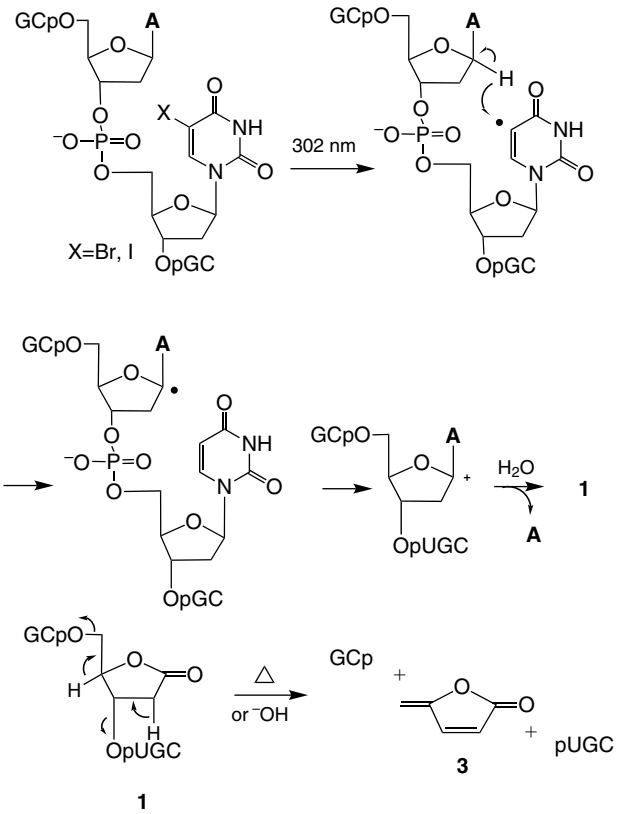

SCHEME 6.2

ribonolactone-containing site, such as **1**, readily decomposes into a DNA fragment with phosphate termini and generates methylenefuranone (**3**) (Scheme 6.2).[5] This facile heat degradation-inducing DNA strand scission is useful for identifying ribonolactone residues in DNA by PAGE analysis.

The erythrose residue, such as **2,** is produced upon C2′αH abstraction by the uracil-5-yl radical. H abstraction at C2′α was demonstrated by photoreaction of the stereospecifically C2′ deuterated 5-halouracil-containing hexamer, $d(GCA^{X}UGC)_2$ as shown in Scheme 6.3. The kinetic isotope effect (kH/kD) for the formation of the erythrose residue from irradiated ^{Br}U- and ^{I}U-containing strands was 7.5 and 7.2, respectively.[7] These kinetic isotope effects are significantly larger than that of 1.7 for C1′ H abstraction.

When treated with a hot alkaline solution (0.1 N NaOH, 90°C), the erythrose-containing hexamer **2** cleaves into two DNA fragments with phosphoglycoaldehyde termini **4** and **5** (Scheme 6.4) via the retroaldol reaction.[5b] Strands **4** and **5** are reduced to strands **6** and **7** upon treatment with $NaBH_4$. It is proposed that erythrose residues in DNA can be detected by reduction and enzymatic digestion of the products of the retroaldol reaction (Scheme 6.5). After photoirradiation, the yield of erythrose residues is usually greater for DNA that contains ^{I}U than for DNA that contains ^{Br}U, indicating that qualitative differences are present in these reactions.

To investigate the fate of the radical at the C2′ site of DNA, products from the photoirradiation of 2′α-iodo-2′-deoxyuridine (**8**), which generates the deoxyuridine C2′ radical, were analyzed (Scheme 6.6).[8] Several photoproducts, including erythrose, were produced by the irradiated 2′α-iodo-2′-deoxyuridine. Interestingly,

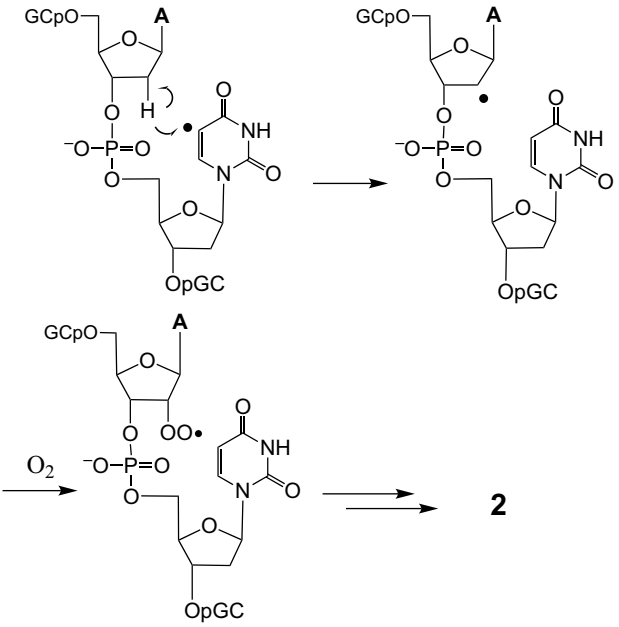

SCHEME 6.3

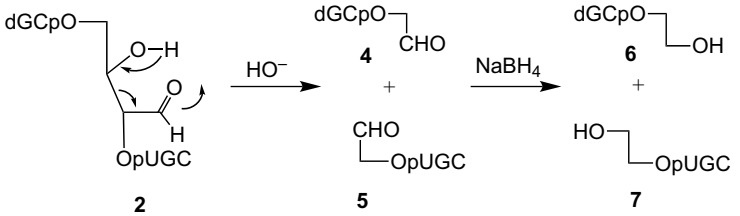

SCHEME 6.4

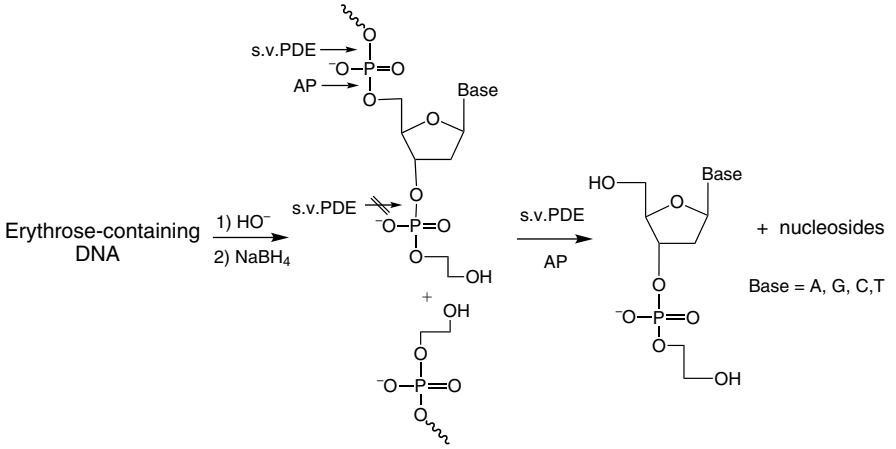

SCHEME 6.5

ribonolactone, the typical oxidation product of C1′ H abstraction, was also produced. That the oxygen atom at C1 of ribonolactone is derived from water indicates that a C1′ cation intermediate is formed from **8** during irradiation. These results indicate that a 1,2 hydride shift occurs from the C1′ to the C2′ cation, which is generated by oxidation of the C2′ radical by the iodide radical (I•) (Scheme 6.6).

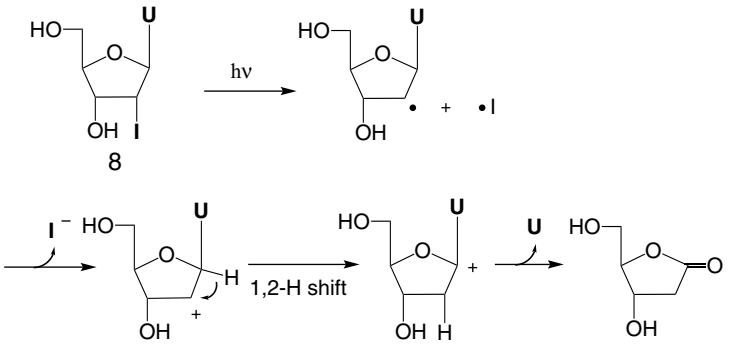

SCHEME 6.6

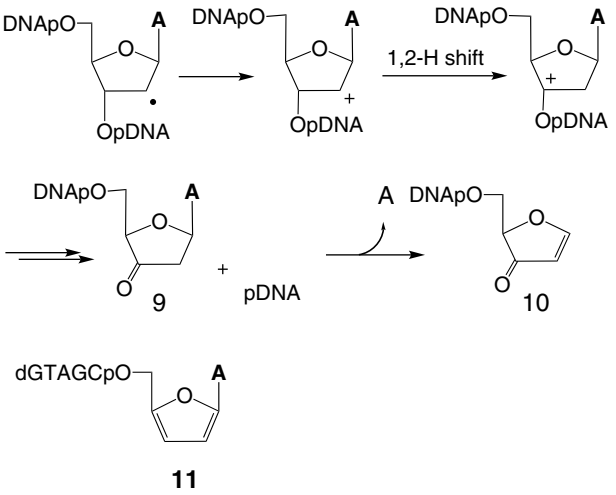

SCHEME 6.7

Photoreaction of a ^{Br}U-containing oligonucleotide under anaerobic conditions reduces the formation of erythrose and increases direct strand cleavage. Product **10** in Scheme 6.7 was detected, and it is suggested that this product is generated from product **9** with the release of adenine. Generation of **10** suggests that a 1,2 hydride shift occurs from the C3′ to the C2′ cation (Scheme 6.7).[9] It has also been reported that furanyladenine (**11**) is formed at 3′-phosphate termini under anaerobic conditions (Scheme 6.7).[10] These results clearly indicate that C2′ H abstraction could also give C1′ and C3′ oxidation products when C2′ radical is oxidized to a C2′ cation and suggest that such a possibility need to be considered in elucidation of the site of H abstraction during the formation of DNA oxidative products.

6.1.2. Photoreaction of 5-Halouracil in A-Form DNA

Exposure to solutions containing high salt concentrations or ethanol induces the A-form of DNA,[11] which contains a deep, narrow major groove. A DNA–RNA hybrid has been shown to form a type of A-form structure, the so-called A-type structure. The DNA–RNA hybrid that is produced during transcription of DNA forms an A-type structure. In A-form DNA, the major photoproduct of irradiation of ^{Br}U- or ^{I}U-containing DNA–RNA hybrid is ribonolactone (Scheme 6.8).[12] Interestingly, erythrose is not a product of the A-form reaction, indicating that C1′ H is selectively abstracted in A-form DNA. The structure of the A^{I}U sequence in the A-type structure is presented in Figure 6.4 and shows that the distance between C1′ and the uracil-5-yl radical is greater than the distance between C2′α and the uracil-5-yl radical. Therefore, there is no direct correlation between distance and selectivity of H abstraction in the A-form.

The feasibility of a transition state of the H abstraction reaction in a DNA duplex structure is an important component of the efficiency of the reaction (Scheme 6.9).

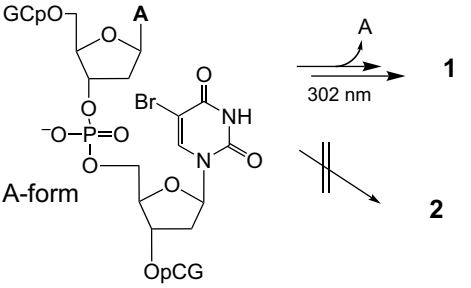

SCHEME 6.8

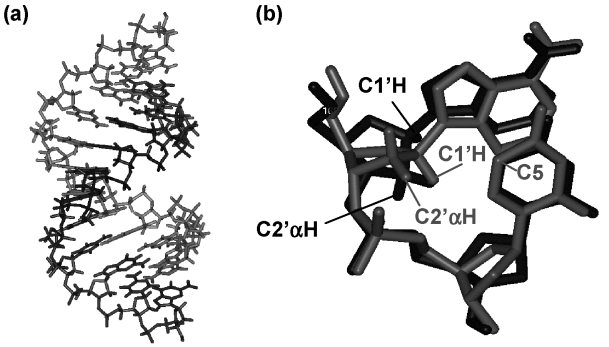

FIGURE 6.4. (**a**) Structure of A-form DNA. (**b**) Close-up view of $A^{Br}U$ step in the A-form (black) and the B-form (red). (See color insert.)

To determine the conformational energy required to achieve a transition state in the A- and B-forms, a putative transition state for H abstraction in a DNA duplex and a DNA–RNA hybrid was constructed and conformational energy was evaluated. The dinucleotide portions of the lowest two minimized structures in each structure that contained the transition state for C1′, C2′α H abstraction in the DNA duplex and C1′ and C2′β H abstraction in the A form DNA–RNA hybrid are shown in Figure 6.5. The AMBER energy for the putative transition structure for C1′ in the DNA–RNA hybrid

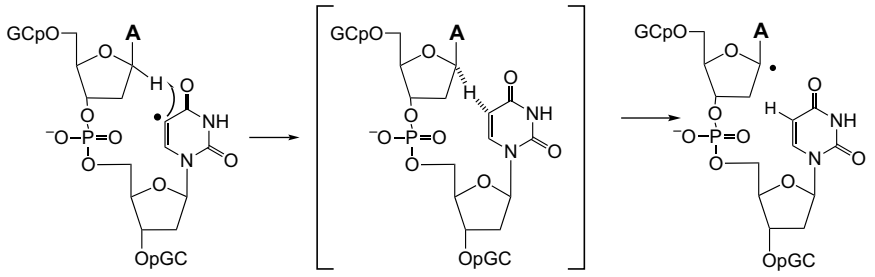

SCHEME 6.9

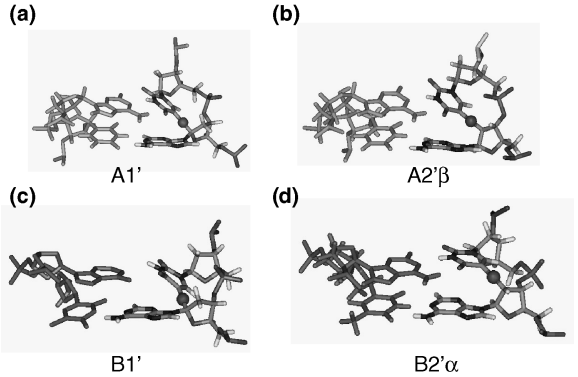

FIGURE 6.5. Estimated transition states of H abstraction in A- (**a**,**b**) and B-form (**c**,**d**) DNA. RNA and DNA are shown in blue and magenta, respectively. A red ball indicates an abstracting H atom. (See color insert.)

was lower than that for C2′α and C2′β H abstraction. These results explain the observed selective C1′ H abstraction in A-form DNA.

6.1.3. Photoreaction of 5-Halouracil in Z-Form DNA

The left-handed Z-form of DNA is one of the characteristic local structures of DNA in X-ray crystallography and has been extensively studied in relation to regulation of gene expression.[13] Formation of the Z-form can effectively reduce torsional stress induced by nucleosome formation. However, the biological relevance of Z-DNA is still unclear, presumably because of its short lifetime under torsional stress caused by unwinding of DNA during transcription.

In Z-DNA, 2′-riboguanosine (**12**) is the major product of irradiated Z-form 5′-(CGCG^{I}UGCG)-3′/5′-(C^{m}GCAC^{m}GCG)-3′ (^{m}G = 8-methylguanine) (Scheme 6.10).[14] Therefore, formation of guanosine from irradiated DNA that contains 5-halouracil is indicative of a Z-DNA structure. Importantly, because guanosine in DNA strands is readily hydrolyzed to **13** by ribonuclease T1, photochemical exposure and subsequent enzymatic hydrolysis could be used to detect the Z-form of DNA (Scheme 6.10). Stereospecific 2′β H abstraction resulting in 2′α-hydroxylation was demonstrated using a stereospecifically deuterated octanucleotide in Z-form DNA. The resulting kinetic isotope effect (1.2) is similar to that for C1′ H abstraction (1.7) and significantly smaller than that for C2′α H abstraction (7.2), suggesting the reaction with a lower level of transition state.[15]

A close-up view of the structure of the GU sequence in Z-DNA is shown in Figure 6.6. The uracil-5-yl radical and the 2′β H are in close proximity, and of Z DNA containing transition state of C2′β H abstraction gave the lowest minimized energy which is consistent with selective C2′βH abstraction.

The photochemical reaction of 5-halouracil in Z-DNA induced by the binding of the N-terminus of ubiquitous RNA editing enzyme, adenosine deaminase 1 (ADAR1), Zα, efficiently resulted in 2′α hydroxylation on the 5′ side of ^{I}U (Figure 6.7). This

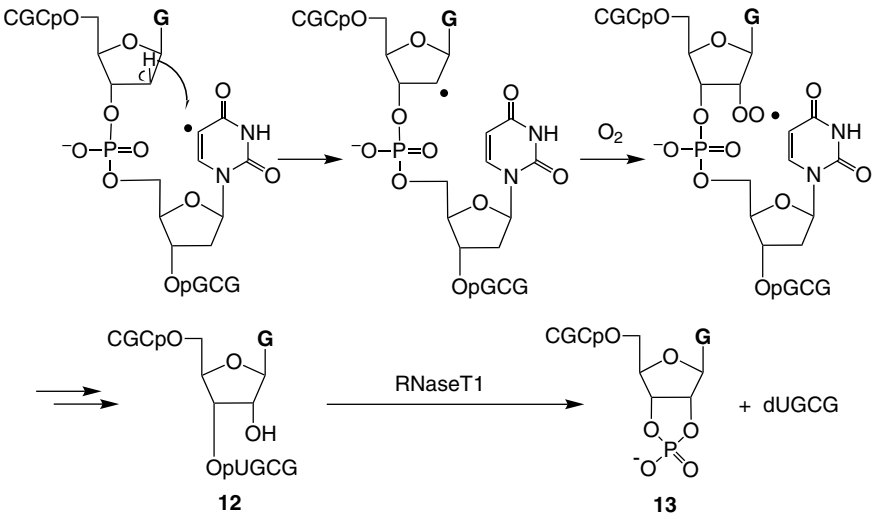

12 13

SCHEME 6.10

suggests that Zα packs tightly in Z-DNA, with the C3′ *endo*-sugar puckering the 2′-deoxyguanosine of the duplex, and promotes specific C2′α H abstraction by the uracil-5-yl radical.[16]

6.1.4. Photoreaction of 5-Halouracil in Bent DNA

DNA bending, which is induced by protein binding, is involved in the regulation of gene expression. For example, the TATA-box binding protein induces DNA bending, which is important for the initiation of prokaryotic transcription.[17] To examine H

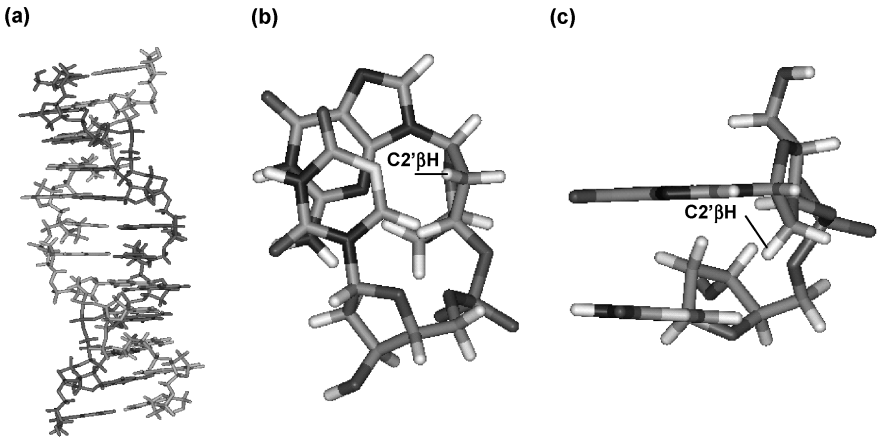

FIGURE 6.6. (**a**) Structure of Z-form DNA. (**b**) Close-up views of the GU sequence and its side view. (**c**) C5 of the uracil-5-yl radical is shaded yellow. (See color insert.)

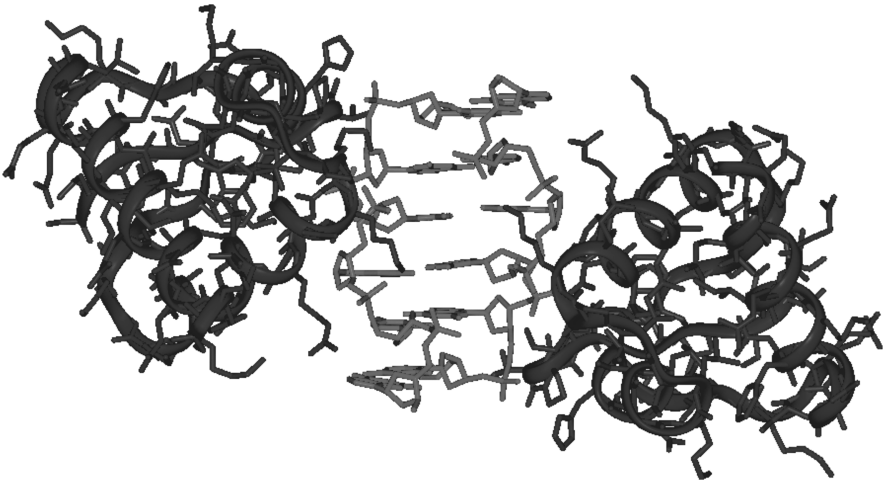

FIGURE 6.7. Structure of the $d(CGCGCG)_2$–Zα complex. (See color insert.)

abstraction in bent DNA, the photoreaction of 5-halouracil-containing DNA in the presence of Sso7d protein was examined.[18] Sso7d is a small chromosomal protein from the hyperthermophilic archaeabacterium, *Sulfolobus solfataricus*. The structure of the complex of Sso7d and $d(GTAATTAC)_2$ was solved by X-ray crystallographic analysis at high resolution (Figure 6.8). The Sso7d protein binds in the minor groove, causing a sharp bending at the TpT step; this kink results from intercalation of the hydrophobic side chains of Val26 and Met29.

Scheme 6.11 depicts the formation of formyluracil- and hydroxymethyluracil-containing oligomers **14**, **15** in the presence of Sso7d.[19] These results clearly indicate that protein-induced DNA bending causes an intrastrand H abstraction from the 5-methyl group of thymine in the same strand. The crystal structure indicates that the 5-methyl group in thymine is in close proximity to the uracil-5-yl radical. This specific intrastrand methyl H abstraction suggests that DNA is similarly kinked by Sso7d in solution and represents a new method for detecting DNA kinks in solution. Sso7d protein was oxidized to Sso7dOH during irradiation with $d(GTAAT^{I}UAC)_2$. Oxidation of Sso7d occurred mainly at the intercalating Val26 and Met 29 residues

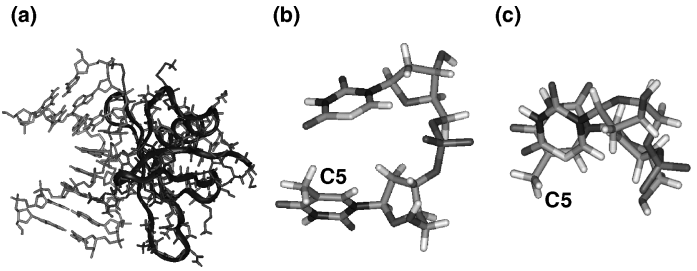

FIGURE 6.8. (**a**) Structure of the Sso7d–DNA complex. (**b**) Close-up view of the TU step and (**c**) its side view. C5 of the uracil-5-yl radical is shaded yellow. (See color insert.)

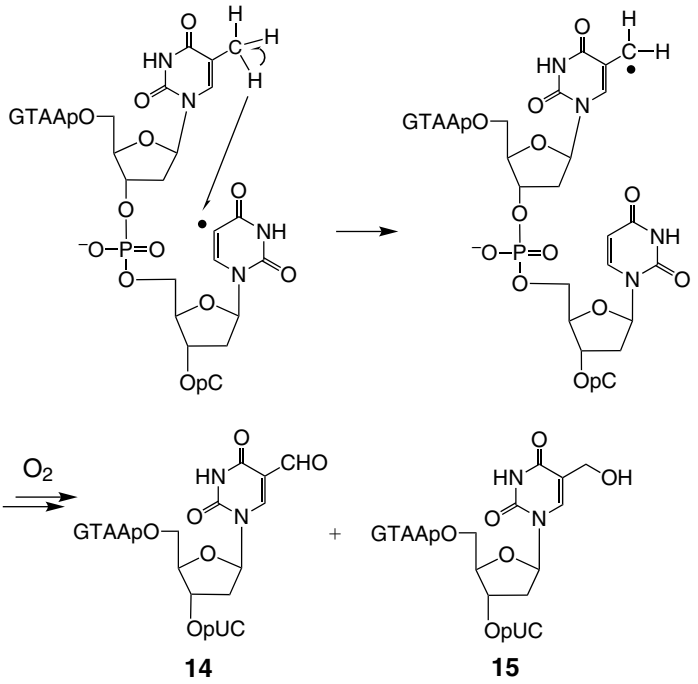

14 **15**

SCHEME 6.11

(78%). The X-ray crystal structure suggests that residues Val26 and Met29 are in close proximity to the uracil-5-yl radical, which is intercalated with the major groove at the bending site. These results suggest that the interaction of DNA and Sso7d in solution closely resembles their crystal structures.

6.1.5. Photoreaction of 5-Halouracil in G Quadruplexes

G quadruplexes are four-stranded DNA structures formed by guanine-rich sequences. Although the formation of G quadruplexes has only been studied *in vitro*, G quadruplexes are attracting attention because of their postulated involvement in a variety of biological processes.[20] The DNA of human telomeres consists of repeat units of the nucleotide sequence, 5′-TTAGGG-3′, which end with a single-stranded segment that overhangs the end of the double-stranded DNA helix. The single-stranded repeat units form four-stranded G quadruplex structures. NMR analysis has demonstrated that a 22-mer of 5′-d[AGGG(TTAGGG)$_3$]-3′ in solution in the presence of Na^+ ions adopts an antiparallel G quadruplex structure in which the opposing GGG columns are antiparallel, with one diagonal and two lateral TTA loops (Figure 6.9).[21]

In contrast, the same 22 mer adopts a completely different G quadruplex architecture in a crystal grown in the presence of K^+ ions: The four core GGG units are parallel and the three linking external loops are located on the exterior of the G quadruplex

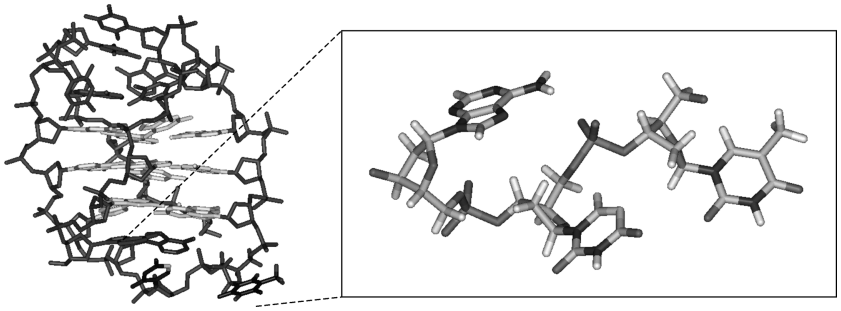

FIGURE 6.9. Structure of human telomere sequence 5′-AGGG(TTAGGG)$_3$-3′ in an NaCl solution and a close-up view of the diagonal TTA loop region. C5 of the uracil-5-yl radical is shaded yellow. (See color insert.)

core.[22] Three groups, including our group, have established that the topology of the human telomere sequence in K^+ solution is that of a completely different hybrid structure.[23]

To explore the structure-dependent abstraction of H atoms in antiparallel and hybrid G quadruplexes, one of the six thymine residues in the 22-mer human telomeric DNA, 5′-d(AGGGT$_1$T$_2$AGGGT$_3$T$_4$AGGGT$_5$T$_6$AGGG)-3′, was substituted for ^{I}U to generate six types of oligodeoxynucleotide.[24] Upon irradiation with UV light, more than 60% of the antiparallel DNA oligomer in which T_4 in the middle of the diagonal loop was substituted with ^{I}U was consumed. Analysis of the products indicated that 2′-deoxyribonolactone was efficiently produced with the release of thymine from the photoirradiated T4-substituted DNA oligomer in the antiparallel structure (Figure 6.10).

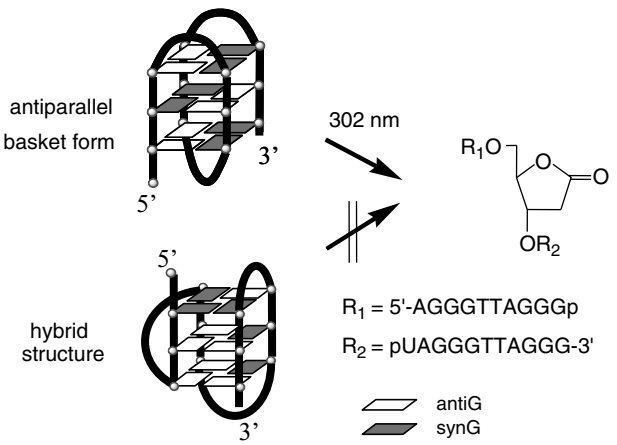

FIGURE 6.10. The ribonolactone residue is formed at the diagonal loop of the antiparallel basket form of the human telomere sequence, 5′-AGGGTTAGGGT^{I}UAGGGTTAGGG-3′, under irradiation at 302 nm. The hybrid structure does not produce ribonolactone residues in the presence of K^+ ions. (See color insert.)

In marked contrast to the large photoreactivity of the antiparallel form, ^{I}U in hybrid form is not consumed (<2%) in the presence of K^+ ions under the same irradiation conditions. The high photochemical reactivity of 5′-AGGGTTAGGGT^{I}UA GGGTTAGGG-3′ in the antiparallel G quadruplex and its poor photoreactivity in the hybrid G quadruplex can be explained by the loop regions of the two structures (Figure 6.10). The hybrid G quadruplex has one external loop and two lateral loops in which neither H atom is directed to the C5 position of uracil. This may explain the low reactivity of the hybrid structure. In contrast, the NMR structure suggests that the uracil-5-yl radical is positioned closer to the 1′-H atom of the adjacent T_3 than the other H atoms in the diagonal loop.[21] Examination of oligonucleotides with various loop structures indicates that this type of efficient formation of ribonolactone residues only occurs at the diagonal loop of the G quadruplex.

Several other guanine-rich sequences have also been proposed to form G quadruplexes.[25] To test the efficacy of the photochemical method of detection of diagonal loops, we examined the photoreactions of the ^{I}U-substituted IgG switch regions and the 5′ termini of the Rb gene. Photoirradiation of 5′-d(AGGGGAGCTGGG G^{I}UAGGTGGGA)-3′ (IgG) and 5′-d(CGGGGGGTT^{I}UTGGGCGGC)-3′ (Rb) indicated that the ribonolactone-containing oligomers were the main products, and that free guanine or thymine was released. The highly efficient production of ribonolactone residues is strongly indicative of the formation of an antiparallel G quadruplex with a diagonal loop by these guanine-rich sequences.[26]

6.1.6. Summary of DNA Structure-Dependent Photoreaction of 5-Halouracil

In Section 6.1, photoreactivity of 5-halouracil in different DNA structures from B-DNA to G-quadruplexes was described. Relationship between DNA structures and photoproducts of 5-halouracil is summarized in Scheme 6.12. These results demonstrate the detailed relationships between the local DNA structures and the products of photoinduced hydrogen abstraction by the resulting uracil-5-yl radicals, and they show that this photochemical method can be used to detect DNA structures.[3]

6.2. PHOTOREACTION OF 5-HALOURACIL FOR DETECTION OF DNA-MEDIATED ELECTRON TRANSFER

The previous chapters have described the dependence of H abstraction by the uracil-5-yl radical on DNA structure and its potential use to elucidate the structure of DNA. This chapter deals with the mechanism by which the uracil-5-yl radical is produced from 5-halouracil. It has been known that π-stacking of DNA mediates electron transfer. Electron transfer plays an important role in repairing damaged DNA.[27] Generation of the uracil-5-yl radical from ^{Br}U is initiated by the acceptance of an electron. Therefore, ^{Br}U has recently been used as a probe to detect DNA-mediated excess electron transfer.[28] The lifetimes of ^{Br}U and estimated as ^{I}U are 7 ns and 1.5 nsec, respectively.[29]

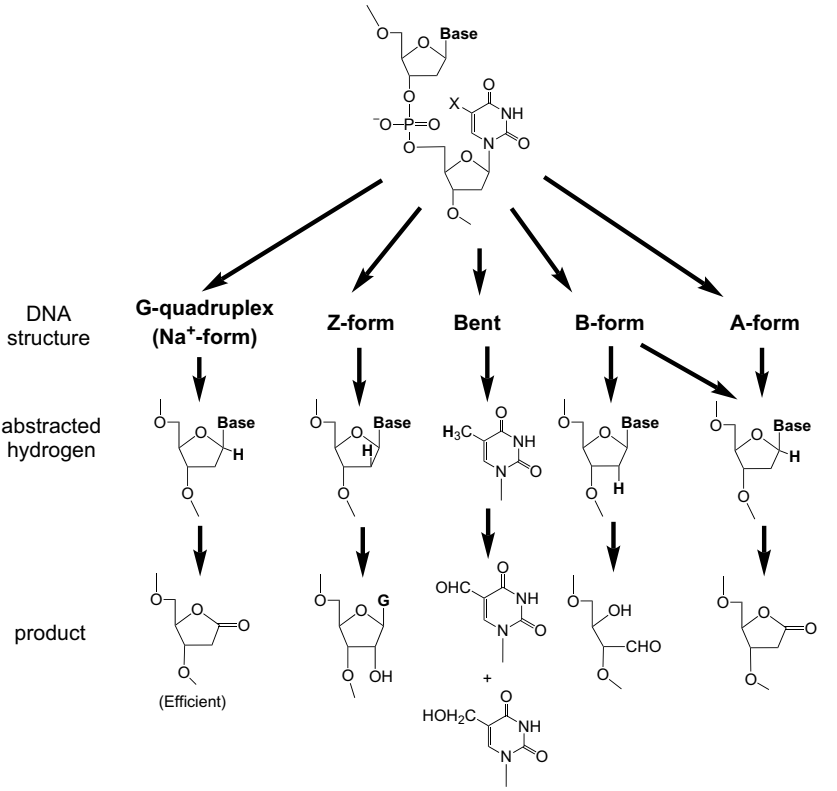

SCHEME 6.12

6.2.1. Electron Transfer in B-DNA

In contrast to $d(GCA^{Br}UGC)_2$, which results in efficient formation of C1′ and C2′ oxidation products after photoirradiation, hexanucleotides that do not have an $A^{Br}U$ sequence, such as 5′-d(GCG^{Br}UCG)-3′/5′-d(CGACGC)-3′, have very poor photoreactivity.[5] This type of $A^{Br}U$ sequence-specific photoreactivity was also observed by Greenberg group.[30] Based on these results, a sequence-specific electron transfer from the adjacent A at the 5′ side to ^{Br}U to form the ^{Br}U anion radical in the duplex structure was initially proposed. As G is a better electron-donating base than A, this reaction has been labeled "contrathermodynamic."[30] Thus, the sequence specificity of a long DNA fragment that contained 5-halouracil was examined. Using PCR, we prepared DNA fragments in which all thymine residues were substituted with ^{Br}U or ^{I}U. The DNA fragments were irradiated with 302-nm UV light and then analyzed on sequencing gels.[31] Surprisingly, specific cleavage at the 5′-(G/C)AA^{X}U^{X}U-3′ and 5′-(G/C)A^{X}U^{X}U-3′ (X = Br or I) sequences in both ^{Br}U- and ^{I}U-containing DNA fragments was observed only after heat treatment. HPLC product analysis of oligonucleotides containing hotspots indicated that the major products were ribonolactone-containing octamers. When oligonucleotides were irradiated in the

presence of $H_2{}^{18}O$, ^{18}O atoms were incorporated into the ribonolactone residues, indicating that H_2O is the source of the carbonyl oxygen of ribonolactone.[31]

As 5′-d(CGAA^{Br}UTGC)-3′/5′-d(GCAATTCG)-3′ produced a ribonolactone-containing product, 5′-d(CGALUTGC)-3′ (L = ribonolactone residue), as a major product with an efficiency similar to that of d(CGAA^{Br}U^{Br}UCG)$_2$, we examined the photoreactivity of various oligonucleotides in which the putative electron donor, G, was replaced with modified purine bases that differed in oxidation potential, namely, hypoxanthine (I), 8-bromoguanine (^{Br}G), 8-methoxyguanine (^{MeO}G), and 7-deaza-guanine (Z) (Figure 6.11).[32]

It was found that the yield of ribonolactone-containing products increased with decreasing ionization potential (IP) of the purine base in the oligonucleotide, namely, $^{Br}G < G < {}^{MeO}G < Z$; almost no ribonolactone was observed in the case of A and I. These results clearly indicate that the G in the 5′-GAA^{Br}U^{Br}U-3′ sequence acts as an electron donor, even though it is not oxidized itself. From these observations, we proposed a mechanism to explain the efficient photoreaction of 5′-GAA^{X}U^{X}U-3′ sequences (Figure 6.12).[32]

In the proposed mechanism, an initial electron transfer occurs from G to the electron-deficient ^{X}U^{X}U step through stacked AA and A. Release of the halide anion from the ^{X}U^{X}U anion radical generates uracil-5-yl radicals, which abstract the C1′ H from the adjacent A of the ^{X}U^{X}U step. One-electron oxidation of the C1′ radical of dA by the cation radical of G produces a C1′ cation and regenerates G. The intervening A bases between G and the ^{X}U^{X}U step are considered to act as a bridge between the electron donor and acceptor for charge separation after electron transfer from G to the ^{X}U^{X}U step, thus preventing rapid back electron transfer. When the number of A/T base pairs between G and the acceptor, ^{X}UT, is zero or one, the back electron transfer is much faster than the release of bromide ions. When two A/T base pairs are present

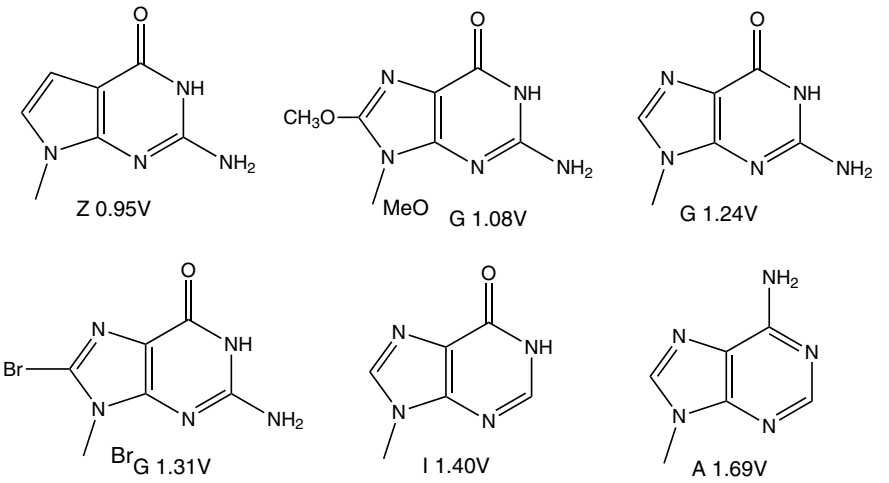

FIGURE 6.11. Chemical structures of purine derivatives and their oxidation potentials. The ionization potential of ^{Br}G was estimated *ab initio*.[32]

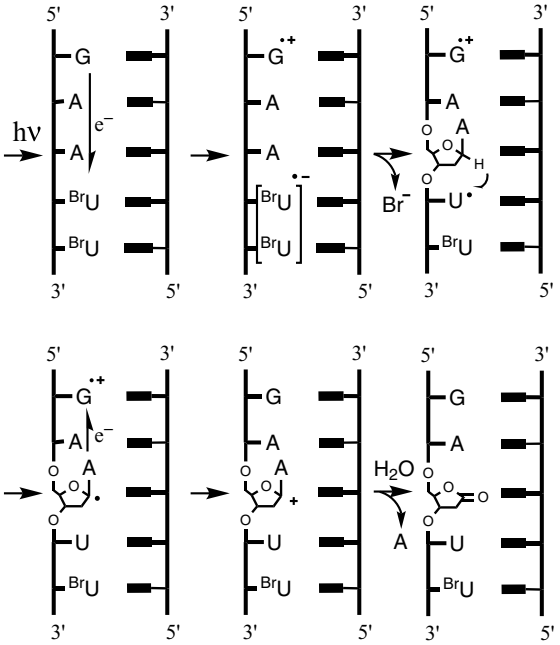

FIGURE 6.12. Proposed reaction mechanism of ^{Br}U in the hot-spot 5′-GAA^{Br}U^{Br}U-3′ sequence.

between G and ^{X}UT, back electron transfer is slow enough to allow the release of bromide ions from the anion radicals of ^{Br}U. These results further confirm that the G located 5′ upstream from ^{Br}U acts as an electron donor for ^{Br}U and that the intervening A/T base pairs act as a bridge for the electron-transfer process (Figure 6.13).

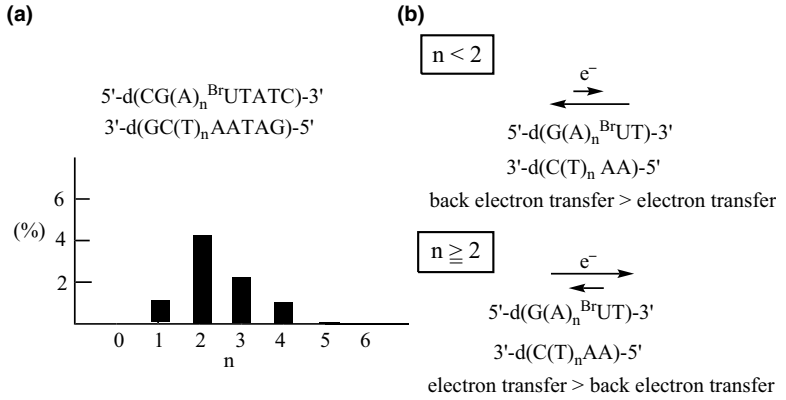

FIGURE 6.13. (**a**) Amount of ribonolactone produced with various numbers (n) of intervening bridge AT base pairs. (**b**) Schematic presentation of electron transfer and back electron transfer in the case of $n < 2$ and $n \geq 2$.

Prevention of back electron transfer by A/T base pairs may be responsible for the results obtained for the $d(GCA^{Br}UGC)_2$.[5a,9]

6.2.2. Electron Transfer in Z-DNA

In the B-form, 5′-$d(C_1G_2C_3G_4{}^{Br}U_5G_6C_7G_8)$-3′/5′-$(C_9{}^{m}G_{10}C_{11}A_{12}C_{13}{}^{m}G_{14}C_{15}G_{16})$-3′ had no photoreactivity, whereas in the Z-form it underwent efficient photoreaction and produced rG-containing DNA. The results clearly indicate that structural changes associated with a B–Z transition increased the photoreactivity of ^{Br}U-containing DNA.[33]. Inspection of the molecular structure of the Z-form suggested that unique four-base π-stacks were formed at the $G_4{}^{Br}U_5C_{11}{}^{m}G_{10}$ sequence (Figure 6.14a), whereas there is a continuous π-stack along each strand in B-DNA (Figure 6.14b). Interestingly, ^{m}G in the complementary strand was oxidized to imidazolone (Im)-containing DNA. Im is an oxidation product of guanine derivatives, and forms a stable base pair with G, suggesting that one of the oxidation products of G causes a CG → GC transversion mutation.[34] The oxidation of ^{m}G in the complementary strand suggests that the $^{m}G_{10}$ in a complementary strand located at the end of the four-base π-stacks acts as an electron donor. In addition, this indicates that the interstrand charge transfer from $^{m}G_{10}$ to $^{Br}U_5$ initiates the photoreaction. A proposed mechanism for the photoreaction of ^{Br}U-containing Z-DNA is shown in Figure 6.14.

In the proposed mechanism, efficient electron transfer from $^{m}G_{10}$ to $^{Br}U_5$ in four-base π-stacks produces cationic and anionic radicals under irradiation. The anionic radical of ^{Br}U eliminates bromine to generate a uracil-5-yl radical, which abstracts H to produce the rG residue. The cation radical of ^{m}G reacts with molecular oxygen to generate Im. Although electron transfer from ^{m}G in the complementary strand would not occur in B-form DNA, electron transfer from adjacent Gs would occur. However, rapid back electron transfer would prevent the reaction from proceeding. Elucidation of these differences in the electronic properties of B- and Z-form DNAs has resulted in the development of a molecular thermometer and biomolecular switching devices that respond inversely to thermal stimuli.[35]

6.2.3. Electron Transfer Between Protein and DNA

In living cells, many proteins interact directly with DNA. Therefore, detection of electron transfer between proteins and DNA is important to understand the mechanisms of DNA damage and repair. Cullis et al.[36] demonstrated that guanine radicals in DNA are reduced by electron transfer from histone. It is well-documented that a photoreactivating enzyme, photolyase, repairs T⟨ ⟩T by a one-electron reduction mechanism. Barton and colleagues proposed that some repair enzymes use electron transfer from redox cofactors to detect oxidative DNA damage.[37]

Electron transfer between a protein and the DNA interface was investigated using Sso7d and DNA that contained ^{Br}U.[38] Photoirradiation of $d(GTAAT^{Br}UAC)_2$ alone mainly resulted in the production of ribonolactone-containing octamers, indicating that electron transfer from 5′G to ^{Br}U initiates the reaction. Compared with

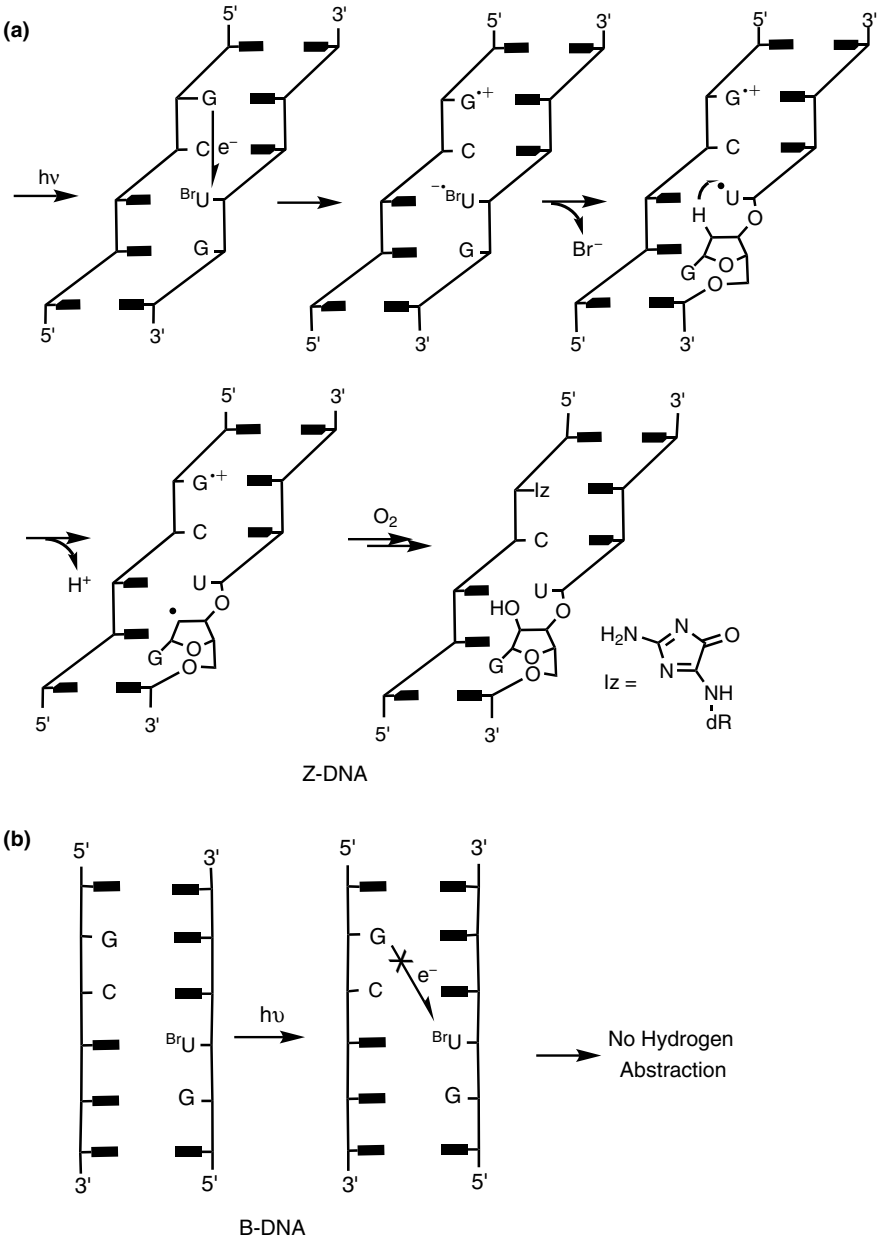

FIGURE 6.14. (**a**) Proposed scheme for efficient electron transfer through a four-base π-stack in Z-form DNA, along with the subsequent elimination of the bromide ion and 2′ hydroxylation. (**b**) Scheme depicting why such electron transfer from G to ^{Br}U does not occur in B-form DNA.

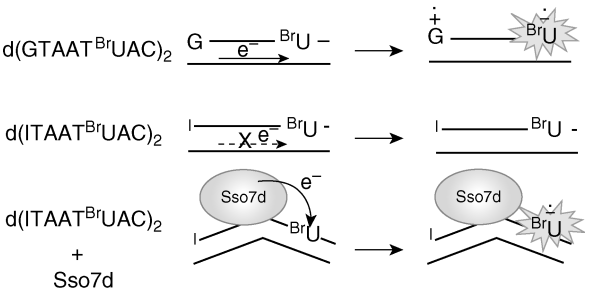

FIGURE 6.15. Electron transfer from Sso7d to ^{Br}U in the 5′-d(ITAAT^{Br}UAC)-3′ sequence. (See color insert.)

d(GTAAT^{Br}UAC)$_2$, d(ITAAT^{Br}UAC)$_2$ had very low photoreactivity. Interestingly, the addition of Sso7d enhanced the photoreactivity of d(ITAAT^{Br}UAC)$_2$ by 10-fold and produced formyluracil and hydroxymethyluracil, which is similar to the results for Sso7d-d(GTAAT^{I}UAC)$_2$ described in Section 6.1.4. These results clearly indicate that Sso7d activates the photoreactivity of d(ITAAT^{Br}UAC)$_2$ by serving as an electron donor to activate ^{Br}U in this DNA strand (Figure 6.15).

Product analysis showed that Trp-24 of Sso7d, which is located at the DNA–protein interface, is oxidized to produce *N*′-formylkynurenine during photoirradiation, indicating that Trp-24 acts as an electron source (Figure 6.16).

To provide further confirmation of electron transfer from Sso7d to DNA, the photochemical repair of a thymine dimer (T⟨⟩T) by Sso7d was examined. It was found that under UV irradiation at 295 nm for 1 h, d(GTAAT⟨⟩TAC)$_2$ was efficiently repaired only in the presence of Sso7d, and produced 5′-d(GTAATTAC)-3′, indicating that electron transfer from Sso7d repaired the T⟨⟩T dimer (Scheme 6.13). During this reaction, Trp-24 was not oxidized to the same extent as in the Sso7d-d(ITAAT^{Br}AC)$_2$ system. The results indicate that the anion radical of the repaired TT sequence is oxidized by the cation radical of Trp-24 and that a so-called ''circular electron transfer'' mechanism operates in this system.

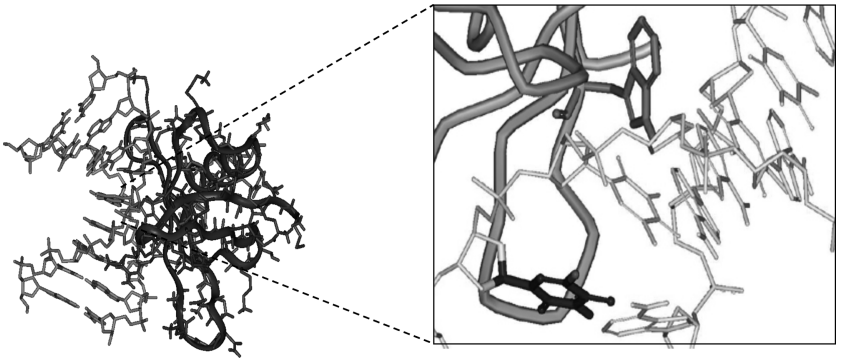

FIGURE 6.16. Close-up view of the structure of the Sso7d-d(GTAATTAC)$_2$ complex. Trp24 moiety (electron donnor) and ^{Br}U (acceptor) are shown in pink and blue, respectively. (See color insert.)

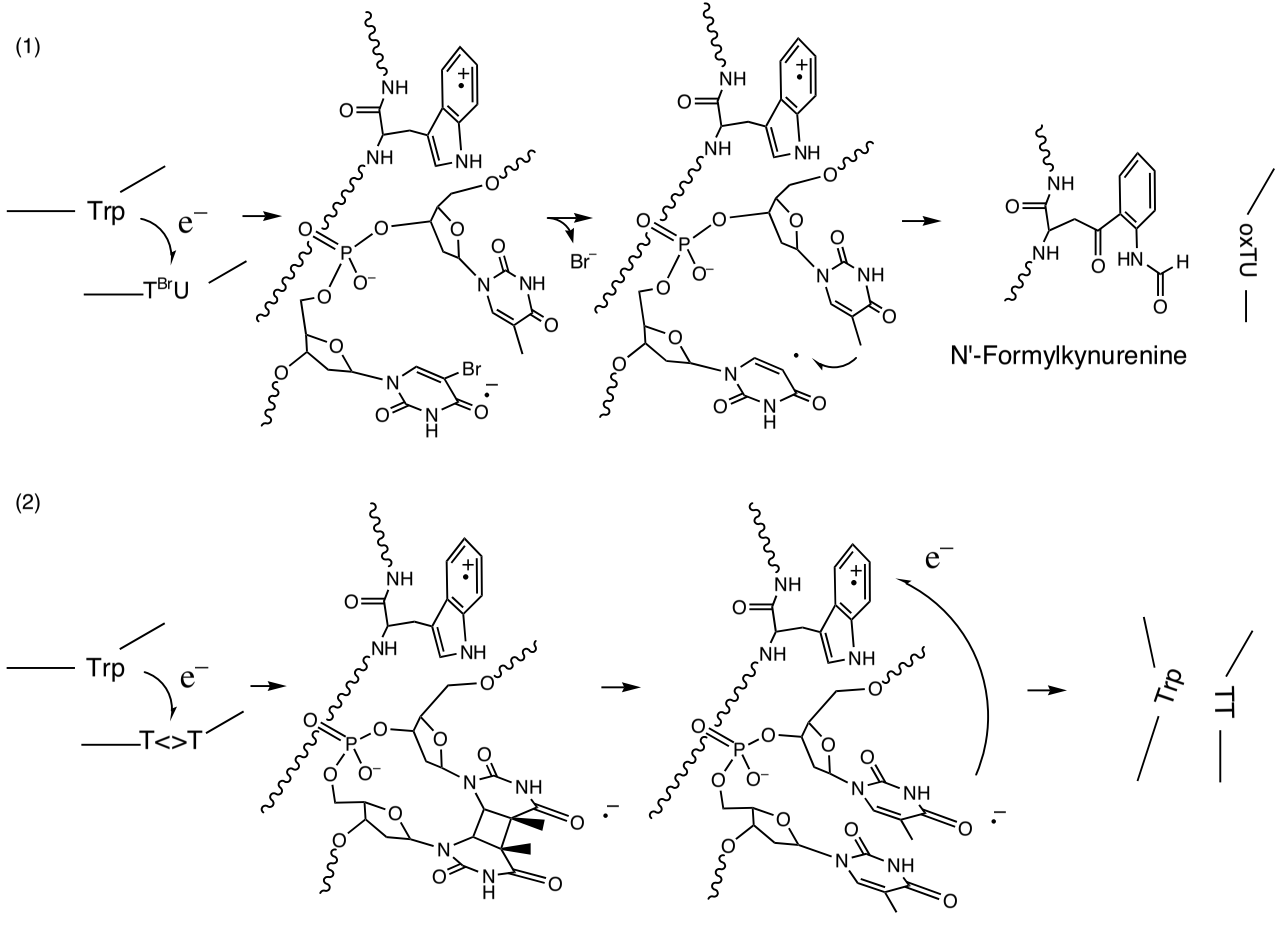

SCHEME 6.13

6.2.4. Photoreactivity of ^{I}U

The analogous hotspot sequences, 5′-(G/C)AA^{I}U^{I}U-3′ and 5′-(G/C)A^{I}U^{I}U-3′, were observed during photoirradiation of ^{I}U-substituted duplex DNA.[31] The Greenberg group has observed A^{I}U sequence specificity of photoreaction of ^{I}U in a 32-mer oligonucleotide and suggested that electron transfer is involved in this photoreaction.[30] These results clearly indicate that an electron transfer mechanism is operating in the ^{I}U-containing hotspot sequence. Although homolytic cleavage is expected to occur in ^{I}U-containing DNA, with some sequences such as 5′-d(GCG^{I}UCG)-3′/5′-d(CGACGC)-3′, the photoreactivity of the ^{I}U-containing oligonucleotide differs from that of the ^{Br}U-containing oligonucleotide and produces ribonolactone and erythrose upon photoirradiation.

To investigate the distance dependency of donors and acceptors, the photoreactivities of various oligonucleotides containing the 5′-G(A)n^{I}UT-3′ sequence were examined.[39] As shown in Figure 6.17, the amount of free adenine increased as the number of A/Ts increased from zero to two, and gradually decreased when more than three A/Ts were present. This reactivity of ^{I}U can be explained by an electron transfer mechanism analogous to the distance dependency of ^{Br}U-containing oligomers (Figure 6.13). However, a significantly different reactivity for ^{I}U relative to that of ^{Br}U was observed when the number of As was 0, 6, or 7 (Figure 6.17a). With ^{Br}U, almost no reactivity was observed in such sequences. Moreover, substitution of the electron-donating G for hypoxantin (I) completely eliminated the electron transfer process (Figure 6.17b). These results are indicative of the coexistence of a distance-independent homolytic process during the generation of the uracil-5-yl radical by ^{I}U photoreaction.

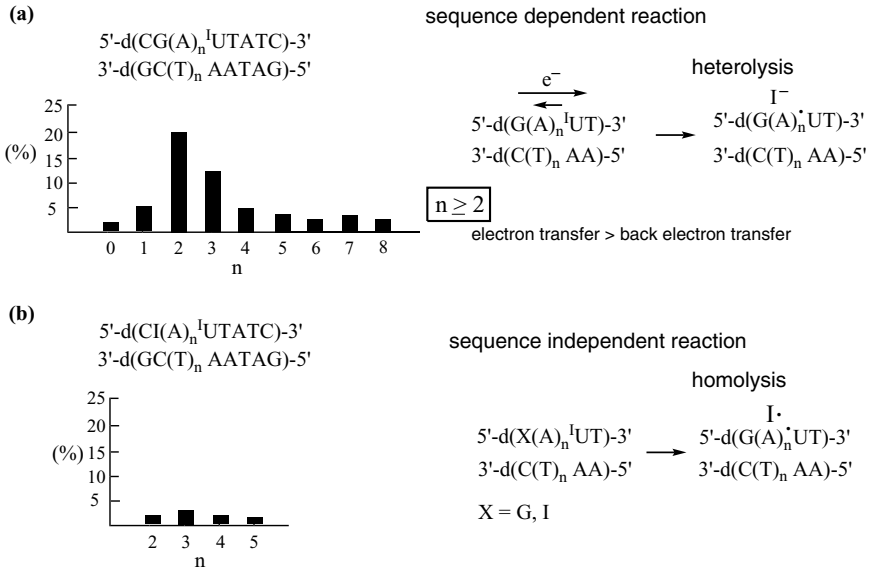

FIGURE 6.17. Amount of free bases produced with various numbers (*n*) of intervening bridge AT base pairs. (**a**) G-containing oligomer and (**b**) ^{I}U-containing oligomer.

It was demonstrated that both homolytic and heterolytic pathways are involved in the C–I bond cleavage mechanism of ^{I}U in DNA duplexes. In addition, the ratio of these pathways is highly dependent on the sequence of the DNA. Previously, we found that ^{I}U and ^{Br}U have different sequence dependencies in that the photoreaction occurs at the G^{I}U sequence but not at the G^{Br}U sequence. These results imply that the G^{I}U sequence produces H abstraction products via the homolytic pathway.

6.3. CONCLUSIONS

The uracil-5-yl radical generated in DNA abstracts specific H atoms from the deoxyribose backbone and base in accordance with the local DNA conformation. Although there are limited *in vitro* data, it is anticipated that knowledge derived from model systems will facilitate the development of new methods for probing local DNA conformation *in vivo*. Incorporation of 5-halouracil in DNA can be used to map the landscape of the anion radical of DNA. It is clear that excess electrons move around the DNA duplex and that in anion radical situations 5-halouracil prevents rapid back electron transfer and eliminates the halogen anion. Knowledge of these fundamental properties of the 5-halouracils is useful for choosing 5-halouracils for photochemical applications such as photocrosslinking or photofootprinting. For example, when electron donors are not expected to be in close proximity to 5-halouracil after it is incorporated into DNA, ^{I}U is more suitable because the uracil-5-yl radical is efficiently generated via the homolytic pathway.

REFERENCES

1. (a) Howard-Flanders, P.; Boyce, R. P.; Theriot, L. Mechanism of sensitization to ultraviolet light of T1 bacteriophage by the incorporation of 5-bromodeoxyuridine or by preirradiation of the host cell. *Nature* **1962**, *195*, 51–54. (b) Rupp, W. D.; Prusoff, W. H. Incorporation of 5-iodo-2′-deoxyuridine into bacteriophage T1 as related to ultra-violet sensitization or protection. *Nature* **1964**, *202*, 1288–1290. (c) Dewey, W. C.; Sedita, B. A.; Humphrey, R. M. Radiosensitization of X chromosome of chinese hamster cells related to incorporation of 5-bromodeoxyuridine. *Science* **1966**, *152*, 519–521.
2. (a) Blatter, E. H.; Ebright, Y. W.; Ebright, R. H. Identification of an amino acid-base contact in the GCN4-DNA complex by bromouracil-mediated photocrosslinking. *Nature* **1992**, *359*, 650–652. (b) Willis, M. C.; Hicke, B. J.; Uhlenbeck, O. C.; Cech, T. R.; Koch, T. H. Photocrosslinking of 5-iodouracil-substituted RNA and DNA to proteins. *Science* **1993**, *262*, 1255–1257. (c) Holz, B.; Dank, N.; Eickhoff, J. E.; Lipps, G.; Krauss, G.; Weinhold, E. Identification of the binding site for the extrahelical target base in N6-adenine DNA methyltransferases by photo-cross-linking with duplex oligodeoxyribonucleotides containing 5-iodouracil at the target position. *J. Biol. Chem.* **1999**, *274*, 15066–15072.
3. (a) Xu, Y.; Sugiyama, H. Photochemical approach to probing different DNA structure. *Angew. Chem. Int. Ed.* **2006**, *45*, 1354–1362. (b) Xu, Y.; Tashiro, R.; Sugiyama, H. Photochemical determination of different DNA structures. *Nat. Protoc.* **2007**, *2*, 78–87.

4. (a) Ito, T.; Rokita, S. E. Excess elecrotron transfer from an internally conjugated aromatic amine to 5-bromo-2′-deoxyuridine in DNA. *J. Am. Chem. Soc.* **2003**, *125*, 11480–11481. (b) Ito, T.; Rokita, S. E. Reductive electron injection into duplex DNA by aromatic amines. *J. Am. Chem. Soc.* **2004**, *126*, 15552–15559. (c) Kaden, P.; Mayer-Enthart, E.; Trifonov, A.; Fiebig, T.; Wagenknecht, H. A. Real-time spectroscopic and chemical probing of reductive electron transfer in DNA. *Angew. Chem. Int. Ed.* **2005**, *44*, 1636–1639. (d) Wagenknecht, H. A. Reductive electron transfer and transport of excess electrons in DNA. *Angew. Chem. Int. Ed.* **2003**, *42*, 2454–2460. (e) Wagner, C.; Wagenknecht, H. A. Reductive electron transfer in phenothiazine-modified DNA is dependent on the base sequence. *Chem. Eur. J.* **2005**, *11*, 1871–1876.
5. (a) Sugiyama, H.; Tsutsumi, Y.; Saito, I. Highly sequence-selective photoreaction of 5-bromouracil-containing deoxyhexanucleotides. *J. Am. Chem. Soc.* **1990**, *112*, 6720–6721. (b) Sugiyama, H.; Tsutsumi, Y.; Fujimoto, K.; Saito, I. Photoinduced deoxyribose C2′ oxidation in DNA. Alkali-dependent cleavage of erythrose-containing sites via a retroaldol reaction. *J. Am. Chem. Soc.* **1993**, *115*, 4443–4447.
6. Fujimoto, K.; Ikeda, Y.; Ishihara, S.; Saito, I. Deoxyribonolactone formation in photoirradiation of 5-bromouracil-containing oligonucleotides by direct C1′ hydrogen abstraction. *Tetrahedron Lett*. **2002**, *43*, 2243–2245.
7. Sugiyama, H.; Fujimoto, K.; Saito, I.; Kawashima, E.; Sekine, T.; Ishido, Y. Evidence for intrastrand C2′ hydrogen abstraction in photoirradiation of 5-halouracil-containing oligonucleotides by using stereospecifically C2′-deuterated deoxyadenosine. *Tetrahedron Lett*. **1996**, *37*, 1805–1808.
8. Sugiyama, H.; Fujimoto, K.; Saito, I. Stereospecific 1,2-hydride shift in ribonolactone formation in the photoreaction of 2′-iododeoxyuridine. *J. Am. Chem. Soc.* **1995**, *117*, 2945–2946.
9. Tallman, K. A.; Tronche, C.; Yoo, D. J.; Greenberg, M. M. Release of superoxide from nucleoside peroxyl radicals, a double-edged sword? *J. Am. Chem. Soc.* **1998**, *120*, 4903–4909.
10. Fujimoto, K.; Ikeda, Y.; Saito, I. Direct strand cleavage via furanyladenine formation in anaerobic photoirradiation of 5-bromouracil-containing oligonucleotides. *Tetrahedron Lett*. **2000**, *41*, 6455–6459.
11. (a) Dickerson, R. E. DNA structure from A to Z. *Methods Enzymol*. **1992**, *211*, 67–111. (b) Dickerson, R. E.; Drew, H. R.; Conner, B. N.; Wing, R. M.; Fratini, A. V.; Kopka, M. L. The anatomy of A-, B-, and Z-DNA. *Science* **1982**, *216*, 475–485. (c) Zimmerman, S. B.; Pheiffer, B. H. A direct demonstration that the ethanol-induced transition of DNA is between the A and B forms: an X-ray diffraction study. *J. Mol. Biol.* **1979**, *135*, 1023–1027.
12. Sugiyama, H.; Fujimoto, K.; Saito, I. Preferential C1′ hydrogen abstraction by an uracilyl radical in a DNA–RNA hybrid. *Tetrahedron Lett*. **1997**, *38*, 8057–8060.
13. (a) Herbert, A.; Rich, A. The biology of left-handed Z-DNA. *J. Biol. Chem.*, **1996**, *271*, 11595–11598.(b) Schwartz, T.; Rould, M. A.; Lowenhaupt, K.; Herbert, A.; Rich, A. Crystal structure of the Zα domain of the human editing enzyme ADAR1 bound to left-handed Z-DNA. *Science* **1999**, *284*, 1841–1845.(c) Herbert, A.; Schade, M.; Lowenhaupt, K.; Alfken, J.; Schwartz, T.; Shlyakhtenko, L. S.; Lyubchenko, Y. L.; Rich, A. The Zalpha domain from human ADAR1 binds to the Z-DNA conformer of many different sequences. *Nucleic Acids Res*. **1998**, *26*, 3486–3493.(d) Berger, I.; Winston, W.; Manoharan, R.; Schwartz, T.; Alfken, J.; Kim, Y. G.; Lowenhaupt, K.; Herbert, A.; Rich, A. Spectroscopic characterization of a DNA-binding domain, Z alpha, from the editing enzyme, dsRNA

adenosine deaminase: Evidence for left-handed Z-DNA in the Z alpha-DNA complex. *Biochemistry* **1998**, *37*, 13313–13321.(e) Wang, A. H.; Quigley, G. J.; Kolpak, F. J.; Crawford, J. L.; van Boom, J. H.; van der Marel, G.; Rich, A. Molecular structure of a left-handed double helical DNA fragment at atomic resolution. *Nature* **1979**, *282*, 680–686. (f) Rich, A.; Zhang, S. Timeline Z-DNA the long road to biological function. *Nat. Rev. Genet.* **2003**, *4*, 566–572.

14. Kawai, K.; Saito, I.; Sugiyama, H. Conformation-dependent photochemistry of 5-halouracil-containing DNA: Stereospecific 2′-hydroxylation of deoxyribose in Z-form DNA. *J. Am. Chem. Soc.* **1999**, *121*, 1391–1932.
15. Kawai, K.; Saito, I.; Kawashima, E.; Ishido, Y.; Sugiyama, H. Intrastrand 2′β hydrogen abstraction of 5′-adjacent deoxyguanosine by deoxyuridin-5-yl in Z-form DNA. *Tetrahedron Lett*. **1999**, *40*, 2589–2592.
16. Oyoshi, T.; Kawai, K.; Sugiyama, H. Efficient C2′-hydroxylation of deoxyribose in protein-induced Z-form DNA. *J. Am. Chem. Soc.* **2003**, *125*, 1526–1531.
17. Kim, Y.; Geiger, J. H.; Hahn, S.; Sigler, P. B. Crystal structure of a yeast TBP/TATA-box complex. *Nature* **1993**, *365*, 512–520.
18. (a) Gao, Y.-G.; Su, S-Y.; Robinson, H.; Padmanabhan, S.; Lim, L.; Wang, A. H-J. The crystal structure of the hyperthermophile chromosomal protein Sso7d bound to DNA. *Nat. Struct. Biol.* **1998**, *5*, 782–785. (b) Agback, P.; Baumann, H.; Knapp, S.; Ladenstein, R.; Hard, T. Architecture of nonspecific protein–DNA interactions in the Sso7d-DNA complex. *Nat. Struct. Biol.* **1998**, *5*, 579–584.
19. Oyoshi, T.; Wang, A. H.-J.; Sugiyama, H. Photoreactivity of 5-iodouracil-containing DNA-Sso7d complex in solution: the protein-induced DNA kink causes intrastrand hydrogen abstraction from the 5-methyl of thymine at the 5′ side. *J. Am. Chem. Soc.* **2002**, *124*, 2086–2087.
20. (a) Sundquist, W. I.; Klug, A. Telomeric DNA dimerizes by formation of guanine tetrads between hairpin loops. *Nature* **1989**, *342*, 825–829.(b) Sen, D.; Gilbert, W. A sodium-potassium switch in the formation of four-stranded G4-DNA. *Nature* **1990**, *344*, 410–414. (c) Kang, C.; Zhang, X.; Ratliff, R.; Moyzis, R.; Rich, A. Crystal structure of four-stranded Oxytricha telomeric DNA. *Nature* **1992**, *356*, 126–131.
21. Wang, Y.; Patel, D. J. Solution structure of the human telomeric repeat d[AG3(T2AG3)3] G-tetraplex. *Structure* **1993**, *1*, 263–282.
22. Parkinson, G. N.; Lee, M. P.; Neidle, S. Crystal structure of parallel quadruplexes from human telomeric DNA. *Nature* **2002**, *417*, 876–880.
23. (a) Xu, Y.; Noguchi, Y.; Sugiyama, H. The new models of the human telomere d[AGGG $(TTAGGG)_3$] in K^+ solution. *Bioorg. Med. Chem.* **2006**, *14*, 5584–5591.(b) Ambrus, A.; Chen, D.; Dai, J.; Bialis, T.; Jones, R. A.; Yang, D. Human telomeric sequence forms a hybrid-type intramolecular G-quadruplex structure with mixed parallel/antiparallel strands in potassium solution. *Nucleic Acids Res*. **2006**, *34*, 2723–2735. (c) Luu, K. N.; Phan, A. T.; Kuryavyi, V.; Lacroix, L.; Patel, D. J. Structure of the human telomere in K^+ solution: An intramolecular (3 + 1) G-quadruplex scaffold. *J. Am. Chem. Soc.* **2006**, *128*, 9963–9970.
24. Xu, Y.; Sugiyama, H. Highly efficient photochemical 2′-deoxyribonolactone formation at the diagonal loop of a 5-iodouracil-containing antiparallel G-quartet. *J. Am. Chem. Soc.* **2004**, *126*, 6274–6279.
25. (a) Murchie, A. I. H.; Lilley, D. M. Retinoblastoma susceptibility genes contain 5′ sequences with a high propensity to form guanine-tetrad structures. *Nucleic Acids Res.*

1992, *20*, 49–53.(b) Simonsson, T.; Pecinka, P.; Kubista, M. DNA tetraplex formation in the control region of c-myc. *Nucleic Acids Res.* **1998**, *26*, 1167–1172. (c) Siddiqui-Jain, A.; Grand, C. L.; Bearss, D. J.; Hurley, L. H. Direct evidence for a G-quadruplex in a promoter region and its targeting with a small molecule to repress c-MYC transcription. *Proc. Natl. Acad. Sci. USA.* **2002**, *99*, 11593–11598.

26. Xu, Y.; Sugiyama, H. Formation of the G-quadruplex and i-motif structures in retinoblastoma susceptibility genes (Rb). *Nucleic Acids Res.* **2006**, *34*, 949–954.
27. (a) Kelley, S. O.; Barton, J. K. Electron transfer between bases in double helical DNA. *Science* **1999**, *283*, 375–381. (b) Sancar, A. Structure and function of DNA photolyase and cryptochrome blue-light photoreceptors. *Chem. Rev.* **2003**, *103*, 2203–2237.
28. (a) Ito, T.; Rokita, S. E. Excess electron transfer from an internally conjugated aromatic amine to 5-bromo-2′-deoxyuridine in DNA. *J. Am. Chem. Soc.* **2003**, *125*, 11480–11481. (b) Lewis, F, D.; Wu, Y. Dynamics of superexchange photoinduced electron transfer in duplex DNA. *J. Photochem. Photobiol. Photochem. Rev.* **2001**, *2*, 1–16.
29. Rivera, E.; Schuler, R. H. Intermediates in the reduction of 5-halouracils by e_{aq}^{-1}. *J. Phys. Chem.* **1983**, *87*, 3966–3971.
30. Chen, T.; Cook, G. P.; Koppisch, T.; Greenberg, M. M. Investigation of the origin of the sequence selectivity for the 5-halo-2′-deoxyuridine sensitization of DNA to damage by UV-irradiation. *J. Am. Chem. Soc.* **2000**, *122*, 3861–3866.
31. Watanabe, T.; Bando, T.; Xu, Y.; Tashiro, R.; Sugiyama, H. Efficient generation of 2'-deoxyuridin-5-yl at 5′-(G/C)AA^{X}U^{X}U-3′ (X = Br, I) sequences in duplex DNA under UV irradiation. *J. Am. Chem. Soc.* **2005**, *127*, 44–45.
32. Watanabe, T.; Tashiro, R.; Sugiyama, H. Photoreaction at 5′-(G/C)AA^{Br}UT-3′ sequence in duplex DNA: Efficient generation of uracil-5-yl radical by charge transfer. *J. Am. Chem. Soc.* **2007**, *129*, 8163–8168.
33. Tashiro, R.; Sugiyama, H. Unique charge transfer properties of the four-base π-stacks in Z-DNA. *J. Am. Chem. Soc.* **2003**, *125*, 15282–15283.
34. (a) Kino, K.; Saito, I.; Sugiyama, H. Product snalysis of GG-specific photooxidation of DNA via electron transfer: 2-Aminoimidazolone as a major guanine oxidation product. *J. Am. Chem. Soc.* **1998**, *120*, 7373–7374.(b) Ikeda, H.; Saito, I. 8-Methoxydeoxyguanosine as an effective precursor of 2-aminoimidazolone, a major guanine oxidation product in one-electron oxidation of DNA. *J. Am. Chem. Soc.* **1999**, *121*, 10836–10837. (c) Kino, K.; Sugiyama, H. Possible cause of GC → CG transversion mutation by guanine oxidation product, 2-aminoimidazolone. *Chem. Biol.* **2001**, *8*, 369–378.
35. (a) Tashiro, R.; Sugiyama, H. A nanothermometer based on the different π stackings of B- and Z-DNA. *Angew. Chem. Int. Ed.* **2003**, *42*, 6018–6020. (b) Tashiro, R.; Sugiyama, H. Biomolecule-based switching devices that respond inversely to thermal stimuli. *J. Am. Chem. Soc.* **2005**, *127*, 2094–2097.
36. Cullis, P. M.; Jones, G. D. D.; Symons, M. C. R.; Lea, J. S. Electron transfer from protein to DNA in irradiated chromatin. *Nature* **1987**, *330*, 773–774.
37. (a) Boon, E. M.; Livingston, A. L.; Chimiel, N. H.; David, S. S.; Barton, J. K. DNA-mediated charge transport for DNA repair. *Proc. Natl. Acad. Sci. U.S.A.* **2003**, *100*, 12543–12547. (b) Yavin, E.; Boal, A. K.; Stemp, E. D.; Boon, E. M.; Livingston, A. L.; O'Shea, V. L.; David, S. S. Long-range electron transfer special feature: protein-DNA charge transport: Redox activation of a DNA repair protein by guanine radical. *Proc. Natl. Acad. Sci. U.S.A.* **2005**, *102*, 3546–3551.

38. Tashiro, R.; Wang, A. H.-J.; Sugiyama, H. Photoreactivation of DNA by an archaeal nucleoprotein Sso7d. *Proc. Natl. Acad. Sci. U.S.A.* **2006**, *103*, 16655–16659.

39. Tashiro, R.; Nakamura, K.; Sugiyama, H. Photoreaction of iodouracil in DNA duplex; C–I bond is cleaved via two different pathways ''Homolysis and Heterolysis.'' *Tetrahedron Lett*. **2008**, *49*, 428–431.

7

KINETICS OF LONG-RANGE OXIDATIVE ELECTRON TRANSFER THROUGH DNA

KIYOHIKO KAWAI AND TETSURO MAJIMA

The Institute of Scientific and Industrial Research (SANKEN), Osaka University, Ibaraki, Osaka 567–0047, Japan

7.1. INTRODUCTION

Double-helical DNA carries information controlling our heredity by means of linear sequence of its nucleotide, G, A, C, and T. The oxidation potential of nucleotides increases in the order of G: 1.47 < A: 1.96 < C ~ T: 2.1 (V versus NHE),[1] and thus G is the most subjective to one-electron oxidation.[2] As a consequence, one-electron oxidation of DNA leads to the formation of G radical cation ($G^{\bullet+}$), a hole, in DNA. Based on the gel electrophoresis strand cleavage experiments, it has been demonstrated that a hole can migrate through DNA over long distance (> 100 Å).[3–7] A model of a multistep hole transfer mechanism, in which G acts as charge carriers, is the most widely adopted to describe the long-range hole-transfer process. The kinetics of hole transfer process in DNA was first reported by Lewis et al.,[7] who determined the kinetics of single-step hole transfer between Gs across A–T base pair. We have established the method for the observation of long-range hole transfer through DNA and determined the rate constants of hole transfer through various sequence patterns.[8–10] Based on the determined rate constants, we can now estimate the hole transfer kinetics for a certain sequence and length of DNA. In other words, DNA can be considered to have additional information—that is, how fast a hole can migrate through it—and it would be possible to read out the sequence information of

Radical and Radical Ion Reactivity in Nucleic Acid Chemistry, Edited by Marc M. Greenberg

DNA by measuring the hole transfer kinetics. In this chapter, we will present an overview of our strategy for the measurements of long-range hole transfer kinetics through DNA and will summarize our efforts in reading out the stored information of DNA, especially the sequence information about single-nucleotide polymorphisms (SNPs), by measuring the hole transfer kinetics.[11]

7.2. DIRECT OBSERVATION OF LONG-RANGE OXIDATIVE ELECTRON TRANSFER

DNA is a versatile molecule that can be used to construct nanometer-sized higher-ordered assemblies and architectures based on the stored information.[12–15] In view of the potential use of DNA as a molecular wire for electrochemical biosensor and nanoelectronic devices, mechanistic studies of charge transfer in DNA have attracted considerable attention.[3–10, 16–52] Additionally, there has been much interest in understanding whether the charge transfer through DNA is relevant to biological consequences.[53–59]

The mechanism of the hole transfer process in DNA has been intensively studied both theoretically and experimentally. Hole transfer through DNA π-stack arrays has been mainly investigated by strand cleavage analysis using polyacrylamide gel electrophoresis strand cleavage experiments, which has provided information about the relative rates of hole migration against reaction of $G^{\bullet+}$ with water and/or molecular oxygen as a function of base sequence.[3–7] However, the gel electrophoresis technique is not suitable for the investigation of the kinetics and dynamics of hole transfer process through DNA.

Time-resolved measurements during the laser flash photolysis (LFP) are useful techniques to investigate the kinetics of charge transfer process in DNA. The kinetic study of single-step hole transfer in DNA was reported by Lewis et al.[7, 30–34] by means of time-resolved transient absorption measurements in which stilbene was used as a photosensitizer. They determined the hole transfer rate from G to GG across A–T base pair(s) by monitoring the decay of stilbene radical anion. By means of two-photon ionization of 2-aminopurine followed by monitoring the transient absorption of 2-aminopurine radical cation and $G^{\bullet+}$, Shafirovich et al.[28, 29] have investigated the distance dependence of single-step hole transfer from the radical cation of 2-aminopurine to G across variable numbers of AT base pairs. These methods were limited to the measurements of kinetics of the single-step or short-distance hole transfer in DNA. In this section, we present our strategy for the measurements of long-range hole transfer kinetics through DNA using LFP transient absorption measurement techniques.

7.2.1. Hole Injection

We used naphthalimide (NI) as a photosensitizer to inject a hole into DNA upon laser flash excitation.[8–10, 41–46] NI is likely to stack well with neighboring nucleobases because of its hydrophobicity and planar structure (Figure 7.1a). NI

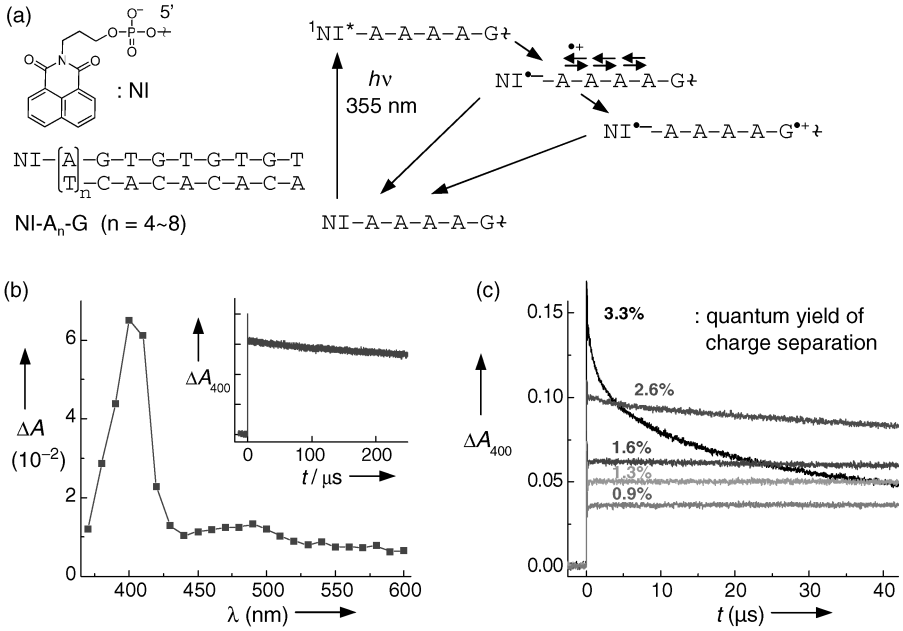

FIGURE 7.1. (**a**) Chemical structure of naphthalimide (NI) attached to the 5′-end of DNA, sequences of the NI-modified DNA, and the kinetic scheme for photoinduced one-electron oxidation of A, hole transfer through As, hole trapping at G, and charge recombination in DNA. (**b**) Transient absorption spectrum for NI–A_6–G, observed 200 ns after laser flash excitation (100 μM DNA in 20 mM Na phosphate buffer (pH 7.0) and 100 mM NaCl). **Inset**: Time profile monitored at 400 nm. (**c**) Decay profiles for NI–A_n–G ($n = 4$–8) monitored at 400 nm, following excitation of NI with a 355-nm laser pulse. (See color insert.)

shows an absorption peak at wavelength around 340 nm, and it can be selectively excited with a 355-nm laser pulse because DNA shows no absorption at wavelength longer than 310 nm. Photophysical properties of naphthalimide (NI) have been well-characterized by Kelly and co-workers. From the reduction potential of −1.01 V (versus NHE) and singlet-state energy of 3.4 eV for NI,[60,61] reduction potential of NI in the singlet excited state is calculated to be 2.4 eV (versus NHE), which means that NI in the singlet excited state can oxidize both G–C base pair and A–T base pair ($E_{ox} = 1.47$ and 1.96 V versus NHE for G and A, respectively[1]). Therefore, when NI was attached to A-stretch sequences, irradiation of the NI site with a 355-nm laser flash triggers the electron transfer between NI in the singlet excited state and adjacent A to give NI radical anion ($NI^{\bullet -}$) and A radical cation ($A^{\bullet +}$), respectively. Previously we have demonstrated that hole transfer between adjacent As proceeds with a rate constant of $>10^9\ s^{-1}$ and can compete with the charge recombination to produce a long-lived charge-separated state.[41] That is, a part of a hole escapes from the initial charge recombination process between $NI^{\bullet -}$ and $A^{\bullet +}$ via fast sequential hole transfer between As, and then the hole is trapped at G. Once G radical cation ($G^{\bullet +}$) is generated

far from $NI^{\bullet -}$, charge recombination proceeds mainly by a strongly distance-dependent super-exchange mechanism, thus forming a long-lived charge-separated state.

DNA conjugates, NI–A_n–G sequences, were designed to investigate the effect of the number of As on the charge separation process via hole transfer between As (Figure 7.1a).[9] Figure 7.1b shows the transient absorption spectrum observed at 200 ns for NI–A_6–G after the excitation of NI with a 355-nm laser pulse. A strong absorption around 400 nm and weak absorption around 500 nm were observed. These two absorption bands can be assigned to an NI radical anion ($NI^{\bullet -}$)[60, 61] and to $G^{\bullet +}$ or deprotonated $G^{\bullet +}$ ($G^{\bullet}(-H^{+})$),[2] respectively. This result clearly shows that the charge separation between NI and G occurred upon the excitation of NI within the laser pulse duration of 10 ns. The yields of formation of the charge-separated state, which was determined from the absorption of $NI^{\bullet -}$ observed after the excitation, decreased with increasing of the distance between NI and G, but weakly depended upon the distance; this was consistent with our previous report using naphthaldiimide as a photosensitizer[41] (Figure 7.1c). The weak distance dependence of the charge separation yields indicates that the charge separation process between NI and G occurred through sequential hole transfer processes between As. Except for NI–A_4–G sequence, the charge-separated state persisted for several hundred microseconds. Because NI is close to G in the case of the NI–A_4–G sequence, charge recombination between $NI^{\bullet -}$ and $G^{\bullet +}$ occurred in this time scale mainly through a super-exchange mechanism. These results clearly demonstrated that hole transfer between As is useful for rapid hole injection into DNA. In order to ensure the formation of the long-lived charge-separated state upon laser excitation, NI was attached to DNA via six consecutive A–T base pairs in the following sections.

7.2.2. Observation of Long-range Hole Transfer

Our approach for the time-resolved transient absorption measurements of the long-range hole transfer is schematically depicted in Figure 7.2.[8] NI was attached to the six consecutive A–T base pairs at one end of the duplex in order to inject a hole on G nearest to NI via fast hole transfer between As upon laser irradiation. Phenothiazine (PTZ), which has a lower oxidation potential than G (PTZ: $E_{ox} = 0.76$ V versus NHE[62, 63]), was attached at the other end of the duplex as a hole trap. PTZ is a suitable molecule for probing the hole transfer process in this system because the ground-state absorption of PTZ at wavelength shorter than 320 nm allows us to excite NI site selectively with 355-nm laser pulse. In addition, the PTZ radical cation ($PTZ^{\bullet +}$) shows a strong absorption around 520 nm and almost no spectral overlap with $NI^{\bullet -}$. Thus the kinetics hole transfer between Gs through the DNA can be measured by monitoring the formation of transient absorption of $PTZ^{\bullet +}$ at 520 nm.

Excitation of the NI site of $(GT)_4$ with a 355-nm laser resulted in the immediate formation of NI radical anion ($NI^{\bullet -}$) with a peak at 400 nm and $G^{\bullet +}$ or $G^{\bullet}(-H^{+})$ with a broad absorption around 500 nm (Figure 7.3). Then, a transient absorption spectrum with a peak at 520 nm, assigned to $PTZ^{\bullet +}$, emerged in the several-microsecond time scale, which corresponded to the hole transfer through DNA to the PTZ site. Time profiles of the transient absorption of $PTZ^{\bullet +}$ monitored at 520 nm for $(GT)_n$

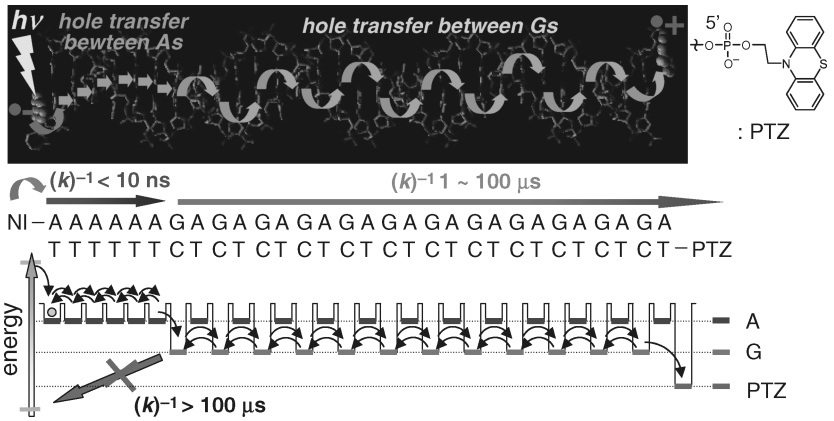

FIGURE 7.2. Strategy for the kinetic study of long-distance hole transfer process. Molecular representation for 30-mer DNA conjugated with naphthalimide (NI) and phenothiazine (PTZ), which work as a photosensitizer and hole acceptor, respectively, and schematic illustration for hole injection via hole transfer between As and long-distance hole transfer process via hole transfer between G through DNA. (See color insert.)

and $(GA)_n$ sequences are shown in Figures 7.4a and 7.4b, respectively. With increasing number of GA and GT repeats, the formation rate of $PTZ^{\bullet+}$ for these sequences slightly decreased. Assuming an average distance of 3.4 Å between base pairs, total distance reaches 100 Å for $n = 12$ for both $(GA)_n$ and $(GT)_n$ sequences. Namely, these results clearly show the direct observation of long-distance hole transfer over 100 Å.

Apparent hole-transfer rate constants (k_a) for $(GT)_n$ and $(GA)_n$ sequences were obtained by single exponential fits of the formation of $PTZ^{\bullet+}$. Though it may be

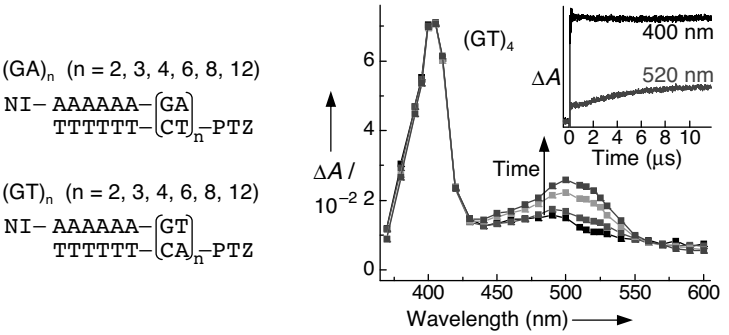

FIGURE 7.3. Transient absorption spectra observed at 200 ns (black), 2 (red), 5 (green), and 10 μs (blue) after a 355-nm laser flash (4 ns, 20 mJ $pulse^{-1}$) with excitation of the NI site during the laser flash photolysis of NI- and PTZ-modified DNA $(GT)_4$. **Inset**: Time profiles observed at 400 (black) and 520 nm (blue) assigned to the transient absorption peak for $NI^{\bullet-}$ and $PTZ^{\bullet+}$, respectively. Sample solution contained 100 μM duplex DNA, 20 mM Na phosphate buffer (pH 7.0), and 100 mM NaCl. (See color insert.)

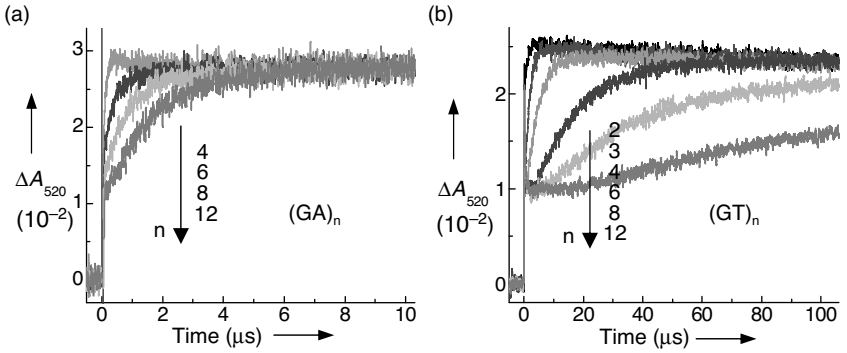

FIGURE 7.4. Time profiles of the transient absorption monitored at 520 nm assigned to $PTZ^{\bullet+}$ after the 355-nm laser flash excitation for (**a**) $(GA)_n$ and (**b**) $(GT)_n$ sequences. Sample solution contained 100 μM duplex DNA, 20 mM Na phosphate buffer (pH 7.0), and 100 mM NaCl. (See color insert.)

inappropriate to analyze the data with single-exponential fitting because long-range hole transfer occurs through multistep processes, simple analysis based on single-exponential fitting was applied to approximately evaluate the observed long-range hole-transfer process. If the hole transfer from $G^{\bullet+}$ nearest NI to PTZ occurs by random walk process via multistep hole transfer processes between Gs, the observed rate constant k_a follows Eq. (7.1):

$$k_a = k_0 N^{-\eta} \tag{7.1}$$

where k_0 is the rate constant of the single-step hole transfer between Gs, N is a hopping number, and η is a proportional factor that takes the value of 2 in the ideal case of random walk process. Plots of ln k_{ht} versus ln N are shown in Figure 7.5.[21, 64–66] The η value of 2.0 ± 0.1 for both $(GT)_n$ and $(GA)_n$ sequences obtained from the slopes was nearly the

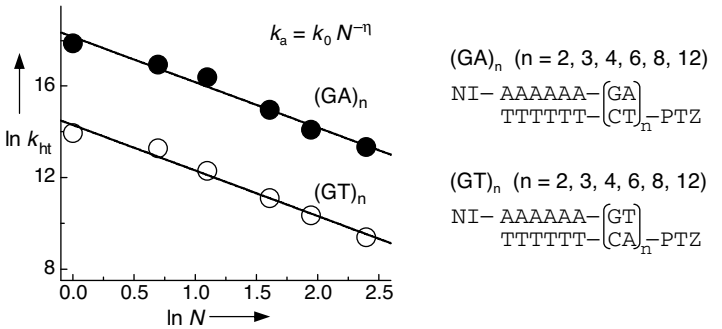

FIGURE 7.5. Plots of ln k_{ht} versus ln N for $(GA)_n$ (filled circle) and $(GT)_n$ (open circle) sequences. Apparent rate constants of hole transfer (k_{ht}) were obtained with a single exponential fit of the time profiles of the formation of $PTZ^{\bullet+}$ monitored at 520 nm, and N corresponds to the hopping number.

same as the ideal value, providing the kinetic evidence that the long-distance hole transfer occurs though the multistep hole transfer process between Gs.

7.3. SEQUENCE DEPENDENCE OF OXIDATIVE ELECTRON TRANSFER

Consistent with the gel electrophoresis strand cleavage experiments, the long-range hole transfer process through DNA was demonstrated spectroscopically to proceed via a sequential hole transfer process between Gs as presented in the previous section.[8] Thus, it would be possible to describe the kinetics of long-range hole transfer through DNA based on the rate constants of each hole transfer process between Gs. Accordingly, given a certain sequence and length of DNA, a unique hole transfer kinetic would be obtained. In other words, it might be possible to read out the sequence information of DNA by measuring the rate constants of hole transfer though DNA. In this section, we present the measurement of the rate constants of hole transfer between Gs (k_{ht}) through various intervening base pairs and discuss the factors that determine the hole transfer rate between Gs.

7.3.1. Intervening Sequences Between Gs

The sequences used for the determination of the k_{ht} are schematically shown in Figure 7.6.[9] Time profiles of the transient absorption of $PTZ^{\bullet+}$ after the flash excitation of NI was monitored. The formation profiles of $PTZ^{\bullet+}$ corresponds to the hole transfer from G nearest to NI to PTZ and includes several kinds of hole

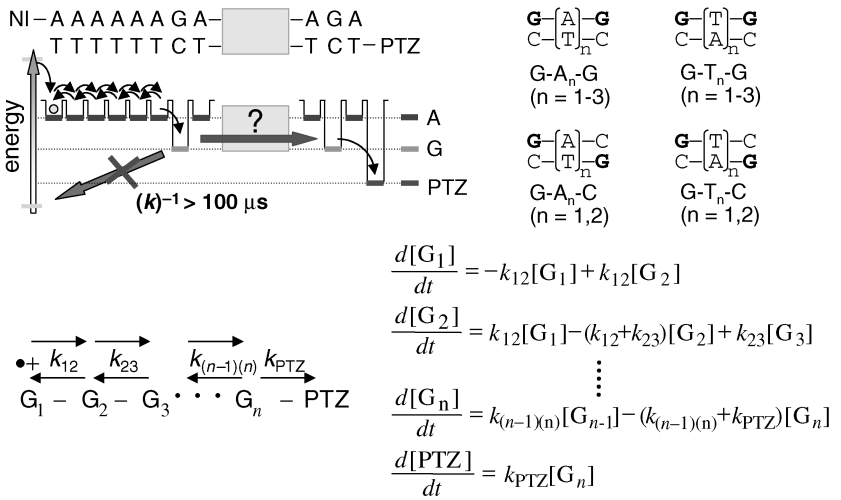

FIGURE 7.6. Schematic representation, kinetic model, and simultaneous differential equations for hole transfer process through DNA of various sequence patterns. (See color insert.)

transfer steps. Therefore, rate constants of the single-step hole transfer between Gs (k_{ht}) through various intervening base pairs were determined from the kinetic modeling. The example of kinetic modeling and the simultaneous differential equations are shown in Figure 7.6. All the hole transfer rates measured in this section were summarized in Table 7.1. The k_{ht} increased in the order G–A–G > G–T–C, G–A–C > G–T–G. It is known that the energy gap between the donor and bridge states affects the electronic coupling—that is, the electron transfer rate in the donor–bridge–acceptor system.[67] Considering that the ionization potential of A (A: $E_{ox} = 1.96$ V versus NHE[1]) is lower than that of T (T: $E_{ox} = 2.1$ V versus

TABLE 7.1. Rate Constants (k_{ht}) for Hole Transfer through DNAs

		k_{ht} [s^{-1}]
•+ –G–A–G– –C–T–C–	k_{GAG}	4.8×10^7
•+ –G–A–A–G– –C–T–T–C–	k_{GAAG}	9.7×10^4
•+ –G–A–A–A–G– –C–T–T–T–C–	k_{GAAAG}	1.4×10^4
•+ –G–T–G– –C–A–C–	k_{GTG}	4.6×10^5
•+ –G–T–T–G– –C–A–A–C–	k_{GTTG}	3.6×10^4
•+ –G–T–T–T–G– –C–A–A–A–C–	k_{GTTTG}	9.1×10^3
•+ –G–A–C– –C–T–G–	k_{GAC}	1.4×10^6
•+ –G–A–A–C– –C–T–T–G–	k_{GAAC}	4.5×10^4
•+ –G–T–C– –C–A–G–	k_{GTC}	1.6×10^6
•+ –G–T–T–C– –C–A–A–G–	k_{GTTC}	3.1×10^4
•+ –G–C–G– –C–G–C–	k_{GC}	2.2×10^8

NHE[1]), the hole transfer for G–A–G sequence is expected to be faster than that for G–T–G sequence. In addition, the π-stacking between the base pairs is considered to be of crucial importance in the charge transfer processes through DNA. Thus, the hole transfer rate through the two-ring purine A is expected to be faster than that through single-ring pyrimidine T. Our results are in good agreement with the prediction, and similar results were reported in other photoinduced electron transfer system.[32] The hole transfer rate through G–T–C and G–A–C sequences in which one G is stacked with A and the other G is stacked with T showed intermediate values between G–A–G and G–T–G sequences. It is noteworthy that hole transfer between Gs occurs in an interstrand fashion as well as in an intrastrand fashion.

7.3.2. Distance Between Gs

Distance dependence of hole transfer is conventionally evaluated by Eq. (7.2):

$$k_{\mathrm{ht}} = k_0 \exp(-\beta r) \tag{7.2}$$

where k_0 is the preexponential factor, β is the attenuation factor of k_{ht}, and r is the distance between hole donor and acceptor (here the distance between Gs). Time profiles of $PTZ^{\bullet+}$ monitored at 520 nm for G–A_n–G (n = 1–3) are shown in Figure 7.7a. Apparently, the formation rate constant decreased with increasing of the distance between Gs, demonstrating that each hole transfer process between Gs proceeds by a super-exchange mechanism. Plots of ln k_{ht} versus r for G–A_n–G and G–T_n–G provide the β value (Figure 7.7b). Interestingly, a considerable decrease of ln k_{ht} from $n = 1$ to $n = 2$ ($\beta = 1.8\ \text{Å}^{-1}$) and a slight decrease from $n = 2$ to $n = 3$ ($\beta = 0.6\ \text{Å}^{-1}$) were found for G–$A_n$–G, whereas a linear relationship was obtained for G–T_n–G sequence ($\beta = 0.6\ \text{Å}^{-1}$). The slope of the plot for $n = 2$–3 of G–A_n–G ($\beta = 0.6\ \text{Å}^{-1}$) was almost the same as that of G–T_n–G. The β value of $0.6\ \text{Å}^{-1}$ is

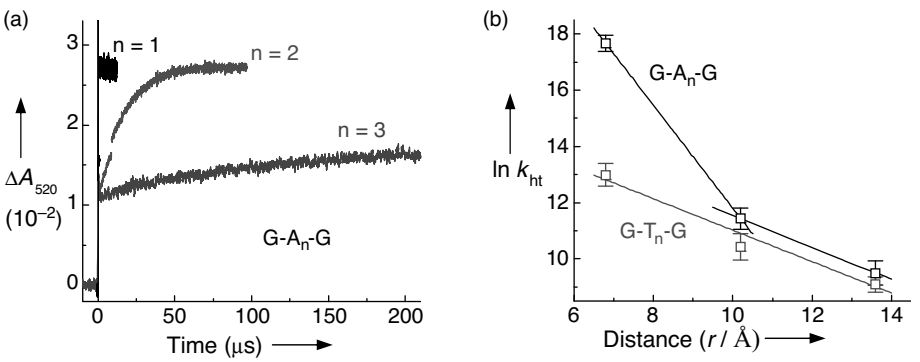

FIGURE 7.7. (**a**) Time profiles of the transient absorption of $PTZ^{\bullet+}$ monitored at 520 nm for G–A_n–G ($n = 1$–3). (**b**) Plots of logarithm of the hole transfer rate versus distance between Gs (r) for G–A_n–G (black) and G–T_n–G (red). (See color insert.)

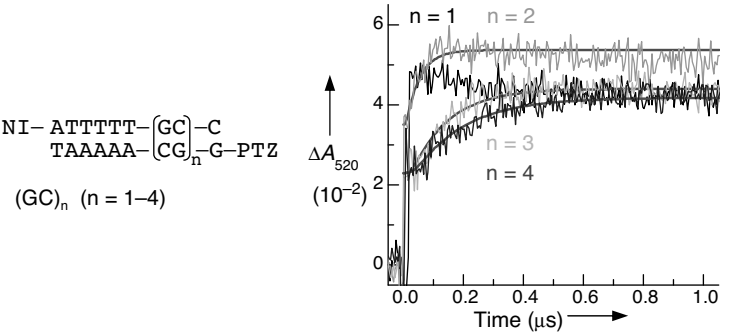

FIGURE 7.8. Sequences and time profiles of the transient absorption of $PTZ^{\bullet+}$ monitored at 520 nm during the 355-nm laser flash photolysis of an Ar-saturated solution of NI- and PTZ-modified DNAs with GC repeat sequences. (See color insert.)

consistent with the β values previously reported for single-step charge transfer in DNA.[39, 68, 69] Thus, the mechanism of hole transfer might be different for G–A–G compared with other sequences resulting in an especially faster kinetic than expected.

7.3.3. GC Repeat Sequences

The k_{ht} was also measured for GC repeat sequence in which G–C base pair are adjacent to each other.[10] The sequences used for the determination of the k_{ht} through GC repeat sequence are shown in Figure 7.8. Interestingly, the hole transfer through GC repeat sequence proceeded much faster compared with sequences having intervening A–T base pair between Gs, and in the case of the shortest sequence (GC)-3 the hole moved faster than the time resolution of our experimental setup. The formation rate of $PTZ^{\bullet+}$ decreased with increasing number of GC repeats, and a kinetic analysis for (GC)-*n* ($n = 5, 7, 9$) provided a k_{ht} value of $2.2 \times 10^8\,s^{-1}$ for hole transfer rate through GC repeat sequence.

Xu et al.[49] reported the conductance for GC repeat sequences by using direct electrical measurements where the conductance is inversely proportional to the length. On the other hand, the conductance decreases exponentially with a decay constant of $0.43\,\text{Å}^{-1}$ by inserting A–T base pairs into GC repeat domains. Our results are consistent with the conductance measurements reported by Xu et al. showing that a hole is mainly carried by G having the lowest HOMO among the four nucleobases and that the hole transfer rate between Gs strongly depends on the distance or the number of intervening A–T base pair between Gs.

7.4. KINETIC SNP DISCRIMINATION BASED ON OXIDATIVE ELECTRON TRANSFER

Single-nucleotide polymorphisms (SNPs) are single nucleotide differences in a gene.[70, 71] A single Watson–Crick base pair in the wild-type DNA is replaced by

the other base pair in the SNP mutant DNA. The SNPs of a gene are related to the risks of various diseases and differences in drug responses. Consequently, detecting the SNPs in a gene has become more important from a clinical point of view.[72,73] Although several enzyme-coupled SNP typing methods based on the high fidelity of DNA polymerase have been reported, a new conceptual method is required for the new solution in SNP typing[74] due to the difficulty in discriminating the small difference in the sequence between the wild-type and SNP mutant DNAs. Thus, several techniques for SNP genotyping on the chemical basis have been reported.[74,75] Chemical SNP typing methods usually employ allele-specific oligonucleotides that hybridize to the target SNP sequence. Hybridization of the oligonucleotides results in a full matched duplex formation for the wild-type target, whereas the mismatched duplex forms for the SNP mutant target. Utilizing the mismatched DNA duplex formation like this, several DNA mismatch detection methods have been developed.[76] Most of the reported methods so far rely on the hybridization assay based on the difference in the thermal stability between the full matched DNA and corresponding mismatched DNA. However, those methods could not be applied to the long DNA molecules because it is difficult to distinguish a difference in the thermostability induced by a single-base mismatch embedded in the thermostable long DNA duplex.[74]

Since the π-stacking between the base pairs is considered to be crucially important in the charge transfer processes through DNA, it was suggested that once the π-stacking of the DNA bases is perturbed by the presence of a mismatch, the efficiency of charge transfer through DNA would be significantly decreased. Therefore, measurements of long-range hole transfer rates through DNA may offer a unique approach for the detection of a single-base mismatch, especially effective in a long DNA molecule. The mechanisms of hole transfer through DNA containing a mismatch have been examined by experimental and theoretical studies. Indeed, based on gel electrophoresis experiments, Giese and co-workers demonstrated that the presence of a mismatched G decreases the hole transfer efficiency.[25,26] Schuster and co-workers reported that the hole transfer efficiency across TT tandem mismatches is decreased, while the hole transfer efficiency is not altered across the AA tandem mismatches.[37]

Depending on the charge transport through the π-stack of the DNA duplex, electrochemical detection of the mismatched DNA, which enables SNP discrimination, has been demonstrated.[77,78] Kelley et al.[77] developed a strategy for the electrochemical detection of a single-base mismatch based on charge transport through the DNA films.[77] They reported that the signal obtained from the redox-active intercalators bound to DNA modified on gold faces exhibits a remarkable sensitivity to the presence of a mismatched DNA base within the immobilized duplex. Recently, Okamoto et al.[78] developed a new SNP photoelectrochemical detection method that relied on the photoinduced hole transfer in a DNA duplex immobilized on a gold electrode. They designed the DNA probes that contain anthraquinone as a photosensitizer that was hybridized with the target DNA. They reported that the cathodic photocurrent signal markedly changes, depending on the presence of a mismatch. Thus, the charge transfer process provides a method for a mismatch detection or an SNP discrimination. However, these electrochemical detections access the relative values of the electrode response that may be significantly affected by the

experimental conditions. Thus, it is desired to develop a new method for distinguishing the mismatched sequence from the fully matched sequence based on the absolute values.

As described in the previous sections, we can now estimate the unique hole transfer rate through DNA of a certain sequence and length. By further elucidating the kinetics through mismatched sequences, it may be possible to transform the information about a DNA mismatched sequence into an absolute value of rate constant. In this section, we describe the kinetic SNP discrimination approach based on the measurements of the kinetics of the hole transfer through mismatched DNA.

7.4.1. Sequence Design

The DNA sequences used for the measurements of the hole transfer rates through mismatches are given in Figure 7.9.[11] The 12- or 13-base-pair assembly contains the following three parts: the charge injection part (photosensitizer NI and consecutive adenine sequence), the charge detection part (GC repeats and PTZ), and bridge parts with two Gs separated by one or two bases. Eighteen assemblies were prepared.

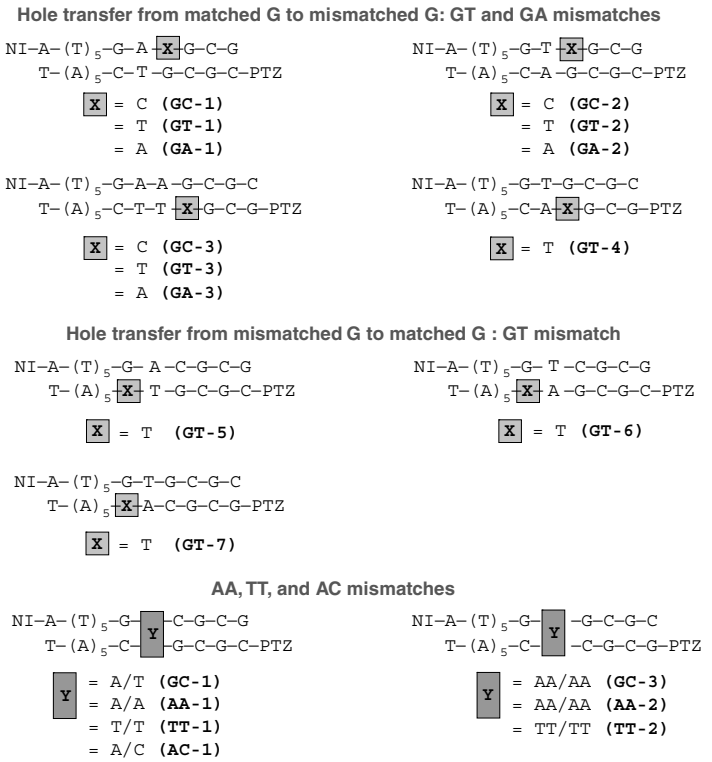

FIGURE 7.9. Sequences of NI- and PTZ-modified DNA used for the investigation of hole transfer through mismatched sequences. (See color insert.)

They were classified into three groups: hole transfer from matched G to mismatched G (GT and GA mismatches), hole transfer from mismatched G to matched G (GT mismatch), and hole transfer through AA, TT, and AC mismatches (Figure 7.9).

7.4.2. GT and GA Mismatches

The formation of the absorption of $PTZ^{\bullet+}$ monitored at 520 nm for the fully matched sequences, GC-1,GC-2, and GC-3, was in good agreement with the results of the kinetic modeling using the hole transfer rates between the fully matched Gs reported in the previous section.[9, 10] The kinetics of the hole transfer between Gs is slowed by the introduction of a GT or GA mismatch. Employing the kinetic modeling based on the assumption that the back hole transfer from the mismatched G to G through the intervening AT base pairs is slow compared to the rapid hole transfer through the GC repeats, we determined the rate constants of the hole transfer from G to the mismatched G (Table 7.2). The k_{ht} is slowed by about an order of magnitude by the GT or GA mismatch (Table 7.2). It is noteworthy that a 2.7-fold difference in k_{ht} between GT-1 and GT-2 was observed, which is caused by the inversion of the AT base pair to the TA base pair between matched G and GT mismatch. Similar to the GT mismatch, a change in the intervening base pair between Gs also results in a 1.7-fold difference in k_{ht} for the GA mismatch. The hole transfer from the mismatched G to the matched G across the AT or TA sequence was also examined (GT-5 and GT-6). Interestingly, the hole transfer rate constants from the mismatched G to a matched G is four- to five-fold faster than those in the fully matched sequences (GC-1 and GC-2). Comparing the GT-5 and GT-6, a 1.3-fold difference in the hole transfer rate was observed, resulting from a change in the intervening base pair between Gs, consistent with the kinetics from the matched G to mismatched G. Taken together, these results indicate that the hole transfer from matched G to the mismatched G is slower than that for fully matched assembly, while the hole transfer from the mismatched G to matched G is faster than that for fully matched assembly.

7.4.3. AA, TT, and AC Mismatches

The hole transfer rates between Gs across AA, TT, and AC mismatch were also measured. Interestingly, replacement of an AT base pair with TT or AC mismatch slowed the hole transfer kinetics, while hole transfer rate between the Gs across AA mismatch is similar to or rather faster than those across fully matched sequences (Table 7.2). As mentioned in the previous section, Lewis et al.[67] demonstrated that the hole transfer kinetics between the Gs depends on the intervening bridge base between the Gs, and the lower oxidation potential bases produce a small tunneling energy gap and increase the hole transfer rate. The AA mismatches, which have a lower oxidation potential and a higher stacking ability than T,[1] producing smaller tunneling energy gaps, may lead to the increase of the hole transfer rate. On the other hand, the TT mismatch, which has a higher oxidation potential and a lower stacking ability producing higher tunneling energy gaps than A, may lead to the suppression of the hole transfer rate.[67]

TABLE 7.2. Rate Constants (k_{ht}) for Hole Transfer through Mismatched DNAs

		k_{ht} [s^{-1}]
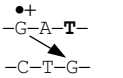	$k_{GT\text{-}1}$	7.1×10^4
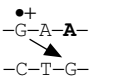	$k_{GA\text{-}1}$	9.2×10^4
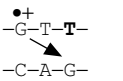	$k_{GT\text{-}2}$	1.9×10^5
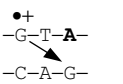	$k_{GA\text{-}2}$	1.6×10^5
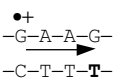	$k_{GT\text{-}3}$	1.0×10^4
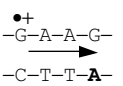	$k_{GA\text{-}3}$	9.5×10^3
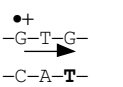	$k_{GT\text{-}4}$	5.0×10^5
	$k_{GT\text{-}5}$	5.2×10^6
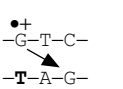	$k_{GT\text{-}6}$	6.9×10^6
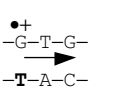	$k_{GT\text{-}7}$	8.2×10^6
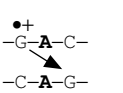	$k_{AA\text{-}1}$	9.7×10^5
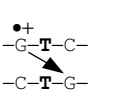	$k_{TT\text{-}1}$	1.6×10^5
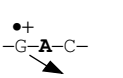	$k_{AC\text{-}1}$	1.3×10^5
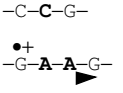	$k_{AA\text{-}2}$	1.3×10^5
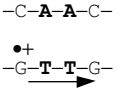	$k_{TT\text{-}2}$	2.7×10^4

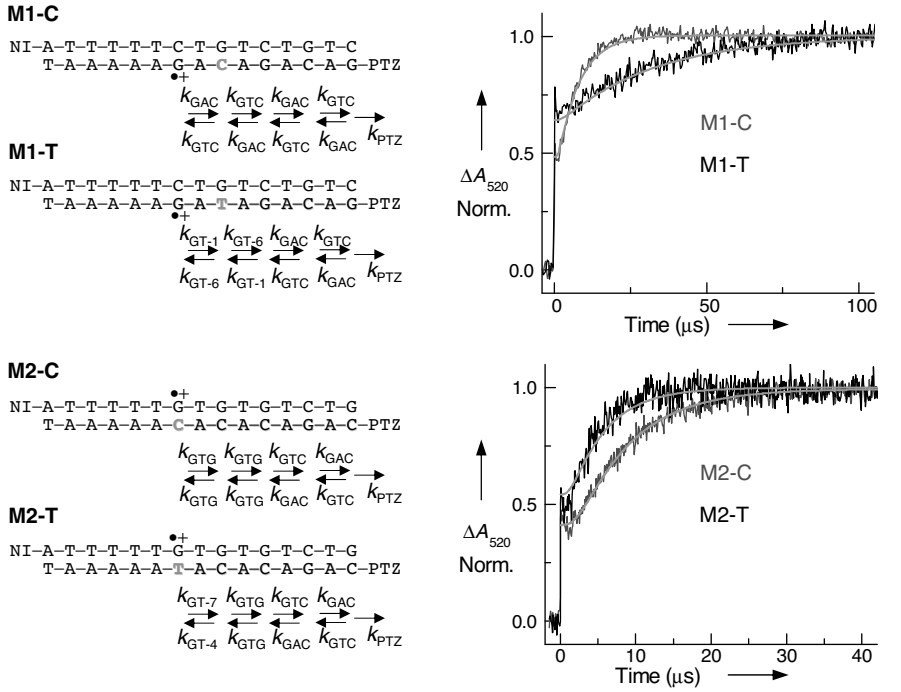

FIGURE 7.10. Discrimination of mismatch DNA related to SNP by hole transfer kinetics through DNAs. Bold letters shown in blue indicate the SNP sequences. Time profiles of the transient absorption of $PTZ^{\bullet+}$ at 520 nm during the 355-nm laser flash photolysis of Ar-saturated aqueous solution containing 100 mM NaCl and 20 mM sodium phosphate (pH 7.0) at a strand concentration of 50 μM. The green smooth curves superimposed on the curves are the fit derived from the kinetic model using the hole transfer rates depicted in Tables 7.1 and 7.2. (See color insert.)

7.4.4. Kinetic SNP Typing

For the kinetic discrimination of SNPs, we investigated whether the information about the SNP sequences can be transformed into the absolute values of hole transfer rate constants. The sequences used in this study are shown in Figure 7.10. DNAs modified with NI and PTZ at the 5′ end which have an A consecutive sequence and a part of the coding sequences for the nuclear LIM interactor-interacting factor 2 and DNA-binding domain T-box 22, carrying SNP rs12392145 (M1) and rs1965744 (M2) C to T substitution, were employed in this study. These SNPs were chosen as a model for the kinetic SNP discrimination because we can carry out the kinetic modeling using the rate constants determined in this chapter. First, the time-resolved transient absorption measurement and kinetic modeling of M1-C and M1-T were performed. Of special interest, the decreased hole transfer kinetics were observed for the M1-T with a mismatch, in agreement with the kinetic modeling. We then examined M2-C and M2-T using the transient absorption method and kinetic

modeling. Interestingly, the hole transfer rate constants for the M2-T with a mismatch was higher compared to that of fully matched M2-C, consistent with the kinetic modeling. These results demonstrate that it is possible to discriminate SNP sequences based on the absolute values of hole transfer rate constants.[11]

7.5. CONCLUSIONS

In this chapter, we described our approach for the measurements of the rate constants of long-range hole transfer through DNA. Time-resolved transient absorption measurements unequivocally demonstrated that long-range hole transfer through DNA proceeds via a series of short-range, hole transfer processes between Gs. The hole transfer rate constants for various sequence patterns were determined, and it became possible to estimate how fast a hole migrate along DNA of a certain sequence and length based on these rate constants. In view of discriminating the SNPs based on the hole transfer rate constants, we also extended our work for mismatched DNA. It was demonstrated that the information about a DNA mismatched sequence can be transformed into an absolute value of rate constant that allows the discrimination of the SNPs. Further improvement in the quantum yield of the charge injection and the hole detection method may open the door to the readout of the sequence information of DNA by measuring the rate constants of hole transfer through DNA.

ACKNOWLEDGMENTS

We are deeply indebted to Dr. Tadao Takada, Miss Yasuko Osakada, and Dr. Mamoru Fujitsuka for their contributions to these studies. This work has been partly supported by a Grant-in-Aid for Scientific Research (Project 17105005, 18750148, and others) from MEXT of Japanese Government.

REFERENCES

1. Seidel, C. A. M.; Schulz, A.; Sauer, M. H. M. Nucleobase-specific quenching of fluorescent dyes. 1. Nucleobase one-electron redox potentials and their correlation with static and dynamic quenching efficiencies. *J. Phys. Chem.* **1996**, *100*, 5541–5553.
2. Steenken, S.; Jovanovic, S. V. How easily oxidizable is DNA? One-electron reduction potentials of adenosine and guanosine radicals in aqueous solution. *J. Am. Chem. Soc.* **1997**, *119*, 617–618.
3. Meggers, E.; Michel-Beyerle, M. E.; Giese, B. Sequence dependent long range hole transport in DNA. *J. Am. Chem. Soc.* **1998**, *120*, 12950–12955.
4. Henderson, P. T.; Jones, D.; Hampikian, G.; Kan, Y. Z.; Schuster, G. B. Long-distance charge transport in duplex DNA: The phonon-assisted polaron-like hopping mechanism. *Proc. Natl. Acad. Sci. U.S.A.* **1999**, *96*, 8353–8358.
5. Nunez, M. E.; Hall, D. B.; Barton, J. K. Long-range oxidative damage to DNA: Effects of distance and sequence. *Chem. Biol.* **1999**, *6*, 85–97.

6. Nakatani, K.; Dohno, C.; Saito, I. Chemistry of sequence-dependent remote guanine oxidation: Photoreaction of duplex DNA containing cyanobenzophenone-substituted uridine. *J. Am. Chem. Soc.* **1999**, *121*, 10854–10855.
7. Lewis, F. D.; Liu, X. Y.; Liu, J. Q.; Miller, S. E.; Hayes, R. T.; Wasielewski, M. R. Direct measurement of hole transport dynamics in DNA. *Nature* **2000**, *406*, 51–53.
8. Takada, T.; Kawai, K.; Fujitsuka, M.; Majima, T. Direct observation of hole transfer through double-helical DNA over 100 Å. *Proc. Natl. Acad. Sci. U.S.A.* **2004**, *101*, 14002–14006.
9. Takada, T.; Kawai, K.; Fujitsuka, M.; Majima, T. Contributions of the distance-dependent reorganization energy and proton-transfer to the hole-transfer process in DNA. *Chem. Eur. J.* **2005**, *11*, 3835–3842.
10. Osakada, Y.; Kawai, K.; Fujitsuka, M.; Majima, T. Charge transfer through DNA nanoscaled assembly programmable with DNA building blocks. *Proc. Natl. Acad. Sci. U.S.A.* **2006**, *103*, 18072–18076.
11. Osakada, Y.; Kawai, K.; Fujitsuka, M.; Majima, T. Kinetics of charge transfer in DNA containing a mismatch. *Nucleic Acids Res.* **2008**, *36*, 5562–5570.
12. Rothemund, P. W. K. Folding DNA to create nanoscale shapes and patterns. *Nature* **2006**, *440*, 297–302.
13. Tanaka, K.; Clever, G. H.; Takezawa, Y.; Yamada, Y.; Kaul, C.; Shionoya, M.; Carell, T. Programmable self-assembly of metal ions inside artificial DNA duplexes. *Nat. Nanotech.* **2006**, *1*, 190–194.
14. Storhoff, J. J.; Mirkin, C. A. Programmed materials synthesis with DNA. *Chem. Rev.* **1999**, *99*, 1849–1862.
15. Shih, W. M.; Quispe, J. D.; Joyce, G. F. A 1.7-kilobase single-stranded DNA that folds into a nanoscale octahedron. *Nature* **2004**, *427*, 618–621.
16. Nakatani, K.; Dohno, C.; Saito, I. Modulation of DNA-mediated hole-transport efficiency by changing superexchange electronic interaction. *J. Am. Chem. Soc.* **2000**, *122*, 5893–5894.
17. Nakatani, K.; Dohno, C.; Saito, I. Design of a hole-trapping nucleobase: Termination of DNA-mediated hole transport at N-2-cyclopropyldeoxyguanosine. *J. Am. Chem. Soc.* **2001**, *123*, 9681–9682.
18. Dohno, C.; Nakatani, K.; Saito, I. Guanine of the third strand of C.GG triplex serves as an effective hole trap. *J. Am. Chem. Soc.* **2002**, *124*, 14580–14585.
19. Dohno, C.; Ogawa, A.; Nakatani, K.; Saito, I. Hole trapping at N6-cyclopropyldeoxyadenosine suggests a direct contribution of adenine bases to hole transport through DNA. *J. Am. Chem. Soc.* **2003**, *125*, 10154–10155.
20. Bixon, M.; Jortner, J. Charge transport in DNA via thermally induced hopping. *J. Am. Chem. Soc.* **2001**, *123*, 12556–12567.
21. Jortner, J.; Bixon, M.; Langenbacher, T.; Michel-Beyerle, M. E. Charge transfer and transport in DNA. *Proc. Natl. Acad. Sci. U.S.A.* **1998**, *95*, 12759–12765.
22. Conwell, E. M.; Rakhmanova, S. V. Polarons in DNA. *Proc. Natl. Acad. Sci. U.S.A.* **2000**, *97*, 4556–4560.
23. Conwell, E. M.; Bloch, S. M.; McLaughlin, P. M.; Basko, D. M. Duplex polarons in DNA. *J. Am. Chem. Soc.* **2007**, *129*, 9175–9181.
24. Candeias, L. P.; Steenken, S. Structure and acid–base properties of one-electron-oxidized deoxyguanosine, guanosine, and 1-methylguanosine. *J. Am. Chem. Soc.* **1989**, *111*, 1094–1099.

25. Giese, B.; Wessely, S. The influence of mismatches on long-distance charge transport through DNA. *Angew. Chem., Int. Ed. Engl.* **2000**, *39*, 3490–3491.
26. Giese, B.; Wessely, S. The significance of proton migration during hole hopping through DNA. *Chem. Commun.* **2001**, 2108–2109.
27. Giese, B.; Amaudrut, J.; Kohler, A. K.; Spormann, M.; Wessely, S. Direct observation of hole transfer through DNA by hopping between adenine bases and by tunnelling. *Nature* **2001**, *412*, 318–320.
28. Shafirovich, V.; Dourandin, A.; Geacintov, N. E. Proton-coupled electron-transfer reactions at a distance in DNA duplexes: Kinetic deuterium isotope effect. *J. Phys. Chem. B* **2001**, *105*, 8431–8435.
29. Shafirovich, V.; Cadet, J.; Gasparutto, D.; Dourandin, A.; Huang, W. D.; Geacintov, N. E. Direct spectroscopic observation of 8-oxo-7,8-dihydro-2′-deoxyguanosine radicals in double-stranded DNA generated by one-electron oxidation at a distance by 2-aminopurine radicals. *J. Phys. Chem. B* **2001**, *105*, 586–592.
30. Lewis, F. D.; Liu, X. Y.; Liu, J. Q.; Hayes, R. T.; Wasielewski, M. R. Dynamics and equilibria for oxidation of G, GG, and GGG sequences in DNA hairpins. *J. Am. Chem. Soc.* **2000**, *122*, 12037–12038.
31. Lewis, F. D.; Kalgutkar, R. S.; Wu, Y. S.; Liu, X. Y.; Liu, J. Q.; Hayes, R. T.; Miller, S. E.; Wasielewski, M. R. Driving force dependence of electron transfer dynamics in synthetic DNA hairpins. *J. Am. Chem. Soc.* **2000**, *122*, 12346–12351.
32. Lewis, F. D.; Liu, J.; Zuo, X.; Hayes, R. T.; Wasielewski, M. R. Dynamics and energetics of single-step hole transport in DNA hairpins. *J. Am. Chem. Soc.* **2003**, *125*, 4850–4861.
33. Lewis, F. D.; Zhu, H.; Daublain, P.; Cohen, B.; Wasielewski, M. R. Hole mobility in DNA a tracts. *Angew. Chem., Int. Ed.* **2006**, *45*, 7982–7985.
34. Lewis, F. D.; Zhu, H.; Daublain, P.; Fiebig, T.; Raytchev, M.; Wang, Q.; Shafirovich, V. Crossover from superexchange to hopping as the mechanism for photoinduced charge transfer in DNA hairpin conjugates. *J. Am. Chem. Soc.* **2006**, *128*, 791–800.
35. Barnett, R. N.; Cleveland, C. L.; Joy, A.; Landman, U.; Schuster, G. B. Charge migration in DNA: Ion-gated transport. *Science* **2001**, *294*, 567–571.
36. Sanii, L.; Schuster, G. B. Long-distance charge transport in DNA: Sequence-dependent radical cation injection efficiency. *J. Am. Chem. Soc.* **2000**, *122*, 11545–11546.
37. Schlientz, N. W.; Schuster, G. B. Long-distance radical cation migration in duplex DNA: The effect of contiguous A.A and T.T mismatches on efficiency and mechanism. *J. Am. Chem. Soc.* **2003**, *125*, 15732–15733.
38. Okamoto, A.; Tanaka, K.; Saito, I. Rational design of a DNA wire possessing an extremely high hole transport ability. *J. Am. Chem. Soc.* **2003**, *125*, 5066–5071.
39. Kawai, K.; Takada, T.; Tojo, S.; Ichinose, N.; Majima, T. Observation of hole transfer through DNA by monitoring the transient absorption of pyrene radical cation. *J. Am. Chem. Soc.* **2001**, *123*, 12688–12689.
40. Kawai, K.; Takada, T.; Tojo, S.; Majima, T. Kinetics of weak distance-dependent hole transfer in DNA by adenine-hopping mechanism. *J. Am. Chem. Soc.* **2003**, *125*, 6842–6843.
41. Takada, T.; Kawai, K.; Cai, X.; Sugimoto, A.; Fujitsuka, M.; Majima, T. Charge separation in DNA via consecutive adenine hopping. *J. Am. Chem. Soc.* **2004**, *126*, 1125–1129.
42. Kawai, K.; Osakada, Y.; Takada, T.; Fujitsuka, M.; Majima, T. Lifetime regulation of the charge-separated state in DNA by modulating the oxidation potential of guanine in DNA through hydrogen bonding. *J. Am. Chem. Soc.* **2004**, *126*, 12843–12846.

43. Takada, T.; Kawai, K.; Fujitsuka, M.; Majima, T. High-yield generation of a long-lived charge-separated state in diphenylacetylene-modified DNA. *Angew. Chem., Int. Ed.* **2006**, *45*, 120–122.

44. Takada, T.; Kawai, K.; Fujitsuka, M.; Majima, T. Rapid long-distance hole transfer through consecutive adenine sequence. *J. Am. Chem. Soc.* **2006**, *128*, 11012–11013.

45. Kawai, K.; Osakada, Y.; Sugimoto, A.; Fujitsuka, M.; Majima, T. Hole transfer rates in A-form DNA/2-OMeRNA hybrid. *Chem. Eur. J.* **2007**, *13*, 2386–2391.

46. Kawai, K.; Osakada, Y.; Fujitsuka, M.; Majima, T. Mechanism of charge separation in DNA by hole transfer through consecutive adenines. *Chem. Eur. J.* **2008**, *14*, 3721–3726.

47. Nakajima, S.; Akiyama, K.; Kawai, K.; Takada, T.; Ikoma, T.; Majima, T.; Tero-Kubota, S. Spin-correlated radical pairs in synthetic hairpin DNA. *ChemPhysChem* **2007**, *8*, 507–509.

48. Gervasio, F. L.; Boero, M.; Parrinello, M. Double proton coupled charge transfer in DNA. *Angew. Chem., Int. Ed.* **2006**, *45*, 5606–5609.

49. Xu, B.; Zhang, P.; Li, X.; Tao, N. Direct conductance measurement of single DNA molecules in aqueous solution. *Nano Letters* **2004**, *4*, 1105–1108.

50. Cohen, H.; Nogues, C.; Naaman, R.; Porath, D. Direct measurement of electrical transport through single DNA molecules of complex sequence. *Proc. Natl. Acad. Sci. U.S.A.* **2005**, *102*, 11589–11593.

51. Hihath, J.; Xu, B.; Zhang, P.; Tao, N. Study of single-nucleotide polymorphisms by means of electrical conductance measurements. *Proc. Natl. Acad. Sci. U.S.A.* **2005**, *102*, 16979–16983.

52. Nogues, C.; Cohen, S. R.; Daube, S.; Apter, N.; Naaman, R. Sequence dependence of charge transport properties of DNA. *J. Phys. Chem. B* **2006**, *110*, 8910–8913.

53. Gorodetsky, A. A.; Boal, A. K.; Barton, J. K. Direct electrochemistry of endonuclease III in the presence and absence of DNA. *J. Am. Chem. Soc.* **2006**, *128*, 12082–12083.

54. Yavin, E.; Stemp, E. D. A.; O'Shea, V. L.; David, S. S.; Barton, J. K. Electron trap for DNA-bound repair enzymes: A strategy for DNA-mediated signaling. *Proc. Natl. Acad. Sci. U.S.A.* **2006**, *103*, 3610–3614.

55. Yavin, E.; Boal, A. K.; Stemp, E. D. A.; Boon, E. M.; Livingston, A. L.; O'Shea, V. L.; David, S. S.; Barton, J. K. Protein–DNA charge transport: Redox activation of a DNA repair protein by guanine radical. *Proc. Natl. Acad. Sci. U.S.A.* **2005**, *102*, 3546–3551.

56. Boon, E. M.; Livingston, A. L.; Chmiel, N. H.; David, S. S.; Barton, J. K. DNA-mediated charge transport for DNA repair. *Proc. Natl. Acad. Sci. U.S.A.* **2003**, *100*, 12543–12547.

57. Kawai, K.; Takada, T.; Nagai, T.; Cai, X.; Sugimoto, A.; Fujitsuka, M.; Majima, T. Long-lived charge-separated state leading to DNA damage through hole transfer. *J. Am. Chem. Soc.* **2003**, *125*, 16198–16199.

58. Kawai, K.; Osakada, Y.; Fujitsuka, M.; Majima, T. Consecutive adenine sequences are potential targets in photosensitized DNA damage. *Chem. Biol.* **2005**, *12*, 1049–1054.

59. Kawai, K.; Osakada, Y.; Fujitsuka, M.; Majima, T. Hole transfer in DNA and photosensitized DNA damage: Importance of adenine oxidation. *J. Phys. Chem. B* **2007**, *111*, 2322–2326.

60. Rogers, J. E.; Kelly, L. A. Nucleic acid oxidation mediated by naphthalene and benzophenone imide and diimide derivatives: Consequences for DNA redox chemistry. *J. Am. Chem. Soc.* **1999**, *121*, 3854–3861.

61. Rogers, J. E.; Weiss, S. J.; Kelly, L. A. Photoprocesses of naphthalene imide and diimide derivatives in aqueous solutions of DNA. *J. Am. Chem. Soc.* **2000**, *122*, 427–436.

62. Tierney, M. T.; Sykora, M.; Khan, S. I.; Grinstaff, M. W. Photoinduced electron transfer in an oligodeoxynucleotide duplex: Observation of the electron-transfer intermediate. *J. Phys. Chem. B* **2000**, *104*, 7574–7576.

63. Tierney, M. T.; Grinstaff, M. W. Synthesis and characterization of fluorenone-, anthraquinone-, and phenothiazine-labeled oligodeoxynucleotides: 5′-probes for DNA redox chemistry. *J. Org. Chem.* **2000**, *65*, 5355–5359.

64. Giese, B.; Wessely, S.; Spormann, M.; Lindemann, U.; Meggers, E.; Michel-Beyerle, M. E. On the mechanism of long-range electron transfer through DNA. *Angew. Chem., Int. Ed. Engl.* **1999**, *38*, 996–998.

65. Kendrick, T.; Giese, B. Charge transfer through DNA triggered by site selective charge injection into adenine. *Chem. Commun.* **2002**, 2016–2017.

66. Behrens, C.; Burgdorf, L. T.; Schwogler, A.; Carell, T. Weak distance dependence of excess electron transfer in DNA. *Angew. Chem., Int. Ed.* **2002**, *41*, 1763–1766.

67. Lewis, F. D.; Liu, J.; Weigel, W.; Rettig, W.; Kurnikov, I. V.; Beratan, D. N. Donor-bridge-acceptor energetics determine the distance dependence of electron tunneling in DNA. *Proc. Natl. Acad. Sci. U.S.A.* **2002**, *99*, 12536–12541.

68. Lewis, F. D.; Wu, T. F.; Zhang, Y. F.; Letsinger, R. L.; Greenfield, S. R.; Wasielewski, M. R. Distance-dependent electron transfer in DNA hairpins. *Science* **1997**, *277*, 673–676.

69. Lewis, F. D.; Wu, Y.; Hayes, R. T.; Wasielewski, M. R. DNA-mediated electron transfer across synthetic T.A.T triplex structures. *Angew. Chem., Int. Ed.* **2002**, *41*, 3485–3487.

70. Wang, D. G.; Fan, J.-B.; Siao, C.-J.; Berno, A.; Young, P.; Sapolsky, R.; Ghandour, G.; Perkins, N.; Winchester, E.; Spencer, J.; Kruglyak, L.; Stein, L.; Hsie, L.; Topaloglou, T.; Hubbell, E.; Robinson, E.; Mittmann, M.; Morris, M. S.; Shen, N.; Kilburn, D.; Rioux, J.; Nusbaum, C.; Rozen, S.; Hudson, T. J.; Lipshutz, R.; Chee, M.; Lander, E. S. Large-scale identification, mapping, and genotyping of single-nucleotide polymorphisms in the human genome. *Science* **1998**, *280*, 1077–1082.

71. Brookes, A. J. The essence of SNPs. *Gene* **1999**, *234*, 177–186.

72. Schafer, A. J.; Hawkins, J. R. DNA variation and the future of human genetics. *Nat. Biotech.* **1998**, *16*, 33–39.

73. McCarthy, J. J.; Hilfiker, R. The use of single-nucleotide polymorphism maps in pharmacogenomics. *Nat. Biotech.* **2000**, *18*, 505–508.

74. Nakatani, K. Chemistry challenges in SNP typing. *ChemBioChem* **2004**, *5*, 1623–1633.

75. Zeglis Brian, M.; Barton Jacqueline, K. DNA base mismatch detection with bulky rhodium intercalators: Synthesis and applications. *Nat. Protoc.* **2007**, *2*, 357–371.

76. Saiki, R. K.; Walsh, P. S.; Levenson, C. H.; Erlich, H. A. Genetic analysis of amplified DNA with immobilized sequence-specific oligonucleotide probes. *Proc. Natl. Acad. Sci. USA* **1989**, *86*, 6230–6234.

77. Kelley, S. O.; Boon, E. M.; Barton, J. K.; Jackson, N. M.; Hill, M. G. Single-base mismatch detection based on charge transduction through DNA. *Nucleic Acids Res.* **1999**, *27*, 4830–4837.

78. Okamoto, A.; Kamei, T.; Saito, I. DNA hole transport on an electrode: Application to effective photoelectrochemical SNP typing. *J. Am. Chem. Soc.* **2006**, *128*, 658–662.

8

RADICAL INTERMEDIATES DURING REDUCTIVE ELECTRON TRANSFER THROUGH DNA

Reji Varghese and Hans-Achim Wagenknecht
Institute of Organic Chemistry, University of Regensburg, D-93040 Regensburg, Germany

8.1. INTRODUCTION

The regularly stacked aromatic heterocycles inside DNA let Eley and Spivey propose over 40 years ago that DNA the might serve as a pathway for charge migration.[1] In the early 1990s, Barton and co-workers phrased provocatively that DNA might serve as a molecular wire and pushed the research in this area quite significantly.[2,3] They reported about many donor–acceptor systems and derived mechanisms to describe photoactivated charge transfer in DNA.[2–4] In fact, one of the first publications of the Barton group described a reductive electron transfer over 40 Å between an intercalating Ru(II) complex and an Rh(III) complex, both covalently attached to the two opposite 5′-ends of the short duplex. Since then, the subject grew to an important research field considering DNA as a charge-transporting biopolymer for potential applications in biotechnology, nanotechnology. The biological relevance of charge transfer as the precursor for DNA radicals enroute to DNA damages is obvious. However, the role of charge transfer in sensing DNA damages and repair by proteins has been proposed recently and supported by experimental results.[5] In the 1990s, the enormous interest in DNA-mediated charge transfer was motivated mainly by the interest in the mechanisms regarding the formation of oxidative DNA damage, which may cause apoptosis, mutations, and cancer.[6–10] Thus, most research groups have focused their work on the photochemically induced or initiated oxidation of DNA,

Radical and Radical Ion Reactivity in Nucleic Acid Chemistry, Edited by Marc M. Greenberg

in which one electron is removed from the DNA and transferred to the photoexcited charge donor. Such a process can be termed chemically as an oxidative hole transfer. From the extensive investigations, it is now well established that a positive charge can move through DNA over a significant distance (at least 200 Å) and that guanines or adenines serve as the hole carrier in form of radical cations as intermediates in this charge transfer process (details are discussed in Chapter 7).[11–13] It is still a matter of debate as to how far the positive charge can actually be transferred, especially in the presence of DNA-binding proteins or inside the nucleosomes, and how DNA dynamics influence these processes.

Reductive electron transfer occurs if an electron from the photoexcited donor is injected into the DNA. In contrast to the broad knowledge about the oxidative hole transfer in DNA, the mechanistic details of the transfer of excess electrons remained unclear until the early 2000s. Although the knowledge has been increased significantly over the last few years (as described in this chapter), a well-defined donor–acceptor system for time-resolved spectroscopic investigation is still elusive but obligatory to bring out the clear picture of the dynamics of these processes. The motivation to study the reductive mode of DNA-mediated charge transfer was the vision that these processes could play a growing role in biotechnological applications. For instance, reductive electron transfer through DNA in a self-assembled monolayer together with an electrochemical readout is suitable for the sensitive detection of single-base mutations.[14] Moreover, the knowledge about reductive electron transfer in DNA has the potential to be considered for the development of nanotechnological applications, such as new DNA-based electronic devices.[15] Here, the research moves away from the natural biological role of DNA to a supramolecular architecture that features unique properties that cannot be found in other nanowires. Mainly the self-assembly of the regular helix as encoded by the DNA base sequence looked very attractive for the advanced nanostructures and nanomachines.[16, 17]

Assuming the analogy between the oxidative and reductive mode of charge transfer, a hopping mechanism was also proposed for the DNA-mediated transfer of excess electrons over long distances.[18] Despite the problem with all experimentally determined redox potentials of DNA bases, mainly that the absolute values vary significantly depending on the solvent and that the applied experimental method influences the result, the relative reducibility of DNA bases follows the order T $\approx$ uridine (dU) $>$ C $\gg$ A $>$ G,[19, 20] showing that the pyrimidines C and T (or dU) are reduced more easily than the purines A and G. Thus, it was suggested that an electron hopping occurs over all base pairs (T–A and C–G) involving the pyrimidine radical anions $C^{\bullet -}$ and $T^{\bullet -}$ as intermediate electron carriers.[18]

In this chapter we briefly discuss the current knowledge about the reductive electron transfer and the involvement of charged radical intermediates that originates from γ-pulse radiolysis studies (Section 8.2), photochemical assays that involves the chemical trapping of the excess electron (Section 8.3), and time-resolved spectroscopic studies of electron donor–acceptor modified DNA (Section 8.4). Finally, we give an outlook for the further studies toward molecular electronics using metallated DNA (M-DNA, Section 8.5).

8.2. γ-PULSE RADIOLYSIS STUDIES

Before any of the photochemical assays were developed in order to study reductive electron transfer in DNA, most of the knowledge came from γ-pulse radiolysis studies carried out mainly by Sevilla and co-workers.[21–30] These studies were performed in frozen ice or glassy aqueous LiBr solutions of duplex DNA using randomly intercalated electron-poor aromatic heterocycles like mitoxantrone (**MX**, Figure 8.1). Solvated electrons that have been generated by γ-radiation reduce the DNA in order to initiate the DNA-mediated electron transfer to the doped acceptors. It is important to point out that solvated electrons are thermodynamically able to potentially reduce all four of the natural DNA bases. The actual intermediate charged radicals inside DNA bases were studied by ESR spectroscopy since the radical intermediates are formed in a sufficiently high steady-state concentration. However, the major disadvantage of this experimental setup is that the electron injection (by the solvated electrons) and the electron trapping (on the intercalators) do not occur site-selectively. Hence any result regarding the distance dependence has to be based on the average distance between the non-covalently bound intercalators. Nevertheless, a few remarkable deductions can be drawn from these studies, as followed.

Below 77 K, reductive electron transfer in DNA occurs via a superexchange mechanism. This mechanism has been known for years for the description of oxidative hole transfer processes through the DNA. A rather simplified view of the superexchange mechanism tells us that the electron tunnels in one coherent step from the donor to the acceptor and never resides on any of the DNA bases as part of the bridge between donor and acceptor.[31,32] According to an again simplified consideration of

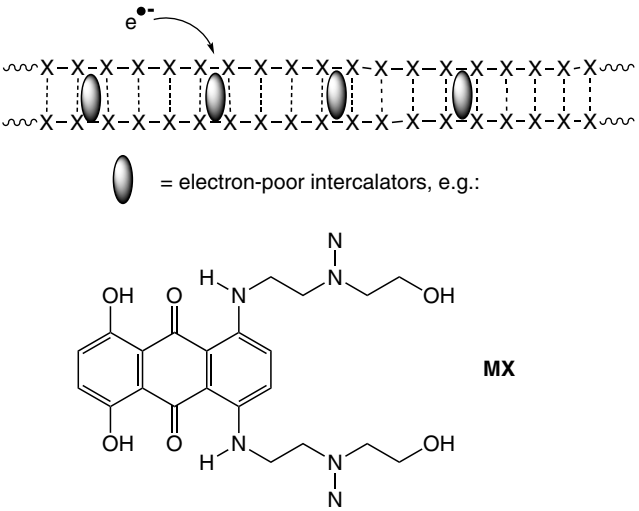

FIGURE 8.1. Principle of the γ-pulse radiolysis studies using mitoxantrone (**MX**), and acridine as non-covalently bound electron acceptors.

the Marcus equation,[33] the rate k_{ET} of such a single-step process depends exponentially on the distance R between donor and acceptor, $k_{ET} \propto \exp(-\beta \bullet R)$, where β represents the critical parameter that characterizes the distance dependence of electron transfer and depends on the nature of the bridge and its coupling with donor and acceptor (DNA in this case). In order to give an idea about the numbers, typical values of β for charge transfer through proteins are found typically in the range of 1.0–1.4 $Å^{-1}$.[34–36]

Coming back to the γ-pulse radiolysis studies, the average value of the distance dependence of the electron transfer rate was found to be $\beta = 0.9\ Å^{-1}$ and not to be temperature-dependent. In comparison with the β value in proteins, representing rather unordered structures by electronical means, the β value in DNA clearly indicates that DNA at 77 K is not an especially effective medium for reductive electron transfer, although duplex DNA looks indeed electronically well-ordered. This result stands in agreement with oxidative hole transfer via the superexchange mechanism (see Chapter 7). The distance dependence of the electron transfer rate varies remarkably on the base composition of the applied synthetic duplexes. The β values of electron tunneling were found to be 0.75 $Å^{-1}$ in poly(dA–dT)·poly(dA–dT) and 1.4 $Å^{-1}$ for poly (dI–dC)·poly(dI–dC), each measured in D_2O. The β value for random-sequence DNA (calf-thymus DNA) lies somewhere in the middle, 0.92 $Å^{-1}$ in D_2O. Comparable measurements in H_2O gave a β of 0.83 $Å^{-1}$, indicating a moderate isotope effect that could be the result of deuteron or proton transfer from inosine (I) or guanine to the cytosine radical anion $C^{\bullet -}$ which significantly slows but does not stop electron transfer. However, this interpretation contradicts significantly the superexchange mechanism. Accordingly, the electron should never reside on the DNA bridge between donor and acceptor and the cytosine radical anion $C^{\bullet -}$ should not occur as an observable intermediate.

Above 130 K, it was shown that irreversible deuteration of the thymine radical anion $T^{\bullet -}$ in D_2O competes with electron tunneling and acts as an irreversible sink for the electron. The one-electron-reduced cytosine ($C^{\bullet -}$) was not observable. Above 170 K the electron transfer mechanism changes completely to a thermally activated process which involves also the cytosine radical anion $C^{\bullet -}$ as the intermediate electron carrier. Protonation of $C^{\bullet -}$ by the complementary base guanine was suggested. It was found that this proton transfer is reversible and thermally activated, suggesting that the proton transfer in a C–G radical anion base pair does not limit significantly the range of electron hopping in DNA.

Anderson and Wright[37] used nitroacridines and nitroquinolines as randomly bound electron acceptors in their γ-pulse radiolysis experiments.[23] In accordance with the previously discussed results, those studies revealed that electron migration in DNA is a highly activation-energy-controlled process. The work by Bernhard and co-workers in this field is discussed separately in Chapter 2. They showed that crystalline DNA at 4 K acts as an extraordinary efficient trap for electrons.[24] Interestingly, the qualitative features of the recorded spectra are consistent with a radical population dominated by one-electron-reduced cytosine. In a similar fashion, Pezeshk et al.[39] concluded that injected electrons in the duplex DNA can travel over many base pairs before being trapped at one of the pyrimidine bases, probably via proton transfer.

8.3. PHOTOCHEMICAL ASSAY FOR REDUCTIVE ELECTRON TRANSFER AND CHEMICAL TRAPPING

It looks reasonable to study electron transfer in DNA in a photochemical or photoinduced fashion: (i) The starting time for the electron transfer is clearly defined by the absorption of a photon. (ii) The photoexcitation pumps a significant amount of energy driving force into the electron donor and shifts the endergonic process toward an exergonic situation. Electron transfer does not occur without light. Hence for the investigations of photoinduced charge transfer processes through DNA, it is necessary to modify oligonucleotides with suitable photochemically activatable compounds. The whole spectrum of different methods of the building-block strategy via the phosphoramidite chemistry as well as protocols for postsynthetic oligonucleotide modifications were applied or further developed in order to prepare best possible structurally well-defined DNA systems. Recent studies of photoinduced electron transfer in DNA were carried out using a broad variety of organic chromophores (Figure 8.2), including derivatives of flavine (**Fl**), naphthalene diamine (**Nd**), stilbene diether (**Sd**), phenothiazine (**Pz**), pyrene (**Py**), thymine (**Tx**), ethidium (**Et**), and thiazole orange (**To**). All photoexcitable electron donors were covalently attached to oligonucleotides in order to ensure the site-selective injection of electrons into the DNA, which is a prerequisite for the clear elucidation of the distance and sequence dependence of the electron transfer processes. They differ significantly in their structures and, more importantly, in their redox properties. In principle, the photoexcited flavine and naphthalene diamine nucleotide analogs or surrogates could reduce all four DNA bases, whereas stilbene diether, thymine, phenothiazine, and pyrene nucleoside analogs or surrogates are able to reduce selectively the pyrimidine bases C and T in order to initiate an electron hopping process within the DNA. On the other hand, ethidium and thiazole orange represent important exceptions in this series of chromophores since their photoexcited states are not able to reduce any of the DNA bases in order to initiate electron hopping. Hence, a suitable acceptor is crucial and has to be provided to promote the electron transfer process.

The major part of the photochemical assays focus on the chemical trapping of the transferred excess electron. It is important to point out that the quantification of the resulting DNA strand cleavages that can be performed by either gel electrophoresis or HPLC analysis allows us only to compare the electron transfer efficiency but does not give any information about the rates and dynamics of electron transfer. Only the comparative application of radical clocks as chemical electron traps that work on different timescales allows us to potentially elucidate some information about the timescale ranges of the electron transfer processes that occurs prior to the electron trapping. The two different chemical electron traps that have been employed to investigate the excess electron transfer do not really fit into these criteria. They are (Figure 8.3): (i) a special T–T dimer lacking the phosphodiester bridge (**$\hat{\mathbf{T}}\hat{\mathbf{T}}$**)[38–40] and (ii) 5-bromo-2′-deoxyuridine (**Br–dU**).[41–44] Even though both radical clocks lead to a strand cleavage at or nearby the actual site of electron trapping the kinetic regime of the radical intermediate is significantly different. The exact dynamics have only been determined with the isolated nucleoside monomers. Accordingly, the radical

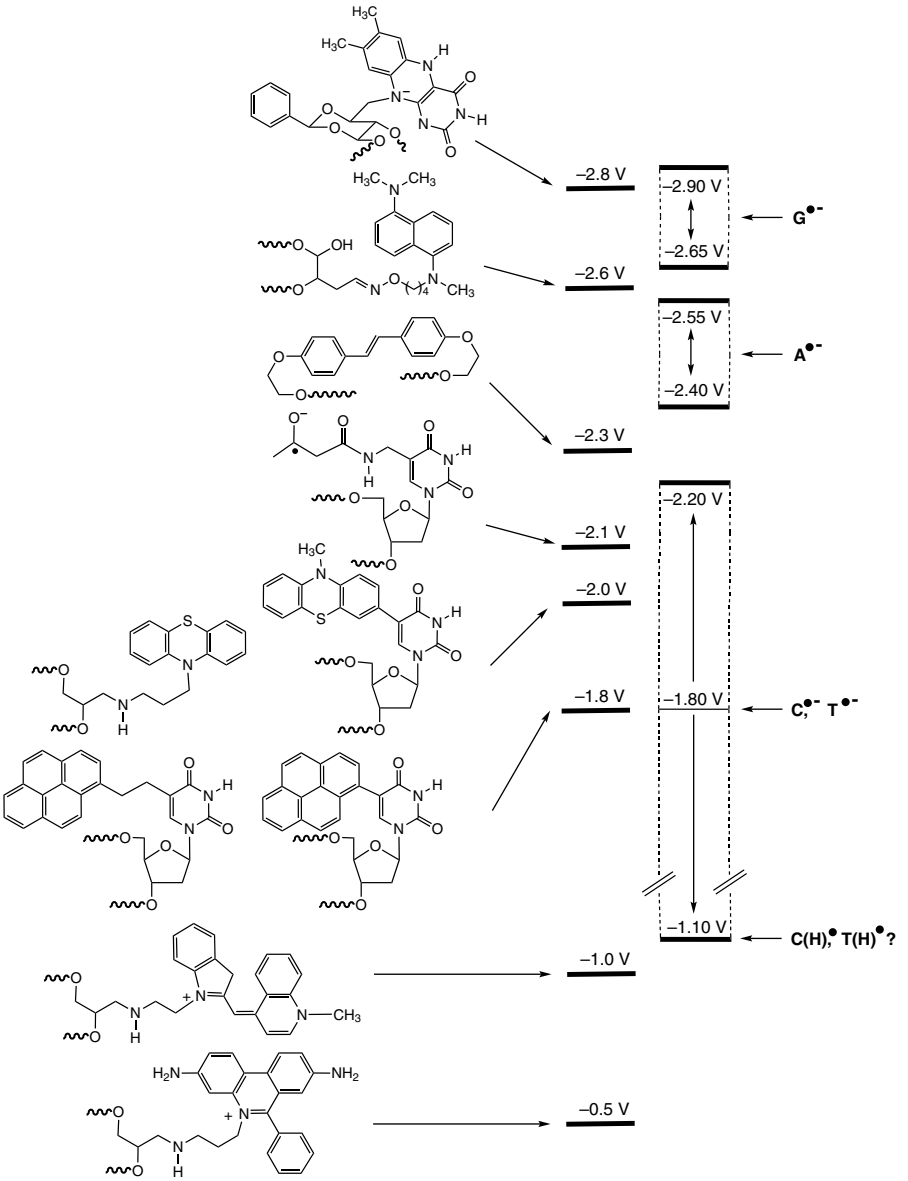

FIGURE 8.2. Estimated reduction potentials of chromophores that have been applied for the investigation of reductive electron transfer, in comparison to the ranges of the reduction potentials of the DNA bases. Except for ethidium and thiazole orange, the chromophores are thermodynamically able to photoinitiate an electron hopping process. Electron transfer from ethidium and thiazole presumably via the superexchange mechanism can only occur if a suitable electron acceptor is present as a second modification of the duplex.

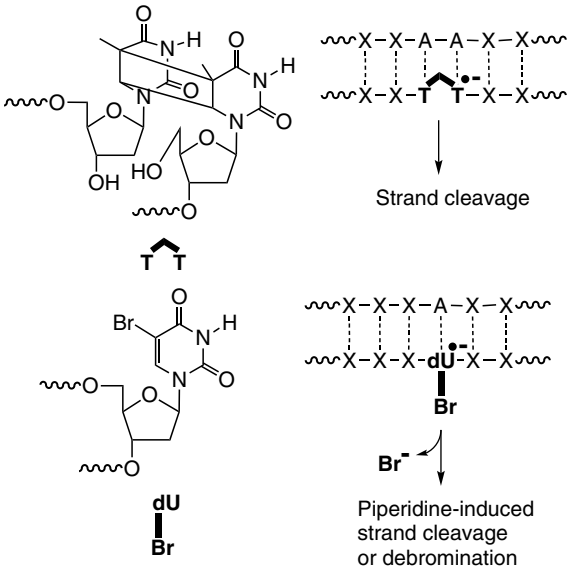

FIGURE 8.3. The $\hat{\mathbf{T}}\mathbf{T}$ dimer and **Br–dU** as chemical electron traps.

anion of **Br–dU** loses its bromide with a rate of $7\ ns^{-1}$ [45] or even faster, whereas the radical anion of the natural (!) T–T dimer splits with a much slower rate of $556\ ns^{-1}$.[46] It is important to note that **Br–dU** induces a strand cleavage only after piperidine treatment at elevated temperature. More recently, Carell and co-workers analyzed the electron transfer efficiency by using simply the debromination reaction from the **Br-dU** to the dU moiety within the oligonucleotide without further cleavage.[47]

In addition to the difference in the kinetics, there is another important difference between the two electron traps. The cleavage of the $\hat{\mathbf{T}}\mathbf{T}$ dimer involves an electron-transfer-induced cycloreversion of the cyclobutane ring system. Hence there still exists an electron even after the cleavage which can subsequently be transferred either back to the electron donor, to a second $\hat{\mathbf{T}}\mathbf{T}$ modification site, or somewhere else. Thus, it is important to point out that the cleavage of the $\hat{\mathbf{T}}\mathbf{T}$ dimer does not consume this excess electron. It is a redoxneutral reaction. In contrast, the **Br–dU** electron trap consumes the electron during the trapping process. Greenberg and co-workers as well as Sugiyama and co-workers investigated in detail the mechanism of UV-induced cleavage of duplex DNA containing 5-bromodeoxyuridine under anaerobic conditions by product analysis and kinetic isotope effect measurements using gel electrophoresis,[48,49] as discussed in Chapters 5 and 6. They suggest that the strand breaks result from abstraction of the C-2′ H atom from the 5′-adjacent nucleotide that forms a 2′-deoxyuridin-5-yl radical yielding an alkaline labile lesion. The ribolactone product was identified after UV irradiation of **Br–dU** in duplex DNA.[44] DFT calculations have shown that the base pairing does not change the reactive nature of the intermediate uracil-5-yl radical, suggesting that the photosensitization properties of halogenated uracils should be effective also in duplex DNA.[50]**Br–dU** was

originally used in the radical-induced photocrosslinking in DNA and between DNA and bound proteins.[51]

This significant difference in the mechanism has important consequences for the elucidation of the distance dependence and DNA base sequence dependence of the excess electron transfer efficiency since the hopping rates are expected to occur on the fast nanosecond or even picosecond timescale. In this regard, it is understandable that in the DNA assay of Carell and co-workers the amount of **T^T** dimer cleavage depends little on the distance to the donor, flavine derivatives (**Fl**) in this case.[38, 39] On the other hand, Rokita et al. and our group have observed a significant dependence of strand cleavage efficiency on the intervening DNA base sequences when **Br–dU** is used as the electron acceptor.[41, 42] This is even more remarkable since the electron donors, the naphthalene diamine (**Nd**) and phenothiazine-modified uridine (**Pz–dU**), represent significantly different photoexcitable electron donors with respect to their reduction potential as well as their interaction with the DNA. Therefore, **Br–dU** seems to be more meaningful as a kinetic electron trap since the timescale is suitable for the resolution of details of a presumably fast electron transfer process.

The photochemical DNA assay by the group of Carell and co-workers[38, 39] is based on knowledge about the repair mechanism of DNA photolyases,[52–54] and the corresponding model compounds.[55–57] Accordingly, the DNA system consists of two DNA modifications (Figure 8.4).[58, 59] (i) Flavine derivatives (**Fl**) were synthetically incorporated into oligonucleotides either as an artificial DNA base into duplex

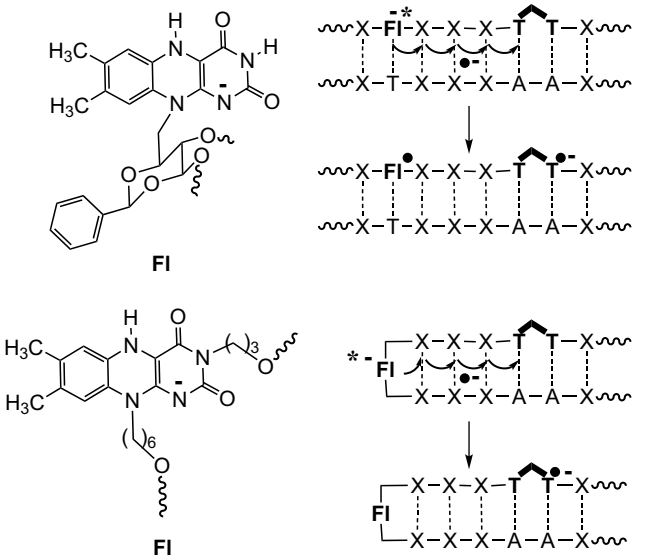

FIGURE 8.4. Photochemical assays for the investigation of electron transfer in DNA consisting of (i) flavine derivatives (**Fl**) either incorporated as an artificial DNA base and electron donor into duplex DNA or as a cap into DNA hairpins and (ii) the **T^T** dimer as the electron trap.

DNA or as a cap into DNA hairpins.[60] Notably the reduced, deprotonated, and photoexcited flavine represents one of the most potent reductants in biological systems with a redox potential of −2.8 V that is capable of reducing all four DNA bases.[46] (ii) Additionally, the above-mentioned **T̂T** dimer was incorporated into the oligonucleotides, and it is important to mention that the **T̂T** dimer lacks the connecting phosphodiester bridge between the 3′-and the 5′-hydroxy groups of the two 2′-deoxyribofuranoside moieties.[61] As a result, cycloreversion of the **T̂T** dimmer, which is initiated by the one-electron reduction, yields a strand break of the oligonucleotide which can easily be analyzed and quantified by HPLC. Based on the constant irradiation conditions and the assumption that the electron injection efficiency is the same in all DNA duplexes, the observed yields of **T̂T** dimer cleavage have been attributed to the different electron transfer efficiencies. Such investigations have been performed in DNA duplexes,[61] in stable DNA hairpins,[64] and in DNA–PNA hybrids.[63] It was shown that the amount of **T̂T** dimer cleavage depends rather weakly on the distance to the flavine. In addition, the electron transfer efficiency was found to be independent of both DNA sequences (A–T versus C–G base pairs) and electron transfer direction (3′ → 5′ versus 5′ → 3′). In fact, the yields of **T̂T** dimer cleavage were found essentially to be the same for electron transfer in the 5′ → 3′ direction as well as in the 3′ → 5′ direction if the sequence composition of both duplexes is the same in an antiparallel DNA–PNA hybdrid. In short, these observations fit pretty well into the model of a thermally activated electron hopping process that stands clearly in agreement with the previously discussed γ-pulse radiolysis studies.

The next photochemical DNA assay comes from the group of Rokita and coworkers (Figure 8.5).[64,65] They employed naphthalene diimide derivatives (**Nd**) as electron donors were attached covalently and regioselectively to abasic sites in DNA. Even though the **Nd** chromophore is structurally different from the **Fl** chromophore, the former is comparable to the latter electronically since **Nd** has an excited-state reduction potential of ∼2.6 V which is also able to reduce any of the four DNA bases. In contrast to the previously described Carell's work, **Br–dU** was used as the chemical electron trap. The different electron traps in combination with comparable potent reductants as electron donors make the two DNA systems interesting alternatives with respect to the resolution of electron transfer efficiencies. Accordingly, Rokita and

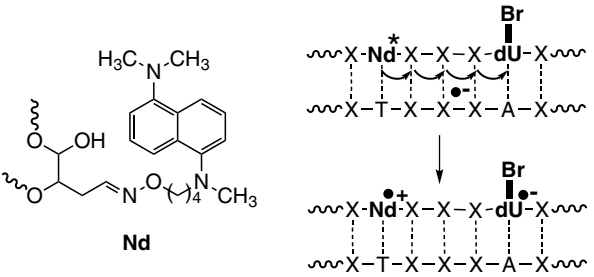

FIGURE 8.5. Photochemical assay for electron transfer in DNA consisting of a naphthalene diamine derivative (**Nd**) as the donor and **Br–dU** as the kinetic electron trap.

co-workers detected a significant distance and sequence dependence of the electron transfer efficiency. The distance-dependent strand cleavage in Rokita's set of experiments exhibits a slope of 0.3 $Å^{-1}$, although it must be mentioned that the β value is not the appropriate parameter to describe the distance dependence of electron hopping. Moreover, G–C base pairs inhibit the electron transfer efficiency significantly. As discussed in more detail using the result of our own group and in accordance with radical studies by Steenken et al.,[66] the authors suspected that protonation of the cytosine radical anion ($C^{\bullet -}$) limits participation of cytosine and leaves thymine as the only major and efficient electron carrier in DNA ($T^{\bullet -}$). Moreover, interstrand crossing and, particularly, orientation can also significantly influence the efficiency of excess electron transfer.

In our group, **Pz** was used as the photochemical electron donor (Figure 8.6).[67, 68] Since the reduction potential of **Pz** in the excited state is −2.0 V, the selective photoreduction of thymine and cytosine is possible within the DNA. In order to inject the electron selectively through a uridine radical anion ($C^{\bullet -}$, structurally very similar to the thymine radical anion $T^{\bullet -}$), we synthesized the **Pz**-modified uridine (**Pz–dU**) and incorporated it as an analogue of T into oligonucleotides. In our investigation we used **Br–dU** as the electron acceptor that was placed either two, three, or four base pairs away from the **Pz–dU** group. The intervening base pairs were chosen to be either T–A or C–G. Interestingly, we observed both a distance and a sequence dependence of DNA-mediated electron transfer efficiency in both sets of duplexes: The DNA duplexes with the intervening T–A base pairs show significantly higher cleavage

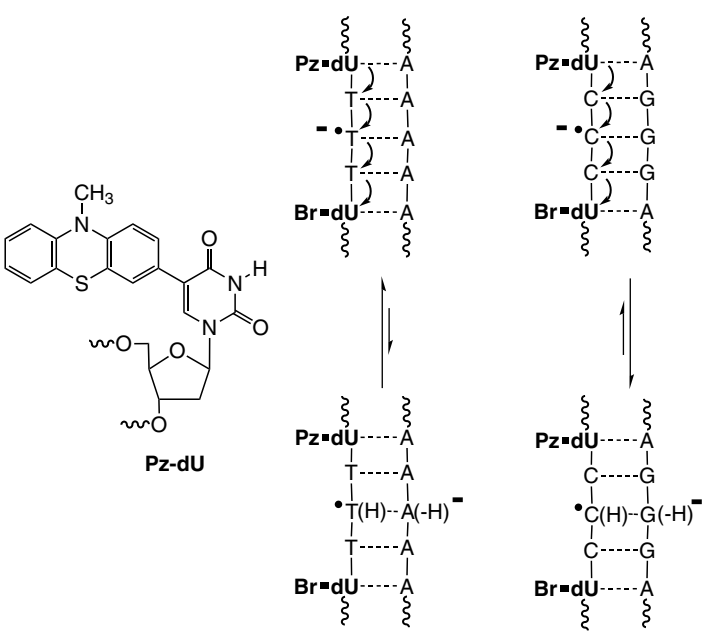

FIGURE 8.6. Photochemical assays for the investigation of electron transfer in DNA-based on the **Pz–dU** as the electron donor and **Br–dU** as electron trap.

efficiencies compared to the C–G base pairs. In fact, in our DNA system three intervening C–G base pairs transfer the electron as efficiently as just one intervening T–A base pair. Similar to the results of Rokita and co-workers, our results imply that the cytosine radical anion $C^{\bullet -}$ is not likely to play a major role as an intermediate electron carrier during electron hopping.

The next photochemical DNA system goes back to the cleavage of the $\hat{\mathbf{T}}\mathbf{T}$ dimer which is a redox neutral process as already pointed out above. This means that subsequent to the $\hat{\mathbf{T}}\mathbf{T}$ dimer cleavage, the excess electron could be transferred further away. In fact, Giese and Carell and co-workers have shown in their joined set of experiments that a single electron that has been injected into DNA can cleave more than one $\hat{\mathbf{T}}\mathbf{T}$ dimer in the same DNA duplex. Accordingly, they called it the "catalytic electron."[40] In contrast to the organic chromophores that have been introduced as electron donors above, the design of the electron injector in this study is different. That means the electron injection does not occur from a photoexcited state but instead from a ground-state radical that has been formed by photoinitiation. This is an important detail for the mechanistic description since back electron transfer does not provide any thermodynamic preference. It is based on a photoinitiated Norrish-type cleavage of the *tert*-butyl ketone attached to **Tx** and subsequent electron transfer to the thymine part of the modified nucleotide (Figure 8.7). The photolysis of the ketone moiety and the formation of the thymine radical anion have been experimentally supported by ESR measurements. The measured ESR signals are similar to those that have been obtained for the unsubstituted thymine radical in frozen solution. The less negative redox potential of thymine compared to those of dialkyl ketones provides the thermodynamic driving force to reduce an adjacent thymine base.

The most recent study by Carell et al. reveals the importance considering the timescales of the radical clocks in order to resolve and experimentally obtain sequence

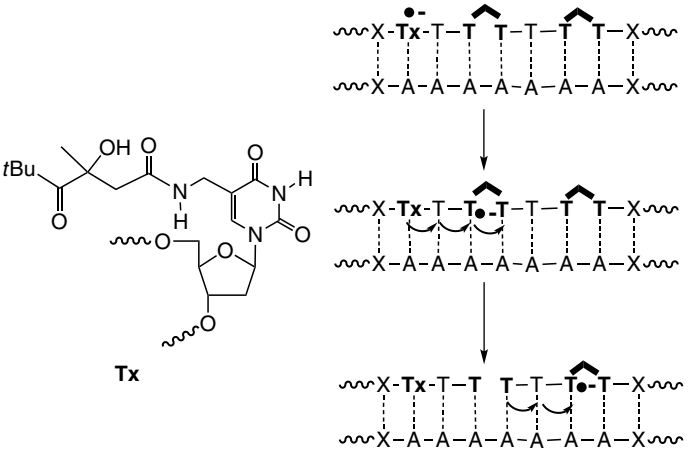

FIGURE 8.7. for The "catalytic" electron: Photochemical assay based on **Tx** as the electron injector the $\hat{\mathbf{T}}\mathbf{T}$ dimer as electron trap.

and distance dependence of the electron transfer efficiencies in DNA.[69] As already investigated by this group, the splitting of $\hat{\mathbf{TT}}$ dimer was found to be too slow ($10^6\,s^{-1}$) compared to the electron hopping (10^8–$10^9\,s^{-1}$). On the other hand, **Br–dU** is a very fast radical clock (10^8–$10^{10}\,s^{-1}$) and in this case a significant dependence of the electron transfer efficiency with respect to intervening sequence and distance was observed by other groups, as discussed above. Carell et al. investigated the influence of the radical clock further by applying 8-bromo-2-deoxyguanosine (**Br–dG**) and 8-bromo-2-deoxyadenosine (**Br–dA**) in addition to **Br–dU** in **Fl**-modified DNA hairpins (Figure 8.8). These radical clocks have been previously investigated by Majima and co-workers spectroscopically[70] and by Chatgilialoglu and co-workers chemically.[71] Even though the exact reduction potentials of the halogenated DNA bases are not known, the authors assumed the following order of potentials for the bases **Br–dU** > **Br–dA** = **Br–dG**. Accordingly, the most efficient (fastest) debromination was observed with **Br–dU**, followed by **Br–dA** and **Br–dG**. According to the literature, the reaction rates of the brominated bases are approximately $10^{10}\,s^{-1}$.[72] The results of this set of experiments show that for the multistep process of reductive electron transfer in DNA consisting of electron injection, electron transfer, and electron trapping; the latter step can in fact represent the rate-limiting step. Very importantly, it has also been observed in the latter set of experiments that electron transfer efficiency dropped by 50% after the replacement of a single intervening T–A base pair by a C–G base pair. However, this difference could only be observed with the fastest radical clock (**Br–dU**). The latter result supports again the idea of a proton-coupled electron transfer (PCET) mechanism that influences G–C base pairs more significantly than A–T base pairs. Even more remarkable is the observation that the

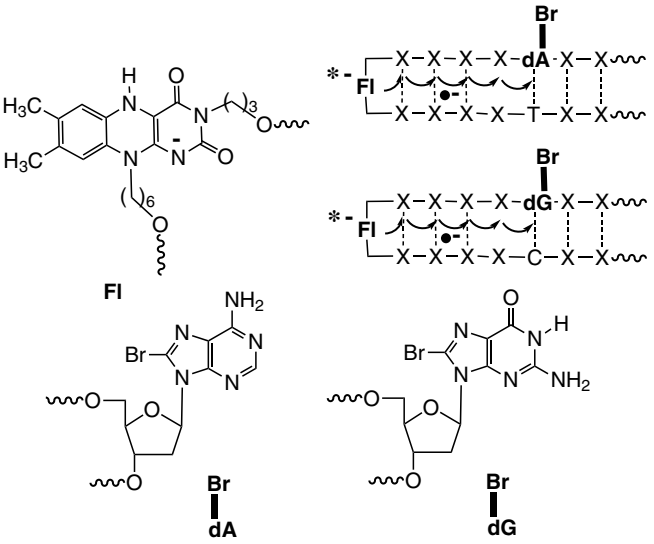

FIGURE 8.8. Photochemical assay consisting of a flavine derivative (**Fl**) incorporated as a cap into DNA hairpins with different radical clock (**Br–dU** and **Br–dA**) as acceptors.

position of the G–C base pair between electron donor and acceptor seems to play a significant role, too. Obviously, as observed in the cases of electron trapping in 5′-TTT-3′ and 5′-TCT-3′ sequences,[73] and in analogy to hole trapping in GG doublets, a modulation of the redox potential of the donor and acceptor by stacking interactions with the adjacent DNA bases is observed to be significant.[74]

8.4. SPECTROSCOPIC INVESTIGATION OF PHOTOINDUCED REDUCTIVE ELECTRON TRANSFER IN DNA

Four years after Barton's first publication on reductive electron transfer,[75] Shafirovich's group reported a nanosecond time-resolved study of electron injection into DNA by using a benz[*a*]pyrene-modified guanosine adduct and by applying non-covalently bound methyl viologen (**Mv**) as the electron acceptor.[76] A main drawback of the latter study is the non-site-selective electron trapping and hence lack of an interpretation of the sequence and distance dependence of electron transfer. The most important spectroscopic investigations on DNA-mediated reductive electron transfer processes were carried out using either stilbene diether-capped DNA hairpins or pyrene-modified DNA duplexes which will be described in this section.

Lewis, Wasielewski, and co-workers investigated the energetic and kinetics of the photoinduced electron injection into stilbene diether (**Sd**) capped DNA hairpins (Figure 8.9).[77–80] Based on the oxidation potential (1.16 V versus NHE) and the singlet energy ($E_{00} = 3.45$ eV) of **Sd** the reduction of cytosine and thymine to the corresponding radical anions in DNA should be exergonic whereas the reduction of adenine and guanine should be endergonic. Hence, **Sd** was used in combination with thymine, cytosine, and **Br–dU** as electron acceptors. The dynamics of the electron injection were followed by picosecond time-resolved laser spectroscopy. It is remarkable that the electron injection rates are larger using thymine ($7.7 \times 10^{11}\ s^{-1}$) as the electron acceptor in comparison to cytosine ($3.3 \times 10^{11}\ s^{-1}$) and reveals the higher reduction potential for C than for T in duplex DNA. This result is in accordance with

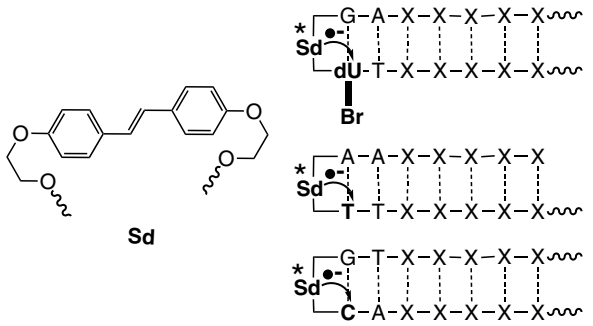

FIGURE 8.9. Photochemical assay for the spectroscopic investigation of electron injection and transfer in DNA consisting of stilbene diether (**Sd**)-capped DNA hairpins in combination with **Br–dU**, thymine, and cytosine as first electron acceptor intermediates.

recent femtosecond time-resolved studies on the reduction of cytosine and thymine using 2-aminopurine as the electron donor,[81] as well as recent calculations of single DNA base electron affinities,[82] but not with recent calculations carried out by Rösch and co-workers.[73] Interestingly, Lewis et al. detected a small difference of the electron injection rate using cytosine as the electron acceptor in two different base-paired situations (C–G versus C–I). The C–G base pair has a stronger hydrogen-bonding network compared to the C–I base pair. As a result, the electron injection into the C–G base pair is slower ($3.3 \times 10^{11}\,s^{-1}$) than the electron injection into the C–I base pair ($1.4 \times 10^{12}\,s^{-1}$). This indicates a small influence of the reduction potential of cytosine by the hydrogen-bonding strength. In fact, all measured rates for charge separation (electron injection) and charge recombination could be correlated with the reduction potentials of the base pairs that are adjacent to the stilbene diether chromophore. This correlation follows the order **Br–dU** < T < C < A < G. A decrease in reduction potential yields a more exergonic charge separation and an increased rate of charge separation. This result shows that **Br–dU**, which has been considered mainly as a kinetic electron trap as described in the previous section, also should exhibit the characteristics of a thermodynamic electron sink with a lower reduction potential. This result is supported by calculations of the electron affinities of pyrimidine base that increase in the order T < U < **F–dU** < **Cl–dU** < **Br–dU**.[83]

Pyrene-labeled oligonucleotides were used initially by Netzel and co-workers to investigate how the quenching efficiency of the photoexcited pyrene emission (Py^*) depends on the flanking DNA base sequence.[84] The authors established the following order for the quenching efficiencies: A < G < T < C. Hence, if the energetics are favorable, the locally excited state of pyrene (Py^*) can act as a precursor state for an electron transfer to the DNA bases yielding the charge-separated state which consists of the pyrenyl radical cation $Py^{\bullet+}$ and the corresponding base radical anion. Based on the redox potential (1.5 V versus NHE) and the singlet energy of pyrene ($E_{00} = 3.25$ eV), and the reduction potential of -1.1 and -1.2 V for uracil and cytosine respectively, the driving force of the electron transfer was estimated to be 0.5–0.6 eV. However, the reduction potentials of nucleobases probably do not refer to the pyrimidine radical anions, $C^{\bullet-}$ and $T^{\bullet-}$, but rather to their protonated neutral forms, C(H) and T(H). Recently, Fiebig et al. reported a time-resolved study of the reduction of thymine and cytosine by photoexcited 2-aminopurine and derived redox potentials (versus NHE) of -1.8 V and -1.9 V for the nonprotonated pairs $C^{\bullet-}$–C and $T^{\bullet-}$–T, respectively.[81] The significant pH dependence of the electrochemical redox potentials suggests that proton transfer is substantially involved in the reductive electron transfer in DNA and must be interpreted as a proton-coupled or at least proton-driven electron transfer. Steady-state and time-resolved fluorescence measurements provided evidence for an electron transfer occurring from the photoexcited Py^* selectively to the pyrimidine bases cytosine or thymine which has been supported by the nanosecond fluorescence lifetime measurements with 5-pyren-1-yl)-2-deoxyuridine (**Py–dU**).

The photoexcited state of pyrene is also able to induce a hole transfer in DNA by oxidizing nearby guanines. In particular, the photoexcitation of the pyrene group in 8-(pyren-1-yl)-2-deoxyguanosine (**Py–dG**) results in the formation of the guanine radical cation as a result of an intramolecular hole transfer ($Py^{\bullet-}$–$dG^{\bullet+}$) representing

an electron transfer in the opposite direction compared to **Py–dU**. In this case also, charge transfer assignment has been proven by picosecond transient absorption experiments using benzo[*a*]pyrenyl-2-deoxyguanosine conjugates. Based on $E_{00} = 3.25\,\text{eV}$ for Py^* and using $E_0(Py/Py^{\bullet -}) = -1.9\,\text{V}$ and $E(dG^{\bullet +}/dG) = 1.3\text{V}$, the driving force ΔG of this charge transfer process in Py–dG is max. -0.1 eV.

In a more recent study, Netzel and co-workers investigated the excited-state dynamics in DNA hairpins equipped with a 5-(2-pyren-1-yl-ethylenyl)-2-deoxyuridine (**Pe–dU**). In comparison with the previously mentioned **Py–dU**, the ethylenyl linker in **Pe–dU** electronically decouples the pyrene chromophore from the uridine moiety and thereby facilitates the interpretation and the assignment of the pyrene radical intermediates in the spectroscopic studies. **Br–dU** was considered as the thermodynamic electron trap (Figure 8.10).[84] The hairpins were 18–24 bases long with a central tetra-T loop and a single **Pe–dU** substitution in the central region of their stems. Nine different DNA hairpins were analyzed with respect to their corresponding $Pe^{\bullet +}$–$dU^{\bullet -}$ states as the electron transfer product upon photoexcitation of the pyrene group at 355 nm. In particular, the results imply that externally injected electrons can migrate back and forth between the $Pe^{\bullet +}$–$dU^{\bullet -}$ state and the adjacent thymines and the **Br–dU** group. The authors did not investigate the final electron trapping by strand cleavage at the **Br–dU** site.

Most recently, we synthesized **Py–dU** and 5-(pyren-1-yl)-2-deoxycytidine (**Py–dC**) to investigate the properties and dynamics of intramolecular electron transfer in these nucleosides by steady-state fluorescence and femtosecond transient absorption spectroscopy in aqueous media at different pH values (Figure 8.11).[85–87] Both nucleosides, Py–dC and Py–dU, were compared as models for electron transfer in DNA and more importantly to address the question of PCET. Most importantly, we detected a huge difference in the basicity of the generated pyrimidine radical anions which implies significance for the understanding of electron migration in DNA as originally put forward by Steenken.[66] Our investigations showed clearly that the

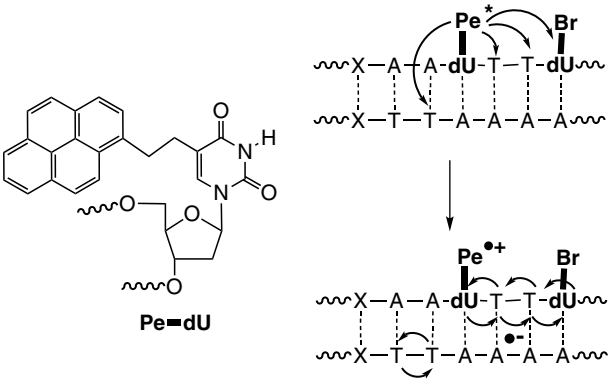

FIGURE 8.10. Electron injection, electron transfer and back electron transfer in photochemical DNA hairpins consisting of the **Pe–dU** nucleotide and **Br–dU** as the major electron acceptors.

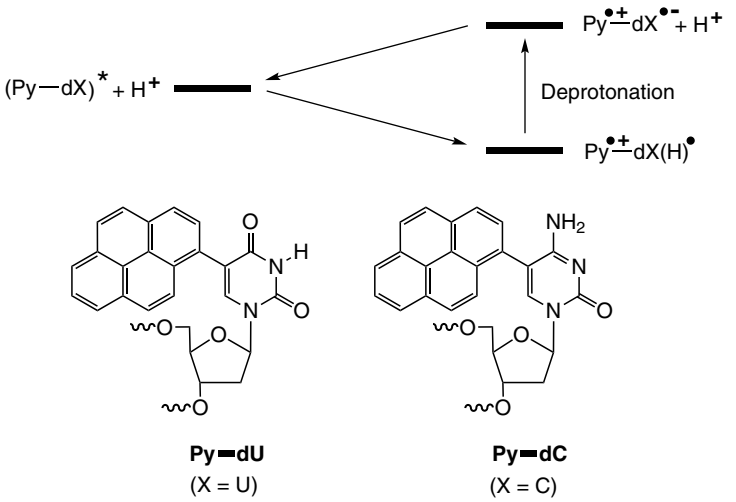

FIGURE 8.11. 5-(Pyren-1-yl)-2-deoxyuridine (**Py–dU**) and 5-(pyren-1-yl)-2-deoxycytidine (**Py–dC**) as model nucleosides for the spectroscopic investigation of the intermediate electron carriers and the question of proton-transfer process during reductive electron transfer in DNA.

$C^{\bullet -}$ is being protonated even in basic aqueous solution on a picosecond timescale or even faster. We observed only a small energetic difference between the electron transfer rates for the formation of $U^{\bullet -}$ (comparable to $U^{\bullet -}$v) versus $C^{\bullet -}$. The time-resolved measurements at pH 5 reveal that the intramolecular electron transfer and protonation occurs within 4.7 ps and 40 ps in Py–dU and Py–dC, respectively. In addition, these results suggest that protonation of the $C^{\bullet -}$ may also occur in DNA. In contrast, efficient intramolecular electron transfer could be observed in Py–dU. Although the situation in water cannot be directly compared with DNA, they provide strong evidence that protonation of $C^{\bullet -}$ by the complementary DNA base guanine or the surrounding water molecules will occur rapidly. During this time the hydrogen-bonding interface can readjust and stabilize the excess electron on the base by separating its spin from charge. Although these processes must be microscopically reversible, they may limit or ultimately terminate electron migration in DNA. From the above observations, we propose that only $T^{\bullet -}$ but not $C^{\bullet -}$ can participate as an intermediate charge carrier for excess electron migration in DNA. However, we suggested that $C^{\bullet -}$ cannot play a major role as an intermediate charge carrier. This result is supported also by the study of Majima et al., which showed that the reduction potential is lowered by the base pairing with guanine.[88] In contrast, $T^{\bullet -}$ can act as a stepping stone for electron hopping in DNA since protonation of these radical anions does not occur.

Going from the isolated model nucleosides **Py–d**U and **Py–dC** to the corresponding modified DNA duplexes, one must consider the fact of diverse conformational states present in DNA and the dependence of electron transfer rate on the microscopic environment. One might not observe single kinetic rate constants for DNA-mediated electron transfer but rather a distribution of rates. In fact, from recent studies of

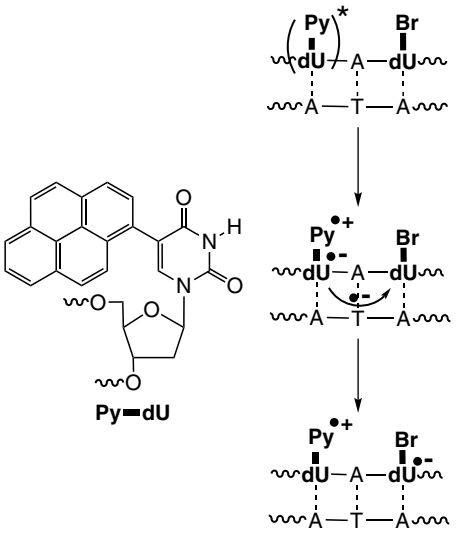

FIGURE 8.12. Photochemical assays with **Py–dU** and **Br–dU** for the combined spectroscopic and chemical investigation of electron transfer in DNA.

oxidative hole transfer in DNA, it is known that DNA has to be considered as a structurally flexible medium and DNA-mediated electron transfer cannot be reduced to a static donor–bridge–acceptor situation. This structural scenario was termed the "base gating effect".[89] In particular, there is strong experimental evidence for an involvement of base stacking fluctuations and hydrogen-bonding interactions (not necessarily proton transfer) inside the DNA helix which we observed during the combination of spectroscopic investigation of reductive electron transfer in the **Py–dU**-modified DNA samples and chemical probing using the **Br–dU** radical clock (Figure 8.12).

Important conclusions were deduced from this latter combination of spectroscopic and chemical studies: (i) The electron injection process in the **Py–dU/Br–dU**-functionalized duplexes show only minor variations due to conformational fluctuations because it occurs between the covalently connected Py and dU moieties. (ii) The charge-separated state $Py^{\bullet+}$–$dU^{\bullet-}$ which is formed after excitation and subsequent electron injection exhibits a strong kinetic dispersion in its lifetimes which is consistent with multiconformational DNA. In fact, DNA as a conformationally flexible medium yields a wide range of electron transfer rate constants. (iii) It became clear that probing both the early time events and the product states is absolutely crucial for obtaining conclusive mechanistic insights. Moreover, the electron injection rates may not simply correlate with the strand degradation as the chemical result of DNA-mediated electron transfer since the electron transfer is a multistep process on various timescales. (iv) Finally, the electron shift from the $Py^{\bullet+}$–$dU^{\bullet-}$ state to the **Br–dU** moiety occurs on the timescale of several hundred picoseconds, thereby competing with charge recombination in these duplexes. It is reasonable to assume that subsequent migration steps during further electron hopping will be faster since

the Coulomb interaction between the excess electron and $Py^{\bullet+}$ decreases drastically with distance. Hence, our results provide a lower limit for the rate of reductive electron transfer between single bases in DNA.

All the photochemical studies described so far in Sections 8.3 and 8.4 focused on the reductive electron transfer interpreted as a hopping process. All results suggest conclusively a thermally activated electron-hopping mechanism over the intervening base pairs. Both pyrimidine radical anions, $T^{\bullet-}$ and $C^{\bullet-}$, can play the role of intermediate charge carriers (Figure 8.14). The electron hopping via $T^{\bullet-}$ seems to be more favorable since the reduction potential of T is slightly lower than that of C in double-helical B-DNA (according to our studies). Moreover, $C^{\bullet-}$ and $T^{\bullet-}$ exhibit a large difference in terms of their basicity. Thus, protonation of $C^{\bullet-}$ by the complementary DNA bases or the surrounding water molecules probably interferes with the electron hopping (Figure 8.13). As a result, it can be assumed that the protonation of $C^{\bullet-}$ in C–G base pairs decreases the efficiency and rate of electron transfer but does not stop electron migration in DNA. However, the occurrence of PCET, especially if the electron resides on C–G base pairs, a rises important doubts about the applicability of reductive electron transfer in nanotechnological applications and devices that would require long distances between the electron injector and the acceptor.

Ethidium (**Et**) and thiazole orange (**To**) behave remarkably different from the above-mentioned electron donors since the photoexcited state of both chromophores are not able neither to oxidise nor to reduce any of the DNA bases.[90–92] Hence, it is expected that the reductive electron transfer in those systems follows the superexchange mechanism, but only if a suitable electron acceptor is present as the second modification site. A well-known acceptor represents methyl viologen ($E(Mv^{2+}/Mv^{\bullet+}) = \sim 0.42$ V), especially in combination with photoexcited Et^* as the electron donor[93] because the radical that is formed after the one-electron reduction is spectroscopically observable. Unfortunately, incorporation of viologens into DNA remains elusive due to the instability viologens under DNA workup conditions.[94] In a more convincing set of experiments, we have incorporated **Et** as an artificial DNA base substitute and combined it either with 7-deazaguanine (**dZ**) as the hole acceptor or with 5-nitroindole (**Ni**) as the electron acceptor.[95] Hence this DNA assay allows for the first time a direct spectroscopic comparison of DNA-mediated reductive electron

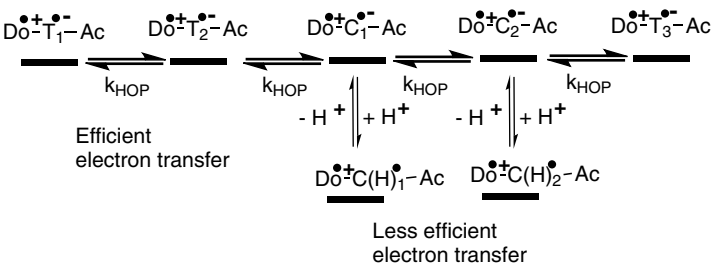

FIGURE 8.13. DNA-mediated reductive electron transfer via electron hopping over cytosines and thymines and the influence of proton transfer.

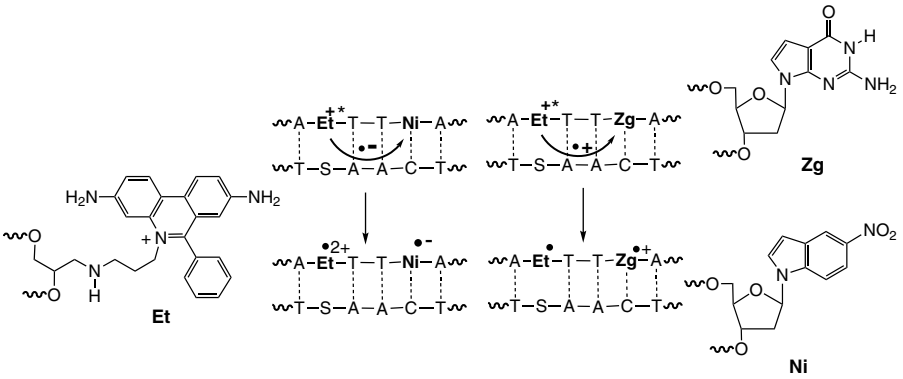

FIGURE 8.14. DNA assay for the direct spectroscopic comparison of oxidative hole transfer in **Et/Zg**-modified DNA and reductive electron transfer in **Et/Ni**-modified DNA (S = abasic site analogue) via the superexchange mechanism.

transfer and oxidative hole transfer in a structurally and electronically very similar donor–acceptor system. The charge acceptors were placed in a distance of one up to three intervening base pairs from the **Et** base (Figure 8.14). Over three base pairs, the fluorescence quenching drops down to less than 10% for both types of charge transfer. This observation stands in agreement with a Marcus-type of charge transfer and is typically limited to a distance of three to four base pairs. Fluorescence measurements revealed lifetimes in the nanonsecond range and a distance dependence of $\beta = 0.3\ \text{Å}^{-1}$ for the DNA-mediated reductive electron transfer between **Et*** and **Ni**, and $\beta = 0.41\ \text{Å}^{-1}$ for the DNA-mediated oxidative hole transfer between **Et*** and **dZ**.

Among the powerful and broadly applied cyanine dyes, such as Cy3 and Cy5,[96] thiazole orange (**To**) exhibits an oxidation potential ($To^+/To^{\bullet 2+}$) of 1.4 V (versus NHE).[97] Together with $E_{00} = 2.4$ V for **To**, the excitation is not sufficient for the photoreduction or photooxidation of DNA, similar to the **Et** dye. We recently presented the fluorescent properties of **To** as an artificial DNA base in combination with short-range reductive electron transfer.[98] In contrast to the previously discussed **Et** chromophore that has a high tendency to intercalate into the base stack, the **To** chromophore tends to bind in the minor groove and can only be forced into intercalation using high salt concentrations in the applied buffer solution. Due to the covalent fixation of the **To** dye as a DNA base surrogate, the **To**-modified oligonucleotides do not exhibit a significant increase of fluorescence upon hybridization with the counterstrand. However, if 5-nitroindole is present as a second artificial DNA base (two base pairs away from the **To** dye), the fluorescence increase upon DNA hybridization can be observed. The fluorescence quenching occurs mainly in the single strand and is caused by a short-range photoinduced electron transfer (Figure 8.15). A similar result has been observed with the commercially available **Cy3** label. In fact, it enables the **Cy3** fluorophore to display the DNA hybridization by a fluorescence increase that is normally not observed with this dye. **To** and **Cy3** represents electron donors for the nonintercalative mode of reductive electron transfer.

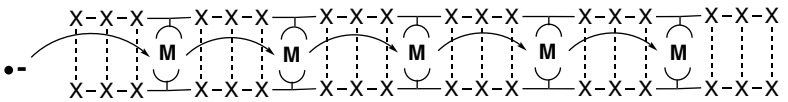

FIGURE 8.15. Electron transfer in DNA over metal ions as artificial stepping stones and intermediate charge carriers.

8.5. TOWARD DNA DEVICES FOR MOLECULAR ELECTRONICS: IS M-DNA AN OPTION?

For the realization of the concept of molecular and supramolecular electronics with the use of π-conjugated systems, a detailed understanding of the organization and interaction of π-conjugated systems is essential.[99] In this regard, DNA plays an important role as a bioorganic material since the unique supramolecular properties of DNA provides a suitable basis in order to use duplex DNA or DNA like architecture as structural scaffold for electronic devices. In principle, both oxidative hole transfer and reductive electron transfer could be applied in molecular electronics. However, one of the major drawbacks of the former with respect to the electronic devices is the DNA irreversible damage that occurs as a side product of the guanine radical cation. On the other hand, excess electron transfer has significantly higher potential because of the proposed lack of DNA damage and the involvement of all base pairs (A–T and C–G) during the electron hopping process. A few measurements of the electronic conductivity of DNA have already been carried out, and they have shown that electrons can transfer through the DNA even though in most systems the observed conductivity is very poor.[15] Taken together with the results from the photoinduced electron transfer experiments in which a diffusive thermal electron hopping can occur over a few nanometers, it becomes clear that electron transfer through longer single DNA molecules (>20 nm) requires more research effort. Hence in order to use DNA as a molecular wire, it is necessary to develop DNA-inspired materials that contain the DNA-typical structural features but exhibit improved electron transfer capabilities. At the moment it looks most promising in this respect to involve metal ions in coordination with DNA.[100] There are three possible ways to develop metal-containing DNA (M-DNA).[101–103] (1) Metal-mediated base pairing in which nucleoside mimics as chelators replace the hydrogen-bonding interface by metal-mediated base pairing. (2) Metals complexed along the DNA duplex: This very general approach utilizes the polyanionic character of the phosphodiester-linked oligonucleotide in order to coordinate metal ions along the DNA helix. The exact position of the metal ions is unclear. (3) Metals coating the duplex: New methods allow the full coating of the DNA duplex with metals for electrochemical devices. Among these structural approaches, option (1) would be superior for the development of M-DNA-based molecular electronics due to the advantage that the metal ions can be placed site-selectively in the interior of the DNA duplex. Until now, experimental examples for this proposal are rare in the literature. One of the most recent examples showed that metal binding (Hg^{2+} and Ag^{+}) to mismatched base pairs effects negatively the DNA-mediated charge transfer.[104]

8.6. CONCLUSIONS

In summary, it has become almost apparent that photoinduced electron transfer occurs via a thermally activated electron hopping mechanism or via the superexchange mechanism, depending on the potential of the photoexcitated state of the electron donor. Both mechanistic regimes are influenced by the DNA dynamics such as base fluctuations up to situation that can be considered as base gating. Despite these efforts in understanding electron migration in DNA, a well-defined donor–acceptor DNA system for time-resolved spectroscopic investigations is still elusive. With such a system, the rates of electron transfer could be measured directly by the absorption of the product radical. The electron hopping in DNA occurs via a mixed cytosine and thymine hopping with some preference for the thymine radical anion as the intermediate electron carriers. The transfer equilibrium of the cytosine radical anion $C^{\bullet -}$ in C–G base pairs decreases the electron transfer efficiency and rate but does not stop the electron migration completely. However, the PCET problem raises important questions and doubts about the applicability of reductive electron transfer in nanotechnological applications and devices that would require long distances between the electron injector and the acceptor. Future experiments include the application of metal-mediated base pairs as artificial charge carriers during electron transfer through M-DNA.

REFERENCES

1. Eley, D.D.; Spivey, D.I. Semiconductivity of organic substances, part 9.-nucleic acid in the dry state *Trans. Faraday Soc.* **1962**, *58*, 411–415.
2. Holmlin, R.E.; Dandliker, P.J.; Barton, J.K. Charge transfer through the DNA base stack *Angew. Chem. Int. Ed. Engl.* **1997**, *36*, 2714–2730.
3. O'Neill, M.A.; Barton, J.K. DNA-Mediated charge transport chemistry and biology *Top. Curr. Chem.* **2004**, *236*, 67–115.
4. Boon, E.M.; Barton, J.K. Charge transport in DNA *Curr. Opin. Struct. Biol.* **2002**, *12*, 320–329.
5. Augustyn, K.E.; Merino, E.J.; Barton, J.K. A role for DNA-mediated charge transport in regulating p53: oxidation of the DNA-bound protein from a distance *Proc. Natl. Acad. Sci. U.S.A.* **2007**, *104*, 18907–18912.
6. O'Neill, P.; Fielden, E.M. Primary Free Radical Processes in DNA *Adv. Radiat. Biol.* **1993**, *17*, 53–120.
7. Armitage, B. Photocleavage of nucleic acids *Chem. Rev.* **1998**, *98*, 1171–1200.
8. Burrows, C.J.; Muller, J.G. Oxidative nucleobase modifications leading to strand scission *Chem. Rev.* **1998**, *98*, 1109–1151.
9. Wang, D.; Kreutzer, D.A.; Essigmann, J.M. Mutagenicity and repair of oxidative DNA damage: insights from studies using defined lesions *Mutat. Res.* **1998**, *400*, 99–115.
10. Kawanashi, S.; Hiraku, Y.; Oikawa, S. Mechanism of guanine-specific DNA damage by oxidative stress and its role in carcinogenesis and aging *Mutat. Res.* **2001**, *488*, 65–76.

11. Longe-range charge transfer in DNA I, *Top. Curr. Chem.* **2004**, *236*, whole issue.
12. Longe-range charge transfer in DNA II, *Top. Curr. Chem.* **2004**, *237*, whole issue.
13. Wagenknecht, H.-A. In *Charge transfer in DNA—from mechanism to application*, Wagenknecht, H.-A., Ed.; Wiley-VCH, Weinheim, 2001, pp. 1–26.
14. Drummond, T.G.; Hill, M.G.; Barton, J.K. Charge transport in DNA, *Nat. Biotechnol.* **2003**, *21*, 1192–1199.
15. Porath, D.; Cuniberti, G.; Felice, R.D. Charge transport in DNA-based devices, *Top. Curr. Chem.* **2004**, *237*, 183–228.
16. Seeman, N.C. From genes to machines: DNA nanomechanical devices, *Trends Biochem. Sci.* **2005**, *30*, 119–125.
17. Seeman, N.C.; Lukeman, P.S. Nucleic acid nanostructures: bottom-up control of geometry on the nanoscale, *Rep. Prog. Phys.* **2005**, *68*, 237–270.
18. Giese, B. Long-distance electron transfer through DNA, *Annu. Rev. Biochem.* **2002**, *71*, 51–70.
19. Seidel, C.A.M.; Schulz, A.; Sauer, M.H.M. Nucleobase-specific quenching of fluorescent dyes. 1. nucleobase one-electron redox potentials and their correlation with static and dynamic quenching efficiencies, *J. Phys. Chem.* **1996**, *100*, 5541–5553.
20. Steenken, S.; Telo, J.P.; Novais, H.M.; Candeias, L.P. One-electron-reduction potentials of pyrimidine bases, nucleosides, and nucleotides in aqueous solution. Consequences for DNA redox chemistry, *J. Am. Chem. Soc.* **1992**, *114*, 4701–4709.
21. Li, X.; Cai, Z.; Sevilla, M.D. Investigation of proton transfer within DNA base pair anion and cation radicals by Density Functional Theory (DFT), *J. Phys. Chem. B* **2001**, *105*, 10115–10123.
22. Cai, Z.; Sevilla, M.D. Studies of excess electron and hole transfer in DNA at low temperatures, *Top. Curr. Chem.* **2004**, *237*, 103–128.
23. Anderson, R.F.; Wright, G.A. Energetics and rate of electron transfer in DNA from base radical anions to electron-affinic intercalators in aqueous solution, *Phys. Chem. Chem. Phys.* **1999**, *1*, 4827–4831.
24. Debije, M.G.; Milano, M.T.; Bernhard, W.A. DNA responds to ionizing radiation as an insulator, not as a molecular wire, *Angew. Chem. Int. Ed.* **1999**, *38*, 2752–2756.
25. Messer, A.; Carpenter, K.; Forzley, K.; Buchanan, J.; Yang, S.; Razskazovskii, Y.; Cai, Z.; Sevilla, M.D. Electron spin resonance study of electron transfer rates in DNA: determination of the tunneling constant for single-step excess electron transfer, *J. Phys. Chem. B* **2000**, *104*, 1128–1136.
26. Cai, Z.; Gu, Z.; Sevilla, M.D. Electron spin resonance study of the temperature dependence of electron transfer in DNA: competitive processes of tunneling, protonation at carbon, and hopping, *J. Phys. Chem. B* **2000**, *104*, 10406–10411.
27. Razskazovskii, Y.; Swarts, S.G.; Falcone, J.M.; Taylor, C.; Sevilla, M.D. Competitive electron scavenging by chemically modified pyrimidine bases in bromine-doped DNA: relative efficiencies and relevance to intrastrand electron migration distances, *J. Phys. Chem. B* **1997**, *101*, 1460–1467.
28. Cai, Z.; Sevilla, M.D. Electron spin resonance study of electron transfer in DNA: inter-double-strand tunneling processes, *J. Phys. Chem. B* **2000**, *104*, 6942–6949.
29. Adhikary, A.; Becker, D.; Collins, S.; Koppen, J.; Sevilla, M.D. C5′- and C3′-sugar radicals produced via photo-excitation of one-electron oxidized adenine in 2′-deoxyadenosine and its derivatives, *Nucleic Acids Res.* **2006**, *34*, 1501–1511.

30. Adhikary, A.; Malkhasian, A.Y.S.; Collins, S.; Koppen, J.; Becker, D.; Sevilla, M.D. UVA-visible photo-excitation of guanine radical cations produces sugar radicals in DNA and model structures, *Nucleic Acids Res.* **2005**, *33*, 5553–5564.
31. Bixon, M.; Giese, B.; Wessely, S.; Langenbacher, T.; Michel-Beyerle, M.E.; Jortner, J. Long-range charge hopping in DNA, *Proc. Natl. Acad. Sci. U.S.A.* **1999**, *96*, 11713–11716.
32. Jortner, J.; Bixon, M.; Langenbacher, T.; Michel-Beyerle, M.E. Charge transfer and transport in DNA, *Proc. Natl. Acad. Sci. U.S.A.* **1998**, *95*, 12759–12765.
33. Marcus, R.A.; Sutin, N. Electron transfers in chemistry and biology, *Biochim. Biophys. Acta* **1985**, *811*, 265–322.
34. Wasielewski, M.R. Photoinduced electron transfer in supramolecular systems for artificial photosynthesis, *Chem. Rev.* **1992**, *92*, 435–461.
35. Isied, S.S.; Ogawa, M.Y.; Wishart, J.F. Peptide-mediated intramolecular electron transfer: long-range distance dependence, *Chem. Rev.* **1992**, *92*, 381–394.
36. Winkler, J.R.; Gray, H.B. Electron transfer in ruthenium-modified proteins, *Chem. Rev.* **1992**, *92*, 369–379.
37. Pezeshk, A.; Symons, M.C.R.; McClymont, J.D. Electron movement along DNA strands: use of intercalators and electron paramagnetic resonance spectroscopy, *J. Phys. Chem.* **1996**, *100*, 18562–18566.
38. Behrens, C.; Cichon, M.K.; Grolle, F.; Hennecke, U.; Carell, T. Excess electron transfer in defined donor-nucleobase and donor-DNA-acceptor systems, *Top. Curr. Chem.* **2004**, *236*, 187–204.
39. Carell, T.; von Meltzer, M. In *Charge transfer in DNA—from mechanism to application*; Wagenknecht, H.-A., Ed., Wiley-VCH, Weinheim, 2001, pp. 77–92.
40. Giese, B.; Carl, B.; Carl, T.; Carell, T.; Behrens, C.; Hennecke, U.; Schiemann, O.; Feresin, E. Excess electron transport through DNA: a single electron repairs more than one UV-induced lesion, *Angew Chem. Int. Ed.* **2004**, *43*, 1848–1851.
41. Rokita, S. E.; Ito, T. In *Charge transfer in DNA—from mechanism to application*; Wagenknecht, H.-A., Ed.; Wiley-VCH, Weinheim, 2001, pp. 133–152.
42. Wagenknecht, H.-A.; Fiebig, T. In *Charge transfer in DNA—from mechanism to application*, Wagenknecht, H.-A., Ed., Wiley-VCH, Weinheim, 2001, pp. 197–224.
43. Swanson, B.J.; Kutzer, J.C.; Koch, T.H. Photoreduction of 5-bromouracil. Ionic and free-radical pathways, *J. Am. Chem. Soc.* **1981**, *103*, 1274–1276.
44. Watanabe, T.; Bando, T.; Xu, Y.; Tashiro, R.; Sugiyama, H. Efficient generation of 2′-deoxyuridin-5-yl at 5′-(G/C)AAXUXU-3′ (X = Br, I) sequences in duplex DNA under UV irradiation, *J. Am. Chem. Soc.* **2004**, *127*, 44–45.
45. Rivera, E.; Schuler, R.H. Intermediates in the reduction of 5-halouracils by e_{aq}^{-1}, *J. Phys. Chem.* **1983**, *87*, 3966–3971.
46. Scannell, M.P.; Fenick, D.J.; Yeh, S.-R.; Falvey, D.E. Model studies of DNA photorepair: reduction potentials of thymine and cytosine cyclobutane dimers measured by fluorescence quenching, *J. Am. Chem. Soc.* **1997**, *119*, 1971–1977.
47. Manetto, A.; Breeger, S.; Chatgilialoglu, C.; Carell, T. Complex sequence dependence by excess-electron transfer through DNA with different strength electron acceptors, *Angew. Chem. Int. Ed.* **2006**, *45*, 318–321.
48. Chen, T.; Cook, G.P.; Koppisch, A.T.; Greenberg, M.M. Investigation of the origin of the sequence selectivity for the 5-halo-2′-deoxyuridine sensitization of DNA to damage by UV-irradiation, *J. Am. Chem. Soc.* **2000**, *122*, 3861–3866.

49. Sugiyama, H.; Tsutsumi, Y.; Saito, I. Highly sequence-selective photoreaction of 5-bromouracil-containing deoxyhexanucleotides, *J. Am. Chem. Soc.* **1990**, *112*, 6720–6721.
50. Li, X.; Sevilla, M.D.; Sanche, L. DFT investigation of dehalogenation of adenine-halouracil base pairs upon low-energy electron attachment, *J. Am. Chem. Soc.* **2003**, *125*, 8916–8920.
51. Ito, S.; Saito, I.; Matsuura, T. Acetone-sensitized photocoupling of 5-bromouridine to tryptophan derivatives via electron-transfer process, *J. Am. Chem. Soc.* **1980**, *102*, 7535–7541.
52. Taylor, J.-S. Unraveling the molecular pathway from sunlight to skin cancer, *Acc. Chem. Res.* **1994**, *27*, 76–82.
53. Carell, T.; Burgdorf, L.T.; Kundu, L.M.; Cichon, M. The mechanism of action of DNA photolyases, *Curr. Opin. Chem. Biol.* **2001**, *5*, 491–498.
54. Sancar, A. Structure and function of DNA photolyase and cryptochrome blue-light photoreceptors, *Chem. Rev.* **2003**, *103*, 2203–2238.
55. Sanders, D.B.; West, O. A Model for the enzyme-substrate complex of DNA photolyase and photodamaged DNA, *J. Am. Chem. Soc.* **1999**, *121*, 5127–5134.
56. Pauvert, M.; Laine, P.; Jonas, M.; Wiest, O. Toward an artificial oxidative DNA photolyase, *J. Org. Chem.* **2004**, *69*, 543–548.
57. Chinnapan, D.J.-F.; Sen, D. A deoxyribozyme that harnesses light to repair thymine dimers in DNA, *Proc. Natl. Acad. Sci. U.S.A.* **2004**, *101*, 65–69.
58. Carell, T.; Butenandt, J. Towards artificial DNA-repair enzymes: incorporation of a flavin amino acid into DNA-binding oligopeptides, *Angew. Chem. Int. Ed. Engl.* **1997**, *36*, 1461–1464.
59. Behrens, C.; Ober, M.; Carell, T. Excess electron transfer in flavin-capped DNA-hairpins, *Eur. J. Org. Chem.* **2002**, 3281–3289.
60. Schwögler, A.; Carell, T. Toward catalytically active oligonucleotides: Synthesis of a flavin nucleotide and its incorporation into DNA, *Org. Lett.* **2000**, *2*, 1415–1418.
61. Kundu, L.M.; Burgdorf, L.T.; Kleiner, O.; Batschauer, A.; Carell, T. Cleavable substrate containing molecular beacons for the quantification of DNA-photolyase activity, *ChemBioChem* **2002**, *3*, 1053–1060.
62. Behrens, C.; Carell, T. Excess electron transfer in flavin-capped, thymine dimer containing DNA hairpins, *Chem. Commun.* **2003**, 1632–1633.
63. Cichon, M.; Haas, C.H.; Grolle, F.; Mees, A.; Carell, T. Efficient interstrand excess electron transfer in PNA:DNA hybrids, *J. Am. Chem. Soc.* **2002**, *124*, 13984–13985.
64. Ito, T.; Rokita, S.E. Excess electron transfer from an internally conjugated aromatic amine to 5-bromo-2′-deoxyuridine in DNA, *J. Am. Chem. Soc.* **2003**, *125*, 11480–11481.
65. Ito, T.; Rokita, S.E. Criteria for efficient transport of excess electrons in DNA, *Angew. Chem. Int. Ed.* **2004**, *43*, 1839–1842.
66. Steenken, S. Electron-transfer-induced acidity/basicity and reactivity changes of purine and pyrimidine bases. Consequences of redox processes for DNA base pairs, *Free Radical Res. Commun.* **1992**, *16*, 349–379.
67. Wagner, C.; Wagenknecht, H.-A. Reductive electron transfer in phenothiazine-modified DNA is dependent on the base sequence, *Chem. Eur. J.* **2005**, *11*, 1871–1876.

68. Babaric, J.; Wagenknecht, H.-A. DNA as a supramolecular scaffold for the helical arrangement of a stack of 1-ethynylpyrene chromophores, *Org. Biomol. Chem.* **2006**, *4*, 2088–2090.

69. Manetto, A.; Breeger, S.; Chatgilialoglu, C.; Carell, T. Complex sequence dependence by excess-electron transfer through DNA with different strength electron acceptors, *Angew. Chem. Int. Ed.* **2006**, *45*, 318–321.

70. Kimura, T.; Kawai, K.; Tojo, S.; Majima, T. One-electron attachment reaction of B- and Z-DNA modified by 8-bromo-2′-deoxyguanosine, *J. Org. Chem.* **2004**, *69*, 1169–1173.

71. Champdore, M.D.; Napoli, L.D.; Montesarchio, D.; Piccialli, G.; Caminal, C.; Mulazzani, Q. G.; Navacchia, M.L.; Chatgilialoglu, C. Excess electron transfer in G-quadruplex, *Chem. Commun.* **2004**, 1756–1757.

72. Patterson, L.K.; Bansal, K.M. Pulse radiolysis studies of 5-halouracils in aqueous solutions, *J. Phys. Chem.* **1972**, *76*, 2392–2399.

73. Voityuk, A.A.; Michel-Beyerle, M.-E.; Rösch, N. Energetics of excess electron transfer in DNA, *Chem. Phys. Lett.* **2001**, *342*, 231–238.

74. Sugiyama, H.; Saito, I. Theoretical studies of GG-specific photocleavage of DNA via electron transfer: significant lowering of ionization potential and 5′-localization of HOMO of stacked GG bases in B-form DNA, *J. Am. Chem. Soc.* **1996**, *118*, 7063–7068.

75. Murphy, C.J.; Arkin, M.R.; Jenkins, Y.; Ghatlia, N.D.; Bossmann, S.H.; Turro, N.J.; Barton, J.K. Long-range photoinduced electron transfer through a DNA helix, *Science* **1993**, *262*, 1025–1029.

76. Shafirovich, V.Y.; Dourandin, A.; Luneva, N.P.; Geacintov, N.E. Migration and trapping of photoinjected excess electrons in double-stranded B-form DNA but not in single-stranded DNA, *J. Phys. Chem. B* **1997**, *101*, 5863–5868.

77. Egli, M.; Tereshko, V.; Mushudov, G.N.; Sanishvili, R.; Liu, X.; Lewis, F.D. Face-to-face and edge-to-face interactions in a synthetic DNA hairpin with a stilbenediether linker, *J. Am. Chem. Soc.* **2003**, *125*, 10842–10849.

78. Lewis, F. D.; Wasielewski, M. R. In *Charge transfer in DNA—from mechanism to application*, Wagenknecht, H.-A., Ed.; Wiley-VCH, Weinheim, 2001, pp. 93–116.

79. Lewis, F.D.; Liu, X.; Miller, S.E.; Hayes, R.T.; Wasielewski, M.R. Dynamics of electron injection in DNA hairpins, *J. Am. Chem. Soc.* **2002**, *124*, 11280–11281.

80. Lewis, F.D.; Liu, X.; Wu, Y.; Miller, S.E.; Wasielewski, M.R.; Letsinger, R.L.; Sanishvili, R.; Joachimiak, A.; Tereshko, V.; Egli, M. Structure and photoinduced electron transfer in exceptionally stable synthetic DNA hairpins with stilbenediether linkers, *J. Am. Chem. Soc.* **1999**, *121*, 9905–9906.

81. Fiebig, T.; Wan, C.; Zewail, A.H. Femtosecond charge transfer dynamics of a modified DNA base: 2-aminopurine in complexes with nucleotides, *ChemPhysChem* **2002**, *3*, 781–788.

82. Wesolowski, S.S.; Leininger, M.L.; Pentchev, P.N.; Schaefer, H.F. III; Electron affinities of the DNA and RNA bases, *J. Am. Chem. Soc.* **2001**, *123*, 4023–4028.

83. Wetmore, S.D.; Boyd, R.J.; Eriksson, L.A. A theoretical study of 5-halouracils: electron affinities, ionization potentials and dissociation of the related anions, *Chem. Phys. Lett.* **2001**, *343*, 151–158.

84. Manoharan, M.; Tivel, K.L.; Zhao, M.; Nafisi, K.; Netzel, T.L. Base-sequence dependence of emission lifetimes for D141018-30-6NA oligomers and duplexes covalently

labeled with pyrene: relative electron-transfer quenching efficiencies of A, G, C, and T nucleosides toward pyrene, *J. Phys. Chem.* **1995**, *99*, 17461–17472.

85. Mayer, E.; Valis, L.; Huber, R.; Amann, N.; Wagenknecht, H.-A. Preparation of pyrene-modified purine and pyrimidine nucleosides via Suzuki-Miyaura cross-couplings and characterization of their fluorescent properties, *Synthesis* **2003**, 2335–2340.
86. Amann, N.; Pandurski, E.; Fiebig, T.; Wagenknecht, H.-A. A model nucleoside for electron injection into DNA: 5-pyrenyl-2-deoxyribose, *Angew. Chem. Int. Ed.* **2002**, *41*, 2978–2980.
87. Raytchev, M.; Mayer, E.; Amann, N.; Wagenknecht, H.-A.; Fiebig, T. Ultrafast proton-coupled electron-transfer dynamics in pyrene-modified pyrimidine nucleosides: model studies towards an understanding of reductive electron transport in DNA, *ChemPhysChem* **2004**, *5*, 706–712.
88. Kawai, K.; Yokoohji, A.; Tojo, S.; Majima, T. Effects of base pairing on the one-electron reduction rate of cytosine, *Chem. Commun.* **2003**, 2840–2841.
89. Shao, F.; Augustyn, K.; Barton, J.K. Sequence dependence of charge transport through DNA domains, *J. Am. Chem. Soc.* **2005**, *127*, 17445–17452.
90. Wan, C.; Fiebig, T.; Kelley, S.O.; Treadway, C.; Barton, J.K.; Zewail, A.H. Femtosecond dynamics of DNA-mediated electron transfer, *Proc. Natl. Acad. Sci. U.S.A.* **1999**, *96*, 6014–6019.
91. Kelley, S.O.; Barton, J.K. DNA-mediated electron transfer from a modified base to ethidium: π-stacking as a modulator of reactivity, *Chem. Biol.* **1998**, *5*, 413–425.
92. Dunn, D.A.; Lin, V.H.; Kochevar, I.E. Base-selective oxidation and cleavage of DNA by photochemical cosensitized electron transfer, *Biochemistry* **1992**, *31*, 11620–11625.
93. Amann, N.; Huber, R.; Wagenknecht, H.-A. Phenanthridinium as an artificial base and charge donor in DNA, *Angew. Chem. Int. Ed.* **2004**, *43*, 1845–1847.
94. Gaballah, S.T.; Kerr, C.E.; Eaton, B.E.; Netzel, T.L. Synthesis of 5-(2,2′-bipyridinyl and 2, 2′-bipyridinediiumyl)-2′deoxyuridine nucleosides: precursors to metallo-DNA conjugates, *Nucleosides Nucleotides Nucleic Acids* **2002**, *21*, 547–560.
95. Valis, L.; Wang, Q.; Raytchev, M.; Buchvarov, I.; Wagenknecht, H.-A.; Fiebig, T. Base pair motions control the rates and distance dependencies of reductive and oxidative DNA charge transfer, *Proc. Natl. Acad. Sci. U.S.A.* **2006**, *103*, 10192–10195.
96. Mishra, A.; Behera, R.K.; Behera, P.K.; Mishra, B.K.; Behera, G.B. Cyanines during the 1990s: a review, *Chem. Rev.* **2000**, *100*, 1973–2011.
97. Hosoi, K.; Hirano, A.; Tani, T. Dynamics of photocreated positive holes in silver bromide microcrystals with adsorbed cyanine dyes, *J. Appl. Phys.* **2001**, *90*, 6197–6204.
98. Menacher, F.; Rubner, M.; Berndl, S.; Wagenknecht, H.-A. Thiazole orange and Cy3: improvement of fluorescent DNA probes with use of short range electron transfer, *J. Org. Chem.* **2008**, *73*, 4263–4266.
99. Schenning, A.P.H.J.; Meijer, E.W. Supramolecular electronics; nanowires from self-assembled -conjugated systems, *Chem. Commun.* **2005**, 3245–3258.
100. Carell, T.; Behrens, C.; Gierlich, J. Electrontransfer through DNA and metal-containing DNA, *Org. Biomol. Chem.* **2003**, *1*, 2221–2228.
101. Clever, G.H.; Kaul, C.; Carell, T. DNA–metal base pairs, *Angew. Chem. Int. Ed.* **2007**, *47*, 6222–6236.

102. Wagenknecht, H.-A. Metal-mediated DNA base pairing and metal arrays in artificial DNA: towards new nanodevices, *Angew. Chem. Int. Ed.* **2003**, *42*, 3204–3206.

103. Shionoya, M.; Tanaka, K. Artificial metallo-DNA: a bio-inspired approach to metal array programming, *Curr. Opin. Chem. Biol.* **2004**, *8*, 592–597.

104. Ito, T.; Nikaido, G.; Nishimoto, S-i. Effects of metal binding to mismatched base pairs on DNA-mediated charge transfer, *J. Inorg. Biochem.* **2007**, *101*, 1090–1093.

9

LOW-ENERGY ELECTRON INTERACTION WITH DNA: BOND DISSOCIATION AND FORMATION OF TRANSIENT ANIONS, RADICALS, AND RADICAL ANIONS

LÉON SANCHE[1]

Centre de Recherche en Radiothérapie, Faculté de Médecine, Université de Sherbrooke, Sherbrooke, Québec, Canada, J1H 5N4

[1]Department of Physics and Astronomy, The Open University, Walton Hall, Milton Keynes, MK7 6AA

9.1. INTRODUCTION

The biological effects of high-energy radiation are not produced by the mere impact of the primary particles in cellular medium, but rather by intermediate secondary species generated along radiation tracks.[1] These species are created at different times after the initial energy deposit in irradiated cells. Reactive species formed at early times are transformed into others, and so on, until stable chemical conditions in the cell are reached. At this point, the cell responds to the chemical transformations in its environment. Thus, to arrive at a complete description of the biological effects of radiation, the entire sequence of events leading to the final chemical state of the cell must be known and the mechanisms involved must be understood. This sequence of events occurs on a timescale ranging from attoseconds to macroscopic times. Efforts to establish these various steps have led to the development of several disciplines involved with the investigation of the primary physical interactions and the chemical stages. Fields of

Radical and Radical Ion Reactivity in Nucleic Acid Chemistry, Edited by Marc M. Greenberg

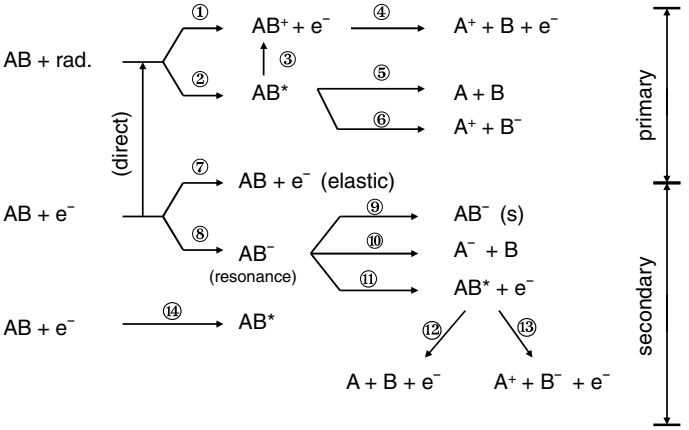

FIGURE 9.1. Reactions induced by primary ionizing radiation and secondary electrons on a molecule AB.

research involving the intermediate stage between radiation physics and chemistry have been more difficult to develop owing particularly to the presence of ultra short-lived species generated within the irradiated cell at times shorter than a picosecond.

Although in radiobiological physics and chemistry the molecules concerned are large and complex, this introduction first attempts to describe femtosecond events in a simple manner. Such events can be divided into three major groups: primary, secondary, and reactive. The first two are considered in Figure 9.1 for the case of a simple hypothetical diatomic molecule AB which could be considered to be located in a cell. Single reactions producing multiple charges are omitted from this figure.

The primary ionizations and excitations may be considered to occur as the result of the propagation within the irradiated substance of the initial charged particles or of other fast charged particles produced by the primary radiation (e.g., photoelectrons, Compton electrons, δ-rays, etc.). As one of these particles passes near a molecule AB, this latter is perturbed by the rapid change of electromagnetic field produced by the moving charge. Since this perturbation leaves the energy and momentum of the fast moving charge practically unchanged, the interaction can be described within the first Born approximation.[2–4] It follows that the energy dependence of the probability amplitudes for primary reactions 1–6 in Figure 9.1 can essentially be obtained from optical data[5] or high-energy electron-energy-loss experiments.[6] About 80% of the energy deposited leads to reaction 1 producing cations and secondary electrons (SE).[7] When the molecular ions are formed in a dissociative state, they can proceed to reaction 4. SE have energies much less than those of the primaries. The major portion of the energy distribution lies below 30 eV with a most probable energy between 9 and 10 eV.[8,9] *Thus by this interaction, low-energy electrons (LEE, $E < 30$ eV) are created in large numbers (i.e., $\sim 3 \times 10^4$/ MeV of deposited energy) and carry a large portion of the primary radiation energy*. The rest of the absorbed radiation energy (∼20%) produces excited molecules (reaction 2) which may dissociate to produce neutral (reaction 5) or

ionized (reaction 6) atoms (Figure 9.1). If the energy of the molecular excited state lies within its own ionization continuum, it may autoionize (reaction 3), yielding one or many SE.

Reactions 7–14 in Figure 9.1 represent the interactions of SE with another molecule AB. Apart from reaction 7 (elastic scattering), SE lose energy by reproducing some or any of reactions 1–6, depending on their energies. Geminate recombination (reaction 14) is also considered in Figure 9.1, as a way to produce excited molecules. In the case of SE, the relative and absolute magnitudes of each process (reactions 1–6) are much different from those for the equivalent reactions produced by the primary particles. This arises from the fact that at low energies, multiple electron scattering *among molecules* can no longer be neglected in the condensed phase. Besides, the molecular orbitals are strongly perturbed by the presence of slow electrons, allowing for exchange interactions and multiple electron scattering *within the molecules*. This perturbation not only favors optically forbidden transitions, but leads to energetically localized phenomena such as electron resonances (i.e., formation of transient anions, reaction 8).[9, 10] These can lead to reactions 9–11 in Figure 9.1[11–19]—that is, resonance stabilization (reaction 9), dissociative electron attachment (DEA) (reaction 10) and vibrational and electronic excitation (reaction 11). If dissociative, an electronically excited state AB^* formed by autoionization of AB^- can separate into neutral and ionic products (reactions 12 and 13). In both the gas phase and condensed phase, the magnitude of these processes often dominates all other energy losses by LEE at the resonance energies.[10–13] Transient anions have typical lifetimes lying between 10^{-15} and 10^{-3} s, though their effects may generally be seen to occur within the femtosecond timescale.[14–16]

Electron–molecule interactions below ~30 eV can be described in terms of nonresonant or direct scattering (vertical arrow in Figure 9.1 leading to reactions 1–6) or via resonance scattering[10] (i.e., the formation of transient anions) depicted by pathway 8 leading to reactions 9–13 in Figure 9.1. Thus, electrons of energy of less than 30 eV can damage molecules by direct scattering or via transient anion formation. Geminate recombination (reaction 14) can also lead to fragmentation via pathways 5 and 6 in Figure 9.1. Direct scattering occurs at all energies above the energy threshold for the observed phenomenon, because the interaction potential is always present. *Since this latter interaction changes slowly with incident electron energy, direct scattering produces a smooth, usually rising, signal that does not exhibit any particular features in the electron energy dependence of the yield of molecular fragments resulting from LEE impact (i.e., the yield function).* In contrast, resonance scattering occurs only when the incoming electron occupies a previously unfilled orbital, which exists at a precise energy,[12, 13] so as to form a transient anion. At a resonance energy, the formation of a product is usually enhanced, so that *the yield function exhibits a pronounced maximum superimposed on an increasing monotonic background from direct scattering*.

Electron resonances are well-described in the literature, and many reviews contain information relevant to this scattering phenomenon.[10–19] There are two major types of electron resonances or transient anions.[10] If the additional electron occupies a previously unfilled orbital of the target in its ground state, then the transitory anion

state is referred to as a "shape" or single-particle resonance. The term "shape" indicates that the electron trapping is due to the shape of the electron–molecule potential. When the transitory anion involves two electrons that occupy previously unfilled orbitals, this transitory state is referred to as a "core-excited" or two-particle, one-hole resonance. In principle, such resonances may lie below or above the energy of their parent neutral state. In the former case, the incoming electron is captured essentially by the electron affinity of an electronically excited state of the molecule. In the latter case, the capture is aided by the angular momentum barrier from the nonzero momentum partial wave content of the attaching electron; in this case the resonance state is called a core-excited shape resonance.

A third group of reactions is also expected to occur within times shorter than a picosecond. Radical anions, cations, and neutrals created by dissociative processes 4–6 and 10–13 can possess energies of a few electron volts and can react rapidly with surrounding molecules in cells. Such reactive scattering is well known from gas-phase experiments[20] and has recently been demonstrated to occur in condensed organic matter[21] including biomolecular films.[22]

In a cell, the number of possibilities is much larger than those shown in Figure 9.1, but the basic principles remain the same. Reactive species created within femtoseconds produce new compounds and damage biomolecules within irradiated cells. In the vicinity of cellular DNA, these species arise from DNA itself, water, and other biomolecules in close contact with DNA such as histone proteins. They can cause mutagenic, genotoxic, and other potentially lethal DNA lesions,[23–26] such as base and sugar modifications, base release, single-strand breaks (SSB), and cluster lesions, including a combination of two single modifications—for example, double-strand breaks (DSB) and cross-links (CL).[26, 27]

This chapter focuses on the study of reactions 2, 5, 6, 8, and 10–13 in Figure 9.1, when they are initiated by the collision of LEE with the DNA molecule. These reactions are usually localized on the molecular subunits of DNA (i.e., the bases and the sugar and phosphate groups). The immediate products are usually not thermalized and are extremely short-lived. They include ions, excited vibrational and electronic states, neutral radicals, and transient anions of the subunits. To date, these reactions have been investigated by measuring the neutral and anion radicals formed by LEE impact on DNA as well as strand breaks and base release. The experimental techniques behind these observations are reviewed in the present chapter. The experimental results obtained are also reviewed, and examples of those which are most instructive are given. The abbreviations used in this chapter are collected at the end of the text. The theoretical studies, which have greatly helped in the interpretation of the experimental results, are reviewed in Chapter 1 of this book.

9.2. EXPERIMENTAL METHODS

9.2.1. Deposition of Thin DNA Films

The DNA molecule consists[28] of two polynucleotide antiparallel strands having the form of a right-handed helix. Depending on the genetic information encoded within

the molecule, it may contain thousands up to billions of atoms. Within DNA, the strands are composed of repeated sugar–phosphate units, which are covalently linked to the sugar moiety of the backbone. The bases guanine (G) and adenine (A), as well as cytosine (C) and thymine (T), are chemically linked to the sugar–phosphate backbone and are hydrogen-bonded to each other to form a double helix. A short double-stranded segment of DNA is illustrated in Figure 9.2. With such a complex and massive molecule, LEE investigations must be performed in the condensed phase, on thin films grown on a conductive substrate, so as to avoid charging of the surface by the incident electrons. Even as a thin film condensed on a substrate in ultra-high vacuum (UHV),

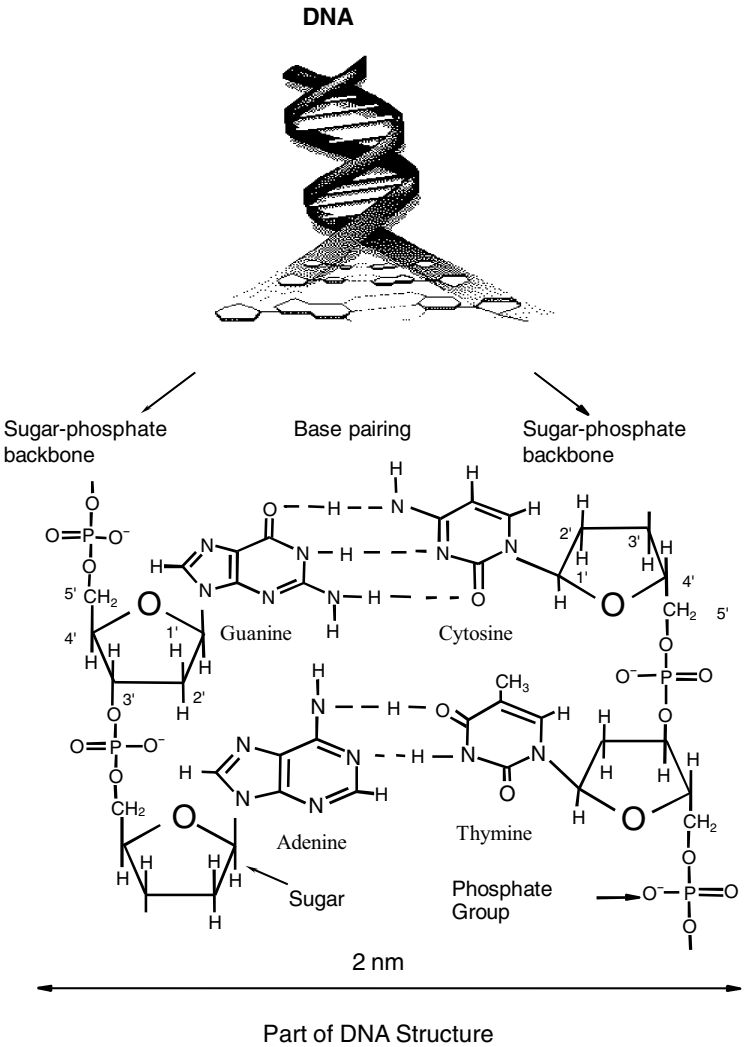

FIGURE 9.2. Segment of DNA containing the four bases.

DNA still contains, on average, 2.5 water molecules per nucleotide.[29] These H_2O molecules, which easily fit in the grooves of the helix, are an integral part of the DNA structure. The negative charge on one of the oxygens of the phosphate group is counterbalanced by a cation. The nature of the latter depends on the buffer used in the procedure to prepare a solution of DNA (i.e., Na^+ if the salt is NaCl). In B-type DNA, the crystallographic (averaged) structure resembles that of a twisted ladder with base pairs defining the rungs and the backbone providing the side support. The helical pitch—that is, the distance for a full turn of the helix—is 3.4 nm and there are 10 rungs per turn. The base pairs lie in a plane perpendicular to the helix axis. In A-type DNA, however, the vertical stacking is appreciably smaller. There are 11 base pairs per turn and the pitch is 2.8 nm. Moreover, in A-type DNA, there is an important tilt of 20° of the plane of the base pairs with respect to the helix axis. In the cell, DNA is in the B form, whereas in its dehydrated state the molecule adapts the A configuration.[28]

For compounds that might be decomposed by sublimation into vacuum, such as DNA, two different techniques have been developed to prepare thin biomolecular films on metal substrates. When multilayer films are required, the molecules are placed in a solution, a small aliquot is deposited on a tantalum substrate, and the solvent is removed by lyophilization.[30] The sample preparation and manipulations are performed within a sealed glove box under a pure dry nitrogen atmosphere. The average film thickness is usually estimated from the amount of biomolecular material deposited and its density.[30] Relatively thick films of DNA of about five monolayers (ML) are prepared to ensure that the measured signal arises from electron interaction with biomolecules that lie close to the film–vacuum interface.

When only a single layer of DNA is needed, a uniform and clean layer can be chemisorbed on a gold substrate by the technique utilized to prepare self-assembled monolayers (SAM).[31, 32] The gold substrate is usually prepared by vacuum evaporation of high-purity gold (99.9%) onto freshly cleaved preheated mica slides.[32] These slides are dipped for at least 24 h in an aqueous solution of highly purified thiolated DNA. After removal of the mica–Au–oligo slide from the solution, it is rinsed with a copious amount of nanopure water and dried under nitrogen flow. Each slide is divided into smaller samples, which are afterwards mounted on a multiple sample holder, such as that shown in Figure 9.3. With this procedure, one monolayer [32, 33] is chemically anchored to the gold substrate via a phosphothiolate modification on one or many nucleotides (i.e., substitution of the double-bonded oxygen atoms by double-bonded sulfur at the phosphorus). Considering that the chemisorbed oligos are well-ordered and densely packed, an upper limit for the surface coverage (i.e., 1.7×10^{14} oligos/cm^2)[34] is obtained, regardless of the nature and number of the bases. The reproducibility of the results obtained so far[32–34] suggests that the surface coverage can be estimated within an error of 20%. Owing to the bonding selectivity of chemisorption, SAM of DNA can be prepared without significant amounts of impurities. Furthermore, molecular orientation within the layer is fairly well-defined.[31] (Two orientations are possible.) Terminal thiolation of DNA would give an upright orientation of the DNA relative to the gold surface, while thiolation throughout the DNA strand would place the strand parallel to the surface of the substrate. Because of all these characteristics, SAM films of DNA are particularly useful in the determination of absolute yields and

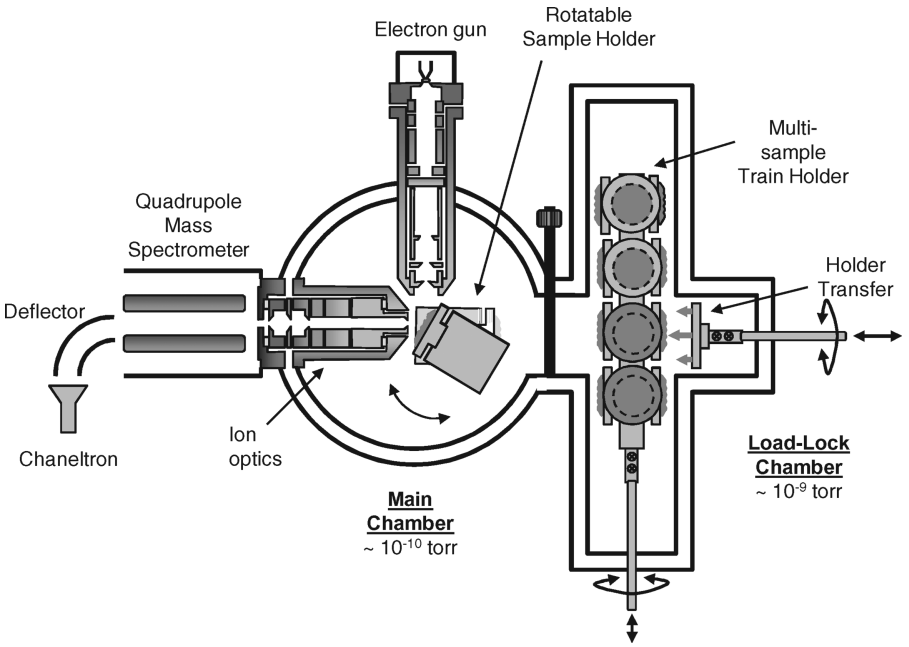

FIGURE 9.3. Schematic overview of the type of apparatus used to investigate the desorption of ions and neutral species induced by electron impact on thin biomolecular films. The films are usually formed by the condensation of molecules evaporated from an oven in front of a metal substrate or by lyophilization outside vacuum. The samples are fitted to a rotary holder.

cross sections for specific damages. When extracting attenuation lengths (AL) or cross sections from electron-scattering experiments on thin molecular films, by far the most difficult parameter to determine and control is the film thickness and its variation along the plane of the supporting substrate. This problem is particularly acute in the case of vacuum-dried DNA films,[30, 35–38] where clustering of the DNA molecules induces variations in the thickness of the film. These variations translate into uncertainty in the determination of the cross sections for strand break (SB) by LEE impact.[30] SAM virtually eliminate this major source of error, since in the layer the molecules are uniformly oriented with a regular density over the substrate to which they are chemisorbed[31].

Other techniques to prepare DNA as a target for LEE impact experiments are presently being developed. Those with which LEE induced damage has already been measured are mentioned here. Denifl et al.[39] have been able to study the negative ions formed via free electron attachment to nucleobases embedded in helium clusters. In their experiments, pure and mixed clusters of adenine and thymine have been formed by pickup of isolated molecules by cold helium droplets. It may soon become possible to seed short DNA strands in such a cooled helium beam. Another approach being developed by Tanabe et al.[40] consists of collimating charged biomolecules as an ion beam in an accelerator. The results of their study of LEE collisions with short oligonucleotide anions and cations are reported in Section 9.3.2.

9.2.2. Electron Bombardment

Once prepared as thin films, the DNA samples are placed either directly into an UHV chamber or into a load lock UHV chamber. A schematic diagram of a system having a load-lock chamber is shown in Figure 9.3. The load-lock chamber (10^{-9} torr) is equipped with a multisample holder, to which 16 samples can be mounted and individually transported into a rotary target holder in the main chamber (10^{-10} torr). In this chamber, an electron source consisting of a modified LEE gun is focused on a 2-mm^2 spot on the film. The energy distribution of the electrons emitted from the gun is approximately 0.4 eV full width at half-maximum FWHM with a beam current adjustable between 1 nA and 1 μA. Electrons from 0.1 to 100 eV impinge onto the film at an incident angle of 70° with respect to the surface normal. The electron energy scale is calibrated by taking 0 eV as the onset of electron transmission through the film, with an estimated uncertainty of ±0.3 eV.[41] Because energy shifts in this onset are related to electron trapping, this calibration method allows one to verify that measurements are obtained from uncharged films; alternatively, with this method it is possible to obtain an estimate of charge accumulation during electron impact.[42] To avoid charging a film with the electron beam, its thickness must be smaller than the effective range (12–14 nm) for damaging DNA with LEE[30] and the penetration depth of 5–30 eV electrons (15–30 nm in liquid water or amorphous ice).[43] Under these conditions, most of the electrons from the beam are transmitted through the DNA film under single inelastic scattering conditions, and thus only small quantities of damaged DNA can be obtained.

To produce much larger amounts of degraded DNA, one can use a defocused LEE beam to irradiate large quantities of the molecules, spread out over a large surface area. In such an irradiator, recently developed by Zheng et al.,[44] the molecules under investigation are spin-coated onto the inner surface of tantalum cylinders. Up to 10 cylinders can be placed on a rotary platform housed in an UHV system, where their inner walls are bombarded by a diverging beam of LEE having an energy distribution of 0.5 eV FWHM. The electrons first reach a cylindrical mesh grid and then are accelerated to any desired energy by a voltage applied between the grid and the cylinder. After irradiation, the cylinders are removed from UHV and the samples are dissolved in an appropriate solvent. With this type of irradiator, the number of molecules that can be irradiated by LEE in a single bombardment period is about two orders of magnitude larger than that with a conventional electron gun.

Other types of electron sources, such as the tip of a scanning tunneling microscope (STM)[45] or SE emitted from a metal substrate,[27] can be used to irradiate DNA samples with LEE. When a sufficiently thin (<5 nm) biomolecular film is lying on a metal substrate, absorption of energy by the film upon exposure to X rays is minimal. Under these conditions, the induced damage may be considered to result from electrons emitted from the substrate with the energies of the measured SE distribution. The latter is usually broad but contains essentially LEE for photon energies less than 1.5 keV. For example, the energy spectrum of $Al_{k\alpha}$ X-ray induced SE emission from tantalum has a peak at 1.4 eV and an average energy of 5.8 eV.[27] The tip of an STM also produces electrons with a broad energy range, but in this case the maximum energy can be controlled by the bias potential.[45,46]

9.2.3. Electron-Stimulated Desorption (ESD) of Ions and Neutral Species

As shown in Figure 9.3, neutral and ionic species desorbing from a DNA film can be analyzed by mass spectrometry. Whereas ions that emerge from the film can be focused by electrostatic lenses located in front of the mass spectrometer (MS), neutral species spread in all directions. So, to obtain reasonable signals for the desorbing neutral species, they are usually ionized close to the target surface by a laser[47, 48] and then the resulting ions are focused into the MS (i.e., in the example of Figure 9.3, into quadrupole rods). However, in order to determine the absolute desorption yields of neutral products, their formation must be related to a pressure rise within a relatively small volume. In this case, the MS measures in a small UHV chamber the partial-pressure increase due to the desorption of a specific fragment induced by LEE impact on a thin film.[32–34] At steady state, the number of fragments desorbed per unit time, $N_d/\Delta t$, is equal to the relative partial pressure increase, ΔRPP, times a conversion that is given by SN_0/RT, where S is the true nominal pumping speed of the system, N_0 is Avogadro's number, R is the universal gas constant, and T is the temperature of the system.[34] The effective number of a specific fragment desorbed per incident electron is proportional to the effective desorption cross section via the constant (N/a), where N is the initial number of target molecules in the irradiated area a.[34, 49]

In certain systems, grids are inserted between the electrostatic lenses to analyze the energies of desorbing ions from the film by the retarding potential method. Relative ion yields can be obtained from three different operating modes[14]: (1) the ion-yield mode, in which the ion current at a selected mass is monitored as a function of incident electron energy (i.e., ion yield functions), (2) the ion-energy mode, in which the ion current is measured for a fixed electron energy as a function of the retarding potential, and (3) the standard mass mode, in which a mass spectrum over a selected range is recorded for a fixed electron energy.

9.2.4. Analysis by Electrophoresis and High-Performance Liquid Chromatography (HPLC)

Once the irradiated samples are extracted from the UHV system, the fragments remaining in the films can, in principle, be identified by various standard methods of chemical analysis. However, the quantity of recovered material and fragments produced by the type of apparatus shown in Figure 9.3 are so small that an efficient method of damage amplification is required to observe any type of fragmentation. One method of damage amplification consists of using a film of plasmid DNA, in which a small modification at the molecular level can cause a large conformal change. A single bond rupture in the backbone of a plasmid of a few thousand base pairs can cause a conformational change in the geometry of DNA, and hence be detected efficiently by agarose gel electrophoresis, after irradiation by a focused LEE beam. The product in each electrophoresis band can be (a) quantified and identified CL, supercoiled (undamaged), nicked circle, corresponding to SSB, and (b) full-length linear, corresponding to DSB or short linear forms.[30, 35] The procedure can be repeated at different electron energies and irradiation times.

The huge amplification factor for SB and CL does not exist for other types of DNA damage, so that the quantity of fragments produced from a collimated electron beam is not sufficient for chemical analysis. To produce sufficient degraded material a LEE irradiator of the type described in the Section 9.2.2 can be used to bombard much more material. This technique allows the total mixture of products resulting from LEE bombardment of DNA and its subunits to be analyzed by HPLC/UV and gas chromatography/MS.[44, 50] When analysis is performed only by HPLC, the identification of the products and their yields is determined by calibration with authentic reference compounds.[44]

9.2.5. Analysis by Scanning Probe Microscopies

With an STM or an atomic force microscope (AFM), images of DNA molecules can be recorded in air and in vacuum.[45, 46, 51–57] AFM images can also easily be obtained in aqueous electrolytes.[53, 58] Thus, both techniques have the potential to visualize damage induced to DNA. STM has the advantage that electrons from the tip can be used as a source, but problems of reproducibility are encountered owing to the lower conductivity of DNA relative to the substrate, which forces the STM tip closer to the substrate, thereby leading to mechanical displacement of DNA.[59] DNA damage may also contribute to poor reproducibility. As shown in reference 37, LEE can damage DNA even in the usual 0- to 4-eV operating range of the STM. However, when problems of reproducibility, LEE damage, and artifacts are circumvented, high-resolution STM images of details of the structure within DNA can be obtained so that individual nucleosides can be distinguished.[56]

As shown in Figure 9.4, with the AFM technique, very clear images of plasmid DNA can be recorded and radiation-induced SSB and DSB can clearly be identified as circular or linear shapes, respectively.[55] The twisted or supercoiled configurations in the figure represent the plasmid. As seen in the work of Mougin et al.,[60] the visibility of damage is substrate-dependent.

9.3. EX VACUO ANALYSIS OF DNA DAMAGE

9.3.1. Plasmid DNA

DNA in the supercoiled configuration was first bombarded with electrons of energies lower than 100 eV by Folkard et al.,[61] who found threshold energies for SSB and DSB at 25 and 50 eV, respectively. Later, Boudaiffa et al.[35, 36, 62, 63] bombarded with 5-eV to 1.5-keV electrons dry samples of pGEM®-3Zf(−) plasmid DNA films. Their samples were analyzed by electrophoresis to measure the production of circular and linear forms of DNA corresponding to SSB and DSB, respectively. By measuring the relative quantities of these forms in their 5-ML sample as a function of exposure to electrons, these authors obtained the total effective cross section ($\sim 4 \times 10^{-15}$ cm^2) for pGEM DNA of 3197 base pairs and an effective range ($\sim$13 nm) for the loss of the initial supercoiled configuration, at 10, 30, and 50 eV.[30] Such experiments also allowed

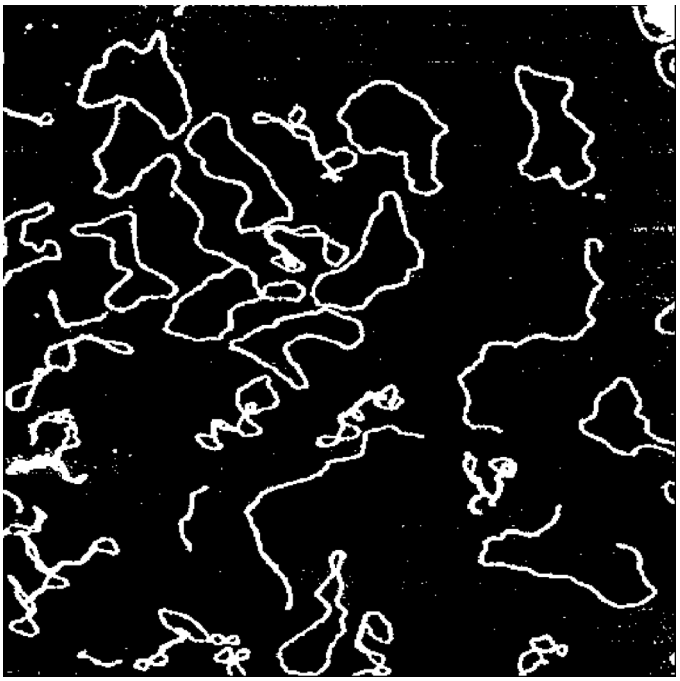

FIGURE 9.4. Tapping mode AFM image of plasmid DNA irradiated with alpha particles at a dose of 2500 Gy in a Tris-EDTA medium deposited on mica ($2 \times 2\,\mu m^2$).

Boudaiffa et al. to delineate the regime under which the measured yields were linear with electron exposure. It is within this regime that the incident electron energy dependence of damage to DNA was recorded more continuously between 5 and 100 eV.[35, 36, 62] Figure 9.5 shows the measured yields of SSB and DSB induced by 5- to 100-eV electrons. At each electron energy, the error bar corresponds to the standard deviation of the average reported value.

Whereas in Figure 9.5, the DSB yield begins near 6 eV, the apparent SSB yield threshold near 4–5 eV is due to the cutoff of the electron beam at low energies. Both yield functions have a peak around 10 eV, a pronounced minimum near 14–15 eV followed by an increase between 15 and 30 eV, and a roughly constant yield up to 100 eV. From the explanations in the introduction, it becomes obvious that the SSB and DSB yield functions can be divided into two scattering regimes. One regime is below 15 eV, where the electron DNA interaction occurs essentially via electron resonances; the other regime is above 15 eV, where, as shown by the dotted line, the major portion of the yield increases monotonically and saturates above 50 eV. This latter behavior is characteristic of direct scattering. Broad resonances between 20 and 40 eV are superimposed on this direct scattering background.

Transient anion formation in the yield functions of SSB and DSB appears more clearly in Figure 9.6. The major peak near 10 eV is seen to be a superposition of broad resonances located at different energies. These yield functions can be understood from

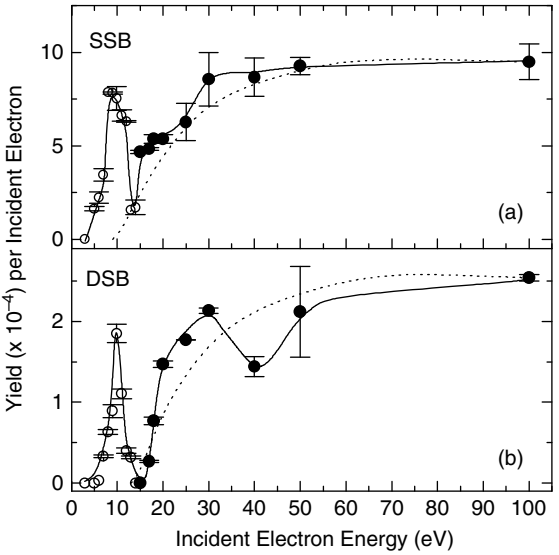

FIGURE 9.5. Open and solid symbols are the measured quantum yields (events per incident electron) for the induction of single-strand breaks (SSB) (**a**) and double-strand breaks (DSB) (**b**) in DNA films by 4- to 100-eV electron impact. The solid curves through the data are guides to the eye. The dotted curves symbolize the general electron energy dependence of the cross sections for various nonresonant damage mechanisms, such as ionization, normalized here to the measured strand break yields at 100 eV.

the results of the fragmentation induced by LEE to the various subunits of the DNA molecule, including its structural water. In fact, the strong energy dependence of DNA strand breaks below 15 eV can be attributed to the initial formation of transient anions of specific DNA subunits decaying into the DEA and/or dissociative electronic excitation channels,[35,36] as exemplified in Figure 9.1 by reactions 10–12. However, because the DNA subunits—which include the phosphate and sugar groups, the bases, and structural H_2O—can all be fragmented via electron resonances between 5 and 13 eV, it was not possible, without more detailed investigation, to unambiguously specify the component responsible for the yields of SSB and DSB reported in Figures 9.5 and 9.6.

Since the data in Figures 9.5 and 9.6 were recorded in a regime of linear yield with electron exposure, each SSB or DSB is the result of a single electron collision. To explain the induction of two strand breaks by one electron, it has been suggested that below ~16 eV, DSB occurs via molecular dissociation on one strand initiated by the decay of a transient anion, followed by reaction of at least one of the fragmentation products on the opposite strand.[35,62] This hypothesis was supported by experiments in condensed films that contain water or molecular oxygen mixed with small linear and cyclic hydrocarbons.[21,22,64–66] In such films, electron-initiated fragment reactions (such as hydrogen abstraction, dissociative charge transfer, and reactive scattering) were found to occur over distances comparable to the DNA double-strand diameter (~2 nm).

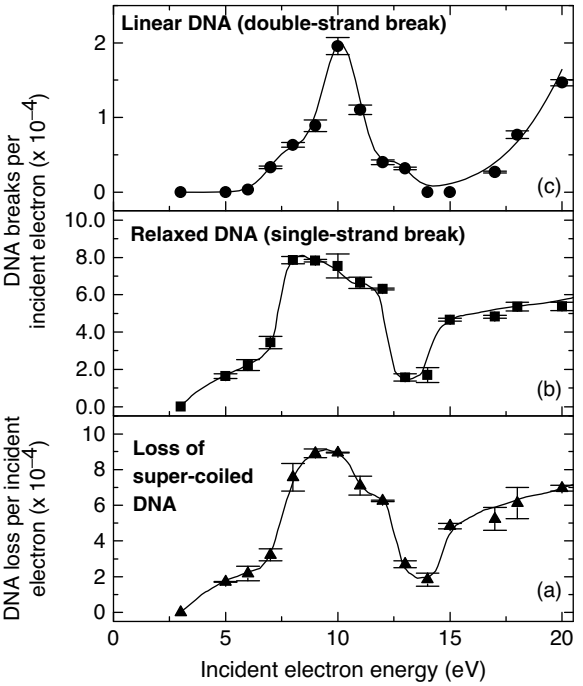

FIGURE 9.6. Measured yields, per incident electron of 5–20 eV, for the loss of the supercoiled DNA form (**a**), induction of SSBs (**b**), and DSBs (**c**) in dry DNA films. The error bars correspond to one standard deviation from six measurements. (Reprinted with permission from Boudaiffa et al., *Science* **2000**, *287*, 1658–1660, Copyright 2000 American Association for the Advancement of Science.)

Owing to problems associated with beam defocusing and film charging, it was only after the development of more efficient techniques to purify DNA that the electron energy range below 4 eV was investigated by Martin et al.[37] The increase in sensitivity of DNA to LEE damage allowed Martin et al. to use electron current of only 2.0 nA and exposure times shorter than 20 s to irradiate the samples of plasmid DNA. As in previous experiments, the different forms of DNA were separated by gel electrophoresis and the percentage of each form was quantified by fluorescence. Exposure response curves were obtained for several incident electron energies. As an example, the inset of Figure 9.7 shows the dependence of the percentage yields of circular DNA on irradiation time for 0.6-eV incident electrons. The energy dependence of the yields of SSB per incident electron was determined from the amounts of circular DNA resulting from a 10-s exposure. As shown in the bottom Figure 9.7, the linear form (DSB) was *not detected* below 5 eV.

Two peaks, with maxima of 1.0 $(\pm 0.1) \times 10^{-2}$ and 7.5 $(\pm 1.5) \times 10^{-3}$ SSB per incident electron, are seen in Figure 9.7 at electron energies of 0.8 eV and 2.2 eV, respectively. The error bars in the yield function show the standard deviation from three to eight exposure experiments, each performed on separately prepared samples.

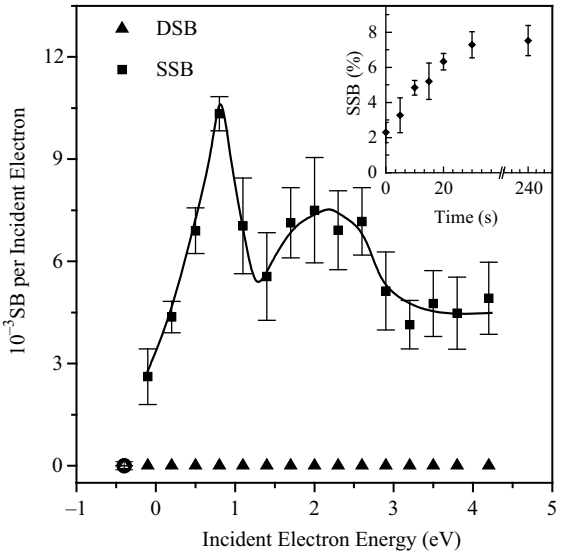

FIGURE 9.7. Yields of SSBs and DSBs induced by 0- to 4.2-eV electrons on supercoiled plasmid DNA films. The inset shows the dependence of the percentage of circular DNA (i.e., SSB) on irradiation time for a beam of 0.6-eV electrons of 2 nA.

At about 1 eV below the first electronic excitation threshold of any molecule, only transient anions can lead to bond dissociation. *Therefore, the peaks in* Figure 9.7 *provide unequivocal evidence for the role of shape resonances in the DNA strand breaking process.* Martin et al.[37] compared these results with those obtained in the gas phase with the DNA bases. With a model that simulates the electron capture cross section as it might appear in DNA owing to the π^* single-particle anion states of the bases, these authors reproduced in magnitude and line shape the yield function seen in Figure 9.7. The attachment energies were taken from the transmission measurements[67] and the maxima were scaled to reflect the inverse energy dependence of the electron capture cross sections. Assuming an equal number of each base in DNA, the contributions from each base were simply added. The lowest peak in the modeled capture cross section, which occurs at 0.39 eV in the gas phase, was shifted by 0.41 eV at higher energy to match that in the SSB yield, and its magnitude was normalized. The relationship between the resonances in the bases and SSB in DNA offered support for the charge transfer mechanism of Barrios et al.,[68] meaning that an anionic potential energy surface connects the initial π^* anion state of the base to a dissociative σ^* anion state of the phosphate group.

Following these observations, Panajotovic et al.[69] determined effective cross sections for production of SSB in plasmid DNA [pGEM 3Zf(−)] by electrons of 10 eV and energies between 0.1 and 4.7 eV. The effective cross sections were derived from the slopes of the yield *versus* exposure curves measured by electrophoresis. They reported values in the range of 10^{-15}–10^{-14} cm^2, which translate into effective cross sections on the order of 10^{-18} cm^2 per nucleotide. The cross sections within the

0- to 4-eV range were similar in magnitude to those found at higher energies (10–100 eV), indicating that *the sensitivity of DNA to electron impact is universal and not limited to any particular energy range*.

The structural changes in plasmid DNA (pUC18, 2686 base pairs) adsorbed onto graphite following LEE irradiation in air were investigated by Mochiji et al.[45] by STM. They observed networks or islands of DNA consisting of entangled molecules and compared the shapes of the DNA before and after electron irradiation with tip biases in the range 8–40 V. At electron energies of 8 and 13 eV, the dominant change was the extension of the DNA islands, which was suggested to be caused by relaxation of DNA molecules via strand breaks or unraveling of the double helix. Higher-energy electrons of 18 eV and 38 eV degraded the area of DNA islands due to the electron-induced desorption of fragments. As electron dose increased, SB and desorption were found to compete with cross-linking. As a result, the two types of change, extension and degradation, became saturated at high electron doses. Although the data of Mochiji et al. were not recorded in the linear regime of the dose response, their results could be fairly well correlated to those of direct LEE beam experiments described in this section, which were performed under single-collision conditions.

More recently, Grant et al.[57] measured the damage to 48,500-base-pair λ-DNA deposited on gold-coated mica surfaces. The damage was induced by field-emitted electrons from an STM tip in air and visualized with both scanning tunneling and atomic force spectroscopies. Collecting DNA images from an STM that simultaneously detects light emission from the tip region, they observed changes in the structure after the first scan. Then, using an AFM whose stiff tip can be operated in both the tapping-mode AFM and STM imaging modes, they measured the damage to DNA caused by LEE from the tip of the STM by reimaging the same area in the AFM tapping mode. In their images, the bias-dependent change in DNA film thickness (i.e., the height of the tip) was correlated to DNA SB. The damage was most obvious in the light-emission images, although no height information was obtained. In this case, they interpreted the spreading of the dark area as DNA torn apart by SSB. They observed a nonmonotonic dependence of layer reduction on bias voltage. Comparing their result with those of Martin et al.[37] on DNA damage as a function of electron energy, they observed striking similarities: the maximum near 0.8 V, the minimum near 1.2 V, and the increase at 2.0 V, seen in Figure 9.7. Their results stand as unequivocal evidence of the ability of AFM and STM to investigate LEE-induced DNA damage.

9.3.2. Small Oligonucleotides

To obtain more detailed information on the mechanisms of DNA damage, the products arising from LEE impact on thin films of short strands of the molecule, namely the tetramers GCAT and its abasic forms and CGTA, were analyzed by HPLC. These tetramers, which constitute the simplest form of DNA containing the four bases, made the analysis of degradation products much easier than with the longer single-strand (ss) and double-strand (ds) configurations of DNA. The samples were irradiated by 10-eV electrons from the LEE irradiator, described in Section 9.2. The HPLC analysis was first focused on SB and nonmodified subunits of the tetramers CGTA and GCAT,

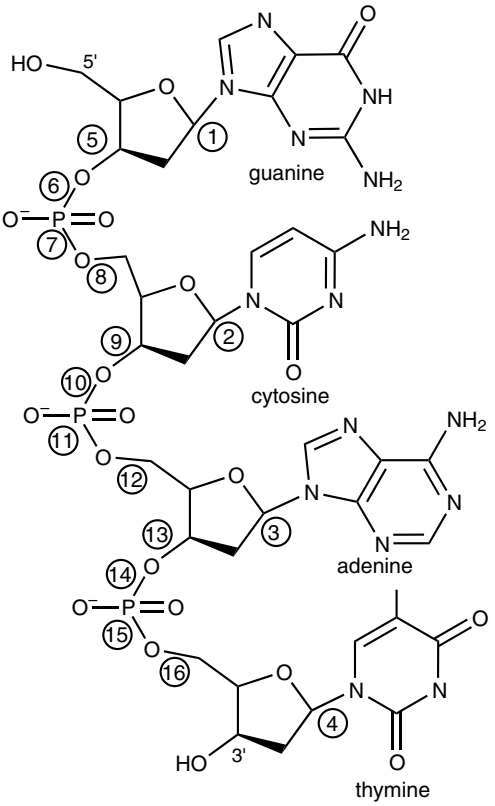

FIGURE 9.8. Nomenclature of oligonucleotide GCAT with numbered sites of cleavage giving nonmodified products.

which included monomeric components (nucleobases, nucleosides, and mononucleotides) and oligonucleotide fragments (dinucleotides and trinucleotides).[70] The incident electron current and irradiation time were adjusted to give an exposure well within the linear regime of the dose response curves and an equal number of electrons to each sample. The nomenclature of GCAT with the potential sites of cleavage yielding nonmodified fragments is shown in Figure 9.8.

The reaction of LEE with the tetramers led to the release of all four nonmodified nucleobases with a bias for the release of nucleobases from terminal positions.[70] For example, the release of T from the internal positions of CGTA was threefold less than from the terminal position of GCAT. The release of unaltered nucleobases from tetramers is likely caused by *N*-glycosidic bond cleavage via DEA from initial electron capture by the base as previously shown in the cleavage of thymidine to thymine in the condensed.[50] and gas phase.[71]Table 9.1 gives the amount of nonmodified fragments formed in both CGTA and GCAT, based on the HPLC analysis of several bombarded samples.[70] The numbers in the last column correspond to the cleavage positions given in Figure 9.8.

TABLE 9.1. Yield of LEE-Induced Products of Irradiated Tetramers[a]

CGTA (16.8 nmol)		GCAT (16.8 nmol)		
Product	Yield (nmol)	Product	Yield (nmol)	Break Position
		Nucleobases		
C	0.27 ± 0.05	G	0.22 ± 0.03	1
G	n.d.[b]	C	0.03 ± 0.05	2
T	0.12 ± 0.02	A	0.11 ± 0.01	3
A	0.35 ± 0.07	T	0.35 ± 0.02	4
		Nucleosides and Mononucleotides		
Cp	0.29 ± 0.06	Gp	0.11 ± 0.01	8
dC	0.06 ± 0.01	dG	0.00 ± 0.01	6
pA	0.19 ± 0.04	pT	0.23 ± 0.01	13
dA	0.05 ± 0.01	dT	0.10 ± 0.01	15
		Dinucleotides and Trinucleotides		
CGp	0.19 ± 0.04	GCp	0.16 ± 0.01	12
CG	n.d.	GC	n.d.	10
pTA	0.11 ± 0.02	pAT	0.22 ± 0.01	9
TA	n.d.	AT	n.d.	11
CGTp	0.20 ± 0.04	GCAp	0.31 ± 0.02	16
CGT	n.d.	GCA	0.04 ± 0.01	14
pGTA	0.23 ± 0.05	pCAT	0.27 ± 0.01	5
GTA	n.d.	CAT	n.d.	7
Total	2.06 ± 0.07		2.15 ± 0.08	

[a]Each fragment is written from 5′ to 3′ with d denoting the deoxyribose unit and p indicating the terminal phosphate group (5′-before or 3′-after the DNA base) with the deoxyribose. The numbers in the last column correspond to the sites of cleavage indicated in Figure 9.8.
[b]Nondetected fragment.

For each tetramer, there are eight possible dinucleotide and trinucleotide fragments resulting from 3′ or 5′ cleavage of the four internal phosphodiester bonds. Fragments with a phosphate group were easily detected; but as seen in Table 9.1, the corresponding fragments without a terminal phosphate were minor or not detected in the initial product mixture (CG, TA, CGT, and GTA). Finally, the same pattern of cleavage was observed for the loss of mononucleotides from terminal positions of the tetramers. Although this cleavage gave fragments with and without a terminal phosphate, the yield of fragments with a phosphate was much greater than that without a phosphate. So, the formation of six major nonmodified fragments out of a total of 12 possible fragments for each tetramer indicated that *LEE induces the cleavage of phosphodiester bonds to give nonmodified fragments with a terminal phosphate rather than a terminal hydroxyl group*.

Based on previous interpretations of SB in DNA,[26] Zheng et al.[70] postulated that rupture of the phosphodiester bond was initiated by the formation of a dissociative transient anion on the phosphate group. The two possible pathways leading to cleavage

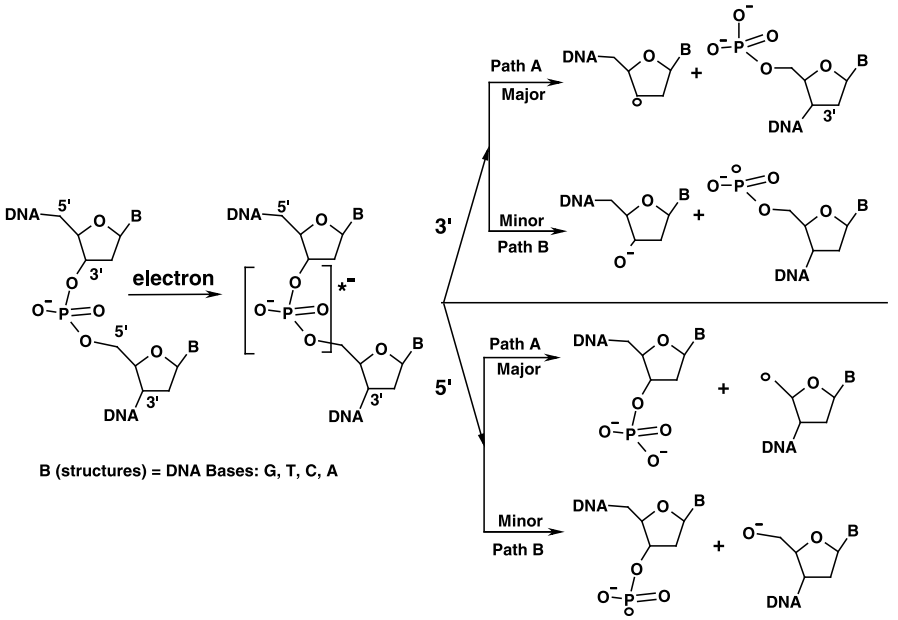

FIGURE 9.9. Proposed pathways for phosphodiester bond cleavage of DNA via LEE impact.

of the phosphodiester bond are shown in Figure 9.9. Pathway A involves scission of the C–O bond and gives carbon-centered radicals (C5′ or C3′ radicals) and phosphate anions as termini, whereas pathway B results in cleavage of the P–O bond giving alkoxyl anions together with phosphoryl radicals. *Thus, the results of Table 9.1 demonstrate that cleavage of the phosphodiester bond primarily takes place via C–O bond cleavage leading to the formation of a sugar radical and a terminal phosphate anion (pathway A)*. The cleavage of C–O and P–O bonds, leading to the formation of phosphoryl radicals and dephosphorylated C3′ radicals of the sugar moiety, was previously reported in ESR studies of argon ion and γ-irradiated hydrated DNA.[72–74] The ESR spectra also showed that C–O bond cleavage was the dominant process. In view of the greater bond dissociation energy of the C–O (335 kJ/mol) compared to that of P–O (80 kJ/mol),[75] these data appear difficult to explain. However, according to reaction A of Figure 9.9, the bond-breaking process takes place by electron attachment into an unfilled orbital lying at a much higher energy (i.e., 10 eV = 960 kJ/mol) than the thermodynamic threshold of C–O bond dissociation. In this case, phosphodiester bond cleavage would not depend on bond energy considerations, but rather on the availability of dissociating anionic states at the energy of the impinging electron.

In subsequent investigations, Zheng et al. measured the yields of the products listed in Table 9.1 as a function of electron energy for GCAT.[76] From 4 to 15 eV, scission of the backbone gave nonmodified fragments containing a terminal phosphate, with negligible amounts of fragments without the phosphate group. This indicated that *phosphodiester bond cleavage involves cleavage of the C–O bond rather than the P–O bond within the entire 4- to 15-eV range*. The incident electron energy dependence of

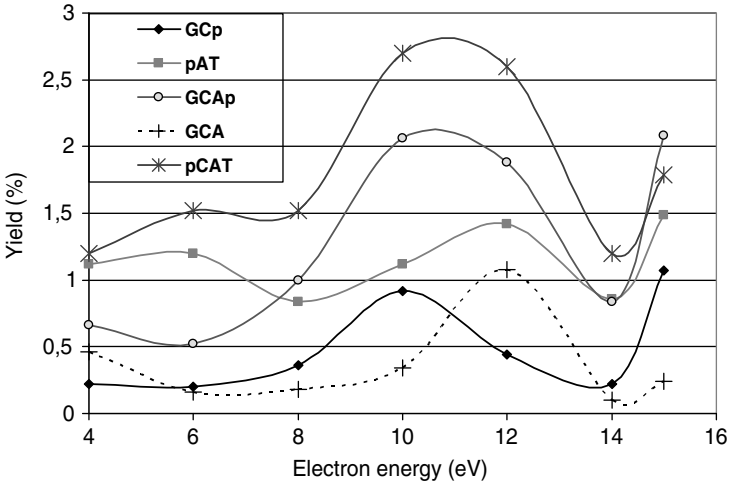

FIGURE 9.10. Dependence of the yield of oligonucleotide fragments on the energy of 4- to 15-eV electrons. Each point is the average of eight individual measurements.

the yield of various fragments caused by SB (i.e., rupture of the C–O bond) is shown as an example in Figure 9.10. Many of the yield functions of fragments other than those reported in Figure 9.10 also exhibited a maximum near 6 eV, a large peak at 10–12 eV, and finally a dip at 14 eV.

The maxima were interpreted as due to the formation of transient anions leading to fragmentation. According to the pathways of Figure 9.9, these transient anions decayed by DEA (reactions 8 and 10 in Figure 9.1). Below 15 eV, these resonances dominated bond dissociation processes. All four nonmodified bases were released from the tetramer within the 4- to 15-eV range, by cleavage of the *N*-glycosidic bond.[76]

As seen from comparison between Figures 9.5, 9.6, and 9.10, the strong maximum at 10–12 eV in the GCAT field functions has been observed in the yield functions for SSB and DSB in films of dry plasmid DNA.[35] Above 14 eV, electron resonances are not expected to dominate the electron scattering process, so that the yields in Figure 9.10 above this energy represent mostly fragmentation via direct electronic excitation of dissociative states (reactions 2, 5, and 6 in Figure 9.1).

The broad peaks at 6 and 10–12 eV in Figure 9.10, which correspond to those in the yield functions for damage to plasmid DNA (Figures 9.5 and 9.6), can be ascribed to the formation of core-excited resonances or core-excited shape resonances, since the lifetime of such resonances is usually sufficiently long at those energies to promote dissociation of the anion.[11] *A priori* scission of the C–O bond leading to SB can occur by direct electron capture on the phosphate group or via electron transfer from a base to the phosphate moiety. However, transfer of a core-excited resonant or core-excited shape resonant state from a subunit to another is unlikely because it requires a three-electron jump.[77] For shape resonances, the lifetime is usually too short above ~5 eV for dissociation,[11, 12] but electron detachment or transfer is highly probable due to the

TABLE 9.2. Comparison of Damage Yield of Tetramer at Electron Energies of 6, 10, and 15 eV (Standard Deviation = 10%)

	6 eV			10 eV			15 eV		
Yield (%)	Strand Break	Base Release	Total	Strand Break	Base Release	Total	Strand Break	Base Release	Total
XCAT	0.72	0.39	1.11	1.11	0.45	1.56	9.89	1.14	11.03
GCXT	0.80	0.60	1.40	4.56	0.56	5.12	2.34	0.78	3.12
GCAT	4.76	1.96	6.72	9.54	5.92	15.46	10.30	4.72	15.02

considerable overlap between the wave functions for an additional electron on each basic DNA subunit.

To provide additional information on the hypothesis of electron transfer from a base to the phosphate group of DNA, Zheng et al.[78] analyzed the products induced by 4- to 15-eV electrons incident on two abasic forms of the tetramer GCAT, that is, XCAT and GCXT, where X represents the base replaced by a hydrogen atom. With the exception of the missing base, the same fragments were observed in the mixture of products from irradiated GCAT tetramers with[78] or without[76] an abasic site. Table 9.2 provides a comparison of the yields expressed as the percentage of SB and base release in the sample of tetramer from bombardment at 6, 10, and 15 eV. Yield functions for both abasic forms were produced from such yields for all fragments recorded at seven different energies between 4 and 15 eV. The yield of each fragment resulting from SB induced by 6-, 10-, and 15-eV electrons is shown in Figure 9.11 as a percentage of the total damage to a particular tetramer. The percentage of fragments corresponding to bond cleavage at different positions along the chain is given for bombardment of XCAT, GCXT, and GCAT. It is obvious that at 6 eV, when G is absent (i.e., in XCAT), there is no cleavage of the phosphodiester bond at the position lacking the base moiety. Similarly, when A is removed (i.e., in GCXT), there is practically no dissociation of the C–O bonds on either side of A. *Thus, at 6 eV, G and A must be present within GCAT to produce C–O bond rupture next to the base (positions 5, 12, and 13 in* Figure 9.8*). It is difficult to explain this result without invoking electron capture by G and A followed by electron transfer to the corresponding phosphate group*. This phenomenon is not observed at 10 and 15 eV, with the exception of bond rupture at position 13, which decreases from 10% in GCAT to 1% in GCXT at 10 eV.

Since electron transfer from a DNA base π^* to a C–O σ^* orbital had been shown theoretically to occur at energies below 3 eV,[68,79] Zheng et al.[78] suggested that the incident 6-eV electron electronically excites a base before transferring to the C–O orbital. They based their suggestion on the existence of electronically excited states of the DNA bases within the 3.5- to 6-eV range measured by electron-energy-loss spectroscopy[80]. For example, LEE energy-loss spectra of thymine exhibit electronically excited states at 3.7, 4.0, and 4.9 eV ascribed to excitation of the triplet $1^3A'$ ($\pi \rightarrow \pi^*$), $1^3A''$ ($n \rightarrow \pi^*$), and ($\pi \rightarrow \pi^*$) transitions.[80] Excitation of these states by 6-eV electrons forming a core-excited shape resonance on T would produce electrons of energies below 3 eV, which could then transfer to the phosphate–sugar

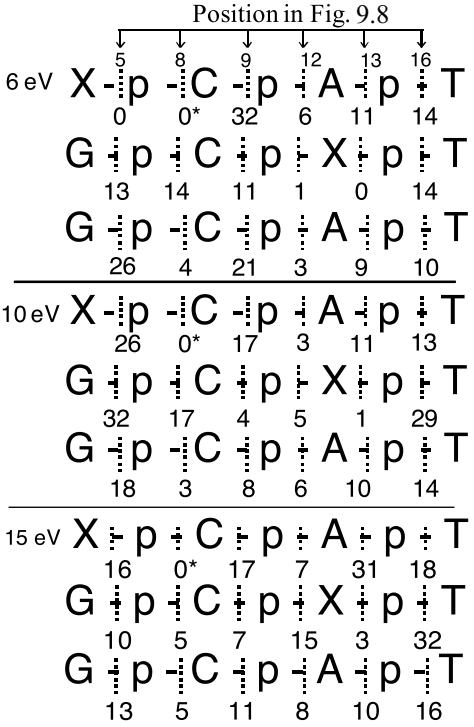

FIGURE 9.11. Percentage distribution of strand breaks by sites of cleavage, induced by 6-, 10-, and 15-eV electrons. *Xp was not detected by HPLC, and the yield was considered to lie below the detection limit.

backbone. In other words, the 6-eV resonance would decay by leaving one hole and one electron in a previously empty orbital on the base and the excess electron would be coupled to an empty σ^* CO orbital on the backbone via through-bond interaction. This hypothesis implies a strong decay of core-excited resonances into electronically inelastic channels, a phenomenon that has recently been demonstrated theoretically by Winstead and McKoy.[81] Zheng et al. denoted this decay channel as the "electron transfer channel." Energy-loss electrons could also transfer into π^* orbitals of adjacent bases, which lie in the range of 0.29 to 4.5 eV,[67] before transferring to the backbone. Thus, by resonance decay to the electron transfer channel following excitation of the bases, electrons having energies in the range for transfer[79] would be created and lead to C–O bond scission. If the transient anion and/or the final electronically excited state on the DNA base are dissociative, it could lead to scission of the *N*-glycosidic bond, thus causing base release or simply leaving DNA with a modified base. Alternatively, the transferring electron could temporarily localize at or near the *N*-glycosidic bond and form a shape resonance at a lower energy, which could be dissociative. In fact, the results in Table 9.2 may be representative of coupling of such electrons between the bases followed by scission of the *N*-glycosidic bond. They also reinforce the hypothesis of electron transfer to the phosphate group.

It is seen from Table 9.2 that removing a base in GCAT causes a drastic reduction in the quantity of damage at 6 and 10 eV. For example, at 6 eV, SB are reduced by a factor of about 6 and base release by a factor of 3.3 and 5 for GCXT and XCAT, respectively. In a classical picture, where the damage caused by electron capture by DNA bases is simply additive and rupture of all the *N*-glycosidic and C–O phosphodiester bonds are given the same probability, we would expect that the amount of SB and base release in the abasic tetramers to decrease by ∼25% (i.e., to be 3.57% and 1.47%, respectively). This nonlinear decrease in damage caused by introduction of an abasic site is also reflected in the yield functions from GCXT for all fragments recorded by Zheng et al.[78] This suggests that the magnitude of damage in GCAT is caused by a collective effect that appears to be strongly suppressed by removal of G or A. In other words, electron–molecule scattering within DNA must be highly sensitive to the number of bases and the overall topology of GCAT. Although we have no information on the topology of these tetramers, recent calculations of LEE-DNA scattering showed that the ordering of DNA bases, in a helical configuration within the molecule, strongly influences the electron capture probability by these components.[82, 83] More specifically, the electron capture probability by DNA bases for partial waves of certain momentum was found to increase up to one order of magnitude, owing to constructive interference of these partial waves within DNA.

The hypothesis that internally scattered electron waves in DNA would have a considerable influence on SB was recently tested in more extensive calculations by Caron et al.[84] These authors performed high-level R-matrix calculations of electron scattering from the DNA bases, which were next used as input parameters in multiple electron scattering calculations within dsDNA. The result they obtained for the average scattered electron current along the axis of A and B forms of DNA (i.e., inside DNA) is shown in Figure 9.12, as a function of the energy of electrons approaching perpendicular to the axis. For the A form, this current is found to maximize at 1.0 and 2.3 eV. The full curve exhibits two additional peaks at 5 and 7 eV, which if unresolved would produce a broad maximum around 6 eV. These results can be compared to those of experiments with thin films of DNA, where a peak appears at 6 eV in Figure 9.10a, shoulder appears at 6 eV in Figure 9.6, and the yield function for SSB exhibits maxima at 0.8 and 2.2 in Figure 9.7 and at 10 eV in Figures 9.6 and 9.10.[35, 37, 76, 85] In the analysis of LEE-induced products from tetramer films, the yield function for base release was also found to exhibit peaks at 6 and 10 eV.[76] As shown in Figures 9.5 and 9.6, below 15 eV the yield function for the induction of DSB was found to be dominated by a single peak located at 10 eV.[35, 36] Thus, by including both the shape resonance wavefunctions and constructive interference due to base stacking, the calculations of Caron et al.[84] can represent fairly well the energy dependence of the yield of SSB if we logically assume that the electron must be initially scattered inside DNA to produce most of the damage. The validity of the agreement between experiment and theory was tested by modifying DNA to its B form, which exists in solution but not in UHV. In this case, the two lower peaks move closer to each other and little correlation is found with the experimental values as seen by the dashed curve in Figure 9.12. Furthermore, the collective effect observed by Zheng et al. at 6 eV in their analysis of the products induced by LEE incident on GCAT and the

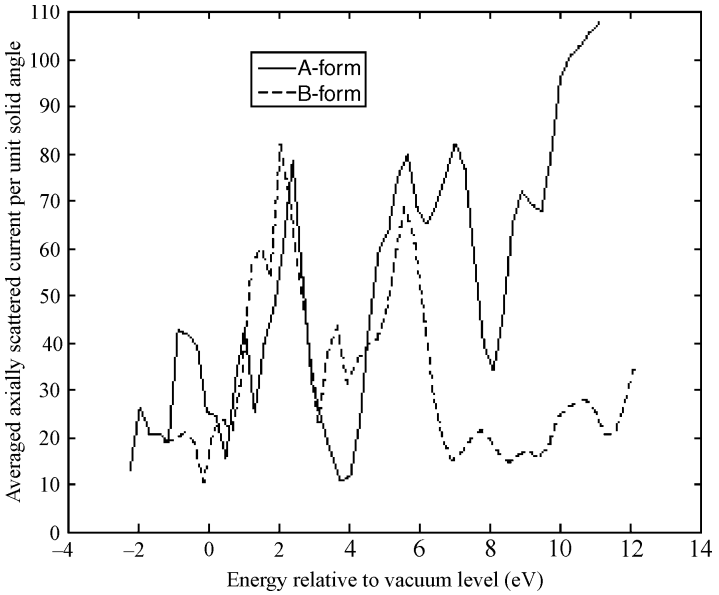

FIGURE 9.12. Electron energy dependence of the average axially scattered current for two mutually orthogonal electron beams incident on the decamers GCGAATTGGC in the A and B forms.

two abasic forms of the tetramer (see Table 9.2) could be related to coherent enhancement and strong electron scattering along the axis around 6 eV (Figure 9.12), which exhibits an eightfold increase in magnitude in going from 4 to 6 eV. *Such phenomena should be highly sensitive to base removal, since they are directly related to base stacking*.

The maximum at 10 eV in the electron energy dependence of the calculated axially scattered current averaged on all bases for the A form also correlates well with the strong maximum found experimentally in the yield function for SSB and DSB induced by LEE impact on plasmid DNA.[35, 36] However, the position of this peak was found to be highly sequence-dependent. Thus comparison with data obtained with plasmid DNA, which is longer and has a different sequence, was not considered to be valid by Caron et al.[84]

The results shown in Figure 9.12 may also provide some explanation for the relatively large cross section of 10^{-17} cm^2 per base pair[69] for damage caused by a single anion dissociative state at 0.8 and 2.2 eV, respectively. In fact, this value is almost as large as that measured at 100 eV in the same DNA where a plethora of ionization and dissociation channels are available.[36, 69] Coherent enhancement of the electron wavefunction within DNA seen in Figure 9.12 may therefore be responsible for increasing the electron capture cross section of transient anion states responsible for SSB at low energies.

Recently, Li et al. undertook a systematic study of 11-eV electron-induced damage to a small ss homo-oligonucleotide of increasing length.[86] The yields of products

arising from the reaction of LEE with dThd, pT, Tp, pTp, pTpT, TpTp, pTpTp, and TpTpT showed that the addition of a phosphate to the terminal positions of the monomers and dimers resulted in a considerable increase in total damage as estimated from HPLC analysis by UV absorption. Their results indicated that terminal phosphate groups efficiently capture 11-eV electrons and that these events caused considerable damage. This effect could be correlated to electron-beam experiments performed on thin films of NaH_2PO_4 [87] and tetrahydrofuran.[88] The results of these experiments show that the phosphate group has a very large cross section (10^{-15} cm^2)[87] for 7- to 12-eV electron-induced fragmentation, much larger than that of the furyl ring.[88, 89]

The finding that terminal phosphate groups increase total damage while decreasing base release and phosphodiester cleavage suggests that the initial capture of electrons by phosphate group does not lead to formation of transient anions that cause base release and phosphodiester cleavage. The work of Li et al.[86] therefore confirms the hypothesis[68] that the electron must first attach to the base in order to break the *N*-glycosidic bond or transfer to the P=O π^* to break the phosphodiester C–O bond. Furthermore, since continuous stretches of DNA do not have terminal phosphate groups, direct capture of LEE by the phosphate group followed by the formation of products from the phosphate should probably be considered as a minor process.

9.3.3. Self-Assembled Monolayers (SAM) of DNA

DNA damage has also been measured by LEE impact on SAM of the molecule. The cross section for the decomposition of oligonucleotides with the sequences $G_6T_3G_6$ and dT_{25} by $\sim$ 1-eV and 3-eV electrons was reported by Solomun et al.[90–92] The single-stranded oligonucleotides were immobilized on a gold surface in a microarray format. Before and after electron irradiation, the ssDNA was hybridized with its complementary strand labeled with a fluorescent molecular probe. The decomposition of the oligonucleotides was correlated with the decrease of the fluorescence signal after LEE bombardment. In the case of dT_{25}, Solomun et al. estimated (assuming 10^{13} oligonucleotides/cm^2) a value for the total damage cross section of about 1.5×10^{-16} cm^2 or 6×10^{-18} cm^2 per nucleotide at 1 eV[90] and 4×10^{-16} cm^2 or 1.6×10^{-17} cm^2 per nucleotide at 3 eV.[92] These values compare well with the cross section of 5×10^{-17} cm^2 (i.e., 4×10^{-18} cm^2 per nucleotide) at electron energy of 12 eV obtained by Dugal et al.[32] in measurements of neutral fragment desorption from SAM of single-stranded oligonucleotides made of 12 bases. The cross sections of Dugal et al. and Solomun et al. can also be compared to the average value of about 10^{-18} cm^2 per nucleotide from the experiment of Panajotovic et al.[69] on dsDNA. The smaller value obtained with DNA in the double-helix configuration may imply that ssDNA is more endangered during replication, transcription, or even translation stages than predicted by the current radiation damage models.

In a different type of experiment, Cai et al.[93] measured the induction of SB induced by electrons of 8–68 eV in SAM of oligonucleotides. From their results they extracted effective cross sections and attenuation lengths (AL) for SB. A 50-base-long thiolated oligonucleotide (OligoS), 5′-$(GCTA)_{12}GC(CH_2)_3$-SS-$(CH_2)_3$-OH-3′, was labeled at the 5′-end with ^{32}P and chemisorbed at 3′-sulfur(S) end onto a gold substrate.

The oriented OligoS layer,[94, 95] having its 5′-end lying at the film-vacuum interface, was exposed to electrons with a constant incident current of 50 ± 2 nA for 3–10 min. Radioactivity measurements of an irradiated portion of the 5′-oligonucleotide fragments (5′-OligoS-F) solution were first used to derive the total yield of LEE-induced 5′-OligoS-F, while the rest was concentrated. Fragments from concentrated 5′-OligoS-F were separated by electrophoresis and quantified by phosphor imaging. Molecular weight ladders for identification of the fragments were finally generated by random depurination. The results obtained from such manipulations, within the linear portion of the exposure response curve, showed that, after subtracting the background from sample manipulation, the percentage yield of LEE-induced 5′-OligoS-F decreased exponentially with increasing length. This dependence was observed for LEE energies of 8, 12, 18, 28, 38, 48, 58, and 68 eV. The results showed no significant base preference for SB, suggesting that above 12 eV, the mechanism for inducing SB is fairly independent of the nature of the bases or it operates on the sugar–phosphate backbone rather than the DNA bases. This result is consistent with the results of Zheng et al.,[78] discussed in the previous subsection, from which no sequence-dependent electron transfer mechanism could be inferred from yields of SSB recorded above 12 eV.

Considering that the effective current density for SB decreases exponentially as a function of the electron penetration depth,[96] Cai et al. derived the average effective cross section per nucleotide for producing SB and electron AL in these films.[93] The derived AL and cross sections are listed in Table 9.3. The cross section per nucleotide for SB from ssDNA at 12 eV has a magnitude of about 1.7×10^{-17} cm^2, which is essentially the same as that reported by Solomun et al.[92] at 1 eV for total damage, which could include forms of damage other than SB. This agreement lends confidence to the experiments of these two groups, particularly since according to the measurements of Panajotovic et al.,[69] the cross sections for SSB in DNA are similar at 3 and 10 eV. The value of the cross section obtained by Cai et al. (1.7×10^{-18} cm^2) for SSB in ssDNA induced by 12-eV electrons is nevertheless larger than that obtained at about

TABLE 9.3. Attenuation Length and Effective Cross Section for Strand Breaks (SB) in SAM of Oligonucleotides Chemisorbed on Gold as a Function of Electron Energy

Incident Electron Energy (eV)	Attenuation Length (nm)[a]	Effective Cross Section for SB ($\times 10^{-17}$ cm^2)[b]
8	2.5 ± 0.6	0.3 ± 0.1
12	1.9 ± 0.3	1.7 ± 0.5
18	1.6 ± 0.3	2.8 ± 0.9
28	1.5 ± 0.3	2.0 ± 0.7
38	1.2 ± 0.2	2.6 ± 0.8
48	1.0 ± 0.2	3.2 ± 1.1
58	1.0 ± 0.2	4.4 ± 1.4
68	0.8 ± 0.1	5.1 ± 1.6

[a]The errors represent the sum of the uncertainty range of the fitting parameter b and 10% absolute error in gel quantification.

[b]The errors represent the sum of the uncertainty range of the fitting parameter a and 25% absolute error in the measurements.

the same energy ($\sim 10^{-18}$ cm^2 per nucleotide) by Panajotovic et al.[69] in the case of multilayers of physisorbed dsDNA.

When renormalized to the more accurate cross section at 10 eV obtained by Panajotovic et al.,[69] the experimental cross sections for LEE-induced damage to DNA recorded by Boudaïffa et al.[30] give the following values: At 10, 30, and 50 eV, the cross sections per nucleotide in a five-layer-thick film of plasmid DNA become 1.7×10^{-18}, 1.9×10^{-18}, and 2.1×10^{-18} cm^2, respectively; that is, they are at least one order of magnitude lower than those derived by Cai et al.[93] at 8, 28, and 48 eV. The difference lies outside the error limits of both experiments and could here also indicate that ssDNA is more fragile toward LEE impact than dsDNA. Nevertheless, other reasons can be invoked to explain these differences. Since the results of Panajotovic et al. and Boudaïffa et al. were obtained with 5-ML film of DNA, they constitute an effective cross section, but not an absolute cross section per nucleotide. Such an effective cross section contains non-negligible contributions from energy-loss electrons. Furthermore, variation of film thickness and clustering as well as the lower purity in the plasmid experiment should lower the absolute cross sections. The different topology of an oligonucleotide versus a supercoiled plasmid of DNA may also contribute to the differences.

9.4. ELECTRON-STIMULATED DESORPTION (ESD) OF ANION RADICALS FROM DNA FILMS

9.4.1. Plasmid and Linear DNA

Further comprehension of the mechanisms leading to LEE-induced DNA damage came from the experiments of Pan et al.,[97] who directly measured ESD of anions from plasmid and 40-base-pair synthetic dsDNA within the 3- to 20-eV range. Resonant structures were observed with maxima at 9.4 ± 0.3, 9.2 ± 0.3, and 9.2 ± 0.3 eV, in the yield functions of H^-, O^-, and OH^-, respectively. The yield functions for H^- desorption, from synthetic and plasmid double-stranded DNA, are shown in Figures 9.13A and 9.13B, respectively. The yield functions for O^- and OH^- desorption exhibit a similar behavior. The prominent 9-eV feature observed in all anion yield functions is a typical signature of the DEA process. The maxima in the H^-, O^-, and OH^- yield functions from DNA can be correlated with the maximum seen between 8 and 10 eV in the SSB yield and the one occurring at 10 eV in the DSB yield induced by LEE impact on films of supercoiled DNA in Figure 9.5.[35,36] Curves C, D, and E in Figure 9.13 represent the yield functions for the desorption of H^- from films of thymine,[98] amorphous ice,[99] and α-tetrahydrofuryl alcohol.[100] The results obtained for the three other bases are similar to that shown for thymine.[98] Those obtained from THF and other DNA backbone sugar-like analogues[100] are essentially the same as the curve E in Figure 9.13. The H^- peak from amorphous water in D is too weak to be associated with DEA to the structural water of DNA. It is also found near 7 eV, an energy too low to be associated with the H^- peak from DNA, unless the strong hydrogen bonding in DNA[28] shifts the H_2O^-

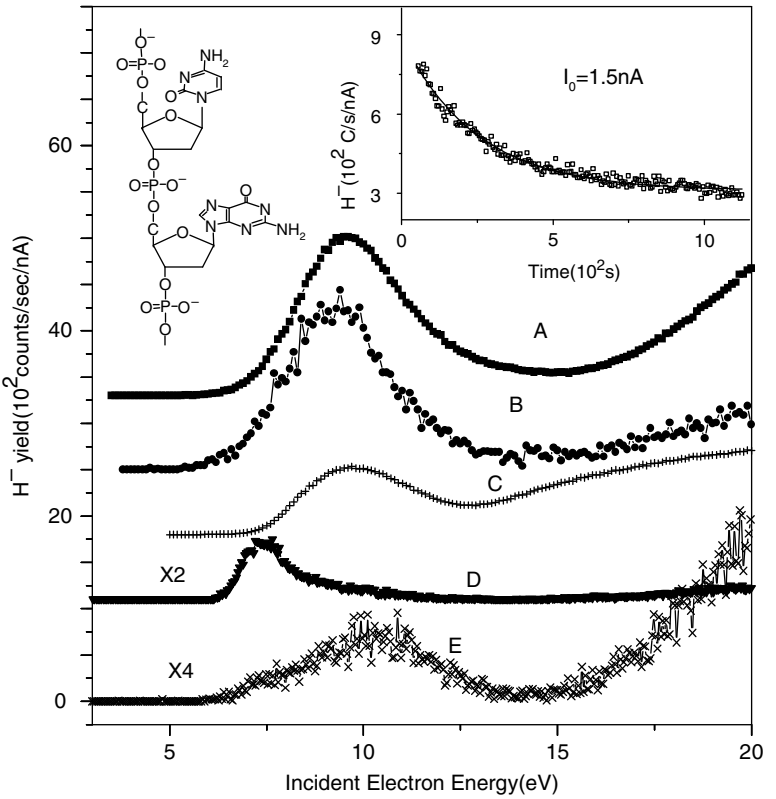

FIGURE 9.13. The H^- yield function from thin films of: (**A**) double-stranded linear DNA, 40 base pairs, (**B**) supercoiled plasmid DNA, (**C**) thymine, (**D**) ice, and (**E**) a deoxyribose analogue. The zero-count baseline of curves A–D has been displaced for clarity. The dependence of the magnitude of the H^- signal from DNA on time of exposure to the electron beam is shown in the insert.

resonance to a considerably higher energy. In contrast, comparison of curve C with curves A and B in Figure 9.13 indicates that the bases are an important source of desorbed H^- with an intensity about three times larger than the one arising from the sugar ring (curve E). A similar conclusion can be reached from comparison with gas-phase H^-/D^- abstraction from the carbon positions in thymine.[101] Hence, comparison of line shapes and magnitude of the yield functions in both phases suggests that LEE-induced H^- desorption from DNA below 15 eV occurs mainly via DEA to the bases with a possible contribution from the deoxyribose ring. Considering the results of Zheng et al.[76, 78] discussed in Section 9.3, we can conclude that when a transient anion forms on a base, it can decay either by DEA, leading to H^- production and base release or by electron transfer to the backbone.

Similar comparisons between the anion yield functions from basic DNA constituents and those of O^- and OH^- from DNA films[97] indicate that O^- production arises

from temporary electron localization on the phosphate group. The yield function for OH^- desorption resembles that of O^-, but has a lower intensity. As explained in the next section, detailed analysis of SAM of DNA indicates that the OH^- signal arises also from the phosphate group when the counterion is a proton.

9.4.2. SAM of DNA

ESD of anions from SAM of DNA was investigated by Pan and Sanche.[38] Their measurements, which were performed with thiolated DNA chemisorbed on gold, allowed both the mechanism and site of OH^- production to be determined. The following four different samples were prepared with 40-mer oligonucleotides 5′-GGT ACC AGG CCT ACT ACG ATT TAC GAG TAT AGC GAG CTC G-3′ with and without its complementary strand. A sulfur atom (1S) was substituted at one end of a backbone in the single (ss)- and double (ds)-stranded configurations (1S-ssDNA and 1S-dsDNA). In other samples, five sulfur atoms (5S) were substituted in the backbone in the ss and ds configurations (5S-ssDNA or 5S-dsDNA). Since the orientation of the DNA molecule with respect to the surface of the substrate depends on the anchoring position, when ssDNA or dsDNA is linked to the substrate at one end (3′ or 5′), the samples have a tendency to stand perpendicular to the gold surface.[102] On the other hand, when the 5S-ssDNA or 5S-dsDNA is anchored on the surface at five different positions along the chain, it lies parallel to the surface.[49] According to the molecular structure, the SAM of ssDNA have a terminal sugar with OH at the 3′ position, whereas in the case of dsDNA, one chain is terminated with OH's at the 3′ and 5′ positions of the sugar and the other has only one terminal sugar with OH at the 3′ position.

The yield functions of OH^- for the four different DNA SAM configurations are shown in curves A to D of Figure 9.14. They all have a threshold at about 2.0 eV, the lowest energy among all anions (i.e., H^-, O^-, OH^-, CH_2^-, CH_3^-, CN^-, OCN^-, $OCNH^-$) detected in this type of experiment.[103] The 1S SAM yield functions (curves A and B of Figure 9.14) consist essentially of a broad maximum located around 7 eV, whereas for the 5S SAM (curves C and D), superposition of peaks lying at 5.5 and 6.7 eV is observed followed by a very broad tail extending from 8 to 14 eV. In principle, OH^- could arise from temporary electron localization on a subunit of DNA or on H_2O molecules retained by DNA. However, purposely condensing D_2O molecules on these SAM considerably diminished the OD^- signal as seen from curve E in Figure 9.14, indicating that the OD^- electron-stimulated yield from additional D_2O is negligible. The OH^- signal could also arise from DEA to a molecule synthesized by the electron beam during the bombardment. In this case, however, the OH^- signal would increase as a function of time contrary to observation (see inset of Figure 9.14). Reactive scattering[21,22] could also occur from a reaction between the O^-, produced via DEA to the phosphate group, and the adjacent deoxyribose unit. In this case, the OH^- yield function would bear a resemblance to that for O^- production from which it is derived. In contrast, the O^- yield functions represented by curve F in Figure 9.14 are different from those shown in curves A to D. Since OH is present in DNA only at the terminal sugar and phosphate groups of the backbone, these comparisons leave the possibility

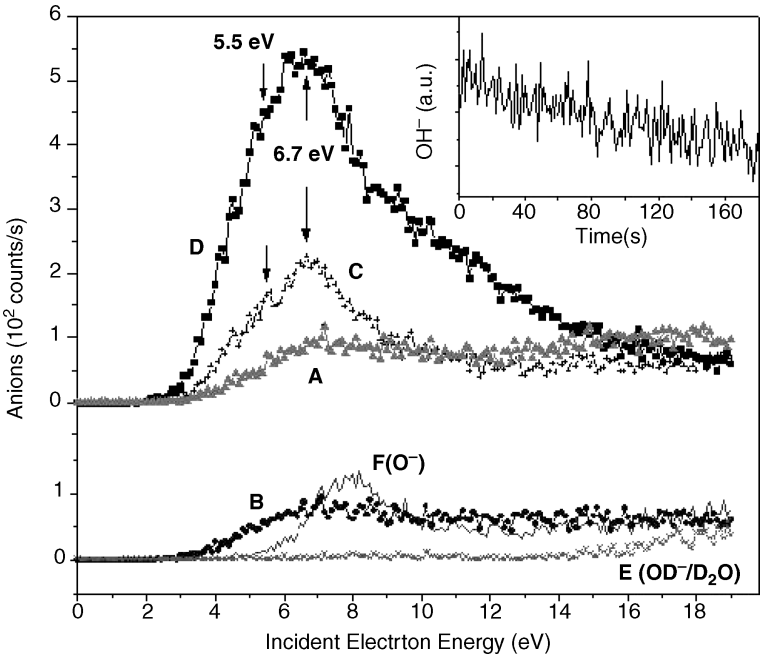

FIGURE 9.14. Dependence of the OH^- yields on incident electron energy for a SAM of (**A**) 1S-ssDNA, (**B**) 1S-dsDNA, (**C**) 5S-ssDNA; and (**D**) 5S-dsDNA. **E** represents the yield of desorbed OD^- from a six-monolayer water film on Pt, and **F** represents the desorbed O^- yield from a 5S-ds DNA film. The inset shows the time dependence of the OH^- signal from a 1S-ssDNA film recorded at an incident electron energy of 7 eV.

of dissociation of a local transient anion at these two positions—that is, DEA via the reactions

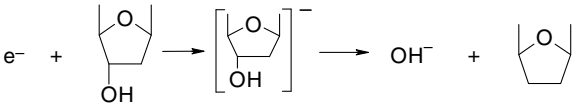

at the 3′ end,

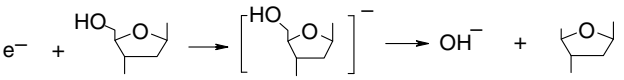

at the 5′ end, and

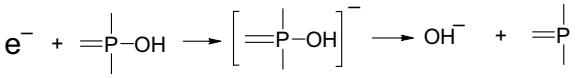

within the backbone.

Considering that the ESD technique is essentially sensitive to constituents near the vacuum–DNA interface, the first reaction would be favored for DNA standing

perpendicular to the gold surface, whereas the last reaction would be prominent for DNA lying parallel to the surface. The results of Figure 9.14 clearly show that the molecules parallel to the surface give the strongest signal. Thus, the last reaction is favored, indicating that below 19 eV, electron impact on DNA with OH in the phosphate unit (i.e., the phosphate with H^+ as a counterion) produces most of the OH^- via DEA to this unit in the backbone. The phosphate-counterion part of DNA therefore plays a significant role in LEE induced DNA damage.

9.4.3. The Oligonucleotide GCAT and Its Abasic Forms

ESD of anions from thin films of GCAT and its four abasic forms has been investigated by Ptasińska and Sanche.[104, 105] For all forms, the H^-, O^-, and OH^- yield functions between 6- and 12-eV impact energies exhibited resonant peaks indicative of DEA to the molecules. Above 14 eV, nonresonant DD dominated the ESD yields. The yield functions for OH^- from GCAT[104] and its abasic forms[105] are shown in Figure 9.15. Similar curves were obtained for H^- and O^- yields.[105] The differences in relative magnitude between GCAT and its abasic forms are illustrated in Table 9.4. The energy-integrated intensities between 3 and 15 eV are shown in this table, along with the relative yield of H^-, O^-, and OH^- from each abasic tetramer considering the yield from GCAT to be 100%.

In their studies, Ptasińska and Sanche[104] compared the anion yield functions obtained from GCAT to those recorded for corresponding anions from isolated subunits of DNA—that is, the nucleobases and sugar in the gas phase and the phosphate group in the condensed phase.[106–117] The DEA processes found in the gas phase were still present within GCAT, but DEA from some transient anions were suppressed, particularly at low energies, because of the existence of chemical and/or hydrogen bonds within DNA or insufficient kinetic energy of the dissociating stable anions to desorb from the film. Additionally, the surrounding medium was found to

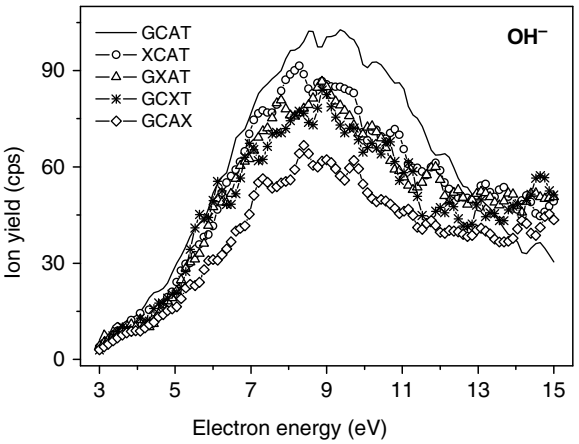

FIGURE 9.15. LEE-stimulated desorption yield of OH^- from the GCAT tetramer and its abasic forms.

TABLE 9.4. Measured H^-, O^-, and OH^- LEE-Induced Desorption Signals (in Arbitrary Units) from Thin Films of the Tetramer GCAT and Its Abasic forms[a]

	Form	Area (a.u)	(Percentage)
H^-	GCAT	702223.0	100
	XCAT	586589.6	83.5
	GXAT	591955.6	84.3
	GCXT	694797.8	99.0
	GCAX	621214.1	88.5
O^-	GCAT	752.2	100
	XCAT	545.9	72.6
	GXAT	581.0	77.2
	GCXT	667.4	88.7
	GCAX	519.4	69.1
OH^-	GCAT	716.4	100
	XCAT	643.8	89.9
	GXAT	613.1	85.6
	GCXT	589.2	82.3
	GCAX	466.9	65.2

[a]The percentage of the signal for each anion is given in the last column taking the yield from GCAT to be 100%.

favor specific dissociation processes (e.g., the formation of OH^-) that had not been observed in gas-phase studies. An example of comparison with gas-phase data from isolated bases is shown in Figure 9.16. This figure shows the CNO^- yield obtained from summing the signal from all bases in the gas phase [106, 107] along with that observed for GCAT films. The CNO^- anion was observed only for pyrimidines, C and T.[107] The lower-energy peaks seen in the gas-phase experiments are not observed in the case of the tetramer. Thus, it appears that CNO^- formations are inhibited by sugar bonding at the N1 position in DNA; however, the low kinetic energies of the CNO^- fragments could also prevent desorption from the surface.

In contrast to the yield of SB and base release, the magnitude of anion desorption does not depend very much on the presence of an abasic site in GCAT,[105] as seen from Table 9.4. From a purely classical point of view, if the anion signals arose exclusively from initial electron attachment on a base and if each base were given an equal weight for producing these anion yields, we should observe the anion signals from the abasic tetramers to be 75% of that from GCAT. For H^- the signal averaged for all abasic tetramers is higher (88%) than this value, whereas for O^- it averages close to 75%; for OH^- the averaged signal is 81% of that from GCAT. These results clearly indicate *the absence* of quantum interference or coherent effects in the interaction of the incident electron with DNA leading to DEA (i.e., the OH^- and O^- yields are merely proportional to the number of bases). The yield is on average remarkably higher than 75% for H^-. The additional contribution possibly arises from the sugar group, which is not expected to be considerably affected by the creation of an abasic site. In fact, in the results of experiments with 40-base pair and plasmid DNA, shown in Figure 9.13, the H^- signal is observed to arise from both the bases and the sugar

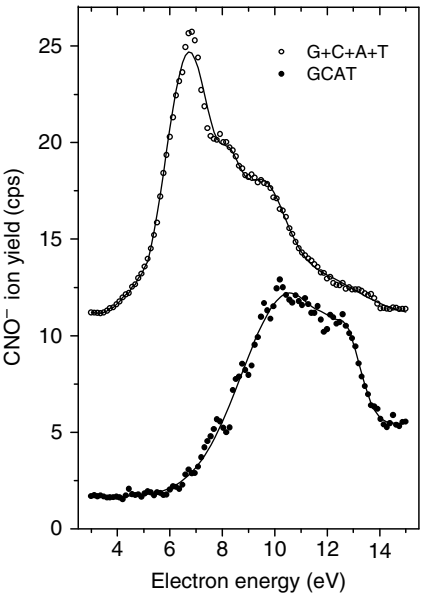

FIGURE 9.16. CNO^- ion yield function from a film of GCAT and the summation of ion yields for corresponding anions observed from nucleobases in the gas phase (G + C + A + T).

group.[97] The results of Figures 9.13 to 9.15 demonstrate that both the O^- and OH^- signals arise from DEA to the phosphate group. If such DEA processes arose only from direct attachment to the phosphate group, no significant decrease would be observed in the O^- and OH^- signals from the abasic tetramers in Table 9.4, unless the resonance parameters on the corresponding phosphate transient anion are severely affected by base removal. Thus, electron transfer may also be involved in OH^- and O^- desorption.

9.5. ESD OF NEUTRAL RADICALS FROM SHORT DNA STRANDS

Dugal et al.[32,33] and Abdoul-Carime et al.[34,49] measured the yields of neutral fragments induced by 1- to 30-eV electrons impinging on SAM of oligonucleotides made of 6–12 bases. The oligomers were chemisorbed lying flat on a gold surface via the sulfur-bonding technique described in Section 9.2.1. Their results showed that LEE-impact dissociation of DNA led mostly to the desorption of $CN^\bullet$, $OCN^\bullet$, and/or H_2NCN neutral species from the bases. No sugar moieties were detected, nor were any phosphorus-containing fragments or entire bases detected. These results were obtained from the MS measurements, explained in Section 9.2.3, of the partial pressure near the target during its bombardment in UHV by a 10^{-8}-A electron beam. In Figure 9.17, the black square and the white dots represent the electron-energy dependence of neutral $CN^\bullet$ and $OCN^\bullet$ (and/or H_2NCN) yields, respectively. The fragments desorbed per incident electron from oligomers[49] that consist of nine cytosine bases are shown in the upper panel; those desorbed from oligomers consisting of six cytosine and three thymine bases, C_6T_3, are shown in the lower panel. The curves

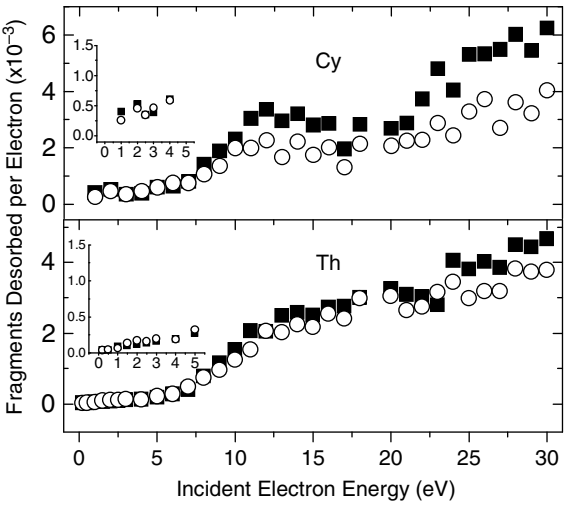

FIGURE 9.17. Incident-electron energy dependence of neutral CN (solid square) and OCN (and/or H_2NCN) (open circle) fragment desorption yields per incident electron from C_9 (**upper panel**) and C_6-$(T)_3$ (**bottom panel**) oligonucleotides chemisorbed on a gold substrate. The spread in the data is estimated to be 20%.

in Figure 9.17 present broad maxima superimposed on a smoothly rising signal. According to the explanation in the introduction, the continuously rising signal is due to direct electronic excitation (reactions 2 and 5 in Figure 9.1). The broad peak is due to resonant excitation to dissociative electronic neutral states (reactions 8, 11, 12) and DEA (reactions 8 and 10).[32, 34, 49] At such relatively high energies (i.e., from 7 to 15 eV for all oligomers), the broad maxima likely reflect the formation of core-excited resonances that are dissociative in the Franck–Condon region. This interpretation is supported by (1) the electron-energy losses in solid-phase DNA bases[80, 118] in the 7- to 15-eV range, which are attributed to the promotion of π- or σ-orbitals to higher-energy ones, and (2) the observation of resonant formation of H^- and CN^- at, respectively, 9–10 and 16 eV and 10–15 eV in the ESD yields from thin films of DNA bases.[98, 119] Moreover, the 5-eV threshold of neutral species production coincides with the threshold for electronic excitation. In summary, the results of Figure 9.17 indicate that transient anions formed on the DNA bases not only decay by DEA and electron transfer, but also can do so by electron emission outside DNA or transfer inside DNA while leaving the base in a dissociative electronically excited state, as inferred from the results of Zheng et al.[78] In such a process a single electron could cause base damage and a strand break by transfer to the phosphate group. Interestingly, in dsDNA, if interstrand electron transfer occurs or if the extra negative charge is canceled by interstrand proton transfer, the extra electron on the strand adjacent to the damaged base could trigger DEA on the phosphate group. *In this case, the two strands could be damaged with an electron of 10 eV or even lower energy.*

From the various results of Abdoul-Carime et al.,[32–34, 49, 120, 121] it has been possible to determine effective cross sections or absolute desorption yields per base for base damage induced by LEE impact on homo-oligonucleotides

(i.e., oligonucleotides that consist of only one type of base).[34, 49] As the strand length increased in homo-oligonucleotides from six to nine bases, a decrease in the yield per base was observed; that decrease was attributed to the greater probability of dissociation at the terminal bases.[49, 120] Above nine units, no change larger than 5% of the signal was found. This percentage lies below experimental uncertainties so that the probability of fragmentation of a given base in an oligo can be considered to be constant in strands that contain $\geq$9 bases. Thus, in a nonamer or longer oligonucleotide, such measurements provided an absolute determination of the sensitivity of a base to LEE impact. With these absolute yields, it became possible to calculate the expected yields for a specific hetero-oligonucleotide by simply adding the yield for each base contained in the strand. Such projected yields, for $\geq$9-mer oligonucleotides, necessarily assume that the damage is solely dependent on the chemical identity of the base and does not depend on the environment of the base or sequence. Experimentally, different results were obtained below 15 eV by Abdoul-Carime et al., indicating that the environment of the bases or their sequences play a role in DNA damage induced by LEE.[120, 121]

The production of neutral radicals was also measured by Tanabe et al.[40] from gaseous negatively charged oligonucleotides consisting of 2–14 bases. The damage was created by impact of 1- to 100-eV electrons on the oligonucleotides in merging beams within an electrostatic storage ring. The nature of the radicals was not identified, but the rate of neutral particles emitted in the collisions was measured as a function of one to four negative charges and number of bases in the oligonucleotide. The rate started to increase from definite threshold energies. These energies increased regularly with ion charges in steps of about 10 eV starting at about 10 eV for a single electron charge. They were almost independent of the length and sequence of DNA. The neutral radicals came from breaks of DNA, rather than from electron detachment.[40] The 10-eV step of the increasing threshold energy approximately agreed with the plasmon excitation energy.[122] From these experiments, Tanabe et al.[40] deduced that plasmon excitation is closely related to the reaction mechanism.

In a similar type of experiment, Tanabe et al.[123] investigated collisions between electrons of 1–15 eV and the deoxyoligonucleotide cations d (AA), d (GG), d (CC), d (TT), d (GA), d (AC), d (AT), d (GT), deoxyadenosine, and deoxyguanosine. They measured the yields of neutral-particle production *vs* electron energy. The results were compared with those obtained from longer homooligonucleotide cations containing up to four DNA bases. With compounds containing A and G, a strong resonance was observed around 4 eV in the neutral yield functions. In this case, the intermediate state is not a transient anion because the initial target is a ground-state cation. The resonance reaction they observed can be generally written as $e + M^+ \rightarrow M^* \rightarrow [M\text{-}f] + f$, where M^+ is the target cation, M^* is a transient doubly electronically excited state, and f denotes the unidentified fragment they detect along with the [M-f] residue. In their experiment, this resonance occurs when base stacking is present in the oligonucleotide. The more thymines there are present in the oligonucleotides, the more hampered the resonance, since the presence of thymines aborts base stacking in the systems they studied. The resonant electron excitations appear to be strongly coupled with conformational transitions.

9.6. FUTURE TRENDS AND MEDICAL APPLICATIONS

9.6.1. Cellular DNA

At the experimental level, our knowledge of LEE–DNA interactions is derived from a multitude of experiments with different target complexity, ranging from gaseous DNA subunits, or their analogues, to plasmid DNA. LEE damage to gaseous DNA subunits has been previously reviewed,[26] and LEE-induced damage to the range of short DNA strands to plasmid DNA is reviewed in this chapter. Such a range in target complexity is necessary to systematically understand how known fundamental principles of the interaction of LEE with simple molecules apply to more complex ones up to plasmid DNA containing over 6000 nucleotides. In fact, this approach must be extended to even more complex systems, if we are to understand fully LEE interactions with DNA in living cells.

Although the experiments with dry films of pure DNA and its basic constituents in vacuum are essential to unveil basic mechanisms of damage, they do not correspond to cellular conditions. It is now well established that the processes induced by LEE impact on a molecule are highly dependent on its environment. It is therefore crucial if we are to apply our knowledge of LEE–biomolecule interactions to practical problems in radiation protection and therapy to show how the fundamental mechanisms, derived from gaseous and thin film studies, are affected and modified within the environment of the cell. We therefore expect that, as the field evolves, the complexity of targets investigated under LEE bombardment will further increase, up to a point, where the action of LEE in cells can be deduced with appreciable certainty. The obvious next step toward a *systematic comprehension of cellular damage* appears to be the investigation of DNA in the presence of specific cell constituents, which lie close to or are bonded to DNA (i.e., water and histone and DNA-binding proteins). Research in this direction has recently been initiated by Ptasińska and Sanche[124] and Solomon and Skalicky.[92]

The former authors measured the yields of the anions H^-, O^-, and OH^- desorbed by 3- to 20-eV electrons from GCAT films under hydrated conditions.[124] They deposited 3 ml of water on GCAT films—an amount corresponding, on average, to 5.25 H_2O molecules per nucleotide at the surface of the oligomer film.[125] Assuming a uniform water distribution, such two-component films represent DNA with the addition of 60% of the first hydration shell. Below 15 eV, the anions were found to emanate principally from a new type of dissociative core-excited transient anions formed via electron capture by a DNA–H_2O complex. The formation of transient anions from GCAT–H_2O complexes was most obvious in the O^- and OH^- yield functions.

As an example, in Figure 9.18, the yield function for O^- desorbed from pure GCAT is compared to that from isotopically labeled D_2O/GCAT mixture films. The 9-eV resonance in GCAT (bottom curve) is replaced by a new one peaking near 11–12 eV (circles) and having a reduced width (i.e., 3.3-eV FWHM) compared to the 4-eV FWHM peak in the yield function for O^- desorption from GCAT. The possibility that O^- desorbs from weakly bonded water molecules can be excluded owing to the fact that (1) all yield functions (H^-, O^-, OH^-) for the H_2O/GCAT film do not resemble

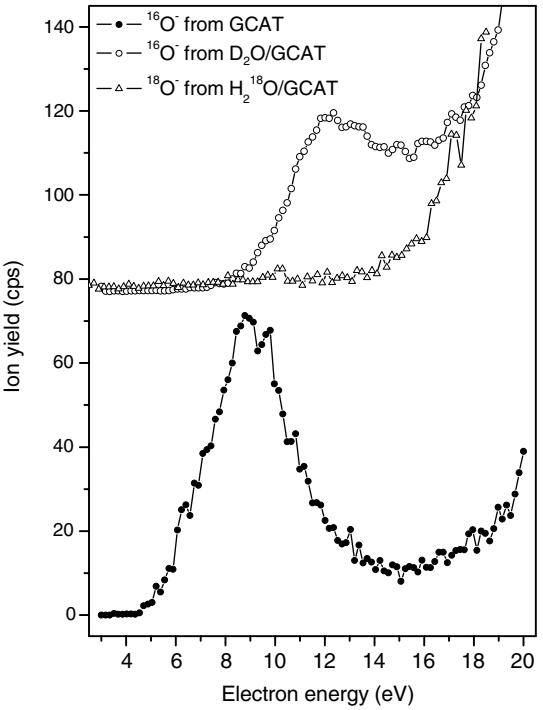

FIGURE 9.18. The O^- ion yield as a function of incident electron energy obtained from pure GCAT (*lower curve*), D_2O/GCAT, and $H_2{}^{18}O$/GCAT films. The baseline of the curves for anions desorbed from mixed films has been shifted vertically for clarity.

those observed from pure films of H_2O and D_2O;[99, 126] (2) the signals from mixture films decrease with exposure to the electron beam as opposed to that of pure water ice films[99]; and (3) the magnitudes of the O^- and OH^- yields[99] are much larger in the case of H_2O/GCAT mixture films.

As seen from Figure 9.18, when $^{18}O^-$ is measured from coverage of GCAT with $H_2{}^{18}O$, the 11- to 12-eV resonance completely disappears. Similar results were obtained with the OH^- signal: The $^{18}OH^-$ yield function did not exhibit a resonance peak for GCAT covered with $H_2{}^{18}O$. These results indicate that O^- and OH^- at 11–12 eV emanate from the complex—in the case of OH^-, with a hydrogen atom from the added water and, for desorption of both anions, an oxygen atom from GCAT. This conclusion is not surprising, since it is already known from the results of Figures 9.14 and 9.15 that LEE impact on dry desalted DNA results in OH^- desorption from the protonated phosphate group.[26, 38] As expected from the experiment of Falk et al.[127, 128] on the binding energy of water to DNA, the binding site of H_2O is located at the negatively charged oxygen of the phosphate group. Such a complex permits the formation of a transient anion located on the phosphate group having the nomenclature $O_2P–O^-H^{+(}$ (^{18}OH) for $H_2{}^{18}O$ deposition on GCAT. The transient anion dissociates

via the rupture of the P–O^- bond.[124] O^- desorbs leaving behind $H^{18}OH$. When hydrogen is retained by O^-, OH^- desorbs.

The investigations of Ptasińska and Sanche[124] further indicated that H^- desorbs upon LEE impact by dissociation of a transient anion of the complex, thus causing bond cleavage on the H_2O portion at this site. Hence, both H_2O and the tetramer are perturbed by their mutual binding interaction and consequently the stable anions resulting from temporary electron attachment. The signature of the perturbation imposed on the tetramer portion is seen in the O^- and OH^- yield functions, whereas that imposed on the H_2O molecule appears in the H^- signal. Interestingly, in these experiments DNA was not shielded by the water overlayers; on the contrary, the DEA yields increased by a factor of 1.6 on average.

The effect of protein binding to DNA on total damage induced by 3-eV electrons was recently investigated by Solomon and Skalicky.[92] Using the SAM technique, HPLC purified thiolated oligonucleotides with the structure 5′-SH-$(CH_2)_6$-$(dT)_{25}$-3′ were deposited onto gold-coated glass chips resulting in immobilized ssDNA monolayers about 4 nm thick. A fluorescent dye-marked complementary strand, Cy5-dA_{25}, was used as a probe to monitor DNA damage. If hybridization occurred, $(dT)_{25}$ was considered to be intact, so that monitoring the fluorescence intensity from the probe on the chip after LEE bombardment allowed these authors to measure the yield of damage versus fluence as explained in Section 9.3.3. Such exposure curves were obtained for the oligonucleotide with and without binding of the single-strand binding *E. coli* protein. The cross sections for total damage were found to be 1.6×10^{-17} cm^2/nucleotide and 3.8×10^{-18} cm^2/nucleotide in the case of pure DNA and the protein–DNA complex, respectively. Since the two molecules in the complex are tightly wrapped around each other, this fourfold decrease in damage may simply be due to the physical shielding of the oligonucleotide by the protein against LEE impact. However, it is also possible that a portion of this protective effect arises from the bonding interaction between the two molecules. Since at 3 eV the only mechanism that leads to bond breaking in DNA is DEA, such a binding interaction could decrease LEE-induced damage via a reduction of the lifetime and capture cross section of the transient anion involved in the process.

Another way to get closer to cellular conditions may be to develop techniques to investigate LEE-induced DNA damage under atmospheric conditions corresponding to different levels of hydration. Such conditions are quite different from those of UHV, where DNA retains only structural H_2O (i.e., two water molecules per nucleotide) within its structure and thus adopts the compressed A-form. Cellular DNA is mainly in the B-form and contains about 20 bound water molecules per nucleotide in the first ($\Gamma < 9$; Γ is defined as the number of water molecules per nucleotide) and second ($9 < \Gamma < 20$) layers of hydration.[29, 125] The first layer consists of contiguous surface water, while the second layer represents amorphous water.

Cai et al.[129] have already developed a technique to investigate DNA damage resulting from SE emission from a metal surface exposed to soft X rays in ambient atmosphere. Thick and thin films of pGEM®-3Zf(−) plasmid DNA deposited on a tantalum foil were exposed to soft X rays of effective energy of 14.8 keV for various times in air under controlled relative humidities ($\Gamma \approx 6$ and 21). In the thick film, DNA

damage was induced chiefly by X-ray photons whereas in the thin film, essentially only X-ray-induced SE emitted from the tantalum produced the damage to DNA. The SE emission from the metal was found to enhance the yields for SSB, DSB, and CL by a factor of 3.8 ± 0.5, 2.9 ± 0.7, and 7 ± 3 at $\Gamma \approx 6$ and 6.0 ± 0.8, 7 ± 1, and 3.9 ± 0.9 at $\Gamma \approx 21$, respectively. Unfortunately, with 14.8-keV mean energy photons incident on a metal, the SE emitted have wide energy distribution that contains both high and LEE. Lower X-ray energy sources ($E < 1.5$ keV), which emit essentially LEE, are presently being developed for operation in ambient or controlled atmospheres.[130] Irradiation of thin DNA films with SE emitted from such a source should make possible the investigation of LEE interactions under atmospheric conditions.

Another promising approach to investigate LEE-induced damage to DNA, in environments closer to those of the cell, resides in the use of an STM tip as an electron source.[45, 57] With STM, the electron energy is not well-defined as in the case of SE from a metal bombarded with X rays, but the upper limit of electron energy can be varied by changing the bias voltage on the tip. STM images of LEE damage to DNA in air have already been reported.[45, 57] Further investigations are now needed to solve problems related to identification and quantification of the damage.

Finally, it should be mentioned that there seems to be no major technical problem in performing experiments with cells under high-vacuum conditions to investigate the basic mechanisms of LEE-induced damage, as recently shown by Ptasińska and Sanche.[131] These authors measured the electron energy dependence of ion yields of the anions H^-, CH_3^-/NH^-, O^-/NH_2^-, and OH^- from whole dried samples of human blood and red blood cell under high vacuum. The yield functions exhibited resonant structures that could be attributed to DEA.

9.6.2. Application to Diagnostic Procedures

The major impetus to investigate the processes induced by LEE within DNA has arisen from their potential role in radiosensitivity. Since LEE possess a large portion of the energy deposited by high-energy radiation, any modification of their energy deposits at crucial cellular sites is expected to have a strong radioprotective or radiosensitizing action. Thus, parameters that affect LEE-induced DNA damage are expected to be highly relevant to radiotherapy and radioprotection, including estimates of cellular damage induced in medical diagnostic procedures using high-energy radiation.

For example, studies with X ray of the type[129] suggested in Section 9.6.1 may provide a molecular basis for understanding the enhanced biological effects at interfaces in the presence of high-molecular-weight (i.e., high-Z) materials, such as metal prosthesis, during diagnostic X-ray procedures. At the interface between the metal and tissue, the dose may become quite high due to SE of low energy, which interact mostly near the interface. Taking only the dose imparted by the slow SE emitted from a tantalum substrate, LEE enhancement factors (LEEEF) for monolayer DNA deposited on tantalum can be estimated from the data of Cai et al.[27] Here the LEEEF is defined as the ratio of the yield of products in monolayer DNA induced by the LEE (slow SE, $E \leq 10$ eV) emitted from the metal substrate versus the yield of products induced by the photons. The LEEEF for 1.5-keV photons was derived by

Cai et al.[27] to be at least 0.2 for both SSB and DSB from X-ray-generated photoelectron experiments with plasmid DNA deposited on tantalum. This value is low but, as the energy of X rays increases, the attenuation in single-layered DNA decreases, such that the contribution of SE from the metal to the yield of products becomes concomitantly larger. Extrapolation of the LEEEF at higher X-ray energies was made by considering the X-ray absorption coefficient, the total quantum yield of LEE on photon energy,[132] and the spectrum for LEE obtained *versus* photon energy.[133] The extrapolated LEEEF for X rays from 1.5 keV to 150 keV (i.e., to energies of medical diagnostic X rays) indicates that SE emitted from tantalum with an average energy of ~5 eV are 20–30 times more efficient in damaging DNA than are X-ray photons of 40–130 keV. This result indicates that LEE may be involved in the loosening of metal implants from the bio-organic linker of patients undergoing X-ray diagnostic procedures.

9.6.3. Application to Radiotherapy: Bromouracil (BrU)

Fifty years ago, Zemenhof, DeGiovanni, and Greer[134] observed that bacterial cells containing DNA in which thymidine has been replaced by BrdU become more sensitive to ionizing radiation. This report led to an important application: the treatment of tumors by combining incorporation of halogenated pyrimidines into DNA with exposure to ionizing radiation. Since then, much work has been devoted to understanding the detailed mechanisms by which such radiosensitizers operate. One of the proposed mechanisms involves the role of hydrated electrons, which are generated in aqueous irradiated biological systems. It was suggested that these hydrated electrons first reduce the halouracil molecules to form $(\text{halouracil})^-$, followed by dissociation of this anionic species into the corresponding stable halogen anion and the reactive uracil-5-yl radical.[135, 136] These reactive radicals then enhance DNA damage and strand breaks.[137, 138] Thus, the substitution of the CH_3 group in thymine by a halogen atom may substantially enhance radiation damage to DNA via its reaction with thermalized electrons.

Following early investigations with solvated electrons, a relatively large number of experiments have been performed both in the gas[139–145] and condensed phases[146–148] to study the interaction of LEE with halogenated pyrimidines. Similar experiments were also performed with SAM of BrdU-containing oligonucleotides.[33, 34, 49] Measurements have included not only mass spectrometric detection of the yields of ion and neutral species induced by LEE impact, but also recordings of electronic and vibrational HREEL spectra from gaseous bromouracil.[140] All experiments with bromouracil clearly indicated that the radiosensitivity of bromouracil is much more complex than previously anticipated. Resonant electron mechanisms lead to complex molecular decompositions over the entire electron energy range between 0 and 7 eV, and they induce formation of different anions and radical fragments (compared to thymine) via different dissociation pathways. If formed within DNA, some of these fragments may react and thus lead to lethal clustered damage in addition to that already occurring in unsensitized DNA.

Perhaps the most striking evidence of the huge enhancement of LEE damage obtained from Br substitution lies in the early results of Klyachko et al.[146] shown in

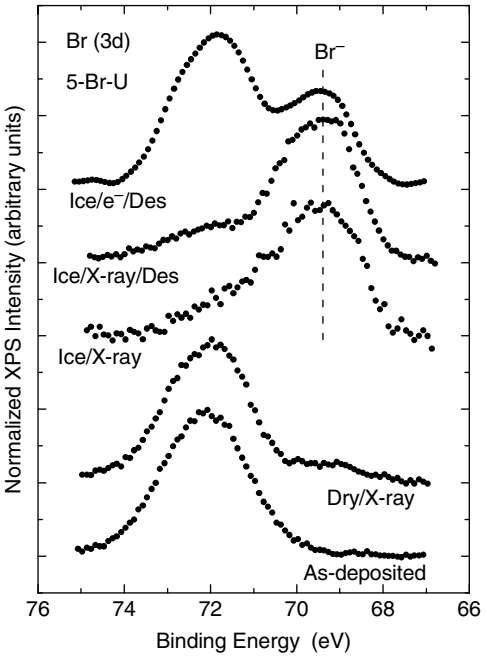

FIGURE 9.19. The XPS spectra of Br(3*d*) in 5-BrU. The XPS spectra are presented from bottom to top: Freshly deposited dry film, dry film irradiated with X rays, wet film irradiated with X rays, wet film irradiated with X rays and measured after water desorption, and wet film irradiated with LEE and measured after water desorption. Vertical lines mark the peaks of halogen anions.

Figure 9.19. This figure exhibits the X-ray photoelectron spectra of bromouracil films of different preparations deposited on a MoS_2 substrate. The bottom curve was recorded from an unirradiated ~100-Å film of bromouracil. The upper curve was recorded after exposure to 2×10^{16} electrons/cm^2 of 3 eV and the others after exposure to 6×10^{16} photons/cm^2. The peak at 72-eV binding energy corresponds to the photoelectron distribution emitted from the Br(3*d*) level in bromouracil. The curve labeled Dry/X-ray was obtained from the same film bombarded essentially by the SE of low energies emitted from the MoS_2 substrate. It exhibits an additional peak at 69.4 eV corresponding to the $Br^-(3d)$ level. The two other curves labeled Ice/X-ray and Ice/X-ray/Des were obtained from ~100-Å films made of intercalated alternative layers of water ice and bromouracil. In this case, the X-ray Br(3*d*) signal almost completely disappears and is replaced by the signal from the $Br^-(3d)$ level. To produce the Ice/X-ray/Des and Ice/e^-/Des curves, the H_2O molecules were evaporated from the sample before XPS analysis. Klyachko et al.[146] estimated from these results the effective cross sections for Br^- production. For the dry samples they obtained a value of 9×10^{-19} cm^2, which increased to 2×10^{-16} cm^2 for LEE bombardment of wet samples. From the latter value and the distribution of SE from the substrate, a lower limit of 10^{-15} cm^2 can be estimated from their data for Br^- formation via DEA to

bromouracil assuming that the distribution of SE from the substrate peaks at 1.4 eV as in the experiment of Cai et al.[27]

Thus, the sensitization properties of halouracils are related not only to hydrated electrons, but also to low-energy SE via DEA. However, according to theory,[149] *the high propensity of LEE to fragment bromouracil and deoxybromouridine (BrUdR) at very low energy (<1 eV) may only exist in single-stranded DNA*. This theoretical prediction was confirmed for the case of solvated electrons by Cecchini et al.[150] Single- and double-stranded oligonucleotides, as well as DNA containing mismatch bubble regions, were irradiated with γ rays in a solution where the different radicals produced could be controlled by scavengers. Such a control allowed these researchers to investigate the action of solvated electrons and determine the effects of BrUdR substitution for thymidine in these DNA targets. *BrUdR did not sensitize complementary double-stranded DNA, but it greatly sensitized single-stranded DNA*. However, when the BrUdR was present in a single-stranded bubble of a double-stranded oligonucleotide, the non-base-paired nucleotides adjacent to the BrUdR as well as several unpaired sites on the opposite unsubstituted strand were strongly sensitized. Since LEE and solvated electrons fragment BrUdR by the same fundamental DEA mechanism,[135, 147–149, 151] these results suggest that the strong radiosensitizing action of such electrons is likely limited to single-stranded regions, such as those found in transcription bubbles, replication forks, DNA bulges, and the loop region of telomeres.

These findings may have profound implications for the clinical use of BrUdR as a radiosensitizer as well as for the development of targeted radiosensitizers.[150, 152] When injected into a patient, BrUdR quickly replaces thymidine in the DNA of fast growing cancer cells. If afterward the patient is administered ionizing radiation, the damage resulting from the presence of BrUdR in the parental strand of tumoral DNA at replication forks during irradiation should be distributed randomly in the genome in a population of asynchronously replicating cells. However, administering another drug to increase the S-phase cycle of the cancer cells (i.e., the replication cycle) should increase the probability of exposure of bromouracil in its ssDNA form. Such a modality, derived from a fundamental understanding of radiosensitivity, is therefore expected to increase the efficiency of BrUdR as a radiosensitizer in cancer treatment.

9.6.4. Application to Radiotherapy: Gold Nanoparticles (GNP)

Recently, there has been considerable interest in the potential use of GNP as radiosensitizers in the treatment of cancer with ionizing radiation.[153–155] For such treatments, GNP have two interesting properties: They increase the absorption of radiation energy and, for diameters near 2 nm, they accumulate preferentially in cancer cells.[156, 157] Hainfeld et al.[158] demonstrated that EMT-6 mammary tumors implanted in BALB/c mice, which received an intravenous injection of 1.35 g GNP/kg, could be completely eradicated 30 days after irradiation with 250-kVp X rays, whereas in the control animals, only injected with GNP, the tumor continued to grow at the same rate as with no treatment. X-ray radiation alone only slowed down tumor. This impressive result showed the ability of 110-keV average energy X rays to destroy

tumor cells efficiently and preferentially in the presence of GNP. Although the mechanisms leading to tumor regression in the study of Hainfeld et al.[158] were not identified, it was obvious that a larger portion of the energy of the primary ionizing photons is transferred to the tumor due to the increased absorption of X rays by GNP.

Unfortunately, the amount of GNP (1.35 g/kg) administered to mice in the experiments of Hainfeld et al.[158] is much too large for application in radiotherapy. Moreover, treatment with low-energy photons is not common; patients are usually irradiated with 1- to 18-MeV photons from cobalt sources or electron accelerators.[7] Thus, for GNP to have potential for general use in radiotherapy, the amount administered to the tumor must be decreased considerably while maintaining as large as possible the radiosensitizing effect. Furthermore, the radiobiological effectiveness of GNP needs to be high for 1- to 18-MeV radiation. In practice, the first condition may be met by targeting GNP to the nucleus, particularly the DNA of cancer cells. The second condition depends on the mechanisms responsible for the large decrease in the tumor volume after X-ray irradiation observed in mice that were treated with GNP.[158] For instance, sensitivity to radiation could be increased by the binding of GNP to DNA. Alternatively, the presence of GNP could cause an increase in the production of short-range secondary particles having penetration depths similar to the diameter of the DNA molecule. In both these scenarios, the attachment of GNP to DNA could increase the local effect through enhanced DNA damage.

These questions prompted considerable effort to understand DNA damage in the presence of GNP. Foley et al.[159] investigated the indirect effect of radiation (i.e., essentially DNA damage induced by OH radicals). Supercoiled DNA in solution bound to GNP in a GNP:DNA ratio of 100 : 1 was irradiated by 100 kVp X. The maximum enhancement in damage was about a factor of two for doses of 0.5 to 2 Gy, in good agreement with the dose calculations of Cho.[160] The X-ray source used by Foley et al.[159] emitted a continuum of photons in the range 10–100 keV.

Later, Carter et al.[161] also investigated the indirect effect of radiation. A Monte Carlo method was developed to investigate the generation and transport of electrons in plasmid DNA dissolved in water. They chose to model the small gold nanoparticles that were available experimentally (3-nm-gold nanoparticles) chemisorbed on DNA [$\sim$500-nm-long and 1.5-nm-diameter supercoiled DNA (scDNA)]. In the simulation, X rays from a 100-kVp tungsten source interacted directly with water and gold. They also probed experimentally the nanoscale spatial profile of energy deposition created by GNP in aqueous solution with the inclusion of radical scavengers in the solution to reduce the diffusion distance of hydroxyl radicals, all the way down to a few nanometers or less from DNA. The resolution afforded by the scavengers makes it possible to characterize the profile of electron energy deposition of the GNP. The average calculated enhancement of DNA damage due to GNP caused by hydroxyl radicals was found to be $\sim$20%, which was much lower than that observed experimentally (150%).

The direct effect of radiation (i.e., DNA damage by LEE and other secondary products formed from the initial radiation interaction with DNA) was investigated by Zheng et al.[162] Thin films of pGEM-3Zf(−) plasmid DNA were bombarded by 60-keV electrons with and without bonded GNP. DNA SSBs and DSBs were measured by

agarose gel electrophoresis. The probabilities for formation of SSBs and DSBs from exposure of 1 : 1 and 2 : 1 gold nanoparticle:plasmid mixtures to fast electrons increased by a factor of about 2.5 compared to neat DNA samples. For monolayer DNA adsorbed on a thick gold substrate, the damage increased by an order of magnitude. The results suggested that the enhancement of radiosensitivity is due to the production of additional low-energy secondary electrons caused by the increased absorption of ionizing radiation energy by the metal, in the form of GNP or a thick gold substrate. Since LEE are created in large numbers by any kind of ionizing radiation, the authors concluded that *the radiosensitizing properties of GNP should be universal and should exist for any type of high-energy radiation, including the 1- to 18-MeV photon beams commonly used in radiotherapy*. Furthermore, since on average only one GNP per DNA molecule was needed to obtain the increase in damage, the results of Zheng et al.[162] indicate that the targeting of the DNA of cancer cells with GNP may offer a novel approach applicable to radiotherapy treatments.

9.7. CONCLUSIONS

Considering the results reviewed in the present chapter and those from various theoretical calculations, it now appears possible to provide a unified model of relatively complex electron interaction with DNA in the 0- to 15-eV range, which is consistent with all observations and calculations. *A priori*, the incoming electron can scatter directly from DNA or via the formation of transient anions. However, owing to the wave nature of the electron and the topology and size of the DNA, electron scattering from DNA is more complex below 15 eV. In this energy range, with the exception of neutral radical formation, LEE-induced damage proceeds essentially via resonance scattering preceded or not by electron diffraction. In its first encounter with DNA, the incoming electron can interact simultaneously with a number of successive DNA subunits. Depending on electron energy, topology of the DNA, and surrounding medium, this interaction results in constructive or destructive interference of the electron wavefunction. The effect of constructive interference is more pronounced at very low energies ($E_0 < 4$ eV), where the electron wavelength compares to the inter-unit distances within DNA (3–4 nm). As diffraction takes place, the additional electron can localize on a subunit (SU) and form a local transient anion $[SU]^-$, which can be a shape, a core-excited, or a core-excited shape resonance. At energies well below the first electronically excited states of DNA, only shape resonance can be produced and it is in this energy range that shape resonances possess a sufficiently long lifetime to cause dissociation of molecular bonds via DEA. *In fact, since electronic excitation is not possible, the only mechanism capable of breaking bonds is DEA*. At energies close to and above that required to produce the first electronically excited state, core-excited, and core-excited shape resonances can be formed. Both types of transient anions are well localized on specific SU, since their motion within the molecule requires a three-electron jump. On the other hand, shape resonances are considered to be too short-lived at these higher energies to cause dissociation. *Thus, above the*

electronic excitation threshold, core-excited resonances are usually considered to be responsible for DEA

Core-excited resonances can decay into:

1. the elastic channel $[e(E_0) + \mathrm{SU} \rightarrow \mathrm{SU}^- \rightarrow \mathrm{SU} + e(E_0)]$,
2. inelastic channels $[e(E_0) + \mathrm{SU} \rightarrow \mathrm{SU}^- \rightarrow \mathrm{SU}^* + e(E)]$, and
3. DEA $[e(E_0) + \mathrm{SU} \rightarrow \mathrm{SU}^- \rightarrow (\mathrm{SU} - \mathrm{F}) + \mathrm{F}^-$ or $e(E_0) + \mathrm{SU} \rightarrow \mathrm{SU}^- \rightarrow (\mathrm{SU} - \mathrm{F})^- + \mathrm{F}]$,

where F denotes a fragment]. In case 2 the additional electron of initial energy E_0 and final energy E leaves the SU in an excited state of energy $E_0 - E$. If SU^* is an electronically excited dissociative state, then bond scission can occur $[\mathrm{SU}^* \rightarrow (\mathrm{SU} - \mathrm{F}) + \mathrm{F}]$. Thus, both DEA and electronically inelastic decay channels can directly break bonds within DNA. Such bond scissions can lead to the production of small reactive neutral and anion radicals and base release or simply be limited to rupture of the backbone of DNA.

Owing to the possibility of nonthermal electron transfer, bond dissociation within DNA cannot be explained only in terms of immediate resonance decay via channels (2) and (3). In other words, the SU that initially captures the electron is not necessarily the one that dissociates due to the presence of an additional electron. According to experimental and theoretical evidence, the incoming electron has a high probability of being first captured by a base and thereafter following the pathways depicted in Figure 9.20. As shown in this figure, the incoming electron first forms a transient anion of a base at an energy E_0. The transient anion can decay into the three previously mentioned channels (1, 2, and 3 in Figure 9.20), but in cases 1 and 2 the electron can be emitted into the continuum (e_c^-) or transferred (e_t^-) within DNA. The branching ratios between these two possibilities depend on the matching of the departing electron wavefunction to the electron states of the continuum and those within the DNA. As mentioned previously, owing to internal diffraction, the magnitude of the square of the

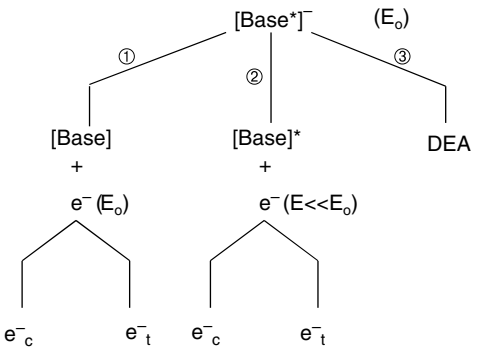

FIGURE 9.20. Decay channels of a transient anion formed on a DNA base.

electron wavefunction can be much larger at very low energies. Thus, we expect the "electron transfer channel" to be strongly favored below 4 eV; whereas at higher energies (e.g., $E_0 > 7$ eV), autoionization into the continuum should considerably increase. Thus electron transfer has a high probability to proceed via pathway 1 in Figure 9.20 for $E_0 < 4$ eV or via pathway 2 as long as electrons reduce their energy below 4 eV (i.e., $E < 4$ eV) by exciting electronically a base. *According to the results presented in this chapter, electron transfer occurs from the base to the phosphate group of the backbone*: A large portion of the H^- yield is produced via DEA to DNA (channel 3), whereas the O^- and OH^- yields can be produced via channel 1, followed by electron transfer to the phosphate group which undergoes DEA. Below 4 eV, SSB are produced via channel 1 followed by electron transfer to the phosphate group and DEA, leading to C–O bond scission. At higher energies, channel 2 becomes accessible to produce electrons of lower energies which can repeat the process just described for $E_0 < 4$ eV.

The strong decrease in strand break and base release, previously observed at 6-eV electron energy upon formation of an abasic site in ssDNA, can be explained from decay into channel 2. Via this channel, highly coherent lower-energy electrons whose wavefunctions are highly sensitive to the molecular arrangement of the oligonucleotide are emitted within DNA. When electron coherence is reduced or destroyed within DNA, owing to molecular rearrangement following creation of an abasic site, electron emission in the continuum is considerably increased followed by a corresponding large decrease in bond scission within DNA, as observed in the experiments of Zheng et al.[78] As a general rule, creating very LEE within DNA has a tendency to be followed by electron transfer to the backbone and cause rupture of the C–O bond. Owing to the high sensitivity of the amplitude of the electron wavefunction to diffraction, below 4 eV the damage becomes highly sensitive to the topology of DNA.

ACKNOWLEDGMENTS

The writing of this review chapter was financed by the Canadian Institutes of Health Research (CIHR). The author would like to thank Francine Lussier for her skilled assistance in the preparation of this manuscript, and he is grateful to Drs. Marc Michaud and David R. Haines for helpful suggestions and corrections.

ABBREVIATIONS

A	Adenine
AFM	Atomic force microscope
AL	Attenuation lengths
BrU	Bromouracil
BUdR	Deoxybromouridine

C	Cytosine
CL	Cross-links
d	Deoxyribose
DD	Dipolar dissociation
DEA	Dissociative electron attachment
DNA	Deoxyribonucleic acid
ds	Double strand
DSB	Double-strand break(s)
ESD	Electron-stimulated desorption
eV	Electron volts
FWHM	Full width at half-maximum
G	Guanine
GNP	Gold nanoparticles
HPLC	High-performance liquid chromatography
HREEL	High-resolution electron energy loss
keV	Kilo-electron volts
LEE	Low-energy electron(s) (0–30 eV)
LEEEF	Low-energy electron enhancement factor
MFP	Mean free path(s)
ML	Monolayer(s)
MS	Mass spectrometer
p	Phosphate
SAM	Self-assembled monolayer(s)
SB	Strand breaks
SE	Secondary electron(s)
ss	Single strand
SSB	Single-strand break(s)
STM	Scanning tunneling microscope
SU	Subunit
T	Thymine
THF	Tetrahydrofuran
UHV	Ultra-high vacuum
UV	Ultraviolet

REFERENCES

1. von Sonntag, C. *The Chemical Basis for Radiation Biology*; Taylor and Francis, London, 1987.
2. Mott, N. F.; Massey, H. S. W. *Theory of Atomic Collisions*; Clarendon, Oxford, 1965.
3. Inokuti, M.; Itikawa, Y.; Turner, J. E. Addenda: Inelastic collisions of fast charged particles with atoms and molecules—The Bethe theory revisited. *Rev. Mod. Phys.* **1978**, *50*, 23–35.
4. Inokuti, M. Inelastic collisions of fast charged particles with atoms and molecules—The Bethe theory revisited. *Rev. Mod. Phys.* **1971**, *43*, 297–347.

5. Hatano, Y. The chemistry of synchrotron radiation. In Fielden, E. M.; Fowler, J. P.; Hendry, J. H.; Scott, D., Eds.; *Proceedings of the 8th International Congress of Radiation Research*, Vol. *2;* Taylor and Francis, Edinburgh, 1987, pp. 86–92.
6. Koch, E. E.; Otto, A. Vacuum ultra-violet and electron energy loss spectroscopy of gaseous and solid organic compounds. *Int. J. Radiat. Phys. Chem.* **1976**, *8*, 113–150.
7. Inokuti, M. *Atomic and Molecular Data Needed for Radiotherapy and Radiation Research*, TECDOC-799; IAEA Press, Vienna, 1995.
8. Pimblott, S. M.; LaVerne, J. A. Production of low-energy electrons by ionizing radiation. *Rad. Phys. Chem.* **2007**, *76*, 1244–1247.
9. Moretto-Capelle, P.; Le Padellec, A. Electron spectroscopy in proton collisions with dry gas-phase uracil base. *Phys. Rev. A* **2006**, *74*, 062705.
10. Schulz, G. J. Resonances in electron impact on atoms. *Rev. Mod. Phys.* **1973**, *45*, 378–422; Schulz, G. J. Resonances in electron impact on diatomic molecules. *Rev. Mod. Phys.* **1973**, *45*, 423–486.
11. Hotop, H.; Ruf, M. W.; Llan, M.; Fabrikant, II. Resonance and threshold phenomena in low-energy electron collisions with molecules and clusters. *Adv. At. Mol. Opt. Phys.* **2003**, *49*, 85–216.
12. Allan, M. Study of triplet states and short-lived negative ions by means of electron impact spectroscopy. *J. Electr. Spectr. Rel. Phenom.* **1989**, *48*, 219–351.
13. Sanche, L. Primary interactions of low-energy electrons in condensed matter. In *Excess Electrons in Dielectric Media*, Jay-Gerin, J. -P.; Ferradini, C., Eds.; CRC Press, Boca Raton, FL, **1991**, pp. 1–42.
14. Sanche, L. Interactions of low-energy electrons with atomic and molecular solids. *Scanning Microsc*. **1995**, *9*, 619–656.
15. Christophorou, L. G. *Electron–Molecule Interactions and Their Applications*, Vol. *2;* Academic Press, New York, 1984.
16. Massey, H. S. W. *Negative Ions*; Cambridge University Press, London, 1976, Chapter 11
17. Palmer, R. E.; Rous P. Resonances in electron scattering by molecules on surfaces. *Rev. Mod. Phys.* **1992**, *64*, 383–440.
18. Sanche, L. Electron resonances in desorption induced by electronic transitions. *Surf. Sci.* **2000**, *451*, 82–90.
19. Bass, A. D.; Sanche, L. Interactions of low-energy electrons with atomic and molecular solids. In *Charged Particle and Photon Interactions with matter: Chemical, Physicochemical and Biological Consequences with Applications*; Hatano, Y.; Mozumder, A., Eds.; Marcel Dekker, New York, 2004, pp. 207–258.
20. Bowers, M. T. *Gas-Phase Ion Chemistry*, Vol. *2;* Academic Press, New York, 1979.
21. Sanche, L.; Parenteau, L. Surface reactions between O_2 and hydrocarbons induced by dissociative electron attachment. *J. Chem. Phys.* **1990**, *93*, 7476–7482.
22. Huels, M. A.; Parenteau, L.; Sanche, L. Reactive scattering of 1–5 eV O^- in films of tetrahydrofuran. *J. Phys. Chem. B* **2004**, *108*, 16303–16312.
23. Ward, J. F. *Advances in Radiation Biology 5*, Academic Press, New York, 1977.
24. Yamamoto, O. In *Aging Carcinogenesis and Radiation Biology*; Smith, K.; Ed.; Plenum, New York, 1976, pp. 165–192.
25. Fuciarelli, A. F.; Zimbrick, J. D., editors. *Radiation Damage in DNA: Structure/Function Relationships at Early Times*; Batelle, Columbus; OH, 1995.

26. Sanche, L. Low energy electron-driven damage in biomolecules. *Eur. Phys. J. D* **2005**, *35*, 367–390.
27. Cai, Z.; Cloutier, P.; Hunting, D.; Sanche, L. Comparison between X-ray photon and secondary electron damage to DNA in vacuum. *J. Phys. Chem. B* **2005**, *109*, 4796–4800.
28. Adams, R. L. P.; Knowler, J. T.; Leader, D. P. *The Biochemistry of the Nucleic Acids*, 10th ed.; Chapman and Hall, New York, 1986.
29. Swarts, S.; Sevilla, M.; Becker, D.; Tokar, C.; Wheeler, K. Radiation-induced DNA damage as a function of hydration. I. Release of unaltered bases. *Radiat. Res.* **1992**; *129*, 333–344.
30. Boudaïffa, B.; Cloutier, P.; Hunting, D.; Huels, M. A.; Sanche, L. Cross sections for low-energy (10–50 eV) electron damage to DNA. *Radiat. Res.* **2002**, *157*, 227–234.
31. Porter, M. D.; Bright, T. B.; Allara, D. L.; Chidsey, C. E. D. Spontaneously organized molecular assemblies. 4. Structural characterization of *n*-alkyl thiol monolayers on gold by optical ellipsometry, infrared spectroscopy, and electrochemistry. *J. Am. Chem. Soc.* **1987**, *109*, 3559–3568.
32. Dugal, P.; Huels, M. A.; Sanche, L. Low-energy (5–25 eV) electron damage to homo-oligonucleotides. *Radiat. Res.* **1999**, *151*, 325–333.
33. Dugal, P.; Abdoul-Carime, H.; Sanche, L. Mechanisms of low energy (0.5–30 eV) electron-induced pyrimidine ring fragmentation within thymine and halogen-substituted single strands of DNA. *J. Phys. Chem. B* **2000**, *104*, 5610–5617.
34. Abdoul-Carime, H.; Dugal, P. C.; Sanche, L. Damage induced by 1–30 eV electrons on thymine and bromouracil substituted oligonucleotides. *Radiat. Res.* **2000**, *153*, 23–28.
35. Boudaiffa, B.; Cloutier, P.; Hunting, D.; Huels, M. A.; Sanche, L. Resonant formation of DNA strand breaks by low energy (3–20 eV) electrons. *Science* **2000**, *287*, 1658–1660.
36. Huels, M. A.; Boudaïffa, B.; Cloutier, P.; Hunting, D.; Sanche, L. Single, double, and multiple strand breaks induced in DNA by 3–100 eV electrons. *J. Am. Chem. Soc.* **2003**, *125*, 4467–4477.
37. Martin, F.; Burrow, P. D.; Cai, Z.; Cloutier, P.; Hunting, D. J.; Sanche, L. DNA strand breaks induced by 0–4 eV electrons: The role of shape resonances. *Phys. Rev. Lett.* **2004**, *93*, 068101.
38. Pan, X.; Sanche, L. Mechanism and site of attack for direct damage to DNA by low-energy electrons. *Phys. Rev. Lett.* **2005**, *94*, 198104.
39. Denifl, S.; Zappa, F.; Mähr, I.; Lecointre, J.; Probst, M.; Märk, T. D.; Scheier, P. Mass spectrometric investigation of anions formed upon free electron attachment to nucleobase molecules and clusters embedded in superfluid helium droplets. *Phys. Rev. Lett.* **2006**, *97*, 043201.
40. Tanabe, T.; Noda, K.; Saito, M.; Starikov, E. B.; Tateno, M. Regular threshold-energy increase with charge for neutral-particle emission in collisions of electrons with oligonucleotide anions. *Phys. Rev. Lett.* **2004**, *93*, 043201.
41. Nagesha, K.; Gamache, J.; Bass, A. D.; Sanche, L. An improved electron transmission method for measuring electron trapping cross sections at the surface of dielectric films. *Rev. Sci. Instrum.* **1997**, *68*, 3883–3888.
42. Marsolais, R. M.; Deschênes, M.; Sanche, L. Low energy electron transmission method for measuring charge trapping in dielectric films. *Rev. Scient. Instr.* **1989**, *60*, 2724–2732.

43. Meesungnoen, J.; Jay-Gerin, J. -P.; Filali-Mouhim, A.; Mankhetkorn, S. Low-energy electron penetration range in liquid water. *Radiat. Res.* **2002**, *158*, 657–660.
44. Zheng, Y.; Cloutier, P.; Wagner, J. R.; Sanche, L. An irradiator to study the damage induced to large non-volatile molecules by low-energy electrons. *Rev. Sci. Instrum.* **2004**; *75*, 4534–4540.
45. Mochiji, K.; Hashimoto, H.; Tanaka, Y.; Ninomiya, N.; Takeo, M. Scanning tunneling microscope observation of plasmid DNA under electron irradiation at 8–40 eV. *Phys. Rev. B* **2007**, *75*, 094302.
46. Allison, D. P.; Thundat, T.; Jacobsen, K.; Bottomley, L. A.; Warmack, R. J. Imaging entire genetically functional DNA molecules with the scanning tunneling microscope. *J. Vac. Sci. Technol. A* **1993**, *11*, 816–819.
47. Bass, A. D.; Arumainayagam, C.; Sanche, L. Revisiting the electron stimulated desorption of anions from thin films of CF_2Cl_2. *Int. J. Mass Spectrom.* **2008**, *277*, 251–255.
48. Kimmel, G. A.; Orlando, T. M. Low-energy (5–120 eV) electron-stimulated dissociation of amorphous D_2O ice: D(2S), $O(3P_{2,1,0})$, and $O(1D_2)$ yields and velocity distributions. *Phys. Rev. Lett.* **1995**, *75*, 2606–2609.
49. Abdoul-Carime, H.; Dugal, P. C.; Sanche, L. DIET of neutral fragments from chemisorbed biological molecular systems. *Surf. Sci.* **2000**, *451*, 102–107.
50. Zheng, Y.; Cloutier, P.; Hunting, D. J.; Wagner, J. R.; Sanche, L. Glycosidic bond cleavage of thymidine by low-energy electrons. *J. Am. Chem. Soc.* **2004**, *126*, 1002–1003.
51. Hansma, H. G.; Vesenka, J.; Siegerist, C.; Kelderman, G.; Morrett, H.; Sinsheimer, R. L.; Elings, V.; Bustamante, C.; Hansma, P. K. Reproducible imaging and dissection of plasmid DNA under liquid with the atomic force microscope. *Science* **1992**, *256*, 1180–1184.
52. Jing, T. W.; Jeffrey, A. M.; DeRose, J. A.; Lyubchenko, Y. L.; Shlyakhtenko, L. S.; Harrington, R. E.; Appella, E.; Larsen, J.; Vaught, A.; Rekesh, D.; et al. Structure of hydrated oligonucleotides studied by *in situ* scanning tunneling microscopy. *Proc. Natl Acad. Sci. USA* **1993**, *90*, 8934–8938.
53. Hansma, H. G.; Bezanilla, M.; Zenhausern, F.; Adrian, M.; Sinsheimer, R. L. Atomic force microscopy of DNA in aqueous solutions. *Nucleic Acids Res.* **1993**, *21*, 505–512.
54. Maeda, Y.; Matsumoto, T.; Kawai, T. Observation of single- and double-stranded DNA using non-contact atomic force microscopy. *Appl. Surf. Sci.* **1999**, *140*, 400–405.
55. Boichot, S.; Fromm, M.; Cunniffe, S.; O'Neill, P.; Labrune, J. C.; Chambaudet, A.; Delain, E.; Le Cam, E. Investigation of radiation damage in DNA by using atomic force microscopy, *Radiat. Prot. Dosim.* **2002**, *99*, 143–145.
56. Tanaka, H.; Kawai, T. Visualization of detailed structures within DNA. *Surf. Sci.* **2003**, *539*, L531–L536.
57. Grant, P.; Jiao, Y.; Bechhoefer, J. Room temperature STM imaging in air can damage DNA, even at low tunneling biases and currents. Abstract, APS March meeting, 2008.
58. Hansma, G. H.; Hoh, J. H. Biomolecular imaging with the atomic force microscope. *Annu. Rev. Biophys Biomol Struct.* **1994**, *23*, 115–139.
59. Dunlap, D. D.; García, R.; Schabtach, E.; Bustamante, C. Masking generates contiguous segments of metal-coated and bare DNA for scanning tunneling microscope imaging. *Proc. Natl Acad. Sci. USA* **1993**, *90*, 7652–7655.

60. Mougin, A.; Babak, V. G.; Palmino, F.; Bêche, E.; Baros, F.; Hunting, D. J.; Sanche, L.; Fromm, M. TDAB-induced DNA plasmid condensation on the surface of a reconstructed boron doped silicon substrate. *Surf. Sci.* **2008**, *602*, 142–150.
61. Folkard, M.; Prise, K. M.; Vojnovic, B.; Davies, S.; Roper, M. J.; Michael, B. D. Measurement of DNA damage by electrons with energies between 25 and 4000 EV. *Int. J. Radiat. Biol.* **1993**, *64*, 651–658.
62. Boudaïffa, B.; Cloutier, P.; Hunting, D.; Huels, M. A.; Sanche, L. Les électrons de très faible énergie produisent des lésions de l'ADN. *Méd. Sci.* **2000**, *16*, 1281–1283.
63. Boudaiffa, B.; Hunting, D. J.; Cloutier, P.; Huels, M. A.; Sanche, L. Induction of single and double strand breaks in plasmid DNA by 100 to 1500 eV electrons. *Int. J. Radiat. Biol.* **2000**, *76*, 1209–1221.
64. Bass, A. D.; Parenteau, L.; Huels, M. A.; Sanche, L. Reactive scattering of O^- in organic films at sub-ionization collision energies. *J. Chem. Phys.* **1998**, *109*, 8635–8643.
65. Huels, M. A.; Parenteau, L.; Sanche, L. Substrate sensitivity of dissociative electron attachment to physisorbed aniline. *Chem. Phys. Lett.* **1997**, *279*, 223–229.
66. Sieger, M. T.; Simpson, W. C.; Orlando, T. M. Production of O_2 on icy satellites by electronic excitation of low-temperature water ice. *Nature* **1998**, *394*, 554–556.
67. Aflatooni, K.; Gallup, G. A.; Burrow, P. D. Electron attachment energies of the DNA bases. *J. Phys. Chem. A* **1998**, *102*, 6205–6207.
68. Barrios, R.; Skurski, P.; Simons, J. Mechanism for damage to DNA by low-energy electrons. *J. Phys. Chem. B* **2002**, *106*, 7991–7994.
69. Panajotovic, R.; Martin, F.; Cloutier, P.; Hunting, D. J.; Sanche, L. Effective cross sections for single strand break production in plasmid DNA by 0.1 to 4.7 eV electrons. *Radiat. Res.* **2006**, *165*, 452–459.
70. Zheng, Y.; Cloutier, P.; Hunting, D. J.; Sanche, L.; Wagner, J. R. Chemical basis of DNA sugar–phosphate cleavage by low-energy electrons. *J. Am. Chem. Soc.* **2005**, *127*, 16592–16598.
71. Abdoul-Carime, H.; Gohlke, S.; Fischbach, E.; Scheike, J.; Illenberger, E. Thymine excision from DNA by subexcitation electrons. *Chem. Phys. Lett.* **2004**, *387*, 267–270.
72. Becker, D.; Bryant-Friedrich, A.; Trzasko, C.; Sevilla, MD. Electron spin resonance study of DNA irradiated with an argon-ion beam: Evidence for formation of sugar phosphate backbone radicals. *Radiat. Res.* **2003**, *160*, 174–185.
73. Becker, D.; Razskazovskii, Y.; Callaghan, M.; Sevilla, M. D. Electron spin resonance of DNA irradiated with a heavy-ion beam ($^{16}O_8+$): evidence for damage to the deoxyribose phosphate backbone. *Radiat. Res.* **1996**, *146*, 361–368.
74. Shukla, L.; Pazdro, R.; Becker, D.; Sevilla, M. D. Sugar radicals in DNA: Isolation of neutral radicals in gamma-irradiated DNA by hole and electron scavenging. *Radiat. Res.* **2005**, *163*, 591–602.
75. Range, K.; McGrath, M. J.; Lopez, X.; York, D. M. The structure and stability of biological metaphosphate, phosphate, and phosphorane compounds in the gas phase and in solution. *J. Am. Chem. Soc.* **2004**, *126*, 1654–1665.
76. Zheng, Y.; Cloutier, P.; Hunting, D. J.; Wagner, J. R.; Sanche, L. Phosphodiester and *N*-glycosidic bond cleavage in DNA induced by 4–15 eV electrons. *J. Chem Phys.* **2006**, *124*, 64710.

77. Rowntree, P.; Sambe, H.; Parenteau, L.; Sanche, L. Formation of anionic excitations in the rare-gas solids and their coupling to dissociative states of adsorbed molecules. *Phys. Rev. B* **1993**, *47*, 4537–4554.

78. Zheng, Y.; Wagner, R.; Sanche, L. DNA damage induced by low energy electrons: Electron transfer and diffraction. *Phys. Rev. Lett.* **2006**, *96*, 208101.

79. Berdys, J.; Anusiewicz, I.; Skurski, P.; Simons, J. Damage to model DNA fragments from very low-energy (<1 eV) electrons. *J. Am. Chem. Soc.* **2004**, *126*, 6441–6447 and references therein.

80. Lévesque, P. L.; Michaud, M.; Cho, W.; Sanche, L. Absolute electronic excitation cross sections for low-energy electron (5–12 eV) scattering from condensed thymine. *J. Chem. Phys.* **2005**, *122*, 224704.

81. Winstead, C.; McKoy, V. Resonant channel coupling in electron scattering by pyrazine. *Phys. Rev. Lett.* **2007**, *98*, 113201.

82. Caron, L. G.; Sanche, L. Low-energy electron diffraction and resonances in DNA and other helical macromolecules. *Phys. Rev. Lett.* **2003**, *91*, 113201.

83. Caron, L. G.; Sanche, L. Diffraction in resonant electron scattering from helical macromolecules: A- and B-type DNA. *Phys. Rev. A* **2004**, *70*, 032719 and Diffraction in resonant electron scattering from helical macromolecules: Effects of the DNA backbone. *Phys. Rev. A* **2005**, *72*, 32726.

84. Caron, L. G.; Tonzani, S.; Greene, C. H.; Sanche, L.;Diffraction in low-energy electron scattering from DNA: Bridging gas phase and solid state theory. *Phys. Rev. A* **2008**, *78*, 042710 (13 pages).

85. Sanche, L. Mechanisms of low-energy electron damage to condensed biomolecules and DNA. *Radiat. Prot. Dosim.* **2002**, *99*, 57–62.

86. Li, Z.; Zheng, Y.; Cloutier, P.; Sanche, L.; Wagner, R. Low energy electron induced DNA damage: Effects of terminal phosphate and base moieties on the distribution of damage. *J. Am. Chem. Soc.* **2008**, *130*, 5612–5613.

87. Pan, X.; Sanche, L. Dissociative electron attachment to DNA basic constituents: The phosphate group. *Chem. Phys. Lett.* **2006**, *421*, 404–408.

88. Park, Y. S.; Cho, H.; Parenteau, L.; Bass, A. D.; Sanche, L. Cross sections for electron trapping by DNA and its component subunits I: Condensed tetrahydrofuran deposited on Kr. *J. Chem. Phys.* **2006**, *125*, 074714.

89. Jäggle, C.; Swiderek, P.; Breton, S. -Ph,; Michaud, M.; Sanche, L. Products and reaction sequences in tetrahydrofuran exposed to low-energy electrons. *J. Phys. Chem. B* **2006**, *110*, 12512–22.

90. Solomun, T.; and Illenberger, E. A fluorescence-based method for detection of electron damage to DNA. *Chem. Phys. Lett.* **2004**, *396*, 448–451.

91. Solomun, T.; Hultschig, C.; Hultschig, C.; Illenberger, E. Microarray technology for the study of DNA damage by low-energy electrons. *Eur. Phys. J. D* **2005**, *35*, 437–441.

92. Solomun, T.; Skalicky, T. The interaction of a protein-DNA surface complx with low-energy electrons. *Chem. Phys. Lett*. **2008**, *453*, 101–104.

93. Cai, Z.; Dextraze, M.-E,; Cloutier, P.; Hunting, D.; Sanche, L. Induction of strand breaks by low energy electrons (8–68 eV) in a self-assembled monolayer of oligonucleotides: Effective cross-sections and attenuation lengths. *J. Chem. Phys.* **2006**, *124*, 024705.

94. Petrovykh, D. Y.; Kimura-Suda, H.; Tarlov, M. J.; Whitman, L. Quantitative characterization of DNA films by X-ray photoelectron spectroscopy. *J. Langmuir* **2004**, *20*, 429–440.

95. Ray, S. G.; Daube, S. S.; Naaman, R. On the capturing of low-energy electrons by DNA. *Proc. Natl. Acad. Sci. USA* **2005**, *102*, 15–19.

96. Sanche, L.; et al. Elastic scattering of electrons and positrons. *J. Int. Commission Radiat. Unit* (ICRU Report 77, ISSN 1473–6691) **2007**, *7*, 1–151.

97. Pan, X.; Cloutier, P.; Hunting, D.; Sanche, L. Dissociative electron attachment to DNA. *Phys. Rev. Lett.* **2003**, *90*, 208102–1.

98. Abdoul-Carime, H.; Cloutier, P.; Sanche, L. Low-energy (5–40 eV) electron-stimulated desorption of anions from physisorbed DNA bases. *Radiat. Res.* **2001**, *155*, 625–633.

99. Pan, X.; Abdoul-Carime, H.; Cloutier, P.; Bass, A. D.; Sanche, L. D^-, O^- and OD^- desorption induced by low-energy (0–20 eV) electron impact on amorphous D_2O films. *Radiat. Phys. Chem.* **2005**, *72*, 193–199.

100. Antic, D.; Parenteau, L.; Lepage, M.; Sanche, L. Low energy electron damage to condensed phase deoxyribose analogues investigated by electron stimulated desorption of H^- and electron energy loss spectroscopy. *J. Phys. Chem.* **1999**, *103*, 6611–6619.

101. Ptasińska, S.; Denifl, S.; Grill, V.; Märk, T. D.; Scheier, P.; Gohlke, S.; Huels, M. A.; Illenberger, E. Bond-selective H^- ion abstraction from thymine. *Angew. Chem. Int. Ed.* **2005**, *44*, 1647–1650.

102. Aqua, T.; Naaman, R.; Daube, S. S. Controlling the adsorption and reactivity of DNA on Gold. *Langmuir* **2003**, *19*, 10573–10580.

103. Pan, X.; Michaud, M.; Sanche, L.;Unpublished observations.

104. Ptasińska, S.; Sanche, L. On the mechanism of anion desorption from DNA induced by low energy electrons. *J. Chem. Phys.* **2006**, *125*, 144713.

105. Ptasińska, S.; Sanche, L. Dissociative electron attachment to abasic DNA. *Phys. Chem. Chem. Phys.* **2007**, *9*, 1730–1735.

106. Abdoul-Carime, H.; Langer, J.; Huels, M. A.; Illenberger, E. Decomposition of purine nucleobases by very low energy electrons. *Eur. Phys. J. D* **2005**, *35*, 399–404.

107. Denifl, S.; Ptasińska, S.; Probst, M.; Hrušák, J.; Scheier, P.; Märk, T. D. Electron attachment to the gas-phase DNA bases cytosine and thymine. *J. Phys. Chem. A* **2004**, *108*, 6562–6569.

108. Denifl, S.; Ptasińska, S.; Cingel, M.; Matejcik, S.; Scheier, P.; Märk, T. D. Electron attachment to the DNA bases thymine and cytosine. *Chem. Phys. Lett.* **2003**, *377*, 74–80.

109. Ptasińska, S.; Denifl, S.; Gohlke, S.; Scheier, P.; Illenberger, E.; Märk, T. D. Decomposition of thymidine by low-energy electrons: Implications for the molecular mechanisms of single-strand breaks in DNA. *Angew. Chem. Int. Ed.* **2006**, *45*, 1893–1896.

110. Burrow, P. D.; Gallup, G. A.; Scheer, A. M.; Denifl, S.; Ptasińska, S.; Märk, T. D.; Scheier, P. Vibrational Feshbach resonances in uracil and thymine. *J. Chem. Phys.* **2006**; *124*, 124310.

111. Zappa, F.; Denifl, S.; Mähr, I.; Lecointre, J.; Rondino, F.; Echt, O.; Märk, T. D.; Scheier, P. Electron impact ionization of thymine clusters embedded in superfluid helium droplets. *Eur. Phys. J. D* **2007**, *43*, 117–120.

112. Hubert, D.; Beikircher, M.; Denifl, S.; Zappa, F.; Matejcik, S.; Bacher, A.; Grill, V.; Märk, T. D.; Scheier, P. High resolution dissociative electron attachment to gas phase adenine. *J. Chem. Phys.* **2006**, *125*, 084304.

113. Ptasińska, S.; Denifl, S.; Grill, V.; Märk, T. D.; Illenberger, E.; Scheier, P. Bond- and site-selective loss of H- from pyrimidine bases. *Phys. Rev. Lett.* **2005**, *95*, 093201.

114. Ptasińska, S.; Denifl, S.; Mróz, B.; Brobst, M.; Grill, V.; Illenberger, E.; Scheier, P.; Märk, TD. Bond selective dissociative electron attachment to thymine. *J. Chem. Phys.* **2005**, *123*, 124302.

115. Sulzer, P.; Ptasińska, S.; Zappa, F.; Mielewska, B.; Milosavljevic, A. R.; Scheier, P.; Mark, T. D.; Bald, I.; Gohlke, S.; Huels, M. A.; Illenberger, E. Dissociative electron attachment to furan, tetrahydrofuran, and fructose. *J. Chem. Phys.* **2006**, *125*, 044304.

116. Abdoul-Carime, H.; Gohlke, S.; Illenberger, E. Site-specific dissociation of DNA bases by slow electrons at early stages of irradiation. *Phys. Rev. Lett.* **2004**, *92*, 168103.

117. Ptasińska, S.; Denifl, S.; Scheier, P.; Illenberger, E.; Märk, T. D. Bond- and site-selective loss of H atoms from nucleobases by very-low-energy electrons (<3 eV). *Angew. Chem. Int. Ed.* **2005**, *44*, 6941–6943.

118. Crewe, A. V.; Isaacson, M.; Johnson, D. Electron energy loss spectra of the nucleic acid bases. *Nature* **1971**, *231*, 262–263.

119. Herve du Penhoat, M. A.; Huels, M. A.; Cloutier, P.; Jay-Gerin, J-P.; Sanche, L. Electron stimulated desorption of H^- from thin films of thymine and uracil. *J. Chem. Phys.* **2001**, *114*, 5755–5764.

120. Abdoul-Carime, H.; Sanche, L. Sequence-specific damage induced by the impact of 3–30 eV electrons on oligonucleotides. *Radiat. Res.* **2001**, *156*, 151–157.

121. Abdoul-Carime, H.; Sanche, L. Fragmentation of short single DNA strands by 1–30 eV electrons: Dependence on base identity and sequence. *Int. J. Radiat. Biol.* **2002**, *78*, 89–99.

122. Ladik, J.; Früchtl, H.; Otto, P.; Jäger, J. Approximate calculation of the collective excited states of a cytosine stack. *J. Mol. Struct.* **1993**, *97*, 215–219.

123. Tanabe, T.; Starikov, E. B.; Noda, K.; Saito, M. Resonant neutral-particle emission after collisions of electrons with base-stacked oligonucleotide cations in a storage ring. *Chem. Phys. Lett.* **2006**, *430*, 380–385.

124. Ptasińska, S.; Sanche, L. Dissociative electron attachment to hydrated single DNA strands. *Phys. Rev. E* **2007**, *75*, 031915.

125. Tao, N. J.; Lindsay, S. M.; Rupprecht, A. Structure of DNA hydration shells studied by Raman spectroscopy. *Biopolymers* **1989**, *28*, 1019–1030.

126. Simpson, W. C.; Sieger, M. T.; Orlando, T. M.; Parenteau, L.; Nagesha, K.; Sanche, L. Dissociative electron attachment in nanoscale ice films: Temperature and morphology effects. *J. Chem. Phys.* **1997**, *107*, 8668–8677.

127. Falk, M.; Hartman, K. A.; Lord, R. C. Hydration of deoxyribonucleic acid. II. An infrared study. *J. Am. Chem. Soc.* **1963**, *85*, 387–390.

128. Falk, M. Hydration of purines, pyrimidines, nucleosides, and nucleotides. *Can. J. Chem.* **1965**, *43*, 314–318.

129. Cai, Z.; Cloutier, P.; Hunting, D.; Sanche, L. Enhanced DNA damage induced by secondary electron emission from a tantalum surface exposed to soft X-rays. *Radiat. Res.* **2006**, *165*, 365–371.

130. Brun, E.; Cloutier, P.; Fromm, M.; Sicard-Roselli, C.; Sanche, L. Direct and indirect effects in the radiosensitization of DNA by gold nanoparticles and surfaces irradiated with soft X-ray. *J. Phys. Chem. B*. **2009**, in press.

131. Ptasińska, S.; Sanche, L. Low energy electron stimulated desorption of ions from whole human blood. *Int. J. Mass Spectrom.* **2007**, *263*, 179–184.

132. Henke, B. L.; Knauer, J. P.; Premaratne, K. The characterization of x-ray photocathodes in the 0.1–10-keV photon energy region. *J. Appl. Phys.* **1981**, *52*, 1509–1520.

133. Henke, B. L.; Smith, J. A.; Attwood, D. T. 0.1–10-keV x-ray-induced electron emissions from solids—Models and secondary electron measurements. *J. Appl. Phys.* **1977**, *48*, 1852–1866.

134. Zamenhof, S.; DeGiovanni, R.; Greer, S. Induced gene unstabilization. *Nature* **1958**, *181*, 827–829.

135. Zimbrick, J. D.; Ward, J. F.; Myers, L. S., Jr. Studies on the chemical basis of cellular radiosensitization by 5-bromouracil substitution in DNA. *Int. J. Radiat. Biol.* **1969**, *16*, 505–523.

136. Simpson, L. D.; Zimbrick, J. D. E. S. R. studies of halogenated pyrimidines in gamma-irradiated alkaline glasses. *Int. J. Radiat. Biol.* **1975**, *28*, 461–475.

137. Ling, L. L. Ward J F, Radiosensitization of Chinese hamster V79 cells by bromodeoxyuridine substitution of thymidine: enhancement of radiation-induced toxicity and DNA strand break production by monofilar and bifilar substitution. *Radiat. Res.* **1990**, *121*, 76–83.

138. Katouzian-Safadi, M.; Charlier, M. Radiolysis of 5-bromouracil-substituted DNA. *J. Chim. Phys.* **1997**, *94*, 326–331.

139. Abouaf, R.; Pommier, J.; Dunet, H. Negative ions in thymine and 5-bromouracil produced by low energy electrons. *Int. J. Mass Spectrom.* **2003**, *226*, 397–403.

140. Abouaf, R.; Pommier, J.; Dunet, H. Electronic and vibrational excitation in gas phase thymine and 5-bromouracil by electron impact. *Chem. Phys. Lett.* **2003**, *381*, 486–494.

141. Scheer, A.; Aflatooni, K.; Gallup, G. A.; Burrow, P. D. Bond breaking and temporary anion states in uracil and halouracils: Implications for the DNA bases. *Phys. Rev. Lett.* **2004**, *92*, 68102.

142. Abdoul-Carime, H.; Huels, M. A.; Brüening, F.; Illenberger, E.; Sanche, L. Dissociative electron attachment to gas phase 5-bromouracil. *J. Chem. Phys.* **2000**, *113*, 2517–2521.

143. Denifl, S.; Matejcik, S.; Gstir, B.; Hanel, G.; Probst, M.; Scheier, P.; Märk, T. D. Electron attachment to 5-chloro uracil. *J. Chem. Phys.* **2003**, *118*, 4107–4114.

144. Abdoul-Carime, H.; Huels, M. A.; Illenberger, E.; Sanche, L. Sensitizing DNA to secondary electron damage: Resonant formation of oxidative radicals from 5-Halouracils. *J. Am. Chem. Soc.* **2001**, *123*, 5354–5355.

145. Abdoul-Carime, H.; Huels, M. A.; Illenberger, E.; Sanche, L. Formation of negative ions from gas phase halouracils by low-energy (0–18 eV) electron impact. *Int. J. Mass Spectrom.* **2003**; *228*, 703–716.

146. Klyachko, D. V.; Huels, M. A.; Sanche, L. Halogen anion formation in 5-halo-uracil films: X rays vs subionization electrons. *Radiat. Res.* **1999**, *151*, 177–187.

147. Hervé, du; Penhoat, M. -A.; Huels, M. A.; Cloutier, P.; Jay-Gerin, J. -P.; Sanche, L. Electron stimulated desorption of H^- from thin films of 5-halouracils. *Phys. Chem. Chem. Phys.* **2003**, *5*, 3270–3277.

148. Hervé, du; Penhoat, M. -A,; Huels, M. A.; Cloutier, P.; Jay-Gerin, J. -P.; Sanche, L. Anion fragment formation in 5-Halouracil films induced by 1–20 eV electron impact. *J. Phys. Chem. B* **2004**, *108*, 17251–17260.

149. Li, X.; Sanche, L.; Sevilla, M. D. Dehalogenation of 5-halouracils after low energy electron attachments: A density functional theory investigation. *J. Phys. Chem. A* **2002**, *106*, 11248–11253.

150. Cecchini, S.; Girouard, S.; Huels, M. A.; Sanche, L.; Hunting, D. J. Single-strand-specific radiosensitization of DNA by bromodeoxyuridine. *Radiat. Res.* **2004**, *162*, 604–615.

151. Abdoul-Carime, H.; Limão-Vieira, P.; Gohlke, S.; Petrushko, I.; Mason, N. J.; Illenberger, E. Sensitization of 5-bromouridine by slow electrons. *Chem. Phys. Lett.* **2004**, *393*, 442–447.

152. Sevilla, M. Research breakthrough: DNA strandedness controls halouracil radiosensitization. *Radiat. Res.* **2004**, *162*, 603.

153. Herold, D. M.; Das, I. J.; Stobbe, C. C.; Iyer, R. V.; Chapman, J. D. Gold microspheres: a selective technique for producing biologically effective dose enhancement. *Int. J. Radiat. Biol.* **2000**, *76*, 1357–1364.

154. Whyman, R. Gold nanoparticles. A renaissance in gold chemistry. *Gold Bull.* **1996**, *29*, 11–15.

155. Chen, W.; Zhang, J. Using nanoparticles to enable simultaneous radiation and photodynamic therapies for cancer treatment. *J. Nanosci. Nanotechnol.* **2006**, *6*, 1159–1166.

156. Anshup; Venkataraman, J. S.; Subramaniam, C.; Kumar, R. R.; Priya, S.; Kumar, T. R. S.; Omkumar, R. V.; John, A.; Pradeep, T. Growth of gold nanoparticles in human cells, *Langmuir* **2005**, *21*, 11562–11567.

157. Niidome, T.; Nakashima, K.; Takahashi, H.; Niidome, Y. Preparation of primary amine-modified gold nanoparticles and their transfection ability into cultivated cells. *Chem. Commun.* **2004**, 1978–1979.

158. Hainfeld, J. F.; Slatkin, D. N.; Smilowitz, H. M. The use of gold nanoparticles to enhance radiotherapy in mice. *Phys. Med. Biol.* **2004**, *49*, N309–N315.

159. Foley, E.; Carter, J. D.; Shan, F.; Guo, T. Enhanced relaxation of nanoparticle-bound supercoiled DNA in X-ray radiation. *Chem. Commun.* **2005**, 3192–3194.

160. Cho, S. H. Estimation of tumour dose enhancement due to gold nanoparticles during typical radiation treatments: A preliminary Monte Carlo study. *Phys. Med. Biol.* **2005**, *50*, N163–N173.

161. Carter, J. D.; Cheng, N. N.; Qu, Y.; Duarez, G. D.; Guo, T. Nanoscale energy deposition by X-ray absorbing nanostructures. *J. Phys. Chem. B* **2007**, *111*, 11622–11625.

162. Zheng, Y.; Hunting, D. J.; Ayotte, P.; Sanche, L. Radiosensitization of DNA by gold nanoparticles irradiated with high-energy electrons. *Radiat. Res.* **2008**, *168*, 19–27.

10

ELECTRON-AFFINIC RADIOSENSITIZERS

PETER WARDMAN

Gray Institute for Radiation Oncology and Biology, University of Oxford, Oxford OX3 7DQ, United Kingdom

10.1. INTRODUCTION

The radiosensitivity of cells and tissues can be modulated by a wide variety of chemicals, but only very few compounds are used clinically as drugs in conjunction with radiotherapy of cancer with the aim of therapeutic gain, or as putative radioprotective agents—for example, for use as a preventative measure or after accidental exposure to radiation. Chemical sensitizers for radiotherapy have been recently reviewed,[1] while drugs which have been included in clinical trials cover quite a wide spectrum, a class that has received a great deal of attention are compounds designed to overcome the resistance of hypoxic cells to radiation.[2] This is because between two and three times the radiation dose is needed to kill cells at very low oxygen tensions or in anoxia compared to well-oxygenated cells. This differential has long been postulated to be a significant factor in prognosis following radiotherapy.[3] In the last two decades, several unequivocal demonstrations of the link between tumor hypoxia and prognosis in the treatment of common cancers by radiation, as well as indications that hypoxia is a factor in metastatic spread and in tumor biology more generally,[4] has reinforced the importance of addressing the problem of tumor hypoxia.[5–7]

One class of chemicals has completely dominated the field of hypoxic cell radiosensitizers. These are compounds that are electron-affinic, of which oxygen itself is an example, and nitroaromatic compounds comprise by far the largest class.

Radical and Radical Ion Reactivity in Nucleic Acid Chemistry, Edited by Marc M. Greenberg

The chemistry of electron-affinic radiosensitizers is therefore almost synonymous with the chemistry of nitroarenes, and because the compounds clearly act through free-radical mechanisms, as noted below, a review[8] of the properties and behavior of nitroarene radical-anions would provide a good background to the chemistry of electron-affinic radiosensitizers. In the present context, the main focus is on the interaction of nitroarene and other electron-affinic molecules with radicals obtained on ionization of DNA, or from reactions of, for example, hydroxyl radicals with DNA. A major theme is the distinction between electron-transfer and radical-addition reactions (of course the latter may precede the former, as in "inner-sphere" electron transfer). Major clinical interest in nitroimidazole radiosensitizers grew in the 1980s, and reviews of electron-affinic radiosensitizers from a mechanistic point of view record knowledge at that time.[9–12] This chapter presents an updated overview and, with the benefit of hindsight, some revision to the views expressed earlier. While there has been limited activity in this area since the 1980s, as evidenced by the sparse coverage of the topic in the standard text describing free-radical-induced DNA damage[13] compared to the discussion in the earlier monograph by the same author,[14] such an overview now seems timely.

In writing this chapter, the author is acutely aware that some references are now very dated, but a feature of the field is that data have been presented in diverse journals and conference proceedings, some of which are not now readily available. It is hoped that presenting this overview may be helpful to those seeking answers to the many outstanding questions that remain in this area and may stimulate the further work that is obviously needed.

10.2. TYPICAL ELECTRON-AFFINIC RADIOSENSITIZERS

10.2.1. Classes of Electron-Affinic Radiosensitizers

The concept of electron-affinic radiosensitizers followed soon after the application of pulse radiolysis to observe directly intermediates in irradiated water by microsecond kinetic spectrophotometry. It was noted that chemicals which enhanced the radiosensitivity of bacteria also has a high reactivity toward the hydrated electron, e^-_{aq}.[15] Of course, examination of tabulated data show many compounds share this property.[16] However, early applications of pulse radiolysis included direct observations of electron transfer involving radicals,[17] represented by

$$A^{\bullet -} + B \rightarrow A + B^{\bullet -} \qquad (10.1)$$

which is obviously driven by differences in electron affinity between A and B. The "electron affinity hypothesis" soon developed into models where such differences were important—for example, possibly facilitating electron trapping to prevent charge recombination in DNA.[18]

The earliest electron-affinic compounds tested involved conjugated double bonds and ketyl functions, but a complication was noted in that some such compounds (e.g., *N*-ethylmaleimide) were also thiol-depleting reagents (thiols are radioprotectors).[15]

Later compounds included much more powerful oxidants, especially quinones such as 2-methyl-1,4-naphthoquinone (which also reacts quite rapidly with thiols, as discussed below)[19] and 9,10-anthraquinone-2-sulfonate.[18] Ketyl functionality in some early sensitizers and electron-affinic molecules studied in model experiments by pulse radiolysis[17] led to 4-nitroacetophenone (Figure 10.1, **1**) being evaluated as a radiosensitizer, and this proved to be a breakthrough,[20,21] because a more water-soluble (Mannich base) derivative (Figure 10.1, **2**) enabled efficacy *in vivo* to be demonstrated.[22]

The nitroaromatic moiety, as in the prototypical 4-nitroacetophenone, proved the cornerstone of the vast majority of hypoxic cell radiosensitizers. Its identification as an active pharmacophore quickly led to demonstration of radiosensitizing activity in 5-nitrofurans such as nitrofurazone (Figure 10.1, **3**) and nitrofurantoin (**4**),[23] and in the 5-nitroimidazole, metronidazole (Flagyl) (**5**),[24] which was quite widely used in humans against a variety of anaerobic organisms and protozoa. Hoffman-La Roche had assessed many 2-nitroimidazoles as potential substitutes for metronidazole, and Ro 07-0582 (misonidazole, Figure 10.1, **6**) had been the subject of human studies; since more active a radiosensitizer than metronidazole *in vitro*,[25] it became the focus of a very large number of laboratory and clinical investigations worldwide. A related compound, benznidazole (**7**), is used in the treatment of Chagas' disease and received limited clinical evaluation as a radiosensitizer.

Numerous alternatives to misonidazole have been evaluated as radiosensitizers in biological models and ones that reached clinical evaluation represent the compounds of most interest for new chemical studies. Some differ only marginally from misonidazole, mainly in the *N*-1 sidechain to modify the biodistribution characteristics. Thus etanidazole (SR 2508) (Figure 10.1, **8**) was hypothesized to be less neurotoxic than misonidazole because of lower lipophilicity, although at an early date the desmethyl (and more hydrophilic) metabolite of misonidazole, Ro 05-9963 (**9**), was shown to have similar toxicity to its parent.[26] Most clinical interest in recent years focused on the 5-nitroimidazole, nimorazole (**10**), better tolerated than misonidazole, and with clear, although modest, clinical effectiveness.[2] High hopes for pimonidazole (**11**) (Ro 03-0799) from studies[27] *in vitro* which suggested improved efficacy were not realized,[26] possibly because of pH-induced concentration gradients associated with its basic sidechain, which led to over-optimistic expectations from the resulting enhanced efficacy *in vitro* (see below). Of other nitroarene structures, the nitrotriazole sanazole (**12**) (AK-2123) has been evaluated in humans as a radiosensitizer.[28,29] It should be noted that although the structures of these compounds include a diversity of substituents, the key functionality is the nitroarene moiety, and most of the rest of the molecules serve only to modify the solubility and biodistribution of the radiosensitizers. Lipophilicity can be varied over quite a wide range without detectable effect on radiosensitization efficiency, at least *in vitro*,[30] and the importance of this property *in vivo* is probably considerably less than, for example, with the efficacy of 5-nitroimidazoles as antitrichomonal agents.[31]

Approaches seeking to target the radiosensitizing moiety to DNA include nitroarenes with dual functionality, which bind to DNA via either (a) a reductively activated alkylating moiety such as the aziridine substituent in RSU1069 (**13**) or its prodrug

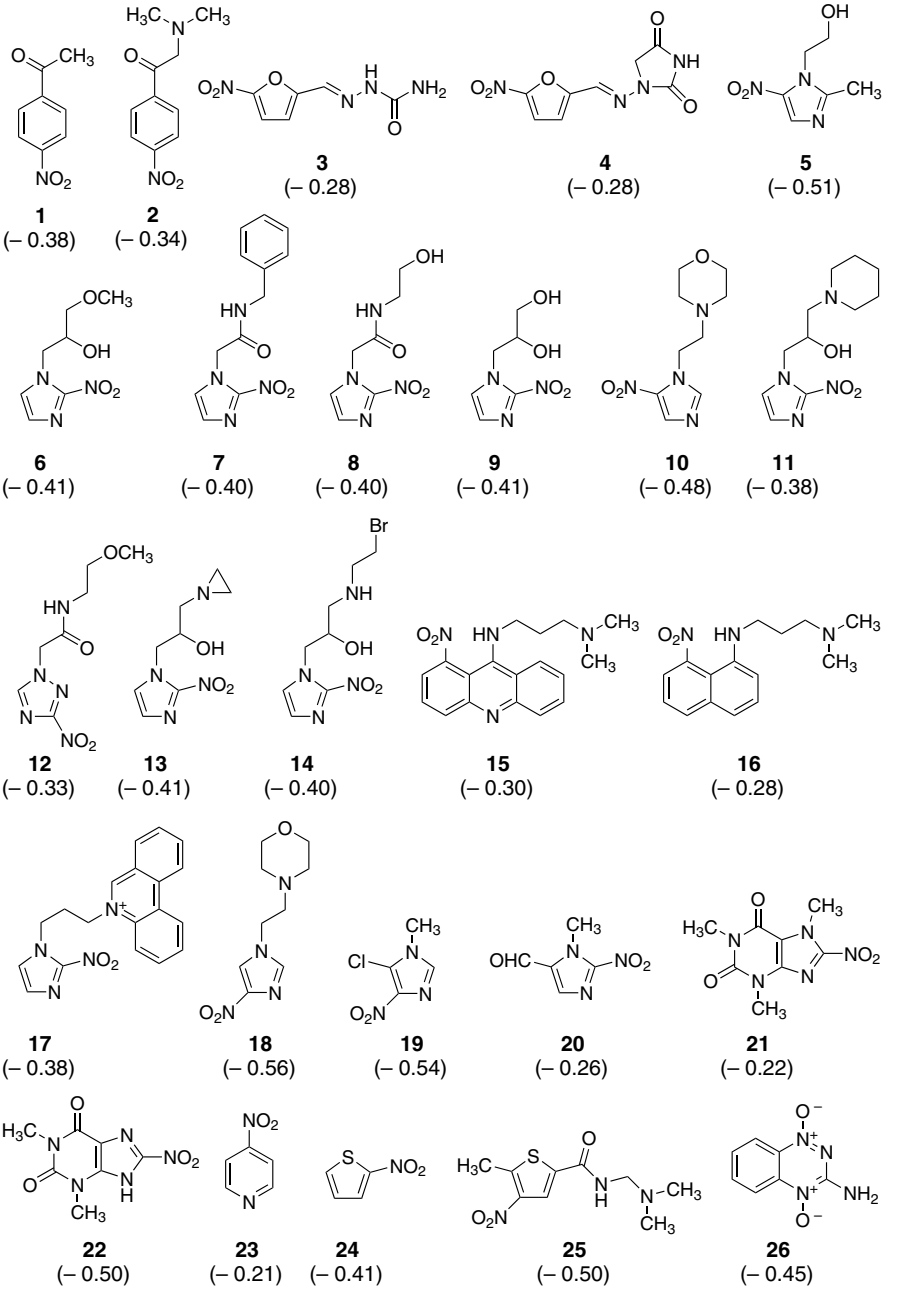

FIGURE 10.1. Structures of representative electron-affinic radiosensitizers discussed in the text. Values in parentheses are estimates of the reduction potentials in water at pH 7 for reduction of the compound to the radical, in volts versus NHE.

RB6145 (**14**), (b) nitroacridine and nitroquinoline intercalators such as nitracrine[32] (**15**) or the related "5-quinacrine"[33] (**16**), or (c) nitroarenes linked to intercalators such as phenanthridium,[34] for example, "2-NLP-3" (**17**). Figure 10.1 also includes a representative selection (**18–25**) of other nitroarenes evaluated as radiosensitizers, mainly to illustrate the range of reduction potentials of such compounds, as discussed below.

The *N*-oxide moiety as an alternative to the nitro group is of most interest in the context of hypoxia-selective bioreductive drugs (not involving radiation treatment). Of these, tirapazamine (Figure 10.1, **26**) has received considerable clinical attention.[35] However, together with the related quinoxaline di-*N*-oxides, tirapazamine and its analogues are also of relevance to the radiosensitizer field because of their interactions with DNA radicals.[36–38] This topic is discussed further in Chapter 5.

10.2.2. The Electron-Affinity Scale

The concept of electron-affinity had driven early research on radiosensitizers, and polarographic half-wave reduction potentials were an early measure helping identify candidate drugs.[23] However, polarography and cyclic voltammetry usually involves nonreversible behavior for the reduction of nitroaromatic compounds in water near physiological pH, and true thermodynamically reversible reduction potentials for the oxidant/radical one-electron couples proved to be of most value in correlating biological activity (including toxicity) with measures of electron affinity, as described below. At about the time of emerging interest in this area, radiation chemists had utilized pulse radiolysis to establish thermodynamically reversible electron-transfer equilibria involving oxidants such as quinones and their radical-anions—that is, the position of electron-transfer reactions represented by Eq. (10.1) but which were reversible equilibria even in water:

$$A^{\bullet -} + B \rightleftarrows A + B^{\bullet -} \tag{10.2}$$

It was possible to measure the equilibrium constant K_2 by fast absorption spectrophotometry, yielding values of ΔG_2 and hence ΔE_2, the difference in the reduction potentials of the one-electron couples:

$$\Delta E_2(\text{volts}) = E(B/B^{\bullet -}) - E(A/A^{\bullet -}) = \approx 0.059 \log K_2 \tag{10.3}$$

If the reduction potential of one of the partners in the equilibrium was known, then the other could be determined. It was possible to calculate the value for some quinones and hence establish a scale of electron affinity for radiosensitizers,[39] and viologens also proved useful because of their facile electrochemistry, radical stability, and high extinction coefficients of the radicals.[40]

The reduction potentials can be (and are probably best) described as mid-point potentials rather than standard potentials, since they are often pH-dependent around the physiological pH range. The values are thermodynamically reversible and can be used in, for example, correlations of the Marcus type (see below). The standard is

versus the normal hydrogen electrode (NHE). An introduction to the experimental measurements and the dependence on pH is accompanied by a data compilation, which, although now dated, has proven to be of value.[41]

10.2.3. Reduction Potentials of Typical Radiosensitizers

Values of (one-electron) reduction potentials for the nitroarene/radical couples at pH 7 are given in Figure 10.1 for the prototypical radiosensitizers. (These have been slightly adjusted from the original publications since it was recognized that dimerization of the radical-cation formed on reduction of benzyl viologen, a widely used redox indicator, increased the reduction potential measured electrochemically.[42]) For comparison, on this scale, oxygen has $E(O_2(1\ M)/O_2^{\bullet -}) \sim -0.18$ V versus NHE, noting that O_2 is at the nonstandard state of 1 M concentration to permit facile comparison of relative electron affinities. Radiosensitization behavior is a feature of nitroaromatic compounds with reduction potentials for the oxidant/radical couple of approximately -0.2 to -0.6 V versus NHE at pH 7; higher values are likely to result in too high metabolic sensitivity for useful behavior, as noted below.

The redox properties may vary widely with position of the nitro substituent—for example, in the imidazole ring (compare **5** with **6** and **10** with **18**), and electron-withdrawing or –donating substituents can have large, and sometimes unwanted, effects. While the chlorine substituent in **19** increases the reduction potential somewhat, much more important is the activation by the nitro group of nucleophilic displacement by thiols (catalyzed by glutathione-*S*-transferases in the case of GSH).[43] The carboxaldehyde substituent in **20** has a greater effect in increasing the reduction potential, but also activates the *nitro* group toward similar displacement reaction with thiols.[44] The implications of reactivity toward thiols, illustrated in Figure 10.2 with compounds known to react with thiols at a significant rate under physiologically relevant conditions,[19,43,44] are discussed below.

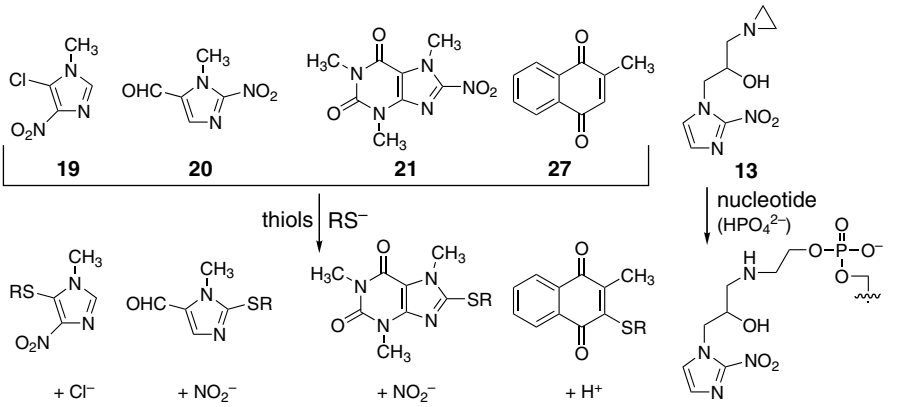

FIGURE 10.2. Radiosensitizers with additional functionality, showing reactions with thiols or other nucleophiles.

As discussed in detail elsewhere,[8,41] mid-point potentials in water are frequently pH-dependent, reflecting the prototropic behavior of the molecule (both ground state and radical). Thus the nitro radical-anions of both misonidazole (Figure 10.1, **6**) and metronidazole (**5**) protonate with pK_a for dissociation of the protonated conjugate $\sim$ 5.7 and 6.1, respectively.[45] Even basic sites distant from the nitroarene moiety, such as the piperidino nitrogen in pimonidazole (**11**), show an increase in pK_a in the radical compared to ground state (in this case, with a three-carbon chain greatly weakening the inductive effect of the nitroarene moiety, by only $\sim$0.5, but still with measurable effects on mid-point potential).[8] Much more dramatic effects are seen in comparing 8-nitrocaffeine (**21**) with the close analogue (**22**), where ionization of the imidazolyl N–H function in the latter, with p$K_a = 2.3$, is accompanied by a large decrease in mid-point reduction potential at pH 7 (and radiosensitization efficiency).[27] Along with irreversible behaviour, such prototropic equilibria give rise to generally poor correlations of thermodynamically reversible one-electron reduction potentials with electrochemical measurements, particularly in aprotic solvents.[46]

The effects of substituents on redox properties, which is also reflected in spin distributions in the radical-anions,[39] can be predicted using well-known Hammett-type relationships. Thus several families of nitroarenes showed reduction potentials (oxidant/radical couple) at pH 7 with a dependence on the Hammett sigma substituent "constant" σ of the form

$$E_m = \text{constant} + \rho\sigma \tag{10.4}$$

where the coefficient ρ was in the range 0.11–0.18 V and the constant term varies with nitroarene and position of the nitro group.[47] Substituents also influence prototropic behavior, in turn influencing pH-dependent mid-point potentials, but these can be accounted for where appropriate. Thus the shift in mid-point potentials at pH 7 of derivatives of nitracrine (**15**) substituted *para* to the nitro group were well predicted by an equation that took into account the effect of the substituent on the pK_a of the ring (acridine) nitrogen[47]:

$$\Delta E_m \approx 0.17(\sigma_p^- - \sigma_m) \tag{10.5}$$

which explained why halogen (Cl, F) substitution *decreased* the reduction potential even though they are electron-withdrawing substituents.

A few other examples (**23**–**25**) of nitroarenes based on other aromatic moieties are included in Figure 10.1. Clearly, a wide choice of redox-active pharmacophore is available, even restricting choice to nitroarenes.

10.2.4. Typical Biological Effects of Electron-Affinic Radiosensitizers in Mammalian Cells and Tissues

Briefly, hypoxic cell radiosensitizers restore the radiosensitivity (typically measured by clonogenic survival *in vitro* or tumor regrowth delay *in vivo*) of anoxic or hypoxic

cells some way toward that of well-oxygenated cells. (The presence of oxygen normally renders cells two to three times more radiosensitive, in terms of radiation dose needed to achieve the same biological response such as clonogenic cell survival, compared to cells that are anoxic.) Typical electron-affinic radiosensitizers are less efficient than oxygen in terms of concentration needed to achieve a response, and they typically show no detectable, or negligible, additional increase in radiosensitivity of well-oxygenated cells. They are thus selective in their mode of action, although whether this simply reflects kinetic competition for initial reaction with DNA radicals is debatable and indeed seems unlikely. This selectivity is different from that of some other types of radiosensitizer, such as the halogenated pyrimidines, which radiosensitize but with selectivity toward rapidly proliferating cells rather than hypoxia.

The radiosensitizing effect reflects damage to DNA. As with measuring effects on cell survival, analysis is complicated by the effects on damage (irrespective of radiation) of high concentrations of nitroarenes (usually too high to be clinically relevant). This is related to hypoxia-selective, reductively activated damage through the production of metabolites that bind to proteins and DNA, such as nitrosoarenes or hydroxylamines.[48] Rapid lysis techniques can help resolve the dual effects of radiosensitization and enzyme-catalyzed reduction. Compounds such as misonidazole enhance DNA single-strand breaks (SSBs) in mammalian cells irradiated in anoxia or in the presence of low concentrations of oxygen, in a manner which parallels survival.[49] Radiation-induced double-strand breaks (DSBs) were sensitized by misonidazole in *E. coli*[50] and in mouse L cells,[51] correlating with survival. The dual-function (alkylating) nitroimidazole RSU-1069 (Figure 10.1, **13**) induces SSBs and DSBs in mammalian cells without radiation, unlike misonidazole under the same conditions.[52]

The study of the enhancement of damage in models such as mixtures of calf thymus DNA and misonidazole is complicated by the inevitable scavenging of hydroxyl radicals by the radiosensitizer unless unrealistically high concentrations of DNA are used. In one such model system, oxygen enhanced DNA SSBs threefold, but misonidazole did not; however, it enhanced the yield of 3′-phosphoglycolate end groups.[53]

10.2.5. Quantitative Structure–Activity Relationships Between Chemical Properties and Biological Efffects

Expressed in concentrations of radiosensitizer needed to achieve the same radiosensitizing effect—for example, the concentration needed to achieve a level of cell survival which would require (say) 1.6 × the radiation dose for cells irradiated in anoxia alone compared to anoxia plus radiosensitizer—radiosensitization efficiencies of nitroarenes vary by at least three orders of magnitude.[30] It is common in classical medicinal chemistry to attempt to relate drug efficacy in terms of concentration C for a constant response with a free-energy related parameter, such as Hammett σ "constants" or the logarithm of the octanol:water partition coefficient, log P, an approach that Hansch pioneered.[54] It was therefore natural to explore the influence of

reduction potential E and lipophilicity of radiosensitizers by multivariate analysis using equations of the form

$$\log(1/C) = b_0 + b_1E + b_2\log P + b_3(\log P)^2 \tag{10.6}$$

Unsurprisingly, the efficiencies of electron-affinic radiosensitizers did exhibit a strong dependence on reduction potential; over a wide range ($P \geq 0.05$), lipophilicity was clearly much less important, with $\sim 85\%$ of the variance in $\log(1/C)$ explained by the redox parameter E.[30] The "redox coefficient" b_1 varied somewhat with response chosen, but for the simpler equation we have

$$\log(1/C) = b_0 + b_1E \tag{10.7}$$

where $b_1 \approx 7$–$8\ \mathrm{V}^{-1}$ for a radiosensitizing effect of a factor 1.4–1.6. In comparing putative mechanistic models with biological effects, this redox dependence provides a crucial test, as discussed below. However, there are two important caveats.

First, the value of C used is that in the medium the cells are irradiated in, whereas ideally we require the concentration at the target site. Compounds that are weak acids or bases may be concentrated intracellularly, or excluded, in a manner that is well understood since the uncharged forms equilibrate across a lipophilic membrane but protonated bases or dissociated acids do not. Average intracellular concentrations can be measured,[55] and quenching of delayed fluorescence of acridine-stained cells can be used to probe relative concentrations near DNA.[56] Alternatively, typical intracellular/extracellular pH differentials can be used to predict concentration gradients and equations such as (10.6) or (10.7) modified accordingly.[57] Such considerations explained the apparently enhanced radiosensitization efficiency *in vitro* of the weak base pimonidazole (Figure 10.1, **11**) compared to misonidazole (**6**) after allowing for the modest difference in reduction potential at pH 7.

A second caveat, with the benefit of hindsight, is that multiple mechanisms render this simplistic approach unsuitable. It was noted that the redox dependence varied with response,[30] suggestive of more than one mechanism, and indeed some compounds included on the "redox plot" were later found to be thiol-reactive (Figure 10.1, **20** is an example). Some other thiol-reactive radiosensitizers are shown in Figure 10.2, including menadione (**27**). Since thiols compete with nitroarenes (thiol depletion enhances activity[58]), this introduces an obvious complication. With hindsight, the extent of thiol depletion, as well as intracellular uptake, should have been checked for each compound, and indeed efficacy should have been measured with minimal pre-incubation to avoid any enhancement from bioreductive metabolism (which can produce thiol-reactive metabolites or lead to binding to intracellular proteins and other nucleophiles).

Some radiosensitizers were designed to be dual-functional from the start. Thus the aziridinyl 2-nitroimidazole, RSU-1069 (Figure 10.1, **13**), is an alkylating agent. As shown in Figure 10.2, it reacts with phosphate moieties—for example, with dGMP with a rate constant of $\sim 2 \times 10^{-3}\ \mathrm{M}^{-1}\ \mathrm{s}^{-1}$ at 310 K and pH 7.[59] This compound and its prodrug **14** are probably of main interest as potential bioreductively activated

cytotoxins independent of radiation[60]; and although the subject of clinical investigations,[61] they will not be discussed in detail here.

The importance of carefully assessing reactivity (in the absence of radiation) toward thiols and other cellular targets is that experiments *in vitro* normally involve using a vast excess (in mole terms) of radiosensitizer compared to the total cellular thiols (or other target). Hence even exposing a cell population in a typical experiment *in vitro* to, for example, 1 μM reactant might deplete all cellular thiols, leaving much of the reagent to give (now greatly enhanced) radiosensitization, but such results will never translate *in vivo* because the situation is reversed: the body burden of thiols is around 2–5 mmol/kg while any realistic drug is unlikely to be tolerable at much more than 0.2 mmol/kg. Although this point was made many years ago[62] and was repeated recently,[1] there are many examples in the literature of seemingly promising phenomena that seldom progress beyond the earliest phases of *in vivo* evaluation because of what the present author termed "simple arithmetic," since the principle is indeed simple and the arithmetic can be done on the back of a postage stamp.

Notwithstanding these caveats, in considering putative mechanisms of radiosensitization by electron-affinic compounds, we are probably seeking a redox dependence that is around 7 V^{-1} when expressed by equations of the form of Eq. (10.7), or in kinetic parameters, substituting $(1/C)$ by a rate constant k.

10.3. CHARACTERISTICS OF RADICALS FROM ELECTRON-AFFINIC RADIOSENSITIZERS

10.3.1. Formation of Sensitizer Radicals in Model Systems

To interpret reactions of radiosensitizers with, for example, radicals from DNA bases or sugars, it is useful to have "reference" spectra or data for comparison. A variety of methods may be used to generate radicals from nitroarene and similar redox-active radiosensitizers. Radical-anions are conveniently generated by the radiolysis of water, using suitable "scavengers" to transform oxidants to reductants—for example, formate or 2-propanol to generate $CO_2^{\bullet -}$ or $(CH_3)_2C^{\bullet}OH$ from $^{\bullet}OH$ (and $H^{\bullet}$) radicals, with reduction of nitroarenes ($ArNO_2$) by reaction (8) or (9) being typically less than an order of magnitude slower than diffusion-controlled[63]:

$$CO_2^{\bullet -} + ArNO_2 \rightarrow CO_2 + ArNO_2^{\bullet -} \tag{10.8}$$

$$(CH_3)_2C^{\bullet}OH + ArNO_2 \rightarrow (CH_3)_2CO + ArNO_2^{\bullet -} + H^+ \tag{10.9}$$

Generating nitro radical-anions for study by electron spin resonance (ESR) can be accomplished either by cells in suspension[64, 65] or in cell-free systems by reductase enzymes,[66] reductants such as ascorbate,[65] or sugar enolates.[67] The present author has found the latter method rather convenient as a general method of preparing radicals from nitroarenes as well as compounds such as tirapazamine (Figure 10.1, **26**) and viologens: mixing tirapazamine with 0.1 M fructose in 40 mM NaOH gave a good steady-state ESR spectrum of the radical-anion (cf. similar experiments with other

N-oxides[68]). Generation of nitro radical-anions by photoreduction of nitroarenes in the presence of an electron donor such as EDTA is also facile.[69] In all chemical models, high pH ensures long radical lifetimes (and hence higher steady-state concentrations than at low pH) because of prototropic equilibria outlined below.

10.3.2. Spectral Properties of Sensitizer Radicals, Their Protonated Conjugates, and Radical-Adducts

Many mechanistic studies of radiosensitizers involve time-resolved kinetic spectrophotometry or ESR spectroscopy, both steady-state and time-resolved. Unfortunately, the absorption spectra of the radicals obtained on reduction (and radical-adducts) of many of the typical sensitizers shown in Figure 10.1 are rather featureless in the UV–visible range accessible (often ground state absorption limits the useful spectral range). Distinction can be made, however, between the radical-anions, their protonated conjugates, and adducts between, for example, carbon-centered radicals and the nitro moiety. This is most easily seen with 4-nitroacetophenone (Figure 10.1, **1**), the radical-anion of which has absorption maxima at 350 and 545 nm with extinction coefficients $\varepsilon \sim 1.76 \times 10^4$ and $2.9 \times 10^3\,M^{-1}\,cm^{-1}$, respectively.[70] The spectra of both protonated radicals and radical-adducts are much weaker and blue-shifted.

Qualitatively similarly phenomena are seen with the nitroimidazoles of greater interest. Thus the radical-anions of metronidazole and misonidazole (Figure 10.1, **5** and **6**) absorb with maxima at ~ 290 nm, usually obscured by the strong ground state absorbance in this region.[71] However, both radical-anions have an easily accessible absorption between ~ 400 and 450 nm, with $\varepsilon \sim 1050$ or $1120\,M^{-1}$ for metronidazole (440 nm) or misonidazole (430 nm), respectively.[45] This visible absorption is much weaker on protonation of the radical-anion, which can be represented by Eq. (10.10):

$$(ArNO_2^{\bullet -})H^+ \rightleftarrows ArNO_2^{\bullet -} + H^+ \tag{10.10}$$

purposely not distinguishing the site of protonation since the data alone cannot provide this information. For metronidazole or misonidazole, $pK_{10} = 6.1$ or 5.7, respectively.[45]

In the case of nitrobenzene or 4-nitroacetophenone, $pK_{10} = 3.2$ or 2.5–2.7, respectively,[70,72] and this must correspond to protonation on the nitro moiety. With nitroimidazoles, it is an open question whether the values above for pK_{10} correspond to protonation on the nitro group or on the unsubstituted ring nitrogen. The present author has previously favored the latter, although it remains an open question. While the corresponding ground state pK_as for protonation at N-3 in metronidazole and misonidazole differ considerably ($\sim$2.6 and < 0, respectively), it is difficult to reconcile a shift in pK_a of $\sim$3 between radicals from nitrobenzenes and nitroimidazoles with similar spin densities on the nitro group. Furthermore, the conjugate acids of nitrobenzene radical-anions have spectra similar to nitroxide adducts (at oxygen) of carbon-centered radicals.[73] In contrast, nitroimidazole radicals absorb less at $\sim$430–440 nm on protonation, whereas adducts absorb more (see Figure 10.3).

Other authors take a different view; that is, they favor assigning pK_{10} (~ 6 for some nitroimidazole radicals, including **5** and **6**, Figure 10.1) to protonation on oxygen

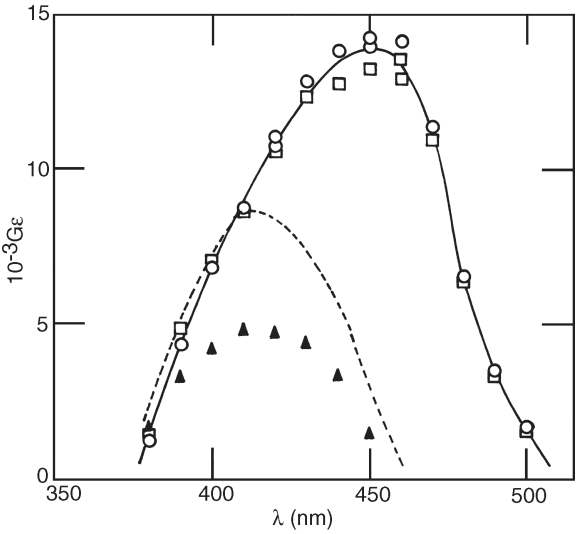

FIGURE 10.3. Absorption spectra observed after reaction of misonidazole (Figure 10.1, **6**) with some radicals, generated by pulse radiolysis. (○) $CH_3C^{\bullet}(H)OCH_2CH_3$, pH 8.3; (□) $CH_3C^{\bullet}(H)OCH_2CH_3$, pH 3.5; (▲) mixture of radicals from reaction of $^{\bullet}OH$ with deoxyribose; (--) spectrum of the radical-anion (from $CO_2^{\bullet -}$). The unit of absorption is the product of the radiation-chemical yield G, in obsolete units of molec $(100\,eV)^{-1}$ ($G = 1$ molec $(100\,eV)^{-1} \sim 0.104\,\mu mol\,J^{-1}$), and the extinction coefficient ε in $M^{-1}\,cm^{-1}$. Unpublished work by the author.

(i.e., the nitro group).[74] Actually, in the case of 2-nitroimidazoles at least, protonation of the radical-anion might well involve a proton "shared" between the imidazole N-3 and the nitro oxygen. For compounds with acidic or basic moieties in substituents [e.g., pimonidazole (Figure 10.1, **11**) or nimorazole (**10**)], the pK_a values for the piperidino- or morpholino- nitrogens will be increased in the radical compared to ground state, influencing the pH profile of reduction potential.[8,41] Regardless of the site of protonation, equilibrium (10.10) controls the lifetimes of nitroimidazole radicals around physiological pH, being accurately first-order in $[H^+]$,[75] such that nitroarene radical-anions are very long-lived at high pH.[74] Protonation of nitroarene radicals also has dramatic effects on the kinetics of electron-transfer reactions generally. Thus unpublished work at the author's Institute by Mr. E. D. Clarke and Dr. I. Wilson showed that the rate of electron transfer from the metronidazole radical to oxygen decreased by a factor of two as the pH was lowered from ∼8 to ∼5 with an apparent pK_a similar to that for equilibrium (10.10). For the nitroimidazole **20** shown in Figure 10.1, p$K_{10} \sim 2.9$ and the rate constant for electron-transfer from the radical from metronidazole (Fig. 1, **5**) to the more powerful oxidant **20** decreases from $\sim 6 \times 10^7\,M^{-1}\,s^{-1}$ at pH ∼8.5 to $< 4 \times 10^6\,M^{-1}\,s^{-1}$ at pH ∼4.5; that is, the pH profile reflects p$K_{10} \sim 6.1$ for metronidazole. These phenomena indicate the need to control pH carefully in experiments involving nitroarenes, and they also illustrate the need to be aware of prototropic equilibria that may be important even at physiological pH.

Some carbon-centered radicals initially *add* to nitroarenes rather than reduce by outer-sphere electron transfer, with major implications in respect of radiosensitizer mechanisms, as discussed below.[76] Figure 10.3 serves to illustrate the typical differences, in the case of nitroimidazoles at least, between radical-anion and radical-adduct spectra. The spectrum of the adduct between $^{\bullet}CH_2OH$ and misonidazole, along with the timescale of heterolysis of the adduct at pH 7, was illustrated earlier.[9] With both $^{\bullet}CH_2OH$ and $CH_3C^{\bullet}(H)OCH_2CH_3$, the visible bands of the radical absorptions are red-shifted in the radical-adducts compared to the radical-anion. In contrast, with 4-nitroacetophenone, the visible band seen in the radical-anion was much diminished in the adduct seen with $^{\bullet}CH_2OH$.[70] The main (UV) absorbance of substituted nitrobenzene radicals is blue-shifted in the radical-adducts compared to the radical-anions.[73] Another study showed a blue shift on going from radical-anion to radical-adduct with 4-nitrobenzoic acid and the OH-adduct of cytosine.[77]

Comparison of the spectra shown in Figure 10.3 suggests that a fraction of the mixture of radicals from reaction of $^{\bullet}OH$ with deoxyribose react with misonidazole to give the radical-anion rather than add, assigning the relatively strong band at 450 nm found with the radical from $^{\bullet}OH$ and diethyl ether to a radical-adduct, clearly resistant to rapid heterolysis (unlike the $^{\bullet}CH_2OH$/misonidazole adduct) since the spectra at pH 3.5 and 8.3 are similar. Obviously, the somewhat featureless nature of these spectra introduces some uncertainty in making such generalizations. However, there are substantial ESR data to support the general principle that α-alkoxyalkyl radicals add to nitroarene radiosensitizers, while strongly reducing radicals such as $CO_2^{\bullet -}$ and $(CH_3)_2C^{\bullet}OH$ form radical-anions with no detectable intermediate, and addition followed by elimination is seen with radicals such as $^{\bullet}CH_2OH$ (but not $^{\bullet}CH_2O^-$). Thus ESR hyperfine coupling from the methylene protons in adducts between nitrobenzenes or nitroalkanes and $^{\bullet}CH_2OH$, and from the ether moiety with $CH_3OC^{\bullet}(H)CH_2CH_3$, was detected in early studies.[78,79] Hyperfine couplings for the nitro ^{14}N are typically ~0.18–0.22 mT higher in nitroxide adduct radicals (with $^{\bullet}CH_2OH$) compared to radical-anions in a series of substituted nitrobenzenes.[73] (In contrast, on protonating the metronidazole radical-anion, the corresponding coupling *decreases* by ~0.13 mT.[80]) A number of key papers[73,76,81,82] and reviews[83,84] present detailed studies.

10.3.3. Factors Influencing the Dissociation of Radiosensitizer Radical-Adducts to Form Radical-Anions

The change of the absorbance of the misonidazole/$^{\bullet}CH_2OH$ adduct over a few tens of microseconds at pH 7 is ascribed to base-catalyzed heterolysis to form the radical-anion, as illustrated in Fig. 10.4a.[9] The rates of heterolysis of radical-adducts are important since the potential competition between fragmentation and reduction of the nitroxyl radical may have important consequences. A detailed study of substituted nitrobenzenes with different alcohol radicals demonstrated four main factors.[73] It is convenient to refer to the general scheme shown in Figure 10.4b. First, the fraction of electron transfer with $CH_3C^{\bullet}(H)OH$ and different *para*-substituted nitrobenzenes varied from ~80% to 90% with strongly electron-withdrawing substituents (e.g., CN,

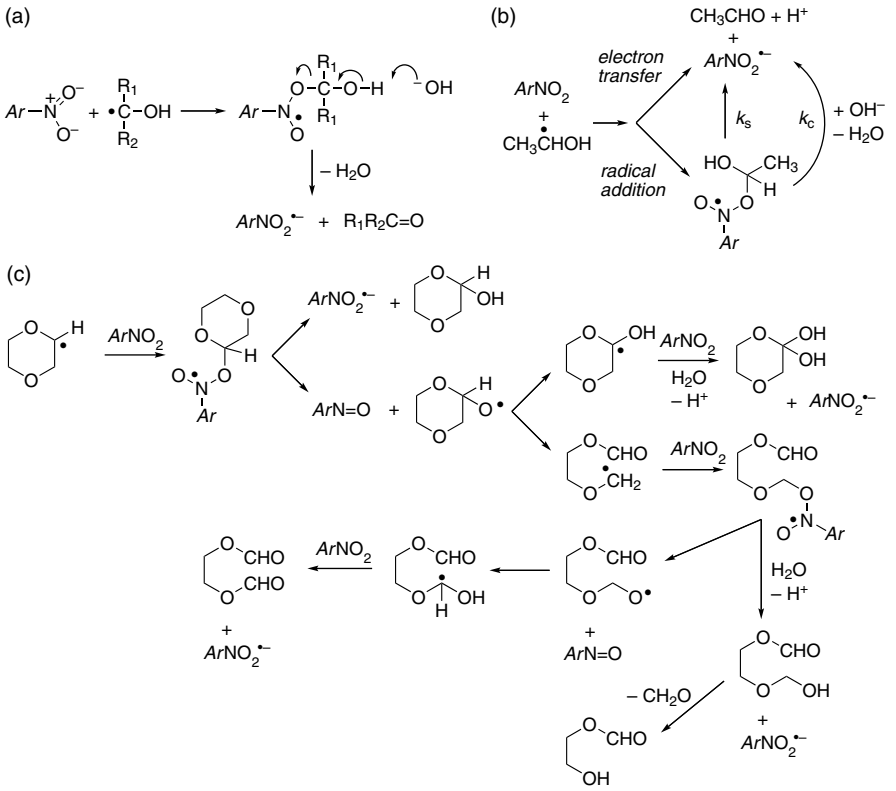

FIGURE 10.4. Formation and dissociation of radical-adducts with nitroarenes ($ArNO_2$). (**a**) General scheme for base-catalyzed heterolysis.[79] (**b**) Scheme illustrating radicals that undergo both electron transfer and radical-addition.[73] (**c**) Scheme illustrating pathways with an α-alkoxyalkyl radical forming an initial adduct that undergoes both heterolysis and homolysis, leading to multiple subsequent products and generating the nitrosoarene.[76]

SO_2CH_3, NO_2) to only ~30–35% with electron-donating substituents (e.g., OCH_3, CH_3). Second (as earlier studies had indicated), adduct fragmentation is base-catalyzed, with $k_c \sim 10^{10}\,M^{-1}\,s^{-1}$. Third, spontaneous heterolysis k_s is strongly influenced by the substituent R on the alcohol; for example, with adducts between 4-nitrobenzonitrile and $RC(H)C^{\bullet}OH$, k_s increased from $\sim 2 \times 10^3\,s^{-1}$ ($R = OHCH_2$) to $\sim 3 \times 10^4\,s^{-1}$ ($R = (CH_3)_3CH_2$), with k_s correlating with the Taft σ^* parameter. Fourth, for the adduct of $CH_3C^{\bullet}(H)OH$ with different nitroarenes, $\log k_s$ was linearly dependent on the reduction potential $E_{m7}(ArNO_2/ArNO_2^{\bullet-})$, with slope $d(\log k_s)/dE_{m7} \sim 7.9\,V^{-1}$.

A later study provided further insight.[76] With certain radicals, *homolysis* of the nitroarene radical-adduct was shown to occur. An example is shown in Figure 10.4c, showing different pathways for the fragmentation of the radical from reaction of $^{\bullet}OH$ with 1,4-dioxane. The two pathways occur to about equal extents. Aside from the biological implications of production of electrophilic nitrosoarenes, such pathways

are of importance since oxyl radicals fragment further as shown, with subsequent reactions with the nitroarene possible.[76]

Recently, further characteristics of the reactions of nitroarenes and other oxidants with α-alkoxyalkyl radicals (e.g., those derived following $^{\bullet}OH$ attack on dioxane or tetrahydrofuran) have been reported.[85] Quinones and viologens oxidize by outer-sphere electron transfer, but nitroarenes formed adducts with rate constants for addition increasing only slightly with reduction potential of the nitroarene: a value of $d(\log k)/dE \sim 2.7\ V^{-1}$ for the radical from dioxane was indicated. The earlier study had found that the radical-adduct between the dioxan radical and 4-nitrobenzonitrile decayed with $k \sim 0.5\ s^{-1}$,[76] and extension to other nitroarenes showed that this value changed little with nitroarene reduction potential.[85]

10.4. REACTIONS OF RADIOSENSITIZERS WITH DNA RADICALS

10.4.1. Reducing Radicals from Pyrimidines and Purines

Electron-affinic radiosensitizers, by definition, are expected to be reactive toward reducing radicals. Around 60% of radiation-induced cell death is associated with $^{\bullet}OH$ radicals (or, at least, can be inhibited by scavengers of this radical), and it is well known that, for example, addition of $^{\bullet}OH$ to pyrimidines at the 5,6 double bond produces predominantly (~60–90%) reducing 6-yl radicals; yields of reducing radicals from reaction of $^{\bullet}OH$ with purines are much lower.[13, 14, 86, 87] Not surprisingly, therefore, attention has focused on interaction of radiosensitizers with 5-hydroxy-pyrimidin-6-yl radicals. It should be noted that it has been common, in order to estimate the yields of reducing radicals, to use oxidants such as methyl viologen (1,1′-dimethyl-4,4′-bipyridinium), reduced to form a stable radical with an intense chromophore. However, this reagent is much more likely to undergo outer-sphere electron-transfer reactions than radical addition, and hence there is not necessarily equivalence between the behavior of a viologen and a nitroarene, since the latter can undergo both radical addition and electron transfer.

10.4.2. Formation of Radical-Adducts Between Nitroarenes and Pyrimidine 6-yl Radicals

A detailed study of reaction of substituted nitrobenzenes with radicals formed from $^{\bullet}OH$ and $H^{\bullet}$ radical adducts to 6-methyluracil and 6-methyl*iso*cytosine characterized the yields of electron transfer and the rate and activation parameters for formation and heterolysis of nitroxyl-type intermediates.[81] Reactions were of the form shown in Figure 10.4b—that is, competition between electron transfer and addition, and with heterolysis of the adduct. Indeed, it was concluded that the behavior of the pyrimidine radicals could be compared with those from simple alcohols discussed above. Thus 5-hydroxyluracil-6-yl resembles $^{\bullet}CH_2OH$, 5-H-6-methyluracil-6-yl is very similar to $CH_3C^{\bullet}HOH$, and 5-OH-6-methyluracil-6-yl is comparable to $HOCH_2C^{\bullet}HOH$.

Several important features of such reactions were noted. First, addition can form *cis* and *trans* adducts, which is likely to be of importance when considering the

possible sites of H-abstraction by the nitroxyl adduct from neighboring sugars (see below). Second, there was a well-defined (linear) redox relationship between the log of the rate constant for heterolysis of the nitroxyls (from 5-H-methyluracil-6-yl) and *para*-substituted nitrobenzenes, with a slope of $6.2\,V^{-1}$ and rate constants ranging from $\sim 2 \times 10^3$ to $\sim 1 \times 10^5\,s^{-1}$. Third, the (initial) fractional yields of radical-anions were quite high, ranging from ~44% to 87%. Fourth, rate constants for initial reactions (formation of the transition state that either dissociates to radical-anion or leads to adduct formation) varied to a lesser extent than heterolysis rates. Thus rate constants for reaction with 5-hydroxy-6-methylisocytosine-6-yl radicals varied between $\sim 2 \times 10^9\,M^{-1}\,s^{-1}$ for 1,4-dinitrobenzene and $\sim 3 \times 10^8\,M^{-1}\,s^{-1}$ for 4-methoxynitrobenzene.[81]

Another important study of reactions of $^{\bullet}OH$ adducts of nucleobases with oxidants showed that representative quinones and viologens reacted with the reducing radicals formed on reaction of $^{\bullet}OH$ with cytosine, thymine, 2′-deoxycytidine, or thymidine with rate constants following a redox dependence typical of outer-sphere electron-transfer reactions.[77] Rate constants with quinones and viologens decreased only slightly (from within an order of magnitude of diffusion-controlled) as the reduction potential of the oxidant decreased from $\sim +0.1$ to -0.25 V, but then decreased sharply with reduction potential, with a slope of log k versus reduction potential (of the oxidant/radical couple in water at pH 7 versus NHE) in the range 11.7–8.5 V^{-1}.

While, as noted above, the fractional yields of reducing radicals after reaction of $^{\bullet}OH$ with purines is much lower than those with pyrimidines, it was possible to measure a clear redox dependence for reaction of the product(s) of $^{\bullet}OH$ radical reaction with 2′-deoxyguanosine and quinones and viologens, with $d(\log k)/dE = \sim 8.5\,V^{-1}$.[77]

In contrast to the behavior with quinones and viologens, there was little redox dependence for reaction of nitroarenes with the $^{\bullet}OH$ adducts of thymine, and there was a shallower ($\sim 6\,V^{-1}$) dependence with nitroarenes and 2′-deoxycytidine compared to the reactions with quinones and viologens ($\sim 11.0\,V^{-1}$).[77] It would be of interest to extend this study over a wider range of reduction potentials and to include nitroimidazoles of clinical interest. However, since close parallels have already been drawn between the behavior of, for example, $^{\bullet}CH_2OH$ and 5-hydroxyluracil-6-yl radicals in their reactivities toward nitroarenes, it may be noted that there was an excellent correlation between log k and reduction potential for reaction of alcohol or ether radicals with five representative nitroimidazoles, over the range ~ -0.57 to ~ -0.24 V, with $d(\log k)/dE = 2.7\,V^{-1}$ for $CH_3C^{\bullet}HOCH_2CH_3$, and $\sim 3.7\,V^{-1}$ for $^{\bullet}CH_2OH$.[88]

There thus seems little doubt that radical-addition of reducing radicals with nitroarene radiosensitizers of clinical interest is characterized by a much shallower redox dependence than found for typical outer-sphere electron-transfer reactions. A biologically important example of the latter involving nitroarenes is the rate of reduction by flavoprotein nitroreductases, associated with cytotoxicity. The simplest model is free (reduced) riboflavin,[89] while reduction of nitroimidazoles by a common oxidoreductase, xanthine oxidase, showed a redox slope of $\sim 14 \pm 1\,V^{-1}$.[90] More

important reductases exhibited similar behavior.[66] Interestingly, the rate constant for the important reaction of nitroarene radicals with oxygen,

$$ArNO_2^{\bullet -} + O_2 \rightarrow ArNO_2 + O_2^{\bullet -} \tag{10.11}$$

is characterized by the equation

$$\log k = 11.0 - 5.44(1 - 0.44\Delta E)^2 \tag{10.12}$$

with $d(\log k)/dE \sim -4.3\,V^{-1}$ around the reduction potentials of interest.[8] This suggests that the reaction is an inner-sphere electron transfer, although to date there appear to be no reports of an intermediate adduct.

10.4.3. Fate of Radical-Adducts of Nitroarenes in Polynucleosides and Polynucleotides

There have been few studies of the interaction between nitroarenes and radicals formed from $^{\bullet}OH$ attack on polynucleotides. A key factor is that replacement of N(1) (H in nucleotides) by the sugar substituent greatly slows heterolysis, such that nitroxyl radical-adducts are much longer lived in polynucleotides (and polynucleosides) than in the radicals formed from the free bases. Bamatraf et al.[77] compared the absorbance change following pulse radiolysis of solutions containing N_2O (to generate principally $^{\bullet}OH$), poly(C), and benzoquinone or nitrofurantoin (Figure 10.1, **4**), with light-scattering intensity associated with strand breaks. It was shown that the nitroxyl radical-adduct of nitrofurantoin decayed with two components. The slower decay was characterized by $k = 2.7\,s^{-1}$, considerably slower than the corresponding decay in the absence of nitroarene ($5.5\,s^{-1}$) and on the same timescale as that associated with strand-break formation revealed by light scattering ($2.6\,s^{-1}$). It was suggested that the faster component with nitrofurantoin might reflect reaction of another isomeric form of the nitroxyl adduct, not leading to strand breaks. The authors noted that in an earlier study,[81] a factor-of-two difference was reported in the stability of the two (*cis* and *trans*) forms of the adduct between 4-nitroacetophenone (Figure 10.1, **1**) and the 5-hydroxy-6-methyl*iso*cytosine-6-yl radical.

Phenomenologically, these reactions can be represented by schemes such as those in Figures 10.5 and 10.6. In Figure 10.5, $^{\bullet}OH$ attack on poly(U) is followed by radical addition, base–sugar radical transfer, and strand breakage, in sequence. In Figure 10.6 (showing attack on deoxycytidine), an alternative abstraction position is shown to illustrate that multiple positions in the sugar, as well as multiple sugars, are candidates for hydrogen abstraction by the nitroxyl radical. (In poly(U), the 2′-OH activates abstraction from this site, which is not a feature in DNA.) Of obvious importance in this regard is the likely differential reactivity toward different sites of nitroarene radical-adducts at the pyrimidine 5,6 bond having *cis* or *trans* conformations. Some pointers as to site of radical attack can be gleaned from the nature of the end groups in strand

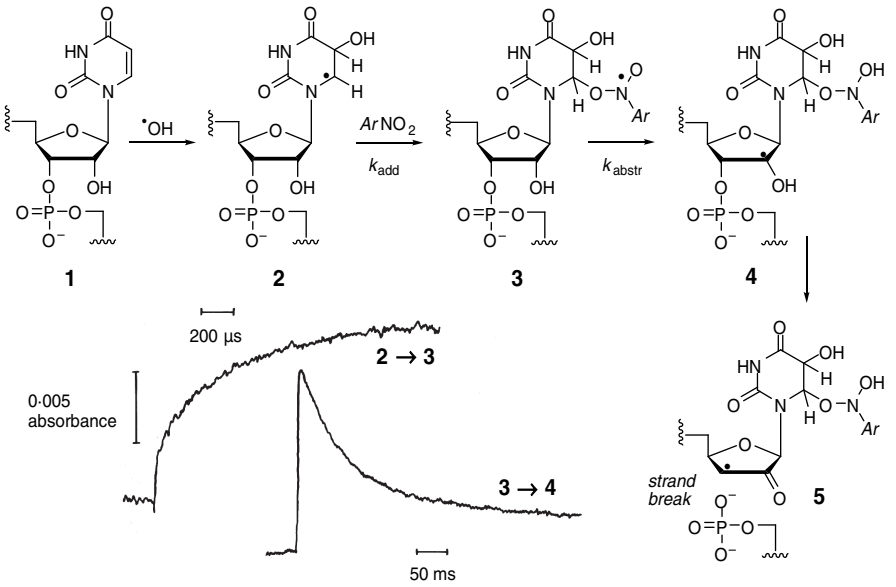

FIGURE 10.5. Possible mechanism for strand break formation in poly(U) (**1**) following formation of a 5-hydroxy-6-yl radical **2**, addition of a nitroarene to form an adduct **3**, and base/sugar radical transfer to form a C-2′ radical **4**, which rapidly loses phosphate to yield a strand break in **5**. **Bottom left**: Absorbance changes at 450 nm following pulse radiolysis (∼9 Gy) of a solution containing poly(U) (0.65 mg/ml), pimonidazole (Figure 10.1, **11**, 25 μM), and N_2O (∼25 mM), pH 6.8 (unpublished work by the author). The formation of the absorbance at 450 nm over ∼2 ms may be associated with reaction **2** → **3**, and the subsequent decay over ∼ 0.5 s may possibly be the abstraction reaction **3** → **4**, although possible reactivity of the C-4′ radical **5** toward the nitroimidazole is a complication.

breaks—for example, 3′-phosphoglycolate end groups, the yield of which was enhanced by misonidazole.[53]

Figure 10.5 also includes, for illustration, results of a preliminary examination of the •OH/poly(U)/pimonidazole (Figure 10.1, **11**) system using pulse radiolysis with absorbance detection. It seems likely, in view of the studies described above, that the fast component is associated with radical-addition, and the slow decay of the absorbance is associated with strand breakage; although lacking light-scattering data, this assignment must be tentative. With only one concentration of pimonidazole used, extraction of rate constants must be at best tentative; but from the limited data, the formation corresponded to $k_{add} \sim 8 \times 10^7\ M^{-1}\ s^{-1}$, and the decay corresponded to $k_{abstr} \sim 12\ s^{-1}$. Interestingly, from a single, similar experiment with misonidazole (Figure 10.1, **6**), formation ($= k_{add}$) was ∼20-fold slower than with pimonidazole. This may be associated with "ion condensation" (and very sensitive to ionic strength), since pimonidazole is a weak base,[27] with the protonated piperidino N dissociating with $pK_a \sim 8.7$ (with profound effects on extracellular/intracellular concentration gradients).[55] Delayed fluorescence from acridine orange was used to probe the relative

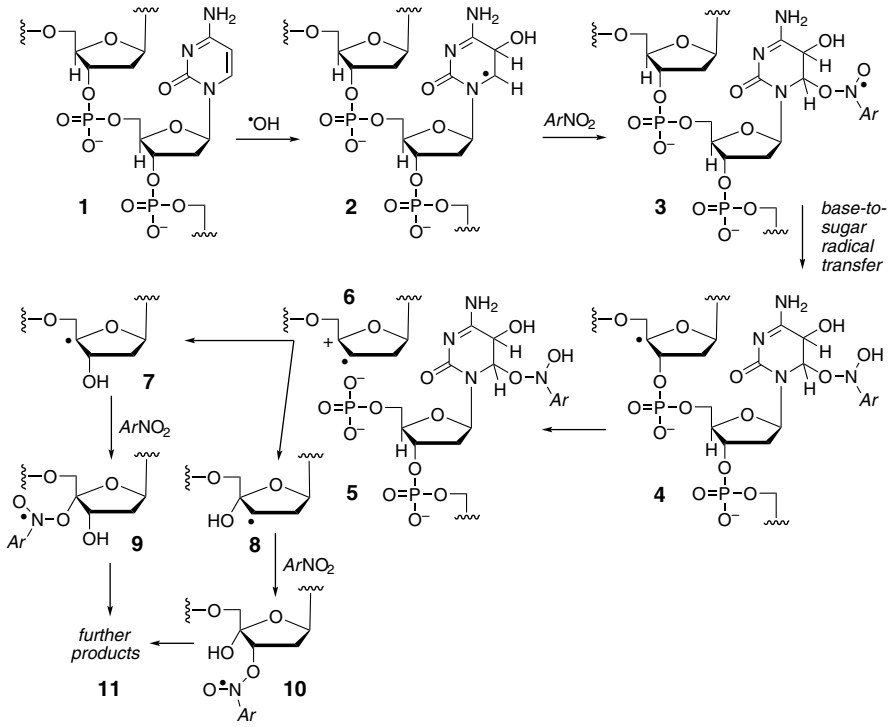

FIGURE 10.6. Possible pathways to formation of single-strand breaks and subsequent reactions following reaction of hydroxyl radicals with a DNA base (illustrated with cytosine) in the presence of nitroarenes radiosensitizers. Addition of •OH to the base **1** is mainly at the 5-position, forming the 6-yl radical **2**. Nitroarenes ($ArNO_2$) add to the 6-position to form a long-lived adduct **3**, which may, as with peroxyl radicals, abstract H from a sugar, for example, to form **4** leading to a strand break with the modified base **5** and sugar radical-cation **6** (abstraction at other sites; e.g., C-3′can also occur). The radical cation **6** reacts with water, forming **7** and **8**, in turn reactive toward nitroarenes, forming initially adducts **9** and **10** and further products **11**. Based upon extensive research surveyed by von Sonntag[13, 14, 86] (cf. references 77 and 113).

effective concentrations of misonidazole and pimonidazole, measurements showing enhanced concentrations of the latter near DNA.[56, 91]

10.4.4. Reactions of Sugar Radicals with Electron-Affinic Radiosensitizers

Oxidation of sugar radicals by nitroarenes, along with early data from model systems, was discussed briefly in earlier reviews,[10, 12] and guidance as to likely reaction pathways can be found by comparison with model alcohol and ether (α-alkoxyalkyl) radicals as discussed above. Fragmentation subsequent to oxidation, either by outer-sphere electron transfer or by radical-addition/elimination, follows well-established pathways—for example, as reviewed by von Sonntag,[13, 14] Pogozelski and Tullius,[92] and Cadet et al.[93]

While considerable advances have been made in understanding the fate of both base- and sugar-peroxyl radicals (i.e., radicals formed by addition of oxygen to carbon-centered radicals), much less is known concerning the analogous reactions involving addition of nitroarenes. Thus in addition to many early studies on radical transfer from base peroxyl radicals,[13,14] and fragmentation of sugar peroxyl radicals,[13,14,92,94] important recent work has identified tandem lesions arising from base peroxyl radicals.[95] Particularly noteworthy is that the peroxyl radical from addition of oxygen to the 5,6-dihydro-2′-deoxyuridin-6-yl radical added to the π bond of the adjacent pyrimidine. Knowledge about the possibility of corresponding reactions involving nitroxyl radicals, either on base or sugar, is sparse, indeed virtually nonexistent.

A recent study showed that the reductant *N*,*N*′-tetramethyl-*p*-phenylenediamine (TMPD) reacted with the *N*-alkoxyaminoxyl radical-adduct formed from reaction with 3,4-dinitrobenzoic acid with the α-alkoxyalkyl radical from $^{\bullet}$OH/1,4-dioxane.[85] Two molecules of the radical-cation $TMPD^{\bullet+}$ were formed for each radical-adduct, whereas reduction to the hydroxylamine requires just one equivalent. The authors suggested that this may reflect nitrosoarene formation (cf. Figure 10.4c). Interestingly, TMPD was far more effective in inhibiting radiation-induced binding of (radiolabeled) nitrofurazone (Figure 10.1, **3**) to DNA than either ascorbate or cysteine.[96] Clearly, there is much to be learned concerning the reactivity of radical-adducts of nitroarenes with both base and sugar radicals, especially in regard to reactions with biologically important reductants and nucleophiles such as thiols and ascorbate.

10.5. RADIOSENSITIZATION BY NITRIC OXIDE: A POINTER TO THE IMPORTANCE OF ADDUCTS IN RADIOSENSITIZATION

10.5.1. Efficiency of Radiosensitization by Nitric Oxide

Although nitric oxide, as a free radical (like oxygen), was selected on this basis for evaluation as a radiosensitizer over 50 years ago[97] and was shown to radiosensitize hypoxic tumor cells,[98] it was neglected for many years. The discovery of nitric oxide as a physiologically important molecule led to its reinvestigation,[99] but only recently did it become apparent that nitric oxide was an extremely efficient radiosensitizer (more efficient than oxygen), giving clear radiosensitization of hypoxic cells with a few tens of nanomolar nitric oxide, at clinically relevant radiation doses.[100]

Nitric oxide is not a good oxidant. It is not straightforward to place it on the same scale of electron affinity or reduction potential such as the values shown in Figure 10.1 for nitroarenes. This is because reduction of singlet $NO^{\bullet}$ gives triplet NO^{-}, protonating to singlet nitroxyl (HNO) with $pK_a \sim 11.4$, and there are further reactions of $^3NO^-$ and ^{1}HNO with $NO^{\bullet}$.[101] An estimate of the reduction potential of the couple ($NO^{\bullet}$, $H^+/^1$HNO) at pH 7 of ~ -0.55 V was derived,[102] much lower than the reduction potential of oxygen (1 M)/$O_2^{\bullet-}$ on the same scale (~ -0.18 V),[41,42] and lower than those of weakly electron-affinic nitroarenes requiring several millimolar nitroarene

to show good radiosensitization.[30] On this basis, nitric oxide is several orders of magnitude more efficient a radiosensitizer than might be expected.

10.5.2. Radical-Addition Reactions of Nitric Oxide

Like oxygen, nitric oxide adds rapidly to radicals. Pulse radiolysis showed that NO$^{\bullet}$ added to the 5-hydroxy-uracil-6-yl radical with a rate constant $k \sim 4\text{–}6 \times 10^9\,M^{-1}\,s^{-1}$ and added to the radical(s) formed on reaction of $^{\bullet}$OH with dGMP with $k \sim 2 \times 10^9\,M^{-1}\,s^{-1}$.[100] The former estimate is two to three times faster than the corresponding reaction with oxygen.[103] Unlike oxygen, the products of radical-addition with NO$^{\bullet}$ are likely to be spin-paired (stable) molecules. Indeed, analysis by HPLC/MS of the stable products formed from $^{\bullet}$OH and uracil in the presence of NO$^{\bullet}$ revealed a product with mass corresponding to the addition of NO$^{\bullet}$, presumably at the 6-position (and presumably a mixture of conformers).[100]

10.5.3. Mechanism of Radiosensitization by Nitric Oxide

In the recent study,[100] evidence was obtained that NO$^{\bullet}$ enhanced the yield of DNA double-strand breaks when mammalian cells were irradiated. (The widely used γ-H2AX assay was used as a surrogate marker for DSBs.) There was a suggestion, which requires confirmation, that the DSBs in cells irradiated in the presence of NO$^{\bullet}$ were repaired more slowly than in cells irradiated either anoxically or in air. Nitric oxide does react slowly with (radioprotective) thiols, but the reaction probably involves a pre-equilibrium with thiolate and is far too slow at submicromolar concentrations of NO$^{\bullet}$ for this to be involved in these experiments.[104] (Thiol reactivity could be a factor in some of the early work with higher concentrations of NO$^{\bullet}$, especially if inadequate deoxygenation was involved, because $NO_2^{\bullet}$ reacts very rapidly with thiols.[105])

Hence, phenomenologically at least, nitric oxide and oxygen share some characteristics in being rather efficient radiosensitizers (in terms of effects on clonogenic survival of cells) and enhancing DNA strand breaks, but the chemical pathways are very probably quite different. To the present author, this suggests that more attention needs to be paid to subsequent processing of damage in cells. It also suggests that we should not neglect information gleaned from another type of "oxygen-mimetic" radiosensitizers: the nitroxyl compounds. Like NO$^{\bullet}$, these add rapidly to radicals and form relatively stable adducts.[106] While the results from some studies doubtless reflect depletion of intracellular thiols,[107] reactivity of nitroxyls toward both DNA base radicals (and base peroxyl radicals)[108] is not dissimilar to the reactions found or expected with nitric oxide. Interest in bioreductive drugs such as tirapazamine, a benzotriazine-1,4-di-*N*-oxide (Figure 10.1, **26**), has also yielded (a) information of relevance concerning the reactions of DNA radicals with another class of oxidant not dissimilar in their reduction potentials to the nitroimidazoles[36–38] and (b) an incidentally useful comparison of reactions of misonidazole with C-1′ nucleoside radicals.[37]

10.6. EFFECTS OF ELECTRON-AFFINIC RADIOSENSITIZERS ON DNA DAMAGE IN CELLULAR SYSTEMS

10.6.1. The Need to Switch Paradigms

In chemical studies, it is the norm to identify the dominant pathways (in yield terms) and to focus on these. "Minor" products are usually deemed unimportant, or "side reactions." In radiation biology, most damage to cellular DNA following irradiation is repaired within a few hours, and so the commonest types of damage might be unimportant: clinical interest focuses on clonogenic capacity. This difference in viewpoints illustrates the need to be cautious in correlating easily measurable effects of radiosensitizer (such as on the initial yield of SSBs) with any particular chemical reaction. The correlation may be valid; but the importance in pathways to radiation-induced cell killing may not be valid, if the damage is subsequently repaired.

10.6.2. Differing Effects of Nitroarene Radiosensitizers in Model Systems and in Mammalian cells

Enhanced yields of thymine glycol are observed when thymine is irradiated in N_2O-saturated solution (to form predominantly $^{\bullet}OH$) in the presence of misonidazole (or other nitroarenes) and quinones in a redox-dependent manner.[109] This is entirely consistent with oxidation of 5-hydroxy-6-yl radicals, either by outer-sphere electron transfer or by addition followed by elimination. In contrast, yields of thymine glycol were not enhanced when HeLa cells were irradiated with misonidazole, although the study involved doses of 250 Gy and higher, which are hardly clinically (or radiobiologically) relevant.

Differences between results with models such as calf thymus DNA or plasmids and cellular systems are common. Thus radiolysis of DNA with misonidazole (Figure 10.1, **6**) in anoxia did not increase strand breaks but enhanced significantly the formation of 3′-phosphoglycolate end groups, while the yield of thymine glycols was not enhanced.[53] (As O'Neill has pointed out,[87] "That the yield of ssb was not enhanced . . . is an indirect indication that the pathway to ssb may involve a competition for the precursor radical between the nitroaromatic and a thiol or some other protective agent. This scenario is identical to that for the lack of an oxygen effect on ssb induction on irradiated plasmid DNA . . . in the absence of thiols.")

10.7. CONCLUSIONS

The two obvious conclusions are that (a) there is a need for further work to understand how electronic-affinic radiosensitizers enhance cell killing by radiation and (b) there is a need for caution in extrapolating the results from simple models to the complexity of the cell. DNA strand breaks are undoubtedly of major importance in radiobiology; and to date, most effort has concentrated on possible pathways by which sensitizers can enhance the yield of breaks, without much regard as to whether the breaks are of a type

easily repaired (for example). A key observation, so far as effects on clonogenic survival go, was a redox relationship or dependence, with a slope for effectiveness versus reduction potential of $\sim$7–8 V^{-1}. It appears that rate constants for the addition of nitroarenes to either base or sugar radicals has a significantly lower redox dependence. However, while the rate-limiting step in the enhancement of strand-break formation by radiosensitizers may be the base-to-sugar hydrogen abstraction by nitroxyl-type radical-adducts, the redox dependence of this reaction has not been established.

Four areas in the emerging models, particularly that involving base radical-addition followed by hydrogen abstraction from sugar by a nitroxyl-type radical, merit further study. The first area lacking information is the interaction of nitroarenes with sugar radicals, particularly the fate of sugar radical-adducts, following the hydrogen abstraction by a base nitroxyl radical; the consequences of deoxyribose oxidation in DNA have been recently reviewed, but there is much to learn in the present context.[110] The second is the extension of the types of study that have been made to date to a wider range of electron-affinic compounds, including (a) quinones with good bioavailability and lacking thiol reactivity and (b) more studies with nitric oxide. (In this context it is important not to overlook the reported effective radiosensitization by quinone-like structures such as the isoindole-4,7-diones[111]; not all the structures examined would be expected to deplete thiols by Michael addition, as with menadione.) The third is to assess in cells which type of DNA damage remains, enhanced by sensitizers, after the normal spectrum of damage processing events have taken place. It might be, for example, that cells deficient in base excision repair are susceptible to radiosensitization by nitric oxide, if the base adducts cannot be "processed." Oxidatively induced bulky DNA lesions, normally repaired by nucleotide excision repair, have been the subject of a recent perspective.[112]

Finally, the fourth area ripe for development is the application of quantum-chemical calculations to model factors that limit accessibility of functional groups in radiosensitizers, or of the adduct radicals derived from them, to particular sites. Thus accessibility of radical attack to H-5′, H-4′, and H-3′ is clear in a model of B-form DNA duplex.[92] There is evident scope for using such approaches to help identify which sites particular radical-adducts might attack and thus have a clearer understanding of the complexity of damge produced.

ACKNOWLEDGMENTS

This work is supported by Cancer Research UK. I am grateful to Dr. Peter O'Neill for helpful discussions.

REFERENCES

1. Wardman, P. Chemical radiosensitizers for use in radiotherapy. *Clin. Oncol. (R. Coll. Radiol.)* **2007**, *19*, 397–417.

2. Overgaard, J. Hypoxic radiosensitization: adored and ignored. *J. Clin. Oncol.* **2007**, *25*, 4066–4074.
3. Gray, L. H.; Conger, A. D.; Ebert, M.; Hornsey, S.; Scott, O. C. A. The concentration of oxygen dissolved in tissues at the time of irradiation as a factor in radiotherapy. *Br. J. Radiol.* **1953**, *26*, 638–648.
4. Bristow, R. G.; Hill, R. P. Hypoxia, DNA repair and genetic instability. *Nat. Rev. Cancer* **2008**, *8*, 180–192.
5. Brown, J. M. Tumor hypoxia in cancer therapy. *Methods Enzymol.* **2007**, *435*, 297–321.
6. Hoogsteen, I. J.; Marres, H. A. M.; van der Kogel, A. J.; Kaanders, J. H. A. M. The hypoxic tumour microenvironment, patient selection and hypoxia-modifying treatments. *Clin. Oncol. (R. Coll. Radiol.)* **2007**, *19*, 385–396.
7. Harrison, L. B.; Chadha, M.; Hill, R. J.; Hu, K.; Shasha, D. Impact of tumor hypoxia and anemia on radiation therapy outcomes. *Oncologist* **2007**, *7*, 492–508.
8. Wardman, P. Chemistry of nitroarene and aromatic *N*-oxide radicals. In *The Chemistry of N-Centered Radicals*; Alfassi, Z. B., Ed.; Wiley, New York, 1998, pp. 615–661.
9. Wardman, P. Radiation chemistry in the clinic: hypoxic cell radiosensitizers for radiotherapy. *Radiat. Phys. Chem.* **1984**, *24*, 293–305.
10. Wardman, P. The mechanism of radiosensitization by electron-affinic compounds. *Radiat. Phys. Chem.* **1987**, *30*, 423–432.
11. Wardman, P. Chemical and biochemical modification of the radiotherapeutic response. In *The Scientific Basis for Modern Radiotherapy (BIR Report 19)*; McNally, N. J., Ed.; British Institute of Radiology, London, 1989, pp. 81–85.
12. Wardman, P. Sensitization and protection of oxidative damage caused by high energy radiation. In *Atmospheric Oxidation and Antioxidants, Vol. III*; Scott, G., Ed.; Elsevier, Amsterdam, 1993, pp. 101–127.
13. von Sonntag, C. *Free-Radical-Induced DNA Damage and Its Repair. A Chemical Perspective*; Springer, Berlin, 2006.
14. von Sonntag, C. *The Chemical Basis of Radiation Biology*; Taylor & Francis, London, 1987.
15. Adams, G. E.; Dewey, D. L. Hydrated electrons and radiobiological sensitization. *Biochem. Biophys. Res. Commun.* **1963**, *12*, 473–477.
16. Buxton, G. V.; Greenstock, C. L.; Helman, W. P.; Ross, A. B. Critical review of rate constants for reactions of hydrated electrons, hydrogen atoms and hydroxyl radicals ($^{\bullet}OH/^{\bullet}O^{-}$) in aqueous solution. *J. Phys. Chem. Ref. Data* **1988**, *17*, 513–886.
17. Adams, G. E.; Michael, B. D.; Richards, J. T. Three stage electron transfer in aqueous and alcoholic solution. *Nature* **1967**, *215*, 1248–1250.
18. Adams, G. E.; Cooke, M. S. Electron-affinic sensitization. I. A structural basis for chemical radiosensitizers in bacteria. *Int. J. Radiat. Biol.* **1969**, *15*, 457–471.
19. Wilson, I.; Wardman, P.; Lin, T.-S.; Sartorelli, A. C. Reactivity of thiols towards derivatives of 2- and 6-methyl-1,4-naphthoquinone bioreductive alkylating agents. *Chem. Biol. Interact.* **1987**, *61*, 229–240.
20. Adams, G. E.; Asquith, J. C.; Dewey, D. L.; Foster, J. L.; Michael, B. D.; Willson, R. L. Electron affinic sensitization. Part II: para-Nitroacetophenone: a radiosensitizer for anoxic bacterial and mammalian cells. *Int. J. Radiat. Biol.* **1971**, *19*, 575–585.

21. Chapman, J. D.; Webb, R. G.; Borsa, J. Radiosensitization of mammalian cells by *p*-nitroacetophenone. I. Characterization in asynchronous and synchronous populations. *Int. J. Radiat. Biol.* **1971**, *19*, 561–573.
22. Denekamp, J.; Michael, B. D. Preferential sensitization of hypoxic cells to radiation *in vivo*. *Nature New Biol*. **1972**, *239*, 21–23.
23. Reuvers, A. P.; Chapman, J. D.; Borsa, J. Potential use of nitrofurans in radiotherapy. *Nature* **1972**, *237*, 402–403.
24. Foster, J. L.; Willson, R. L. Radiosensitzation of anoxic cells by metronidazole. *Br. J. Radiol.* **1973**, *46*, 234–235.
25. Asquith, J. C.; Watts, M. E.; Patel, K.; Smithen, C. E.; Adams, G. E. Electron affinic sensitization. V. Radiosensitization of hypoxic bacteria and mammalian cells *in vitro* by some nitroimidazoles and nitropyrazoles. *Radiat. Res.* **1974**, *60*, 108–118.
26. Dische, S. A review of hypoxic cell radiosensitization. *Int. J. Radiat. Oncol. Biol. Phys.* **1991**, *20*, 147–152.
27. Smithen, C. E.; Clarke, E. D.; Dale, J. A.; Jacobs, R. S.; Wardman, P.; Watts, M. E.; Woodcock, M. Novel (nitro-1-imidazolyl) alkanolamines as potential radiosensitizers with improved therapeutic properties. In *Radiation Sensitizers. Their Use in the Clinical Management of Cancer*; Brady, L. W., Ed.; Masson, New York, 1980, pp. 22–32.
28. Sugie, C.; Shibamoto, Y.; Ito, M.; Ogino, H.; Suzuki, H.; Uto, Y.; Nagasawa, H.; Hori, H. Reevaluation of the radiosensitizing effects of sanazole and nimorazole *in vitro* and *in vivo*. *J. Radiat. Res. (Tokyo)* **2005**, *46*, 453.
29. Dobrowsky, W.; Huigol, N. G.; Jayatilake, R. S.; Kizilbash, N. I.; Okkan, S.; Kagiya, V. T.; Tatsuzaki, H. AK-2123 (Sanazol) as a radiation sensitizer in the treatment of stage III cervical cancer: Results of an IAEA multicentre randomised trial. *Radiother. Oncol.* **2007**, *82*, 24–29.
30. Adams, G. E.; Clarke, E. D.; Flockhart, I. R.; Jacobs, R. S.; Sehmi, D. S.; Stratford, I. J.; Wardman, P.; Watts, M. E.; Parrick, J.; Wallace, R. G.; Smithen, C. E. Structure–activity relationships in the development of hypoxic cell radiosensitizers: I. Sensitization efficiency. *Int. J. Radiat. Biol.* **1979**, *35*, 133–150.
31. Butler, K.; Howes, H. L.; Lynch, J. E.; Pirie, D. K. Nitroimidazole derivatives. Relationship between structure and antitrichomonal activity. *J. Med. Chem.* **1967**, *10*, 891–897.
32. Roberts, P. B.; Denny, W. A.; Wakelin, L. P.; Anderson, R. F.; Wilson, W. R. Radiosensitization of mammalian cells *in vitro* by nitroacridines. *Radiat. Res.* **1990**, *123*, 153–164.
33. Wilson, W. R.; Siim, B. G.; Denny, W. A.; van Zijl, P. L.; Taylor, M. L.; Chambers, D. M.; Roberts, P. B. 5-Nitro-4-(*N*,*N*-dimethylaminopropylamino)quinoline (5-nitraquine), a new DNA-affinic hypoxic cell radiosensitizer and bioreductive agent: comparison with nitracrine. *Radiat. Res.* **1992**, *131*, 257–265.
34. Cowan, D. S. M.; Matejovic, J. F.; Wardman, P.; McClelland, R. A.; Rauth, A. M. Radiosensitizing and cytotoxic properties of DNA-targeted phenanthridine-linked nitroheterocycles of varying electron affinities. *Int. J. Radiat. Biol.* **1994**, *66*, 729–738.
35. Brown, J. M.; Wilson, W. R. Exploiting tumour hypoxia in cancer treatment. *Nat. Rev. Cancer* **2004**, *4*, 437–447.
36. Daniels, J. S.; Gates, K. S.; Tronche, C.; Greenberg, M. M. Direct evidence for bimodal DNA damage induced by tirapazamine. *Chem. Res. Toxicol.* **1998**, *11*, 1254–1257.

37. Hwang, J.-T.; Greenberg, M. M.; Fuchs, T.; Gates, K. S. Reaction of the hypoxia-selective antitumor agent tirapazamine with a C1′-radical in single-stranded and double-stranded DNA: the drug and its metabolites can serve as surrogates for molecular oxygen in radical-mediated DNA damage reactions. *Biochemistry* **1999**, *38*, 14248–14255.
38. Chowdhury, G.; Junnotula, V.; Daniels, J. S.; Greenberg, M. M.; Gates, K. S. DNA strand damage product analysis provides evidence that the tumor cell-specific cytotoxin tirapazamine produces hydroxyl radical and acts as a surrogate for O_2. *J. Am. Chem. Soc.* **2007**, *129*, 12870–12877.
39. Meisel, D.; Neta, P. One-electron redox potentials of nitro compounds and radiosensitizers. Correlation with spin densities of their radical anions. *J. Am. Chem. Soc.* **1975**, *97*, 5198–5203.
40. Wardman, P.; Clarke, E. D. One-electron reduction potentials of substituted nitroimidazoles measured by pulse radiolysis. *J. Chem. Soc., Faraday Trans. 1* **1976**, *72*, 1377–1390.
41. Wardman, P. Reduction potentials of one-electron couples involving free radicals in aqueous solution. *J. Phys. Chem. Ref. Data* **1989**, *18*, 1637–1755.
42. Wardman, P. The reduction potential of benzyl viologen: An important reference compound for oxidant/radical redox couples. *Free Radical Res. Commun.* **1991**, *14*, 57–67.
43. Wardman, P. The kinetics of the reaction of "anomalous" 4-nitroimidazole radiosensitizers with thiols. *Int. J. Radiat. Biol.* **1982**, *41*, 231–235.
44. Wardman, P. Thiol reactivity towards drugs and radicals: some implications in the radiotherapy and chemotherapy of cancer. In *Sulfur-Centered Reactive Intermediates in Chemistry and Biology*; Chatgilialoglu, C., Asmus, K.-D., Eds.; Plenum Press, New York, **1990**, pp. 415–427.
45. Wardman, P. Protonation of the radical-anions of nitro-imidazole radiosensitizers and the formation of radical-adducts. *Int. J. Radiat. Biol.* **1975**, *28*, 585–588.
46. O'Neill, P. One-electron reduction potentials of nitroimidazoles: correlation with polarographic half-wave potentials. *Anal. Proc.* **1980**, *17*, 282–283.
47. Wardman, P. Prediction and measurement of redox properties of drugs and biomolecules. In *Selective Activation of Drugs by Redox Processes*; Adams, G. E., Breccia, A., Fielden, E. M., Wardman, P., Eds.; Plenum Press, New York, 1990, pp. 11–24.
48. Taylor, Y. C.; Evans, J. W.; Brown, J. M. Radiosensitization by hypoxic pretreatment with misonidazole: an interaction of damage at the DNA level. *Radiat. Res.* **1987**, *109*, 364–373.
49. Millar, B. C.; Fielden, E. M.; Steele, J. J. Effect of oxygen-radiosensitizer mixtures on the radiation response of Chinese hamster cells, line V-79-753B, *in vitro*. II. Determination of the initial yield of single-strand breaks in the cellular DNA using a rapid lysis technique. *Radiat. Res.* **1980**, *83*, 57–65.
50. Tilby, M. J.; Loverock, P. S. Measurements of DNA double-strand break yields in *E. coli* after rapid irradiation and cell inactivation: The effects of inactivation technique and anoxic radiosensitizers. *Radiat. Res.* **1983**, *96*, 309–321.
51. Radford, I. R. The level of induced DNA double-strand breakage correlates with cell killing after X-irradiation. *Int. J. Radiat. Biol.* **1895**, *48*, 45–54.
52. Jenner, T. J.; Sapora, O.; O'Neill, P.; Fielden, E. M. Enhancement of DNA damage in mammalian cells upon bioreduction of the nitroimidazole-aziridines RSU-1069 and RSU-1131. *Biochem. Pharmacol.* **1988**, *37*, 3837–3842.

53. Buchko, G. W.; Weinfeld, M. Influence of nitrogen, oxygen and nitroimidazole radiosensitizers on DNA damage induced by ionizing radiation. *Biochemistry* **1993**, *32*, 2186–2193.
54. Hansch, C.; Fujita, T. ρ–σ–π Analysis. A method for the correlation of biological activity and chemical structure. *J. Am. Chem. Soc.* **1964**, *86*, 1616–1626.
55. Dennis, M. F.; Stratford, M. R. L.; Wardman, P.; Watts, M. E. Cellular uptake of misonidazole and analogues with acidic or basic functions. *Int. J. Radiat. Biol.* **1985**, *47*, 629–643.
56. Wardman, P. Chemical properties of "radiation modifiers" of DNA damage and their radiobiological effects. In *Early Effects of Radiation on DNA*; Fielden, E. M., O'Neill, P., Eds.; Springer-Verlag, Berlin, 1991, pp. 249–264.
57. Wardman, P. Molecular structure and biological activity of hypoxic cell radiosensitizers and hypoxic-specific cytotoxins. In *Advanced Topics on Radiosensitizers of Hypoxic Cells*; Breccia, A., Rimondi, C., Adams, G. E., Eds.; Plenum Press, New York, **1982**, pp. 49–75.
58. Hodgkiss, R. J.; Middleton, R. W. Enhancement of misonidazole radiosensitization by an inhibitor of glutathione biosynthesis. *Int. J. Radiat. Biol.* **1983**, *43*, 179–183.
59. Silver, A. R. J.; O'Neill, P. Interaction of the aziridine moiety of RSU-1069 with nucleotides and inorganic phosphate. Implications for alkylation of DNA. *Biochem. Pharmacol.* **1986**, *35*, 1107–1112.
60. Rauth, A. M.; Melo, T.; Misra, V. Bioreductive therapies: an overview of drugs and their mechanisms of action. *Int. J. Radiat. Oncol. Biol. Phys.* **1998**, *42*, 755–762.
61. Overgaard, J. Clinical evaluation of nitroimidazoles as modifiers of hypoxia in solid tumors. *Oncol. Res.* **1994**, *6*, 509–518.
62. Wardman, P.; Clarke, E. D. Redox properties and rate constants in free-radical mediated damage. *Br. J. Cancer* **1987**, *55* (Suppl. VIII), 172–177.
63. Ross, A. B.; Mallard, W. G.; Helman, W. P.; Buxton, G. V.; Huie, R. E.; Neta, P. NDRL-NIST Solution Kinetics Database: Version 3; Notre Dame Radiation Laboratory and National Institute of Standards and Technology, Notre Dame, Indiana and Gaithersburg, Maryland (see also http://www.rcdc.nd.edu/), 1998.
64. Rao, D. N. R.; Jordan, S.; Mason, R. P. Generation of nitro radical anions of some 5-nitrofurans, and 2- and 5-nitroimidazoles by rat hepatocytes. *Biochem. Pharmacol.* **1988**, *37*, 2907–2913.
65. Rao, D. N. R.; Harman, L.; Motten, A.; Schreiber, J.; Mason, R. P. Generation of radical anions of nitrofurantoin, misonidazole and metronidazole by ascorbate. *Arch. Biochem. Biophys.* **1987**, *255*, 419–427.
66. Orna, M. V.; Mason, R. P. Correlation of kinetic parameters of nitroreductase enzymes with redox properties of nitroaromatic compounds. *J. Biol. Chem.* **1989**, *264*, 12379–12384.
67. Ayscough, P. B.; Sargent, F. P.; Wilson, R. Electron spin resonance studies of radical anions. Part II. Aromatic nitro-compounds. *J. Chem. Soc.* **1963**, *1963*, 5418–5425.
68. Inbaraj, J. J.; Motten, A. G.; Chignell, C. F. Photochemical and photobiological studies of tirapazamine (SR 4233) and related quinoxaline 1,4-di-*N*-oxide analogues. *Chem. Res. Toxicol.* **2003**, *16*, 164–170.
69. Moore, D. E.; Chignell, C. F.; Sik, R. H.; Motten, A. G. General of radical anions from metronidazole, misonidazole and azathioprine by photoreduction in the presence of EDTA. *Int. J. Radiat. Biol.* **1986**, *50*, 885–891.

70. Adams, G. E.; Willson, R. L. Ketyl radicals in aqueous solution. Pulse radiolysis study. *J. Chem. Soc., Faraday Trans. 1* **1973**, *69*, 719–729.

71. Whillans, D. W.; Adams, G. E.; Neta, P. Electron-affinic sensitization. VI. A pulse radiolysis and ESR comparison of some 2- and 5-nitroimidazoles. *Radiat. Res.* **1975**, *62*, 407–421.

72. Asmus, K.-D.; Wigger, A.; Henglein, A. Pulsradiolytische Untersuchung einiger Elementarprozesse der Nitrobenzolreduktion. *Ber. Bunsenges. Phys. Chem.* **1966**, *70*, 862–868.

73. Jagannadham, V.; Steenken, S. One-electron reduction of nitrobenzenes by α-hydroxyalkyl radicals via addition/elimination. An example of an organic inner-sphere electron-transfer reaction. *J. Am. Chem. Soc.* **1984**, *106*, 6542–6551.

74. Henry, Y.; Guissani, A.; Hickel, B. Radicals of nitroimidazole derivatives: pH dependence of rates of formation and decay related to acid-base equilibria. *Int. J. Radiat. Biol.* **1987**, *51*, 797–809.

75. Wardman, P. Lifetimes of the radical-anions of medically-important nitroaryl compounds in aqueous solution. *Life Chem. Rep.* **1985**, *3*, 22–28.

76. Nese, C.; Schuchmann, M. N.; Steenken, S.; von Sonntag, C. Oxidation *vs.* fragmentation in radiosensitization. Reactions of α-alkoxyalkyl radicals with 4-nitrobenzonitrile and oxygen. A pulse radiolysis and product analysis study. *J. Chem. Soc., Perkin Trans. 2* **1995**, 1037–1044.

77. Bamatraf, M. M. M.; O'Neill, P.; Rao, B. S. M. Redox dependence of the rate of interaction of hydroxyl radical adducts of DNA nucleobases with oxidants: Consequences for DNA strand breakage. *J. Am. Chem. Soc.* **1998**, *120*, 11852–11857.

78. Griffiths, W. E.; Longster, G. F.; Myatt, J.; Todd, P. F. Electron spin resonance studies of electron-transfer reactions with aromatic nitro-compounds in aqueous media. *J. Chem. Soc. (B)* **1966**, 1130–1132.

79. McMillan, M.; Norman, R. O. C. Electron spin resonance studies. Part XVII. Reactions of some free radicals with nitroalkanes. *J. Chem. Soc. (B)* **1968**, 590–597.

80. Ayscough, P. B.; Elliott, A. J.; Salmon, G. A. *In situ* radiolysis electron spin resonance study of the radical-anions of substituted nitroimidazoles and nitroaromatic compounds. *J. Chem. Soc., Faraday Trans. 1* **1978**, *74*, 511–518.

81. Jagannadham, V.; Steenken, S. One-electron reduction of nitrobenzenes by OH and H radical adducts to 6-methyluracil and 6-methylisocytosine via electron transfer and addition/elimination. Effects of substituents on rates and activation parameters for formation and heterolysis of nitroxyl-type tetrahedral intermediates. *J. Phys. Chem.* **1988**, *92*, 111–118.

82. Jagannadham, V.; Steenken, S. Reactivity of α-heteroatom-substituted alkyl radicals with nitrobenzenes in aqueous solution: An entropy-controlled electron-transfer/addition mechanism. *J. Am. Chem. Soc.* **1988**, *110*, 2188–2192.

83. Steenken, S. One-electron redox reactions between radicals and molecules. Dominance of inner-sphere mechanisms. In *Free Radicals in Synthesis and Biology*; Minisci, F., Ed.; Kluwer Academic Publishers, Dordrecht, 1989, pp. 213–231.

84. Steenken, S. One-electron redox reactions between radicals and organic molecules. An addition/elimination (inner-sphere) path. *Top. Current Chem.* **1996**, *177*, 125–145.

85. Sharma, G.; Rao, B. S. M.; O'Neill, P. Redox dependence of the reactions of α-alkoxyalkyl radical with a series of oxidants. *J. Phys. Chem.* **2009**, *113*, 2207–2211.

86. von Sonntag, C.; Schuchmann, H.-P. Radiation chemistry of the nucleobases. In *Radiation Chemistry: Present Status and Future Trends*; Jonah, C. D., Rao, B. S. M., Eds.; Elsevier: Amsterdam, 2001, pp. 513–551.
87. O'Neill, P. Radiation-induced damage in DNA. In *Radiation Chemistry: Present Status and Future Trends*; Jonah, C. D., Rao, B. S. M., Eds.; Elsevier, Amsterdam, 2001, pp. 585–622.
88. Wardman, P.; Clarke, E. D. Electron transfer and radical-addition in the radiosensitization and chemotherapy of hypoxic cells. In *New Chemo and Radiosensitizing Drugs*; Breccia, A., Fowler, J. F., Eds.; Lo Scarabeo, Bologna, 1985, pp. 21–38.
89. Clarke, E. D.; Wardman, P.; Goulding, K. H. Anaerobic reduction of nitroimidazoles by reduced flavin mononucleotide and by xanthine oxidase. *Biochem. Pharmacol.* **1980**, *29*, 2684–2687.
90. Clarke, E. D.; Goulding, K. H.; Wardman, P. Nitroimidazoles as anaerobic electron-acceptors for xanthine oxidase. *Biochem. Pharmacol.* **1982**, *31*, 3237–3242.
91. Wardman, P.; Dennis, M. F.; White, J. A probe for intracellular concentrations of drugs: delayed fluorescence from acridine orange. *Int. J. Radiat. Oncol. Biol. Phys.* **1989**, *16*, 935–938.
92. Pogozelski, W. K.; Tullius, T. D. Oxidative strand scission of nucleic acids: Routes initiated by hydrogen abstraction from the sugar moiety. *Chem. Rev.* **1998**, *98*, 1089–1107.
93. Cadet, J.; Douki, T.; Gasparutto, D.; Ravanat, J. L. Oxidative damage to DNA: Formation, measurement and biochemical features. *Mutation Res.* **2003**, *531*, 5–23.
94. Breen, A. P.; Murphy, J. A. Reactions of oxyl radicals with DNA. *Free Radic. Biol. Med.* **1995**, *18*, 1033–1077.
95. Hong, I. S.; Carter, K. N.; Sato, K.; Greenberg, M. M. Characterization and mechanism of formation of tandem lesions in DNA by a nucleobase peroxyl radical. *J. Am. Chem. Soc.* **2007**, *129*, 4089–4098.
96. Greenstock, C. L.; Chapman, J. D.; Raleigh, J. A.; Shierman, E.; Reuvers, A. P. Competitive radioprotection and radiosensitization in chemical systems. *Radiat. Res.* **1974**, *59*, 556–571.
97. Howard-Flanders, P. Effect of nitric oxide on the radiosensitivity of bacteria. *Nature* **1957**, *180*, 1191–1192.
98. Gray, L. H.; Green, F. O.; Hawes, C. A. Effect of nitric oxide on the radiosensitivity of tumour cells. *Nature* **1958**, *182*, 952–953.
99. Mitchell, J. B.; Wink, D. A.; DeGraff, W.; Gamson, J.; Keefer, L. K.; Krishna, M. C. Hypoxic mammalian cell radiosensitization by nitric oxide. *Cancer Res.* **1993**, *53*, 5845–5848.
100. Wardman, P.; Rothkamm, K.; Folkes, L. K.; Woodcock, M.; Johnston, P. J. Radiosensitization by nitric oxide at low radiation doses. *Radiat. Res.* **2007**, *167*, 475–484.
101. Lymar, S. V.; Shafirovich, V.; Poskrebyshev, G. A. One-electron reduction of aqueous nitric oxide: a mechanistic revision. *Inorg. Chem.* **2005**, *44*, 5212–5221.
102. Shafirovich, V.; Lymar, S. V. Nitroxyl and its anion in aqueous solutions: spin states, protic equilibria, and reactivities toward oxygen and nitric oxide. *Proc. Natl. Acad. Sci. USA* **2002**, *99*, 7340–7345.
103. Willson, R. L. The reaction of oxygen with radiation-induced free radicals in DNA and related compounds. *Int. J. Radiat. Biol.* **1970**, *17*, 349–358.

104. Folkes, L. K.; Wardman, P. Kinetics of the reaction between nitric oxide and glutathione: Implications for thiol depletion in cells. *Free Radic. Biol. Med.* **2004**, *37*, 549–556.

105. Ford, E.; Hughes, M. N.; Wardman, P. Kinetics of the reactions of nitrogen dioxide with glutathione, cysteine, and uric acid at physiological pH. *Free Radic. Biol. Med.* **2002**, *32*, 1314–1323.

106. Cadet, J.; Téoule, R. Radiation-induced binding of radiosensitizing drugs to DNA. In *Free Radicals and Cancer*; Floyd, R. A., Ed.; Marcel Dekker, New York, 1982, pp. 183–200.

107. Millar, B. C.; Fielden, E. M.; Smithen, C. E. Polyfunctional radiosensitizers. II. Interaction of the biradical (Ro 03-6061) with reducing species. *Radiat. Res.* **1977**, *71*, 516–527.

108. O'Neill, P.; Jenkins, T. C.; Fielden, E. M. Interaction of oxygen and nitroxyls with radiation-induced radicals of DNA and related bases in aqueous solution. *Radiat. Res.* **1980**, *82*, 55–64.

109. Nishimoto, S.; Ide, H.; Wada, T.; Kagiya, T. Radiation-induced hydroxylation of thymine promoted by electron-affinic compounds. *Int. J. Radiat. Biol.* **1983**, *44*, 585–600.

110. Dedon, P. C. The chemical toxicology of 2-deoxyribose oxidation in DNA. *Chem. Res. Toxicol.* **2008**, *21*, 206–219.

111. Infante, G. A.; Guzman, P.; Alvarez, R.; Figueroa, A.; Correa, J. N.; Myers, J. A.; Lanier, L. J.; Williams, T. M.; Burgos, S.; Vera, J.; Neta, P. Radiosensitization by derivatives of isoindole-4,7-dione. *Radiat. Res.* **1984**, *98*, 234–241.

112. Wang, Y. Bulky DNA lesions induced by reactive oxygen species. *Chem. Res. Toxicol.* **2008**, *21*, 276–281.

113. Wardman, P. The importance of radiation chemistry to radiation- and free radical-biology. The 2008 Silvanus Thompson Memorial Lecture. *Br. J. Radiol.* **2009**, *82*, 89–104.

11

REACTIONS OF REACTIVE NITROGEN SPECIES AND CARBONATE RADICAL ANIONS WITH DNA

VLADIMIR SHAFIROVICH, CONOR CREAN, AND NICHOLAS E. GEACINTOV
Chemistry Department and Radiation and Solid State Laboratory, New York University, New York, NY 10003, USA

11.1. INTRODUCTION

Recent epidemiological studies suggest that chronic inflammation and infections are associated with the development of some human cancers.[1–3] Chronic inflammation induces persistent oxidative and nitrosative stress that is associated with the overproduction of oxidative DNA modifications (lesions).[4–6] The latter, if not excised by the cellular DNA repair machinery, can give rise to point mutations, deletions, and rearrangements and, finally, to the development of cancer. The activation of neutrophils and macrophages gives rise to the production of nitric oxide and superoxide radical anions that, in turn, rapidly combine to form the highly toxic peroxynitrite[7]:

$$NO + O_2^{\bullet -} \rightarrow ONOO^-$$

This reaction occurs with a nearly diffusion-controlled rate constant of $6.7 \times 10^9\,M^{-1}s^{-1}$.[8] In neutral solutions, peroxynitrite exists in equilibrium with unstable peroxynitrous acid ($pK_a = 6.5$–6.8)[9,10] that decays with a rate constant[11] of $1.3\,s^{-1}$ at 25 °C to form hydroxyl and nitrogen dioxide radicals with a yield of $x \sim 0.30$[12]:

$$ONOOH \rightarrow x(^{\bullet}NO_2 + {}^{\bullet}OH) + (1-x)(NO_3^- + H^+)$$

Radical and Radical Ion Reactivity in Nucleic Acid Chemistry, Edited by Marc M. Greenberg

In carbonate buffer solutions, the lifetime of peroxynitrite is greatly reduced due to its reaction with free carbon dioxide (rate constant of $2.9 \times 10^4\,M^{-1}s^{-1}$) present in solution[13]:

$$ONOO^- + CO_2 \rightarrow ONOOCO_2^-$$

The nitrosoperoxycarbonate anion formed in this reaction is highly unstable and decomposes to form nitrogen dioxide and carbonate radical anions with a yield of $y \sim 0.33$[12]:

$$ONOOCO_2^- \rightarrow y(^{\bullet}NO_2 + CO_3^{\bullet -}) + (1-y)(NO_3^- + CO_2)$$

In vivo, the concentrations of CO_2 are relatively high due to high levels of bicarbonate in intracellular (12 mM) and interstitial (30 mM) fluids,[14] and the reaction of $ONOO^-$ with CO_2 is expected to be the major pathway of decay of peroxynitrite in biological systems.[5, 15]

Among the radicals that are believed to be formed under inflammatory conditions, hydroxyl radicals, carbonate radical anions, and nitrogen dioxide radicals are strong one-electron oxidants,[16] which can potentially damage biomolecules.[17] These radicals exhibit different reactivities toward DNA. Hydroxyl radicals with a reduction potential[16] of $E^0 = 1.9$ V versus NHE are extremely strong electrophiles that rapidly and unselectively react with DNA mostly via addition to the double bonds of nucleobases and by abstraction of hydrogen atoms from the 2-deoxyribose moieties.[18–20] The chemistry and genotoxic effects of $^{\bullet}OH$ radicals generated by ionizing radiation, or derived from Fenton reactions, have been studied extensively.[21–23] In this work we focus on oxidative damage due to the reactions of $CO_3^{\bullet -}$ and $^{\bullet}NO_2$ radicals with DNA. These reactions result in the formation of highly mutagenic oxidation and nitration products and will be considered in the next Sections.

11.2. SITE-SELECTIVE OXIDATION OF GUANINE BASES IN DNA BY CARBONATE RADICAL ANIONS

Carbonate radical anions with the reduction potential[24] of $E^0 = 1.59$ V versus NHE can selectively and rapidly oxidize biomolecules by one-electron abstraction mechanisms.[17] In contrast, hydrogen atom abstraction by the $CO_3^{\bullet -}$ radicals is generally slow.[17] The conjugate acid ($HCO_3^{\bullet}$) is a strong acid ($pK_a < 0$), and at $pH > 0$ these radicals exist in the anion form, $CO_3^{\bullet -}$.[25] The $CO_3^{\bullet -}$ radicals exhibit a broad absorption band at 600 nm ($\varepsilon_{600} = 1970\,M^{-1}cm^{-1}$)[25] and can be detected in real time by spectroscopic transient absorption methods.[17] The predominant target of $CO_3^{\bullet -}$ attack is guanine, which can be more easily oxidized than any of the other natural nucleobases, thus resulting in diverse mutagenic oxidation products.[6, 26, 27] The reduction potential of guanine neutral radicals at pH 7,[28] E_7, is 1.29 V versus NHE, and its oxidation by $CO_3^{\bullet -}$ radicals by a one-electron mechanism is thus thermodynamically feasible. Indeed, we have demonstrated experimentally that $CO_3^{\bullet -}$ radicals

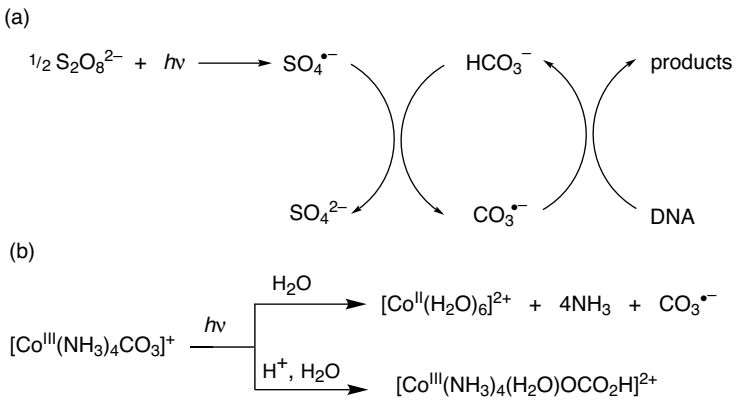

FIGURE 11.1. Photochemical generation of $CO_3^{\bullet -}$ radicals. (Adapted from references 30 and 37.)

can induce the site-selective one-electron oxidation of guanine in 2′-deoxyribo-oligonucleotides in either the single- or double-stranded forms.[29–37]

In these experiments, $CO_3^{\bullet -}$ radicals (Figure 11.1) were generated either by the one-electron oxidation of bicarbonate anions with photochemically generated sulfate radicals,[29–38] or by the photolysis of carbonatotetrammineCo(III) complexes,[37] $[Co(NH_3)_4CO_3]^+$. In the first method, irradiation with either steady-state [30, 33, 36–38] or pulsed UV light (e.g., 308-nm XeCl excimer laser pulses [29, 31, 32, 34, 35]) of a buffered solution containing bicarbonate and persulfate anions induces the dissociation of the $S_2O_8^{2-}$ ions to sulfate radical anions, $SO_4^{\bullet -}$ (Figure 11.1A). In turn, the one-electron oxidation of the HCO_3^- ions by $SO_4^{\bullet -}$ radicals generates $CO_3^{\bullet -}$ radicals. This method is suitable for the generation of $CO_3^{\bullet -}$ radicals at pH $\geq$ 7.5. At pH $<$ 7.5, the HCO_3^- anions are transformed to CO_2 and thus the yield of $CO_3^{\bullet -}$ radicals decreases as the pH is decreased, because $SO_4^{\bullet -}$ radicals can oxidize both the HCO_3^- and CO_3^{2-} anions, but not CO_2.[17] In the second method, UV irradiation of $[Co(NH_3)_4CO_3]^+$ complexes (Figure 11.1B) induces charge transfer from coordinated CO_3^{2-} anions to Co(III) followed by a rapid hydrolysis of the Co(II) complex and the formation of free $CO_3^{\bullet -}$ radicals.[39–41] Using this method, $CO_3^{\bullet -}$ radicals can be generated within a wide pH range (3–13).[39–42] We found that $CO_3^{\bullet -}$ radicals, regardless of the method of generation, exhibit the same reactivities toward DNA and produce the same end-products.[37]

Laser kinetic spectroscopy methods can be used to monitor the kinetics of one-electron oxidation of guanine in DNA by $CO_3^{\bullet -}$ radicals in real time.[29, 31, 34, 35, 37] In typical experiments, the decay of the $CO_3^{\bullet -}$ transient absorbance at 600 nm is correlated with the appearance of a narrow absorption band near 315 nm. This band is characteristic of the guanine radical cation, $G^{\bullet +}$, or the guanine neutral radical, $G(-H)^{\bullet}$, species, which have similar absorption spectra.[43] The free nucleoside radical cation, $dG^{\bullet +}$, is a weak acid[43] ($pK_a = 3.9$) that, according to the results of pulse radiolysis studies, deprotonates at pH 7.0 with a rate constant of $1.8 \times 10^7\ s^{-1}$.[44] In double-stranded DNA, depending on the position within a DNA strand, the rate

constant of deprotonation ($\geq 3 \times 10^6\ s^{-1}$) is smaller than that of free $dG^{\bullet+}$,[44] but is of sufficient magnitude to entail the complete deprotonation of $G^{\bullet+}$ in the millisecond time range when G in DNA is oxidized by $CO_3^{\bullet-}$ radical.

The rate constants of oxidation of guanine in DNA by $CO_3^{\bullet-}$ radicals were determined from the analysis of the decay curves of $CO_3^{\bullet-}$ radicals monitored at 600 nm.[29,31,34,35,37] The values of the rate constants measured for double-stranded 20- to 35-mer oligonucleotides with noncontiguous guanines G, or guanines grouped as contiguous GG and GGG sequences, are in a rather narrow range of $(1.5–3.0) \times 10^7\ M^{-1}s^{-1}$. These rate constants exhibit a very weak temperature dependence with activation energies of 7 ± 3 kJ/mol. The lack of dependence of the rate constant on sequence context and the small activation energy indicate that the one-electron oxidation of guanine in DNA by $CO_3^{\bullet-}$ radicals occurs via an inner-sphere mechanism of electron transfer[34,35] that was proposed earlier for the one-electron oxidation of diverse organic molecules such as ascorbate, tryptophan, cysteine, and methionine by $CO_3^{\bullet-}$ radicals.[45]

In contrast, the rate constants of oxidation of guanines in DNA by the aromatic radical cations of the pyrene derivative 7,8,9,10-tetrahydroxytetrahydrobenzo[*a*]-pyrene (BPT) follow the trend 5′-..GGG.. > 5′-..GG.. > 5′-..G. . . that is characteristic of an outer-sphere mechanism of electron transfer.[34,35] However, the distributions of alkali-labile guanine lesions generated by $CO_3^{\bullet-}$ radicals, as well by $BPT^{\bullet+}$ radical cations, are base sequence context-dependent. Guanine oxidation damage is more abundant at the 5′-G in 5′-..GG.. sequences and at the first two 5′-guanines in the 5′-.. GGG.. sequences than in isolated guanines—that is, those that are not flanked by other guanines. These distributions are attributed to (a) the redistribution of guanine radicals along contiguous guanine bases (hole hopping) after electron abstraction from guanine (hole injection) and (b) the subsequent chemical reactions that lead to product formation at a particular guanine in runs of GG or GGG. Such effects are characteristic of the oxidation of DNA by one-electron oxidants generated by the photosensitization of metal complexes,[46,47] anthraquinones,[48,49] naphthalimides,[50] riboflavin,[51,52] 4′-pivaloyl derivatives,[53,54] cyanobenzoyl- and cyanobenzophenone-substituted 2′-deoxyuridine,[55,56] and other chemical one-electron oxidants.[57,58] Saito and co-workers have shown that the enhancement of oxidative guanine damage within runs of of contiguous guanines varies according to 5′-G < 5′-GG < 5′-GGG. This trend is correlated with the calculated gas-phase ionization potentials for guanines in these different sequence contexts.[51,59,60]

11.3. INTRASTRAND CROSS-LINKS BETWEEN G AND T BASES GENERATED BY CARBONATE RADICAL ANIONS

Direct spectroscopic measurements have shown that the DNA-bound G(-H)$^{\bullet}$ radicals generated by $CO_3^{\bullet-}$ radicals do not react with observable rate constants with molecular oxygen,[29,31,37] and their modes of decay involve reactions with other free radicals or nucleophiles.[6,26,27] To reduce the contributions of radical–radical reactions, the $CO_3^{\bullet-}$ radicals were generated in low steady-state concentrations by

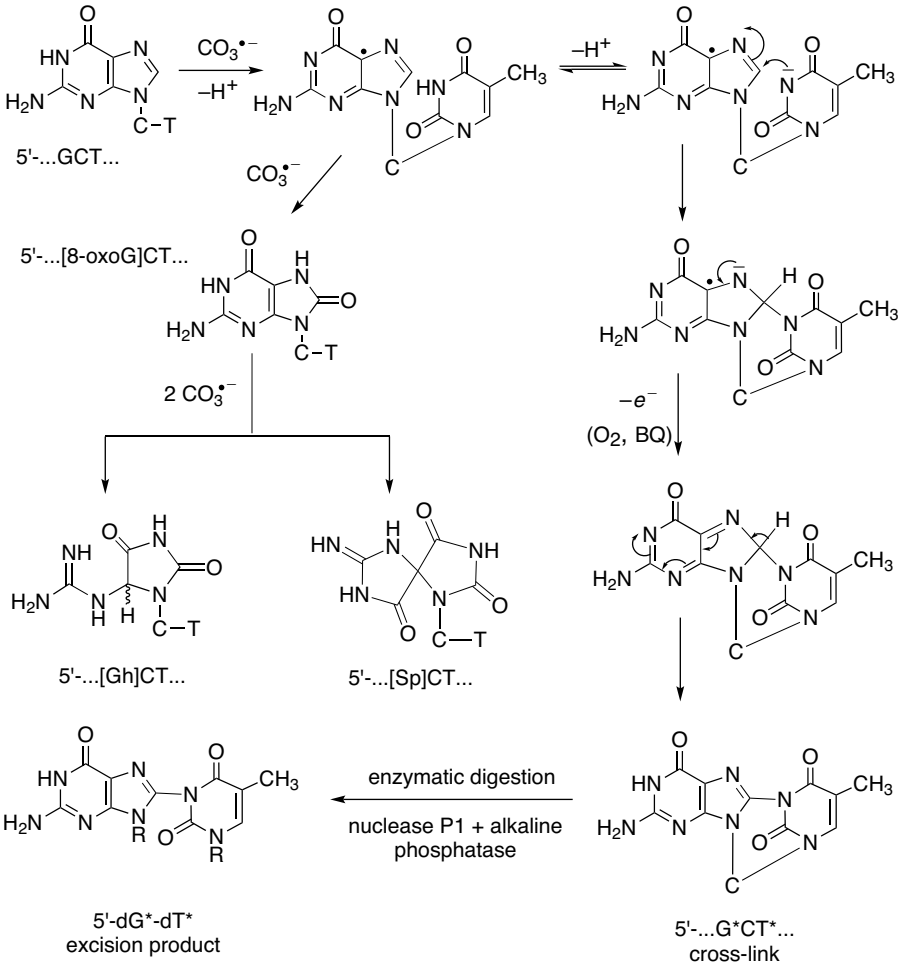

FIGURE 11.2. Lesions derived from the oxidation of guanine by $CO_3^{\bullet -}$ radicals in single-stranded oligonucleotides containing a 5′. . .GCT. . . sequence. (Adapted from references 36 and 37).

continuous illumination methods. Under these conditions, the oxidation of the single-stranded oligonucleotide, 5′-d(CCATCGCTACC), by $CO_3^{\bullet -}$ radicals generates three prominent oligonucleotide reaction products containing guanine lesions.[36, 37] These adducts isolated by anion-exchange HPLC methods and identified by mass spectrometry techniques include guanidinohydantoin (Gh) and two diastereomeric spiroiminodihydantoin (Sp) lesions, as well as a novel intrastrand cross-linked product involving a covalent bond between guanine and thymine (Figure 11.2). The latter was excised from the oligonucleotide adduct by enzymatic digestion with nuclease P1 and alkaline phosphatase and was identified by LC-MS/MS analysis. The positive ion spectra (MS/MS) of the digestion products showed that an excision fragment with

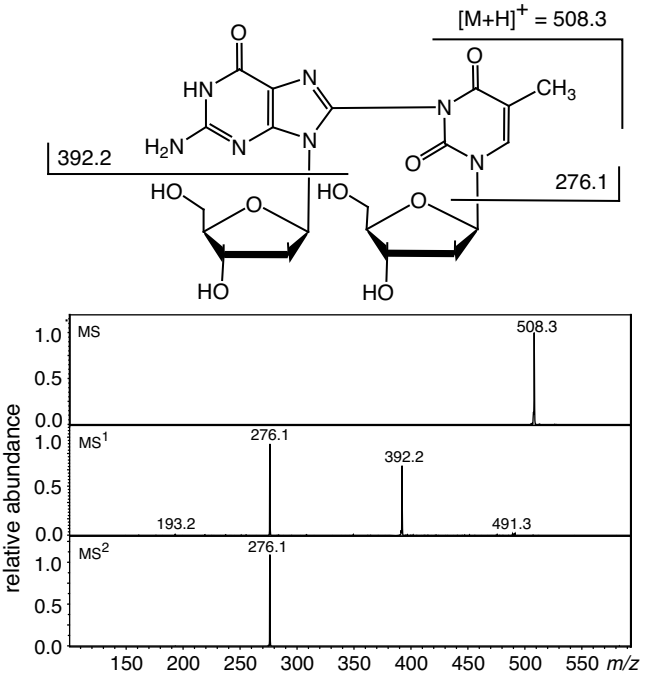

FIGURE 11.3. Positive ion spectra (MS/MS) of the d(G*-T*) product obtained by the enzymatic digestion of the cross-linked products (Figure 11.2). MS spectrum of the molecular ion $[M+H]^+$ at *m/z* 508.3. MS^1 product ion spectrum obtained by fragmentation of the molecular ion $[M+H]^+$ at *m/z* 508.3. MS^2 product ion spectrum obtained by fragmentation of the ion $[M+H-116]^+$ at *m/z* 392.2. (Reproduced with permission from *Nucleic Acids Res.* **2008**, *36*, 742–755. Copyright 2008, Oxford University Press.)

molecular ion $[M+H]^+$ detected at *m/z* 508.3 has a mass that is smaller by 2 Da than the combined masses of dG and dT (Figure 11.3). The fragmentation of the $[M+H]^+$ ion occurs via a consecutive detachment of two sugar residues to yield the ion with *m/z* 276.1 assigned to the G*-T* fragment that has mass equivalent to the sum of the G and T masses minus 2 Da.

The structure of the d(G*-T*) excision fragment is unusual because G and T are not adjacent to one another in the parent oligonucleotide. The precursor of the enzymatic digestion product, 5′-d-(G*pCpT*), has been synthesized via the oxidation of the 5′-d-(GpCpT) trinucleotide and investigated by LC-MS/MS, 1D and 2D NMR methods.[36] The positive ion spectra show the molecular ion $[M+H]^+$ detected at *m/z* 859.1, which has a mass that is smaller by 2 Da than the mass of the parent 5′-d(GpCpT) trinucleotide. In turn, the fragmentation of the $[M+H]^+$ ion yields the ion with *m/z* 276.0 and is assigned to the G*-T* fragment, just as in the case of the ion derived from dG*-dT* cross-linked product. The 1D proton NMR spectra of 5′-d(G*pCpT*) recorded in D_2O clearly show that guanine is linked to the T base via its C8 carbon atom because the guanine H8 proton, which is of course present in the spectrum of the

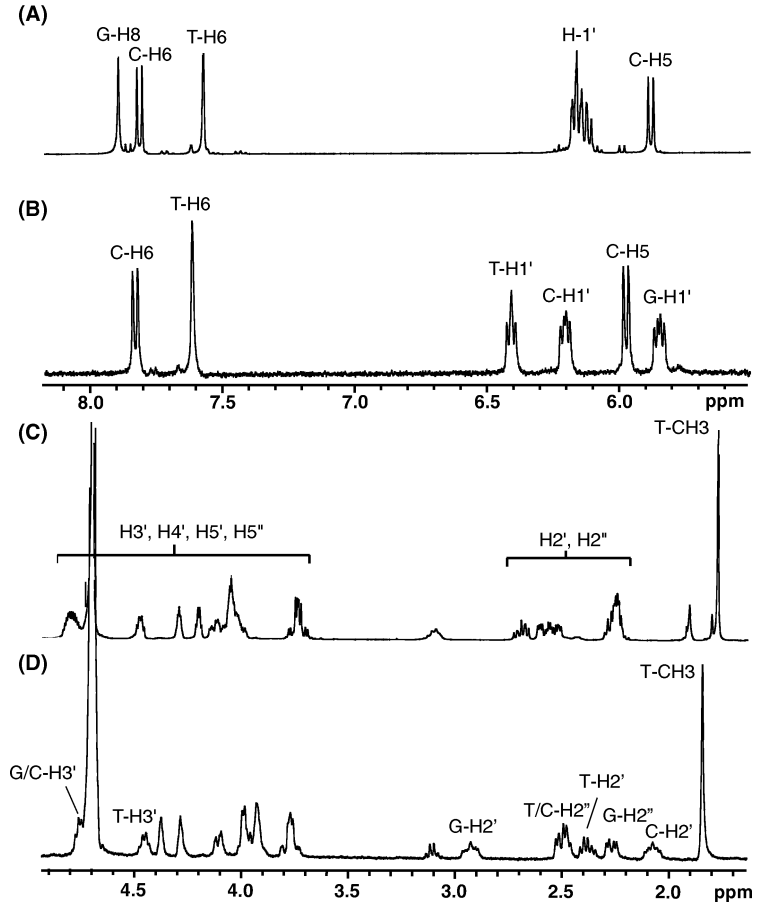

FIGURE 11.4. The 1D proton NMR spectra of the intact 5′-d(GpCpT) (A and C) and 5′-d(G*pCpT*) (B and D) are compared. (Reproduced with permission from *Nucleic Acids Res.* **2008**, *36*, 742–755. Copyright 2008, Oxford University Press.)

intact and original 5′-d(GpCpT) trinucleotide at 7.9 ppm, is absent in the cross-linked product (Figure 11.4). In contrast, the thymine singlets of H6 at 7.61 ppm and methyl group at 1.85 ppm are evident in the 5′-d(G*pCpT*) cross-link and with small shifts in the parent 5′-d(GpCpT) as well. Thus, the covalent bond in the cross-link does not involve the thymine methyl group or the C6 carbon atom. Further analysis of 1D ^{13}C NMR, 2D COSY, HSQC, and HMBC spectra allowed the assignment of most of the resonances and suggests that the covalent link between G and T in 5′-d(G*pCpT*) occurs via the G-C8 and T-N3 atoms.

The efficiency of G-T cross-link formation is strongly dependent on base sequence.[36] The highest efficiency of cross-linking was found in the 5′-d(GpCpT) sequence. In the case of 5′-d(GpT) that lacks intervening C bases, the efficiency of formation of the G*–T* product is almost three times lower. Increasing the number of C

bases between the G and T reaction partners also resulted in a decrease in the efficiency of cross-link formation—for example, when there are two C bridging residues as in the case of the tetranucleotide 5′-d(GCCT). In the case of the 5′-d(GCCCT) sequence that has three bridging C bases, cross-linked products were not detected. Furthermore, the intrastrand 5-d(T*pG*) cross-links were not detected in the dinucleotide 5′-d(TpG) either, although there is a substantial yield in the isomeric 5′-d(GpT). This latter result supports the conclusion, reached on the basis of experiments with the isomeric 5′-d-(GpCpT) and 5′-d(TpCpG), that cross-link formation is more efficient when the T residue is on the 3′-side rather than on the 5′-side of the guanine.

In double-stranded DNA, we found intrastrand cross-links between adjacent G and T bases.[36] Interestingly, enzymatic digestion with nuclease P1 and alkaline phosphatase generates the 5′-d(G*pT*) fragment; that is, this treatment does not excise the sugar residue between the G and T bases.

Thymine is not a unique pyrimidine that can be involved in intrastrand cross-link formation, a reaction initiated by the one-electron abstraction from guanine. Indeed, we found that similar cross-links can be generated by an analogous oxidation of 5′-r(GpCpU) and 5′-d(GpCpU) trinucleotides containing the uracil base instead of thymine.[38] The latter is a demethylated form of thymine (with an H atom instead of a methyl group at C5), in which the N3(H) group remains available for cross-link formation with the C8 site of guanine. In contrast to DNA, where T pairs with A, in RNA uracil is the complementary base to adenine. The positive ion MS/MS spectra of the 5′-r(G*pCpU*) and 5′-d(G*pCpU*) products clearly indicate the presence of covalently linked G*–U* products that have a mass smaller by 2 Da than the sum of masses the G and U bases in both types of trinucleotides. The 5′-d(G*CU*) cross-linked product was characterized by 1D and 2D NMR methods that confirmed its cyclic structure in which the guanine C8 atom is covalently linked to the uracil N3 atom.

Covalent bond formation between G and T (or U) requires the abstraction of two electrons. According to the results of transient absorption measurements, the $CO_3^{\bullet-}$ radical selectively abstracts an electron from a G base.[29–37] However, $CO_3^{\bullet-}$ radicals are not uniquely required for the generation of cross-linked products. Indeed, any one-electron oxidant that has a reduction potential that is sufficient for electron abstraction from guanine (e.g., the $SO_4^{\bullet-}$ radical), as well as photoexcited riboflavin, a typical type I photosensitizer that reacts with guanine via an electron transfer mechanism, also generates the 5′-G*CT* cross-linked products.[36, 38] To gain further insights into the second electron abstraction step, the effect of molecular oxygen on the cross-linking reaction was explored. In the absence of O_2, the yields of the G*–T* (or G*–U*) cross-linked products are negligible.[36, 38] Since the 5′-G*CT* (or 5′-G*CU*) cross-linked products do not contain any added oxygen atoms, molecular oxygen is needed for the oxidation of an intermediate. Indeed, addition of 100 μM 1,4-benzoquinone (BQ) to the solutions extensively purged with argon to remove O_2 restores the generation of 5′-G*CT* (or 5′-G*CU*).[38] Benzoquinone is a moderate one-electron oxidant with a redox potential, $E^0(BQ/BQ^{\bullet-}) = 0.078$ V versus NHE,[61] and it is not surprising that BQ can serve as a surrogate for molecular oxygen, which is a weaker one-electron oxidant ($E^0(O_2/O_2^{\bullet-}) = -0.16$ V versus NHE).[16]

Mechanistically, the formation of the G*–T* (or G*–U*) cross-links can be considered as a one-electron oxidation of guanine by an appropriate oxidant, followed by a nucleophilic addition of the N3 atom of T(or U) to the C8 position of the G(-H)• radical (Figure 11.1). The radical adduct thus formed is further oxidized by oxygen (or another oxidant, such as 1,4-benzoquinone) to yield the G*–T* (or G*–U*) cross-linked products.[38] This mechanism is supported by a significant increase of the cross-linked product yields when the pH is increased to ≥ 10. The deprotonation of T-N3(H) with $pK_a = 9.67$[62] occurring in basic solutions greatly enhances the nucleophilicity of T-N3, and at pH 10 the yield of G*–T* cross-linked product is greater by a factor of 4.8 relative to the yield measured at pH 7.5. The enhancement of cross-linked product yields has also been observed in the case of 5′-GCU sequences[38] because T-N3(H) and U-N3(H) have the same pK_a values.[62] Similar mechanisms have been proposed by Perrier et al.[63] for the formation of cross-linked products between guanine and lysine mediated by the riboflavin photosensitization of d(TpGpT) in aerated solutions containing the KKK tripeptide. These authors suggested that the cross-linking reaction occurs via a nucleophilic addition of the ε-amino group of the lysine residue to the C8 atom of the $G^{\bullet+}$ or G(-H)• radicals, followed by the oxidation of the radical adduct formed, an *Nε*-(guanin-8-yl)-lysine cross-link.

11.3.1. Comparisons with Intrastrand Cross-Links Generated by •OH Radicals

The existence of intrastrand cross-links between adjacent G–T bases in oligonucleotides (the so-called tandem lesions) have been previously discovered by Box and co-workers.[64–67] These tandem lesions are generated by the oxidation of oligonucleotides with GT sequences by radiation-induced •OH radicals in deoxygenated solutions. In these products, the intrastrand cross-link involves a covalent bond between guanine C8 and the thymine C5 methyl group (Figure 11.5). The mass of these products is

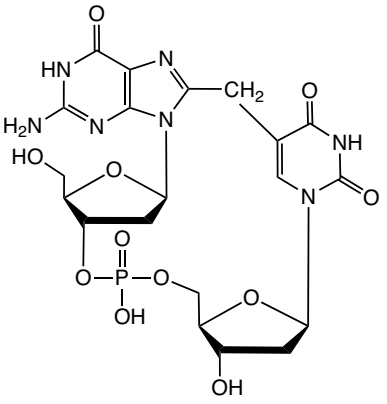

FIGURE 11.5. Tandem lesions generated by the oxidation of oligonucleotides with GT sequences by radiation-induced •OH radicals in deoxygenated solutions.[64–67]

smaller by 2 Da than the mass of the precursor G–T sequences and the mechanism involves the formation of the C-centered 5-(2′-deoxyuridinyl)methyl radical (U-$^{\bullet}CH_2$) intermediate.[68,69] Indeed, it has been shown that the independent generation of U-$^{\bullet}CH_2$ radicals by photolysis of 5-(phenylthiomethyl)-2′-deoxyuridine results in the formation of these G–T tandem lesions. The U-$^{\bullet}CH_2$ radicals rapidly react with O_2, thus suppressing the formation of the covalent bond between U-$^{\bullet}CH_2$ and G-C8.[70] On the other hand, oxygen does not prevent the formation of the M-2 tandem lesions between adjacent A and T bases.[71,72] Greenberg and co-workers[69,71,72] proposed that the reaction of the U-$^{\bullet}CH_2$ radicals with O_2 is reversible [$k(O_2) = 2 \times 10^9\ M^{-1}s^{-1}$, and $k_{-}(O_2) = 3.4\ s^{-1}$] and the small transient concentrations of these radicals present in oxygenated solutions can account for the formation of the tandem lesions. The formation of the 5-(2′-deoxyuridinyl)methyl radical intermediates suggests that the initial cross-linking step can occur via the oxidation of thymine[68,69] mediated by $^{\bullet}OH$ radicals induced by ionizing radiation[64–67] or derived from Fenton reactions.[73]

11.4. END PRODUCTS DERIVED FROM THE REACTIONS OF CARBONATE RADICAL ANIONS WITH GUANINE RADICALS

Laser pulse excitation generates high transient concentrations of free radicals that favor radical–radical combination reactions over nucleophilic addition reactions, which are more favorable under continuous illumination when the radical concentrations are lower. The formation of the Sp and Gh end-products involves several consecutive reactions of intermediates with $CO_3^{\bullet-}$ radicals, while the formation of the G*CT* cross-linked product involves only one carbonate radical (Figure 11.2). Our experiments have demonstrated that the reactions resulting in the formation of Sp/Gh lesions include the intermediate formation of 8-oxo-7,8-dihydroguanine (8-oxoG) (Figure 11.2), which is the product of a two-electron oxidation of guanine.[31] The maximum yield of the 8-oxodG nucleoside enzymatically excised from the 5′-d(CCATCGCTACC) sequence oxidized by $CO_3^{\bullet-}$ radicals, and determined by the HPLC-amperometric detection methods, does not exceed ~2%. The low yield of 8-oxodG is a clear indication that the oxidation of 5′-d(CCATC[8-oxoG]CTACC) is much faster than that of the parent 5′-d(CCATCGCTACC) sequence. Indeed, laser flash photolysis experiments have shown that the rate constant of oxidation of 5′-d(CCATC[8-oxoG]CTACC) by $CO_3^{\bullet-}$ radicals is greater by a factor of ~13 than the value of the analogous rate constant for the oxidation of 5′-d(CCATCGCTACC). Another factor that decreases the transient yields of 8-oxoG lesions is their fast oxidation by G(-H)$^{\bullet}$ radicals. The reduction potential of 8-oxodG(-H)$^{\bullet}$ radicals,[74] $E_7 = 0.74$ V versus NHE, is lower than that of G(-H)$^{\bullet}$ radicals,[28] $E_7 = 1.29$ V versus NHE. Thus, dG(-H)$^{\bullet}$ radicals oxidize 8-oxodG with the relatively large rate constant of $4.6 \times 10^8\ M^{-1}s^{-1}$.[74] The fast reduction of dG(-H)$^{\bullet}$ radicals by 8-oxodG, a reaction that leads to the recovery of the parent dG, provides a very efficient protection of dG against oxidation[75]; this explains why the levels of 8-oxodG are low (less than 0.1% of the dG degradated) in photooxidation reactions of dG mediated by the photexcitation of

riboflavin.[76] However, in double-stranded DNA, the repair of G(-H)$^{\bullet}$ radicals by intermolecular mechanisms is much less efficient than in the case of free nucleosides. Our laser flash photolysis experiments showed that the rate constant for oxidation of 8-oxoG in the duplex containing the 5′-d(CCATC[8-oxoG]CTACC) by the G(-H)$^{\bullet}$ radicals positioned in another duplex ($2.7 \times 10^6\,M^{-1}s^{-1}$) is two orders of magnitude smaller than the rate constant of oxidation of free nucleosides.[77] The intramolecular oxidation of 8-oxoG by G$^{\bullet+}$/G(-H)$^{\bullet}$ radicals can be an alternative mechanism for the repair of the latter radicals in double-stranded DNA. However, the kinetic parameters of this reaction remain unknown. The further oxidation of 5′-d(CCATC[8-oxoG]CTACC) by $CO_3^{\bullet-}$ radicals results in the formation of the Sp/Gh lesions only (cross-linked adducts were not detectable) and that, therefore, the sequence 5′-d(CCATC[8-oxoG]CTACC) is likely to be an intermediate in the oxidation of 5′-d(CCATCGCTACC) by $CO_3^{\bullet-}$ radicals when guanine is transformed to either Sp or Gh after oxidation (Figure 11.2).

A deeper understanding of the mechanistic aspects of the consecutive three-electron oxidation of the G(-H)$^{\bullet}$ radicals by $CO_3^{\bullet-}$ radicals was gained by studying the formation of Sp lesions from the free nucleoside[33] (2′,3′,5′-tri-*O*-acetylguanosine) and in DNA duplexes derived from the self-complementary sequence,[37] 5′-d(AACGCGAATTCGCGTT) in $H_2{}^{18}O$ buffer solutions. In the latter experiments, the Sp lesions were enzymatically excised from the oxidized DNA in the form of 5′-d(C[Sp]). Analysis of the tri-*O*-acetyl-Sp and 5′-d(C[Sp]) nucleosides by LC-MS/MS methods showed that both oxygen atoms added to the C5 and C8 positions of the oxidized guanine intermediates originate from the $C^{16}O_3^{\bullet-}$ radicals (Figure 11.6). In agreement with these observations, the oxidation of the 8-oxoG derivatives by $CO_3^{\bullet-}$ radicals generates the Sp products containing only one additional O-atom that originates from $C^{16}O_3^{\bullet-}$ radicals. In contrast, Sp nucleoside products are found to contain ^{18}O atoms when the reactions are carried out in buffer solutions that contain carbonic anhydrase[79] that enhances isotope exchange between $HC^{16}O_3^-$ and $H_2{}^{18}O$. These experiments clearly show that the reaction mechanisms leading to Sp oxidation products involve consecutive bimolecular combination reactions of $CO_3^{\bullet-}$ radicals with G(-H)$^{\bullet}$ and 8-oxoG(-H)$^{\bullet}$ radicals (Figure 11.6). The primary products of these radical–radical combination reactions can be considered as monoesters of the carbonic acid (H_2CO_3). The classical works of Polanyi,[80] Ingold,[81] and co-workers showed that, in the acid–base hydrolysis of esters, the ^{18}O atoms from water are transferred to the acid component and not to the alcohol product. In agreement with this mechanism of ester hydrolysis, the O atoms in Sp originate from the $CO_3^{\bullet-}$ radicals and not from H_2O (Figure 11.6). Therefore, the combination reactions of $CO_3^{\bullet-}$ radicals with G(-H)$^{\bullet}$ and 8-oxoG(-H)$^{\bullet}$ radicals can be formally considered as a transfer of O^- from $CO_3^{\bullet-}$ to these radicals. The O^- transfer mechanism has been proposed earlier on the basis of pulse radiolysis experiments for the reactions of $CO_3^{\bullet-}$ radicals with the inorganic radicals, $^{\bullet}NO_2$, $SO_3^{\bullet-}$, and $^{\bullet}NO$ that result in the formation of CO_2, NO_3^-, SO_4^{2-}, and NO_2^- anions.[82,83] In contrast, metal complexes such as $IrCl_6^{2-}$ induce the consecutive abstraction of two electrons from 8-oxoG, followed by the addition of water molecules to the carbo-cation intermediates. Thus the oxygen atoms in the Sp residues originate from water.[84]

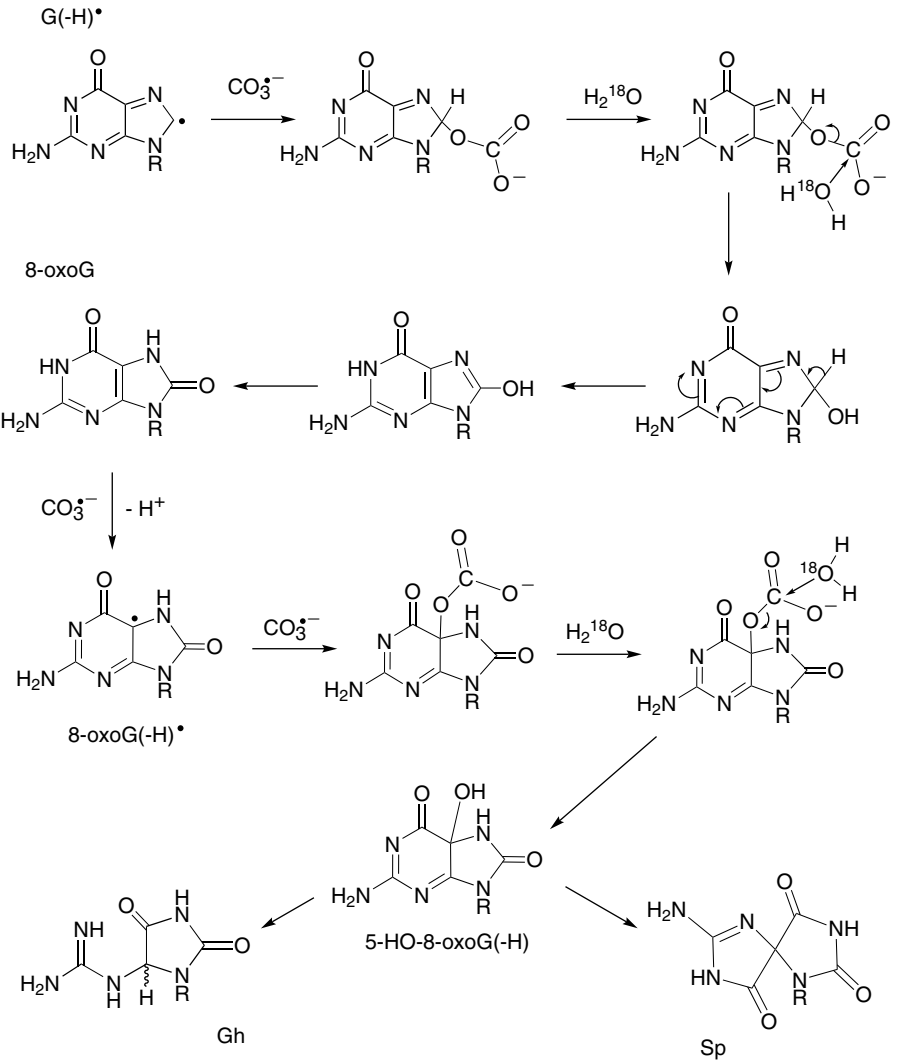

FIGURE 11.6. The O^- transfer mechanism of the combination of $CO_3^{\bullet -}$ radicals with G(-H)• and 8-oxoG(-H)• radicals to form the Sp and Gh lesions. The isotope exchange between $C^{16}O_3^{\bullet -}$ and $H_2{}^{18}O$ is very slow,[78] and both O-atoms added to the C5 and C8 positions of the G intermediates originate from the $C^{16}O_3^{\bullet -}$ radicals (not from $H_2{}^{18}O$). (Adapted from references 33 and 37.)

The hydrolysis of the monoesters derived from the combination of the 8-oxoG(-H)• and $CO_3^{\bullet -}$ radicals can generate the 5-HO-8-oxoG intermediate that is considered to be a precursor of the Sp and Gh products.[84, 85] The subsequent transformation of this 5-HO-8-oxoG intermediate to form either Sp or Gh lesions depends on the pH of the soluion. Tannenbaum and co-workers[86] proposed that the partitioning

of 5-HO-8-oxoG(-H) into either Sp or Gh is determined by the different reactivities of the deprotonated and protonated forms of this adduct ($pK_a \sim 5.8$). Decreasing the pH below 5.8 favors pyrimidine ring opening, followed by the formation of the Gh lesions; in contrast, the acyl shift leading to the Sp lesions dominates at pH > 5.8. This pH dependence qualitatively agrees with the enhancement of the yield of Gh products at low pH that has been reported for the oxidation of 8-oxoG by either peroxynitrite,[86] photoexcited riboflavin, $IrCl_6^{2-}$,[87,88] or Cr(VI) complexes.[89]

11.5. COMBINATION OF GUANINE RADICALS AND NITROGEN DIOXIDE RADICALS GENERATES NITRATION PRODUCTS

The reduction potential of nitrogen dioxide radicals[16] of $E^0 = 1.04$ V versus NHE is less than the reduction potential of guanine neutral radicals,[28] $E_7 = 1.29$ V versus NHE. Thus, the oxidation of guanine by $^{\bullet}NO_2$ radicals is thermodynamically unfavorable. Indeed, our laser flash photolysis experiments have shown that $^{\bullet}NO_2$ radicals do not react with guanine with observable rates and, in turn, G(-H)$^{\bullet}$ radicals positioned in single-stranded oligonucleotides oxidize NO_2^- anions with the rate constant of $\sim 1 \times 10^6\ M^{-1}s^{-1}$.[90] However, $^{\bullet}NO_2$ radicals can combine with radical intermediates generated by the oxidation of guanine with stronger oxidants than $^{\bullet}NO_2$ (e.g., with $CO_3^{\bullet-}$ radicals) to form diverse nitration products. To explore these radical-to-radical addition reactions, we developed two photochemical methods for the generation of controlled fluxes of G(-H)$^{\bullet}$ and $^{\bullet}NO_2$ radicals (Figure 11.7). The first method (Figure 11.7A) involves the competitive oxidation of NO_2^- and HCO_3^- anions by photochemically generated $SO_4^{\bullet-}$ radicals to form $^{\bullet}NO_2$ and $CO_3^{\bullet-}$ radicals.[30,32] The G(-H)$^{\bullet}$ radicals derived from the site-selective one-electron oxidation of guanines by $CO_3^{\bullet-}$ radicals rapidly combine with $^{\bullet}NO_2$ radicals to form guanine nitration products. In the second method (Figure 11.7B), $^{\bullet}NO_2$ radicals are generated by the one-electron reduction of NO_3^- anions by hydrated electrons derived from the selective two-photon ionization of 2-aminopurine (2AP), a nucleic acid base analogue site-specifically positioned in DNA.[90] The 2AP absorption band in the UV region is characterized by a broad maximum at 305 nm, which is beyond the threshold of absorption of DNA at ~300 nm. Therefore, the canonical DNA bases are not photoionized by 308-nm nanosecond laser pulses of the XeCl excimer laser used in these experiments. The 2AP radicals are ionized first to the radical cation, $2AP^{\bullet+}$, that deprotonates to form the neutral radical, 2AP(-H)$^{\bullet}$. These 2AP radicals selectively oxidize nearby G bases to form G(-H)$^{\bullet}$ radicals, a process that is completed within 100 μs after the incidence of the ~10-ns duration 308-nm excimer laser pulse. Subsequently, the combination of the G(-H)$^{\bullet}$ and $^{\bullet}NO_2$ radicals occurs on millisecond timescales and can be directly monitored by transient absorption laser kinetic spectroscopy. These transient absorption experiments showed that the decay of the narrow absorption band of the G(-H)$^{\bullet}$ radicals at 315 nm is correlated with the growth of the characteristic absorption band of the nitration products at 385 nm. The combination of the G(-H)$^{\bullet}$ and $^{\bullet}NO_2$ radicals occurs with similar rate constants ($\sim 4.4 \times 10^8\ M^{-1}s^{-1}$) in both single- and double-stranded DNA.[90]

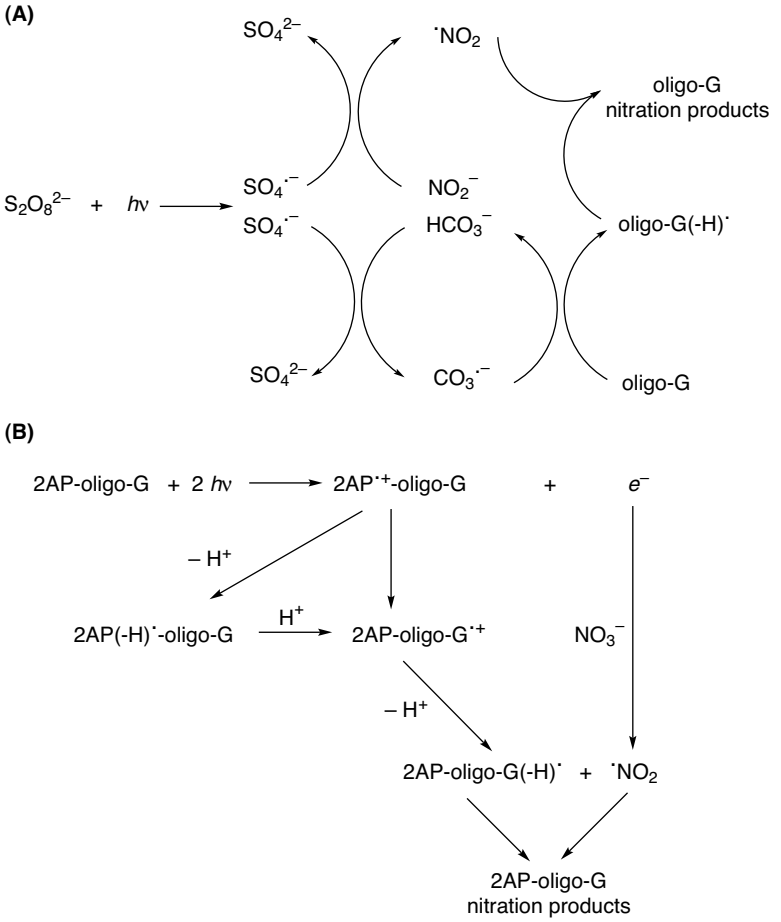

FIGURE 11.7. Two methods of site-selective nitration of guanines in DNA by photochemically generated $^{\bullet}NO_2$ radicals. (Adapted from references 30, 32, and 90.)

The $^{\bullet}NO_2$ radicals, regardless of the method of their generation, produce the same nitrated end products.[30, 32, 90] These products were isolated by HPLC and identified by mass spectrometry methods. We found that the combination of the G(-H)$^{\bullet}$ and $^{\bullet}NO_2$ radicals occurs via addition of $^{\bullet}NO_2$ radicals to either the C8 or the C5 positions of G(-H)$^{\bullet}$ radicals (Figure 11.8). In the $^{\bullet}NO_2$ radical, the unpaired electron is delocalized on the N and the O atoms[91] and, in principle, both the N and the O atoms can participate in the formation of chemical bonds with a target radical. Here, we found that the formation of end products occurs via formation of the N–C bond between $^{\bullet}NO_2$ and G(-H)$^{\bullet}$ radicals. Addition of $^{\bullet}NO_2$ to the C8 position of G(-H)$^{\bullet}$ radical generates the well-known 8-nitroguanine (8-nitroG) lesions, whereas the attack at the C5 position produces unstable adducts that rapidly decompose to 5-guanidino-4-nitroimidazole (NIm) lesions (Figure 11.8). The maximum yields of the nitroproducts

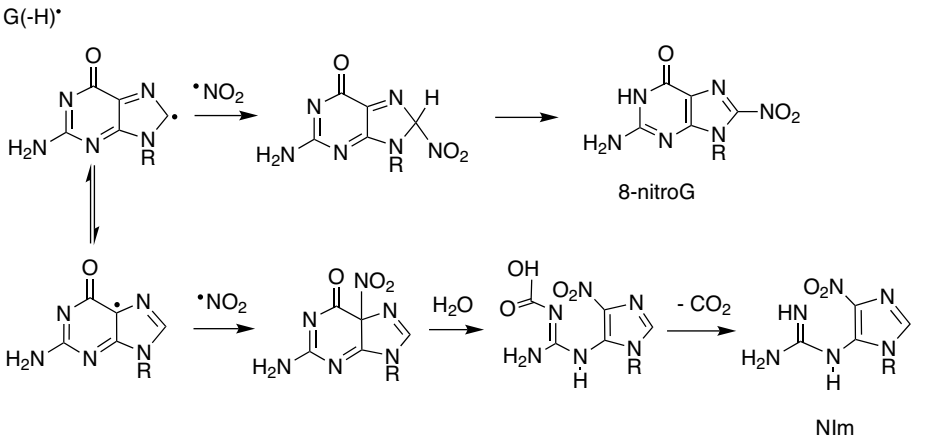

FIGURE 11.8. Formation of nitration products via the combination of G(-H)• with •NO_2 radicals. (Adapted from references 30, 32, and 90.)

(NIm + 8-nitro-G) were typically in the range of 20–40%, depending on the number of guanine residues in the sequence. The ratio of the 5-guanidino-4-nitroimidazole and 8-nitro-G lesions gradually decreases from 3.4 in the model compound, 2′,3′,5′-tri-*O*-acetylguanosine, to 2.1 – 2.6 in the single-stranded oligodeoxynucleotides, and to 0.8–1.1 in the duplexes.

In contrast, the oxidation of 8-oxodG ($E_7 = 0.74$ V versus NHE) by •NO_2 radicals ($E^0 = 1.04$ V versus NHE) is thermodynamically feasible and occurs with a rate constant of $5.3 \times 10^6\,M^{-1}s^{-1}$.[92] Our laser flash photolysis experiments showed that the combination of the 8-oxoG(-H)• and •NO_2 radicals occurs with similar rate constants ($\sim 4.3 \times 10^8\,M^{-1}s^{-1}$) in both single- and double-stranded DNA.[90] The products of these radical–radical addition reactions are mostly the diastereomeric Sp lesions (Figure 11.9). In the case of 8-oxoG(-H)• radicals, the C5 nitro (or nitrite) adduct formed is unstable. The hydrolysis of this adduct can occur via a nucleophilic addition of the water molecule to C5, followed by the release of the NO_2^- anion and the formation of the 5-HO-8-oxoG(-H) intermediate, which is believed to be the precursor of the Sp lesions (Figure 11.9). According to this mechanism, the 5-HO-8-oxoG(-H) adduct, and hence the Sp end products, contain the oxygen atom from $H_2{}^{18}O$ (not from •$N^{16}O_2$). The subsequent transformation of the 5-HO-8-oxoG(-H) intermediate depends on the solution pH and results in the formation of either Sp or Gh lesions.[37, 84, 86, 87, 89] The proposed mechanism (Figure 11.9) explains two important observations: (i) The combination of •NO_2 and 8-oxoG(-H)• radicals occurs with a rate constant typical for radical-radical addition reactions, and (ii) the O atom in the oxidation product originates from water. An alternative mechanism is the electron transfer from 8-oxoG(-H)• to •NO_2 with the formation of the intermediate 8-oxoG $(-H)^+$ cation and NO_2^- anion. Addition of $H_2{}^{18}O$ to the 8-oxoG$(-H)^+$ cation proposed by Burrows and co-workers during the course of 8-oxoG oxidation by $IrCl_6^{4-}$ leads to the 5-HO-8-oxoG(-H) precursor of the Gh and Sp lesions containing the ^{18}O-isotope

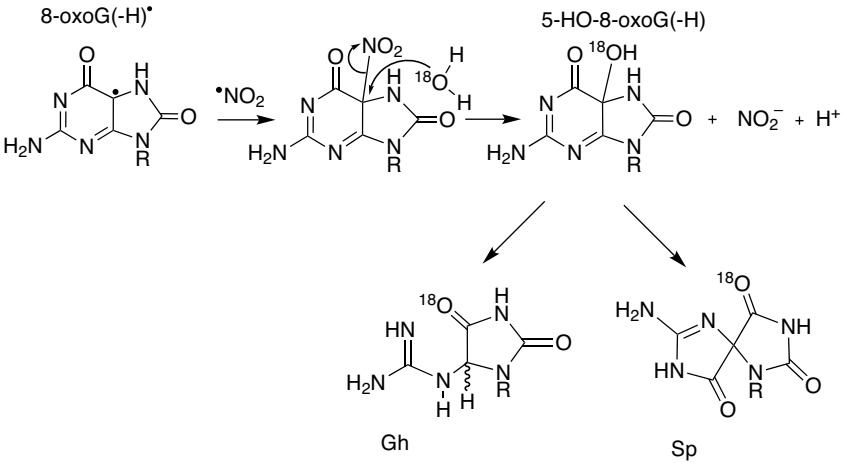

FIGURE 11.9. Formation of oxidation products via the combination of 8-oxoG(-H)• with $^{\bullet}NO_2$ radicals. (Adapted from reference 90.)

that originates from water molecules.[84,93] However, such an electron transfer mechanism cannot explain the high rate constants for the combination reaction measured here experimentally for both the 8-oxoG(-H)• radicals and the G(-H)• radicals ($\sim 4.3 \times 10^8\,M^{-1}s^{-1}$). The electron transfer reactions of $^{\bullet}NO_2$ radicals are typically slow due to a small self-exchange rate constant and high internal reorganization energy in the $^{\bullet}NO_2/NO_2^-$ system.[94] These factors account for the lower reactivity of $^{\bullet}NO_2$ radicals in bimolecular outer-sphere electron transfer reactions in comparison with typical electron acceptors, such as aromatic radical cations.[92]

11.6. THE ROLE OF SUPEROXIDE AND PEROXYL RADICALS IN THE GENERATION OF GUANINE LESIONS

The overproduction of alkyl peroxyl radicals (ROO•) is one of the key events that occur as a result of the inflammatory response in tissues that arises from an enhancement of lipid peroxidation.[95] The hydroperoxyl radical, $HO_2^{\bullet}$, is a special radical in the family of peroxyl radicals, because it not only has the oxidizing properties of other ROO• radicals, but also can participate in reduction reactions.[96] The $HO_2^{\bullet}$ radical is a weak acid with $pK_a = 4.8$ and therefore exists in neutral solution predominantly as the superoxide radical anion, $O_2^{\bullet -}$.[97] The enhanced production of $O_2^{\bullet -}$ radicals under inflammatory conditions occurs as a result of the activation of microphages.[5] As an electron donor with a redox potential[16] of $E^0 = -0.16$ V versus NHE, superoxide is easily oxidized by electron acceptors with an appropriate reduction potential.[97] However, due to their oxidative properties, $O_2^{\bullet -}$ radicals can also contribute to the formation of oxidation end products via radical–radical addition reactions.[96] To explore these radical combination pathways, we developed a photochemical

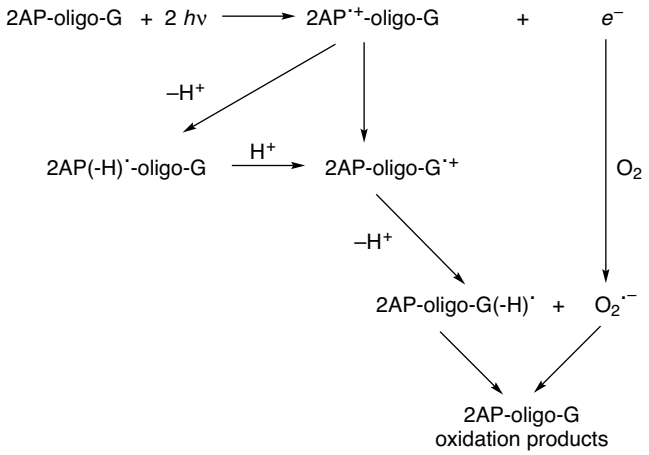

FIGURE 11.10. Photochemical generation of G(-H)$^{\bullet}$ and $O_2^{\bullet -}$ radicals in DNA. (Adapted from reference 77.)

method to generate G(-H)$^{\bullet}$ and $O_2^{\bullet -}$ radicals in DNA.[77] In this method (Figure 11.10), hydrated electrons derived from the two-photon ionization of the 2AP residues are rapidly and quantitatively scavenged by dissolved molecular oxygen to form $O_2^{\bullet -}$ radicals.[97]

Our laser flash photolysis experiments have shown that the combination of the G(-H)$^{\bullet}$ and $O_2^{\bullet -}$ radicals in single- and double-stranded oligonucleotides occurs with the same rate constant $\sim 4.7 \times 10^8\ M^{-1}s^{-1}$.[77] Addition of Cu,Zn-superoxide dismutase (Cu,Zn-SOD), which reacts with $O_2^{\bullet -}$ radicals with nearly diffusion-controlled rates,[98,99] dramatically enhances the lifetimes of the DNA-bound G(-H)$^{\bullet}$ radicals from 4–7 ms to 0.2–0.6 s in the presence of micromolar concentrations of Cu,Zn-SOD ($\sim$5 μM).[77] This remarkable increase in the G(-H)$^{\bullet}$ lifetimes is a clear indication that the reaction partner of G(-H)$^{\bullet}$ radicals is indeed the superoxide anion. The combination of G(-H)$^{\bullet}$ with $O_2^{\bullet -}$ radicals involves the following reaction pathways: (i) repair of G(-H)$^{\bullet}$ radicals by an electron transfer mechanism resulting in the formation of the intact guanine base G and O_2, and (ii) formation of oxidation end products via radical–radical addition mechanisms.[77] The latter products were isolated by HPLC and identified by mass spectrometry methods. Our experiments showed that these products in both single- and double-stranded DNA are mostly 2,5-diamino-4*H*-imidazolone lesions (Iz) and minor amounts of 8-oxoG lesions (Figure 11.11). Addition of $O_2^{\bullet -}$ to the C5 position of G(-H)$^{\bullet}$, followed by a rapid protonation of the adduct formed, generates the 5-HOO-G(-H) hydroperoxide. Cleavage of this unstable intermediate occurs via the opening of the pyrimidine ring at the C5–C6 bond, leading to an unstable intermediate that is easily hydrated at the 7,8-C=N double bond. Ring-chain tautomerization of the carbinolamine results in the opening of the imidazole ring with a subsequent intramolecular cyclization of the guanidine residue resulting in the Iz lesions, which are slowly hydrolyzed to

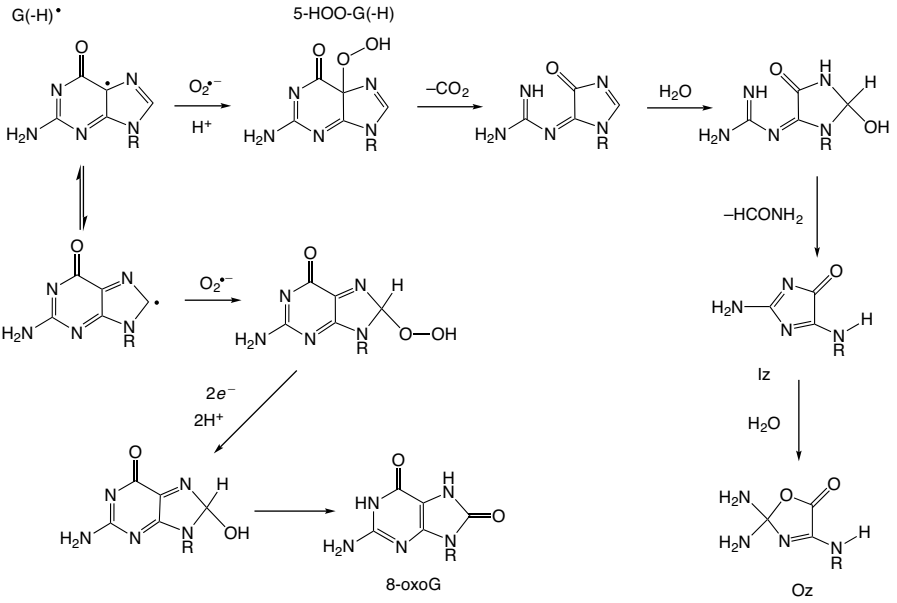

FIGURE 11.11. Formation of 8-oxoG and Iz lesions via the combination of the G(-H)• radicals with $O_2^{\bullet -}$ in DNA. (Adapted from reference 77.)

form 2,2-diamino-4-amino-2,5-dihydrooxazol-5-one (Oz) derivatives. In agreement with this mechanism the ^{18}O-labeling experiments showed that the O atom in the Iz lesion originates from oxygen.[100] Moreover, we found that in the presence of 1,4-benzoquinone added in small concentrations at a level of $\sim 100\,\mu M$, the yields of the Iz lesions become negligible because the addition of BQ can eliminate $O_2^{\bullet -}$ and G(-H)• radicals. First, BQ rapidly reacts with $O_2^{\bullet -}$ with a rate constant of $9 \times 10^8\,M^{-1}s^{-1}$.[97] Second, the $BQ^{\bullet -}$ radical thus produced ($E^0 = 0.078$ V versus NHE)[61] can rapidly reduce the G(-H)• radical ($E_7 = 1.29$ V versus NHE),[28] because of the significant difference in the redox potentials of these species.

In contrast, the ^{18}O-labeling experiments reveal that there are two pathways of 8-oxoG formation, including either the addition of $O_2^{\bullet -}$ to the C8 position of G(-H)• radicals (Figure 11.11) or the hydration of the $G^{\bullet +}$/G(-H)• radicals.[77,101] The two-electron reduction of the 8-HOO-G(-H) hydroperoxide formed leads to 8-oxoG in which the O atom originates from $^{16}O_2$, which is reduced to $O_2^{\bullet -}$ by hydrated electrons. Alternatively, $O_2^{\bullet -}$ radicals can be generated by the oxidation of hydrogen peroxide by Fe^{3+} ions. Indeed, the appearance of the ^{18}O atom in 8-oxoG has been detected during the course of oxidation of human A549 lung epithelial cells by $H_2{}^{18}O_2$.[102] In laser pulse excitation experiments, a decrease in the $^{16}O_2^{\bullet -}$ concentrations (by removal of $^{16}O_2$ from the solutions) favors the hydration of guanine radicals by $H_2{}^{18}O$ that results in the formation of 8-HO-G• radicals.[77] Pulse radiolysis experiments showed that 8-HO-dG• radicals generated by the addition of hydroxyl radicals to dG are strong reductants that are easily oxidized by weak oxidants

such as methylviologen, $Fe(CN)_6^{3-}$, oxygen,[103] and benzoquinone,[104] potentially resulting in the formation of 8-oxodG. According to this mechanism, the O atom in 8-oxodG originates from $H_2{}^{18}O$. Cadet and co-workers[101] showed that 8-oxodG derived from the oxidation of calf thymus DNA by excited riboflavin, a typical type I photodynamic agent, contains O atoms from $H_2{}^{18}O$. The transient concentrations of the radical species (and $O_2^{\bullet -}$) in these experiments with continuous excitation should be orders of magnitude lower than in our laser flash photolysis experiments, and thus the hydration can compete with the combination reactions of guanine radicals with superoxide radicals.

The combination of $O_2^{\bullet -}$ with 8-oxoG(-H)$^\bullet$ radicals in double- and single-stranded DNA occurs with the rate constant of $(1.0–1.3) \times 10^8\,M^{-1}s^{-1}$.[105] The major end products of this reaction are the dehydroguanidinohydantoin lesions (Gh_{ox}) derived from the addition of $O_2^{\bullet -}$ to the C5 position of 8-oxoG(-H)$^\bullet$, followed by the decomposition of the 5-HOO-8-oxoG(-H) hydroperoxide (Figure 11.12). According to this mechanism, the cleavage of 5-HOO-8-oxoG(-H) occurs via the opening of the pyrimidine ring at the C5–C6 bond in 5-HOO-8-oxoG(-H), thus leading to an unstable intermediate that is easily decomposed with the release of CO_2 and the formation of Gh_{ox}.[105] The Gh_{ox} lesions are unstable and slowly hydrolyze to oxaluric acid (Oa). In the presence of Cu,Zn-SOD, the yields of the Gh_{ox} lesions become negligible. Under these conditions, the 8-oxoG radicals do not exhibit any observable reactivities with oxygen ($k < 10^2\,M^{-1}s^{-1}$), they decay on the time interval of several seconds, and the major reaction products are the diastereomeric Sp lesions that are derived via the hydration of 8-oxoG(-H)$^\bullet$.[105]

In contrast to $HO_2^\bullet/O_2^{\bullet -}$ radicals, the ROO$^\bullet$ radicals derived from lipid peroxidation have only oxidizing properties.[96] The reduction potential of these radicals,[106, 107] $E_7 = 1.0–1.1$ V versus NHE, is lower than the reduction potential of G(-H)$^\bullet$ radicals,[28] $E_7 = 1.29$ V versus NHE, and the oxidation of guanine by ROO$^\bullet$ radicals is thus thermodynamically unfavorable. The bond dissociation energies (BDE) of the ROO–H bonds are ~88 kcal/mol, regardless of the exact structure of R.[108] This value is lower than the BDE of a guanine–hydrogen bond (94.3 ± 0.5 kcal/mol).[109] Hence, even within the uncertainties in the BDE values, it is unlikely that H-atom abstraction from G residues by ROO$^\bullet$ radicals can occur with observable rates. In agreement with these thermodynamic expectations, our experiments have shown that the major role of ROO$^\bullet$ radicals in the oxidation of guanine is their combination with G(-H)$^\bullet$ radicals.[110] In these experiments, the peroxyl radicals were generated by the addition of O_2 to C-centered radicals of polyunsaturated fatty acids, such as arachidonic acid (ArAc). Our laser flash photolysis experiments showed that ArAc peroxyl radicals are unstable and spontaneously generate $O_2^{\bullet -}$ radicals (Figure 11.13). The formation of $O_2^{\bullet -}$ radicals was directly monitored by the reduction of tetranitromethane[96, 97] and occurs with a rate constant of $3.4 \times 10^4\,s^{-1}$.[110]

The major products derived from the reactions of G(-H)$^\bullet$ radicals and ArAc peroxyl radicals are the Iz, Gh_{ox}, and diastereomeric Sp lesions. The mechanisms of the Iz (Figure 11.11) and Gh_{ox} (Figure 11.12) generation suggest that at least a fraction of these lesions is produced as a result of combination reactions of G(-H)$^\bullet$ [or 8-oxoG(-H)$^\bullet$] radicals with $O_2^{\bullet -}$ derived from the unimolecular decay of the lipid peroxyl

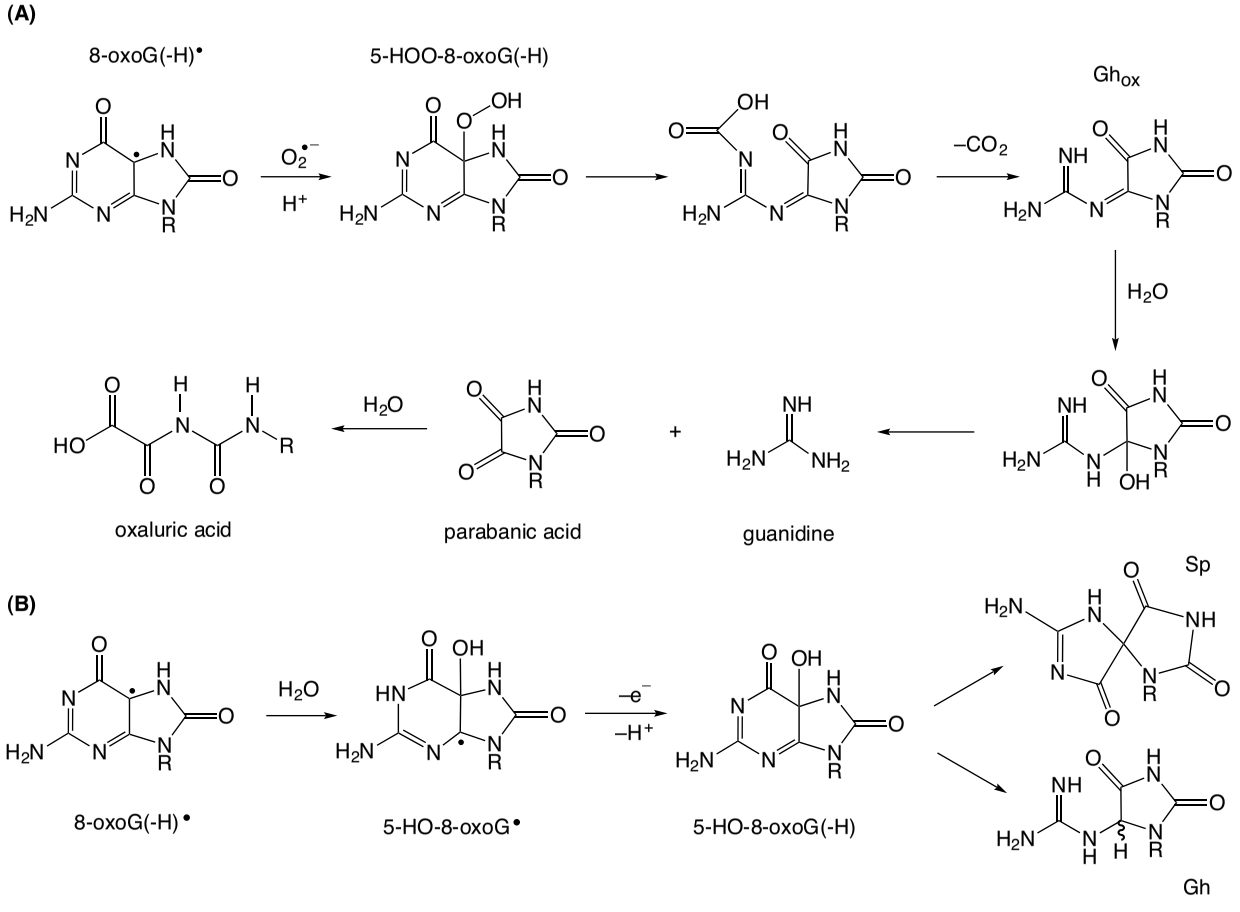

FIGURE 11.12. Distribution of reaction products of 8-oxoG(-H)• radicals in aqueous DNA solutions. (**A**) Formation of the oxaluric acid lesions via the combination reaction of 8-oxoG(-H)• with $O_2^{\bullet -}$ radicals. (**B**) Reaction pathways leading to the spiroiminodihydantoin and guanidinohydantoin adducts in the absence of superoxide radicals (Adapted from reference 105.)

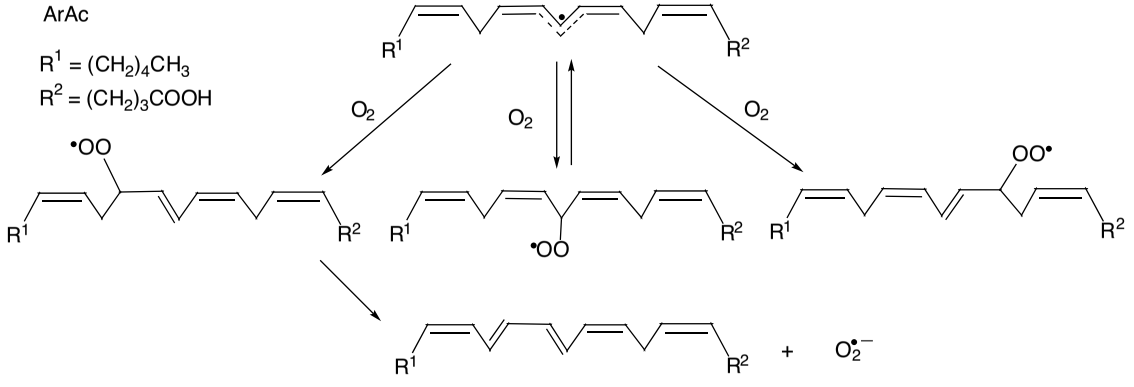

FIGURE 11.13. Reactions of peroxyl radicals derived from C-centered radicals of arachidonic acid. (Adapted from reference 110.)

radicals (Figure 11.13). To estimate the relative contributions of these pathways to the observed formation of the end products, we used 1,4-benzoquinone that, according to our previous results, completely suppresses the formation of the Iz lesions arising from the combination of the $O_2^{\bullet -}$ and G(-H)$^\bullet$ radicals.[77] Here, we found that in the presence of BQ the yields of the Iz and Gh_{ox} lesions decrease by a factor of only $\sim$2 at the BQ concentration of 50 μM. Increasing [BQ] to 100 μM does not further diminish these values. These observations indicate that the combination of $O_2^{\bullet -}$ and G(-H)$^\bullet$ [or 8-oxo-G(-H)$^\bullet$] radicals is responsible for the formation of about one-half of the Iz (or Gh_{ox}) products and that the other half is associated with the combination of ROO$^\bullet$ with G(-H)$^\bullet$ [or 8-oxoG(-H)$^\bullet$] radicals.

11.7. BIOLOGICAL IMPLICATIONS AND FUTURE PROSPECTS

The final oxidative modifications arising from the initial one-electron abstraction from guanine in DNA by carbonate radicals are determined by further reactions of guanine radicals with free radicals or nucleophiles. Of the guanine lesions considered in this work, only 8-oxoG and the 8-nitroG lesions have been detected in humans.[111] Detailed studies by several groups have shown that the levels of 8-oxoG in normal human cells are in the range of 0.3–4.2 per 10^6 molecules of intact G bases.[112, 113] The accurate measurement of the enhanced levels of 8-oxoG in tissues under inflammatory conditions is a difficult problem due to the efficient removal of these lesions by base excision repair enzymes. The enhanced levels of 8-nitroG bases that easily depurinate in DNA have been detected in tissues and biological fluids of patients with various diseases including chronic hepatitis C,[114, 115] intrahepatic cholangiocarcinoma,[116, 117] nasopharyngeal carcinoma,[118] malignant fibrous histiocytoma,[119, 120] *Helicobacter pylori* infection,[121, 122] and inflammatory bowel disease.[123, 124] Further research should be focused on the detection of 5-guanidino-4-nitroimidazole lesions which, in *in vitro* experiments, are formed with nearly the same proportions as 8-nitroG lesions, but do not undergo depurination. At a formal level, both 8-oxoG and 8-nitroG are products of a two-electron oxidation of guanine. Indeed, the formation of 8-nitroG occurs in two steps, electron abstraction from guanine ("first hit"), followed by the combination of $^\bullet NO_2$ radicals ("second hit"); in other words, the interaction of guanine with two free radicals ("two hits") is required for the formation of nitration products. In contrast, the formation of 8-oxoG requires only one-electron abstraction from guanine (a "single hit"), and molecular oxygen that is ubiquitous in cells can abstract the second electron after the hydration of the guanine radicals. The formation of the intrastrand G*–T* cross-links involves a similar sequence of events, a one-electron oxidation of guanine ("single hit"), nucleophilic addition of T-N3 to G-C8, followed by oxidation of the radical adduct by O_2 (or BQ). This mechanism of formation of G*–T* cross-links may be operative *in vivo*, and further research should be directed toward determining whether these intrastrand cross-linked lesions are also formed in cellular DNA.

The Iz (or Oz, the Iz hydrolysis product) and Sp lesions are products of the four-electron oxidation of guanine. However, the formation of the Iz lesions requires

only "two hits" of G by free radicals: the one-electron oxidation of guanine followed by combination of guanine radicals with the superoxide radical anion, a three-electron oxidant. Recently, the Oz lesions have been detected at a level of 2–6 molecules of Oz per 10^7 molecules of intact G in liver DNA of diabetic and control rats maintained on a diet high in animal fat.[125] The formation of the Sp lesions *in vitro* can occur via the intermediate formation of 8-oxoG. Since the levels of 8-oxoG in cells are quite low,[112,113] the further oxidation of 8-oxoG to Sp seems to be unlikely because guanine is present in concentrations that are a factor of $\sim 10^6$ greater than that of 8-oxoG. Under inflammatory conditions, the best candidates for such reactions are $^{\bullet}NO_2$ and $ROO^{\bullet}$ radicals that do not react with G bases, but can potentially oxidize 8-oxoG. Recently, the Sp lesions have been detected in *Escherichia coli* treated with Cr(VI).[126] The search for Sp lesions *in vivo*, especially in tissues under inflammatory conditions, is a critically important task that might further clarify the pathways of oxidatively generated damage in DNA generated by reactive intermediates that are products of the inflammatory response.

ACKNOWLEDGMENTS

This work was supported by the National Institute of Environmental Health and Sciences (5 R01 ES 011589-07). The content is solely the responsibility of the authors and does not necessarily represent the official views of the National Institute of Environmental Health and Sciences or the National Institutes of Health.

REFERENCES

1. Kuper, H.; Adami, H. O.; Trichopoulos, D. Infections as a major preventable cause of human cancer. *J. Intern. Med.* **2000**, *248*, 171–183
2. Balkwill, F.; Mantovani, A. Inflammation and cancer: Back to Virchow? *Lancet* **2001**, *357*, 539–545.
3. Coussens, L. M.; Werb, Z. Inflammation and cancer. *Nature* **2002**, *420*, 860–867.
4. Grisham, M. B.; Jourd'heuil, D.; Wink, D. A. Review article: Chronic inflammation and reactive oxygen and nitrogen metabolism—implications in DNA damage and mutagenesis. *Aliment. Pharmacol. Ther.* **2000**, *14* (Suppl. 1), 3–9.
5. Dedon, P. C.; Tannenbaum, S. R. Reactive nitrogen species in the chemical biology of inflammation. *Arch. Biochem. Biophys.* **2004**, *423*, 12–22.
6. Cadet, J.; Douki, T.; Ravanat, J. L. One-electron oxidation of DNA and inflammation processes. *Nat. Chem. Biol.* **2006**, *2*, 348–349.
7. Beckman, J. S.; Beckman, T. W.; Chen, J.; Marshall, P. A.; Freeman, B. A. Apparent hydroxyl radical production by peroxynitrite: Implications for endothelial injury from nitric oxide and superoxide. *Proc. Natl. Acad. Sci. USA* **1990**, *87*, 1620–1624.
8. Huie, R. E.; Padmaja, S. The reaction of NO with superoxide. *Free Radic. Res. Commun.* **1993**, *18*, 195–199.
9. Løgager, T.; Sehested, K. Formation and decay of peroxynitrous acid: A pulse radiolysis study. *J. Phys. Chem.* **1993**, *97*, 6664–6669.

10. Pryor, W. A.; Squadrito, G. L. The chemistry of peroxynitrite: A product from the reaction of nitric oxide with superoxide. *Am. J. Physiol.* **1995**, *268*, L699–L722.
11. Koppenol, W. H.; Moreno, J. J.; Pryor, W. A.; Ischiropoulos, H.; Beckman, J. S. Peroxynitrite, a cloaked oxidant formed by nitric oxide and superoxide. *Chem. Res. Toxicol.* **1992**, *5*, 834–842.
12. Goldstein, S.; Lind, J.; Merenyi, G. Chemistry of peroxynitrites as compared to peroxynitrates. *Chem. Rev.* **2005**, *105*, 2457–2470.
13. Lymar, S. V.; Hurst, J. K. Rapid reaction between peroxonitrite ion and carbon dioxide: Implications for biological activity. *J. Am. Chem. Soc.* **1995**, *117*, 8867–8868.
14. Carola, R.; Harely, J. P.; Noback, C. R. *Human Anatomy and Physiology*; McGraw-Hill, New York, 1990.
15. Pacher, P.; Beckman, J. S.; Liaudet, L. Nitric oxide and peroxynitrite in health and disease. *Physiol. Rev.* **2007**, *87*, 315–424.
16. Stanbury, D. M. Reduction potentials involving inorganic free radicals in aqueous solution. *Adv. Inorg. Chem.* **1989**, *33*, 69–138.
17. Neta, P.; Huie, R. E.; Ross, A. B. Rate constants for reactions of inorganic radicals in aqueous solution. *J. Phys. Chem. Ref. Data* **1988**, *17*, 1027–1284.
18. Breen, A. P.; Murphy, J. A. Reactions of oxyl radicals with DNA. *Free Radic. Biol. Med.* **1995**, *18*, 1033–1077.
19. Burrows, C. J.; Muller, J. G. Oxidative nucleobase modifications leading to strand scission. *Chem. Rev.* **1998**, *98*, 1109–1151.
20. Pogozelski, W. K.; Tullius, T. D. Oxidative strand scission of nucleic acids: Routes initiated by hydrogen abstraction from the sugar moiety. *Chem. Rev.* **1998**, *98*, 1089–1107.
21. Steenken, S. Purine bases, nucleosides, and nucleotides: Aqueous solution redox chemistry and transformation reactions of their radical cations and e^- and OH adducts. *Chem. Rev.* **1989**, *89*, 503–520.
22. Cadet, J.; Delatour, T.; Douki, T.; Gasparutto, D.; Pouget, J. P.; Ravanat, J. L.; Sauvaigo, S. Hydroxyl radicals and DNA base damage. *Mutat. Res.* **1999**, *424*, 9–21.
23. Cadet, J.; Douki, T.; Gasparutto, D.; Ravanat, J. L. Oxidative damage to DNA: Formation, measurement and biochemical features. *Mutat. Res.* **2003**, *531*, 5–23.
24. Huie, R. E.; Clifton, C. L.; Neta, P. Electron transfer reaction rates and equilibria of the carbonate and sulfate radical anions. *Radiat. Phys. Chem.* **1991**, *38*, 477–481.
25. Czapski, G.; Lymar, S. V.; Schwarz, H. A. Acidity of the carbonate radical. *J. Phys. Chem. A* **1999**, *103*, 3447–3450.
26. Pratviel, G.; Meunier, B. Guanine oxidation: One- and two-electron reactions. *Chem. Eur. J.* **2006**, *12*, 6018–6030.
27. Cadet, J.; Douki, T.; Ravanat, J. L. Oxidatively generated damage to the guanine moiety of DNA: Mechanistic aspects and formation in cells. *Acc. Chem. Res.* **2008**, *41*, 1075–1083.
28. Steenken, S.; Jovanovic, S. V. How easily oxidizable is DNA? One-electron reduction potentials of adenosine and guanosine radicals in aqueous solution. *J. Am. Chem. Soc.* **1997**, *119*, 617–618.
29. Shafirovich, V.; Dourandin, A.; Huang, W.; Geacintov, N. E. Carbonate radical is a site-selective oxidizing agent of guanines in double-stranded oligonucleotides. *J. Biol. Chem.* **2001**, *276*, 24621–24626.

30. Shafirovich, V.; Mock, S.; Kolbanovskiy, A.; Geacintov, N. E. Photochemically catalyzed generation of site-specific 8-nitroguanine adducts in DNA by the reaction of long-lived neutral guanine radicals with nitrogen dioxide. *Chem. Res. Toxicol.* **2002**, *15*, 591–597.
31. Joffe, A.; Geacintov, N. E.; Shafirovich, V. DNA lesions derived from the site-selective oxidation of guanine by carbonate radical anions. *Chem. Res. Toxicol.* **2003**, *16*, 1528–1538.
32. Joffe, A.; Mock, S.; Yun, B. H.; Kolbanovskiy, A.; Geacintov, N. E.; Shafirovich, V. Oxidative generation of guanine radicals by carbonate radicals and their reactions with nitrogen dioxide to form site specific 5-guanidino-4-nitroimidazole lesions in oligodeoxynucleotides. *Chem. Res. Toxicol.* **2003**, *16*, 966–973.
33. Crean, C.; Geacintov, N. E.; Shafirovich, V. Oxidation of guanine and 8-oxo-7,8-dihydroguanine by carbonate radical anions: Insight from oxygen-18 labeling experiments. *Angew. Chem., Int. Ed. Engl.* **2005**, *44*, 5057–5060.
34. Lee, Y. A.; Yun, B. H.; Kim, S. K.; Margolin, Y.; Dedon, P. C.; Geacintov, N. E.; Shafirovich, V. Mechanisms of guanine oxidation in DNA by carbonate radical anion, a decomposition product of nitrosoperoxycarbonate. *Chem. Eur. J.* **2007**, *13*, 4571–4581.
35. Lee, Y. A.; Durandin, A.; Dedon, P. C.; Geacintov, N. E.; Shafirovich, V. Oxidation of guanine in G, GG, and GGG sequence contexts by aromatic pyrenyl radical cations and carbonate radical anions: Relationship between kinetics and distribution of alkali-labile lesions. *J. Phys. Chem. B* **2008**, *112*, 1834–1844.
36. Crean, C.; Uvaydov, Y.; Geacintov, N. E.; Shafirovich, V. Oxidation of single-stranded oligonucleotides by carbonate radical anions: Generating intrastrand cross-links between guanine and thymine bases separated by cytosines. *Nucleic Acids Res.* **2008**, *36*, 742–755.
37. Crean, C.; Lee, Y. A.; Yun, B. H.; Geacintov, N. E.; Shafirovich, V. Oxidation of guanine by carbonate radicals derived from photolysis of carbonatotetramminecobalt(III) complexes and the pH dependence of intrastrand DNA cross-links mediated by guanine radical reactions. *ChemBioChem* **2008**, *9*, 1985–1991.
38. Crean, C.; Geacintov, N. E.; Shafirovich, V. Intrastrand G-U cross-links generated by the oxidation of guanine in 5′-d(GCU) and 5′-r(GCU). *Free Radic. Biol. Med.* **2008**, doi: 10.1016/j.freeradbiomed.2008.07.008.
39. Cope, V. W.; Hoffman, M. Z. Photochemical generation of carbonate anion radicals in neutral aqueous solution. *J. Chem. Soc. Chem. Commun.* **1972**, 227–8.
40. Chen, S.-N.; Cope, V. W.; Hoffman, M. Z. Behavior of $CO_3^{\bullet -}$ radicals generated in the flash photolysis of carbonatoamine complexes of cobalt(III) in aqueous solution. *J. Phys. Chem.* **1973**, *77*, 1111–1116.
41. Ferraudi, G.; Perkovic, M. Mechanism of CoO_3H generation in the charge-transfer photochemistry of $Co(NH_3)_4CO_3^+$. A picosecond to microsecond flash photochemical investigation of the reaction intermediates. *Inorg. Chem.* **1993**, *32*, 2587–2590.
42. Kuimova, M. K.; Cowan, A. J.; Matousek, P.; Parker, A. W.; Sun, X. Z.; Towrie, M.; George, M. W. Monitoring the direct and indirect damage of DNA bases and polynucleotides by using time-resolved infrared spectroscopy. *Proc. Natl. Acad. Sci. USA* **2006**, *103*, 2150–2153.
43. Candeias, L. P.; Steenken, S. Structure and acid–base properties of one-electron-oxidized deoxyguanosine, guanosine, and 1-methylguanosine. *J. Am. Chem. Soc.* **1989**, *111*, 1194–1099.

44. Kobayashi, K.; Tagawa, S. Direct observation of guanine radical cation deprotonation in duplex DNA using pulse radiolysis. *J. Am. Chem. Soc.* **2003**, *125*, 10213–10218.

45. Huie, R. E.; Shoute, L. C.; Neta, P. Temperature dependence of the rate constants for reactions of the carbonate radical with organic and inorganic reductants. *Int. J. Chem. Kinet.* **1991**, *23*, 541–552.

46. Hall, D. B.; Holmlin, R. E.; Barton, J. K. Oxidative DNA damage through long-range electron transfer. *Nature* **1996**, *382*, 731–735.

47. Nunez, M. E.; Hall, D. B.; Barton, J. K. Long-range oxidative damage to DNA: Effects of distance and sequence. *Chem. Biol.* **1999**, *6*, 85–97.

48. Ly, D.; Kan, Y.; Armitage, B.; Schuster, G. B. Cleavage of DNA by irradiation of substituted anthraquinones: Intercalation promotes electron transfer and efficient reaction at GG steps. *J. Am. Chem. Soc.* **1996**, *118*, 8747–8748.

49. Schuster, G. B. Long-range charge transfer in DNA: Transient structural distortions control the distance dependence. *Acc. Chem. Res.* **2000**, *33*, 253–260.

50. Saito, I.; Takayama, M.; Sugiyama, H.; Nakatani, K.; Tsuchida, A.; Yamamoto, M. Photoinduced DNA cleavage via electron transfer: Demonstration that guanine residues located 5′ to guanine are the most electron-donating sites. *J. Am. Chem. Soc.* **1995**, *117*, 6406–6407.

51. Saito, I.; Nakamura, T.; Nakatani, K.; Yoshioka, Y.; Yamaguchi, K.; Sugiyama, H. Mapping of the hot spots for DNA damage by one-electron oxidation: Efficacy of GG doublets and GGG triplets as a trap in long-range hole migration. *J. Am. Chem. Soc.* **1998**, *120*, 12686–12687.

52. Yoshioka, Y.; Kitagawa, Y.; Takano, Y.; Yamaguchi, K.; Nakamura, T.; Saito, I. Experimental and theoretical studies on the selectivity of GGG triplets toward one-electron oxidation in B-form DNA. *J. Am. Chem. Soc.* **1999**, *121*, 8712–8719.

53. Meggers, E.; Kusch, D.; Spichty, M.; Wille, U.; Giese, B. Electron transfer through DNA in the course of radical-induced strand cleavage. *Angew. Chem., Int. Ed. Engl.* **1998**, *37*, 460–462.

54. Meggers, E.; Michel-Beyerle, M. E.; Giese, B. Sequence dependent long range hole transport in DNA. *J. Am. Chem. Soc.* **1998**, *120*, 12950–12955.

55. Nakatani, K.; Fujisawa, K.; Dohno, C.; Nakamura, T.; Saito, I. p-Cyano substituted 5-benzoyldeoxyuridine as a novel electron-accepting nucleobase for one-electron oxidation of DNA. *Tetrahedron Letters* **1998**, *39*, 5995–5998.

56. Nakatani, K.; Dohno, C.; Saito, I. Chemistry of sequence-dependent remote guanine oxidation: Photoreaction of duplex DNA containing cyanobenzophenone-substituted uridine. *J. Am. Chem. Soc.* **1999**, *121*, 10854–10855.

57. Muller, J. G.; Hickerson, R. P.; Perez, R. J.; Burrows, C. J. DNA damage from sulfite autoxidation catalyzed by a nickel(II) peptide. *J. Am. Chem. Soc.* **1997**, *119*, 1501–1506.

58. Hickerson, R. P.; Prat, F.; Muller, J. G.; Foote, C. S.; Burrows, C. J. Sequence and stacking dependence of 8-oxoguanine oxidation: Comparison of one-electron vs singlet oxygen mechanisms. *J. Am. Chem. Soc.* **1999**, *121*, 9423–9428.

59. Sugiyama, H.; Saito, I. Theoretical studies of GG-specific photocleavage of DNA via electron transfer: Significant lowering of ionization potential and 5′-localization of HOMO of stacked GG bases in B-form DNA. *J. Am. Chem. Soc.* **1996**, *118*, 7063–7068.

60. Yoshioka, Y.; Kawai, H.; Sato, T.; Yamaguchi, K.; Saito, I. Ab initio molecular orbital study on the G-selectivity of GGG triplet in copper(I)-mediated one-electron oxidation. *J. Am. Chem. Soc.* **2003**, *125*, 1968–1974.
61. Wardman, P. Reduction potentials of one-electron couples involving free radicals in aqueous solution. *J. Phys. Chem. Ref. Data* **1989**, *18*, 1637–16755.
62. Knobloch, B.; Linert, W.; Sigel, H. Metal ion-binding properties of (N3)-deprotonated uridine, thymidine, and related pyrimidine nucleosides in aqueous solution. *Proc. Natl. Acad. Sci. USA* **2005**, *102*, 7459–7464.
63. Perrier, S.; Hau, J.; Gasparutto, D.; Cadet, J.; Favier, A.; Ravanat, J. L. Characterization of lysine-guanine cross-links upon one-electron oxidation of a guanine-containing oligonucleotide in the presence of a trilysine peptide. *J. Am. Chem. Soc.* **2006**, *128*, 5703–5710.
64. Box, H. C.; Budzinski, E. E.; Dawidzik, J. D.; Wallace, J. C.; Evans, M. S.; Gobey, J. S. Radiation-induced formation of a crosslink between base moieties of deoxyguanosine and thymidine in deoxygenated solutions of d(CpGpTpA). *Radiat. Res.* **1996**, *145*, 641–643.
65. Box, H. C.; Budzinski, E. E.; Dawidzik, J. B.; Gobey, J. S.; Freund, H. G. Free radical-induced tandem base damage in DNA oligomers. *Free Radic. Biol. Med.* **1997**, *23*, 1021–1030.
66. Budzinski, E. E.; Dawidzik, J. B.; Rajecki, M. J.; Wallace, J. C.; Schroder, E. A.; Box, H. C. Isolation and characterization of the products of anoxic irradiation of d(CpGpTpA). *Int. J. Radiat. Biol.* **1997**, *71*, 327–336.
67. Box, H. C.; Budzinski, E. E.; Dawidzik, J. B.; Wallace, J. C.; Iijima, H. Tandem lesions and other products in X-irradiated DNA oligomers. *Radiat. Res.* **1998**, *149*, 433–439.
68. Box, H. C.; Dawidzik, J. B.; Budzinski, E. E. Free radical-induced double lesions in DNA. *Free Radic. Biol. Med.* **2001**, *31*, 856–868.
69. Greenberg, M. M. Elucidating DNA damage and repair processes by independently generating reactive and metastable intermediates. *Org. Biomol. Chem.* **2007**, *5*, 18–30.
70. Romieu, A.; Bellon, S.; Gasparutto, D.; Cadet, J. Synthesis and UV photolysis of oligodeoxynucleotides that contain 5-(phenylthiomethyl)-2′-deoxyuridine: A specific photolabile precursor of 5-(2′-deoxyuridilyl)methyl radical. *Org. Lett.* **2000**, *2*, 1085–1088.
71. Hong, I. S.; Greenberg, M. M. Efficient DNA interstrand cross-link formation from a nucleotide radical. *J. Am. Chem. Soc.* **2005**, *127*, 3692–3693.
72. Hong, I. S.; Ding, H.; Greenberg, M. M. Oxygen independent DNA interstrand cross-link formation by a nucleotide radical. *J. Am. Chem. Soc.* **2006**, *128*, 485–491.
73. Hong, H.; Cao, H.; Wang, Y.; Wang, Y. Identification and quantification of a guanine-thymine intrastrand cross-link lesion unduced by Cu(II)/H_2O_2/ascorbate. *Chem. Res. Toxicol.* **2006**, *19*, 614–621.
74. Steenken, S.; Jovanovic, S. V.; Bietti, M.; Bernhard, K. The trap depth (in DNA) of 8-oxo-7,8-dihydro-2′deoxyguanosine as derived from electron-transfer equilibria in aqueous solution. *J. Am. Chem. Soc.* **2000**, *122*, 2373–2374.
75. Ravanat, J. L.; Saint-Pierre, C.; Cadet, J. One-electron oxidation of the guanine moiety of 2′-deoxyguanosine: Influence of 8-oxo-7,8-dihydro-2′-deoxyguanosine. *J. Am. Chem. Soc.* **2003**, *125*, 2030–2031.

76. Girault, I.; Ravanat, J.-L.; Fier, C.; Fontecave, M.; Cadet, J.; Decout, J.-L. 5-deazaflavins: New very efficient DNA photosensitisers, synthesis of oligonucleotide conjugates. *Nucleosides Nucleotides* **1999**, *18*, 1345–1347.

77. Misiaszek, R.; Crean, C.; Joffe, A.; Geacintov, N. E.; Shafirovich, V. Oxidative DNA damage associated with combination of guanine and superoxide radicals and repair mechanisms via radical trapping. *J. Biol. Chem.* **2004**, *279*, 32106–32115.

78. Mills, G. A.; Urey, H. C. The kinetics of isotopic exchange between carbon dioxide, bicarbonate ion, carbonate ion and water. *J. Am. Chem. Soc.* **1940**, *62*, 1019–1026.

79. Silverman, D. N.; Tu, C. K. Carbonic anhydrase catalyzed hydration studied by carbon-13 and oxygen-18 labeling of carbon dioxide. *J. Am. Chem. Soc.* **1976**, *98*, 978–984.

80. Polanyi, M.; Szabo, C. Mechanism of hydrolysis. Alkaline saponifications of amyl acetate. *Trans. Faraday Soc.* **1934**, *30*, 508–512.

81. Datta, S. C.; Day, J. N. E.; Ingold, C. K. Mechanism of hydrolysis of carboxylic esters and of esterification of carboxylic acids. Acid hydrolysis of an ester with heavy oxygen as isotopic indicator. *J. Chem. Soc.* **1939**, 838–840.

82. Lilie, J.; Hanrahan, R. J.; Henglein, A. O^- transfer reactions of the carbonate radical anion. *Radiat. Phys. Chem.* **1978**, *11*, 225–227.

83. Czapski, G.; Holcman, J.; Bielski, B. H. J. Reactivity of nitric oxide with simple short-lived radicals in aqueous solutions. *J. Am. Chem. Soc.* **1994**, *116*, 11465–11469.

84. Luo, W.; Muller, J. G.; Rachlin, E. M.; Burrows, C. J. Characterization of spiroimino-dihydantoin as a product of one-electron oxidation of 8-oxo-7,8-dihydroguanosine. *Org. Lett.* **2000**, *2*, 613–616.

85. McCallum, J. E.; Kuniyoshi, C. Y.; Foote, C. S. Characterization of 5-hydroxy-8-oxo-7,8-dihydroguanosine in the photosensitized oxidation of 8-oxo-7,8-dihydroguanosine and its rearrangement to spiroiminodihydantoin. *J. Am. Chem. Soc.* **2004**, *126*, 16777–16782.

86. Niles, J. C.; Wishnok, J. S.; Tannenbaum, S. R. Spiroiminodihydantoin and guanidino-hydantoin are the dominant products of 8-oxoguanosine oxidation at low fluxes of peroxynitrite: Mechanistic studies with ^{18}O. *Chem. Res. Toxicol.* **2004**, *17*, 1510–1519.

87. Leipold, M. D.; Muller, J. G.; Burrows, C. J.; David, S. S. Removal of hydantoin products of 8-oxoguanine oxidation by the *Escherichia coli* DNA repair enzyme, FPG. *Biochemistry* **2000**, *39*, 14984–14992.

88. Kornyushyna, O.; Berges, A. M.; Muller, J. G.; Burrows, C. J. In vitro nucleotide misinsertion opposite the oxidized guanosine lesions spiroiminodihydantoin and guanidinohydantoin and DNA synthesis past the lesions using *Escherichia coli* DNA polymerase I (Klenow fragment). *Biochemistry* **2002**, *41*, 15304–15314.

89. Sugden, K. D.; Campo, C. K.; Martin, B. D. Direct oxidation of guanine and 7,8-dihydro-8-oxoguanine in DNA by a high-valent chromium complex: A possible mechanism for chromate genotoxicity. *Chem. Res. Toxicol.* **2001**, *14*, 1315–1322.

90. Misiaszek, R.; Crean, C.; Geacintov, N. E.; Shafirovich, V. Combination of nitrogen dioxide radicals with 8-oxo-7,8-dihydroguanine and guanine radicals in DNA: Oxidation and nitration end-products. *J. Am. Chem. Soc.* **2005**, *127*, 2191–2200.

91. Behar, D.; Fessenden, R. W. Electron spin resonance studies of inorganic radicals in irradiated aqueous solutions. I. Direct observation. *J. Phys. Chem.* **1972**, *76*, 1710–1721.

92. Shafirovich, V.; Cadet, J.; Gasparutto, D.; Dourandin, A.; Geacintov, N. E. Nitrogen dioxide as an oxidizing agent of 8-oxo-7,8-dihydro-2′-deoxyguanosine but not of 2′-deoxyguanosine. *Chem. Res. Toxicol.* **2001**, *14*, 233–241.

93. Ye, Y.; Muller, J. G.; Luo, W.; Mayne, C. L.; Shallop, A. J.; Jones, R. A.; Burrows, C. J. Formation of ^{13}C-, ^{15}N-, and ^{18}O-labeled guanidinohydantoin from guanosine oxidation with singlet oxygen. Implications for structure and mechanism. *J. Am. Chem. Soc.* **2003**, *125*, 13926–13927.
94. Stanbury, D. M. In *Electron Transfer Reactions*, Vol. 253; Isied, S. S., Ed.; American Chemical Society, Washington, D.C., 1997, pp. 165–182.
95. Marnett, L. J. Oxy radicals, lipid peroxidation and DNA damage. *Toxicology* **2002**, *181–182*, 219–222.
96. von Sonntag, C.; Schuchmann, H.-P. The elucidation of peroxyl radical reactions in aqueous solution with the help of radiation–chemical methods. *Angew. Chem. Int. Ed. Engl.* **1991**, *30*, 1229–1253.
97. Bielski, B. H. J.; Cabelli, D. E.; Arudi, R. L.; Ross, A. B. Reactivity of perhydroxyl/superoxide radicals in aqueous solution. *J. Phys. Chem. Ref. Data* **1985**, *14*, 1041–1100.
98. Klug, D.; Rabani, J.; Fridovich, I. A direct demonstration of the catalytic action of superoxide dismutase through the use of pulse radiolysis. *J. Biol. Chem.* **1972**, *247*, 4839–4842.
99. Rotilio, G.; Bray, R. C.; Fielden, E. M. A pulse radiolysis study of superoxide dismutase. *Biochim. Biophys. Acta* **1972**, *268*, 605–609.
100. Cadet, J.; Berger, M.; Buchko, G. W.; Joshi, P. C.; Raoul, S.; Ravanat, J.-L. 2,2-Diamino-4-[(3,5-di-*O*-acetyl-2-deoxy-β-D-*erythro*-pentofuranosyl)amino]-5-(2*H*)-oxazolone: A novel and predominant radical oxidation product of 3′,5′-di-*O*-acetyl-2′-deoxyguanosine. *J. Am. Chem. Soc.* **1994**, *116*, 7403–7404.
101. Kasai, H.; Yamaizumi, Z.; Berger, M.; Cadet, J. Photosensitized formation of 7, 8-dihydro-8-oxo-2′-deoxyguanosine (8-hydroxy-2′-deoxyguanosine) in DNA by riboflavin: A nonsinglet oxygen-mediated reaction. *J. Am. Chem. Soc.* **1992**, *114*, 9692–9694.
102. Hofer, T.; Seo, A. Y.; Prudencio, M.; Leeuwenburgh, C. A method to determine RNA and DNA oxidation simultaneously by HPLC-ECD: Greater RNA than DNA oxidation in rat liver after doxorubicin administration. *Biol. Chem.* **2006**, *387*, 103–111.
103. Candeias, L. P.; Steenken, S. Reaction of $HO^{\bullet}$ with guanine derivatives in aqueous solution: Formation of two different redox-active OH-adduct radicals and their unimolecular transformation reactions. Properties of $G(-H)^{\bullet}$. *Chem. Eur. J.* **2000**, *6*, 475–484.
104. Simic, M. G.; Jovanovic, S. V.In *Mechanisms of DNA Damage and Repair: Implications for Carcinogenesis and Risk Assessment*, Vol. 38; Simic, M. G., Grossman, L., Upton, A. C., Eds.; Plenum Press, New York, 1986; pp. 39–49.
105. Misiaszek, R.; Uvaydov, Y.; Crean, C.; Geacintov, N. E.; Shafirovich, V. Combination reactions of superoxide with 8-oxo-7,8-dihydroguanine radicals in DNA: Kinetics and end-products. *J. Biol. Chem.* **2005**, *280*, 6293–6300.
106. Das, T. N.; Dhanasekaran, T.; Alfassi, Z. B.; Neta, P. Reduction potential of the *tert*-butylperoxyl radical in aqueous solutions. *J. Phys. Chem. A* **1998**, *102*, 280–284.
107. Jovanovic, S. V.; Jankovic, I.; Josimovic, L. Electron-transfer reactions of alkylperoxy radicals. *J. Am. Chem. Soc.* **1992**, *114*, 9018–9021.
108. Luo, Y. R.; Kerr, A.In *CRC Handbook of Chemistry and Physics*, 87th ed.; Lide, D. R., Ed.; CRC Press, Boca Raton, FL, 2006, pp. 9–60.
109. Steenken, S.; Jovanovic, S. V.; Candeias, L. P.; Reynisson, J. Is "frank" DNA-strand breakage via the guanine radical thermodynamically and sterically possible? *Chem. Eur. J.* **2001**, *7*, 2829–2833.

110. Crean, C.; Geacintov, N. E.; Shafirovich, V. Pathways of arachidonic acid peroxyl radical reactions and product formation with guanine radicals. *Chem. Res. Toxicol.* **2008**, *21*, 358–373.

111. Neeley, W. L.; Essigmann, J. M. Mechanisms of formation, genotoxicity, and mutation of guanine oxidation products. *Chem. Res. Toxicol.* **2006**, *19*, 491–505.

112. Collins, A.; Gedik, C.; Vaughan, N.; Wood, S.; White, A.; Dubois, J.; Duez, P.; Dehon, G.; Rees, J.-F.; Loft, S.; Moller, P.; Paulsen, H.; Riis, B.; Weimann, A.; Cadet, J.; Douki, T.; Ravanat, J.-L.; Sauvaigo, S.; Faure, H.; Morel, I.; Morin, B.; Epe, B.; Phoa, N.; Hartwig, A.; Pelzer, A.; Dolara, P.; Casalini, C.; Giovannelli, L.; Lodovici, M.; Olinski, R.; Bialkowski, K.; Foksinski, M.; Gackowski, D.; Durackova, Z.; Hlincikova, L.; Korytar, P.; Sivonova, M.; Dusinska, M.; Mislanova, C.; Vina, J.; Lloret, A.; Moller, L.; Hofer, T.; Nygren, J.; Gremaud, E.; Herbert, K.; Chauhan, D.; Kelly, F.; Dunster, C.; Lunec, J.; Cooke, M.; Evans, M.; Patel, P.; Podmore, I.; White, A.; Wild, C.; Hardie, L.; Olliver, J.; Smith, E. Comparative analysis of baseline 8-oxo-7,8-dihydroguanine in mammalian cell DNA, by different methods in different laboratories: An approach to consensus. *Carcinogenesis* **2002**, *23*, 2129–2133.

113. Collins, A. R.; Cadet, J.; Moller, L.; Poulsen, H. E.; Vina, J. Are we sure we know how to measure 8-oxo-7,8-dihydroguanine in DNA from human cells? *Arch. Biochem. Biophys.* **2004**, *423*, 57–65.

114. Horiike, S.; Kawanishi, S.; Kaito, M.; Ma, N.; Tanaka, H.; Fujita, N.; Iwasa, M.; Kobayashi, Y.; Hiraku, Y.; Oikawa, S.; Murata, M.; Wang, J.; Semba, R.; Watanabe, S.; Adachi, Y. Accumulation of 8-nitroguanine in the liver of patients with chronic hepatitis. C. *J. Hepatol.* **2005**, *43*, 403–410.

115. Kaito, M.; Horiike, S.; Tanaka, H.; Fujita, N.; Adachi, Y. Accumulation of 8-nitroguanine in the liver of chronic hepatitis C patients without sustained virological response after completion of interferon therapy. *J. Gastroenterol.* **2006**, *41*, 713–714.

116. Pinlaor, S.; Sripa, B.; Ma, N.; Hiraku, Y.; Yongvanit, P.; Wongkham, S.; Pairojkul, C.; Bhudhisawasdi, V.; Oikawa, S.; Murata, M.; Semba, R.; Kawanishi, S. Nitrative and oxidative DNA damage in intrahepatic cholangiocarcinoma patients in relation to tumor invasion. *World J. Gastroenterol.* **2005**, *11*, 4644–4649.

117. Pinlaor, S.; Hiraku, Y.; Yongvanit, P.; Tada-Oikawa, S.; Ma, N.; Pinlaor, P.; Sithithaworn, P.; Sripa, B.; Murata, M.; Oikawa, S.; Kawanishi, S. iNOS-dependent DNA damage via NF-κB expression in hamsters infected with *Opisthorchis viverrini* and its suppression by the antihelminthic drug praziquantel. *Int. J. Cancer* **2006**, *119*, 1067–1072.

118. Ma, N.; Kawanishi, M.; Hiraku, Y.; Murata, M.; Huang, G. W.; Huang, Y.; Luo, D. Z.; Mo, W. G.; Fukui, Y.; Kawanishi, S. Reactive nitrogen species-dependent DNA damage in EBV-associated nasopharyngeal carcinoma: The relation to STAT3 activation and EGFR expression. *Int. J. Cancer* **2008**, *122*, 2517–2525.

119. Hoki, Y.; Murata, M.; Hiraku, Y.; Ma, N.; Matsumine, A.; Uchida, A.; Kawanishi, S. 8-Nitroguanine as a potential biomarker for progression of malignant fibrous histiocytoma, a model of inflammation-related cancer. *Oncol. Rep.* **2007**, *18*, 1165–1169.

120. Hoki, Y.; Hiraku, Y.; Ma, N.; Murata, M.; Matsumine, A.; Nagahama, M.; Shintani, K.; Uchida, A.; Kawanishi, S. iNOS-dependent DNA damage in patients with malignant fibrous histiocytoma in relation to prognosis. *Cancer Sci.* **2007**, *98*, 163–168.

121. Ma, N.; Adachi, Y.; Hiraku, Y.; Horiki, N.; Horiike, S.; Imoto, I.; Pinlaor, S.; Murata, M.; Semba, R.; Kawanishi, S. Accumulation of 8-nitroguanine in human gastric epithelium

induced by *Helicobacter pylori infection. Biochem. Biophys. Res. Commun.* **2004**, *319*, 506–510.

122. Kawanishi, S.; Hiraku, Y.; Pinlaor, S.; Ma, N. Oxidative and nitrative DNA damage in animals and patients with inflammatory diseases in relation to inflammation-related carcinogenesis. *Biol. Chem.* **2006**, *387*, 365–372.
123. Ding, X.; Hiraku, Y.; Ma, N.; Kato, T.; Saito, K.; Nagahama, M.; Semba, R.; Kuribayashi, K.; Kawanishi, S. Inducible nitric oxide synthase-dependent DNA damage in mouse model of inflammatory bowel disease. *Cancer Sci*. **2005**, *96*, 157–163.
124. Sawa, T.; Ohshima, H. Nitrative DNA damage in inflammation and its possible role in carcinogenesis. *Nitric Oxide* **2006**, *14*, 91–100.
125. Matter, B.; Malejka-Giganti, D.; Csallany, A. S.; Tretyakova, N. Quantitative analysis of the oxidative DNA lesion, 2,2-diamino-4-(2-deoxy-β-D-*erythro*-pentofuranosyl)amino]-5(2*H*)-oxazolone (oxazolone), *in vitro* and *in vivo* by isotope dilution-capillary HPLC-ESI-MS/MS. *Nucleic Acids Res.* **2006**, *34*, 5449–5460.
126. Hailer, M. K.; Slade, P. G.; Martin, B. D.; Sugden, K. D. Nei deficient *Escherichia coli* are sensitive to chromate and accumulate the oxidized guanine lesion spiroiminodihydantoin. *Chem. Res. Toxicol.* **2005**, *18*, 1378–1383.

12

PRINCIPLES AND APPLICATIONS OF ELECTROCHEMICAL OXIDATION OF NUCLEIC ACIDS

H. Holden Thorp and Julie M. Sullivan
Department of Chemistry, University of North Carolina, Chapel Hill, NC 27599, USA

12.1. INTRODUCTION

Modification of the nucleic acid bases through chemical or oxidative means can cause a disturbance to the cellular machinery leading to the malfunction or death of cells. The oxidation of DNA has been established as an important source of genomic instability, and there is evidence that the oxidation products of nucleic acids, specifically the oxidation of the guanine nucleobase, is implicated in carcinogenesis and aging.[1,2]

Electrochemical methods have been used to study the mechanism of oxidative DNA damage and electrode surfaces have been developed into sensitive sensor systems for the detection of nucleic acid mismatches.[3–5] Electrochemical studies are attractive because they do not require labeling or amplification of the target and can allow for the simultaneous detection of multiple sequences.[3,6] Small quantities of material are required for analysis, and modern simulation methods can be used to provide detailed information on the kinetics and thermodynamics of the redox properties of nucleic acids.[7–11] Parallel studies can be performed with spectroscopic techniques and gel electrophoresis to supplement the information received from the electrochemical characterization. Additionally, instrumentation for electrochemical detection is inexpensive, and a variety of electrode types and sizes can be used.[12,13]

Radical and Radical Ion Reactivity in Nucleic Acid Chemistry, Edited by Marc M. Greenberg

While both DNA and RNA are subject to electrochemical oxidation, the majority of work done in this field has focused on the electrochemistry of DNA, and this will be the main focus of this chapter. This chapter will begin with a brief introduction to the principles behind nucleic acid oxidation and electrochemical methods used to explore their oxidative properties. It will then address some of the applications of nucleic acid oxidation, specifically the focusing on work done in a few labs, including ours, on the mechanisms of guanine oxidation and the development of nucleic acid biosensors.

12.2. REACTIVITY OF NUCLEIC ACIDS

12.2.1. Nucleobase Oxidation

Nucleic acids are susceptible to damage in cells by a variety of mechanisms including oxidation. DNA damage via oxidation can occur either at the sugars through hydrogen abstraction or at the nucleobases via radical reactions or electron transfer.[14, 15] The most easily oxidized naturally occurring base in DNA is guanine with a $E_{1/2}$ $[G\ (1+/0)] = 1.29$ V versus NHE (Figure 12.1).[16] Damage usually originates at a guanine nucleobase or migrates to guanine regions.[17, 18] Reaction at the other bases is less common because of their higher redox potential.[14] Adenine is oxidized at 1.42 V versus NHE and the two pyrimidine nucleobases exhibit redox potentials of ~1.6 V versus NHE.[16]

The products of nucleic acid oxidation depend on DNA structure as well as on the method of oxidation, and it has been suggested that there is some dependence on the sequence as well.[19] Nucleotides within the native DNA helix are less reactive than

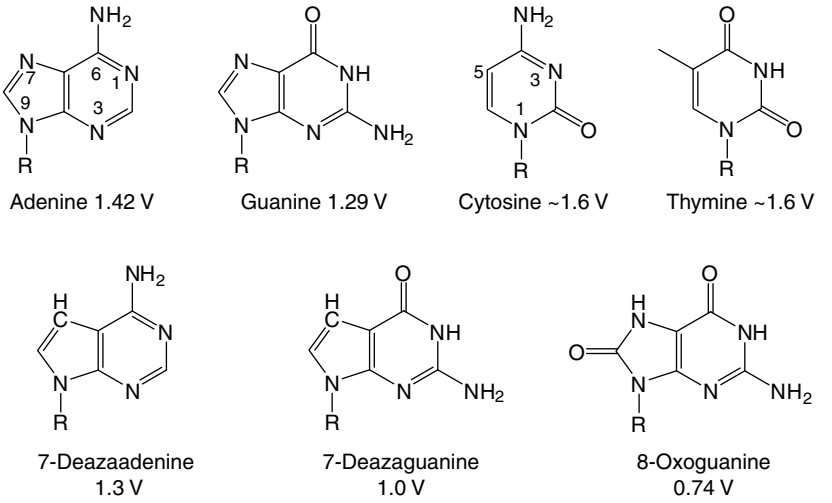

FIGURE 12.1. Chemical structures and oxidation potentials of the native DNA nucleobases and the 7-deazaadenine, 7-deazaguanine, and 8-oxoguanine derivatives. All oxidation potentials are versus NHE. The IUPAC numbering is shown for adenine and cytosine.

those found in single stranded regions because the bases in native DNA are shielded from the electrode surface. The electrochemical properties of peptide nucleic acids (PNAs, which are DNA mimics that bind to complementary DNA and RNA but lack a charged backbone) have also been investigated.[20] The absence of the charged backbone changes the adsorption behavior of the PNA, and it affects the oxidation and reduction of the PNA bases at carbon and mercury electrodes.[20]

Some derivatives of the native nucleobases exhibit even lower oxidation potentials than the parent molecule, with the guanine derivatives 7,8-dihydro-2′-deozyguanosine (8-oxoguanine, 8-oxoG) at 0.74 V versus NHE,[21] and 7-deazaguanine (7-deazaG, Z) at 1.0 versus NHE.[22] A derivative of adenine, 7-deazaadenine (7-deazaA), exhibits lower redox potentials than native adenine with $E_{1/2} = \sim 1.3$ V versus NHE.[23] Due to their reduced redox potentials, these molecules have been used to help understand the mechanism of nucleic acid oxidation.

12.2.2. Mechanism of Guanine Oxidation by Electron Transfer

Guanine nucleobase oxidation can occur under a variety of oxidizing conditions including reactions with hydroxyl and related radicals, one-electron oxidants, alkylating agents, singlet oxygen, as well as intercalating compounds or metal compounds tethered to nucleic acids.[15] Many oxidized products result from guanine oxidation, depending on the degradation pathway. A great deal of effort has been dedicated to understanding the chemical modifications of guanine under different oxidizing conditions. The goal of this research is to understand which lesions can be expected to occur *in vivo* and the biological consequences of these oxidation events. A summary of the oxidation of guanine by electron transfer will be presented here, and a more detailed overview of nucleic acid oxidation reactions can be found in reviews.[14, 19, 24, 25] The isolated guanine base, GMP, dGMP, or guanine found in single-stranded DNA is thought to undergo a one-electron oxidation yielding the radical cation of guanine ($G^{\bullet +}$), which deprotonates rapidly at pH 7due to the low pK_a (3.9) of the radical cation species.[24, 26] The deprotonation is thought to occur from the N1 position of the guanine and results in the formation of neutral radical as shown in Eq. (12.1).[26, 27]

$$G \rightarrow G^{\bullet +} \rightarrow G(\text{-H})^{\bullet} + H^{+} \tag{12.1}$$

The neutral radical can be quenched by reaction with the superoxide radical anion, $O_2^{\bullet -}$, starting a cascade of reactions that results in the formation imidazolone and oxazolone products.[14, 19] In duplex DNA, when $G^{\bullet +}$ is formed, deprotonation is not favored, due to the hydrogen bond interaction between guanine and cytosine at the N1 position.[28] It is thought that the proton is transferred to the N3 position of the base-paired cytosine, allowing the radical cation to retain more positive character than the unpaired nucleotide. Recent studies revealed a kinetic isotope effect for the reaction of $Ru(bpy)_3^{2+}$ with guanine, indicating that proton loss was still the lowest energy pathway for dsDNA.[29–31] Formation of 8-oxoguanine occurs by hydration of the guanine radical cation at the C8 position followed by subsequent oxidation steps,

and it is thought to be due at least in part to the longer-lived guanine radical cation present in dsDNA.[14, 19, 32] The 8-oxoguanine nucleobase can also undergo further oxidation to subsequent products, including imidazolone and oxazolone, making the reaction mechanism difficult to elucidate.[14, 33] Imidazolone is a product of the addition of oxygen to the radical cation, while oxazalone is the product of the hydrolysis of imidazolone. *In vivo*, guanine oxidation has been shown to result in the production of a number of possible reaction products including 8-oxoG, imidazolone, and oxazolone.[14, 34]

12.3. ELECTROCHEMICAL METHODS FOR NUCLEIC ACID OXIDATION

Early studies were performed using dropping mercury electrodes, followed by the use of stationary mercury electrodes and carbon electrodes about a decade later. More recently, carbon (including glassy carbon, carbon paste, and graphite),[35, 36] gold,[37] indium tin oxide (ITO),[7] copper,[38, 39] silver, and platinum electrodes have been used.[12] One of the limitations to most electrodes used in electrochemical techniques is that the nucleic acid bases, nucleosides, and nucleotides are strongly adsorbed to the electrode surface. This property led other researchers to use surfaces where adsorption is much weaker, such as ITO and gold, and to develop indirect oxidation methods to take advantage of the oxidative properties of nucleic acids.[34] Detailed reviews of the electrodes used,[12, 40] and of the adsorption of nucleic acids at electrode surfaces, can be found.[41]

12.3.1. Direct Oxidation

Direct oxidation methods rely on the intrinsic electroactivity of the nucleobases found in DNA and RNA. Early work by Palaček and co-workers pioneered the study of nucleic acids using oscillographic polarography at dropping mercury electrodes with controlled alternating current around 1960[41] and has been widely reviewed.[12, 13, 42] Their work showed that the electrochemical oxidation and reduction signals seen were due to the redox activity of the residues of the bases in DNA and RNA upon interaction with an electrode surface.[12] Reduction signals were produced by the adenine and cytosine residues, while anodic signals were produced by the guanine residues. The potential window for mercury electrodes is usually between 0.2 and -1.8 V versus NHE.[12] The potential windows of most solid electrodes are shifted to more positive values by $\sim$1 V, making them better for studying the oxidation of nucleic acids, while mercury electrodes are better for studying nucleic acid reduction.

Oxidation signals for all four DNA bases have been simultaneously detected at glassy carbon electrodes in phosphate buffered solutions over a wide pH range using differential pulse voltammetry (DPV).[36] While it was previously shown that all four bases could be detected at glassy carbon electrodes using sonovoltammetry, detection was limited to alkaline electrolyte solutions containing pyrimidine bases with

a concentration 10 times higher than that of the purine bases.[43,44] Using differential pulse voltammetry, oxidation peaks were detected in equimolar mixes of the four DNA bases. In the DPV setup, the electrodes were preconditioned by a series of scans in buffer only, which enabled better peak separation and enhancement of the current of the oxidation peaks for all four bases in pH 7.4 phosphate buffer. Detection limits were found to be in the nanomolar range for the purine nucleotides and in the micromolar range for the pyrimidine bases.[36]

Electrochemical detection of nucleotides, ssDNA, and dsDNA using sinusoidal voltammetry at copper microelectrodes has been investigated by Khur and co-workers.[38,39] Their approach utilized the electrocatalytic oxidative properties of sugars and amines at copper surfaces. Ribose sugars and exoycylic amines on the nucleobases are oxidized at 0.4 V in the presence of Cu(II) on the electrode surface. This approach is universal to all types of oligonucleotides because all nucleotides and DNA molecules contain a ribose sugar backbone and primary amines can be found on the nucleobases. Consequently, detection sensitivity is enhanced for longer oligonucleotides, and dsDNA showed a larger electrochemical signal due to the presence of a higher number of sugar residues on the outside of the dsDNA when compared with a single stranded oligo of the same length. Using this technique, picomolar amounts of ss- and dsDNA were detected.[39]

12.3.2. Indirect Oxidation

Indirect methods for the detection of nucleic acid oxidation are based on the detection of electroactive indicators that intercalate or associate with DNA.[8,37,45,46] The complexes used as exogenous electroactive probes are designed to bind to duplex DNA with a higher affinity than single-stranded sequences. Millan and Mikkelsen were the first to demonstrate the viability of a sensor based on detection of an exogenous indicator by observing DNA hybridization to the probe sequences covalently immobilized on glassy carbon or carbon paste electrodes.[47,48] They determined that performing cyclic voltammetry in the presence of $Co(bpy)_3^{3+}$, $Co(phen)_3^{3+}$ or $Os(bpy)_3^{2+}$ (bpy = 2,2′-bipyridine; phen = 1,10 phenanthrolene), reversibly electroactive ($1e^-$) complexes, resulted in larger current responses compared to single-stranded probes due to preconcentration of the metal complex near the electrode surface by electrostatic interaction with the phosphate groups in the minor groove. They were able to use the assay to detect a three-base pair deletion present in 70% of cystic fibrosis (CF) patients and carriers.[48] A similar approach has been developed in which DNA or PNA probes are adsorbed directly onto carbon paste electrodes and chronoamperometry of $Co(phen)_3^{3+}$ associated with duplex DNA is used to detect hybridization.[49,50]

Several groups have used intercalating agents as electrochemical indicators.[37,45,51,52] In an early experiment, Kelley et al. attached double-stranded oligonucleotides to a gold electrode through a 5′-thiol linker and investigated the electrochemistry of methylene blue by cyclic voltammetry.[45] They later used this and other methods to examine the mechanisms behind DNA-bound redox chemistry and DNA-mediated electron transfers.[5,22,45,53]

Threading intercalators, intercalators with bulky subsituents on the periphery of the intercalating moiety, discriminate between double- and single-stranded DNA better than other intercalators because the subsituents bind to the grooves of duplex DNA. Takenaka et al.[37] have used ferrocenylnaphthalene diimide, a threading intercalator, as an electrochemically active ligand to sense dsDNA immobilized onto gold electrodes. This complex was shown to bind preferentially to dsDNA by a factor of 4 over binding to ssDNA. Using DPV, they were able to detect hybridization of a target DNA sequence to an oligonucleotide probe sequence immobilized on gold electrodes at subpicomolar concentrations.

The focus of our laboratory has been the one-electron oxidation of DNA by metal polypyridyl complexes via perpendicular extraction of electrons from DNA.[7,8] We have investigated this process using metal-mediated guanine redox reactions for nucleic acid analysis on ITO electrodes. In this process, the redox mediator is oxidized at the electrode and diffuses in solution where it can exchange an electron with DNA. A schematic illustration of our method is shown in Figure 12.2. The electron transfer is thermodynamically driven through a coupled chemical reaction, and the redox active metal complex acts as a three-dimensional electrode, compared to the two-dimensional electrode surface. Various metal complexes have been used in the redox experiments, including Os,[29,30,54] Re,[46] Fe,[7,54] and Ru.[6,7,10,29,30,54–60]

ITO is a good electrode surface because it is optically transparent, can be fabricated on glass,[61,62] and has a number of special properties that make it useful for electrochemistry. ITO does not significantly adsorb DNA,[63] and it can access potentials up to about 1.4 V (versus Ag/AgCl) in neutral solution.[62] Direct oxidation of guanine at ITO surfaces is extremely slow, even when DNA is directly adsorbed onto the electrode, making signals from the direct oxidation of guanine insignificant.[64,65] The first observation of electrocatalytic current due to the oxidation of guanine in DNA at the ITO surface was first made using the complex $Re(O)_2(py)_4^{2+/+}$,[46] which

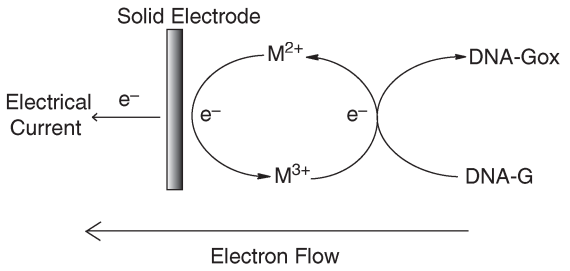

FIGURE 12.2. Schematic illustration of the metal-mediated guanine reaction for nucleic acid analysis on ITO electrodes. The electrode is at a potential that oxidizes the reduced metal mediator [M^{2+}, usually $Ru(bpy)_3^{2+}$] to the oxidized form [M^{3+}, usually $Ru(bpy)_3^{3+}$]. The oxidized form then removes an electron from an unmodified guanine in DNA (DNA-G) and converts it to an oxidized guanine ($DNA\text{-}G_{ox}$), which generates the reduced metal mediator and completes the catalytic cycle. In the absence of guanine, the mediator can only be oxidized once. When DNA is present, the catalytic cycle can turn over many times, resulting in an enhancement of current. (Adapted from reference 74).

has a redox potential similar to that of $Ru(bpy)_2^{3+/2+}$ but is less stable, making the ruthenium complex a better catalyst.[7,66] The redox potential of $Ru(bpy)_3^{3+/2+}$ and guanine are similar ($E_{1/2}$ [G(1+/0)] = 1.1 V versus Ag/AgCl and $E_{1/2}$ [Ru(III/II)] = 1.06 V versus Ag/AgCl. This and related complexes are used to oxidize guanine and related nucleobases by a single electron after generation of the Ru(III) state of the complex.[7] The reaction is monitored as a catalytic current in the oxidation of the complex to $Ru(bpy)_3^{3+}$.[67] In order to use the electrocatalytic signals to obtain kinetic and thermodynamic information on the Ru(III)-guanine reactions, we have developed methods using the digital simulation program DigiSim.[9] The information obtained electrochemically can be supplemented with studies using either optical absorption of the metal complex or gel electrophoresis.[8,55]

Figure 12.3 shows an example of a cyclic voltammogram of $Ru(bpy)_3^{2+}$ in the presence and absence of DNA. Quasi-reversible voltammograms for $Ru(bpy)_3^{2+}$ are detected at conventional scan rates. The oxidative wave detected in the presence of DNA is indicative of a scheme where electronically generated Ru(III) is reduced to Ru(II) by DNA, setting up an electrocatalytic cycle shown in Eqs. (12.2) and (12.3).[7,46]

$$Ru(bpy)_3^{2+} \rightarrow Ru(bpy)_3^{3+} + e^- \tag{12.2}$$

$$Ru(bpy)_3^{3+} + \text{guanine} \rightarrow Ru(bpy)_3^{2+} + \text{guanine}_{ox} \tag{12.3}$$

In this scheme, when the electode is swept through the potential for the Ru(III/II) oxidation, $Ru(bpy)_3^{2+}$ is oxidized at the ITO electrode surface to $Ru(bpy)_3^{3+}$. The oxidized metal complex undergoes a thermal reaction with guanine resulting in the extraction of an electron out of guanine to make the guanine radical cation ($guanine_{ox}$) and regenerate $Ru(bpy)_3^{2+}$, which is then reoxidized by the electrode.[67] The additional current seen in the electrocatalytic wave arises from the reoxidation

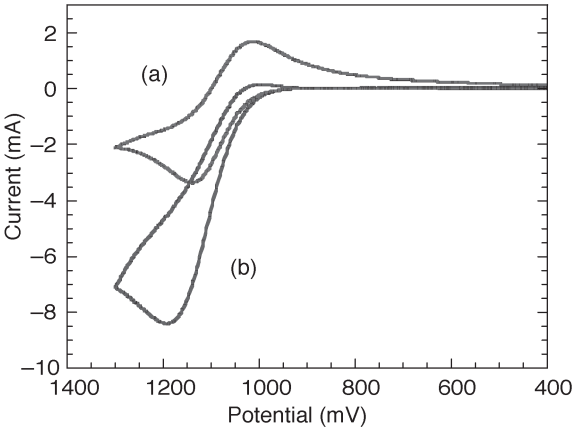

FIGURE 12.3. Cyclic voltammograms at ITO working electrodes of $Ru(bpy)_3^{2+}$ without (**a**) and with (**b**) DNA at 800 mM added salt. The oxidation of guanine is detected as current enhancement in the cyclic voltammogram of $Ru(bpy)_3^{2+}$. All potentials are versus Ag/AgCl.

of $Ru(bpy)_3^{2+}$ that occurs during oxidation of guanine as shown in Eq. (12.3). The return wave due to the reduction of $Ru(bpy)_3^{3+}$ is not seen in the presence of DNA because any $Ru(bpy)_3^{3+}$ generated by the electrode is reduced by DNA and does not accumulate at the electrode.[67] The binding of the positively charged $Ru(bpy)_3^{3+/2+}$ to the negatively charged DNA has been shown to be important in low ionic strength solution, with binding constants of 700 M^{-1} and 3500 M^{-1} for the 2+ and 3+ forms, respectively.[8, 68] The electrostatic binding weakens with an increased $[Na^+]$ and is negligible at high ionic strengths—that is, a 50 mM sodium phosphate solution with 700 mM sodium chloride. Association of the mediator and DNA at low ionic strength enhances the catalytic current and rate of guanine oxidation by an order of magnitude relative to higher ionic strength because of the shortened electron-transfer distance in the Ru–DNA complex. At high ionic strength, binding of the metal complexes is too weak to influence the current response.[7]

Guanine was thought to be the electron donor after experiments showed that catalytic currents were observed in the presence of genomic DNA and poly(GC)·poly(GC) but not in the presence of poly(A)·poly(T).[7, 8] A second experiment with radiolabeled oligonucleotides showed that when the electrode was at potentials able to generate $Ru(bpy)_3^{3+}$, selective cleavage at guanine was seen after base treatment of the oligonucleotides and analysis by gel electrophoresis.[7, 46, 55, 56] The observation of electrocatalysis shown in Figure 12.3 suggested that there are similar redox potentials for the $Ru(bpy)_3^{3+/2+}$ and $G^{1+/0}$ reactions. Using the calculated values for the kinetics of oxidation by a series of substituted metal complexes, we predicted the redox potential for guanine to be 1.1 V versus Ag/AgCl.[7] Later reports by Steenken showed that the redox potential for guanine was 1.07 V versus Ag/AgCl for guanine at pH 7.[16] The use of the ITO–phosphate system allowed our group to apply this method to study the mechanism of guanine oxidation. A large number of groups have also applied the basic principles of nucleic acid oxidation to develop biosensors and investigate the biological implications of electron transport.

12.4. APPLICATIONS OF NUCLEIC ACID OXIDATION

The redox activity of the guanine nucleobase has received the most attention of the four naturally occurring nucleobases due to its involvement in metabolism, aging, and disease. The ability to selectively oxidize guanine over other nucleobases has led to the creation of numerous types of DNA biosensors, ranging from (a) those that use hybridization probes to detect mismatches present in genes causing disease to (b) those that monitor the activity of protein binding to nucleic acids based on changes in sequence.[7, 47, 48, 52, 53, 69–72]

12.4.1. Investigating the Mechanism of Guanine Oxidation

12.4.1.1. Effects of Salt Concentration on DNA Binding. Our laboratory has used the ITO–phosphate system to investigate the mechanisms behind guanine oxidation in DNA. As noted above, we identified guanine as the oxidized moiety in DNA upon

interaction with the redox active $Ru(bpy)_3^{3+}$ complex. Using a digital simulation program, DigiSim,[9] we sought to simulate the observed catalytic currents to develop a kinetic model that would give rate constants for the guanine–Ru(III) electron transfer. The rate constant for the oxidation of guanine in calf thymus DNA by $Ru(bpy)_3^{3+}$ is $9000\,M^{-1}\,s^{-1}$. The reactions simulated were performed in high ionic strength solutions to make the binding of $Ru(bpy)_3^{2+}$ to DNA negligible.[7,8] A similar value was obtained through the use of the COOL algorithm to analyze cyclic square-wave voltammograms.[7]

Studies of the isostructural complex $Os(bpy)_3^{2+}$ in the presence of DNA at low salt concentrations were done to parallel the studies done with $Ru(bpy)_3^{2+}$ and showed a tighter binding of the 3+ form that for the 2+ form due to the higher charge.[68,73] This makes the redox potential for the Os(III/II) couple different for the bound and free forms.[68] The diffusion constant for the bound form was the same as that for DNA, which is lower than that of the free $Os(bpy)_3^{2+}$ complex, indicating that the majority of the electrochemistry occurs through free $Os(bpy)_3^{2+}$.[68,73] Using DigiSim we can model the effect of DNA binding on the catalytic oxidation observed in the $Ru(bpy)_3^{3+/2+}$ couple. From the data obtained for the isostructural $Os(bpy)_3^{2+}$ complex, we can use the known diffusion coefficients and binding constants to determine the electron-transfer rates from guanine to the bound Ru(III).[8,58] An additional effect that arises in the catalytic case that must be considered is that most of the electrode oxidation occurs from the free $Ru(bpy)_3^{2+}$, while DNA oxidation goes through the bound $Ru(bpy)_3^{3+}$. We determined that the effective second-order rate constants at low salt concentrations approached $10^6\,M^{-1}\,s^{-1}$.

Not only does the binding of the metal complex to DNA need to be considered, but the overall probability that a bound $Ru(bpy)_3^{3+}$ will extract an electron from guanine must be considered at low-salt concentrations.[58] To examine the effect of distance on the oxidation of guanine, a 15-mer DNA duplex containing a single guanine in the middle of one strand with no guanines in the complementary strand was used. We considered each of the nucleotides present in the duplex to be a possible "active site," with a total 30 sites possible for the duplex. If electron transfer only occurs at bound guanine residues, then there is a total of one active site; and if binding at every nucleotide produces electron transfer, there are 30 total active sites. Using DigiSim to simulate the current resulting from the oxidation of the 15-mer, models with one active site underestimate the amount of catalytic current, while models with 30 active sites overestimate the current. When a model containing 5 or 10 active sites was used, the data could be adequately simulated, suggesting that electrons are transferred to a bound $Ru(bpy)_3^{3+}$ that was located between 2.5 and 5 base pairs from the guanine.[58] Increasing the number of guanines in the sequence was also shown to predictably increase the number of active sites.[58]

In order to make the $Ru(bpy)_3^{3+}$–guanine electron reaction scheme observed in our laboratory into a practical system for use as a nucleic acid biosensor, we wanted to develop a method for surface immobilization of the nucleic acid.[74] We had previously pursued a number of immobilization schemes involving self-assembled monolayers,[75] electropolymerized films,[76] and porous membranes attached to the ITO surface,[77] and we wanted to investigate a system for immobilizing DNA directly onto an ITO

electrode. Direct attachment of DNA strands prepared by PCR onto the surface was done using irreversible adsorption of the DNA from a 9:1 DMF/water mixture buffered with sodium acetate.[64] The adsorbed DNA did not produce any direct oxidation of guanine using the ITO electrode, but the modified electrodes produced catalytic signals upon the addition of $Ru(bpy)_3^{2+}$ as an electrochemical indicator. Using this method, we were able to detect long strands of DNA at less than 1 fmol, or 44 amol/mm^2 of electrode surface.[64]

Using these modified electrodes, investigated the oxidation kinetics of the guanine in DNA molecules adsorbed onto the surface.[65] From the data collected using chronocoulometry and chronoamperometry on modified electrodes both with and without the $Ru(bpy)_3^{2+}$ complex, the number of electrons transferred to the electrode per guanine was quantified, and the rate constants for both the catalyzed and uncatalyzed reactions could be estimated. Chronocoulometry over 2.5 s shows that roughly two electrons per guanine were transferred to the electrode in both the presence and absence of $Ru(bpy)_3^{2+}$, although the transfer in the absence of catalyst occurred at a much slower rate. This result was consistent with a number of proposed oxidation mechanisms.[33, 78–82] From the kinetics data, we determined that the DNA–Ru^{3+} electron transfer at the surface is similar to that in solution. There is a slightly faster electron-transfer rate at the surface, which is likely due to a distortion of the immobilized DNA that increases the solvent accessibility of the oxidized guanine. Also, at the adsorbed DNA surface, the affinity of the catalyst is a factor of 100 greater than that in solution and is likely due to partial negative charges on the ITO surface, which increase the electrostatic attraction of the cationic catalyst to the DNA-modified ITO surface. Overall, this surface immobilization technique gave results similar to those of the solution experiments, indicating that this was a useful strategy for our investigations.

12.4.1.2. Effects of Sequence and Secondary Structure on DNA Oxidation

Guanine Multiplets. Guanine oxidation is sensitive to the sequence environment. Depending on the structure and surrounding conditions, the radical cation that is initially formed can migrate to a site of lower energy. For example, studies have shown that guanine is the resting site for hole migration from damage originating at other bases and is termed an "electron sink."[18, 83] Also, clustering of guanines in a sequence affects the redox properties of the stacked bases. A number of groups have observed that the 5′-guanine is preferentially oxidized when two adjacent guanines are present in a DNA sequence.[53, 84, 85] *Ab initio* calculations by Sugiyama and coworkers indicated that the 5′-guanine of the 5′-GG-3′ doublet is the more electron-rich site in the doublet.[84] Experimental data using gel electrophoretic techniques showed that bands at the 5′-guanine position of the doublet had a greater intensity than those at the 3′ position.[51, 85–88] Foote and co-workers determined that electrostatic interactions contributed to the lowered potential of the 5′-guanine.[89] In an electrostatic potential map, the carbonyl oxygen and N7 of guanine harbor a high concentration of negative charge. The positioning of these atoms over the 5′-guanine was proposed to create a stabilization effect for the 5′-guanine cation.

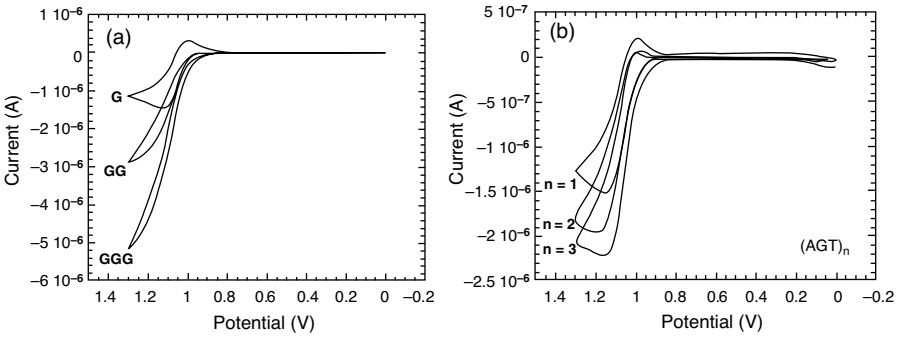

FIGURE 12.4. Cyclic voltammograms of $Ru(bpy)_3^{2+}$ in the presence of DNA at pH 7. (**a**) Added sequences are the duplex forms of **G15** (G singlet), **GG16** (GG doublet), and **GGG17** (GGG triplet). (**b**) Added sequences are the duplex forms of **G15** ($n = 1$), **GxG18** ($n = 2$), **GxGxG21** ($n = 3$), where n is the number of guanines in the sequence. All potentials are versus Ag/AgCl. (Reprinted with permission from reference 55. Copyright 2000 American Chemical Society.)

Our group wanted to determine exactly to what extent the reactivity of the 5′-G is increased by determining the relative rate constants for electron transfer in oligonucleotides that contain a single guanine, guanine doublets, or guanine multiplets, using cyclic voltammetry.[55] A total of three sequences were compared: 5′-AGT (**G15**), 5′-AGGT (**GG16**), and 5′-AGGGT (**GGG17**). Previous work had shown that the lowest reactivity was seen for a guanine with a T on the 3′ side[84]; so to mimic an isolated guanine, the 5′-AGT sequence was used.[55] The voltammograms of $Ru(bpy)_3^{2+}$ in the presence of DNA duplexes, **G15**, **GG16**, and **GGG17**, are shown in Figure 12.4a. The sigmoidal shapes of the voltammograms for **GG16** and **GGG17** represent very rapid electron transfer from guanine to Ru(III). The electron transfer was faster for the doublet and multiplet sequences when compared to the isolated guanine.

In gel electrophoresis experiments, a increased amount of oxidation is seen in the 5′-guanine in ds-DNA compared to ss-DNA.[90] However, cyclic voltammetry experiments with **G15**, **GG16**, and **GGG17** as single-stranded oligonucleotides did not show this same dependence. The absolute current enhancements were greater for the single-stranded DNA than for the duplex because the solvent accessibility is higher in the single-stranded form.[55]

To show that the change in electron transfer rate was due to the sequence context, and not the overall concentration of guanine found in the reaction, we examined the electron transfer in sequences that had two and three isolated guanines. The sequences used were **GxG18** and **GxGxG21**, which are composed of 5′-AGTAGT and 5′AGTAGTAGT, respectively.[55] The voltammograms corresponding to these sequences are seen in Figure 12.4b. The increase in catalytic current for the guanine doublet and multiplet is much greater than the current seen for the same concentration of isolated guanines. This implies a greater intrinsic oxidation rate for guanine doublets and multiplets. Modeling of the voltammograms for sequences containing an isolated guanine using DigiSim yielded a rate constant of $1.4 \times 10^5\ M^{-1}\ s^{-1}$ while

sequences containing a 5′-GG gave an overall rate constant of $7.5 \times 10^5\,M^{-1}\,s^{-1}$.[55] By assuming that the 3′-G of the GG doublet exhibits the same rate constant as the isolated guanine, we estimated the ratio of rate constants for the 5′-G of the GG doublet to the 3′-G to be $k_{GG}/k_G = 12 \pm 2$. Inosine (I), a base that is identical to guanosine but does not contain the exocyclic amine, does not donate electrons to Ru(III), leaving it redox inactive in our system. Experiments using inosine in place of guanosine in oligonucleotides gave the same rate constant for a 5′-IG doublet as for isolated guanine ($k_{IG}/k_G = 1.0 \pm 0.2$) but showed a significant enhancement for a 5′-IG sequence ($k_{GI}/k_G = 2.8 \pm 0.4$).[91] These results supported our assumption that the 3′-G of the GG doublet gives the same rate constant as isolated guanine.

We also studied the effect of placing a 7-deazaguanine (Z) on the 3′ side in doublets with guanine.[55] Studies have shown that 7-deazaguanine is a good electron donor and, as mentioned above, exhibits a redox potential lower than native guanine.[92,93] The stacking of guanine on the 5′ side of a 7-deazaguanine enhances the electron-transfer reactivity, but not to the same extent as native guanine even though 7-deazaguanine has a lower oxidation potential.[55] These results support the hypothesis that the favorable orientation of the N7 position of the 3′ base is an important aspect of the stacking effect.[89]

Single Base Mismatches. The sequence of a nucleic acid can have a large effect on the electron-transfer of nucleic acids.[34,55] We reported a distance dependence for the electron transport between $Ru(bpy)_3^{3+}$ and guanine in duplex DNA.[55] From these results we suspected that secondary structure would also play an important role in determining the reactivity of guanine.[55] Using an oligonucleotide containing an isolated guanine (AGT), we compared the rate constants for oxidation of the guanine base. For the native G:C base pair, the measured rate constant was 200 times less than the rate constant for the single-stranded DNA. We hypothesize that the decrease in the rate constant is due to the protection of the guanine in the double helix. When the oligonucleotide was hybridized to complementary DNA, causing a mismatch across from the guanine residue, intermediate rate constants were seen (Figure 12.5). The oxidation rate constants followed the trend G (single strand) > GA > GG > GT > GC. The relative order of reactivities for mismatches containing 7-deazaguanine and 8-oxoguanine is similar to that of guanine mismatches.[10,94] These mismatches were all distinguishable from one another, and this result was later exploited by our group for the development of DNA biosensors for detecting DNA sequencing platforms.

Barton and co-workers have used duplex DNA oligonucleotide films self-assembled onto a gold electrode surface through a thiol linker to probe nucleic acid structure (Figure 12.6). A redox indicator, methylene blue, was bound to the DNA duplexes and was electrochemically reduced by charge transport through the DNA base stack. The reduced methylene blue acts as a catalyst for the reduction of a $[Fe(CN)_6]^{3-}$ species diffusing in solution, which can then reoxidize the methylene blue creating a catalytic cycle. Using this assay, they are able to detect changes in base-pair stacking of the DNA duplex and have identified all single-base mismatches and several common DNA base damage products.[53]

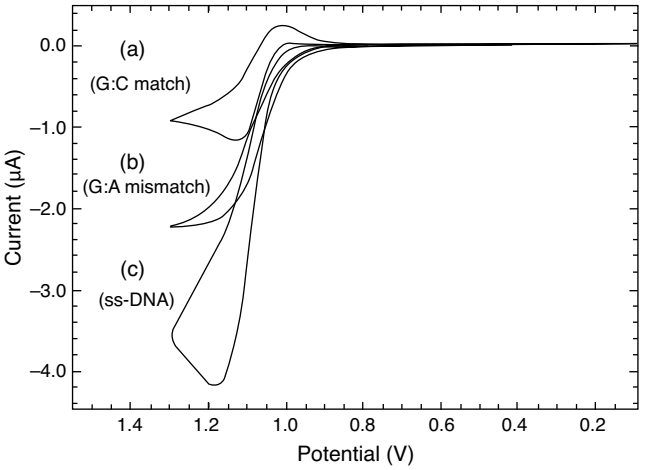

FIGURE 12.5. Cyclic voltammograms of $Ru(bpy)_3^{2+}$ with double-stranded and single-stranded oligonucleotides. (**a**) $Ru(bpy)_3^{2+}$ in the presence of ds-DNA containing one guanine in a GC base pair. (**b**) $Ru(bpy)_3^{2+}$ in the presence of ds-DNA containing a GA mismatch. (**c**) $Ru(bpy)_3^{2+}$ in the presence of ss-DNA containing one guanine. All potentials are versus Ag/AgCl. (Reprinted with permission from reference 7. Copyright 1995 American Chemical Society.)

To determine the primary factors governing the detection of DNA lesions by DNA charge-transfer chemistry and the range of lesions that could be detected, the system devised above was used to examine a wide range of base analogues and DNA damage products.[95] It was determined that charge transfer did not depend on the

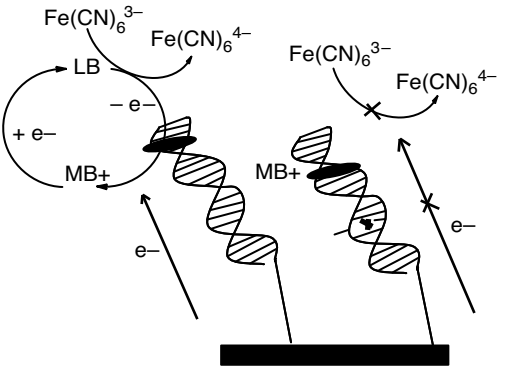

FIGURE 12.6. Electrochemical assay for disruptions in the π-stack of duplex DNA through DNA-mediated charge transport. Electrodes are modified with duplex DNA. Current flows through well-stacked DNA (*left*) to reduce methylene blue (MB^+) to leucomethylene blue (LB). LB is then able to reduce $Fe(CN)_6^{3-}$, regenerating MB, and completing the catalytic cycle. A current enhancement is seen from this catalysis. When the base-stacking is interrupted (*right*), charge transfer does not occur through the base stack, and MB^+ is not reduced. (Adapted from references 5 and 45.)

thermodynamic stability of the helix, but instead on other factors contributing to correct base stacking in the helix. Changes in the hydrogen bonding of Watson–Crick base pairs, or the addition of steric bulk by the modified bases, caused a loss in the efficiency of charge transfer.[95] This technique has also been used to probe an DNA:RNA hybrid containing a 3′-*endo*-locked conformation in the sugar–phosphate backbone.[96]

G Quartets. Guanine-rich sequences, such as those that occur in telomeres at the ends of chromosomes, can form G quartets. In these quartets, multiplet guanines are organized around a central cation in a four-stranded structure.[97] As discussed above, in normal B-form DNA the 5′-guanine in guanine multiplets is electron-rich,[55] and it has been suggested that guanine multiplets are therefore traps for oxidizing equivalents generated in the DNA duplex.[33, 51, 90, 98–101] We sought to study whether G quartets formed from guanine triplets could be traps for oxidizing equivalents, so we studied electron transfer in an oligonucleotide that contains a repeating GGG sequence and forms a G quartet at the appropriate monovalent cation concentration.[54, 97] $Ru(bpy)_3^{3+}$ oxidation produced an enhanced current for the G quartet over that seen for a duplex containing the same number of guanines, with no adjacent guanines.[54, 57] The average rate constants per guanine are $1.9 \times 10^4\,M^{-1}\,s^{-1}$ for the DNA duplex and $3.7 \times 10^4\,M^{-1}\,s^{-1}$ for the G quartet. This is a much smaller ratio than that seen for duplex guanine doublets, which show an increase of a factor of 12 for the 5′-G. We next used gel electrophoresis to determine the extent of oxidation at each guanine to the G quartet with an extra TGT (**G3**) sequence which would be single stranded at the 3′ end. Oxidation was performed using the "flash-quench" technique,[102] where $Ru(bpy)_3^{2+}$ is photolyzed in the presence of a quencher to generate $Ru(bpy)_3^{3+}$, the same oxidant used in the electrochemical measurements. The G-quartet form showed a pattern of 5′ > 3′ > central where the reactivity of the 3′-guanine is enhanced compared to the reactivity pattern usually seen in duplex DNA. This is consistent with the results that are expected for a more solvent-accessible structure. When the **G3** sequence was hybridized to its complement, the enhancement of the 5′-guanine returned.

The measured rate constants for the oxidation of guanines found in duplex, G quartet, and single strands ($1.9 \times 10^4\,M^{-1}\,s^{-1}$, $3.7 \times 10^4\,M^{-1}\,s^{-1}$, and $2 \times 10^5\,M^{-1}\,s^{-}1$, respectively) for the DNA follow the same trend as the average solvent-accessible surface areas (148, 164, and 253 Å, respectively). This result supports the hypothesis that the increase in electron density of the 5′-guanine in B-DNA results form the position of the N7 of the 3′-guanine relative to the π-system of the 5′-guanine which is also consistent with the 7-deazaguanine chemistry. In the G-quartet structure there is no similar alignment of the N7 atoms as is seen in duplex DNA.[57] This is consistent with the results of Schuster et al., where there is less selectivity for the 5′-G in a guanine doublet found in A-form DNA:RNA hybrids.[99] Because adjacent guanines in G quartets are not effective hole traps, formation of the G-quartet structure might protect guanine multiplets from oxidation *in vivo*.[98]

Reactions with Modified Bases. Guanine nucleobase derivatives such as 8-oxoguanine and 7-deazaguanine exhibit a lower oxidation potential than the guanine

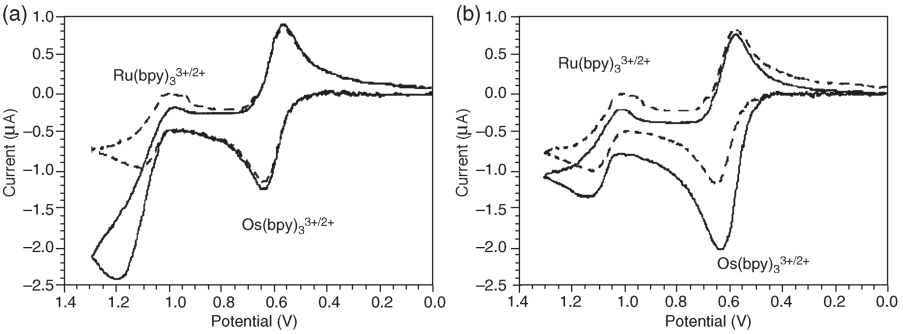

FIGURE 12.7. Cyclic voltammograms of $Ru(bpy)_3^{2+}$ and $Os(bpy)_3^{2+}$ with single-stranded oligonucleotides at pH 7. (**a**) Voltammograms of $Ru(bpy)_3^{2+}$ and $Os(bpy)_3^{2+}$ alone (dashed line) or in the presence of ss-DNA containing guanine (solid line). (**b**) Voltammograms of $Ru(bpy)_3^{2+}$ and $Os(bpy)_3^{2+}$ alone (dashed line) or in the presence of 8-oxoguanine (solid line). All potentials are versus Ag/AgCl. (Adapted from reference 94.)

nucleobase itself.[21, 22, 103] We suspected that this would allow the modified base to be selectively oxidized using a metal complex with a lower redox potential than $Ru(bpy)_3^{2+}$ as a catalyst. We first showed that using $Os(bpy)_3^{2+}$, with a $E_{1/2} = 0.62$ V (versus Ag/AgCl), could selectively catalyze the oxidation of 8-oxoguanine in the presence of guanine.[94] We then used this redox catalyst to probe the secondary structural effects in duplex DNA for detecting mismatch selective oxidation at a single 8-oxoguanine base in oligonucleotides also containing the guanine nucleobase. The current enhancement seen in the presence of the $Os(bpy)_3^{2+}$ catalyst mirrored those obtained with $Ru(bpy)_3^{2+}$ and the native guanine.[7] To confirm that the results seen with $Os(bpy)_3^{2+}$ were due to oxidation of 8-oxoguanine only, cyclic voltammograms of a mixture of $Os(bpy)_3^{2+}$ and $Ru(bpy)_3^{2+}$ were measured as seen in Figure 12.7. When only native guanine is present, as seen in Figure 12.7a, current enhancement is only seen for the $Ru(bpy)_3^{3+/2+}$ wave and not for the $Os(bpy)_3^{3+/2+}$ wave, showing that Os(III) is not an effective oxidant of guanine under conditions where Ru(III) oxidizes guanine effectively. Interestingly, identical results were obtained when a sequence containing a 5′-GG doublet and a 5′-GGG triplet were used, showing the degree of selectivity of Os(III) for 8-oxoguanine. When 8-oxoG is present (Figure 12.7b), enhancement of both the osmium and ruthenium wave is observed.

One of the potential applications of mismatch selectivity detection is its use in the identification of single-base mismatches in clinical samples.[7] The presence of other guanines in a sequence obscures the effect of the mismatch on the target site and is a major limitation of the guainine–Ru(III) reaction. We reasoned that the 8-oxoG-Os (III) reaction might allow for detection of a mismatch at 8-oxoG in the presence of native guanines. The ability to detect the secondary structure dependence for 8-oxoG was tested in a physiologically relevant sequence using an oligomer that is complementary to a site of common genetic mutation for cystic fibrosis.[94, 104] Deletion of a phenylalanine codon (TTT) from this gene is responsible for 70% of all cases of CF.[104] We designed a probe oligonucleotide with the sequence

5′-ATAGGAAACACC-A8GA-GATGATATTTTC, along with a wild-type complement that contains a 5′-TTT triplet opposite the A8GA on the probe. The A8GA sequence gave a relatively small enhancement when hybridized to the full length (+TTT) complement, while the –TTT mutant gave a significant enhancement in current due to the 8-oxoG being placed in a single-stranded A8GA bulge. This experiment provides a strategy for detecting point mutations by designing probes modified with 8-oxoG that can be selectively oxidized by $Os(bpy)_3^{3+}$ in the presence of native guanines.[67]

The modified base 8-oxoguanine was later used to study conformationally controlled electron transfer in DNA molecules using electrochemistry on ITO electrodes.[105] The oligonucleotide (25-mer) used was labeled with an $Os(bpy)_3^{2+}$ on the 5′ end and with a 8-oxoguanine base on the 3′ end. This contrasted our previous studies which had until this time centered on freely diffusing metal complexes undergoing intermolecular reactions with DNA nucleobases.[8, 58, 94] The tethering of $Os(bpy)_3^{2+}$ to the DNA molecule does not effect redox potential of the metal complex. In the presence of an unlabeled complementary DNA sequence, a ds-DNA helix forms and then it places the Os(III) complex at the opposite end of the helix, too far from the 8-oxoG for electron transfer to occur since the potential of the Os(III) is too low to generate nucleobases radicals that would be required for efficient charge transfer over a long distance. Oxidation of 8-oxoG only occurred through bimolecular reaction of the electrogenerated Os(III) of one duplex with the 8-oxoG of another duplex. In the absence of the complementary sequence, the single-stranded sequence folds into a hairpin structure, placing the 8-oxoG close to the Os(III), thereby allowing electron transfer to occur in the same molecule. The electron transfer is detectable by the formation of a catalytic current seen using cyclic voltammetry.

We next wanted to determine if multiple DNA sequences could be simultaneously detected on the same electrode. Two 7-deaza analogues, 7-deazaguanine and 7-deazaadenine, were used to prepare PCR products that could be differentially detected using cyclic voltammetry.[6] The two base analogues have different redox potentials that can be oxidized by corresponding metal complexes with matching potentials, and they can be incorporated into DNA using Taq polymerase with conventional PCR protocols.[106, 107] Current enhancement in the voltammograms of a particular metal complex would be indicative of the presence of the corresponding modified base, which in turn would be a positive signal for the presence of a DNA sequence amplified using this base. Amplification of a gene with 7-deazaguanine renders it more readily oxidized than native DNA, since 7-deazaguanine has a redox potential of 0.75 V compared to 1.1 V for guanine (both potentials versus Ag/AgCl).[10] Thus, the 7-deazaguanine fragment can be selectively oxidized by complexes with lower potentials. Amplification of a separate DNA fragment with 7-deazaadenine produces a fragment that is less readily oxidized than the 7-deazaguanine fragment,[23] so mediators that oxidize the 7-deazaadenine fragment will also oxidize the 7-deazaguanine fragment. In this study, the metal complex $Ru(bpy)_3^{3+}$ is used to oxidize both 7-deaza nucleobases, while the 7-deazaguanine is selectively oxidized by the metal complex $Ru(dmb)_3^{3+}$ (dmb = 4,4′-dimethyl-2,2′-bipyridine) with an $E_{1/2} = 0.86$ V versus Ag/AgCl. The PCR products were immobilized onto an ITO

surface by precipitation from a solution of 9:1 DMF/acetate, resulting in the immobilization of single-stranded DNA. Using this strategy, it was possible to detect the two PCR products on the same electrode: one 330-bp sequence containing 7-deazaadenine and a 1200-bp sequence containing 7-deazaguanine.

12.4.2. Examining Charge Transfer through DNA

Numerous studies have shown that duplex DNA can serve as an effective medium to transport charge.[86, 96, 108–111] Guanines, with their low oxidation potentials, can serve as positive charge carriers in the migration of the radical cation through DNA.[17, 112, 113] Mechanistically, the process of charge transport is not well understood.[108] It exhibits sensitivity to changes in the base stack such as those caused by single-base mismatches,[114] DNA bulges,[115] and protein binding.[116] Barton and co-workers have studied the charge transport through DNA duplexes using redox active intercalators.[45, 111] In an early study, double-stranded 15 base-pair oligonucleotides were attached to a gold electrode through a 5′-hexylthiol linker on one of the strands. They used methylene blue, an aromatic heterocycle that binds strongly to DNA via intercalation to investigate the redox chemistry of molecules within the DNA environment.[45] A number of electrochemical techniques as well as radiolabeling indicated a surface covering of $\geq$75% with the DNA helices stacked at an angle from the electrode surface, showing that the helices were densely packed. The methylene blue intercalator was shown to interact reversibly with the duplex DNA with a binding affinity comparable to the affinity for DNA in solution. An average of 1.4 methylene blue molecules were shown to bind to each DNA helix; and due to the tight packing of the helices on the electrode, the intercalation is restricted primarily to sites near the bulk solution. This leaves the methylene blue about 65 Å from the electrode, indicating that the electrochemical reduction of methylene blue at the surface occurs over a long distance through the DNA duplex (Figure 12.6).[45]

Later work examined the necessity of intercalative stacking of methylene blue for DNA-mediated electrochemistry.[117] The ionic strength of the buffer solution was modulated to change the mode of binding of a covalently bound methylene blue molecule. The methylene blue molecule was attached in a manner that left it tethered at the top of the DNA film. In low salt buffers, the intercalation of the methylene blue molecule is detected electrochemically. At high ionic strength the methylene blue cannot bind to the DNA through intercalation and there is a complete loss of the electrochemical signal in the DNA film. This and recent electrochemical work have indicated that the coupling into the π-stack by redox indicators is important for long-range DNA mediated electrochemistry.[111]

Charge transfer through DNA has also been investigated using photochemical methods for electron transfer with the use of bound intercalators,[22, 51, 86] or redox active binders,[102, 118] to induce oxidation of guanine, followed by visualization with gel-electrophoresis.[119] Electron transport over long distances ($\sim$200 Å) has been identified,[98, 100] and it is thought that this long-range transport may be a factor leading to cellular DNA damage. A more in-depth review of the work done to investigate long-range DNA charge transport can be found in other references.[83, 108]

12.4.3. Electrochemical DNA Biosensors

Biosensors are small devices employing biochemical molecular recognition properties as the basis for a selective analysis.[3] There is a great need for highly sensitive methods for measuring markers of disease found at ultra-low levels, such as those seen in early stages of disease.[3] Existing diagnostic tests to not have the level of sensitivity needed and often detect protein at levels corresponding to later stages of disease. Electrochemical biosensors have been the focus of much research because they produce a simple, inexpensive, sensitive platform for patient diagnosis. Electrochemical analysis has been useful in assays to detect protein binding, lesions, and mutations in DNA, and both direct and indirect methods of electrochemical oxidation have been used by groups to construct nucleic acid biosensors. The minimal elements required to develop a biosensor include a molecular recognition layer and a signal transducer than can be coupled to an appropriate readout device.[4] An in-depth review of these topics can be found.[4] Direct electrical reading of DNA interactions offers great promise for the development of quick, easy-to-use devices for DNA sensing and genetic testing. Many of the methods described previously in this chapter can also be considered to be electrochemical nucleic acid biosensors. This section will focus on a few of the more current sensors that have been developed.

In the majority of sensors used to detect the hybridization of a DNA sequence, a probe molecule made up of a single-stranded DNA oligonucleotide (ss-DNA) is chemically attached to an electrode surface, to create a probe-modified electrode. The electrode is then brought into contact with a solution containing the complementary target ss-DNA sequence to form duplex DNA bound at the electrode surface. The complementary sequence is recognized using an electroactive indicator, which produces a current in response to interaction with duplex DNA and can be used in conjunction with enzyme or redox labels. Most hybridization sensors rely on the ability to convert this recognition event into a useful electrical signal.

Using DNA-modified gold electrodes in a manner similar to that discussed earlier, Barton and co-workers were able to detect changes in DNA structure upon protein binding.[120] Daunomycin was used as a redox indicator and was covalently linked to the top of the DNA film. Binding of the base-flipping enzyme M.*Hha*I or the TATA-box binding protein, which causes the DNA to bend 90°, cause a reduction in the amount of charge transfer to the daunomycin probe.[120] Proteins that bind to the DNA but do not disrupt the base stack do not show a significant reduction in the yield of charge transfer. Binding of the TATA-box protein was determined at micromolar concentrations using macroelectrodes,[120] and it was recently detected at nanomolar concentrations using microelectrodes and Nile Blue as the redox active probe.[121] This technique could be adapted for use in the electrical assay of DNA-binding proteins on a chip. Difficulties with this technique can arise, however, when probe DNA is closely packed on an electrode surface because target DNA can be repelled from the negatively charged surface.

Wong and Gooding[71] have developed an electrochemical DNA biosensor that is able to detect DNA hybridization in real time using long-range charge transfer with an approach they describe as an *in situ* assay. They developed this approach to (i) simplify

the detection of DNA hybridization so that it is compatible with PCR on a chip, (ii) reduce the time needed for detection of a subnanomolar concentration of hybridization to under an hour, and (iii) detect single-base mismatches without extra processing steps.[71] The redox intercalator 2,6-anthraquinonedisulfonic acid (AQDS) was used, which binds to hybridized DNA. Thiolated ss-DNA probes were bound to a gold electrode, and 6-mercapto-1-hexanol was used as a diluent to prevent nonspecific adsorption of DNA and AQDS to the electrode surface and to disperse the DNA probes. To cut back on the time required for sample preparation, detection of hybridization was conducted in the presence of target DNA and the redox intercalator. The detection in the presence of target DNA and indicator can be performed because there is a shift in the reduction electrode potential of the anthraquinone at the ds-DNA-modified electrode that does not occur at a bare or modified electrode.[122, 123] This method was further used to differentiate between complementary target DNA, noncomplementary target DNA, and target DNA with single-base-pair mismatches.[71] The intercalation must occur above the mismatch in order to affect the charge transfer through the DNA duplex.

Kelley and co-workers have developed oligonucleotide-functionalized gold nanoelectrode ensembles (NEE) as a nanoelectrode DNA detection platform.[124] Two- and three-dimensional NEEs that were created feature gold nanowires templated by a polycarbonate membrane. The label-free DNA detection system developed in their laboratory uses a catalytic reaction between two metal complexes, $Ru(NH_3)_6^{3+}$ and $Fe(CN)_6^{3-}$, to detect DNA hybridization. Upon hybridization, there is an increase in the concentration of phosphates at the electrode surface, which increases the local concentration of $Ru(NH_3)_6^{3+}$ and produces a change in the electrocatalytic signal.[125] A thiolated ss-DNA probe containing a portion of the 23S rRNA gene sequence from the target DNA was attached to the NEEs, and the surfaces were analyzed using Ru(III)/Fe(III) electrocatalysis before and after hybridization of the target sequence. Hybridized sequences resulted in an increase in electrocatalytic current, while significant increases in current were not seen for noncomplementary sequences. The three-dimensional NEEs were better suited for biochemical analysis due to the production of larger signals upon hybridization; and they were able to detect target DNA strands down to the picomolar concentrations, with an attamole-level detection limit.

Since initially discovering the electroactivity of nucleic acids on electrodes at the end of the 1950s and in the early 1960s, Paleček has continued to exploit their activity for use in electrochemical sensors.[70, 126–128] His group has recently developed a DNA sensor based on the labeling of DNA reporter probe (RP) molecules with osmium metal complexes covalently bound to thymine bases to create a thymine adduct.[126] By changing the ligands bound to the metal center, they can alter the redox potential of the overall thymine–osmium marker and use it for electrochemical "multicolor" (multipotential) DNA coding (Figure 12.8). The RP contains a stretch of sequence complementary to a DNA of interest (tDNA), and a poly-T tail (T_x). Labeling of the T_x tail with an osmium–ligand complex, where the ligand can be 2,2′-bipyridine, 1,10-phenanthroline, bathophenanthroline disulfonic acid, or *N*,*N*,*N*′,*N*′-tetramethylethylenediamine (TEMED), occurs after blocking of the non-poly-T sequence.

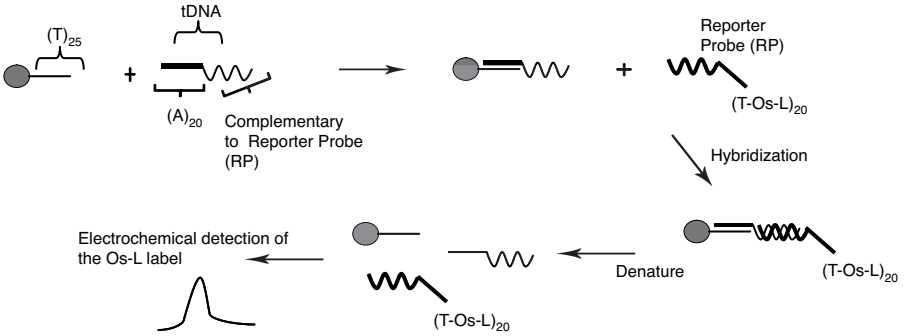

FIGURE 12.8. Scheme showing the DNA sensor developed by Paleček and co-workers based on the labeling of DNA reporter probes (RP) with osmium metal complexes. Target DNA (tDNA) is captured by magnetic beads containing a poly-T sequence (T_{25}) through hybridization of the poly-A region (A_{20}) of the tDNA to the T_{20}. After magnetic separation and washing, a sandwich complex is formed only if there is a complementary sequence between the tDNA and the osmium-reporter probe complex (RP). After washing, heat is applied to denature any bound RP, and the released RP is determined electrochemically. (Adapted from reference 126.)

The tDNA contains the target DNA sequence, along with a poly-A sequence upstream used to complex the tDNA to a magnetic bead. After the target DNA sequence is complexed to the magnetic bead, the reporter probe containing the osmium label is hybridized to the target DNA. After removal of the unbound probe DNA, thermal denaturation is used to separate the reporter probe, target DNA, and magnetic bead, and the released reporter probe is detected using adsorptive transfer stripping square wave voltammetry at a pyrolytic graphite electrode. Using this approach, they were able to determine the identity of the captured probe based upon the potential of the osmium-labeled poly-T tail. Identification of multiple hybridized probes could be differentiated from a single sample.

Electrochemical nanoparticle-based hybridization assays were developed from previous use of nanoparticles in optical bioassays. There are a number of different types of nanomaterials being used, including gold,[129–131] silver,[132, 133] CdS,[72, 134] and other nanoparticles,[135, 136] carbon nanotubes,[137] and magnetic particles.[138, 139] In these systems, the nanoparticles bind to the captured target, followed by dissolution and anodic-stripping electrochemical measurement of the metal tracer.[140] Potentiometric microsensors for monitoring DNA hybridization have been developed using CdS-nanocrystal tags in a sandwich assay.[72] Target DNA (60-mer) is first hybridized to a thiolated probe (20-mer) bound to the gold surface, followed by the capture of a secondary DNA probe (26-mer) coupled to the CdS label. A dilute electrolyte background solution for the potentiometric detection of the released Cd^{2+} with a polymer membrane Cd^{2+}-selective microelectrode is created by dissolving the nanocrystal in H_2O_2. This system displays high selectivity for hybridized complementary DNA strands, with two-base mismatches creating the same response as

a control solution with zero target DNA present. The detection limit for the microelectrode was found to be in the femtomolar range, and it is impressive for an assay that has no preconcentration step.

Wang and co-workers have created numerous nucleic acid biosensors, based on a variety different detection methods.[4, 49, 50, 69, 72, 134, 136, 140–144] They have recently described a label-free aptamer-based system for the detection of target proteins.[142] This system is based on a sandwich assay, with two aptamers involved in identifying the amount of bound thrombin protein, each binding the thrombin protein at different sites. The first DNA aptamer is bound to a magnetic bead and is then exposed to a solution containing the thrombin analyte. The unbound thrombin is then removed by separating the magnetic beads containing the bound thrombin from the supernatant containing any remaining thrombin. A second guanine-rich aptamer is exposed to the bound thrombin, and excess second aptamer is removed in a wash step. The remaining bound secondary aptamer is released from the thrombin under acidic conditions, and it is amplified using PCR. After purification of the PCR products, the resulting DNA is depurinated under acidic conditions, and adsorptive stripping measurements of the free guanine nucleobases were carried out using a graphite pencil electrode.[142] Using this method, the authors were able to detect low femtomolar concentrations of thrombin in solution. The overall quantitation of the thrombin concentration was dependent on the concentration dependence of the guanine oxidation peak that occurs upon the secondary aptamer binding. The amplification of the bound secondary aptamer was also important, and it resulted in an increase in the sensitivity by approximately four orders of magnitude over detection using a sample with no amplification.

Commercial sensor technology based on DNA electrochemistry has been developed by a number of companies.[145–149] The eSensor®,[150] developed by Clinical Micro Sensors, Inc. and Osmetech PLC, contains a number of gold electrodes as well as a reference and auxiliary electrode. The electrodes are printed into a circuit board, and the gold electrodes are coated with a self-assembled monolayer (SAM) of capture probes (Figure 12.9). Unlabeled nucleic acid targets are immobilized onto the surface of the SAM by sequence-specific hybridization to the capture probes. A third probe, a ferrocene-modified signaling probe oligonucleotide, contains a sequence that is complementary to the target probe in the region adjoining the capture probe binding site. This allows the signaling probe to be in close proximity to the monolayer in a sandwich complex, where a nucleic acid target of interest is bound simultaneously by capture probes on the electrode surface and a second probe in the system referred to as a signaling probe.[149] The SAM allows electron transfer to occur between the immobilized ferrocenes and the gold electrode, and it also acts to insulate the electrode from any soluble redox species. The ferrous ion in each ferrocene group undergoes cyclic oxidation and reduction, leading to loss or gain of an electron, which is measured as current at the electrode surface using alternating-current voltammetry.[150] This electron transfer only occurs when the target is hybridized by both the capture probe and the signaling probe. An electronic detection system has been designed to complement the eSensor®, and it can analyze upward of 48 chips

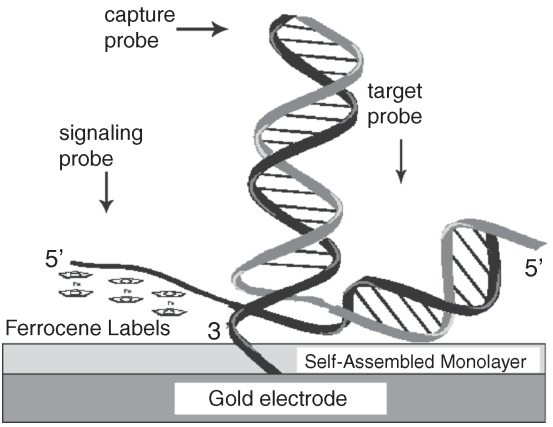

FIGURE 12.9. Sandwich complex used in the eSensor® for detection of DNA hybridization. (Adapted from reference 146.)

at a time. The eSensor® platform has been used to detect human papillomaviruses and have detected 86% of the HPV types contained in clinical samples.[146] It has also been used to detect single-base mismatches found in hereditary hemochromatosis[147, 148] and has been approved by the FDA for detection of the gene for cystic fibrosis.[150]

12.5. CONCLUSION

Both the methods used and the applications for nucleic acid oxidation have seen remarkable advances since the electroactivity of nucleobases was discovered in the last 50 years. Oxidation of cellular components including DNA, RNA, and proteins has been implicated as a cause for human diseases, and it provides an impetus for further research. Improvements in biochemical technology have allowed researchers to use the basic redox properties of nucleic acids to develop sensor technologies that can be used in a variety of applications. Creation of nanoscale devices that are cost-effective, accurate, and portable for diagnostic testing will help to make this technology available to the larger population. The biological importance of charge transport through DNA and proteins is also an area of research that is currently gaining prominence in order to better understand the effect of redox reactions on cellular machinery.

ACKNOWLEDGMENTS

H. H. T. is a consultant to Osmetech PLC. We would like to thank the graduate school at UNC-Chapel Hill for funding J.M.S. with the Linda Dykstra dissertation completion fellowship.

REFERENCES

1. Shigenaga, M. K.; Hagen, T. M.; Ames, B. N. Oxidative damage and mitochondrial decay in aging. *Proc. Natl. Acad. Sci. USA* **1994**, *91*, 10771–10778.
2. D'Errico, M.; Parlanti, E.; Dogliotti, E. Mechanism of oxidative DNA damage repair and relevance to human pathology. *Mutat. Res.* **2008**, *659*, 4–14.
3. Wang, J. Electrochemical biosensors: Towards point-of-care cancer diagnostics. *Biosens. Bioelectron.* **2006**, *21*, 1887–1892.
4. Wang, J. In *Electrochemistry of Nucleic Acids and Proteins—Towards Electrochemical Sensors for Genomics and Proteomics*; Palecek, E., Scheller, F., Wang, J., Eds.; Elsevier, Amsterdam, 2005, pp. 175–190.
5. Drummond, T. G.; Hill, M. G.; Barton, J. K. Electrochemical DNA sensors. *Nat. Biotechnol.* **2003**, *21*, 1192–1199.
6. Yang, I. V.; Ropp, P. A.; Thorp, H. H. Toward electrochemical resolution of two genes on one electrode: Using 7-deaza analogues of guanine and adenine to prepare PCR products with differential redox activity. *Anal. Chem.* **2002**, *74*, 347–354.
7. Johnston, D. H.; Glasgow, K. C.; Thorp, H. H. Electrochemical Measurement of the Solvent Accessibility of Nucleobases Using Electron Transfer between DNA and Metal Complexes. *J. Am. Chem. Soc.* **1995**, *117*, 8933–8938.
8. Johnston, D. H.; Thorp, H. H. Cyclic Voltammetry Studies of Polynucleotide Binding and Oxidation by Metal Complexes: Homogeneous Electron-Transfer Kinetics. *J. Phys. Chem.* **1996**, *100*, 13837–13843.
9. Rudolph, M.; Reddy, D. P.; Feldberg, S. W. Simulator for cyclic voltammetric responses. *Anal. Chem.* **1994**, *66*, 589A–600A.
10. Yang, I. V.; Thorp, H. H. Oxidation of 7-Deazaguanine by One-Electron and Oxo-Transfer Oxidants: Mismatch-Dependent Electrochemistry and Selective Strand Scission. *Inorg. Chem.* **2001**, *40*, 1690–1697.
11. Palecek, E.; Fojta, M. DNA Hybridization and Damage. *Anal. Chem.* **2001**, *73*, 74A.
12. Palecek, E.; Jelen, F. In *Electrochemistry of Nucleic Acids and Proteins—Towards Electrochemical Sensors for Genomics and Proteomics*, Vol. 1; Palecek, E., Shcheller, F., Wang, J., Eds.; Elsevier, Boston, 2005, pp. 74–153.
13. Palecek, E. From polarography of DNA to microanalysis with nucleic acid-modified electrodes. *Electroanalysis* **1996**, *8*, 7–14.
14. Burrows, C. J.; Muller, J. G. Oxidative nucleobase modifications leading to strand scission. *Chem. Rev.* **1998**, *98*, 1109–1152.
15. Thorp, H. H. In *Advances in Inorganic Chemistry*, Vol. 43; Academic Press, Orlando, FL, 1995, pp. 127–177.
16. Steenken, S.; Jovanovic, S. V. How easily oxidizable is DNA? One-electron reduction potentials of adenosine and guanosine radicals in aqueous solution. *J. Am. Chem. Soc.* **1997**, *119*, 617–618.
17. Candeias, L. P.; Steenken, S. Electron-transfer in di(Deoxy)nucleoside phosphates in aqueous-solution—rapid migtation of oxidative damage (Via Adenine) to Guanine. *J. Am. Chem. Soc.* **1993**, *115*, 2437–2440.
18. Melvin, T.; Botchway, S.; Parker, A. W.; O'Neill, P. Migration of photoinduced oxidative damage in models for DNA. *J. Chem. Soc., Chem. Commun.* **1995**, 653–654.

19. Pratviel, G.; Meunier, B. Guanine oxidation: One- and two-electron reactions. *Chem. Eur. J.* **2006**, *12*, 6018–6030.
20. Tomschik, M.; Jelen, F.; Havran, L.; Trnková, L.; Nielsen, P. E.; Palecek, E. Reduction and oxidation of peptide nucleic acid and DNA at mercury and carbon electrodes. *J Electroanal. Chem.* **1999**, *476*, 71–80.
21. Steenken, S.; Jovanovic, S. V.; Bietti, M.; Bernhard, K. The trap depth (in DNA) of 8-oxo-7,8-dihydro-2′deoxyguanosine as derived from electron-transfer equilibria in aqueous solution. *J. Am. Chem. Soc.* **2000**, *122*, 2373–2374.
22. Kelley, S. O.; Barton, J. K. DNA-mediated electron transfer from a modified base to ethidium: [pi]-stacking as a modulator of reactivity. *Chem. Biol.* **1998**, *5*, 413–425.
23. Baik, M.-H.; Silverman, J. S.; Yang, I. V.; Ropp, P. A.; Szalai, V. A.; Yang, W.; Thorp, H. H. Using density functional theory to design DNA base analogues with low oxidation potentials. *J. Phys. Chem. B* **2001**, *105*, 6437–6444.
24. Steenken, S. Purine bases, nucleosides, and nucleotides: Aqueous solution redox chemistry and transformation reactions of their radical cations and e^- and OH adducts. *Chem. Rev.* **1989**, *89*, 503–520.
25. Cadet, J.; Douki, T.; Gasparutto, D.; Ravanat, J.-L. Oxidative damage to DNA: Formation, measurement and biochemical features. *Mutat. Res.* **2003**, *531*, 5–23.
26. Candeias, L. P.; Steenken, S. Structure and acid-base properties of one-electron-oxidized deoxyguanosine, guanosine, and 1-methylguanosine. *J. Am. Chem. Soc.* **1989**, *111*, 1094–1099.
27. Hildenbrand, K.; Schulte-Frohlinde, D. ESR spectra of radicals of single-stranded and double-stranded DNA in aqueous solution. Implications for OH-Induced Strand Breakage. *Free Radic. Res.* **1990**, *11*, 195–206.
28. Kawai, K.; Takada, T.; Tojo, S.; Majima, T. Regulation of one-electron oxidation rate of guanine and hole transfer rate in DNA through hydrogen bonding. *Tetrahedron Lett.* **2002**, *43*, 8083–8085.
29. Weatherly, S. C.; Yang, I. V.; Thorp, H. H. Proton-coupled electron transfer in duplex DNA: Driving force dependence and isotope effects on electrocatalytic oxidation of guanine. *J. Am. Chem. Soc.* **2001**, *123*, 1236–1237.
30. Weatherly, S. C.; Yang, I. V.; Armistead, P. A.; Thorp, H. H. Proton-coupled electron transfer in guanine oxidation: Effects of isotope, solvent, and chemical modification. *J. Phys. Chem. B* **2003**, *107*, 372–378.
31. Murphy, C. F.; Holcomb, D. Unpublished results.
32. Angelov, D.; Spassky, A.; Berger, M.; Cadet, J. High-intensity UV laser photolysis of DNA and purine 2′-deoxyribonucleosides: Formation of 8-oxopurine damage and oligonucleotide strand cleavage as revealed by HPLC and gel electrophoresis studies. *J. Am. Chem. Soc.* **1997**, *119*, 11373–11380.
33. Hickerson, R. P.; Prat, F.; Muller, J. G.; Foote, C. S.; Burrows, C. J. Sequence and stacking dependence of 8-oxoguanine oxidation: Comparison of one-electron vs singlet oxygen mechanisms. *J. Am. Chem. Soc.* **1999**, *121*, 9423–9428.
34. Boussicault, F.; Robert, M. Electron transfer in DNA and in DNA-related biological processes. Electrochemical insights. *Chem. Rev.* **2008**, *108*, 2622–2645.
35. Stempkowska, I.; Ligaj, M.; Jasnowska, J.; Langer, J.; Filipiak, M. Electrochemical response of oligonucleotides on carbon paste electrode. *Bioelectrochemistry* **2007**, *70*, 488–494.

36. Oliveira-Brett, A. M.; Piedade, J. A. P.; Silva, L. A.; Diculescu, V. C. Voltammetric determination of all DNA nucleotides. *Anal. Biochem.* **2004**, *332*, 321–329.
37. Takenaka, S.; Yamashita, K.; Takagi, M.; Uto, Y.; Kondo, H. DNA sensing on a DNA probe-modified electrode using ferrocenylnaphthalene diimide as the electrochemically active ligand. *Anal. Chem.* **2000**, *72*, 1334–1341.
38. Singhal, P.; Kuhr, W. G. Direct electrochemical detection of purine- and pyrimidine-based nucleotides with sinusoidal voltammetry. *Anal. Chem.* **1997**, *69*, 3552–3557.
39. Singhal, P.; Kuhr, W. G. Ultrasensitive voltammetric detection of underivatized oligonucleotides and DNA. *Anal. Chem.* **1997**, *69*, 4828–4832.
40. Brabec, V. Nucleic acid analysis by voltammetry at carbon electrodes. *Bioelectrochem. Bioenerg.* **1981**, *8*, 437–449.
41. Palecek, E. Oscillographic polarography of highly polymerized deoxyribonucleic acid. *Nature* **1960**, *188*, 656–657.
42. Palecek, E. In *Electrochemistry of Nucleic Acids and Proteins—Towards Electrochemical Sensors for Genomics and Proteomics*, Vol. 1; Palecek, E., Shcheller, F., Wang, J., Eds.; Elsevier, Boston, 2005, pp. 1–12.
43. Oliveira Brett, A. M.; Matysik, F.-M. Sonoelectrochemical studies of guanine and guanosine. *Bioelectrochem. Bioenerg.* **1997**, *42*, 111–116.
44. Oliveira Brett, A. M.; Matysik, F.-M. Voltammetric and sonovoltammetric studies on the oxidation of thymine and cytosine at a glassy carbon electrode. *J. Electroanal. Chem.* **1997**, *429*, 95–99.
45. Kelley, S. O.; Barton, J. K.; Jackson, N. M.; Hill, M. G. Electrochemistry of methylene blue bound to a DNA-modified electrode. *Bioconjugate Chem.* **1997**, *8*, 31–37.
46. Johnston, D. H.; Cheng, C.-C.; Campbell, K. J.; Thorp, H. H. Trans-dioxorhenium(V)-mediated electrocatalytic oxidation of DNA at indium tin-oxide electrodes: voltammetric detection of DNA cleavage in solution. *Inorg. Chem.* **1994**, *33*, 6388–6390.
47. Millan, K. M.; Mikkelsen, S. R. Sequence-selective biosensor for DNA based on electroactive hybridization indicators. *Anal. Chem.* **1993**, *65*, 2317–2323.
48. Millan, K. M.; Saraullo, A.; Mikkelsen, S. R. Voltammetric DNA biosensor for cystic fibrosis based on a modified carbon paste electrode. *Anal. Chem.* **1994**, *66*, 2943–2948.
49. Wang, J.; Palecek, E.; Nielsen, P. E.; Rivas, G.; Cai, X.; Shiraishi, H.; Dontha, N.; Luo, D.; Farias, P. A. M. Peptide Nucleic Acid Probes for Sequence-Specific DNA Biosensors. *J. Am. Chem. Soc.* **1996**, *118*, 7667–7670.
50. Wang, J.; Rivas, G.; Fernandes, J. R.; Lopez Paz, J. L.; Jiang, M.; Waymire, R. Indicator-free electrochemical DNA hybridization biosensor. *Anal. Chim. Acta* **1998**, *375*, 197–203.
51. Hall, D. B.; Holmlin, R. E.; Barton, J. K. Oxidative DNA damage through long-range electron transfer. *Nature* **1996**, *382*, 731–735.
52. Marrazza, G.; Chianella, I.; Mascini, M. Disposable DNA electrochemical sensor for hybridization detection. *Biosens. Bioelectron.* **1999**, *14*, 43–51.
53. Boon, E. M.; Ceres, D. M.; Drummond, T. G.; Hill, M. G.; Barton, J. K. Mutation detection by electrocatalysis at DNA-modified electrodes. *Nat. Biotechnol.* **2000**, *18*, 1096–1100.
54. Szalai, V. A.; Singer, M. J.; Thorp, H. H. Site-specific probing of oxidative reactivity and telomerase function using 7,8-dihydro-8-oxoguanine in telomeric DNA. *J. Am. Chem. Soc.* **2002**, *124*, 1625–1631.

55. Sistare, M. F.; Codden, S. J.; Heimlich, G.; Thorp, H. H. Effects of base stacking on guanine electron transfer: Rate constants for G and GG sequences of oligonucleotides from catalytic electrochemistry. *J. Am. Chem. Soc.* **2000**, *122*, 4742–4749.
56. Szalai, V. A.; Thorp, H. H. Electrocatalysis of guanine electron transfer: New insights from submillimeter carbon electrodes. *J. Phys. Chem. B* **2000**, *104*, 6851–6859.
57. Szalai, V. A.; Thorp, H. H. Electron transfer in tetrads: Adjacent guanines are not hole traps in G quartets. *J. Am. Chem. Soc.* **2000**, *122*, 4524–4525.
58. Sistare, M. F.; Holmberg, R. C.; Thorp, H. H. Electrochemical studies of polynucleotide binding and oxidation by metal complexes: Effects of scan rate, concentration, and sequence. *J. Phys. Chem. B* **1999**, *103*, 10718–10728.
59. Holmberg, R. C.; Thorp, H. H. Electrochemical determination of triple helices: electrocatalytic oxidation of guanine in an intramolecular triplex. *Inorg. Chem.* **2004**, *43*, 5080–5085.
60. Farrer, B. T.; Thorp, H. H. Redox pathways in DNA oxidation: Kinetic studies of guanine and sugar oxidation by para-substituted derivatives of Oxoruthenium(IV). *Inorg. Chem.* **2000**, *39*, 44–49.
61. Armstrong, N. R.; Lin, A. W. C.; Fujihira, M.; Kuwana, T. Electrochemical and surface characteristics of tin oxide and indium oxide electrodes. *Anal. Chem.* **1976**, *48*, 741–750.
62. Popovich, N. D.; Wong, S.-S.; Yen, B. K. H.; Yeom, H.-Y.; Paine, D. C. Influence of microstructure on the electrochemical performance of tin-doped indium oxide film electrodes. *Anal. Chem.* **2002**, *74*, 3127–3133.
63. Grover, N.; Thorp, H. H. Efficient electrocatalytic and stoichiometric oxidative cleavage of DNA by oxoruthenium(IV). *J. Am. Chem. Soc.* **1991**, *113*, 7030–7031.
64. Armistead, P. M.; Thorp, H. H. Modification of indium tin oxide electrodes with nucleic acids: Detection of attomole quantities of immobilized DNA by electrocatalysis. *Anal. Chem.* **2000**, *72*, 3764–3770.
65. Armistead, P. M.; Thorp, H. H. Oxidation kinetics of guanine in DNA molecules adsorbed onto indium tin oxide electrodes. *Anal. Chem.* **2001**, *73*, 558–564.
66. Thorp, H. H.; Van Houten, J.; Gray, H. B. Excited-state properties of dioxorhenium(V). Generation and reactivity of dioxorhenium(VI). *Inorg. Chem.* **1989**, *28*, 889–892.
67. Thorp, H. H. In *Long Range Charge Transfer in DNA II*, Vol. 237; Schuster, G. B., Ed.; Springer-Verlag, Berlin, 2004; pp. 159–181.
68. Welch, T. W.; Thorp, H. H. Distribution of metal complexes bound to DNA determined by normal pulse voltammetry. *J. Phys. Chem.* **1996**, *100*, 13829–13836.
69. Ye, Y.; Wen, W.; Xiang, Y.; Qi, X.; La Belle, J. T.; Chen, J. J. L.; Wang, J. Direct electrochemical monitoring of RNase activity. *Electroanalysis* **2008**, *20*, 919–922.
70. Masarik, M.; Cahova, K.; Kizek, R.; Palecek, E.; Fojta, M. Label-free voltammetric detection of single-nucleotide mismatches recognized by the protein MutS. *Anal. Bioanal. Chem.* **2007**, *388*, 259–270.
71. Wong, E. L. S.; Gooding, J. J. Charge transfer through DNA: A selective electrochemical DNA biosensor. *Anal. Chem.* **2006**, *78*, 2138–2144.
72. Numnuam, A.; Chumbimuni-Torres, K. Y.; Xiang, Y.; Bash, R.; Thavarungkul, P.; Kanatharana, P.; Pretsch, E.; Wang, J.; Bakker, E. Potentiometric detection of DNA hybridization. *J. Am. Chem. Soc.* **2008**, *130*, 410–411.

73. Welch, T. W.; Corbett, A. H.; Thorp, H. H. Electrochemical determination of nucleic acid diffusion coefficients through noncovalent association of a redox-active probe. *J. Phys. Chem.* **1995**, *99*, 11757–11763.

74. Thorp, H. H. Cutting out the middleman: DNA biosensors based on electrochemical oxidation. *Trends in Biotechnology* **1998**, *16*, 117–121.

75. Napier, M. E.; Thorp, H. H. Modification of electrodes with dicarboxylate self-assembled monolayers for attachement and detection of nucleic acids. *Langmuir* **1997**, *13*, 6342–6344.

76. Ontko, A. C.; Armistead, P. A.; Kircus, S. R.; Thorp, H. H. Electrochemical detection of single-stranded DNA using polymer-modified electrodes. *Inorg. Chem.* **1999**, *38*, 1842–1846.

77. Napier, M. E.; Thorp, H. H. Electrocatalytic oxidation of nucleic acids at Electrodes modified with nylon and nitrocellulose membranes. *J. Fluoresc* **1999**, *1999*, 181–186.

78. Arkin, M. R.; Stemp, E. D.; Pulver, S. C.; Barton, J. K. Long-range oxidation of guanine by Ru(III) in duplex DNA. *Chem. Biol.* **1997**, *4*, 389–400.

79. Cullis, P. M.; Malone, M. E.; Merson-Davies, L. A. Guanine radical cations are precursors of 7,8-Dihydro-8-oxo-2′-deoxyguanosine but are not precursors of immediate strand breaks in DNA. *J. Am. Chem. Soc.* **1996**, *118*, 2775–2781.

80. Kino, K.; Saito, I.; Sugiyama, H. Product analysis of GG-specific photooxidation of DNA via electron transfer: 2-Aminoimidazolone as a major guanine oxidation product. *J. Am. Chem. Soc.* **1998**, *120*, 7373–7374.

81. Duarte, V.; Muller, J.; Burrows, C. Insertion of dGMP and dAMP during *in vitro* DNA synthesis opposite an oxidized form of 7,8-dihydro-8-oxoguanine. *Nucl. Acids Res.* **1999**, *27*, 496–502.

82. Muller, J.; Duarte, V.; Hickerson, R.; Burrows, C. Gel electrophoretic detection of 7,8-dihydro-8-oxoguanine and 7, 8- dihydro-8-oxoadenine via oxidation by Ir (IV). *Nucl. Acids Res.* **1998**, *26*, 2247–2249.

83. Giese, B. Long-distance electron transfer through DNA. *Annu. Rev. Biochem.* **2002**, *71*, 51–70.

84. Sugiyama, H.; Saito, I. Theoretical studies of GG-specific photocleavage of DNA via electron transfer: Significant lowering of ionization potential and 5′-localization of HOMO of stacked GG bases in B-form DNA. *J. Am. Chem. Soc.* **1996**, *118*, 7063–7068.

85. Saito, I.; Nakamura, T.; Nakatani, K.; Yoshioka, Y.; Yamaguchi, K.; Sugiyama, H. Mapping of the hot spots for DNA damage by one-electron oxidation: efficacy of GG doublets and GGG triplets as a trap in long-range hole migration. *J. Am. Chem. Soc.* **1998**, *120*, 12686–12687.

86. Schuster, G. B. Long-range charge transfer in DNA: Transient structural distortions control the distance dependence. *Acc. Chem. Res.* **2000**, *33*, 253–260.

87. Lewis, F. D.; Liu, X.; Liu, J.; Hayes, R. T.; Wasielewski, M. R. Dynamics and equilibria for oxidation of G, GG, and GGG sequences in DNA hairpins. *J. Am. Chem. Soc.* **2000**, *122*, 12037–12038.

88. Meggers, E.; Michel-Beyerle, M. E.; Giese, B. Sequence dependent long range hole transport in DNA. *J. Am. Chem. Soc.* **1998**, *120*, 12950–12955.

89. Prat, F.; Houk, K. N.; Foote, C. S. Effect of guanine stacking on the oxidation of 8-oxoguanine in B-DNA. *J. Am. Chem. Soc.* **1998**, *120*, 845–846.

90. Kan, Y.; Schuster, G. B. Long-range guanine damage in single-stranded DNA: charge transport through a duplex bridge and in a single-stranded overhang. *J. Am. Chem. Soc.* **1999**, *121*, 10857–10864.

91. Napier, M. E.; Loomis, C. R.; Sistare, M. F.; Kim, J.; Eckhardt, A. E.; Thorp, H. H. Probing biomolecule recognition with electron transfer: Electrochemical sensors for DNA hybridization. *Bioconjugate Chem.* **1997**, *8*, 906–913.

92. Kelley, S. O.; Barton, J. K. Electron transfer between bases in double helical DNA. *Science* **1999**, *283*, 375–381.

93. Wan, C.; Fiebig, T.; Kelley, S. O.; Treadway, C. R.; Barton, J. K.; Zewail, A. H. Femtosecond dynamics of DNA-mediated electron transfer. *Proc. Natl. Acad. Sci. U. S. A.* **1999**, *96*, 6014–6019.

94. Ropp, P. A.; Holden Thorp, H. Site-selective electron transfer from purines to electrocatalysts: Voltammetric detection of a biologically relevant deletion in hybridized DNA duplexes. *Chem. Biol.* **1999**, *6*, 599–605.

95. Boal, A. K.; Barton, J. K. Electrochemical detection of lesions in DNA. *Bioconjugate Chem.* **2005**, *16*, 312–321.

96. Boon, E. M.; Barton, J. K.; Pradeepkumar, P. I.; Isaksson, J.; Petit, C.; Chattopadhyaya, J. An electrochemical probe of DNA stacking in an antisense oligonucleotide containing a C3prime-endo-locked sugar. *Angew. Chem. Int. Ed.* **2002**, *41*, 3402–3405.

97. Williamson, J. R.; Raghuraman, M. K.; Cech, T. R. Monovalent cation-induced structure of telomeric DNA: The G-quartet model. *Cell* **1989**, *59*, 871–880.

98. Núñez, M. E.; Hall, D. B.; Barton, J. K. Long-range oxidative damage to DNA: Effects of distance and sequence. *Chem. Biol.* **1999**, *6*, 85–97.

99. Sartor, V.; Henderson, P. T.; Schuster, G. B. Radical cation transport and reaction in RNA/DNA hybrid duplexes: Effect of global structure on reactivity. *J. Am. Chem. Soc.* **1999**, *121*, 11027–11033.

100. Ly, D.; Sanii, L.; Schuster, G. B. Mechanism of charge transport in DNA: internally-linked anthraquinone conjugates support phonon-assisted polaron hopping. *J. Am. Chem. Soc.* **1999**, *121*, 9400–9410.

101. Kan, Y.; Schuster, G. B. Radical cation transport and reaction in triplex DNA: long-range guanine damage. *J. Am. Chem. Soc.* **1999**, *121*, 11607–11614.

102. Stemp, E. D. A.; Arkin, M. R.; Barton, J. K. Oxidation of guanine in DNA by Ru(phen)2-(dppz)3+ using the flash-quench technique. *J. Am. Chem. Soc.* **1997**, *119*, 2921–2925.

103. Bernstein, R.; Prat, F.; Foote, C. S. On the mechanism of DNA cleavage by fullerenes investigated in model systems: Electron transfer from guanosine and 8-Oxo-guanosine derivatives to C60. *J. Am. Chem. Soc.* **1999**, *121*, 464–465.

104. Riordan, J. R.; Rommens, J. M.; Kerem, B.-s.; Alon, N.; Rozmahel, R.; Grzelczak, Z.; Zielenski, J.; Lok, S.; Plavsic, N.; Chou, J.-L.; Drumm, M. L.; Iannuzzi, M. C.; Collins, F. S.; Tsui, L.-C. Identification of the cystic fibrosis gene: Cloning and characterization of complementary DNA. *Science* **1989**, *245*, 1066–1073.

105. Holmberg, R. C.; Tierney, M. T.; Ropp, P. A.; Berg, E. E.; Grinstaff, M. W.; Thorp, H. H. Intramolecular electrocatalysis of 8-oxo-guanine oxidation: secondary structure control of electron transfer in osmium-labeled oligonucleotides. *Inorg. Chem.* **2003**, *42*, 6379–6387.

106. Seela, F.; Roling, A. 7-Deazapurine containing DNA: efficiency of c7Gd TP, c7Ad TP and c7ld TP incorporation during PCR amplification and protection from endodeoxyribonuclease hydrolysis. *Nucl. Acids Res.* **1992**, *20*, 55–61.

107. McConlogue, L.; Brow, M. A. D.; Innis, M. A. Structure-independent DNA amplification by PCR using 7-deaza-2′-deoxyguanosine. *Nucl. Acids Res.* **1988**, *16*, 9869.

108. Delaney, S.; Barton, J. K. Long-range DNA charge transport. *J. Org. Chem.* **2003**, *68*, 6475–6483.

109. Boon, E. M.; Barton, J. K. Charge transport in DNA. *Curr. Opin. Struct. Biol.* **2002**, *12*, 320–329.

110. Giese, B. Long-distance charge transport in DNA: The Hopping mechanism. *Acc. Chem. Res.* **2000**, *33*, 631–636.

111. Gorodetsky, A. A.; Green, O.; Yavin, E.; Barton, J. K. Coupling into the base pair stack is necessary for DNA-mediated electrochemistry. *Bioconjugate Chem.* **2007**, *18*, 1434–1441.

112. Berlin, Y. A.; Burin, A. L.; Ratner, M. A. On the long-range charge transfer in DNA. *J. Phys. Chem. A* **2000**, *104*, 443–445.

113. Holmlin, R. E.; Dandliker, P. J.; Barton, J. K. Charge transfer through the DNA base stack. *Angew. Chem. Int. Ed.* **1997**, *36*, 2715–2730.

114. Bhattacharya, P. K.; Barton, J. K. The Influence of intervening mismatches on long-range guanine oxidation in DNA duplexes. *J. Am. Chem. Soc.* **2001**, *123*, 8649–8658.

115. Hall, D. B.; Barton, J. K. Sensitivity of DNA-mediated electron transfer to the intervening pi-stack: A probe for the integrity of the DNA base stack. *J. Am. Chem. Soc.* **1997**, *119*, 5045–5046.

116. Rajski, S. R.; Kumar, S.; Roberts, R. J.; Barton, J. K. Protein-modulated DNA electron transfer. *J. Am. Chem. Soc.* **1999**, *121*, 5615–5616.

117. Boon, E. M.; Jackson, N. M.; Wightman, M. D.; Kelley, S. O.; Hill, M. G.; Barton, J. K. Intercalative stacking: A critical feature of DNA charge-transport electrochemistry. *J. Phys. Chem. B* **2003**, *107*, 11805–11812.

118. Stemp, E. D. A.; Barton, J. K. The flash-quench technique in protein-DNA electron transfer: Reduction of the guanine radical by ferrocytochrome c. *Inorg. Chem.* **2000**, *39*, 3868–3874.

119. Augustyn, K. E.; Merino, E. J.; Barton, J. K. A role for DNA-mediated charge transport in regulating p53: Oxidation of the DNA-bound protein from a distance. *Proc. Natl. Acad. Sci. USA* **2007**, *104*, 18907–18912.

120. Boon, E. M.; Salas, J. E.; Barton, J. K. An electrical probe of protein-DNA interactions on DNA-modified surfaces. *Nat. Biotechnol.* **2002**, *20*, 282–286.

121. Gorodetsky, A. A.; Ebrahim, A.; Barton, J. K. Electrical detection of TATA binding protein at DNA-modified microelectrodes. *J. Am. Chem. Soc.* **2008**, *130*, 2924–2925.

122. Wong, E. L. S.; Gooding, J. J. Electronic detection of target nucleic acids by a 2,6-disulfonic acid anthraquinone intercalator. *Anal. Chem.* **2003**, *75*, 3845–3852.

123. Wong, E. L. S.; Erohkin, P.; Gooding, J. J. A comparison of cationic and anionic intercalators for the electrochemical transduction of DNA hybridization via long range electron transfer. *Electrochem. Commun.* **2004**, *6*, 648–654.

124. Gasparac, R.; Taft, B. J.; Lapierre-Devlin, M. A.; Laxareck, A. D.; Xu, J. M.; Kelley, S. O. Ultrasensitive electrocatalytic DNA detection at two- and three-dimensional nanoelectrodes. *J. Am. Chem. Soc.* **2004**, *126*, 12270–12271.

125. Lapierre, M. A.; O'Keefe, M.; Taft, B. J.; Kelley, S. O. Electrocatalytic detection of pathogenic DNA sequences and antibiotic resistance markers. *Anal. Chem.* **2003**, *75*, 6327–6333.

126. Fojta, M.; Kostecka, P.; Trefulka, M.; Havran, L.; Palecek, E. "Multicolor" electrochemical labeling of DNA hybridization probes with osmium tetroxide complexes. *Anal. Chem.* **2007**, *79*, 1022–1029.

127. Fojta, M.; Havran, L.; Vojtiskova, M.; Palecek, E. Electrochemical detection of DNA triplet repeat expansion. *J. Am. Chem. Soc.* **2004**, *126*, 6532–6533.

128. Palecek, E.; Fojta, M.; Jelen, F. New approaches in the development of DNA sensors: Hybridization and electrochemical detection of DNA and RNA at two different surfaces. *Bioelectrochemistry* **2002**, *56*, 85–90.

129. Authier, L.; Grossiord, C.; Brossier, P.; Limoges, B. Gold nanoparticle-based quantitative electrochemical detection of amplified human cytomegalovirus DNA using disposable microband electrodes. *Anal. Chem.* **2001**, *73*, 4450–4456.

130. Ozsoz, M.; Erdem, A.; Kerman, K.; Ozkan, D.; Tugrul, B.; Topcuoglu, N.; Ekren, H.; Taylan, M. Electrochemical genosensor based on colloidal gold nanoparticles for the detection of factor V Leiden Mutation using disposable pencil graphite electrodes. *Anal. Chem.* **2003**, *75*, 2181–2187.

131. Pingarrón, J. M.; Yáñez-Sedeño, P.; González-Cortés, A. Gold nanoparticle-based electrochemical biosensors. *Electrochim. Acta* **2008**, *53*, 5848–5866.

132. Cai, H.; Xu, Y.; Zhu, N.; He, P.; Fang, Y. An electrochemical DNA hybridization detection assay based on a silver nanoparticle label. *The Analyst* **2002**, *127*, 803–808.

133. Gao, M.; Qi, H.; Gao, Q.; Zhang, C. Electrochemical detection of DNA hybridization based on the probe labeled with carbon-nanotubes loaded with silver nanoparticles. *Electroanalysis* **2008**, *20*, 123–130.

134. Wang, J.; Liu, G.; Polsky, R.; Merkoçi, A. Electrochemical stripping detection of DNA hybridization based on cadmium sulfide nanoparticle tags. *Electrochem. Commun.* **2002**, *4*, 722–726.

135. Merkoci, A. Electrochemical biosensing with nanoparticles. *FEBS J.* **2007**, *274*, 310–316.

136. Suwansa-ard, S.; Xiang, Y.; Bash, R.; Thavarungkul, P.; Kanatharana, P.; Wang, J. Prussian blue dispersed sphere catalytic labels for amplified electronic detection of DNA. *Electroanalysis* **2008**, *20*, 308–312.

137. Ma, H.; Zhang, L.; Pan, Y.; Zhang, K.; Zhang, Y. A novel electrochemical DNA biosensor fabricated with layer-by-layer covalent attachment of multiwalled carbon nanotubes and gold nanoparticles. *Electroanalysis* **2008**, *20*, 1220–1226.

138. Zhu, X.; Han, K.; Li, G. Magnetic nanoparticles applied in electrochemical detection of controllable DNA hybridization. *Anal. Chem.* **2006**, *78*, 2447–2449.

139. Kouassi, G. K.; Irudayaraj, J. Magnetic and gold-coated magnetic nanoparticles as a DNA sensor. *Anal. Chem.* **2006**, *78*, 3234–3241.

140. Palecek, E.; Scheller, F.; Wang, J. In *Electrochemistry of Nucleic Acids and Proteins—Towards Electrochemical Sensors for Genomics and Proteomics*, Vol. 1; Palecek, E., Ed.; Elsevier, Amsterdam, 2005, pp. 369–384.

141. Wang, J.; Xu, D.; Kawde, A.-N.; Polsky, R. Metal nanoparticle-based electrochemical stripping potentiometric detection of DNA hybridization. *Anal. Chem.* **2001**, *73*, 5576–5581.

142. Xiang, Y.; Xie, M.; Bash, R.; Chen, J. J. L.; Wang, J. Ultrasensitive label-free aptamer-based electronic detection. *Angew. Chem. Int. Ed.* **2007**, *46*, 9054–9056.

143. Wang, J.; Rivas, G.; Cai, X.; Chicharro, M.; Dontha, N.; Luo, D.; Palecek, E.; Pater, E. Nielsen adsorption and detection of peptide nucleic acids at carbon paste eletrodes. *Electroanalysis* **1997**, *9*, 120–124.

144. Dolinnaya, N. G.; Jan, M. R.; Kawde, A.-N.; Oretskaya, T. S.; Tashlitsky, V. N.; Wang, J. Electrochemical detection of abasic site-containing DNA. *Electroanalysis* **2006**, *18*, 399–404.

145. Roth, K. M.; Peyvan, K.; Schwarzkopf, K. R.; Ghindilis, A. Electrochemical detection of short DNA oligomer hybridization using the CombiMatrix ElectraSense microarray reader. *Electroanalysis* **2006**, *18*, 1982–1988.

146. Vernon, S.; Farkas, D.; Unger, E.; Chan, V.; Miller, D.; Chen, Y.-P.; Blackburn, G.; Reeves, W. Bioelectronic DNA detection of human papillomaviruses using eSensor™: A model system for detection of multiple pathogens. *BMC Infect. Dis.* **2003**, *3*, 12.

147. Umek, R.; Lin, S.; Vielmetter, J.; Terbrueggen, R.; Irvine, B.; Yu, C.; Kayyem, J.; Yowanto, H.; Blackburn, G.; Farkas, D.; Chen, Y. Electronic detection of nucleic acids: Versatile platform for molecular diagnostics. *J. Mol. Diagn.* **2001**, *3*, 74–84.

148. Umek, R.; Lin, S.; Chen Yp, Y.; Irvine, B.; Paulluconi, G.; Chan, V.; Chong, Y.; Cheung, L.; Vielmetter, J.; Farkas, D. Bioelectronic detection of point mutations using discrimination of the H63D polymorphism of the Hfe gene as a model. *Mol. Diagn.* **2000**, *5*, 321–328.

149. Farkas, D. Bioelectronic DNA chips for the clinical laboratory. *Clin. Chem.* **2001**, *47*, 1871–1872.

150. Liu, R. H.; Coty, W. A.; Reed, M.; Gust, G. Electrochemical detection-based DNA microarrays. *IVD Technol.* **2008**, *31*, 31–37.

13

DNA DAMAGE DUE TO DIRADICAL-GENERATING CYCLIZATIONS

SEAN M. KERWIN

Division of Medicinal Chemistry, College of Pharmacy, The University of Texas at Austin, Austin, TX 78712, USA

13.1. INTRODUCTION

The naturally occurring enediyne antitumor agents are among the most cytotoxic natural products known. They are also one of the few classes of small organic molecules that can effect oxidative DNA cleavage in the absence of redox-active metal ions or irradiation. Most of these natural products are of microbial origin, and they can be grouped according to the size of the ring containing the enediyne core. In one family, exemplified by calicheamicin γ_1^I,[1] esperamicin A_1,[2] and dynemicin A[3] (Figure 13.1), the enediyne is constrained to a 10-membered ring. Other examples of this family are uncialamycin,[4] namenamicin,[5] and shishijimicin.[6] In contrast to this family of naturally occurring enediynes, which are produced as isolated chromophores, almost all of the nine-membered enediynes are produced as chromophore–protein complexes. Figure 13.1 shows the structure of the chromophores for some members of this family, neocarzinostatin (NCS),[7,8] C-1027 or lidamycin,[9,10] and N1999A2.[11] Other members of this family include kedarcidin[12] and maduropeptin.[13] Within this family, only N199A2 is produced as the isolated chromophore.

The ability of some naturally occurring enediynes to kill cancer cells *in vitro* at concentrations as low as 10^{-12} M[14] has fueled interest in studying the mechanism of action of these agents and their potential application to cancer chemotherapy. A very early, critical insight into the mechanism of action of these natural products came from

Radical and Radical Ion Reactivity in Nucleic Acid Chemistry, Edited by Marc M. Greenberg

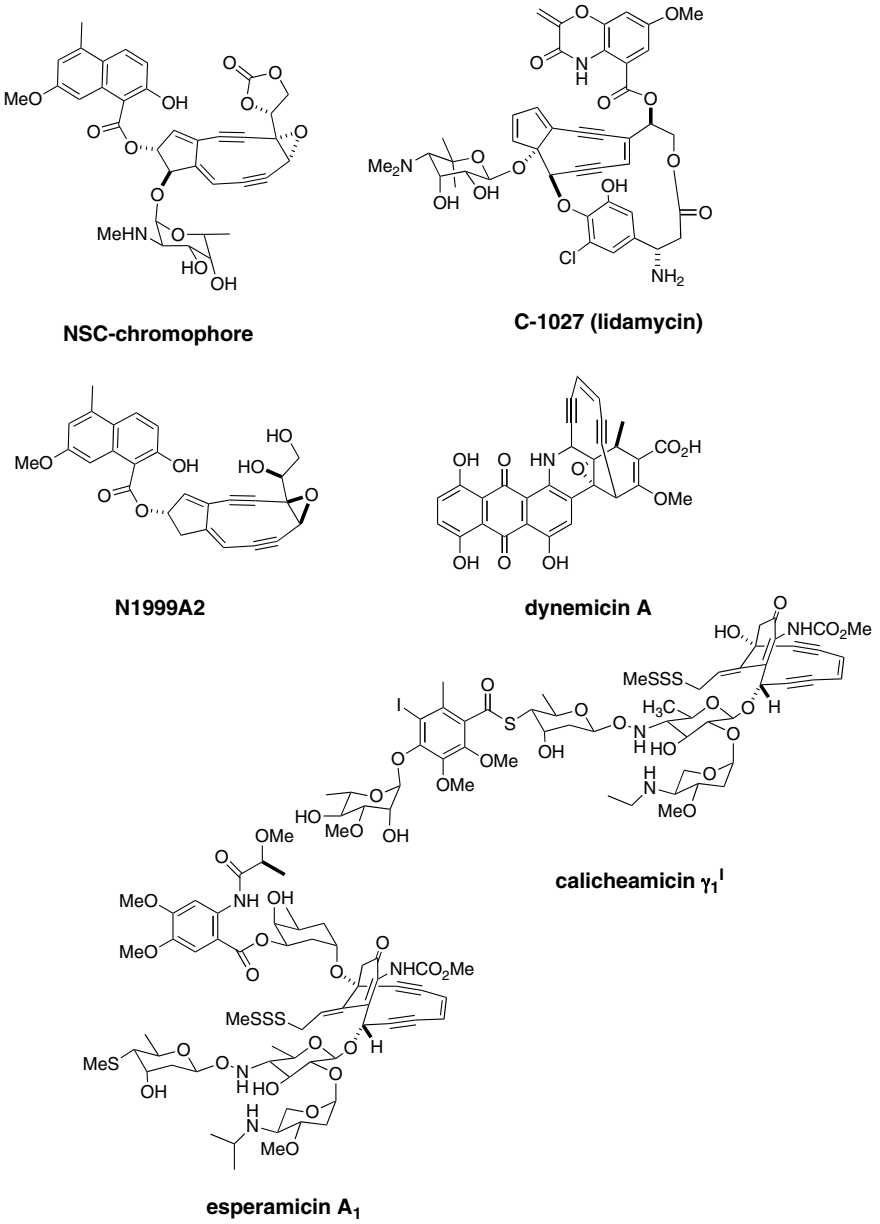

FIGURE 13.1. Structures of naturally occurring enediynes.

the results of prior studies by Bergman, who had demonstrated the thermal rearrangement of enediynes to reactive *p*-benzyne diradicals.[15] The generation of benzenoid diradicals from naturally occurring enediynes, the interaction of these diradicals with DNA, and the chemical and biological aspects of the resulting DNA damage continue

to be very active areas of research. While the enediyne natural products appear too toxic for direct use in cancer chemotherapy, ongoing efforts to develop these enediynes have led to the approval of two drugs, a styrene-maleic acid polymer-coupled NCS (SMANCS)[16] and Mylotarg (gemtuzumab ozogamicin), a conjugate of calicheamicin and a humanized antibody that targets CD33.[17, 18] The search for improved analogues for drug discovery continues through studies directed toward understanding and engineering the biosynthetic pathways for these compounds[19–21] and the design and synthesis of enediynes with improved selectivity, including harnessing other diradical-generating reactions.[22–27]

This chapter will provide a brief overview of the diradical-generating cyclizations of these enediyne natural products. The interaction of these diradicals with DNA will be presented, focusing on the resulting 2-deoxyribose-based DNA radicals and their fate. Finally, alternative diradical-generating systems that have been examined for DNA-cleavage potential will be discussed.

13.2. DIRADICAL-GENERATING CYCLIZATIONS OF ENEDIYNE NATURAL PRODUCTS

13.2.1. Bergman Cyclization

The 10-membered enediynes such as calicheamicin and dynemicin are stable to diradical-generating Bergman cyclization until activated through reduction or nucleophilic attack. In the case of calicheamicin and esperamicin, nucleophilic attack on the trisulfide moiety reveals a sulfhydryl group poised for intramolecular Michael addition to the cyclohexenone core (Figure 13.2A). The resulting rehybridization of the bridgehead carbon from sp^2, in which cyclization is prevented by the strain that would be manifest in the formation of an anti-Brent olefin,[28] to sp^3 triggers the Bergman cyclization, which readily occurs with an activation energy on the order of 19.6 kcal/mole.[29, 30] In contrast to the 28.8 kcal/mol barrier for Bergman cyclization of (*Z*)-hex-3-ene-1,5-diyne,[31] the facility of the Bergman cyclization of the post-activated calicheamicin enediyne core is comparable to the ready cyclization of simple, monocyclic 10-membered enediynes, which has been attributed to the short distance between the two terminal *sp*-hybridized carbons (the c–d distance) in these enediynes.[14] Subsequent studies demonstrate that strain energy, rather than the c–d distance per say, controls the Bergman cyclization rate.[28] Although there is conflicting evidence concerning the role that DNA plays in the triggering nucleophilic addition,[32] recent computational studies have predicted that the product of triggering of calicheamicin bound to the minor groove of duplex DNA is a higher-energy epimer that cyclizes more readily than the thermodynamic epimer predicted to form from triggering in solution.[30]

The reactivity of the benzenoid diradicals derived from enediynes by Bergman cyclization has been attributed to the relatively small energy difference between the singlet and triplet states.[33] Hydrogen atom abstraction from DNA occurs stepwise to generate an intermediate monoradical that reacts very quickly, by hydrogen atom abstraction from either the opposite DNA strand or from solvent.

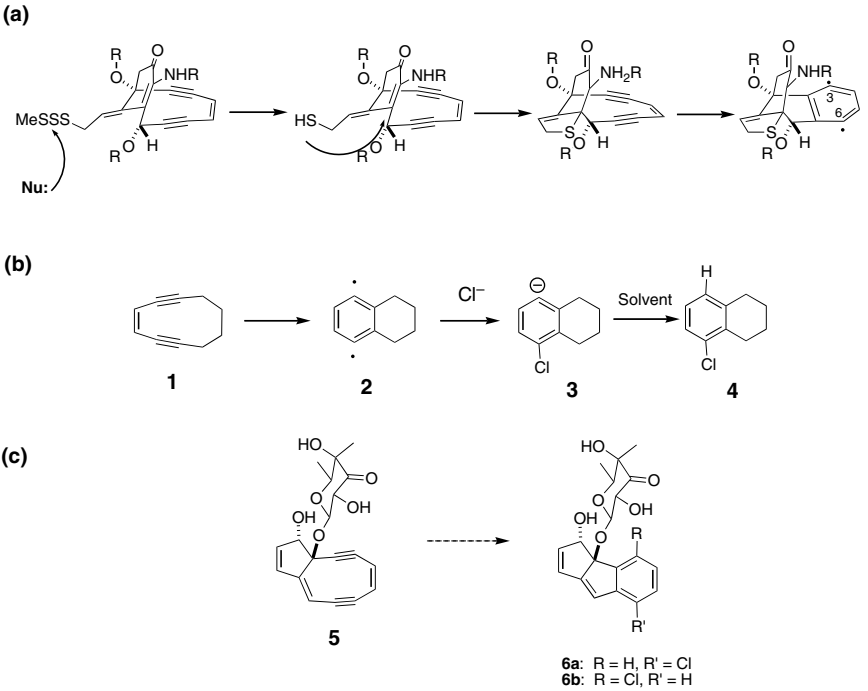

FIGURE 13.2. (**A**) Bergman cyclization of the naturally occurring enediynes. (**B**) Halide ion addition trapping of an enediyne-derived diradical. (**C**) Proposed biosynthetic pathway for the cyanosporasides.

Recently, an alternative reactivity of benzenoid diradicals has been observed in the case of the synthetic 10-membered enediyne **1** (Figure 13.2B).[34] Under physiological temperature in the presence of halide ions, **1** affords the halotetrahydronaphthalenes **4** via nucleophilic trapping of the intermediate benzenoid diradical **2**. Addition of halide ion to **2** affords the anion **3**, which is quickly protonated. Although there is no evidence that this nucleophilic trapping is involved in the mechanism of action of the naturally occurring enediynes such as calicheamicin, it is plausible that this process is involved in the biosynthesis of the cyanosporasides **6a**,**b** (Figure 13.2C).[35,36] These marine natural products, isolated as a 1:1 mixture of positional isomers, may arise from Bergman cyclization of a precursor nine-membered enediyne **5** followed by trapping with chloride.

13.2.2. Enyne Cumulene Cyclization

Although the NCS chromophore lacks the 3-ene-1,5-diyne core common to the 10-membered enediynes such as calicheamicin and esperamicin, thiol addition generates a reactive enyne cumulene system **7** (Figure 13.3A). The diradical-generating cyclization of this activated form of NCS was first proposed by Myers.[8] There are important differences between the benzenoid diradicals generated from the

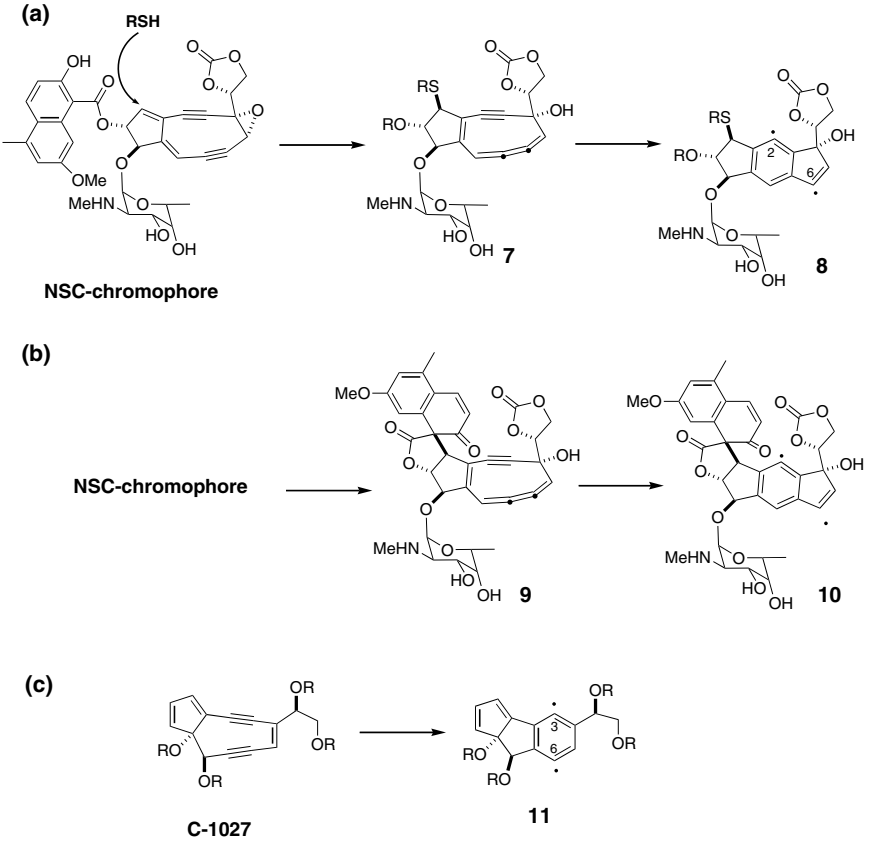

FIGURE 13.3. (**A**) Enyne cumulene cyclization of NCS-chromophore. (**B**) Thiol-independent cyclization of NCS-chromophore. (**C**) Bergman cyclization of nine-membered enediyne natural product C-1027.

10-membered enediynes and the didehydroindene diradicals generated from NCS and related nine-membered enediynes. The activating thiol becomes covalently attached to the NCS and is proximal to the C2 radical center in the resulting didehydroindene diradical **8**. As a result, the reactivity of the diradical is somewhat dependent on the nature of the thiol. This may reflect specific interactions with the thiol side chain and the DNA, the ability of the thiol side chain to quench the C2 radical center through intramolecular hydrogen atom transfer, the quenching of a ribose-centered radical through hydrogen atom abstraction from the thiol side chain, or a combination of these effects.[37] Interestingly, under certain conditions, thiol activation is not required for DNA cleavage by NCS.[38] At bulged DNA sites, NCS undergoes a self-activation involving the intramolecular addition of the naphthoate to form a spirocyclic cumulene intermediate **9** that undergoes cyclization to diradical **10** (Figure 13.3B). Although the DNA cleavage arising from this pathway is not as efficient as that initiated by thiol addition, the selectivity for bulged DNA structures is very high.[39]

Another nine-membered enediyne N1999A2[40] undergoes thiol-dependent activation like NCS. However, nine-membered enediynes C-1027,[41] maduropeptin,[13] and kedarcidin[42] are different; possessing the 3-ene-1,5-diyne moiety, they can spontaneously and directly undergo Bergman cyclization (Figure 13.3C).

13.3. DNA CLEAVAGE CHEMISTRY OF ENEDIYNE NATURAL PRODUCTS

These enediyne natural products are directed toward the minor groove of double-stranded DNA. Within the minor groove, the efficiency and sites of deoxyribose hydrogen atom abstraction by these natural products are a function not only of the identity of the activated enediyne, but also of the conformational aspects of the DNA target that are engendered by sequence or noncanonical base pairing. This gives rise to varying proportions of single-stranded versus double-stranded DNA cleavage events for different enediynes at different DNA sites. The DNA cleavage chemistry of the enediyne natural products has been extensively studied and there are some excellent reviews comparing and contrasting the cleavage chemistry of the enediynes with other DNA cleavage agents that attack the deoxyribose backbone.[43–50] In the following section, an outline of this chemistry is presented, organized by the site of DNA hydrogen atom abstraction by the enediyne.

13.3.1. 1′-Chemistry

The ability of esperamicin A1 to abstract hydrogen from the 1′-deoxyribose position was established by studying the incorporation of tritium into the aromatized enediyne after incubation with site-specifically tritiated DNA.[51] Similarly, a minor lesion produced by NCS-mediated double-stranded DNA cleavage at 5′-AGC·3′-TCG sites was shown to involve hydrogen atom abstraction from the C1′ of the C of AGC by tritium incorporation[52] and deuterium isotope effect.[53] The NCS C2-radical center (see Figure 13.3A) is responsible for abstraction of the C1′ hydrogen,[54,55] while in the case of esperamicin, it is presumably the C3 radical center (see Figure 13.2A) that is involved. PAGE analysis of DNA products formed as a result of cleavage by dynemicin A have also been interpreted as evidence for C1′ hydrogen atom abstraction.[56]

In the presence of oxygen, the resulting C1′ radical **12** forms a peroxyl radical **13** that ultimately gives rise to an abasic, deoxyribonolactone lesion **14** (Figure 13.4).[57] In the context of double-stranded DNA, the deoxyribonolactone lesion is relatively labile,[58] with a half-life of 32–52 h under physiological conditions. Ultimately, under physiological conditions, or more quickly at higher pH, these lesions undergo elimination leading to DNA cleavage, releasing 3′-phosphate- (**15**) and 5′-phosphate-terminated DNA fragments (**17**) and 5-methylenyl-2(5*H*)furanone **16** (Figure 13.4). In addition to leading to DNA strand scission, the deoxyribonolactone lesions **14** are biologically important due to their unique mutational profile[59–62] and their propensity to form covalent DNA–protein cross-links via lactone ring opening by lysine side chains.[63,64]

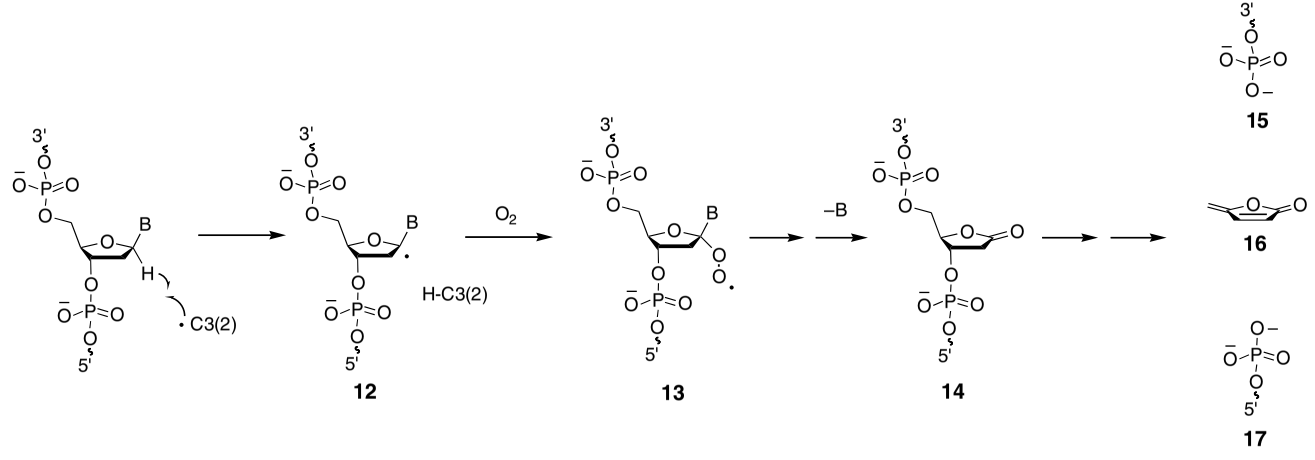

FIGURE 13.4. 1′-Chemistry of enediyne natural product DNA cleavage.

13.3.2. 4′-Chemistry

Abstraction of the deoxyribose C4′ hydrogen by calicheamicin γ_1^I has been established using isotope incorporation studies of a site-specifically deuterated duplex oligodeoxyribonucleotide containing a 5′-AGGATC site.[65] At this site, the C3 radical center of calicheamicin (see Figure 13.2A) abstracts the C4′ hydrogen of the C residue while, on the complementary strand, the corresponding C6 radical center is involved in stereospecific abstraction of a C5′ hydrogen (see below). Similarly, for NCS in the context of double-stranded DNA cleavage at 5′-AGT sites, the C4′ hydrogen of the T residue is abstracted by the activated NCS C2 radical center, while on the opposite DNA strand a C5′ hydrogen atom is abstracted by the C6 radical center (see below).[66] Less direct evidence for C4′ hydrogen atom abstraction in competition with C5′ hydrogen atom abstraction by NCS has been observed in the context of single-stranded cleavage at T of short oligonucleotides containing a 5′-GT step.[67] It has been noted that the presence of a G•T mismatch to the 5′ side of an NCS cleavage site causes a switch from C1′ to C4′ hydrogen atom abstraction.[68] Although esperamicin A_1 selectively abstracts 5′-hydrogen atoms from DNA, other esperamicins derived by chemical hydrolysis of the natural product afford DNA products commensurate with 4′-hydrogen atom abstraction,[69] as does the nine-membered enediyne C-1027.[70]

In contrast to DNA lesions resulting from abstraction of C1′ hydrogen, which lead exclusively to ribonolactone products, the chemistry of DNA lesions resulting from C4′ hydrogen atom abstraction by enediynes (**18**, Figure 13.5) is more complicated. In the case of C4′ hydrogen atom abstraction, a number of DNA products are observed, and their proportions vary with the nature of the activated enediyne, the reaction conditions, and whether the initially formed DNA radical is part of a single- or double-stranded lesion. Although some of these ultimate DNA products, a 4′-hydroxylated abasic site **21**, 5′-phosphate **17**, and 3′-phosphoglycolate-terminated cleavage products **23** (Figure 13.5) are the same as observed for bleomycin-induced DNA cleavage by C4′ oxidation, the mechanism for the formation of these products by enediyne-mediated DNA cleavage is clearly different.

For enediynes, the formation of both 3′-phosphoglycolate-terminated DNA cleavage products **23** and 4′-hydroxylated abasic sites **21** requires oxygen,[52] in contrast to the case of bleomycin, where 4′-hydroxylated sites are formed preferentially under anaerobic conditions.[71] Also in contrast with bleomycin-mediated DNA cleavage, NCS and calicheamicin-mediated 3′-phosphoglycolate DNA cleavage products **23** are only observed in double-strand scission events.[37] However, in the case of NCS, phosphoglycolate products can be formed at single-strand cut sites, but only in the presence of misonidazole, which serves as an oxidant. In the case of a calicheamicin activated by base, the ratio of products **23** and **21** is dependent on the nature and concentration of thiol present. The formation of an additional, 3′-phosphate terminated product **15** observed under these conditions is unaffected by thiols.[72]

A number of different mechanistic proposals have been put forth for the C4′ enediyne cleavage chemistry, some of which are summarized in Figure 13.5. In the case of single-stranded cleavage, it has been proposed that the initially formed 4′-radical **18** is trapped by oxygen to form a 4′-peroxy radical **19**. This radical, in

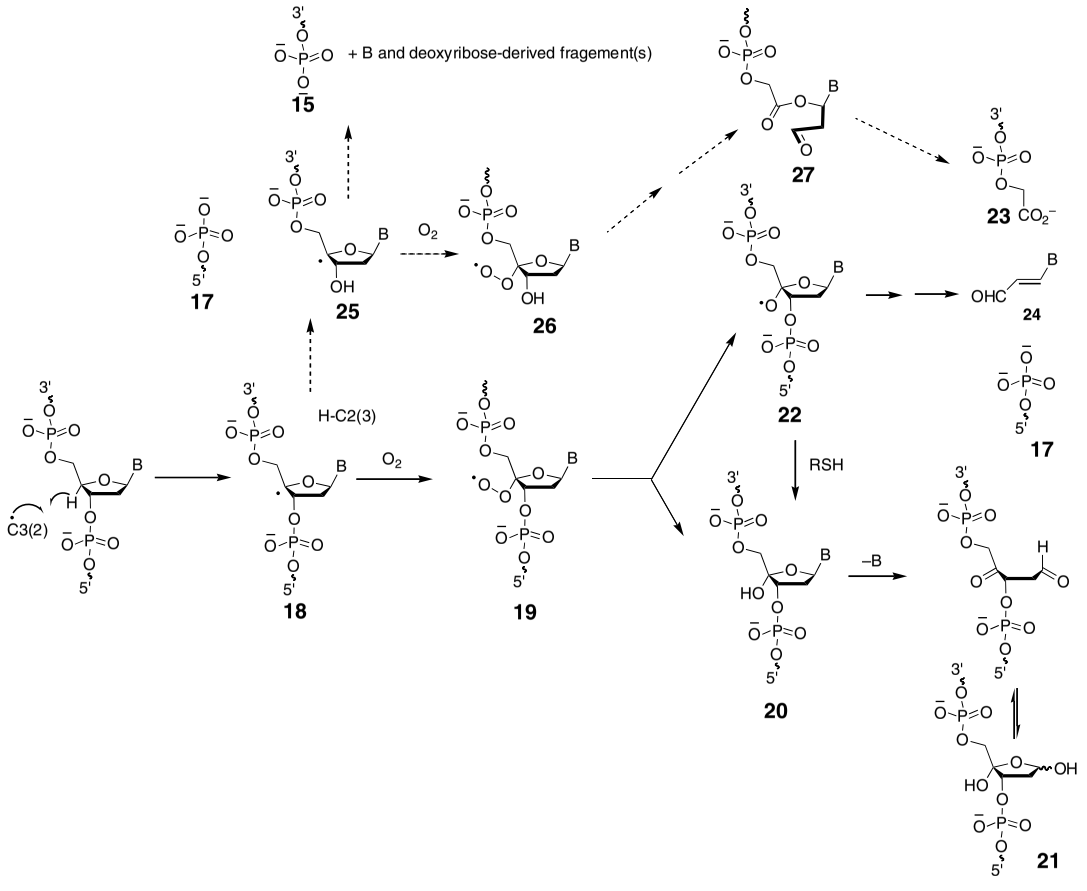

FIGURE 13.5. 4′-Chemistry of enediyne natural product DNA cleavage.

the environment of a single-stranded cleavage event, partitions to the 4′-hydroxylated lesion **20** (major) or to a 4′-oxy radical **22** which, in the presence of thiol, is reduced to afford the same 4′-hydroxylated abasic site **21**.[37] When NCS cleavage is carried out in the presence of misonidazole, the 4′-radical **18** is oxidized directly to the oxy radical **22**, which now can undergo β-fragmentation to ultimately afford the phosphoglycolate **23** in competition with reduction to afford **21**.[37] In the case of double-stranded cleavage events, the dimerization of two adjacent 4′-peroxy radicals **19** is proposed to lead to a tetraoxide that fragments to afford the oxy radical **22**, molecular oxygen, and a corresponding 5′-oxy radical on the opposite strand (see below). Just as in the presence of misonidazole, the efficient formation of the oxy radical **22** in the case of double-strand lesions leads to increased formation of the phosphoglycolate product **23**. Alternatively, the phosphoglycolate product **23** formed in double-strand scission events has been proposed to arise from the peroxy radical **19** via a Criegee-type fragmentation of the corresponding hydroperoxide,[73] although the problematic nature of this fragmentation in the absence of Lewis acid has been noted.[37, 66] Finally, based upon studies of stable precursors to oligodeoxynucleotide C4′ radicals, a mechanism for the formation of phosphogycolate **23** that does not proceed through the 4′-oxy radical **22** or involve a Criegee-type fragmentation has been proposed.[73] Heterolytic bond cleavage of the C4′ radical **18** can lead to formation of a 5′-phosphate-terminated product **17** and a 3′-hydroxy-4′-radical **25**.[74] A second heterolytic event can lead to the 3′-phosphate-terminated product **15**.[72] Alternatively, the C4′ radical **25** can be trapped by oxygen to afford the peroxy radical **26**. A Grob-like fragmentation of the corresponding hydroperoxide leads to the aldehyde **27** that undergoes β-elimination to the 3′-phosphoglycolate **23**.

13.3.3. 5′-Chemistry

The ability of both NCS and calicheamicin to abstract DNA 5′-hydrogens in the context of double-stranded scission events by these agents has been mentioned above. In addition, single-stranded cleavage by NCS also proceeds, for the most part, through 5′-hydrogen atom abstraction, as is the case for esperamicin A_1. Studies employing site-specifically labeled duplex deoxynucleotides have shown that the *pro-S* 5′-hydrogen of cytosine is abstracted by the calicheamicin C6 radical center (Figure 13.6).[65] Similar deuterium-transfer experiments have established the ability of NCS to abstract the 5′-hydrogen from T residues.[75]

The major products of 5′-hydrogen abstraction by NCS are a 3′-phosphate terminated fragment **15** and a 5′-thymidine-5′-aldehyde fragment **30** (Figure 13.6).[44] Trapping of the 5′-radical **28** by O_2[76] leads to a peroxy radical **29** that either is reduced to give 5′-aldehyde **30** (thiol-dependent and major pathway, ~80%) or gives rise to a 3′-phosphoformate **33**. The precise mechanism for the formation of the latter is not clear, and three proposals have been put forth: Criegee-type rearrangement of the initially formed peroxyradical to either **35**[46] or **36**,[77] or β-scission of an oxy radical **31** derived from the peroxy radical (Figure 13.5).[37] The phosphoformate **33** is unstable, and it hydrolyzes to 3′-phosphate **15**. The fragment derived from the deoxyribose has been identified[77] as the 5′-(1,4-dioxo-2-phosphorylbutane) **32**. The elimination

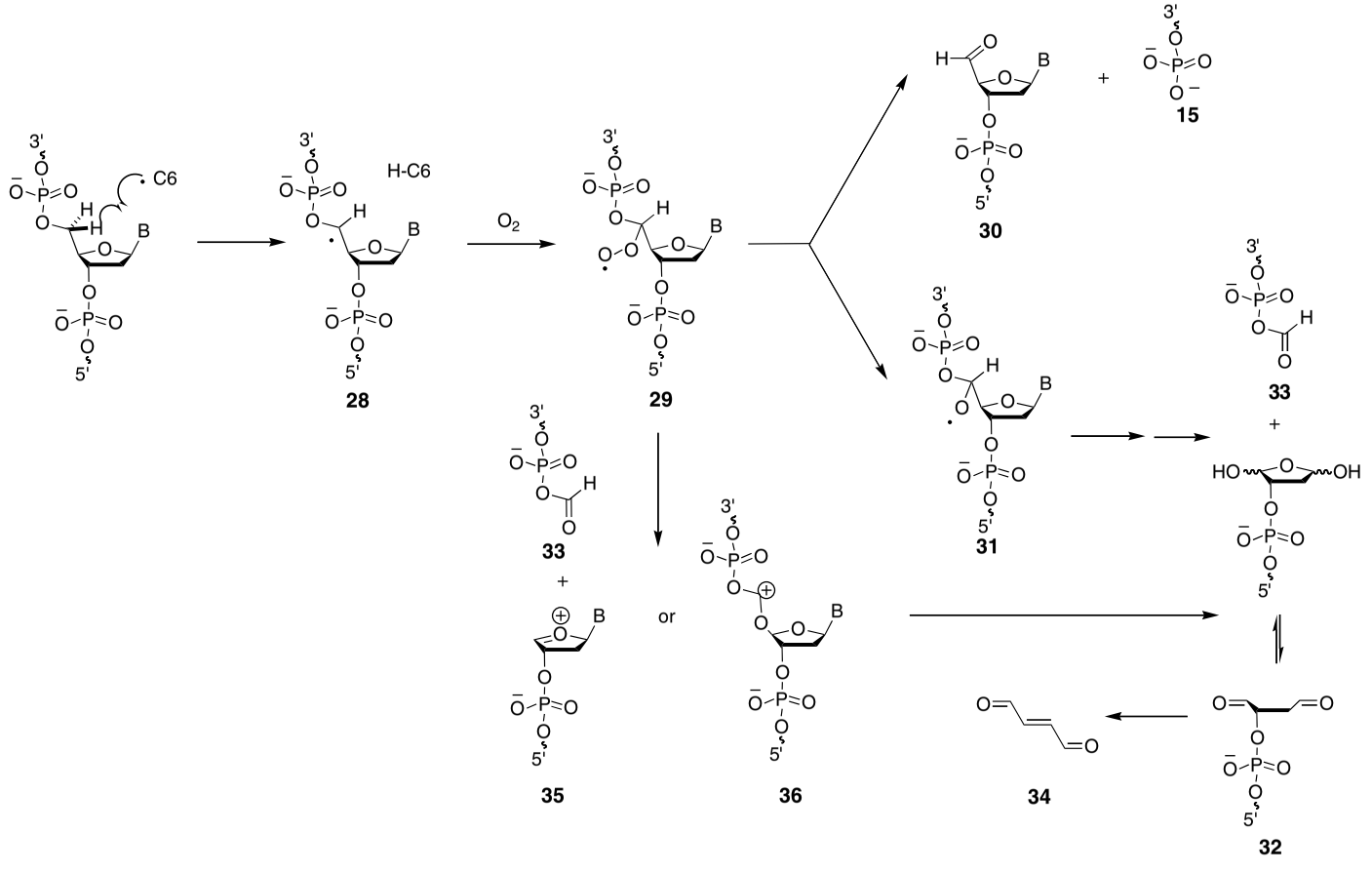

FIGURE 13.6. 5′-Chemistry of enediyne natural product DNA cleavage.

product, 1,4-dioxabut-2-ene (**34**), can itself undergo condensation reactions with DNA bases, leading to hydroxytetrahydrofuro[3,2-*d*]imidazole adducts of dC and dA.[78]

13.4. DNA ADDUCTS AND CROSS-LINKS WITH ENEDIYNE NATURAL PRODUCTS

The ability of NCS to form adducts with DNA had been reported as early as 1983.[79] Separate oligodeoxynucleotides containing either 5′-AGC$_1$/5′-GCT$_2$ or 5′-AGT$_1$/5′-ACT$_2$ target sequences, which form mostly single-strand cleavage products at T$_2$ under aerobic conditions, lead to almost exclusive monoadduct formation under anaerobic conditions.[80] In addition to adducts formed at T$_2$, minor amounts of adducts are also formed at C$_1$ and T$_1$ under these conditions.[80] Bulged DNA substrates also form adducts with NCS under anaerobic conditions.[81] Duplex DNA containing a two-base 5′-AT bulge is selectively cleaved by NCS under aerobic conditions via 5′-hydrogen atom abstraction of the deoxyribose of the 3′-T position; however, under anaerobic conditions, only a DNA adduct is formed at this site.[81] Although the exact structure of the adduct has not been elucidated, it appears to involve covalent attachment of NCS C6 to the 5′C of the bulged T.[82] The adducted DNA, when employed as a template, blocks replication by a variety of DNA polymerases.[83]

Incubation of C1027 with calf thymus DNA leads to the formation of DNA adducts, as shown by the fluorescence spectrum of the DNA product after phenol–chloroform extraction and ethanol precipitation.[80] The amount of adduct formed increases when the incubations are carried out under anaerobic conditions. In a labeled oligonucleotide containing the preferred C1027 cleavage site 5′-GTTA$_1$T/5′-ATA$_2$A$_3$C, monoadducts are formed on the bottom strand. Under anaerobic conditions, the amount of DNA cleavage at A$_1$ and A$_2$ is reduced, and monoadducts on both the top (minor) and bottom (major) strand are formed in addition to interstrand DNA cross-links.[84] Interestingly, under these conditions, cleavage at A$_3$ is unaffected, leading to the speculation that the cleavage chemistry at this site may involve direct α-fragmentation of a 5′-centered DNA radical. To confirm that these adducts and cross-links were initiated by DNA hydrogen atom abstraction, a specifically A$_2$ C1′-deuterated hairpin oligonucleotide was employed, which demonstrated an overall diminution of C-1027-mediated DNA damage ($k_H/k_D = 1.8$) under anaerobic conditions and the disappearance of a product band attributed to the A$_1$–A$_2$ interstrand cross-link.[80] The mechanism proposed for adduct and cross-link formation involves the addition of DNA-centered radicals back onto the cyclized, reduced form of C-1027.

Under anaerobic conditions, calicheamicin also generates both DNA adducts (major) and cross-links (minor). [80] Studies employing a labeled oligonucleotide containing the 5′-TC$_1$CT/5′AGGATC$_2$ target sequence showed that adducts are formed mostly with the bottom strand containing the 5′-AGGATC$_2$ sequence. Interestingly, although the DNA cleavage on the top 5-TC$_1$CT-containing strand is inhibited under anaerobic conditions, there is little evidence of adduct formation on this strand. It is postulated that the enediyne C6 radical center abstracts the 5′-H of C$_1$

from the top strand and the resulting DNA-centered radical is quenched, whereas abstraction of hydrogen from the C_2 of the bottom strand leads to a DNA-centered radical that readily adds back to the cyclized, reduced enediyne.[80]

The significance of enediyne–DNA adduct and cross-link formation on the biological effects of these agents was recently shown.[85] C-1027 induces interstrand DNA cross-links in SV40 DNA in SV40-infected BSC-1 cells. The formation of these cross-links is related to the unique cytotoxic profile of CC-1027, which is equally active against wild-type cells and cells that lack either the *ataxia telangiectasia and Rad3 related* gene [ATR(−)] or the *ataxia telangiectasia mutated* gene [ATM(−)]. In contrast, cells that lack ATM are more sensitive to enediynes such as NSC and calicheamicin as well as ionizing radiation.[86] DeschloroC-1026, an analogue that lacks the ability to form interstrand DNA cross-links, behaves similarly to NCS and calicheamicin in that its cytotoxicity is greater in ATM(−) cells.[85] DesmethylC-1026, an analogue that predominantly forms cross-links and shows little ability for double-strand DNA cleavage, is approximately 2.5-fold more cytotoxic to ATR knockdown cells than to mock-transfected cells.[85]

When NCS is incubated with a RNA–DNA hybrid with a 3′-four base RNA overhang in the presence of thiol and oxygen, an adduct is formed between the activated NCS chromophore and one of the unpaired uridines.[87] The formation of this adduct is thought to involve initial addition of the C6 radical center of the NCS-derived diradical to the 5-position of the uracil base C5–C6 double bond. Trapping of the resulting uracil C6 radical with oxygen is proposed to lead to a peroxy radical that is reduced with thiol to a C6-hydroxyl group. Elimination of water from this C6-hydroxylated C5-C6-dihydrocytosine intermediate regenerates the C5–C6 double bond to form the observed adduct.

13.5. DESIGNED DNA CLEAVAGE AGENTS BASED ON OTHER DIRADICAL-GENERATING CYCLIZATIONS

The remarkable anticancer activity of the enediyne antitumor antibiotics coupled with a need for improved selectivity has spawned numerous approaches to designed enediynes. In contrast to these efforts to refine and harness the Bergman cyclization, a different approach involving the search for alternative diradical-generating cyclizations that may provide enhanced levels of selectivity has also been pursued. In the ideal case, these alternative cyclizations would provide a means of controlling both the rate of diradical production and the reactivity of the diradical species in a tumor-cell-selective manner. In the following section, the alternative diradical-generating cyclizations that have been discovered and harnessed for DNA cleavage chemistry will be described. Specific examples of DNA cleavage agents that employ these alternative cyclizations will also be discussed. Although not nearly as well studied as the naturally occurring enediynes, some of these alternative diradical-generating cleavage agents have been shown to reproduce, to some extent, the cleavage chemistry of the natural products. In addition, these alternative agents also participate in DNA chemistry that is quite distinct from the enediynes.

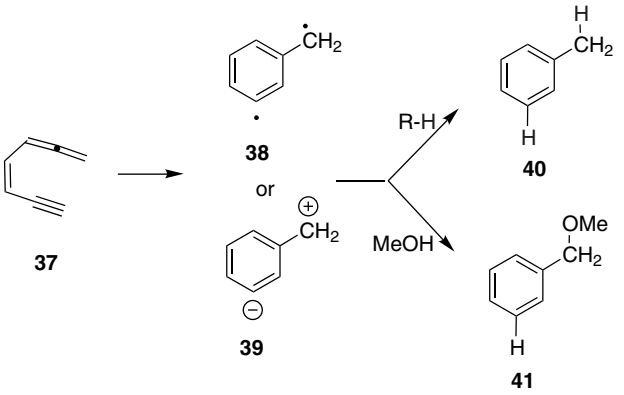

FIGURE 13.7. Myers–Saito cyclization of enyne allenes.

13.5.1. Myers–Saito Cyclization-Based Agents

Inspired by the diradical-generating cyclization of the 9-membered enediyne NCS chromophore, Myers[88] and Saito[89] independently proposed an analogous cyclization of enyne allenes (e.g., **37**) to α,3-didehydrotoluene diradicals **38** (Figure 13.7). Two features distinguish this cyclization from the Bergman enediyne cyclization. First, the intrinsic barrier for the Myers–Saito cyclization is lower than the Bergman cyclization, so much so that simple enyne allenes such as **37** cyclize spontaneously under physiological conditions.[90] Second, the diradical **38** arising from the Myers–Saito cyclization is not a σ,σ-diradical as in the case of Bergman-cyclization-derived *p*-benzyne, but rather a σ,π-diradical in which one of the radical centers is delocalized on to the newly formed aromatic ring. This leads to the prediction that hydrogen atom abstraction by the σ-radical center from deoxyribose is favorable, whereas abstraction by the π-radical is thermodynamically disfavored. As a result, double-stranded DNA cleavage analogous to that observed for enediynes would not be expected from enyne allenes.

In the initial reports of the thermal cyclization of enyne allenes, evidence was obtained for both diradical and polar reaction pathways. Trapping studies in cyclohexadiene afforded the expected toluene product (**40**) of hydrogen atom abstraction, but in methanol, a mixture of hydrogen atom abstraction and polar addition product **41** were obtained (Figure 13.7).[88] Based on computational studies supported by experimental product distribution studies, it has been proposed that both the diradical **38** and zwitterionic **39** forms of the didehydrotoluene intermediate are produced from the common cyclization transition state by a process of post-transition state nonadiabatic transition to the zwitterion, which is the excited state of the diradical.[91,92] In this sense, the enyne allene system is not different from that of the enediynes, which have also been shown to give polar trapping products (see above), but in the latter case, these polar trapping products are proposed to arise from direct nucleophilic attack on the *p*-benzene diradical.

A number of DNA cleavage agents have been designed to exploit the Myers–Saito cyclization. In most cases, the only DNA cleavage activity reported is from supercoiled plasmid cleavage studies, which, although quite sensitive, do not provide much insight into the mechanism of DNA cleavage. In only a few cases have the DNA products of cleavage been resolved by PAGE, and these studies provide evidence for both enediyne-like and unique DNA cleavage chemistry.

The 10-membered cyclic enediyne sulfones **42**, **43**, and **44** were designed to undergo isomerization to the corresponding allenes (e.g., **45**) and subsequent Myers–Saito cyclization.[93] These sulfones were shown to cleave DNA using a plasmid nicking assay, which demonstrated single-strand cleavage with EC_{50}'s (concentration required to cleave 50% of the supercoiled plasmid) in the 100 μM range (Figure 13.8). However, detailed mechanistic studies of the DNA cleavage chemistry for most of these enyne allenes is lacking, and the role of the Myers–Saito-cyclization-derived diradicals is in doubt, given the potential of the allenic sulfones to alkylate DNA.[94]

A series of 10-membered cyclic enediyne thioethers of general structure **46** have been reported to cleave DNA. Treatment of **46** with strong base in organic solvent affords trapping products that are presumably formed through initial isomerization to the enyne allenes **47** followed by Myers–Saito cyclization.[95,96] In supercoiled nicking assays, the DNA cleavage activity of these compounds is pH-dependent, requiring pH > 7.5, which has been attributed to the requirement for base-promoted isomerization to trigger diradical generation. The most active DNA cleavage compounds in this series, the naphthoate **48** and the β-carboline ester **49**, display EC_{50} values of <100 μM at pH 8.5. The products of cleavage of radiolabeled duplex restriction fragments were analyzed by PAGE, and both **48** and **49** showed DNA base-selective cleavage at purines, especially G's.[97] Similarly, the 10-membered enediyne **50** also demonstrated G-selective DNA cleavage after piperidine-heat treatment of the DNA.[98] In both cases, the DNA cleavage was attributed to DNA alkylation.

Due to the lower activation energy for Myers–Saito cyclization versus the Bergman cyclization, even simple, acyclic enyne allenes can generate diradical intermediates under physiological conditions. Thus, the simple enyne allenes **51** and **52** (Figure 13.9) cleave supercoiled plasmid DNA at 37°C, pH 8. Interestingly, both linear and nicked, relaxed products of DNA cleavage were observed, indicative of both double-strand and single-strand DNA cleavage.[99] At lower pH, only products of single-strand cleavage were observed.

The simple, acyclic enyne allene **53** and **54**, its conjugate with the DNA minor groove binding element derived from distamycin A (Figure 13.9) also display DNA cleavage activity. Analysis of the DNA cleavage of a 5′-radiolabeled duplex deoxyribonucleotide by the simple acyclic enyne allene **53** revealed very weak, non-base-selective cleavage indicative of deoxyribose hydrogen abstraction chemistry and a stronger, G-selective cleavage suggesting alkylative depurination.[100] The corresponding distamycin conjugate **54** shows much more potent DNA cleavage activity localized to the 3′-ends of sites that are protected from MPE-Fe(II)-mediated cleavage in the presence of **54**.[100] The cleavage pattern and kinetics supported a mechanism involving hydrogen atom abstraction by the Myers–Saito cyclization-derived diradical, although no details of the DNA cleavage products that would indicate the site of

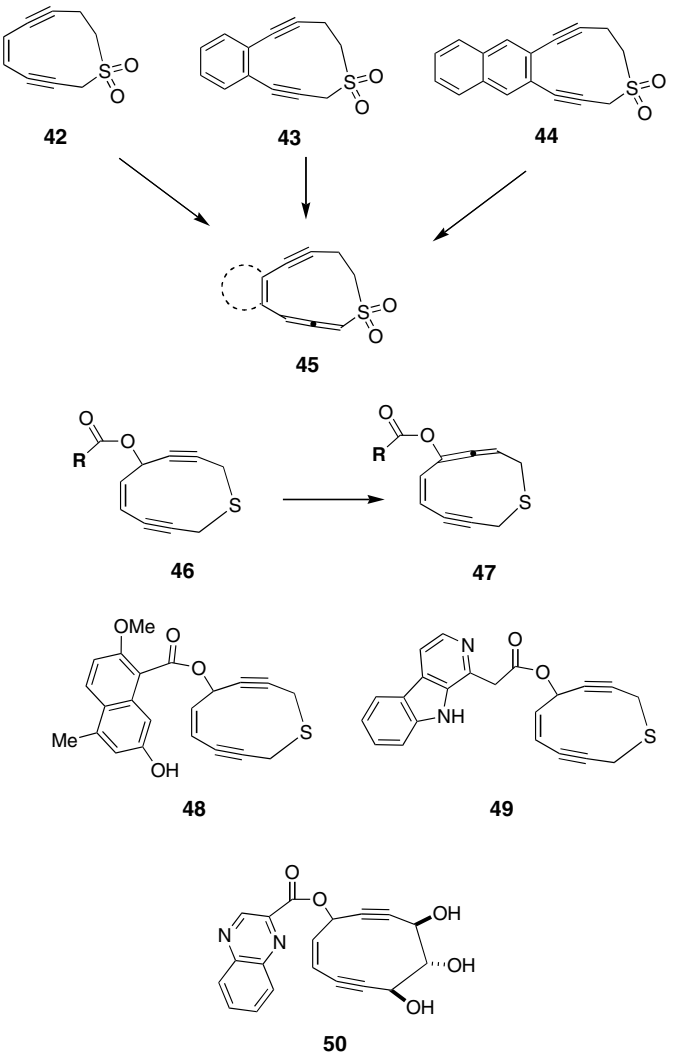

FIGURE 13.8. DNA cleaving agents based on the Myers–Saito cyclizationi of 10-membered cyclic enyne allenes.

hydrogen atom abstraction were reported. No double-strand DNA cleavage was observed for **54**.

13.5.2. C2–C6 Cyclization of Enyne Allenes

In 1995, Schmittel and co-workers described a new thermal cyclization mode of enyne allenes to fulvalene diradicals.[101, 102] The benzannulated enyne allene **55** undergoes the expected Myers–Saito cyclization in the presence of 1,4-cyclohexadiene to afford

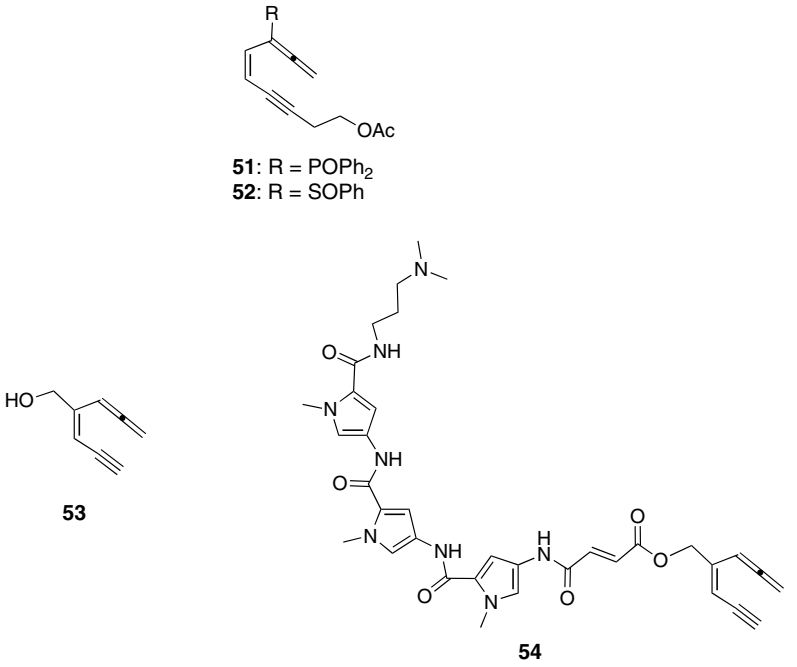

FIGURE 13.9. DNA cleavage agents based on acyclic enyne allenes.

the naphthalene product **57** (Figure 13.10). However, the analogue **56** bearing a toluyl substituent on the alkyne undergoes cyclization to afford the trapped product **58**. Although formally a product of an ene-cyclization of **56**, extensive mechanistic and theoretical studies support the intermediacy of the diradical **59**, which undergoes intramolecular hydrogen atom transfer to afford **58**.[103] The switch between Myers–Saito and this C2–C6 cyclization mode can be controlled by the nature of the alkyne substituent; bulky substituents or those capable of stabilizing the adjacent radical center favor the C2–C6 cyclization.

Both the benzannulated enyne allene **60**[104] and the corresponding phosphonate **61**[105] have been shown to cleave DNA in supercoiled nicking assays. However, while the "ene"-type product of the C2–C6 cyclization-derived diradical (similar to **58**) could be identified in thermolysis studies of **60**, no product of intermolecular trapping from either **60** or **61** was isolated, although mass spectrometric analysis of thermolysis products did show ions corresponding to the addition of two hydrogen atoms. Thus, it is not entirely clear what type of DNA cleavage is occurring with these compounds.

13.5.3. Moore–Cyclization-Based Agents

In 1985, Moore and co-workers described a new synthesis of benzoquinones from alkynylcyclobutenones.[106] Mild thermolysis of cyclobutenones **62** led to the enyne ketenes **63** (Figure 13.11). Depending upon the nature of the alkyne substituent R, the

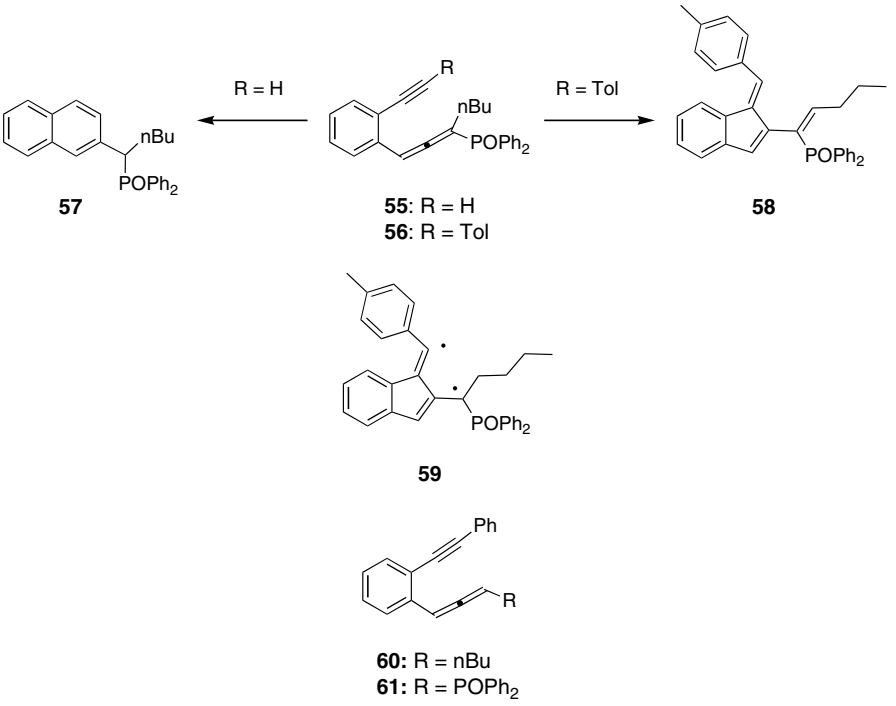

FIGURE 13.10. Myers–Saito and C2–C6 cyclizations of enyne allenes.

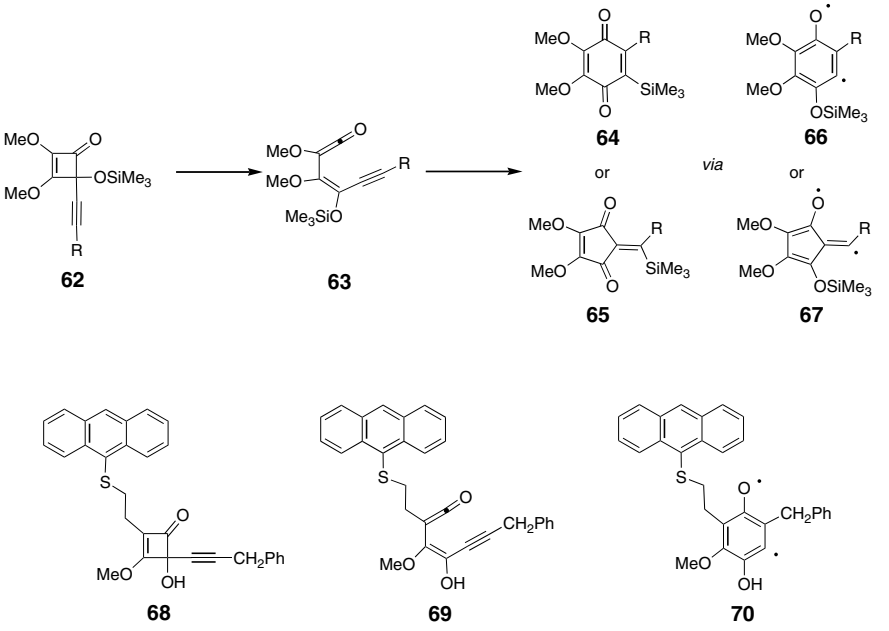

FIGURE 13.11. Moore cyclization of enyne ketenes derived from cyclobutenones.

isolated products were the benzoquinones **64** or the cyclopentenediones **65**. Subsequent experimental studies led to the mechanistic proposal that in both cases, the diradicals **66** or **67** were intermediates,[107] a conclusion that has found support in theoretical studies.[108] Thus, the Moore cyclization of enyne ketenes is an oxa analogue of the Myers–Saito and C2–C6 cyclizations of enyne allenes.

A series of cyclobutenones, including the anthracene derivative **68** (Figure 13.11) were assayed for DNA cleavage activity in a plasmid nicking assay.[109] Compound **68** demonstrated the highest level of activity, affording complete conversion of supercoiled plasmid to the circular, relaxed form at 2.3 mM concentration after 19.5 h at 45°C. The observation that the DNA cleavage was inhibited in the presence of BHT and the isolation of a trace of the benzoquinone trapping product of the diradical **70** under the DNA cleavage reaction conditions lend support for a role of this diradical in the observed cleavage; however, the majority of the isolated trapping products were derived from hydrolysis of the ketene intermediate **69**.

An alternative entry to the enyne ketene system pioneered by Saito involves the photolysis of the diazoketone **71** (Figure 13.12).[110] The resulting carbene **72** can undergo Wolff rearrangement to the ketene **73**, followed by Moore-type cyclization to the diradical **74** (Figure 13.12). In photolyses carried out in organic solvents, this pathway leads to the isolation of the benzoquinone derived by trapping of **74**. In DNA cleavage studies, irradiation of solutions of supercoiled plasmid DNA in the presence of **71** affords nicked, relaxed DNA products. However, subsequent studies revealed that the cleavage is due to the carbene **72** rather than the diradical **74**. Under the conditions of the DNA cleavage reactions, only products derived from trapping the carbene **72** were observed.[111]

13.5.4. Aza-enyne Allene Cyclization-Based Agents

A diradical-generating cyclization analogous to the Myers–Saito cyclization has been observed for *N*-allenyl-*C*-alkynylimines (aza-enyne allenes) **76** (Figure 13.13).[27] Readily available *N*-propargylimine **75** undergoes simultaneous fluoride-mediated desilylation and rearrangement to the allenylimine **76**, which can be observed by NMR. At ambient temperature the imine **76** undergoes aza-Myers–Saito cyclization over the course of minutes to the didehydro-3-picoline **77••**, which in the presence of 1,4-cyclohexadiene is trapped to afford the 3-picoline **78**. In analogy to the enyne allene Myers–Saito cyclization, the polar trapping product **79**, formally derived from

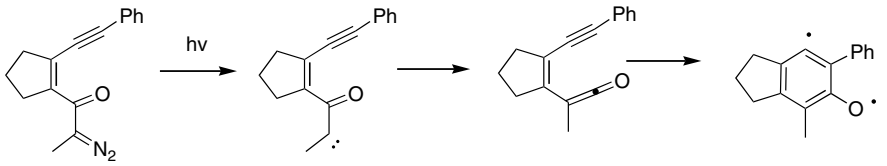

FIGURE 13.12. Moore cyclization of enyne ketene from Wolff rearrangement of an α-ketocarbene.

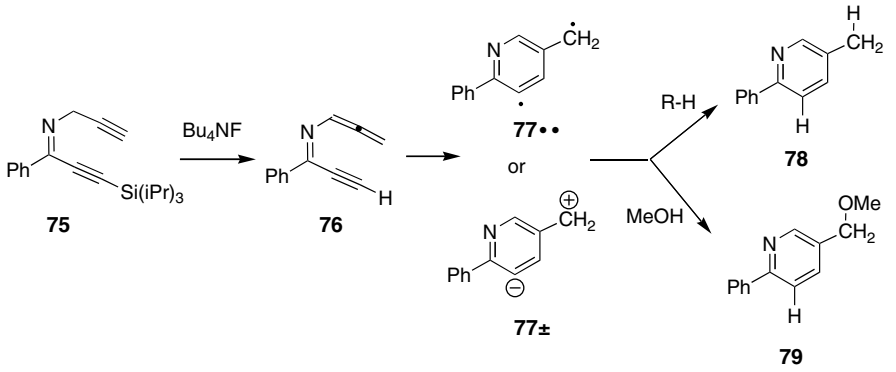

FIGURE 13.13. Aza-Myers–Saito cyclization of an aza-enyne allene derived from an *N*-propargyl-*C*-alkynylimine.

the zwitterionic form of the intermediate **77**±, is formed in the presence of methanol.[27] The facility of the cyclization of **76** is notable; while the enyne allene **37** (Figure 13.7) has a half-life of 20.5 h at 39°C,[90] aza-enyne allene **76** cyclizes completely after just 8 h at 4°C.[27] DFT calculations confirm the relative facility of the aza-Myers–Saito cyclization relative to the parent Myers–Saito cyclization; and they also predict that the corresponding aza-C2–C6 cyclization, although disfavored in the case of **76**, is more competitive with the aza-Myers–Saito cyclization than in the enyne allene case.[27]

A series of *N*-propargyl-2-alkynyl heterocycles have been prepared and evaluated for their ability to cleave DNA through an aza-Myers–Saito or aza-C2–C6 cyclization pathway.[112, 113] The benzimidazole **80** (Figure 13.14) exemplifies this series, in which a propargyl to allene isomerization such as observed for **75** → **76** (Figure 13.13) is facilitated by the presence of an adjacent positively charged nitrogen. Indeed, **80** was found to cleave DNA in a pH-dependent manner; its approximate EC_{50} in a supercoiled plasmid nicking assay is 10 μM at pH 9, but >100 μM at pH 7.[112] In contrast, the benzimidazole **81** (Figure 13.14), which lacks the ability to form an aza-enyne allene, does not cleave DNA at either pH.[112] PAGE analysis of the DNA cleavage by **80** demonstrated a unique cytosine-selective DNA cleavage pattern after piperidine-heat treatment of the DNA.[114] In the absence of piperidine-heat treatment, evidence for covalent adducts formed between the DNA and **80** was observed as low-mobility bands on the PAGE gel.[114] No adduct or DNA cleavage products were observed with **81**.[114] ESI-MS analysis of the covalent adducts formed between short deoxyoligoribonucleotides and **80** provided evidence for bonding between the 2-substituent of **80** and the cytosine exocyclic amino group, as in **87** (Figure 13.14).[115] A mechanistic proposal that invokes direct addition of cytosine to **80** fails to account for the lack of interaction with **81**, the pH dependence of the adduct formation, or the selectivity for cytosine, which is not observed with other, structurally related electrophilic alkynes, which alkylate at G residues.[113] An alternative proposal shown in Figure 13.14 involves initial base-promoted isomerization of **80** to the allene **82** followed by an aza-C2–C6 cyclization. The resulting intermediate can be formulated as either the

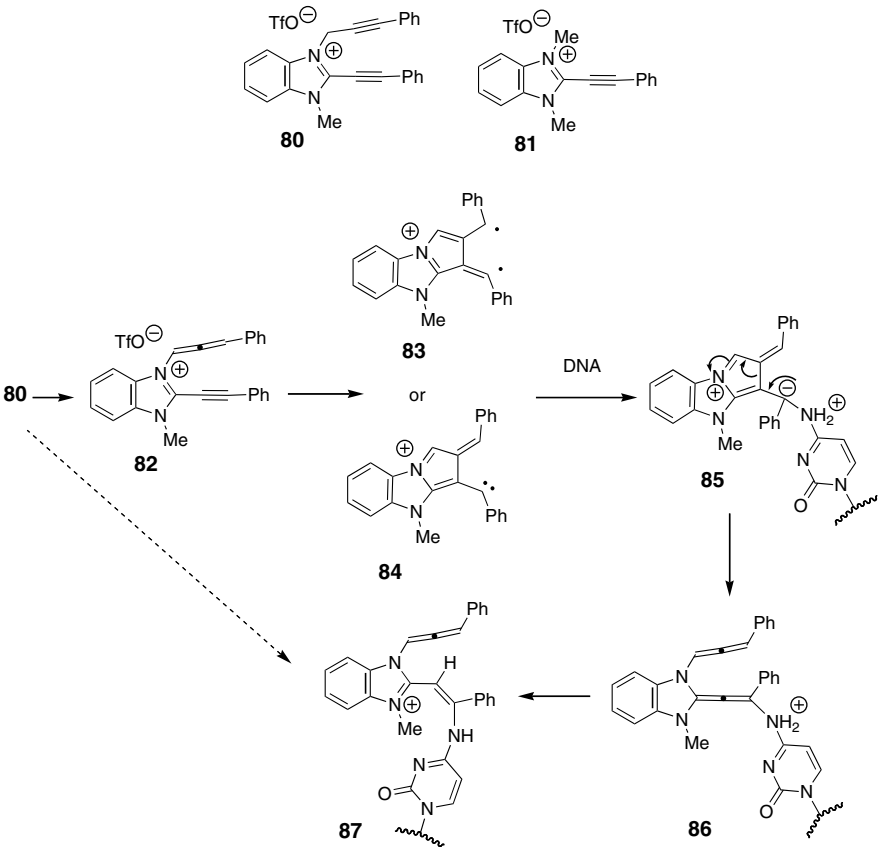

FIGURE 13.14. Imidazole-based DNA cleavage agent based on the aza-C2–C6 cyclization.

diradical **83** or the carbene **84**. Recent computational[116] and experimental evidence[117] support the role for carbene intermediates such as **84** in C2–C6 cyclizations, particularly those involving aza-substituted enyne allenes. Trapping of the carbene **84** as the ylide **85** by nucleophilic addition may be followed by a Grob-like fragmentation to **86**. Prototropic rearrangement then produces the adduct **87**.

The compound **88** (Figure 13.15) is an example of a series of pyridine-based aza-enyne allene precursors that have been examined for DNA cleavage activity.[118] As in the case of the benzimidazole **80**, in supercoiled DNA nicking assays pyridine **88** is more active at pH 8 than at pH 7. The DNA cleavage activity of **88**, with an EC_{50} value at pH 8 of $<10\,\mu M$, is higher that that of the benzimidazole analogue.[118] PAGE analysis of the DNA cleavage products of **88** demonstrate a base- and sequence-neutral cleavage pattern similar to that observed for hydroxyl radical.[118] However, unlike hydroxyl radical, the cleavage due to **88** is not inhibited by DMSO or other hydroxyl radical scavengers.[118] Distamycin A protects against DNA cleavage due to **88**, indicating that cleavage by this compound requires access to the DNA minor groove.[118] Based on PAGE mobility, the groups at the 3′-termini of the DNA cleavage

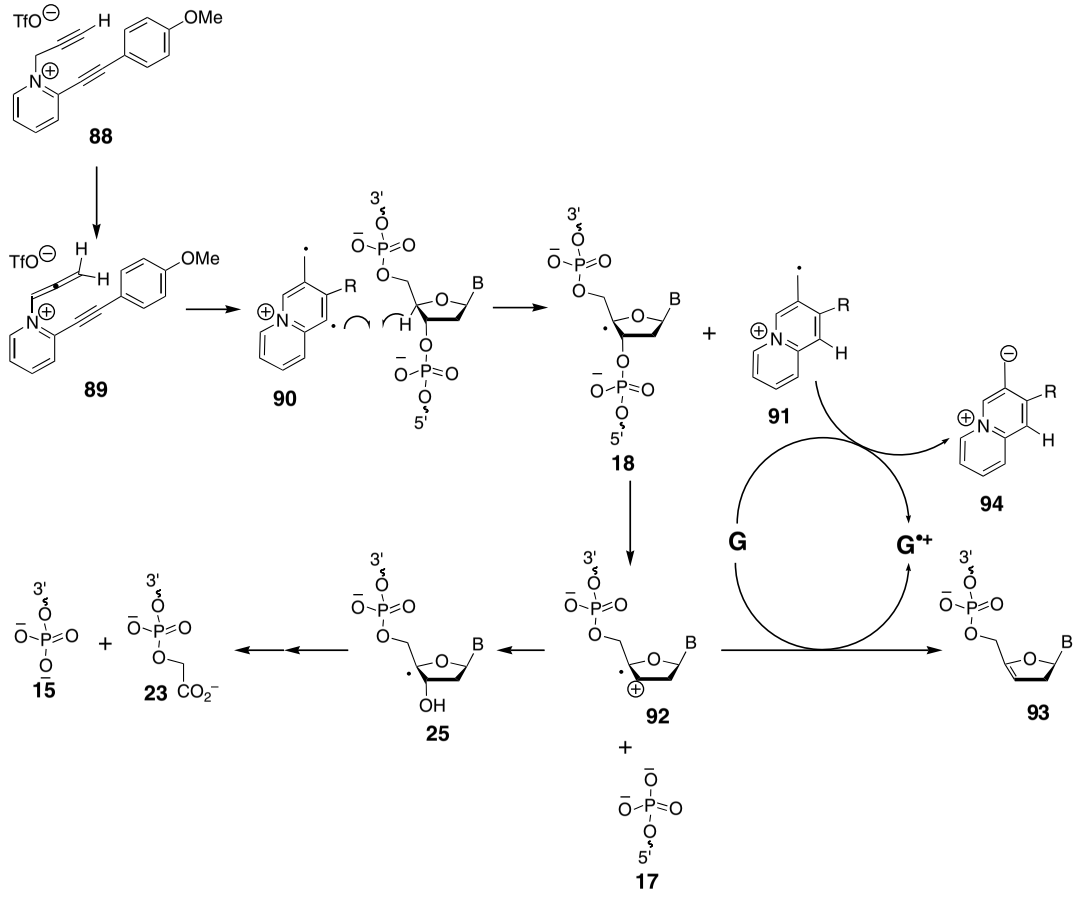

FIGURE 13.15. Pyridine-based DNA cleavage agent based on the aza-Myers–Saito cyclization.

products were identified as 3′-phosphate- (major) and 3′-phosphoglycolate- (minor), with phosphate groups at the 5′-termini.[118] In addition, DNA treated with **88** undergoes a base-promoted, G-specific cleavage that is associated with the formation of 8-oxo-G, with no evidence for DNA-adduct formation.[118]

A mechanistic proposal commensurate with these observations involves isomerization of **88** under basic conditions to the allene **89** followed by an aza-Myers–Saito cyclization to the diradical **90** (Figure 13.15).[118] Abstraction of the C4′ hydrogen atom from DNA by **90** leads to the deoxyribose-centered radical **18** and the drug-derived radical cation **91**. As discussed previously regarding the 4′-chemistry for the naturally occurring enediynes (Figure 13.5), the radical **18** can undergo heterolysis by loss of the 5′-phosphate **17** and formation of a deoxyribose radical cation **92**, which can be trapped by the addition of water to give **25** (Figure 13.15). In turn, radical **25** can give rise to either the 3′-phosphate **15** or 3′-phosphoglycolate **23** (Figure 13.15) products following the same pathway as proposed in Figure 13.5. Here it should be noted that the DNA cleavage due to **88** is nearly exclusively single-stranded scission, and unlike the natural enediynes, the formation of 3′-phosphoglycolate product **23** does not involve double-strand DNA cleavage. However, studies of C4′ deoxyribose radicals **18** generated by photolysis of 4′-acylated nucleotide-containing duplex DNA demonstrate that an alternative pathway exists in which radical cation **92** initiates electron transfer from the DNA bases, resulting in the formation of the enol ether **93** and a guanine radical cation.[119] In the case of the radical cation **92** generated upon DNA cleavage by **88**, this electron transfer may be the source of the observed 8-oxo-G products (Figure 13.15). Alternatively, the radical cation **91** derived from **88** may serve as the oxidant, leading to the zwitterion **94** (Figure 13.15). It is possible that the G-selective cleavage observed from the enyne allenes **48–50** (Figure 13.8) might also be due to a similar electron transfer process.

13.6. CONCLUSIONS

Studies of the DNA cleavage chemistry of the naturally occurring enediynes have provided insights into the chemistry derived from hydrogen atom abstraction from DNA by diradicals. Although much has been learned in the process, there are still some specific aspects of the DNA cleavage chemistry that are unclear. These studies have led to an appreciation of the diverse chemistry of the deoxyribose-centered radicals that are produced by hydrogen atom abstraction by these natural products. The interaction between the DNA and the reduced drug modulates the observed cleavage chemistry and can even lead to relatively efficient DNA adduction and cross-linking, either directly or via the deoxyribose-derived products of DNA cleavage.

Alternative diradical-generating cyclizations have been discovered and applied toward the design of DNA cleavage agents. Although there are only a few examples in which the products of DNA cleavage by these diradicals have been determined, it appears that the interaction of these alternative diradicals with DNA resembles some of the chemistry observed with the natural enediynes and also provides evidence for additional pathways. In addition to potentially leading to more selective

diradical-based DNA cleavage agents for therapy, the study of these alternative diradical-generating systems also provides further insight into factors that contribute to the diverse deoxyribose-radical chemistry of the natural enediynes.

ACKNOWLEDGMENTS

The Robert Welch Foundation, the Foundation for Research, and the National Institutes of Health are gratefully acknowledged for their support. Additional support and resources from the Center for Molecular and Cellular Toxicology (University of Texas at Austin), the Institute of Cellular and Molecular Biology (University of Texas at Austin), and the Center for Research on Environmental Diseases (M. D. Anderson Cancer Center and University of Texas at Austin) are also acknowledged.

REFERENCES

1. Lee, M. D.; Manning, J. K.; Williams, D. R.; Kuck, N. A.; Testa, R. T.; Borders, D. B. Calicheamicins, a novel family of antitumor antibiotics. 3. Isolation, purification and characterization of calicheamicin-β_1^{Br}, calicheamicin-γ_1^{Br}, calicheamicin-α_2^I, calicheamicin-α_3^I, calicheamicin-β_1^I, calicheamicin-γ_1^I and calicheamicin-δ_1^I. *J. Antibiotics* **1989**, *42*, 1070–1087.
2. Golik, J.; Dubay, G.; Groenewold, G.; Kawaguchi, H.; Konishi, M.; Krishnan, B.; Ohkuma, H.; Saitoh, K.; Doyle, T. W. Esperamicins, a novel class of potent antitumor antibiotics. 3. Structures of esperamicins-A1, esperamicin-A^2, and esperamicin- A_1^b. *J. Am. Chem. Soc.* **1987**, *109*, 3462–3464.
3. Konishi, M.; Ohkuma, H.; Matsumoto, K.; Tsuno, T.; Kamei, H.; Miyaki, T.; Oki, T.; Kawaguchi, H.; Vanduyne, G. D.; Clardy, J. Dynemicin A, A novel antibiotic with the anthraquinone and 1,5- diyn-3-ene subunit. *J. Antibiotics* **1989**, *42*, 1449–1452.
4. Davies, J.; Wang, H.; Taylor, T.; Warabi, K.; Huang, X.-H.; Andersen, R. J. Uncialamycin, A New Enediyne Antibiotic. *Org. Lett.* **2005**, *7*, 5233–5236.
5. McDonald, L. A.; Capson, T. L.; Krishnamurthy, G.; Ding, W. D.; Ellestad, G. A.; Bernan, V. S.; Maiese, W. M.; Lassota, P.; Discafani, C.; Kramer, R. A.; Ireland, C. M. Namenamicin, a new enediyne antitumor antibiotic from the marine ascidian polysyncraton lithostrotum. *J. Am. Chem. Soc.* **1996**, *118*, 10898–10899.
6. Oku, N.; Matsunaga, S.; Fusetani, N. Shishijimicins A-C, novel enediyne antitumor antibiotics from the ascidian didemnum proliferum. *J. Am. Chem. Soc.* **2003**, *125*, 2044–2045.
7. Koide, Y.; Ishii, F.; Hasuda, K.; Koyama, Y.; Edo, K.; Katamine, S.; Kitame, F.; Ishida, N. Isolation of a non-protein component and a protein-component from neocarzinostatin (NCS) and their biological-activities. *J. Antibiotics* **1980**, *33*, 342–346.
8. Myers, A. G. Proposed structure of the neocarzinostatin chromophore-methyl thioglycolate adduct: A mechanism for the nucleophilic activation of neocarzinostatin. *Tetrahedron Lett*. **1987**, *28*, 4493–4496.
9. Yoshida, K.; Minami, Y.; Azuma, R.; Saeki, M.; Otani, T. Structure and cycloaromatization of a novel enediyne, C-1027 chromophore. *Tetrahedron Lett*. **1993**, *34*, 2637–2640.

10. Shao, R. G.; Zhen, Y. S. Enediyne anticancer antibiotic lidamycin: Chemistry, biology and pharmacology. *Anti-Cancer Agents Med. Chem.* **2008**, *8*, 123–131.
11. Ando, T.; Ishii, M.; Kajiura, T.; Kameyama, T.; Miwa, K.; Sugiura, Y. A new non-protein enediyne antibiotic N1999A2: Unique enediyne chromophore similar to neocarzinostatin and DNA cleavage feature. *Tetrahedron Lett*. **1998**, *39*, 6495–6498.
12. Leet, J. E.; Schroeder, D. R.; Hofstead, S. J.; Golik, J.; Colson, K. L.; Huang, S.; Klohr, S. E.; Doyle, T. W.; Matson, J. A. Kedarcidin, a new chromoprotein antitumor antibiotic—structure elucidation of kedarcidin chromophore. *J. Am. Chem. Soc.* **1992**, *114*, 7946–7948.
13. Zein, N.; Solomon, W.; Colson, K. L.; Schroeder, D. R. Maduropeptin—An antitumor chromoprotein with selective protease activity and DNA-cleaving properties. *Biochemistry* **1995**, *34*, 11591–11597.
14. Nicolaou, K. C.; Dai, W. M.; Tsay, S. C.; Estevez, V. A.; Wrasidlo, W. Designed enediynes—A new class of DNA-cleaving molecules with potent and selective anticancer activity. *Science* **1992**, *256*, 1172–1178.
15. Jones, R. R.; Bergman, R. G. *p*-Benzyne. Generation as an intermediate in a thermal isomerization reaction and trapping evidence for the 1,4-benzenediyl structure. *J. Am. Chem. Soc.* **1972**, *94*, 660–661.
16. Abe, S.; Otsuki, M. Styrene maleic acid neocarzinostatin treatment for hepatocellular carcinoma. *Curr. Med. Chem. Anticancer Agents* **2002**, *2*, 715–726.
17. Sievers, E. L.; Larson, R. A.; Stadtmauer, E. A.; Filipovich, A.; Locatelli, F.; Peters, C.; Remberger, M.; Michel, G.; Arcese, W.; Dallorso, S.; Tiedemann, K.; Busca, A.; Chan, K. W.; Kato, S.; Ortega, J.; Vowels, M.; Zander, A.; Souillet, G.; Oakill, A.; Woolfrey, A.; Pay, A. L.; Green, A.; Garnier, F.; Ionescu, I.; Wernet, P.; Sirchia, G.; Rubinstein, P.; Chevret, S.; Gluckman, E. Efficacy and safety of gemtuzumab ozogamicin in patients with CD33-positive acute myeloid leukemia in first relapse. *J. Clin. Oncol.* **2001**, *19*, 3244–3254.
18. Bross, P. F.; Beitz, J.; Chen, G.; Chen, X. H.; Duffy, E.; Kieffer, L.; Roy, S.; Sridhara, R.; Rahman, A.; Williams, G.; Pazdur, R. Approval summary: Gemtuzumab ozogamicin in relapsed acute myeloid leukemia. *Clin. Cancer Res.* **2001**, *7*, 1490–1496.
19. Van Lanen, S. G.; Shen, B. Biosynthesis of enediyne antitumor antibiotics. *Curr. Top. Med. Chem.* **2008**, *8*, 448–459.
20. Van Lanen, S. G.; Shen, B. Advances in polyketide synthase structure and function. *Curr. Opin. Drug Discov. Dev.* **2008**, *11*, 186–195.
21. Thorson, J. S.; Sievers, E. L.; Ahlert, J.; Shepard, E.; Whitwam, R. E.; Onwueme, K. C.; Ruppen, M. Understanding and exploiting nature's chemical arsenal: The past, present and future of calicheamicin research. *Curr. Pharm. Design* **2000**, *6*, 1841–1879.
22. Rawat, D. S. Target directed enediynes: Chemical and biological significance. *J. Ind. Chem. Soc.* **2008**, *85*, 130–141.
23. Jones, G. B.; Fouad, F. S. Designed enediyne antitumor agents. *Curr. Pharm. Des.* **2002**, *8*, 2415–2440.
24. Capitani, J. F.; Gaffney, S. M.; Castaldo, L.; Mitra, A. The critical distance for the cycloaromatization reactions of enediynes. *Curr. Top. Med. Chem.* **2008**, *8*, 470–486.
25. Alabugin, I.; Breiner, B.; Manoharan, M. Cycloaromatization reactions: The testing ground for theory and experiment. *Adv. Phys. Org. Chem.* **2008**, *42*, 1–33.

26. Feng, L. P.; Zhang, A. B.; Kerwin, S. M. Enediynes from aza-enediynes: C,N-dialkynyl imines undergo both aza-Bergman rearrangement and conversion to enediynes and fumaronitriles. *Org. Lett.* **2006**, *8*, 1983–1986.
27. Feng, L.; Kumar, D.; Birney, D.; Kerwin, S. M. α,5-didehydro-3-picoline diradicals from skipped aza-enediynes: Computational and trapping studies of an aza-Myers–Saito cyclization. *Org. Lett.* **2004**, *6*, 2059–2062.
28. Magnus, P.; Fortt, S.; Pitterna, T.; Snyder, J. P. Synthetic and mechanistic studies on esperamicin-A1 and calicheamicin-gamma-1 - molecular strain rather than pi-bond proximity determines the cycloaromatization tates of bicyclo[7.3.1] enediynes. *J. Am. Chem. Soc.* **1990**, *112*, 4986–4987.
29. Elmroth, K.; Nygren, J.; Martensson, S.; Ismail, I. H.; Hammarsten, O. Cleavage of cellular DNA by calicheamicin γ_1. *DNA Repair* **2003** *2*, 363–374.
30. Kraka, E. Tuttle, T.; Cremer, D. The reactivity of calicheamicin γ_1^I in the minor groove of DNA: The decisive role of the environment. *Chem. Eur. J.* **2007**, *13*, 9256–9269.
31. Roth, W. R.; Hopf, H.; Horn, C. The energy well of diradicals. 5. 1,3,5-Cyclohexatriene-1,4-diyl and 2,4-cyclohexadiene-1,4-diyl. *Chem. Ber.* **1994**, *127*, 1765–1779.
32. Chatterjee, M.; Smith, P. J.; Townsend, C. A. The role of the aminosugar and helix binding in the thiol-induced activation of calicheamicin for DNA cleavage. *J. Am. Chem. Soc.* **1996**, *118*, 1938–1948.
33. Logan, C. F.; Chen, P. *Ab initio* calculation of hydrogen abstraction reactions of phenyl radical and *p*-benzyne. *J. Am. Chem. Soc.* **1996**, *118*, 2113–2114.
34. Perrin, C. L.; Rodgers, B. L.; O'Connor, J. M. Nucleophilic addition to a *p*-benzyne derived from an enediyne: A new mechanism for halide incorporation into biomolecules. *J. Am. Chem. Soc.* **2007**, *129*, 4795–4799.
35. Buchanan, G. O.; Williams, P. G.; Feling, R. H.; Kauffman, C. A.; Jensen, P. E.; Fenical, W. Sporolides A and B: Structurally unprecedented halogenated macrolides from the marine actinomycete *Salinispora tropica*. *Org. Lett.* **2005**, *7*, 2731–2734.
36. Oh, D. C.; Williams, P. G.; Jensen, P. R.; Fenical, W. Cyanosporasides A and B, chloro- and cyano-cyclopenta[*a*]indene glycosides from the marine *Actinomycete* "*Salinispora pacifica*". *Org. Lett.* **2006**, *8*, 1021–1024.
37. Dedon, P.C.; Goldberg, I. H. Free-radical mechanisms involved in the formation of sequence-dependent bistranded DNA lesions by the antitumor antibiotics bleomycin, neocarzinostatin, and calicheamicin. *Chem. Res. Toxicol.* **1992**, *5*, 317–332.
38. Chin, D. H.; Goldberg, I. H. Generation of superoxide free-radical by neocarzinostatin and its possible role in DNA damage. *Biochemistry* **1986**, *25*, 1009–1015.
39. Kappen, L. S.; Goldberg, I. H. Site-specific cleavage at a DNA bulge by neocarzinostatin chromophore via a novel mechanism. *Biochemistry* **1993**, *32*, 13138–13145.
40. Miyagawa, N.; Sasaki, D.; Matsuoka, M.; Imanishi, M.; Ando, T.; Sugiura, Y. DNA cleavage characteristics of non-protein enediyne antibiotic N1999A2. *Biochem. Biophys. Res. Commun.* **2003**, *306*, 87–92.
41. Yoshida, K.; Minami, Y.; Azuma, R.; Saeki, M.; Otani, T. Structure and cycloaromatization of a novel enediyne, C-1027 chromophore. *Tetrahedron Lett*. **1993**, *34*, 2637–2640.
42. Myers, A. G.; Hurd, A. R.; Hogan, P. C. Evidence for facile atropisomerism and simple (non-nucleophilic) biradical-forming cycloaromatization within kedarcidin chromophore aglycon. *J. Am. Chem. Soc.* **2002**, *124*, 4583–4585.

43. Lee, M. D.; Ellestad, G. A.; Borders, D. B. Calicheamicins—Discovery, structure, chemistry, and interaction with DNA. *Acc. Chem. Res* **1991**, *24*, 235–243.
44. Goldberg, I. H. Mechanism of neocarzinostatin action: Role of DNA microstructure in determination of chemistry of bistranded oxidative damage. *Acc. Chem. Res.* **1991**, *24*, 191–202.
45. Dedon, P. C.; Goldberg, I. H. Free-radical mechanisms involved in the formation of sequence-dependent bistranded DNA lesions by the antitumor antibiotics bleomycin, neocarzinostatin, and calicheamicin. *Chem. Res. Toxicol.* **1992**, *5*, 311–332.
46. Murphy, J. A.; Griffiths, J. A survey of natural-products which abstract hydrogen-atoms from nucleic-acids. *Nat. Prod. Rep.* **1993**, *10*, 551–564.
47. Pratviel, G.; Bernadou, J.; Meunier, B. Carbon–hydrogen bonds of DNA sugar units as targets for chemical nucleases and drugs. *Angew Chem. Int. Ed.* **1995**, *34*, 746–769.
48. Pogozelski, W. K.; Tullius, T. D. Oxidative strand scission of nucleic acids: Routes initiated by hydrogen abstraction from the sugar moiety. *Chem. Rev.* **1998**, *98*, 1089–1107.
49. Povirk, L. F. DNA damage and mutagenesis by radiomimetic DNA-cleaving agents: Bleomycin, neocarzinostatin and other enediynes. *Mutat. Res.* **1996**, *355*, 71–89.
50. Dedon, P. The chemical toxicology of 2-deoxyribose oxidation in DNA. *Chem. Res. Toxicol.* **2008**, *21*, 206–219.
51. Yu, L.; Golik, J.; Harrison, R.; Dedon, P. The deoxyfucose-anthranilate of esperamicin A1 confers intercalative DNA binding and causes a switch in the chemistry of bistranded DNA lesions. *J. Am. Chem. Soc.* **1994**, *116*, 9733–9738.
52. Kappen, L. S.; Chen, C.-Q.; Goldberg, I. H. Atypical abasic sites generated by neocarzinostatin at sequence-specific cytidylate residues in oligodeoxynucleotides. *Biochemistry* **1988**, *27*, 4331–4340.
53. Kappen, L. S.; Goldberg, I. H.; Wu, S. H.; Stubbe, J.; Worth, L., Jr.; Kozarich, J. W. Isotope effects on the sequence-specific cleavage of dC in d(AGC) sequences by neocarzinostatin: Elucidation of chemistry of minor lesions. *J. Am. Chem. Soc.* **1990**, *112*, 2729–2728.
54. Galat, A.; Goldberg, I. H. Molecular-models of neocarzinostatin damage of DNA—Analysis of sequence dependence in 5′-GAGCG-5′CGCTC. *Nucl. Acids Res.* **1990**, *18*, 2093–2099.
55. Gao, X. L.; Stassinopoulos, A.; Rice, J. S.; Goldberg, I. H. Structural basis for the sequence-specific DNA strand cleavage by the enediyne neocarzinostatin chromophore—structure of the post-activated chromophore DNA complex. *Biochemistry* **1995**, *34*, 40–49.
56. Shiraki, T.; Uesugi, M.; Sugiura, Y. C-1′ hydrogen abstraction of deoxyribose in DNA strand scission by dynemicin-A. *Biochem. Biophys. Res. Comm.* **1992**, *188*, 584–589.
57. Kappen, L.; Goldberg, I. H. Identification of 2-deoxyribonolactone at the site of neocarzinostatin-induced cytosine release in the sequence d(AGC). *Biochemistry* **1989**, *28*, 1027–1032.
58. Zheng, Y.; Sheppard, T. L. Half-life and DNA strand scission products of 2-deoxyribonolactone oxidative DNA damage lesions. *Chem. Res. Toxicol.* **2004**, *17*, 197–207.
59. Povirk, L. F.; Goldberg, I. H. Base substitution mutations induced in the Ci gene of lambda-phage by neocarzinostatin chromophore—Correlation with depyrimidination hot-spots at the sequence AGC. *Nucl. Acids Res.* **1986**, *14*, 1417–1426.

60. Kroeger, K. M.; Jiang, Y. L.; Kow, Y. W.; Goodman, M. F.; Greenberg, M. M. Mutagenic effects of 2-deoxyribonolactone in *Escherichia coli.* An abasic lesion that disobeys the A-rule. *Biochemistry* **2004**, *43*, 6723–6733.

61. Faure, V.; Constant, J. F.; Dumy, P.; Saparbaev, M. 2′-Deoxyribonolactone lesion produces G → A transitions in *Escherichia coli*. *Nucl. Acids Res. 32*, **2004**, 2937–2946.

62. Kow, Y. W.; Bao, G.; Minesinger, B.; Jinks-Robertson, S.; Siede, W.; Jiang, Y. L.; Greenberg, M. M. Mutagenic effects of abasic and oxidized abasic lesions in *Saccharomyces cerevisiae*. *Nucl. Acids Res.* **2005**, *33*, 6196–6202.

63. Hashimoto, M.; Greenberg, M. M.; Kow, Y. W.; Hwang, J. T.; Cunningham, R. P. The 2-deoxyribonolactone lesion produced in DNA by neocarzinostatin and other damaging agents forms crosslinks with the base-excision repair enzyme endonuclease III. *J. Am. Chem. Soc.* **2001**, *123*, 3161–3162.

64. DeMott, M. S.; Beyret, E.; Wong, D.; Bales, B. C.; Hwang, J. T.; Greenberg, M. M.; Demple, B. Covalent trapping of human DNA polymerase beta by the oxidative DNA lesion 2-deoxyribonolactone. *J. Biol. Chem.* **2002**, *277*, 7637–7640.

65. Hangeland, J. J.; Devoss, J. J.; Heath, J. A.; Townsend, C. A.; Ding, W. D.; Ashcroft, J. S.; Ellestad, G. A. Specific abstraction of the 5′(*S*)-deoxyribosyl and 4′-deoxyribosyl hydrogen-atoms from DNA by calicheamicin-gamma-1(I). *J. Am. Chem. Soc.* **1992**, *114*, 9200–9202.

66. Frank, B. L.; Worth, L.; Christner, D. F.; Kozarich, J. W.; Stubbe, J.; Kappen, L. S.; Goldberg, I. H. Isotope effects on the sequence-specific cleavage of DNA by neocarzinostatin—kinetic partitioning between 4′-hydrogen and 5′-hydrogen abstraction at unique thymidine sites. *J. Am. Chem. Soc.* **1991**, *113*, 2271–2275.

67. Saito, I.; Kawabata, H.; Fujiwara, T.; Sugiyama, H.; Matsuura, T. A novel ribose C-4′ hydroxylation pathway in neocarzinostatin-mediated degradation of Oligonucleotides. *J. Am. Chem. Soc.* **1989**, *111*, 8302–8303.

68. Kappen, L. S.; Goldberg, I. H. Neocarzinostatin acts as a sensitive probe of DNA microheterogeneity—Switching of chemistry from C-1′ to C-4′ by a G•T mismatch 5′ to the site of DNA damage. *Proc. Natl. Acad. Sci.* **1992**, *89*, 6706–6710.

69. Christner, D. F.; Frank, B. L.; Kozarich, J. W.; Stubbe, J.; Golik, J.; Doyle, T. W.; Rosenberg, I. E.; Krishnan, B. Unmasking the chemistry of DNA cleavage by the esperamicins—Modulation of 4′-hydrogen abstraction and bistranded damage by the fucose anthranilate moiety. *J. Am. Chem. Soc.* **1992**, *114*, 8763–8767.

70. Xu, Y. J.; Xi, Z.; Zhen, Y. S.; Goldberg, I. H. A single binding mode of activated enediyne C1027 generates 2 Types of double-strand DNA lesions—deuterium isotope-induced shuttling between adjacent nucleotide target sites. *Biochemistry* **1995**, *34*, 12451–12460.

71. Rabow, L. E.; McGall, G. H.; Stubbe, J.; Kozarich, J. W. Identification of the source of oxygen in the alkaline-labile product accompanying cytosine release during bleomycin-mediated oxidative degradation of d(CGCGCG). *J. Am. Chem. Soc.* **1990**, *112*, 3203–3208.

72. Lopez-Larraza, D. M.; Moore, K.; Dedon, P. C. Thiols alter the partitioning of calicheamicin-induced deoxyribose 4′-oxidation reactions in the absence of DNA radical repair. *Chem. Res. Toxicol.* **2001**, *14*, 528–535.

73. Giese, B.; Beyrichgraf, X.; Erdmann, P.; Petretta, M.; Schwitter, U. The chemistry of single-stranded 4′-DNA radicals—influence of the radical precursor on anaerobic and aerobic strand cleavage. *Chem. Biol.* **1995**, *2*, 367–375.

74. Dussy, A.; Meggers, E.; Giese, B. Spontaneous cleavage of 4′-DNA radicals under aerobic conditions: Apparent discrepancy between trapping rates and cleavage products. *J. Am. Chem. Soc.* **1998**, *120*, 7399–7403.
75. Meschwitz, S. M.; Goldberg, I. H. Selective abstraction of H-2 from C-5′ of thymidylate in an oligodeoxynucleotide by the radical center at C-6 of the diradical species of neocarzinostatin—Chemical evidence for the structure of the activated drug DNA Complex. *Proc. Natl. Acad. Sci. USA* **1991**, *88*, 3047–3051.
76. Chin, D. H.; Carr, S. A.; Goldberg, I. H. Incorporation of O-18(2) into thymidine 5′-aldehyde in neocarzinostatin chromophore-damaged DNA. *J. Biol. Chem.* **1984**, *259*, 9975–9978.
77. Kawabata, H.; Takeshita, H.; Fujiwara, T.; Sugiyama, H.; Matsuura, T.; Saito, I. chemistry of neocarzinostatin-mediated degradation of d(GCATGC)—Mechanism of spontaneous thymine release. *Tetrahedron Lett*. **1989**, *30*, 4263–4266.
78. Chen, B.; Vu, C. C.; Byrnes, M. C.; Dedon, P.; Peterson, L. A. Formation of 1,4-dioxo-2-butene-derived adducts of 2′-deoxyadenosine and 2′-deoxycytidine in Oxidized DNA. *Chem. Res. Toxicol.* **2006**, *19*, 982–985.
79. Povirk, L. F.; Goldberg, I. H. Covalent adducts of DNA and the non-protein chromophore of neocarzinostatin contain a modified deoxyribose. *Proc. Natl. Acad. Sci. USA* **1982**, *79*, 369–373.
80. Xu, Y. J.; Xi, Z.; Zhen, Y. S.; Goldberg, I. H. Mechanism of formation of novel covalent drug center dot DNA interstrand cross-links and monoadducts by enediyne antitumor antibiotics. *Biochemistry* **1997**, *36*, 14975–14984.
81. Kappen, L. S.; Goldberg, I. H. DNA conformation induced activation of an enediyne for site-specific cleavage. *Science* **1993**, *261*, 1319–1321.
82. Stassinopoulos, A.; Ji, J.; Gao, X.; Goldberg, I. H. Solution structure of a two-base DNA bulge complexed with an enediyne cleaving analog. *Science* **1996**, *272*, 1943–1964.
83. Kappen, L. S.; Goldberg, I. H. Replication block by an enediyne drug–DNA deoxyribose adduct. *Biochemistry* **1999**, *38*, 235–242.
84. Xu, Y. J.; Zhen, Y. S.; Goldberg, I. H. Enediyne C1027 induces the formation of novel covalent DNA interstrand cross-links and monoadducts. *J. Am. Chem. Soc.* **1997**, *119*, 1133–1134.
85. Kennedy, D. R.; Ju, J.; Shen, B.; Beerman, T. A. Designer enediynes generate DNA breaks, interstrand cross-links, or both, with concomitant changes in the regulation of DNA damage responses. *Proc. Natl. Acad. Sci. USA* **2007**, *104*, 17632–17637.
86. Povirk, L. F. DNA damage and mutagenesis by radiomimetic DNA-cleaving agents: Bleomycin, neocarzinostatin and other enediynes. *Mutat. Res.* **1996**, *355*, 71–89.
87. Jiang, Z. H.; Hwang, G. S.; Xi, Z.; Goldberg, I. H. Formation and structure of a novel enediyne-RNA base covalent adduct. *J. Am. Chem. Soc.* **2002**, *124*, 3216–3217.
88. Myers, A. G.; Dragovich, P. S. Design and dynamics of a chemically triggered reaction cascade leading to biradical formation at subambient temperature. *J. Am. Chem. Soc.* **1989**, *111*, 9130–9132.
89. Nagata, R.; Yamanaka, H.; Okazaki, E.; Saito, I. Biradical formation from acyclic conjugated enyne-allene system related to neocarzinostatin and esperamicin-calichemicin. *Tetrahedron Lett*. **1989**, *30*, 4995–4998.
90. Myers, A. G.; Kuo, E. Y.; Finney, N. S. "Thermal generation of a,3-dehydrotoluene from (*Z*)-1,2,4-heptatrien-6-yne" *J. Am. Chem. Soc.* **1989**, *111*, 8097–8059.

91. Cremeens, M. E.; Hughes, T. S.; Carpenter, B. K. Mechanistic studies on the cyclization of (*Z*)-1,2,4-Heptatrien-6-yne in methanol: A possible nonadiabatic thermal reaction. *J. Am. Chem. Soc.* **2005**, *127*(18), 6652–6661.
92. Carpenter, B. K. Electronically nonadiabatic thermal reactions of organic molecules. *Chem. Soc. Rev.* **2006**, *35*, 736–747.
93. Suzuki, I.; Shigenaga, A.; Manabe, A.; Nemoto, H.; Shibuya, M. Synthesis, reactions and DNA damaging abilities of 10-membered enediyne-sulfone and related compounds. *Tetrahedron* **2003**, *59*, 5691–5704.
94. Sakai, Y.; Bando, Y.; Shishido, K.; Shibuya, M. Cycloaromatization of a 10-membered enediyne derivative via an allenic sulfone intermediate and its DNA cleaving activity. *Tetrahedron Lett*. **1992**, *33*, 957–960.
95. Toshima, K.; Ohta, K.; Ohashi, A.; Nakata, M.; Tatsuta, K. Design and synthesis of 1-thia-3,8-diyn-5-ene systems with DNA-cleaving properties related to the neocarzinostatin chromophore. *J. Chem. Soc. Chem. Commun.* **1992**, 1306–1308.
96. Toshima, K.; Ohishi, K.; Tomishima, M.; Matsumura, S. Novel heterocyclic enediynes. Molecular design, chemical synthesis and DNA cleavage. *Heterocycles* **1997**, *45*, 851–855.
97. Toshima, K.; Ohta, K.; Ohashi, A.; Nakamura, T.; Nakata, M.; Matsumura, S. Design, synthesis and DNA-cleaving profiles of hybrids containing the novel enediyne and naturally-occurring DNA intercalators. *J. Chem. Soc., Chem. Comm.* **1993**, 1525–1527.
98. Toshima, K.; Ohta, K.; Kano, T.; Nakamura, T.; Nakata, M.; Kinoshita, M.; Matsumura, S. Novel designed enediynes: Molecular design, chemical synthesis, mode of cycloaromatization and guanine-specific DNA cleavage. *Bioorg. Med. Chem.* **1996**, *4*, 105–113.
99. Nagata, R.; Yamanaka, H.; Murahashi, E.; Saito, I. DNA cleavage by acyclic eneyne-allene systems related to neocarzinostatin and esperamicin-calicheamicin. *Tetrahedron Lett*. **1990**, *31*, 2907–2910.
100. Myers, A. G.; Parrish, C. A. DNA cleavage by an α,3-dehydrotoluene precursor conjugated to a minor groove binding element. *Bioconj. Chem.* **1996**, *7*, 322–331.
101. Schmittel, M.; Strittmatter, M.; Kiau, S. Switching from the Myers reaction to a new thermal cyclization mode in enyne-allenes. *Tetrahedron Lett*. **1995**, *36*, 4975–4978.
102. Schmittel, M.; Strittmatter, M.; Kiau, S. An unprecedented biradical cyclization as an alternative pathway to the Myers–Saito cycloaromatization in the thermal reactions of enyne allenes. *Ang. Chem. Int. Ed.* **1996**, *35*, 1843–1845.
103. Schmittel, M.; Vavilala, C. Kinetic isotope effects in the thermal C-2–C-6 cyclization of enyne-allenes: Experimental evidence supports a stepwise mechanism. *J. Org. Chem.* **2005**, *70*, 4865–4868.
104. Schmittel, M.; Maywald, M.; Strittmatter, M. Synthesis of novel enyne-allenes, their thermal C-2–C-6 cyclization, and the importance of a benzofulvene biradical in the DNA strand cleavage. *Synlett* **1997**, 165–166.
105. Schmittel, M.; Kiau, S.; Siebert, T.; Strittmatter, M. Steric effects in enyne-allene thermolyses: Switch from Myers–Saito reaction to the C2–C6-cyclization and DNA strand cleavage. *Tetrahedron Lett*. **1996**, *37*, 7691–7694.
106. Karlsson, J. O.; Nguyen, N. V.; Foland, L. D.; Moore, H. W. (2-Alkynylethenyl)ketenes—A new benzoquinone synthesis. *J. Am. Chem. Soc.* **1985**, *107*, 3392–3393.
107. Moore, H. W.; Yerxa, B. R. Ring expansions of cyclobutenones—Synthetic utility. *Chemtracts—Org. Chem.* **1992**, *5*, 273–313.

108. Musch, P. W.; Remenyi, C.; Helten, H.; Engels, B. On the regioselectivity of the cyclization of enyne–ketenes: A computational investigation and comparison with the Myers–Saito and Schmittel reaction. *J. Am. Chem. Soc.* **2002**, *124*, 1823–1828.

109. Sullivan, R. W.; Coghlan, V. M.; Munk, S. A.; Reed, M. W.; Moore, H. W. DNA cleavage by 4-alkynyl-3-methoxy-4-hydroxcyclobutenones. *J. Org. Chem.* **1994**, *59*, 2276–2278.

110. Nakatani, K.; Isoe, S.; Maekawa, S.; Saito, I. Photoinduced DNA cleavage by designed molecules with conjugated Ene–yne–ketene functionalities. *Tetrahedron Lett*. **1994**, *35*, 605–608.

111. Nakatani, K.; Maekawa, S.; Tanabe, K.; Saito, I. Alpha-diazo ketones as photochemical DNA cleavers—A Mimic for the radical generating-system of neocarzinostatin chromophore. *J. Am. Chem. Soc.* **1995**, *117*, 10635–10644.

112. David, W. M.; Kumar, D.; Kerwin, S. M. Synthesis of a heterocyclic aza-enediyne and Its DNA-cleavage properties. *Bioorg. Med. Chem. Lett.* **2000**, *10*, 2509–2512.

113. Kumar, D.; David, W. M.; Kerwin, S. M. N-Propargyl-2-Alkynylbenzothiazolium aza-enediynes: Role of the 2-alkynylbenzothiazolium functionality in DNA cleavage. *Bioorg. Med. Chem. Lett.* **2001**, *11*, 2971–2974.

114. Tuntiwechapikul, W.; David, W. M.; Kumar, D.; Salazar, M.; Kerwin, S. M. DNA modification by 4-aza-3-ene-1,6-diynes: DNA cleavage, pH-dependent cytosine-specific interactions, and cancer cell cytotoxicity. *Biochemistry* **2002**, *41*, 5283–5290.

115. Sherman, C. L.; Pierce, S. E.; Brodbelt, J. S.; Tuesuwan, B.; Kerwin, S. M. identification of the adduct between a 4-aza-3-ene-1,6-diyne and DNA using electrospray ionization mass spectrometry. *J. Am. Soc. Mass Spectrom.* **2006**, *17*, 1342–1352.

116. Musch, P. W.; Remenyi, C.; Helten, H.; Engels, B. On the regioselectivity of the cyclization of enyne–ketenes: A computational investigation and comparison with the Myers–Saito and Schmittel reaction. *J. Am. Chem. Soc.* **2002**, *124*, 1823–1828.

117. Schmittel, M.; Steffen, J. P.; Rodriguez, D.; Engelen, B.; Neumann, E.; Cinar, M. E. Thermal C-2–C-6 cyclization of enyne-carbodiimides: Experimental evidence contradicts a diradical and suggests a carbene intermediate. *J. Org. Chem.* **2008**, *73*, 3005–3016.

118. Tuesuwan, B.; Kerwin, S. M. 2-Alkynyl-*N*-propargyl pyridinium salts: Pyridinium-based heterocyclic skipped aza-enediynes that cleave DNA by deoxyribosyl hydrogen-atom abstraction and guanine oxidation. *Biochemistry* **2006**, *45*, 7265–7276.

119. Giese, B. Electron transfer through DNA and peptides. *Bioorg. Med. Chem.* **2006**, *14*, 6139–6143.

14

DNA DAMAGE BY PHENOXYL RADICALS

RICHARD A. MANDERVILLE

Departments of Chemistry and Toxicology, University of Guelph, Guelph, Ontario, Canada N1G 2W1

14.1. INTRODUCTION

Phenols are ubiquitous substances that contain a hydroxyl substituent attached to an aromatic ring. The phenolic compounds shown in Figure 14.1 highlight their structural variation and vast range of biological activities. For example, the essential amino acid tyrosine contributes greatly to the active sites of many enzymes, including ribonucleotide reductases that catalyze the conversion of nucleotides to deoxynucleotides, supplying a pool of deoxynucleoside triphosphates needed for DNA replication and repair.[1,2] Enzymatic hydroxylation of tyrosine by tyrosine hydroxylase generates *L*-dihydroxyphenylalanine (*L*-DOPA),[3] which undergoes decarboxylation to generate dopamine, a critical neurotransmitter in the central nervous system. Dopamine contributes importantly to the neurophysiological control of arousal, initiation of movement, perception, motivation, and emotion.[4] Vitamin E (α-tocopherol) is the major lipid-soluble chain-breaking antioxidant in human blood plasma and has the essential role of inhibiting the oxidation of lipids, thereby preventing lipid peroxidation.[5] A similar role is carried out by the commercial antioxidant, butylated hydroxyanisole (BHA), which is used as a food additive to prevent the oxidation of fats.[6] Dietary polyphenols, such as epicatechin and quercetin, are found in a variety of fruits, vegetables, and beverages (notably red wine and green tea) and are also known for their antioxidant properties.[7] It is believed that the consumption of certain polyphenols provides protection against cardiovascular disease and cancer.[8]

Radical and Radical Ion Reactivity in Nucleic Acid Chemistry, Edited by Marc M. Greenberg

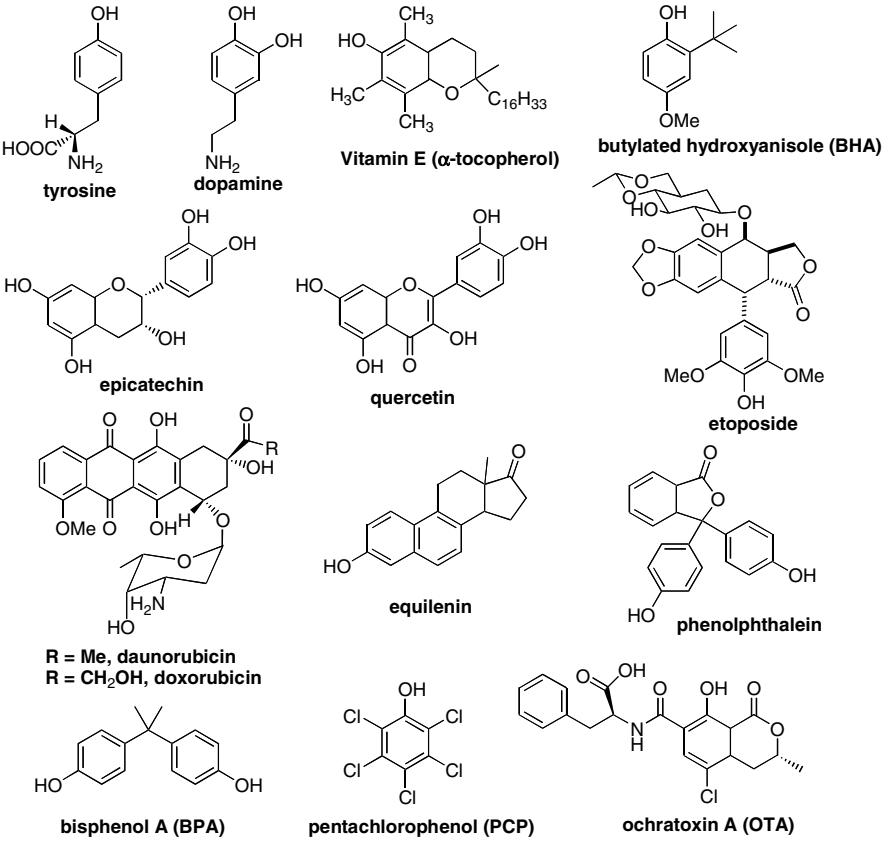

FIGURE 14.1. Structures of natural, commercial, and industrial phenols.

Phenolic compounds are also important drugs. Etoposide and the anthracycline antibiotics, daunorubicin and doxorubicin, are clinically used therapeutics for cancer treatment. Etoposide is a semisynthetic derivative of the natural plant extract podophyllotoxin and acts as a DNA topoisomerase II inhibitor.[9] The proposed mechanism for the cytotoxicity of anthracyclines is the production of reactive oxygen species (ROS) during intracellular metabolism.[10] Equilenin is an estrogen component of Premarin isolated from horse urine (Pregnant Mares' urine); it is widely used in hormone replacement therapy by postmenopausal women to alleviate menopausal symptoms and to protect against osteoporosis.[11] The bis-phenolic compound phenolphthalein is used as a laxative and is also a well-known pH indicator.[12]

Phenolic compounds are also used as monomers for polymer production. Bisphenol A (BPA) is used in the manufacturing of polycarbonate plastics and epoxy resins, which have applications in a variety of consumer products (including baby bottles), in the lining of food cans, and in dental sealants.[13] Chlorophenols are used as germicides, analgesics, antiseptics, weed killers, bactericides, and fungicides; pentachlorophenol (PCP) is an extremely effective wood preservative.[14]

Despite the beneficial effects of some phenolic compounds, they can also be toxic. Chlorophenols, PCP, and the natural chlorophenol ochratoxin A (OTA) exhibit carcinogenicity in animal models and are classified by the International Agency for Cancer Research (IARC) as probable (Group 2B) human carcinogens.[14,15] Ingestion of dietary polyphenols during pregnancy has been linked to the development of specific types of infant leukemia.[16] Use of the anticancer drug etoposide is also associated with the increased risk of developing secondary leukemias,[9] while the anthracycline antibiotics are noted for their cardiotoxicity due to the production of ROS, posing a major problem in their clinical application.[10] Long-term hormone replacement therapy with equine estrogens is also associated with a higher risk of breast, ovarian, and endrometrial cancers.[11] In April 2008, Canada moved to become the first country to set exposure limits on BPA.[17] Polymers that contain BPA are typically sturdy, but it is possible for BPA to be released from polycarbonates that have not completely polymerized. BPA may pose a risk for newborns and infants, and thus the proposed ban in Canada targets polycarbonate baby bottles.[17]

The toxicity of phenols is thought to stem from their oxidative metabolism with formation of the phenoxyl radical regarded as the rate-determining step in phenol-induced toxicity.[18] Generation of the phenoxyl radical in biological systems is known to promote oxidative stress mediated by thiol oxidation, antioxidant depletion, and enhanced ROS production to afford oxidative DNA damage.[19] In this mode of damage, the phenol does not interact with DNA directly and the observed genotoxicity represents an indirect mechanism of action. A direct mode of phenol-induced genotoxicity involves covalent DNA adduction derived from phenoxyl radicals and quinone electrophiles produced by oxidative metabolism of phenols. DNA adduction by quinone electrophiles is a well-developed topic because these α,β-unsaturated carbonyl compounds react readily with the nucleophilic nitrogen atoms of the DNA nucleobases.[20–22] However, in this chapter, attention is focused on covalent DNA adduction by the electrophilic phenoxyl radical that displays ambident (O versus C) electrophilicity in direct radical addition reactions with the nucleobases to afford bulky covalent DNA adducts.[23] While little is known about the biological properties of these types of adducts, they are expected to play an important role in DNA–protein cross-link (DPC) formation[24,25] and the toxicity of phenols in peroxidase-rich tissues.[23] Structural evidence shows a tendency for phenoxyl radical attachment at the purine C8 position, especially C8 of 2′-deoxyguanosine (dG), as noted with hydroxyl radical ($HO^{\bullet}$) in formation of 8-oxo-dG.[23] The synthesis of C-bound C8-PhOH-dG adducts has shed light on their structural, optical, and chemical properties. These experiments provide a basis for future studies aimed at gaining an understanding of the structural and biological impact of DNA adducts derived from phenoxyl radical species.

14.2. OXIDATION OF PHENOLS

The oxidation of phenol is outlined in Scheme 14.1. In dipolar aprotic solvents, such as acetonitrile and *N*,*N*-dimethylformamide (DMF), phenol possesses a one-electron

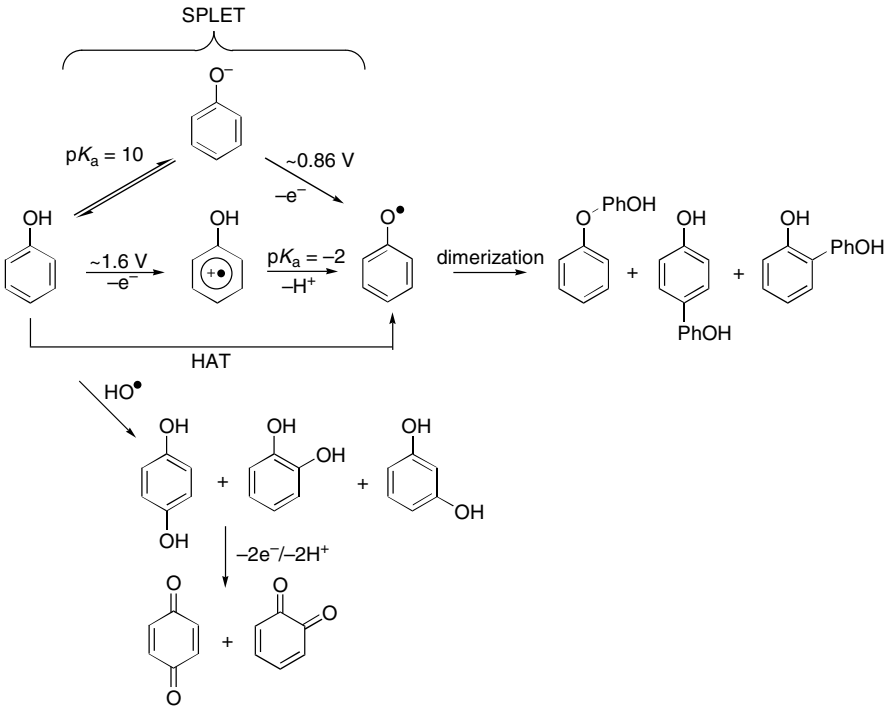

SCHEME 14.1

oxidation potential of ~1.6 V versus NHE.[26] The resulting phenolic radical cation is a very strong acid with a $pK_a \sim -2$,[27] and so typically oxidation is accompanied by proton transfer to afford the neutral phenoxyl radical species. In aqueous media the pK_a of phenol is ~10 and the phenolate undergoes one-electron oxidation much more readily than the protonated species with an oxidation potential of ~0.86 V versus NHE.[26]

Attachment of electron-donating and–withdrawing substituents on the phenolic ring affect both the acid–base behavior and the oxidation potential of the phenol. Electron-donating groups at the *ortho* and *para* positions lower the oxidation potential because of through-resonance between the electron-deficient phenoxyl radical site and the ring substituent. Electron-withdrawing groups increase the oxidation potential but lower the phenolic pK_a by stabilizing the phenolate anion. For example, the pK_a of PCP is ~4.74 and its phenolate has an oxidation potential ~0.99 V versus NHE[26] to afford the PCP-phenolic radical that possesses an absorption spectrum in H_2O at 440 nm and decays via second-order kinetics with $k_d = 9.1 \times 10^8\,M^{-1}s^{-1}$, as evidenced by pulse radiolytic studies.[28]

In terms of rates of phenolic radical production, bimolecular rate constants, k_2, for the H-atom transfer (HAT) reaction of peroxyl radicals with phenols to generate the phenoxyl radical and peroxide are $\sim 10^3\,M^{-1}s^{-1}$ for phenol and $\sim 5 \times 10^6\,M^{-1}s^{-1}$ for compounds related to vitamin E.[29] This HAT process has been well-studied for

phenols bearing electron-donating groups that can act as antioxidants. However, phenols bearing electron-withdrawing groups that do not possess antioxidant properties undergo the HAT process sluggishly, if at all. These electron-deficient phenols favor phenolate formation followed by electron transfer, the so-called sequential proton loss electron transfer (SPLET) mechanism, for phenoxyl radical formation in aqueous solution.[30] Wright and Shadnia predict a rate of ~50 μM per s for phenoxyl radical formation by a SPLET mechanism for 10 μM phenol with a $pK_a = 7$.[31]

Once the neutral phenoxyl radical is formed, it can dimerize by radical coupling processes to generate isomeric dihydroxybiphenyls and diaryl ethers.[32, 33] In nonpolar solvents, the dihydroxybiphenyls are favored and are formed by an initial dimerization of the phenoxyl radicals to produce the isomeric diketo intermediates that enolize to form the final stable products. In aqueous solution, sufficient catalyst is present such that the rate of enolization of the metastable diketo intermediates is very high and absolute rates of dimerization of phenoxyl radical are equal to the rate constant for the diffusion-controlled reaction, $\sim 6 \times 10^9\ M^{-1}s^{-1}$.[32]

The $HO^\bullet$ reacts with substituted benzenes predominantly by addition to the aromatic ring and not by interaction with the substituent.[34] In reaction of $HO^\bullet$ with phenol to yield dihydroxybenzenes, the ratio of the probabilities for attachment of $HO^\bullet$ to one ring position, para : ortho : meta, is 9 : 6 : 1. The $HO^\bullet$ exhibits a strong preference for attachment at the positions activated by the hydroxyl substituent of the phenol, a preference that stems from the electrophilic character of $HO^\bullet$. As pointed out by Raghavan and Steenken, this selectivity is quite remarkable given that the highly reactive $HO^\bullet$ reacts with phenol with a rate constant that is in the upper end of the diffusion-controlled limit ($k = 1.4 \times 10^{10}\ M^{-1}s^{-1}$).[34]

Attachment of $HO^\bullet$ at the activated *para* and *ortho* positions of phenol generates *para*- (hydroquinone) and *ortho*-hydroxyphenol (catechol) that are prone to further oxidation to generate the corresponding quinones. For example, the one-electron oxidation potential of the phenolate of hydroquinone is ~0.17 V versus NHE (compared to ~0.86 V for the phenol phenolate).[26] Hydroquinone reacts rapidly by a HAT reaction to generate the semiquinone, which are transient species in aqueous solution at neutral pH, rapidly disproportionating into the hydroquinone and the *para*-quinone.[31] Quinones are electrophiles that react with biological nucleophiles, including GSH and the nucleobases of DNA,[20–22] and are predicted to play an important role in the toxicity of certain phenolic compounds.[35]

Enzymatic oxidation of phenol also generates phenoxyl radical and quinone intermediates. Many phenols are substrates for peroxidases that in the presence of hydrogen peroxide (H_2O_2) can oxidize the phenol to their corresponding phenoxyl radical.[36] Specific examples of mammalian peroxidase enzymes include: lactoperoxidase (LPO), which is found in milk, saliva, and tears as well as in the mammary glands; eosinophil peroxidase (EPX) and MPO, found in white blood cells; and cyclooxygenase (COX) enzymes that have peroxidase activity and are found in most mammalian cells. In tissues the relative concentration of the phenolic radical compared to the concentration of biochemical reductants is small, and so radical coupling reactions to form dihydroxybiphenyls are unlikely. Instead, the neutral phenoxyl radical is prone to undergo a redox-cycling mechanism by a HAT

reaction with GSH for example, to yield $GS^{\bullet}$, which repeatedly generates the parent phenol as a substrate for peroxidase.[19] Phenols are also substrates for cytochrome P450 enzymes. Certain P450 isoforms such as 3A4 are known to favor *ortho*-hydroxylation of phenols to form the catechol that subsequently undergoes oxidation to furnish the *ortho*-quinone.[37]

14.3. OXIDATIVE DNA DAMAGE

The metabolism of phenols by peroxidase enzymes in the presence of H_2O_2 furnishes phenoxyl radicals that can react with suitable biochemical reductants (glutathione (GSH) and NAD(P)H) to generate the parent phenolic compound and a reductant-derived radical.[12] As outlined in Scheme 14.2, the HAT reaction of phenoxyl radical with GSH generates $GS^{\bullet}$ that reacts with GSH to generate a GSH disulfide anion radical that can reductively activate molecular O_2 to generate the superoxide radical anion ($O_2^{\bullet -}$).[19] Because one molecule of phenol can undergo multiple cycles of oxidation and reduction in a process termed "futile metabolism," it can generate $O_2^{\bullet -}$ in quantities that greatly exceed the concentration of the phenolic compound.[12] This process facilitates $O_2^{\bullet -}$ toxicity leading to the release of free ferrous iron (Fe^{2+}), production of H_2O_2 through spontaneous dismutation of $O_2^{\bullet -}$, and $HO^{\bullet}$ production by the Fenton reaction or Haber–Weiss processes that causes oxidative DNA damage.[38]

Enhanced $O_2^{\bullet -}$ production to stimulate oxidative DNA damage also occurs through hydroxylation of phenols by P450 enzymes to afford catechols (Scheme 14.2),

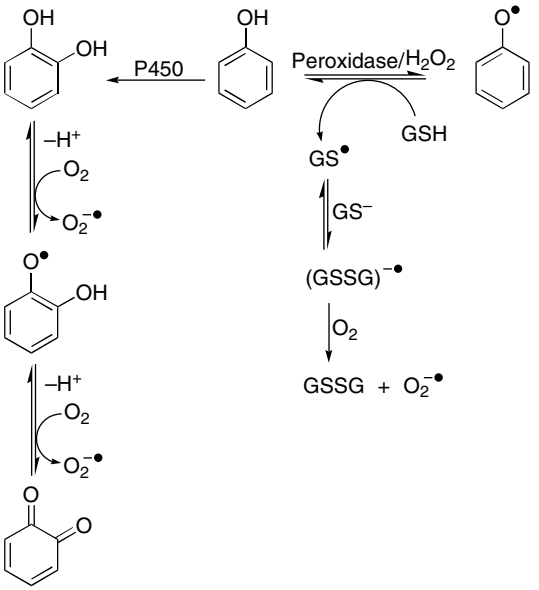

SCHEME 14.2

or hydroquinone metabolites.[20] In the example shown in Scheme 14.2, autoxidation of the catechol generates the semiquinone and *ortho*-quinone intermediates along with $O_2^{\bullet -}$. Reduction of the *ortho*-quinone by P450 reductase or quinone reductase regenerates the semiquinone species that can continue to redox cycle and produce $O_2^{\bullet -}$ for the generation of ROS and subsequent oxidative DNA damage.[20]

Evidence for phenol-mediated oxidative DNA damage includes the finding that inhibition of MPO activity in HL60 cells prevented production of the etoposide phenoxyl radical with the concomitant decrease in etoposide-induced oxidative DNA damage and cleavage of the *MLL* gene known to be associated with acute myeloid leukemia.[9,39] The 4-hydroxylation of equilenin (Figure 14.1) by both P450s 1A1 and 1B1 forms the catechol, which undergoes autoxidation to the 3,4-*ortho*-quinone.[40] Studies carried out *in vitro*[41] and in a rat model[42] show that 4-hydroxyequilenin facilitates oxidative DNA damage. The mutagenicity and carcinogenicity of the chlorophenols PCP and OTA is also thought to be associated with ROS production and oxidative DNA damage.[14] Treatment of rodents and cell cultures with the chlorophenols leads to an increase in 8-oxo-dG levels, DNA strand scission, and other biomarkers for oxidative stress including GSH depletion.[14]

14.4. COVALENT DNA ADDUCTION

Early structural evidence for covalent DNA adduction by phenoxyl radical species was provided by the Dizdaroglu laboratory from efforts to establish the structure of DNA–protein cross-links (DPCs) formed when cells are exposed to ionizing radiation.[43,44] In order to generate authentic cross-link material, N_2O-saturated aqueous mixtures of thymine and tyrosine were treated with ionizing radiation to afford $HO^{\bullet}$. This treatment generated hydroxytyrosines ($HO^{\bullet}$ attachment to the phenolic ring of tyrosine), tyrosine dimers (tyrosyl radical coupling reactions), and a single thymine–tyrosine cross-link resulting from covalent bond formation between the methyl group of thymine and C3 of tyrosine.[43] With an authentic cross-linked component in hand, it was then shown that the same species is produced upon treatment of calf thymus nucleohistone with ionizing radiation.[44] A likely mechanism for formation of the cross-link (Scheme 14.3A) involves addition of the 5-(2′-deoxyuridinyl)methyl radical (produced by HAT from the 5-methyl group of thymine to $HO^{\bullet}$) to the C3 position of the tyrosine ring, requiring the close proximity of the radical to a tyrosine in the DNA–protein complex.[44] Although the alternative mechanism involving combination of the tyrosyl and 5-(2′-deoxyuridinyl)methyl radical species could not be ruled out, it appeared less likely due to the requisite formation of two radical species in close proximity under the low radiation doses used for cross-link formation. Further experiments showed that the same thymine–tyrosine cross-link (Scheme 14.3A) was formed by treating mammalian chromatin with hydrogen peroxide in the presence of iron or copper ions.[45] A cross-link between cytosine and tyrosine was also produced upon radiation,[46] as outlined in Scheme 14.3B.

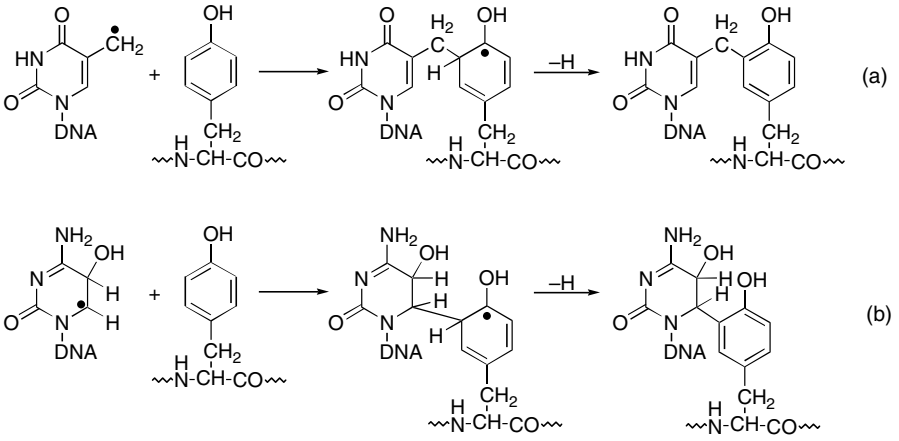

SCHEME 14.3

The HO$^{\bullet}$ can also abstract a single electron from dG to generate the base radical cation (G$^{\bullet+}$) that can subsequently react with tyrosine to form DPCs. This reactivity was initially demonstrated by the Barton Laboratory[24] through the use of flash-quench experiments involving DNA-bound ruthenium complexes in the presence of the tripeptide lysine–tyrosine–lysine (Lys–Tyr–Lys). Irradiation of the ruthenium complex at 436 nm to initiate G$^{\bullet+}$ production was accompanied by the tyrosyl radical at 405 nm. Inspection of the DNA sample by HPLC and MALDI-TOF mass spectrometric analysis showed the presence of a peak with the mass expected for a cross-link between DNA and Lys–Tyr–Lys with covalent selectivity of Tyr for adenine and thymine. Replacement of the central Tyr residue with tryptophan showed that the Lys–Trp–Lys tripeptide failed to react covalently with DNA, suggesting that the tryptophan radical exhibits no reactivity toward the DNA bases, unlike the tyrosyl radical.[24]

On the basis of the above results, Bjorklund and Davis[25] speculated that charge transfer in DNA involving G$^{\bullet+}$ production can lead to the formation of DNA–histone cross-links. To test this prediction, DNA charge-transfer reactions in model nucleosome core particles (NCPs) were investigated by attaching an anthroquinone (AQ) label to the 5′-end of a 162-bp DNA duplex bound to chicken erythrocyte histone protein. The AQ linker has been utilized extensively by the Schuster laboratory[47] to study charge transfer within DNA. Selective photoirradiation of the AQ label at 350 nm introduces a radical cation into the duplex that will migrate through the duplex until it reaches a GG site (deep trap), where the G$^{\bullet+}$ may react with H_2O to generate 8-oxoG lesions.[48] In the presence of histone proteins, Bjorklund and Davis noted that ~69% of all ^{32}P-labeled AQ-tethered DNA was cross-linked to histone proteins as a result of DNA charge transfer.[25] A proposed mechanism for DPC formation is outlined in Scheme 14.4 and involves a tyrosine moiety that is in van der Waals contact with the minor groove of several DNA base pairs. In this proposed mechanism, photoirradiation of AQ triggers G$^{\bullet+}$ formation that has a reduction potential

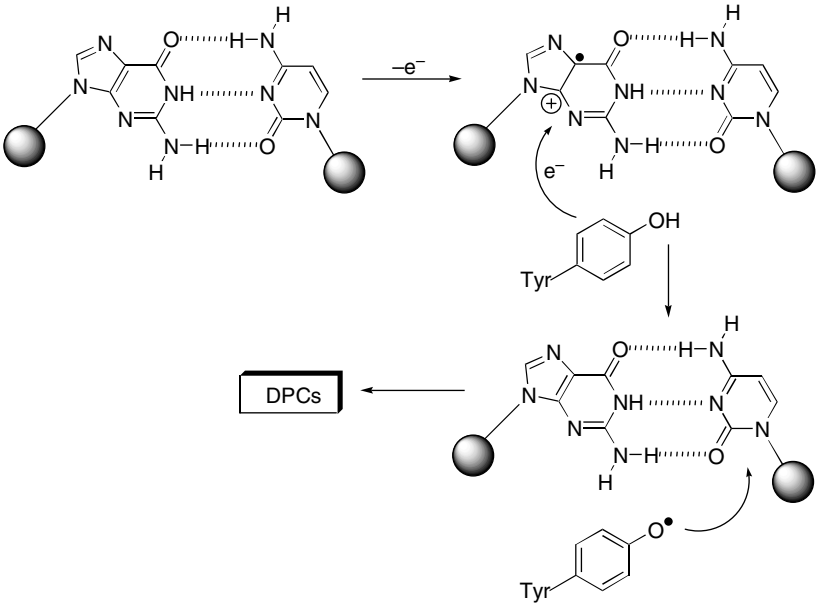

SCHEME 14.4

($E^0 = 1.3$ V versus NHE[49]) high enough to cause spontaneous oxidation of tyrosine ($E^0 = 0.94$ V versus NHE[50]) to generate the tyrosyl radical.[25] Given that tyrosine residues form cross-links with pyrimidines,[43–46] covalent attachment of tyrosyl radical to the pyrimidine 5–6 double bond was proposed.[25]

In the work outlined by Bjorklund and Davis multiple DPCs were produced that could not easily be rationalized by the proposed mechanism outlined in Scheme 14.4.[25] While it was speculated that other protein residues such as lysine may participate in DPC formation, the Wagner laboratory has demonstrated that the AQ radical anion ($AQ^{\bullet -}$) generated during photoirradiation of AQ-tethered oligonucleotides is also capable of forming covalent adducts with DNA residues[51] and may be expected to react with protein residues as well. In the proposed mechanism outlined in Scheme 14.5 charge transfer from thymine to excited AQ generates $AQ^{\bullet -}$ and $T^{\bullet +}$ that is proposed to undergo deprotonation to yield the neutral 5-(2′-deoxyuridinyl)methyl radical that subsequently reacts covalently with $AQ^{\bullet -}$.[51] Likewise, radical coupling reactions between $AQ^{\bullet -}$ and a nearby tyrosyl radical may also yield DPCs in the model DNA–histone system studied by Bjorklund and Davis.

In the above studies on DPC formation it is interesting to note that cross-link formation between the tyrosyl radical and dG has not been reported. This lack of evidence for covalent attachment to dG by a phenoxyl radical is contrasted by results presented by the Burrows laboratory.[52–54] In studies involving oxidative DNA damage by metallosalens, it was discovered that a phenolic radical generated as part of a metallosalicylaldehyde complex undergoes facile addition to the C8 position of dG to form a covalent adduct, such as 8-[Ni(sal-RH)]$^+$-dG shown in Figure 14.2. In our work

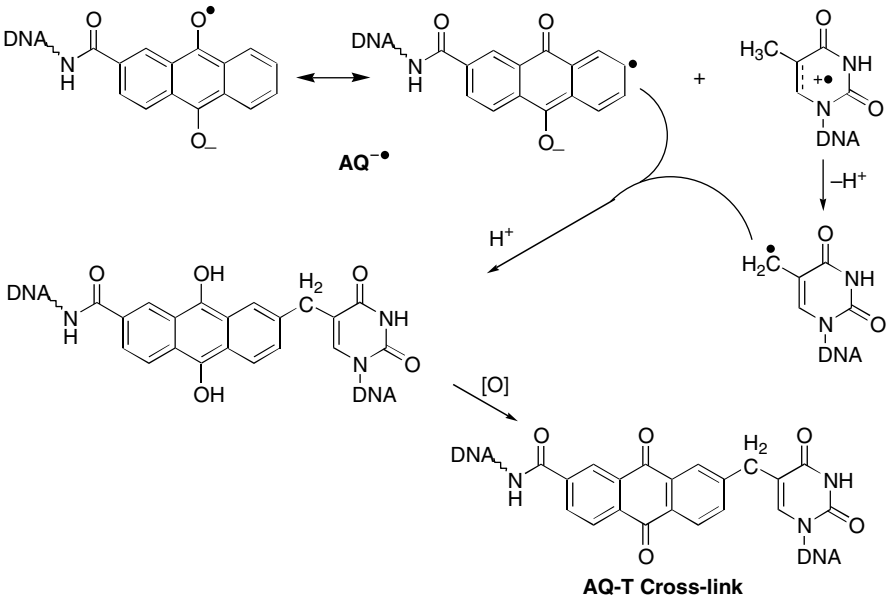

SCHEME 14.5

on DNA adduction by chlorophenol toxins, it was found that metabolic activation of PCP by peroxidase enzymes in the presence of H_2O_2 yielded the 8-PCP-dG adduct (Figure 14.2) resulting from O-attachment to C8 of dG.[55,56] In contrast, the natural product OTA yielded the C-adduct 8-OTA-dG following oxidative activation.[57] These results were consistent with the ambident (O- versus C-attack) reactivity of phenolic radicals in DNA adduction with dG, as outlined in Scheme 14.6.[23] Here, extensive delocalization of the phenolic radical or steric factors that may block O-attachment would favor C-adduct formation, while phenoxyl radicals with the unpaired electron localized on the oxygen atom would favor O-attack.[23] For the C-adducts shown in Figure 14.2, the phenolic O-site in 8-[Ni(sal-RH)]$^+$-dG is bound

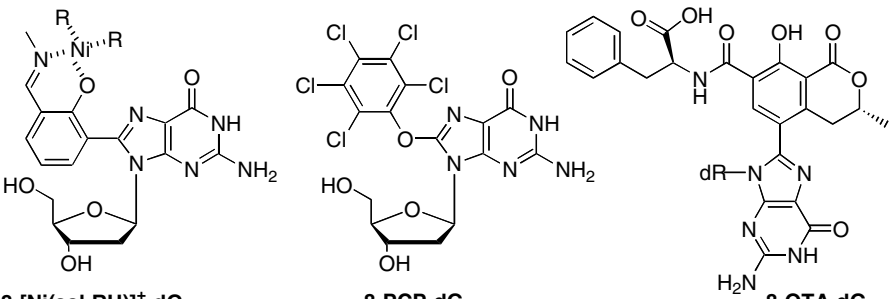

FIGURE 14.2. Structures of C- and O-bound C8-dG adducts of phenols.

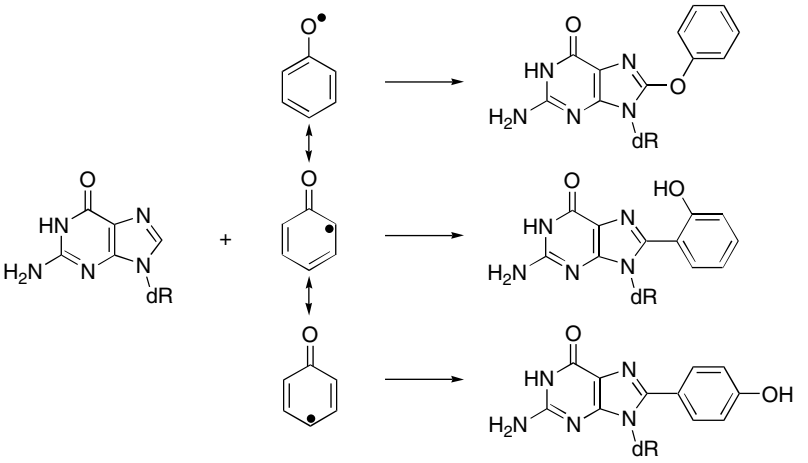

SCHEME 14.6

to a transition metal, while the phenolic OH of 8-OTA-dG is flanked by two carbonyl groups that would hinder O-attachment. For O-attachment by PCP it is known that phenoxyl radicals exhibit a linear correlation with Brown σ^+ constants because of the through-resonance between the electron-deficient phenoxyl radical and the ring substituent.[26] A high positive value of σ^+ suggests that the radical is localized on the oxygen atom, while a negative value suggests extensive radical delocalization. For PCP the σ^+ value is 1.1, while the corresponding value for 4-MeO-PhOH is -0.78.[26] The high positive σ^+ value for PCP suggests that its oxidation will produce a reactive O-centered phenolic radical, which is consistent with 8-PCP-dG (Fig. 14.2) formation.[23]

The C-adducts 8-[Ni(sal-RH)]$^+$-dG and 8-OTA-dG shown in Figure 14.2 are structurally related to a family of 8-aryl-dG adducts, such as those shown in Figure 14.3. Derivatives of 8-Ph-dG (X = H) with various para substituents (X = H, CH_3, CH_2OH, COOH) are derived from aryl hydrazines that are found in the mushroom *Agaricus bisporus* and are metabolized to arenediazonium ions and then to aryl radicals that form C8-purine adducts.[58–60] An interesting aspect of aryl hydrazine reactivity is that the aryl radical intermediates favor attachment to the C8 site of dA,[60] while phenolic radicals favor attachment to C8 of dG.[23] This observation is consistent with the electrophilicity of the phenolic radical that favors attachment to the more electron-rich purine, as noted with electrophilic HO$^\bullet$,[61] while aryl radicals are nucleophilic in nature[62] and hence favor attachment to the more electron-deficient purine dA.

Other C8-aryl adducts (Figure 14.3) include the 8-phenol derivatives, 8-(4″-hydroxyphenyl)-dG (8-*p*-PhOH-dG) and 8-(2″-hydroxyphenyl)-dG (8-*o*-PhOH-dG) that are generated by reaction of phenol with excess nitrite.[63] This reaction generates diazoquinones that break down into hydroxyphenyl radicals that subsequently attach to the purine C8 position. Carcinogenic polycyclic aromatic hydrocarbons (PAHs), such as benzo[*a*]pyrene (BP), also form C8-dG adducts (8-BP-dG,

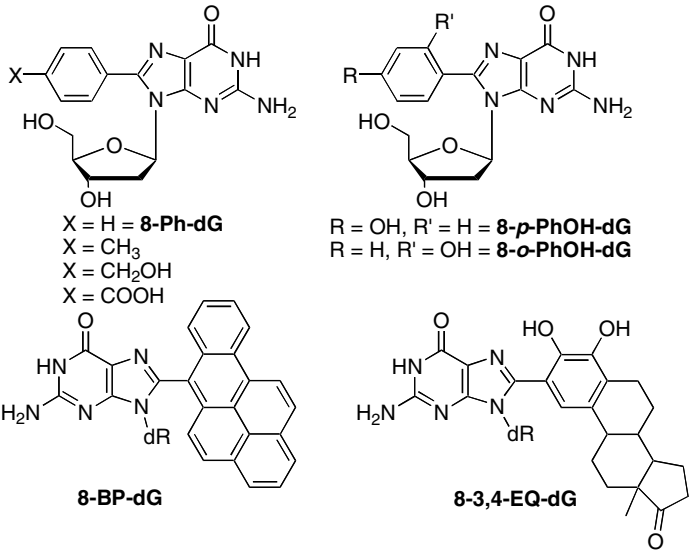

FIGURE 14.3. Structures of C8-aryl-dG adducts.

Figure 14.3) following radical cation production mediated by P450 peroxidase.[64–66] The estrogen 3,4-estronequinone (3,4-EQ) also undergoes metabolic activation to form C8-purine adducts,[67,68] such as 8-3,4-EQ-dG (Figure 14.3); in this case the reactive intermediate is the 3,4-EQ radical anion. Given that a wide range of toxins form C8-aryl-purine adducts that are structurally related to phenolic C-bound adducts, such as 8-OTA-dG (Figure 14.2), our laboratory is interested in gaining an understanding of the structural and electronic properties of C-bound C8-phenolic-dG adducts that are expected to play important roles in the biological activity of certain phenolic toxins.

14.5. CARBON-BOUND C8-PHENOLIC-DEOXYGUANOSINE ADDUCTS

A common property of C8-aryl-purine adducts are their tendency to undergo depurination to form abasic sites.[60,65–68] For example, diazonium ion treatment of calf thymus DNA at pH 7 generated ~30% 8-Ph-dG ($X = CH_3$) and 70% 8-Ph-G ($X = CH_3$), while for $X = CH_2OH$ the corresponding ratios were 7% and 93%, respectively.[60] For 8-BP-dG formation, ~50% had undergone depurination to form 8-BP-G,[65] while 8-3,4-EQ-dG gave way to 8-3,4-EQ-G following 30-min incubation in 1 : 1 DMF:aqueous buffer.[68] The latter result prompted Akanni and Abul-Hajj to propose that 8-3,4-EQ-dG is formed as an intermediate prior to the loss of the deoxyribose sugar.

To gain an understanding of the hydrolytic stability of C8-aryl-dG adducts, first-order rate constants for a number of *p*-substituted 8-Ph-dG adducts, including 8-*p*-PhOH-dG, were determined spectrophotometrically by monitoring formation

of the deglycosylated product at its absorbance maximum. In 0.1 N HCl at 37°C, $t_{1/2}$ ranged from 0.4 min for the phenyl adducts bearing electron-withdrawing CN and CHO substituents up to 1.45 min for 8-*p*-PhOH-dG. In pH 4 at 48.4°C, 8-*p*-PhOH-dG was the most reactive and underwent hydrolysis with $t_{1/2} \sim 22$ min. Protonation of N7 of dG (pK_a for protonated dG is 2.34[69]) is known to accelerate the rate of hydrolysis, as the positively charged purine ring becomes a good leaving group for a heteroatom-assisted S_N1-type hydrolysis reaction.[70–72] Thus, in acid where N7 is protonated, the purine ring bearing electron-withdrawing CN and CHO substituents are better leaving groups and increase the rate of hydrolysis, while in pH 4 where N7 is not initially protonated, electron-withdrawing CN and CHO substituents lower N7 basicity and decrease the rate of hydrolysis. For dG itself, the $t_{1/2}$ is 17.7 min in 0.1 N HCl at 37°C and 2840 min in pH 4.1 at 48°C.[70] Thus, 8-*p*-PhOH-dG undergoes deglycosylation ~12 times faster than dG in 0.1 N HCl and ~129 times faster at pH 4. A rate constant of $3.82 \times 10^{-5}\ s^{-1}$ for $t_{1/2} \sim 302$ h (12.6 days) was also determined for 8-*p*-PhOH-dG at 37°C pH 7. A rate for spontaneous loss of G from duplex DNA at pH 7.4, 37°C is $\sim 3 \times 10^{-11}\ s^{-1}$ ($t_{1/2} = 730$ years).[72] While 8-*p*-PhOH-dG is certainly more reactive than dG toward depurination, it is not as reactive as 8-NO_2-dG ($t_{1/2} \sim 1$ h at 37°C, pH 7.2[73]) and is reasonably stable at physiological pH.

A rationale for the tendency of C8-aryl-purine adducts to undergo deglycosylation at physiological pH is provided in Scheme 14.7. Direct radical attachment to C8 of dG would produce the nucleobase radical intermediate. In the gas phase under vacuum the Kenttämaa laboratory has found that the radical addition reaction by aryl radicals at C8 of purines is always followed by cleavage of the N-sugar bond to eliminate the deoxyribose moiety and produce the free base.[74,75] A competitive HAT process is required for production of the nucleoside adduct that is stable at pH 7, but undergoes deglycosylation under acidic conditions. Candidates for catalysis of the HAT process include phenoxyl radicals,[76] phenyl radicals,[77] and molecular O_2.[78] Given that O_2 would be the most abundant radical species present (1.2 mM for O_2-saturated solution[78]), it is the most likely candidate for abstracting the H atom from the nucleobase radical intermediate to form the aromatized nucleoside adduct and the hydroperoxy radical (HOO•). Rate constants for this HAT process should be $\sim 10^9\ M^{-1}s^{-1}$ based on rate constants for the reaction of O_2 with cyclohexadienyl radical in benzene.[78] The pathways outlined in Scheme 14.7 suggest that the deglycosylation process will dominate when the concentration of O_2 in solution

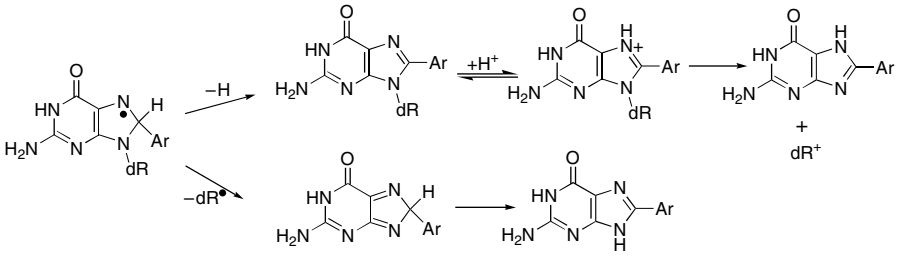

SCHEME 14.7

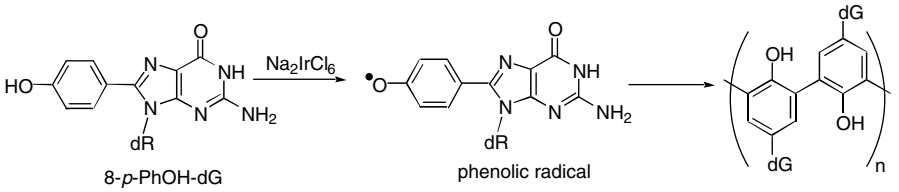

SCHEME 14.8

is sufficiently low, while adduct formation becomes a competitive process in O_2-saturated solution.

As noted for heteroatom (O and N) attachment to C8 of dG to form 8-oxo-dG and C8-arylamine adducts, attachment of the Ph moiety also enhances the 1-electron donor characteristics of the purine nucleoside.[79] The redox properties of 8-*p*-X-Ph-dG (X = OH, OCH_3, CH_3, H, CN, CHO) adducts have been studied by cyclic voltammetry in anhydrous DMF.[79] The C8-aryl adducts exhibited irreversible one-electron oxidation peaks with half-peak potentials ($E_{p/2}$) ranging from 0.85 V versus saturated calomel electrode (SCE) for 8-*p*-PhOH-dG (X = OH) up to 1.11 V/SCE for 8-*p*-CHO-Ph-dG. All adducts were oxidized more readily than dG, which gave $E_{p/2} = 1.14$ V/SCE in DMF.[79]

The results from the electrochemical measurements suggested that the oxidation of 8-*p*-PhOH-dG was coupled with phenol deprotonation to yield the neutral phenolic radical. Consistent with this hypothesis, treatment of 8-*p*-PhOH-dG with the one-electron oxidant Na_2IrCl_6, using conditions developed by Burrows for the oxidation of 8-oxoG,[80] generated polyphenol materials through the intermediacy of the phenolic radical intermediate, as outlined in Scheme 14.8.[79] In contrast to the behavior of 8-*p*-PhOH-dG, treatment of 8-*p*-OMe-Ph-dG with Na_2IrCl_6 gave rise to spiroiminodihydantoin (Sp)-like products (Scheme 14.9), as noted with 8-oxo-dG[80] and C8-arylamine adducts.[81] These results showed that replacement of the phenolic OH in 8-*p*-PhOH-dG with OCH_3 restores the well-established oxidative chemistry of the purine nucleoside and that attachment of the phenolic ring to dG expands the redox chemistry of the nucleoside to generate the phenolic radical instead of the purine radical cation that reacts with water.[79]

The C8-PhOH-purine adducts can also provide insight into the electronic properties of *p*-purine substituent by determining phenolic pK_a values, as utilized historically to determine substituent (σ^-) constants.[82] For 8-*p*-PhOH-N1-Me-dG

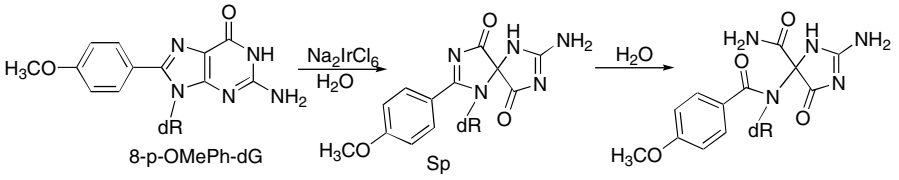

SCHEME 14.9

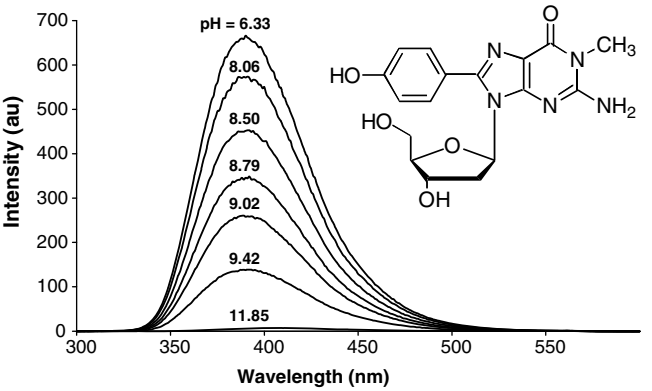

FIGURE 14.4. Emission spectra of 8-*p*-PhOH-N1-Me-dG in water at different pH values. Spectra were recorded with excitation at the absorbance maxima of the adduct (280 nm at pH 6.33–8.79, 292 at pH 9.02–11.85).

a phenolic pK_a of 8.90 was determined from basic pH titrations using the spectrophotometric procedure;[83] a phenolic pK_a for 8-*p*-PhOH-dG could not be determined due to overlap with N1 deprotonation (N1 pK_a of dG is 9.25[69]). The phenolic pK_a of 8-*p*-PhOH-dA is 8.70,[83] confirming that the dA adduct is a stronger acid than the dG adduct, which is consistent with the one-electron oxidation potentials (E^0) for purine nucleosides (1.42 V/NHE for A versus 1.29 V/NHE for G[49]). Calculation of Hammett substituent constants afforded a σ^- of 0.55 for dA and 0.46 for N1-Me-dG,[83] which are comparable to those established for 2-pyridyl (0.55), $CONH_2$ (0.61), $N(CF_3)_2$ (0.53), and C_6F_5 (0.43).[84]

Another interesting aspect of 8-PhOH-purine adducts is that they act as fluorophores (emission at ~390 nm in aqueous buffer at pH 7) and the fluorescence is quenched upon addition of base.[83] For the *p*-isomers the protonation/deprotonation on/off fluorescence switching mechanism may be exploited for the development of nucleobase analogues with fluorescent pH-sensing properties. Figure 14.4 highlights the pH-dependent fluorescence of 8-*p*-PhOH-N1-Me-dG. Similar properties were noted for 8-*p*-PhOH-dA, which prompted the synthesis of 8-*p*-(2-Cl-PhOH)-dA that has a phenolic pK_a of 7.29 and exhibits fluorescent pH-sensing in the physiological pH range.[83]

The optical properties of the 8-*o*-PhOH-purine adducts have provided insight into their ground-state structures at the nucleoside level.[85] These adducts have the ability to phototautomerize, through an excited-state intramolecular proton transfer (ESIPT) process, to generate the keto form. This tautomerization depends on the presence of an intramolecular H-bond between the phenolic OH and the imine nitrogen (N7). In water, 8-*o*-PhOH-dG shows only enol emission at ~395 nm; in hexane, keto emission at ~475 nm is observed.[85] These results show that in water the intramolecular H-bond required for ESIPT is disrupted, while the H-bond is present in the nonpolar hexane solvent. The absorption spectrum of 8-*o*-PhOH-dG in hexane also displayed a shoulder at ~320 nm that was absent in water. In $CHCl_3$

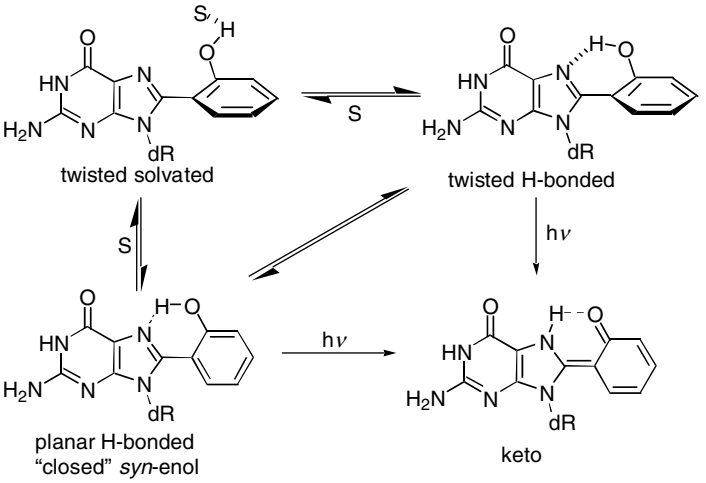

SCHEME 14.10

and MeCN the absorbances at 320 and 280 nm are of almost equal intensity. These results provided insight into the conformational equilibria of 8-*o*-PhOH–purine adducts, which are summarized in Scheme 14.10 for 8-*o*-PhOH-dG. In water, these adducts exist in a solvated (S) nonplanar "twisted" conformation that absorbs at ~280 nm and cannot undergo ESIPT. Desolvation of this structure yields the twisted H-bonded structure that is prevalent in hexane and undergoes ESIPT. In $CHCl_3$, the equilibrium shifts more in favor of the planar H-bonded species that absorbs at ~320 nm and undergoes ESIPT.[85]

Support for the predicted conformations of 8-PhOH–purine adducts derived from optical data was provided by DFT calculations.[86] As shown in Figure 14.5, the adducts adopt a *syn* conformation about the glycosidic bond due to the presence of an O5′−H · · · N3 hydrogen bond, where the *anti* minima are 20–30 kJ mol^{-1} higher in energy. While the deglycosylated nucleobase adducts are planar, the presence of the deoxyribose sugar induces a twist about the carbon–carbon bond connecting the phenol and nucleobase rings. The 8-*o*-PhOH-purine adducts are less twisted (25°) than the corresponding 8-*p*-PhOH-purine adducts (40°) due to stabilization provided by an intramolecular O−H · · · N7 bond. Solvation calculations demonstrate that the structural preference is solvent-dependent, where solvents with hydrogen-bonding abilities disrupt the intramolecular O−H · · · N7 hydrogen bond such that a greater degree of twist is observed, and less polar solvents stabilize the planar structure.[86]

While the structural impact of phenolic adducts has yet to be determined in duplex DNA, the phosphoramidite of 8-Ph-dG has been prepared and used to incorporate the adduct into oligonucleotides using solid-phase DNA synthesis.[87,88] In the 12-mer 5′-d (GCGCCXGCGGTG), where X = 8-Ph-dG, the T_m of the duplex was 5.6°C lower than the normal dG : dC base pair, while the T_m of 8-Ph-dG : dG was 2.1°C higher than that of the mismatched dG : dC base pair.[87] These data suggested that 8-Ph-dG exists

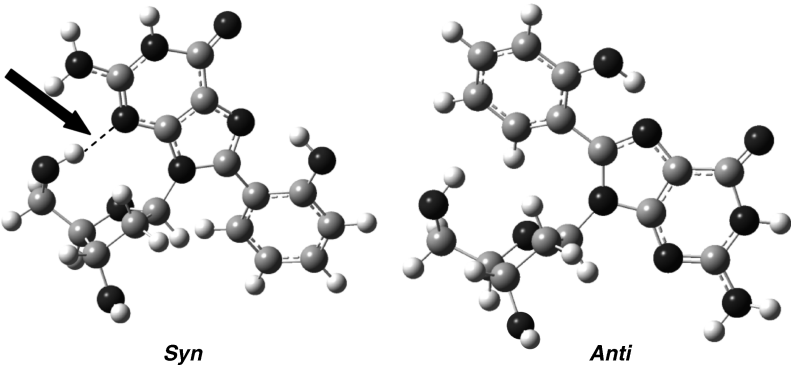

FIGURE 14.5. Fully optimized (B3LYP/6-311 + G(2df,p) low-energy *syn* and *anti* structures of 8-*o*-PhOH-dG. The arrow in the low-energy *syn* structure points to an O5′−H···N3 hydrogen bond that is absent in the *anti* structure that is 20–30 kJ mol^{-1} higher in energy.

primarily in the *anti* conformation when paired with dC, while the *syn* conformation may pair with dGMP. The miscoding properties of 8-Ph-dG have also been assessed using *in vitro* primer extension analysis.[88] Klenow fragment from *E. coli* incorporated predominately the correct base dCMP opposite 8-Ph-dG, while primer extension by mammalian pol α was strongly blocked opposite the lesion. Small amounts of dGMP and dAMP were incorporated opposite the lesion; two-base deletions were also observed, suggesting that 8-Ph-dG is weakly mutagenic and capable of generating G → C and G → T transversions and deletions in cells. These results provide a basis for the determination of substituent effects on the biological impact of C8-aryl-dG adducts.

14.6. CONCLUSIONS

Phenoxyl radicals are an important family of reactive intermediates that initiate oxidative DNA damage and covalent modification of DNA bases. Phenoxyl radicals play a key role in formation of DNA–protein cross-links (DPCs) that arise during times of cellular oxidative stress or when cells are exposed to ionizing radiation. For certain phenoxyl radicals the C8 site of dG is most susceptible to direct radical attachment, wherein the phenoxyl radicals act as ambident electrophiles forming C- and O-adducts. The natural phenolic carcinogen, ochratoxin A (OTA), has been shown by the ^{32}P-postlabeling method to form a C-C8-dG adduct *in vivo*, while the chemical carcinogen pentachlorophenol (PCP) generates an O-C8-dG adduct following activation by peroxidase enzymes. The C-adducts of phenols possess fluorescent pH-sensing properties and undergo oxidative polymerization reactions to afford ortho–ortho C–C oligomeric cross-linked adducts through the intermediacy of phenoxyl radicals. Within duplex DNA, the phenoxyl radical intermediates formed by the oxidation of C-C8-dG adducts of phenols are expected to form covalent cross-links, which may have therapeutic value.

14.7. FUTURE PROSPECTS

The basic biochemistry of covalent lesions formed by phenoxyl radicals remains largely unexplored. This is somewhat surprising given that (i) tyrosine residues play a crucial role in DPC formation that arise in chromatin structures because of oxidative DNA damage and (ii) phenolic toxins undergo bioactivation by peroxidase enzymes to generate phenoxyl radical intermediates that form covalent adducts by direct attachment to DNA nucleobases. Our efforts in this area of research are currently devoted to the site-specific incorporation of C8-dG adducts of phenols into oligonucleotides to assess their structural impact within duplex DNA and determine how C8-phenol-dG adducts influence DNA replication. Within this area of research we are particularly interested in the reactivity of C8-phenol-dG adducts within duplex DNA. Such adducts should act as radical cation sinks and then go on to generate phenoxyl radicals whose chemistry within duplex DNA has not been previously studied.

ACKNOWLEDGMENTS

The research in the author's laboratory was supported by the Natural Sciences and Engineering Research Council (NSERC) of Canada, the Canada Foundation for Innovation, the University of Guelph, and the Ontario Innovation Trust Fund. I also acknowledge with gratitude the contributions of my co-workers to these studies. Their names appear in the references; special thanks are due to Drs. Jian Dai (Wake Forest University, Winston-Salem, North Carolina), Wojciech Gabryelski (University of Guelph), Annie Pfohl-Leszkowicz (National High School of Agriculture, Toulouse, France), and Stacey D. Wetmore (University of Lethbridge, Alberta, Canada).

REFERENCES

1. Jordan, A.; Reichard, P. Ribonucleotide reductases. *Annu. Rev. Biochem.* **1998**, *67*, 71–98.
2. Chang, M. C. Y.; Yee, C. S.; Nocera, D. G.; Stubbe, J. Site-specific replacement of a conserved tyrosine in ribonucleotide reductase with an aniline amino acid: A mechanistic probe for a redox-active tyrosine. *J. Am. Chem. Soc.* **2004**, *126*, 16702–16703.
3. Fitzpatrick, P. F. Tetrahydropterin-dependent amino acid hydroxylases. *Annu. Rev. Biochem.* **1999**, *68*, 355–381.
4. Zhang, A.; Neumeyer, J. L.; Baldessarini, R. J. Recent progress in development of dopamine receptor subtype-selective agents: Potential therapeutics for neurological and psychiatric disorders. *Chem. Rev.* **2007**, *107*, 274–302.
5. Burton, G. W.; Ingold, K. U. Vitamin E: Application of the principles of physical organic chemistry to the exploration of its structure and function. *Acc. Chem. Res.* **1986**, *19*, 194–201.
6. Wright, J. S.; Johnson, E. R.; DiLabio, G. A. Predicting the activity of phenolic antioxidants: Theoretical method, analysis of substituent effects, and application to major families of antioxidants. *J. Am. Chem. Soc.* **2001**, *123*, 1173–1183.

7. Scalbert, A.; Williamson, G. Dietary intake and bioavailability of polyphenols. *J. Nutr.* **2000**, *130*, 2073S–2085S.
8. Yao, L. H.; Jiang, Y. M.; Shi, J.; Tomas-Barberan, F. A.; Datta, N.; Singanusong, R.; Chen, S. S. Flavonoids in food and their health benefits. *Plants Foods Hum. Nutr.* **2004**, *59*, 113–122.
9. Fan, Y.; Schreiber, E. M.; Giorgianni, A.; Yalowich, J. C.; Day, B. W. Myeloperoxidase-catalyzed metabolism of etoposide to its quinone and glutathione adduct forms in HL60 cells. *Chem. Res. Toxicol.* **2006**, *19*, 937–943.
10. Kang, Y. J.; Sun, X.; Chen Y.; Zhou, Z. Inhibition of doxorubicin chronic toxicity in catalase-overexpressing transgenic mouse hearts. *Chem. Res. Toxicol.* **2002**, *15*, 1–6.
11. Okamoto, Y.; Chou, P.-H.; Kim, S. Y.; Suzuki, N.; Laxmi, Y. R. S.; Okamoto, K.; Liu, X.; Matsuda, T.; Shibutani, S. Oxidative DNA damage in *XPC*-knockout and its wild mice treated with equine estrogen. *Chem. Res. Toxicol.* **2008**, *21*, 1120–1124.
12. Sipe, H. J., Jr.; Corbett, J. T.; Mason, R. P. *In vitro* free radical metabolism of phenolphthalein by peroxidases. *Drug. Metab. Disp.* **1997**, *25*, 468–480.
13. Bindhumol, V.; Chitra, K. C.; Mathur, P. P. Bisphenol A induces reactive oxygen species generation in the liver of male rats. *Toxicology* **2003**, *188*, 117–124.
14. Manderville, R. A.; Pfohl-Leszkowicz, A. Genotoxicity of chlorophenols and ochratoxin A. In *Advances in Molecular Toxicology*, Vol. 1; Fishbein J. C., Ed.; Elsevier, Amsterdam, **2006**, pp. 85–138.
15. Pfohl-Leszkowicz, A.; Manderville, R. A. Ochratoxin A: An overview on toxicity and carcinogenicity in animals and humans. *Mol. Nutr. Food Res.* **2007**, *51*, 61–99.
16. Strick, R.; Strissel, P. L.; Borgers, S.; Smith, S. L.; Rowley, J. D. Dietary bioflavonoids induce cleavage in the *MLL* gene and may contribute to infant leukemia. *Proc. Natl. Acad. Sci. USA* **2000**, *97*, 4790–4795.
17. Mullin, R.; Morrissey, S. Momentum builds against bisphenol A. In *C&EN*; Schulz, J. C.; Moore, K. J., Eds.; April 28, **2008**, p. 11.
18. Hansch, C.; McKarns, S. C.; Smith, C. J.; Doolittle, D. J. Comparative QSAR evidence for a free-radical mechanism of phenol-induced toxicity. *Chem.–Biol. Interact.* **2000**, *127*, 61–72.
19. Murray, A. R.; Kisin, E.; Castranova, V.; Kommineni, C.; Gunther, M. R.; Shvedova, A. A. Phenol-induced *in vivo* oxidative stress in skin: Evidence for enhanced free radical generation, thiol oxidation and antioxidant depletion. *Chem. Res. Toxicol.* **2007**, *20*, 1769–1777.
20. Bolton, J. L.; Trush, M. A.; Penning, T. M.; Dryhurst, G.; Monks, T. J. Role of quinones in toxicology. *Chem. Res. Toxicol.* **2000**, *13*, 135–160.
21. Zhao, S.; Narang, A.; Ding, X.; Eadon, G. Characterization and quantitative analysis of DNA adducts formed from lower chlorinated PCB-derived quinones. *Chem. Res. Toxicol.* **2004**, *17*, 502–511.
22. Bolton, J. L.; Thatcher, G. R. J. Potential mechanisms of estrogen quinone carcinogenesis. *Chem. Res. Toxicol.* **2008**, *21*, 93–101.
23. Manderville, R. A. Ambident reactivity of phenoxyl radicals in DNA adduction. *Can. J. Chem.* **2005**, *83*, 1261–1267.
24. Wagenknecht, H.-A.; Stemp, E. D. A.; Barton, J. K. DNA-bound peptide radicals generated through DNA-mediated electron transport. *Biochemistry* **2000**, *39*, 5483–5491.
25. Bjorklund, C. C.; Davis, W. B. Stable DNA-protein cross-links are products of DNA charge transport in a nucleosome core particle. *Biochemistry* **2007**, *46*, 10745–10755.

26. Li, C.; Hoffman, M. Z. One-electron redox potentials of phenols in aqueous solution. *J. Phys. Chem. B* **1999**, *103*, 6653–6656.

27. Dixon, W. T.; Murphy, P. Determination of the acidity constants of some phenol radical cations by means of electron spin resonance. *J. Chem. Soc., Faraday Trans. 2* **1976**, *72*, 1221–1230.

28. Terzian, R.; Serpone, N.; Draper, R.B.; Fox, M.A.; Pelizzetti, E. Pulse radiolytic studies of the reaction of pentahalophenols with OH radicals: formation of pentahalophenoxyl, dihydroxypentahalocyclohexadienyl, and semiquinone radicals. *Langmuir* **1991**, *7*, 3081–3089.

29. Burton, G. W.; Doba, T.; Gabe, E.; Hughes, L.; Lee, F. L.; Prasad, L.; Ingold, K. U. Autoxidation of biological molecules. 4. Maximizing the antioxidant activity of phenols. *J. Am. Chem. Soc.* **1985**, *107*, 7053–7065.

30. Litwinienko, G.; Ingold, K. U. Solvent effects on the rates and mechanisms of reactions of phenols with free radicals. *Acc. Chem. Res.* **2007**, *40*, 222–230.

31. Wright, J. S.; Shadnia, H. Computational modeling of substituent effects on phenol toxicity. *Chem. Res. Toxicol.* **2008**, *21*, 1426–1431.

32. Mahoney, L. R.; Weiner, S. A. A mechanistic study of the dimerization of phenoxyl radicals. *J. Am. Chem. Soc.* **1972**, *94*, 585–590.

33. Ye, M.; Schuler, R. H. Second-order combination reactions of phenoxyl radicals. *J. Phys. Chem.* **1989**, *93*, 1898–1902.

34. Raghavan, N. V.; Steenken, S. Electrophilic reaction of the OH radical with phenol. Determination of the distribution of isomeric dihydroxycyclohexadienyl radicals. *J. Am. Chem. Soc.* **1980**, *102*, 3495–3499.

35. Shadnia, H.; Wright, J. S. Understanding the toxicity of phenols: using quantitative structure–activity relationships and enthalpy changes to discriminate between possible mechanisms. *Chem. Res. Toxicol.* **2008**, *21*, 1197–1204.

36. Walsh, C. *Enzymatic Reaction Mechanisms*; W. H. Freeman, New York, **1979**, p. 488–493.

37. Stresser, D. M.; Kupfer, D. Catalytic characteristics of CYP3A4: Requirement for a phenolic function in *ortho* hydroxylation of estradiol and mono-*O*-demethylated methoxychlor. *Biochemistry* **1997**, *36*, 2203–2210.

38. Josephy, P. D.; Mannervik, B. *Molecular Toxicology*, 2nd ed., Oxford University Press, New York, **2006**, pp. 2–45.

39. Kagan, V. E.; Yalowich, J.; Borisenko, G. G.; Tyurina, Y. Y.; Tyurin, V. A.; Thampatty, P.; Fabisiak, J. P. Mechanism-based chemopreventive strategies against etoposide-induced acute myeloid leukemia: Free radical/antioxidant approach. *Mol. Pharmacol.* **1999**, *56*, 494–506.

40. Spink, D. C.; Zhang, F.; Hussain, M. M.; Katz, B. H.; Liu, X.; Hilker, D. R.; Bolton, J. L. Metabolism of equilenin in MCF-7 and MDA-MB-231 human breast cancer cells. *Chem. Res. Toxicol.* **2001**, *14*, 572–581.

41. Shen, L.; Pisha, E.; Huang, Z.; Pezzuto, J. M.; Krol, E.; Alam, Z.; van Breemen, R. B.; Bolton, J. L. Bioreductive activation of catechol estrogen-ortho-quinones: Aromatization of the B ring in 4-hydroxyequilenin markedly alters quinoid formation and reactivity. *Carcinogenesis* **1997**, *18*, 1093–1101.

42. Zhang, F.; Swanson, S. M.; van Breemen, R. B.; Liu, X.; Yang, Y.; Gu, C.; Bolton, J. L. Equine estrogen metabolite 4-hydroxyequilenin induces DNA damage in the rat mammary tissues: Formation of single-strand breaks, apurinic sites, stable adducts, and oxidized bases. *Chem. Res. Toxicol.* **2001**, *14*, 1654–1659.

43. Margolis, S. A.; Coxon, B.; Gajewski, E.; Dizdaroglu, M. Structure of a hydroxyl radical induced cross-link of thymime and tyrosine. *Biochemistry* **1988**, *27*, 6353–6359.

44. Dizdaroglu, M.; Gajewski, E.; Reddy, P.; Margolis, S. A. Structure of a hydroxyl radical induced DNA-protein cross-link involving thymine and tyrosine in nucleohistone. *Biochemistry* **1989**, *28*, 3625–3628.

45. Nackerdien, Z.; Rao, G.; Cacciuttolo, M. A.; Gajewski, E.; Dizdaroglu, M. Chemical nature of DNA-protein cross-links produced in mammalian chromatin by hydrogen peroxide in the presence of iron or copper ions. *Biochemistry* **1991**, *30*, 4873–4879.

46. Gajewski, E.; Dizdaroglu, M. Hydroxyl radical induced cross-linking of cytosine and tyrosine in nucleohistone. *Biochemistry* **1990**, *28*, 977–980.

47. Schuster, G. B. Long-range charge transfer in DNA: Transient structural distortions control the distance dependence. *Acc. Chem. Res.* **2000**, *33*, 253–260.

48. Joseph, J.; Schuster, G. B. Emergent functionality of nucleobase radical cations in duplex DNA: Prediction of reactivity using qualitative potential energy landscapes. *J. Am. Chem. Soc.* **2006**, *128*, 6070–6074.

49. Steenken, S.; Jovanovic, S. V. How easily oxidizable is DNA? One-electron reduction potentials of adenosine and guanosine radicals in aqueous solution. *J. Am. Chem. Soc.* **1997**, *119*, 617–618.

50. Defelippis, M. R.; Murthy, C. P.; Broitman, F.; Weinraub, D.; Faraggi, M.; Klapper, M. H. Electrochemical properties of tyrosine phenoxyl and tryptophan indolyl radicals in peptides and amino acid analogs. *J. Phys. Chem.* **1991**, *95*, 3416–3419.

51. Bergeron, F.; Nair, V. K.; Wagner, J. R. Near-UV induced interstrand cross-links in anthraquinone–DNA duplexes. *J. Am. Chem. Soc.* **2006**, *128*, 14798–14799.

52. Muller, J. G.; Kayser, L. A.; Paikoff, S. J.; Duarte, V.; Tang, N.; Perez, R. J.; Rokita, S. E.; Burrows, C. J. Formation of DNA adducts using nickel(II) complexes of redox-active ligands: A comparison of salen and peptide complexes. *Coord. Chem. Rev.* **1999**, *185–186*, 761–774.

53. Stemmler, A. J.; Burrows, C. J. The sal-XH motif for metal-mediated oxidative DNA-peptide cross-linking. *J. Am. Chem. Soc.* **1999**, *121*, 6956–6957.

54. Kornyushyna, O.; Stemmler, A. J.; Graybosch, D. M.; Bergenthal, I.; Burrows, C. J. Synthesis of a metallopeptide–PNA conjugate and its oxidative cross-linking to a DNA target. *Bioconjugate Chem.* **2005**, *16*, 178–183.

55. Dai, J.; Wright, M. W.; Manderville, R. A. An oxygen-bonded C8-deoxyguanosine nucleoside adduct of pentachlorophenol by peroxidase activation: Evidence for ambident C8 reactivity by phenoxyl radicals. *Chem. Res. Toxicol.* **2003**, *16*, 817–821.

56. Dai, J.; Sloat, A. L.; Wright, M. W.; Manderville, R. A. Role of phenoxyl radicals in DNA adduction by chlorophenol xenobiotics following peroxidase activation. *Chem. Res. Toxicol.* **2005**, *18*, 771–779.

57. Dai, J.; Wright, M. W.; Manderville, R. A. Ochratoxin A forms a carbon-bonded C8-deoxyguanosine nucleoside adduct: Implications for C8 reactivity by a phenolic radical. *J. Am. Chem. Soc.* **2003**, *125*, 3716–3717.

58. Lawson, T.; Gannett, P. M.; Yau, W.-M.; Dalal, N. S.; Toth, B. Different patterns of mutagenicity of arenediazonium ions in V79 cells and *Salmonella typhimurium* TA102: Evidence for different mechanisms of action. *J. Agric. Food Chem.* **1995**, *43*, 2627–2635.

59. Hiramoto, K.; Kaku, M.; Sueyoshi, A.; Fujise, M.; Kikugawa, K. DNA base and deoxyribose modification by the carbon-centered radical generated from 4-(hydroxymethyl)benzene-diazonium salt, a carcinogen in mushroom. *Chem. Res. Toxicol.* **1995**, *8*, 356–362.

60. Gannett, P. M.; Powell, J. H.; Rao, R.; Shi, X.; Lawson, T.; Kolar, C.; Toth, B. C^8-Arylguanine and C^8-aryladenine formation in calf thymus DNA from arenediazonium ions. *Chem. Res. Toxicol.* **1999**, *12*, 297–304.

61. Burrows, C. J.; Muller, J. G. Oxidative nucleobase modifications leading to strand scission. *Chem. Rev.* **1998**, *98*, 1109–1151.

62. Ramirez-Arizmendi, L. E.; Heidbrink, J. L.; Guler, L. P.; Kenttämaa, H. I. Reactivity of substituted charged phenyl radicals toward components of nucleic acids. *J. Am. Chem. Soc.* **2003**, *125*, 2272–2281.

63. Kikugawa, K.; Kato, T.; Kojima, K. Substitution of *p*- and *o*-hydroxyphenyl radicals at the 8 position of purine nucleosides by reaction with mutagenic *p*- and *o*-diazoquinones. *Mutat. Res.* **1992**, *268*, 65–75.

64. Cavalieri, E. L.; Rogan, E. Role of radical cations in aromatic hydrocarbon carcinogenesis. *Environ. Health Perspect.* **1985**, *64*, 69–84.

65. Rogan, E. G.; Cavalieri, E. L.; Tibbels, S. R.; Cremonesi, P.; Warner, C. D.; Nagel, D. L.; Tomer, K. B.; Cerney, R. L.; Gross, M. L. Synthesis and identification of benzo[*a*]pyrene-guanine nucleoside adducts formed by electrochemical oxidation and by horseradish peroxidase catalyzed reaction of benzo[*a*]pyrene with DNA. *J. Am. Chem. Soc.* **1988**, *110*, 4023–4029.

66. Dai, Q.; Xu, D.; Lim, K.; Harvey, R. G. Efficient syntheses of C^8-aryl adducts of adenine and guanine formed by reaction of radical cation metabolites of carcinogenic polycyclic aromatic hydrocarbons with DNA. *J. Org. Chem.* **2007**, *72*, 4856–4863.

67. Abul-Hajj, Y. J.; Tabakovic, K.; Tabakovic, I. An estrogen–nucleic acid adduct. Electroreductive intermolecular coupling of 3,4-estrone-*o*-quinone and adenine. *J. Am. Chem. Soc.* **1995**, *117*, 6144–6145.

68. Akanni, A.; Abul-Hajj, Y. J. Estrogen-nucleic acid adducts: Dissection of the reaction of 3,4-estrone quinone and its radical anion and radical cation with deoxynucleosides and DNA. *Chem. Res. Toxicol.* **1999**, *12*, 1247–1253.

69. Da Costa, C. P.; Sigel, H. Acid–base and metal ion binding properties of guanyly($3' \rightarrow 5'$) guanosine (GpG^-) and $2'$-deoxyguanyly($3' \rightarrow 5'$)-$2'$-deoxyguanosine[$d(GpG)^-$] in aqueous solution. *Inorg. Chem.* **2003**, *42*, 3475–3482.

70. Hevesi, L.; Wolfson-Davidson, E.; Nagy, J. B.; Nagy, O. B.; Bruylants, A. Contribution to the mechanism of the acid-catalyzed hydrolysis of purine nucleosides. *J. Am. Chem. Soc.* **1972**, *94*, 4715–4720.

71. Zoltewicz, J. A.; Clark, D. F.; Sharpless, T. W.; Grahe, G. Kinetics and mechanism of the acid-catalyzed hydrolysis of some purine nucleosides. *J. Am. Chem. Soc.* **1970**, *92*, 1741–1750.

72. Gates, K. S.; Nooner, T.; Dutta, S. Biological relevant chemical reactions of N7-alkylguanine residues in DNA. *Chem. Res. Toxicol.* **2004**, *17*, 839–856.

73. Tretyakova, N. Y.; Burney, S.; Pamir, B.; Wishnok, J. S.; Dedon, P. C.; Wogan, G. N.; Tannenbaum, S. R. Peroxynitrite-induced DNA damage in the *supF* gene: Correlation with the mutational spectrum. *Mutat. Res.* **2000**, *447*, 287–303.

74. Liu, J.; Petzold, C. J.; Ramirez-Arizmendi, L. E.; Perez, J.; Kenttämaa, H. Phenyl radicals react with dinucleoside phosphates by addition to purine bases and H-atom abstraction from a sugar moiety. *J. Am. Chem. Soc.* **2005**, *127*, 12758–12759.

75. Yang, L.; Nash, J. J.; Yurkovich, M. J.; Jin, Z.; Vinueza, N. R.; Kenttämaa, H. I. Gas-phase reactivity of aromatic σ,σ-biradicals toward dinucleoside phosphates. *Org. Lett.* **2008**, *10*, 1889–1892.

76. Foti, M.; Ingold, K. U.; Lusztyk, J. The surprisingly high reactivity of phenoxyl radicals. *J. Am. Chem. Soc.* **1994**, *116*, 9440–9447.

77. Scaiano, J. C.; Stewart, L. C. Phenyl radical kinetics. *J. Am. Chem. Soc.* **1983**, *105*, 3609–3614.

78. Maillard, B.; Ingold, K. U.; Scaiano, J. C. Rate constants for the reactions of free radicals with oxygen in solution. *J. Am. Chem. Soc.* **1983**, *105*, 5095–5099.

79. Weishar, J. L.; McLaughlin, C. K.; Baker, M.; Gabryelski, W.; Manderville, R. A. Oxidation of a biomarker for phenol carcinogen exposure: Expanding the redox chemistry of 2′-deoxyguanosine. *Org. Lett.* **2008**, *10*, 1839–1842.

80. Luo, W.; Muller, J. G.; Rachlin, E. M.; Burrows, C. J. Characterization of spiroimino-dihydantoin as a product of 7,8-dihydro-8-oxoguanosine oxidation. *Org. Lett.* **2000**, *2*, 613–616.

81. Stover, J. S.; Ciobanu, M.; Cliffel, D. E.; Rizzo, C. J. Chemical and electrochemical oxidation of C8-arylamine adducts of 2′-deoxyguanosine. *J. Am. Chem. Soc.* **2007**, *129*, 2074–2081.

82. Jaffé, H. H. A reexamination of the Hammett equation. *Chem. Rev.* **1953**, *53*, 191–261.

83. Sun, K. M.; McLaughlin, C. K.; Lantero, D. R.; Manderville, R. A. Biomarkers for phenol carcinogen exposure act as pH-sensing fluorescent probes *J. Am. Chem. Soc.* **2007**, *129*, 1894–1895.

84. Hansch, C.; Leo, A.; Taft, R. W. A survey of Hammett substituent constants and resonance and field parameters. *Chem. Rev.* **1991**, *91*, 165–195.

85. McLaughlin, C. K.; Lantero, D. R.; Manderville, R. A. Conformational properties of a phototautomerizable nucleoside biomarker for phenolic carcinogen exposure *J. Phys. Chem. A* **2006**, *110*, 6224–6230.

86. Millen, A. L.; McLaughlin, C. K.; Sun, K. M.; Manderville, R. A.; Wetmore, S. D. Computational and experimental evidence for the structural preference of phenolic C-8 purine adducts. *J. Phys. Chem. A* **2008**, *112*, 3742–3753.

87. Gannett, P. M.; Heavner, S.; Daft, J. R.; Shaughnessy, K. H.; Epperson, J. D.; Greenbaum, N. L. Synthesis, properties, and NMR studies of a C8-phenylguanine modified oligonucleotides that preferentially adopts the Z DNA conformation. *Chem. Res. Toxicol.* **2003**, *16*, 1385–1394.

88. Kohda, K.; Tsunomoto, H.; Kasamatsu, T.; Sawamura, F.; Terashima, I.; Shibutani, S. Synthesis and miscoding specificity of oligodeoxynucleotide containing 8-phenyl-2′-deoxyguansine. *Chem. Res. Toxicol.* **1997**, *10*, 1351–1358.

INDEX

Radical and Radical Ion Reactivity in Nucleic Acid Chemistry, Edited by Marc M. Greenberg